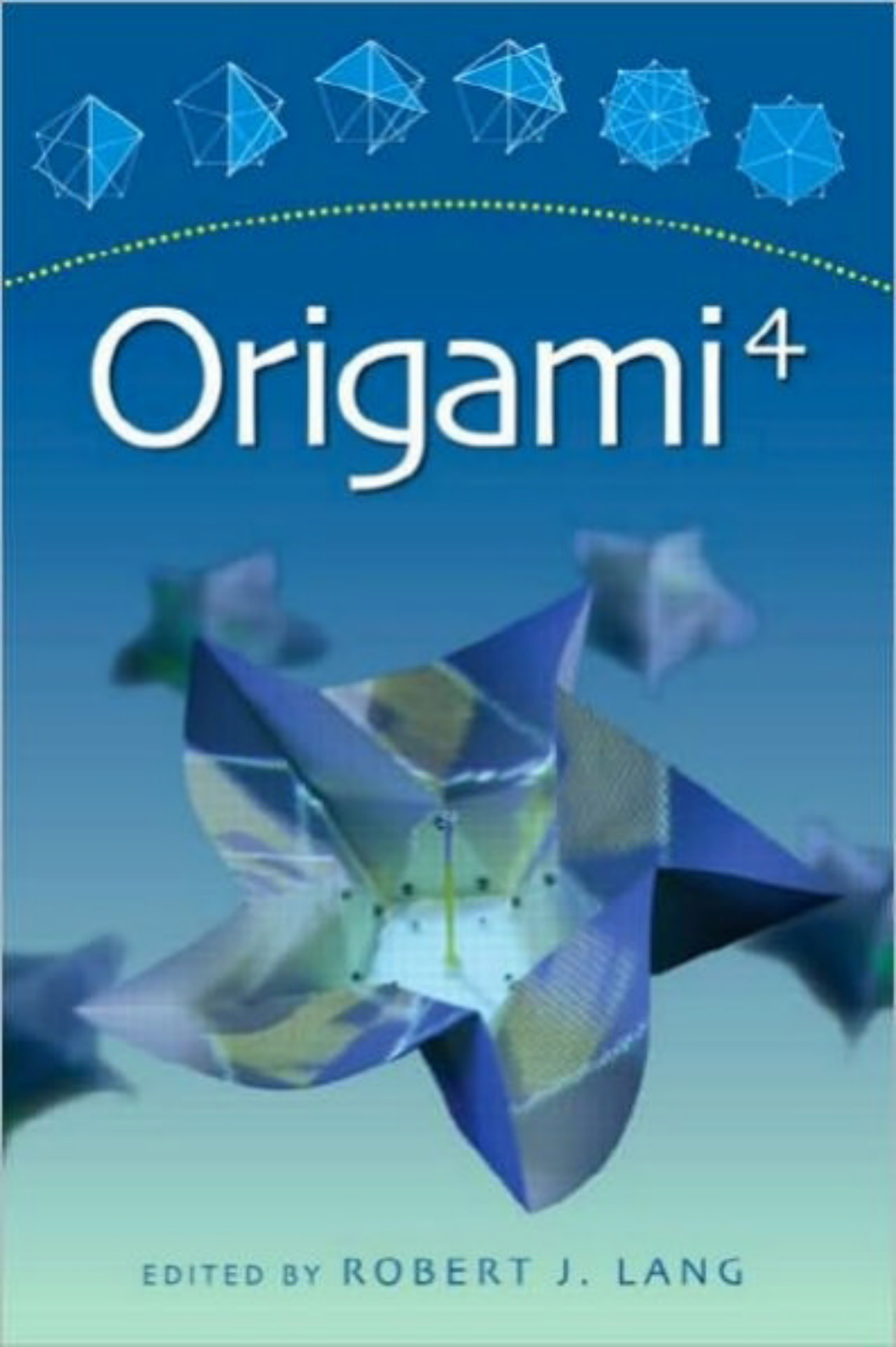
Origami4
EDITED BY ROBERT J. LANG

Origami^4

Origami^4

Fourth International Meeting of Origami Science, Mathematics, and Education

Robert J. Lang, editor

A K Peters, Ltd.
Natick, Massachusetts

Editorial, Sales, and Customer Service Office

A K Peters, Ltd.
5 Commonwealth Road, Suite 2C
Natick, MA 01760
www.akpeters.com

Library of Congress Cataloging-in-Publication Data

International Meeting of Origami Science, Mathematics, and Education (4th : 2006 : Pasadena, Calif.)
Origami 4 : Fourth International Meeting of Origami Science, Mathematics, and Education / Robert J. Lang, editor.
p. cm.
Includes bibliographical references and index.
ISBN 978-1-56881-346-2 (alk. paper)
1. Origami–Mathematics–Congresses. 2. Origami in education–Congresses. I. Lang, Robert J. (Robert James), 1961- II. OrigamiUSA. III. Title. IV. Title: Origami Four.
More CIP info.

QA491.I55 2006
736'.982–dc22

2009013855

Cover illustrations: See "Constructing Regular n-gonal Twist Boxes," Figure 2 (p. 43); "A Brief History of Oribotics," Figure 1 (p. 52); and "Curves and Flats," Figure 4 (p. 13).

Printed in the United States of America
13 12 11 10 09 10 9 8 7 6 5 4 3 2 1

Contents

Preface

The concepts of *origami* and *science* would seem to be about as far apart as you can get within human fields of endeavor: the former, an art, a craft, associated with a Japanese tradition hundreds of years old; the latter, a strict, rationalist way of knowing. But remarkably, both fields extend tendrils of influence into the other, exhibiting connections in manifold ways. And, in fact, they have done so for decades.

For upon closer examination, they are not as far apart as you might think, science and origami, or even science and art in general. While science is generally perceived among the public as the province of white-coated individuals following a rigid set of rules collectively known as "the scientific method," said scientific method is merely a discipline—a set of tools—that bring order to what is still a very human practice. Aesthetic terms like "elegance" pervade science; and while one may create and follow a double-blind protocol to evaluate a hypothesis or use advanced computational and mathematical tools to establish and explore a technology, the moment of scientific inspiration—that moment of "Aha!"—is widely known, if not widely advertised, as an art within the science. Many scientists, mathematicians, and technologists are as motivated by the order, beauty, and elegance within their field as any painter, writer, or sculptor. Scratch a successful scientist, and you will find an artist not far under the surface.

Conversely, the art of origami—folding uncut sheets of paper into beautiful objects—is deeply connected to the worlds of mathematics and science. The laws of origami—folding without cutting—would seem on their surface to be so restrictive as to prevent any significant variety of accomplishment. It is a testimony to the ingenuity of hundreds of origami artists that the opposite is true; there seems to be no limit on the range of artistic expres-

sion possible within origami. But there are absolute limits on the physical structures foldable with origami. Those limits are defined by the underlying mathematics of origami. By exploring, elucidating, and describing those mathematical laws, modern origami artists have found ways to push the art to undreamed-of heights, and to begin to develop computational tools that augment the capabilities of the human artist in order to more fully realize their artistic visions.

At the same time, these mathematical explorations have allowed origami, or more broadly, folded structures, to take on applications in the real world and bring real benefits to the world. Folded structures based on origami principles have found application in space flight, consumer electronics, health, and safety, to name just a few areas where origami has made an unexpected appearance.

These rich connections make origami an ideal vehicle to bridge the supposedly disparate worlds of math and science, and it should be no surprise that origami has found repeated application in education to form connections, to make mathematics accessible, and to provide concrete demonstration of the fact that mathematics is everywhere around us.

The connections between origami, mathematics, science, technology, and education have been a topic of considerable interest now for several decades. While many individuals have happened upon discrete connections among these fields during the twentieth century, the field began to take off when previously isolated individuals began to make further connections with each other through a series of conferences exploring the links between origami and "the outside world." The first such conference, the First International Meeting of Origami Science and Technology was held in Ferrara, Italy, in 1989, and was organized by Professor Humiaki Huzita at the University of Padova. This conference brought together researchers from all over the world, many meeting each other for the first time, and its published proceedings became almost immediately a standard reference for mathematical origami. (And now they are an extremely hard-to-find reference.)

This conference was so successful that a second conference, The Second International Meeting of Origami Science and Scientific Origami, was organized in Ohtsu, Japan, in 1994. It, too, produced a proceedings volume, which also became a key reference for this cross-disciplinary field. It was followed in 2001 by the Third International Meeting on Origami in Science, Mathematics, and Education, held in Monterey, California, whose proceedings were published as a book, *Origami*^{3}, edited by Thomas Hull, and published by A K Peters, Ltd.

The success of these conferences—each year larger and with a more extensive program than the last—and their proceedings led to the Fourth International Meeting on Origami in Science, Mathematics, and Education

(4OSME), held in September, 2006, at the California Institute of Technology in Pasadena, California. The 4OSME brought together an unprecedented number of researchers presenting some 80 papers on fields ranging from mathematics, to technology, to educational uses of origami, to computer programs for the design of origami. Selected papers based on talks presented at that conference make up the book you hold in your hands.

It should be clear now that this book, and the conference that gave rise to it, owe their existence to those pioneering individuals who plumbed the fields of origami, math, science, and education. The contributors to those fields are innumerable, but I should like to acknowledge several people and organizations whose support was absolutely critical. First and foremost, the support of OrigamiUSA, which sponsored the conference, and of the California Institute of Technology, which provided facilities as well as financial support, was invaluable. The program committee, consisting of Tom Hull, Günter Rote, Ryda Rose, Koichi Tateishi, and Toshikazu Kawasaki, performed heroic duties in reviewing (and in many cases, recommending improvements to) both the conference papers and the works in this book. Tom, in particular, played a critical role in bringing this book together in many ways: advice, support, and through his extensive knowledge of origami-math. I must also express my thanks to an anonymous reviewer (you know who you are) who made extensive and helpful recommendations for several of the papers. Last, this book would not exist at all if not for the contributions of the authors, those who gave presentations at 4OSME, and who contributed to this book. My thanks to you all.

Robert J. Lang
General Chair, 4OSME
Editor, *Origami*^{4}
Alamo, California, 2008

Part I

Origami in Design and Art

Paper Nautili: A Model for Three-Dimensional Planispiral Growth

Arle Lommel

The spiral forms of seashells have been of interest to many paper folders in recent years, with models such as the elegant intertwined flaps of Tomoko Fuse and Robert Lang's nautilus. This article describes a novel method for the construction of smoothly curved three-dimensional models of logarithmic spiral shell-like forms that approximate the curves of natural spiral shells.

This model differs from existing models in a number of regards. Rather than intertwining flaps, it is produced by repetition of a relatively simple folding sequence along the length of a tapered strip of folding medium in which a straight line is folded to a curved line, thereby causing the folding medium to buckle into three dimensions with a curve roughly catenary in form.

It should be emphasized that this model was designed initially through practical hands-on experimentation, not via the mathematical model presented herein, which is a post facto explanation of the results. As a result, even if any details of the mathematical model remain underspecified, the practical results demonstrate that the techniques described work well for producing actual models.

The natural basis chosen for this model was the shell of the chambered nautilus. Besides its traditional use as an image of mathematical perfection,

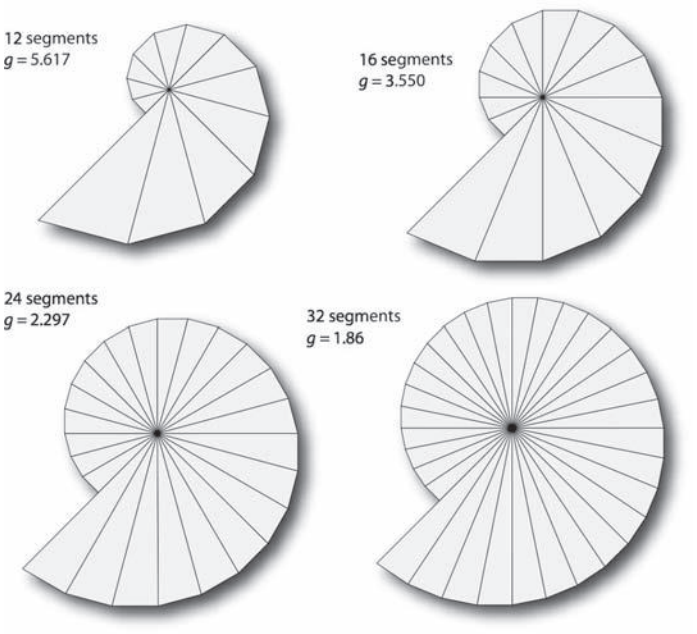

Figure 1. Various spirals produced by rotating similar right triangles about a radial axis.

the nautilus is planispiral (i.e., the spiral coils on a plane and is bilaterally symmetrical) and has a relatively simple catenary-type cross section when cut radially from the axis. It is thus a relatively simple shell form to model when compared to many other whorled shells found in nature.

Contrary to numerous published accounts, the chambered nautilus is not a so-called Golden Mean spiral; like the Golden Mean spiral it is a logarithmic (constant-slope) spiral, but a simple visual examination of both spirals shows that the nautilus has a much lower slope. The fact that so many sources cite it as a Golden Mean spiral demonstrates how powerful the belief in nature's mathematical basis can be, even in the face of manifest evidence to the contrary. One goal in producing this model was to generate a spiral that approximated the actual spiral of the nautilus rather than the idealized (but inaccurate) form that many scholars state that it has.

A useful starting point for designing this model is that any logarithmic spiral can be approximated as a series of similar triangles in which the hypotenuse of one triangle lies on (and is equal in length to) one leg of the previous triangle (see Figure 1). Each triangle differs in size from its neighbors by a fixed ratio. For purposes of this model, a series of right

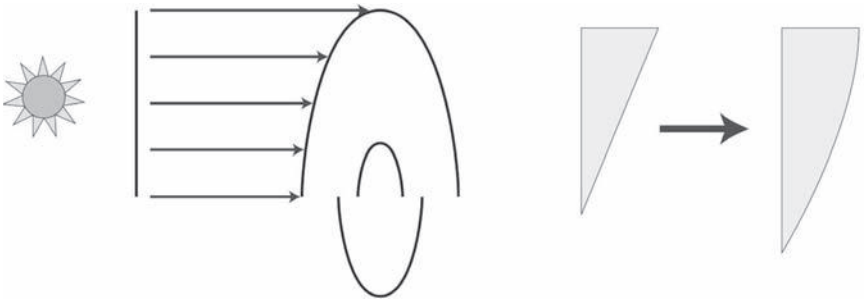

Figure 2. The shadow of right-triangle spiral segments on the curved form of the final model produces segment shapes that can cover the surface of the nautilus model.

triangles is particularly useful, because when right triangles are utilized to model a logarithmic spiral, a simple formula can be used to determine the growth rate per revolution (g) for any number of triangular segments per revolution (n):

$$g = \cos(2\pi/n)^{-n}.$$

This formula produces steeper slopes/growth rates for lower numbers of segments, as shown in Figure 1. As it turns out, measurements of actual nautilus shells yielded growth rates of roughly 3.5, for which the value $g = 3.55$ of a 16-segment spiral model is a good approximation (a Golden Mean spiral, in contrast, has a g roughly equal to 6.9). Therefore, to simplify folding and design, this model of the nautilus adopts the 16-segment model. (It should be noted that *any* arbitrary logarithmic spiral can be produced in this manner, and I have produced 12- and 32-segment models in addition to the 16-segment model described here.)

Having established an appropriate two-dimensional model for the nautilus spiral's growth pattern, the problem of how to generate the three-dimensional structure, which includes roughly catenary radial cross sections, remains. However, this problem can be solved in a simple manner: the needed two-dimensional shapes can be conceived as the shadows of the right-angle triangles on the surface of the desired three-dimensional shape, as shown in Figure 2.

The shadows of the original right triangle sections show the same scaling factor with regard to adjacent segments as in the original two-dimensional model, allowing them to be arranged within an evenly tapered strip of folding medium, as shown in Figure 3.

It is important to note in Figure 3 that the curved segment BC (the shadow-distorted hypotenuse of an original ABC right triangle) is equal in length to the leg of BDE (the curve onto which each segment was projected

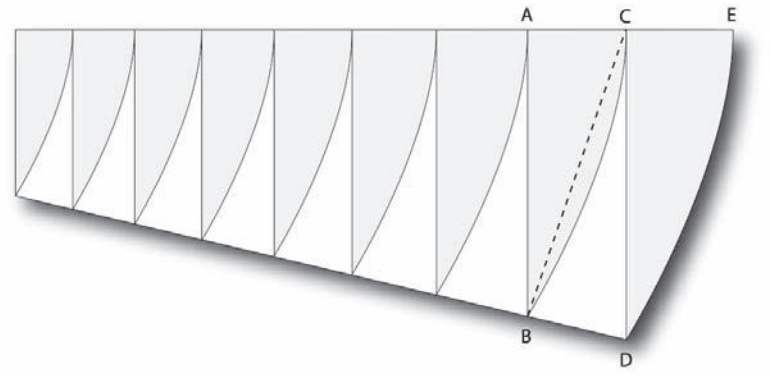

Figure 3. A sequence of distorted triangles that can cover the surface of a nautilus model arranged in a series.

was the same curve), and the straight-line segment BC (shown with a dotted line) is, consequently, shorter than CD. The ratio (r) of the length of the edge of any distorted triangle to the corresponding edge of its larger neighbor is defined as

$$r = g^{1/n}.$$

In the case of the 16-segment model, this yields a scale factor of 1.082. (This simple scaling factor aids in the production of templates for folding the model on a computer since each segment can be copied and scaled to yield the next segment.)

The fact that CD and CB are equal in length suggests a folding sequence that will yield the three-dimensional shape sought in this model. Segment CD is mountain folded and swung back to lie on CB, a process that is repeated on each segment of the model to leave only the gray shaded areas in Figure 3 visible. As the straight line CD is brought to lie on the curve BC, a curved valley fold forms equidistant between CD and BC. As this new fold is formed, the folding medium takes on the catenary-like shape onto which the original triangle sections were projected in Figure 2. Through the repetition of this process, the tips of the triangles (e.g., points B and D in Figure 3) are all brought to lie on the axis of the spiral, causing the overall spiral outline to form. One advantage of this model is that as points C and D are brought together, the valley fold (line CF in the crease pattern shown in Figure 4) automatically forms, similar to folding a straight angle bisector in conventional origami. Although it looks difficult, the folding is actually quite simple and automatic with a small amount of practice.

Figure 4 shows the resulting crease pattern, and Figure 5 shows a completed model made in this fashion from copper cloth.

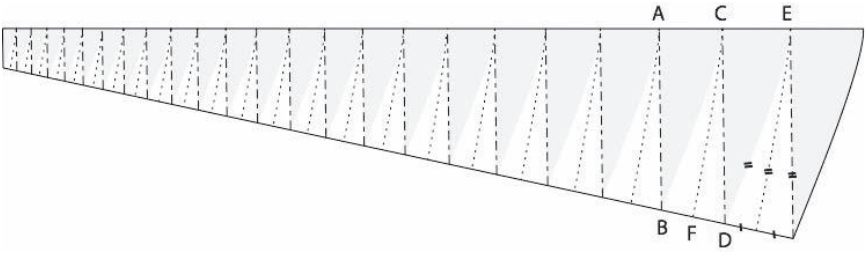

Figure 4. Crease pattern for a half nautilus shell. Gray areas will be visible from the outside of the completed model. Twenty four segments (1.5 revolutions) are shown.

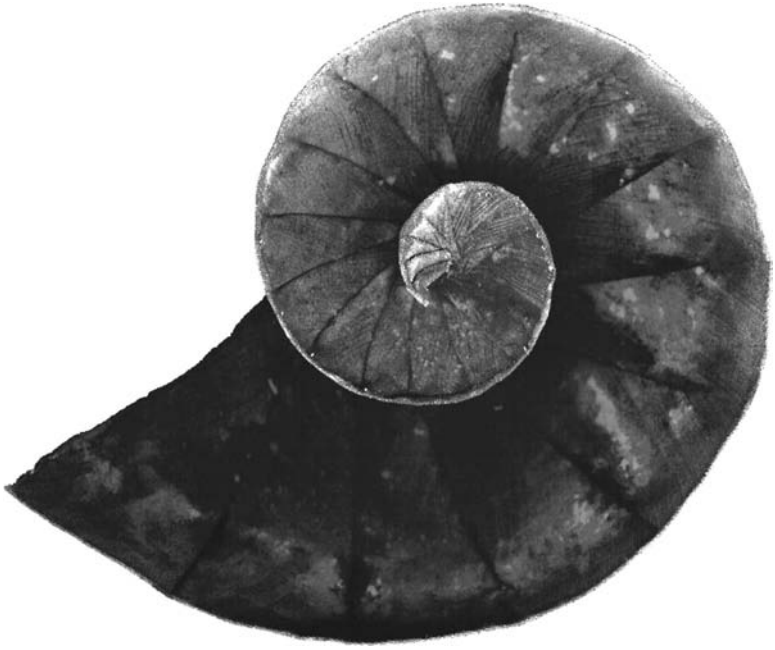

Figure 5. Image of a completed half-shell model folded from copper cloth and chemically treated to variegate the surface.

As a practical matter, shells made following this model can be constructed by using a computer-drawing program (the author uses Adobe Illustrator) to generate a paper template used to place the mountain folds, which are precreased. This crease pattern can produce a half shell (as shown), or it can be reflected along its top edge to produce a bilaterally symmetrical crease pattern that yields a model of a complete shell. Either

model is aesthetically pleasing, although only the half shell model affords a view of both the "inside" and the "outside" of the construction. In addition, the crease pattern can be extended to produce as many spirals as desired, although the folding is impractical below a certain size and adding extra segments on the big end can take up a large amount of folding medium for little additional spiral. If paper is used to fold these models, wet folding is helpful if the final model is to retain its shape, but in the author's experience, woven metal cloth is a superior folding medium for these models due to its malleability and receptiveness to hard creases.

In conclusion, this article has described a folded model that closely resembles an actual nautilus shell in its overall shape and spiral growth. It is constructed using a minimal set of repeated folds (and is thus conceptually elegant). The model is useful because it approximates the structure of an actual shell, rather than just its appearance, and does so in a gracefully curved form. In addition, the fold lines visible on the inside are evocative of the septa within a real nautilus shell, an unintended aesthetic bonus of the design. This novel technique for folding curves has proved capable of accurately modeling a variety of natural planispiral shells in an elegant and natural-seeming manner. To this point, the technique has been applied only to planispiral shells. The author has attempted to apply the technique to the more complex whorls of marine snails and other conically-spiral shells, but the results have not met expectations. Further research may enable the technique to be extended into these more complex shapes, but success is not yet certain.

Curves and Flats

Saadya Sternberg

1 Background: Raising a Pattern, Keeping a Sheet Flat

What is the subject here? The aim is to gain control of this medium, mostly so as to be able to make those faces, my main proving ground. And the medium itself—is what? Clearly it involves *folding curves* (in, as it happens, rectangles of brown wrapping paper spray-glued to thick aluminum foil). Now curve folding, as is known, creates surfaces that won't lie flush to each other, that is, *open folds*; and open folds can be made voluntarily with straight lines too. So maybe our subject is best described as the *manipulation of open folds*, whether curved or not. And gaining control of this subject, taming it, means, for me—as in certain political theories—flattening it: being able to crush, squeeze, twist, bend the thing to the right or left .... In short, I want to be able to restore an *average flatness* to a surface *deformed by curved or open folds*, and then see whether and how such a textured or raised surface can be further manipulated.

But let's start at the beginning. Suppose you put curved folds of any kind in a flat sheet of paper. The paper will no longer lay flat. For that matter, you can easily enough use *straight folds* to create a surface that curves—a cone for example—by means of an angled crimp that originates in the interior of a sheet. But with non-flat surfaces made only via straight-line folds, you can always collapse the surface to a completely flat state (while retaining the initial folds) by adding a finite number of new straight-

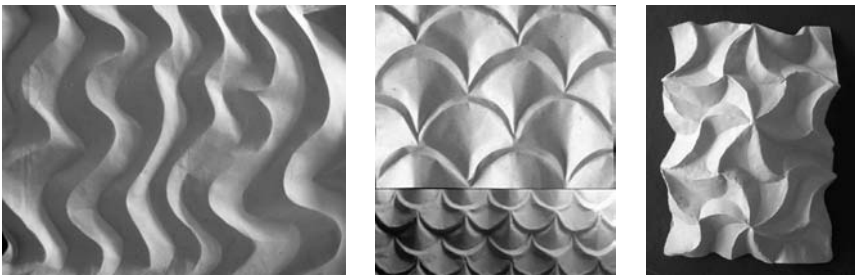

(a) (b) (c)

Figure 1. (a) *Sand Curves.* (b) *Fish Scales.* (c) *Triangle Spirals.*

line folds. Curved surfaces made by *curved* folds cannot be collapsed flat while retaining those folds by *any* finite means, neither by adding straight folds nor by adding curved folds. (Both of these last conjectures seem to me eminently provable.)

If real flatness is not to be had, there is still the next-best thing, *average* flatness. Here the surface has a raised texture of essentially the same height and depth throughout. The surface gives some of the appearance of flatness and shares some of its properties. This article mainly addresses some of the issues involved in making and manipulating surfaces of such a kind.

For a surface with a curved fold to be kept flat on average, a pattern of curves of roughly similar shape must typically be drawn on it. This can be done in one direction, with curves (for instance, waves) running parallel to each other. Can it be done in two? Clearly it can, for one instinctively flattens a cone shape (a surface created by a flat fold) by means of concentric circles. But another, less explored possibility is to divide a flat surface into a lattice of squares, triangles, or hexagons, and to place the identical curve pattern in each. This has the nice effect of shrinking the paper by the same amount in all places, so it is not forced to bend from the plane. And it not only maintains average flatness, but also yields a surface that is similar in outline to the one with which we started. (See the examples in Figure 1.)

However, this trick can't be done with every pattern, only with those that line up or *tessellate*—so that the left line in one tile's pattern turns into a right line in the tile next to it, and ditto for tops and bottoms.

2 Spiral Curvigami Tessellations

One ancient, well-studied pattern that tessellates very nicely is the vortex or spiral, so I want to spend a little time on it.

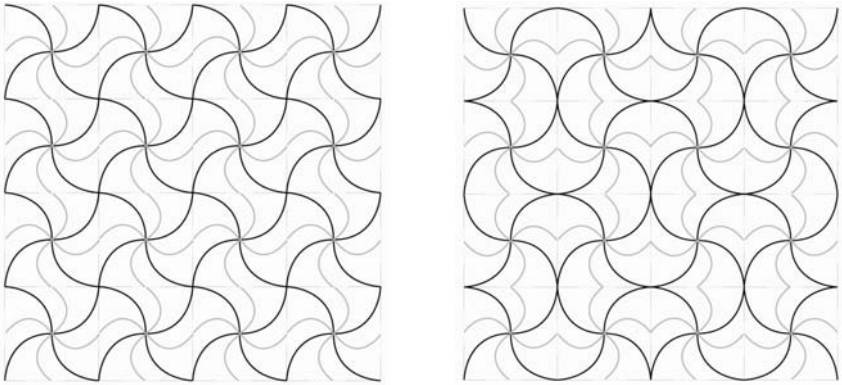

(a) (b)

Figure 2. (a) Regular square spirals. (b) Alternating spirals.

A vortex, whether in a bathtub or a galaxy, is nature's way of pulling material in a plane toward a center in the least objectionable manner, so it's an intuitive choice for shrinking a sheet of paper too. Liquid swirls were considered observationally by Leonardo da Vinci and patterns of ornamental spirals are to be found in the decorative art of many ancient cultures.

In origami too, spirals and vortex-like twist-folds have a distinguished pedigree, having been studied by, among others, S. Fujimoto, T. Kawasaki, Alex Bateman, Tomoko Fuse, Jeremy Shafer, Chris Palmer—indeed it sometimes seems by all the pioneers of the currently exploding field of *origami tessellations*. The spiral tessellations I'm introducing here are necessarily related to some of those more familiar ones in their underlying geometry, and they have other points in common too. But one difference is that the spirals here are drawn on the surface *as curves* and then folded *directly*—causing the paper to condense—rather than being created from straight folds of relatively free material in already condensed paper, folds that are then twisted into spirals. These spiral patterns are, for all that, one type of origami tessellation: they belong to the subset of tessellations that can be formed continuously with a lateral, bidirectional compression of a surface.

With a square and triangular grid, you can make spirals that curve in the same direction (Figure 2(a)) or you can alternate the direction (Figure 2(b)); the pattern will still line up. (With a hexagonal grid more thought is needed to achieve alternation.) Figure 1(c) is from a triangular grid with a unidirectional spiral; Figures 3(c) and 4 use a square grid. In

(a) (b) (c)

Figure 3. (a) *Hexagon Spirals.* (b) *Squeezed Hair.* (c) *Molly.*

these patterns the eye is naturally drawn to the shaded hollows between the ridges, but if you look at the vertices you'll see the pattern's spiral basis. Figure 5(a) is a fancy version of a spiral pattern based on a hexagonal grid; Figure 3(a) and (b) use simple spirals, also from hexagons.

Interestingly, an alternating spiral pattern compresses inward from the sides much less than a unidirectional pattern does. The degree of lateral compressibility is an important issue for any open-fold pattern, although it takes some practice to be able to recognize from a pattern drawing alone how well it will compress. I won't dwell on this subject here, but the issue of tangents, touched on below, bears on compressibility. It should be remembered that when a pattern contains curves it will not compress all the way, in the nice way that a Miura fold does. So the applicability of curving patterns for stents and such may be somewhat limited; but perhaps other uses can be found for them.

Note, too, that a regular division of the plane is not necessary for shrinking a sheet via spirals: any irregular polygonal lattice will do. Figure 6 shows a surface carved at random into irregular polygons, along with a (semiregular) spiral crease pattern for it. It is trivial to prove that any division into regular or irregular polygons will allow a spiral pattern to be created for it, and that the pattern will fold. It is less trivial to prove that a surface so divided and folded can always be made to lay flat—for the possible reason that this may not be true. In my own experiments, since the spiral within each polygon can be twisted with some independence from its neighbors, one always has a certain control over how flat or curved the overall surface will be. On the other hand, when the polygons are of a different size and the spirals in them are of a different height, the concept of average flatness loses some of its clarity.

Figure 4. *Ernestine.*

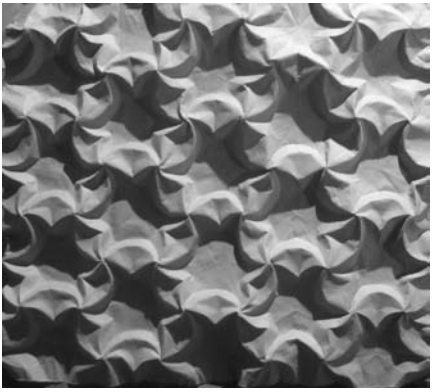

(a)

(b)

Figure 5. (a) *Fancy Hexagon Spirals.* (b) *Ben Gurion.*

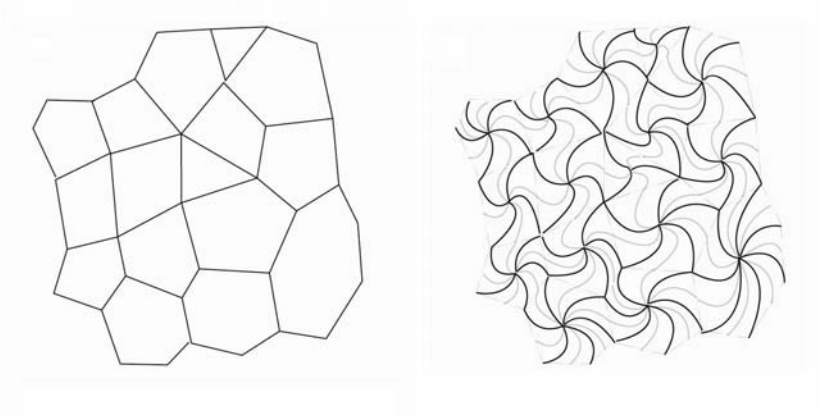

Figure 6. Spirals from an irregular grid.

As an autobiographical note, I came upon this subject of spiral tessellations only when seeking an elegant solution to a sculptural problem that was nagging at me: how to make from paper the dome of a person's head, which curves in two directions at once, as paper is loth to do. Many curve-based tessellations, while they can be kept flat, also introduce some bidirectional flexibility to a sheet of paper. Spiral ones happen fortuitously (see Figure 4) to look like hair.

Finally, to put this discussion of spirals back into perspective: spiral tessellations are just *one* kind of open-fold tessellation that will shrink a surface while preserving average flatness. There are many others (e.g., Figure 1(b)). Surfaces can also be shrunk without any tessellation at all using semiregular (Figure 1(a)) or random-crumple methods; and if edge proportions are allowed to change a great many other options are available. It seems that this field of compressive, flatness-preserving deformations of a sheet is still wide open for exploration in origami.

3 Folding Patterned Sheets

Let's move to our other main area of investigation. Once you have a surface with a raised pattern on it, what can you do with it? Specifically, can the usual origami manipulations done on smooth sheets be done on these textured ones too?

The answer, I'm afraid, is usually "no": most elaborate origami folding will typically be interfered with by the existence of a raised pattern. A counterexample among top-rank models is Roman Diaz' *Tiger's Head* (Fig-

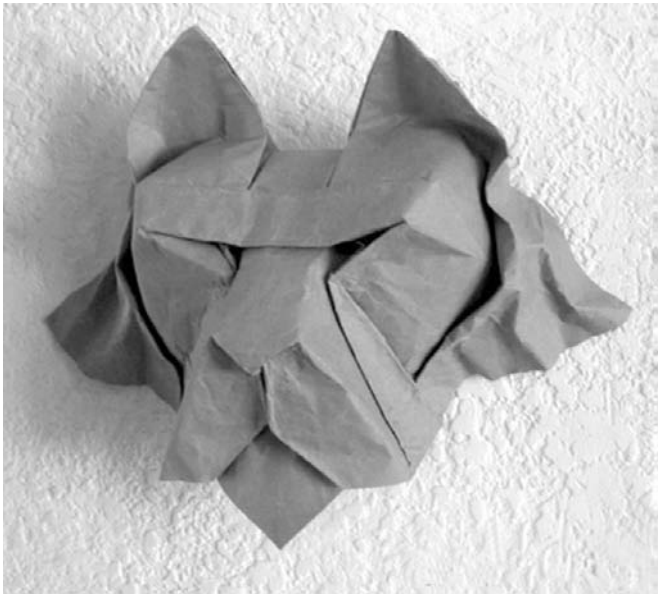

Figure 7. *Tiger's Head*, by Roman Diaz. (Folded by the author.)

ure 7: his design, my fold); but there the curves are put in at the final stage on the free flat edges that remain at that stage. Starting from the outset with a three-dimensional texture poses considerable difficulties for much origami. Having said that, folding a raised and especially a curved pattern around a corner line can create deep furrows and bulges that are visually quite arresting—enough by itself to make a fine model, as the beautiful 1976 Tower form by David Huffman, the great pioneer of curved folding, clearly demonstrates (Figure 8). Here, although the resultant shape has struck many people as wondrously complex, a crease pattern that folds to a similar form is actually quite simple (Figure 3; my reconstruction). I have tried absorbing some of its design principles in my own work (Figure 10).

The *Huffman Tower*, by the way, prompts a question that comes up more generally from various quarters when dealing with curved folds: is there any difference in principle between a curved fold and a straight one? Isn't a sine curve just a zigzag with the corners rounded off? In the case of the *Huffman Tower*, couldn't all the curvy lines have been replaced with straight segments, and the curving surfaces with flat ones? (And how about with my spirals?) This is not an insignificant question, and while the answer may be different in each separate instance it is always worth asking. There are some real differences between curved and straight folding (we await the full list . . .) but the effect of curves can also be so hypnotic

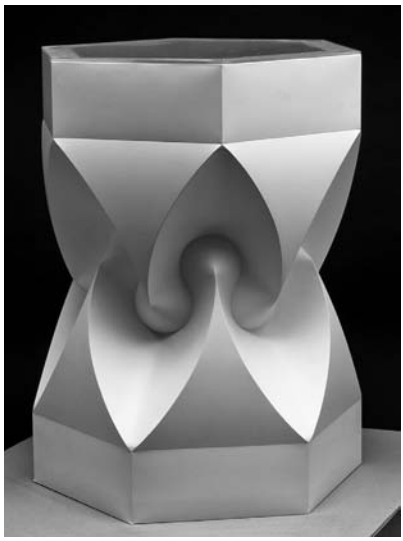

Figure 8. Mathematical paper folding, by David A. Huffman. (Courtesy of the Huffman family. Photo by Tony Grant.)

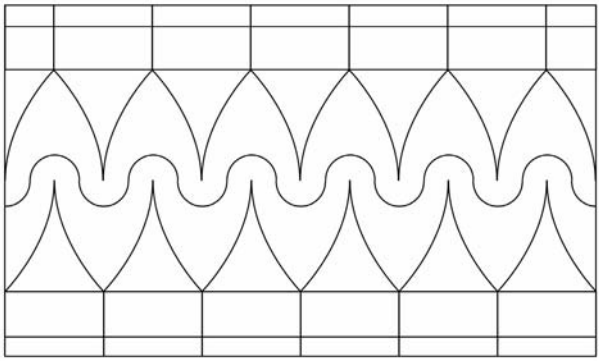

Figure 9. Reconstructed crease pattern for the *Huffman Tower*.

as to make us forget to check whether straight-line analogues exist. But let us leave that aside for now.

I want to consider what happens when a surface that is patterned in the way I've been describing is folded along a line—folded gradually anywhere from zero to 180 degrees. There are four different types of simple encounters of open folds (for now: mountain-valley pairs) with a corner line, and I'd like to show what happens in each.

Figure 10. *Jar of Muses.*

Figure 11 is an open-fold crease pattern, in which you are to imagine (or attempt) folding the more horizontal lines first into open mountain and valley folds, and then bending the pattern successively at each of the four vertical locations.

If you try bending the *straight-line* open-folds at A, the paper will resist. Eventually it will buckle, that is, it will form new fold-lines at awkward and unexpected locations. This is the corrugation effect, used for adding stability to flimsy sheet materials. Note that since the lines that intersect at A are all straight, there is nothing stopping you from folding them all the way into closed folds; A can then be folded without complaint.

At B, the horizontal open-fold lines, which are shown to be straight but may also be curved, meet line B from both sides *at an angle*. (Line B in fact will already be formed by having made the angled open-folds.) Bending the surface here can be done quite easily: the corrugation effect has disappeared. However, the result of such bending is that the height of the surface will compress along B, as the angles turn inward and trade some of their verticality for depth. If the open folds meeting B are straight lines, a 180° bend around B will close these folds completely.

At C, the horizontal lines are *arcs*; a hard fold along C itself encounters the same resistance as at A and for the same reasons. However, the *region* of C taken as a whole behaves just as the single line of B does; in fact it can be considered a stretched out version of B (one dimension stretching

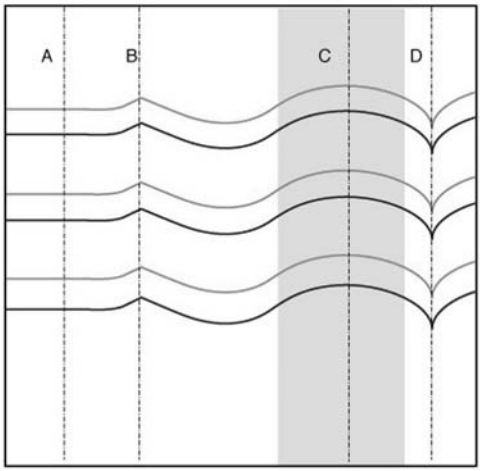

Figure 11. Encounters of curves with straight open folds.

into two!). Thus the entire region of C can be made into a corner that curves gradually, and if the corner is sharpened (edges bent back more), the furrows will deepen just as they did at B. The height will likewise shrink. But because they are curved, the folds will never shut completely. (On the other hand you are able to bend the surface back by more than 180°, indeed by more than 360°.)

At D, the open folds meet the line at a *tangent*: an angle of zero. Consequently there are no angles to rotate inward, and a fold here is not as disruptive to the vertical extension. It may be noted that this property of being able to meet a line at a tangent is one that curves possess and straight segments do not, so this is yet another answer to the question of what differences there are for folding purposes between curves and straights.

None of the above is earth-shaking mathematics, but it does account for many of the simpler cases of raised-pattern folding, so it needs to be stated. Fancier permutations (nonparallel mountains and valleys, mountain + mountain + valley open folds, open folds that meet curves, etc.) are of course possible too.

4 Concluding Thoughts

I think this is enough of a sketch to suggest some of the issues that come up when forming and manipulating curve patterns. I want to conclude with a few thoughts about method and the links and tensions here between art and science.

For experimental work, the ideal medium for curved folding is a foil-backed paper (preferably stiff foil, 50–100 microns thick) rather than paper on which the pattern has been plotted and scored. The reason is not aesthetic—aesthetics may in fact favor plain paper—but rather that foil-paper, which holds a curvy shape without springing, also allows you to erase a line with a fingernail and shift your curve at will. This helps avoid a trap one may fall into, especially if one takes an analytic rather than experimental approach to this field: the assumption that if a curve representing a particular function creates a nice effect, the effect is due to the function and no other curve can accomplish approximately the same thing. You can avoid such fixation by trying out other curves and straight-line variants—but that requires a comfortable medium for doing so. (This of course is not to say there are no specific curves that optimally solve well-defined problems, or that mathematics is not useful for finding them. But for most curved origami sculpture, at least in my experience, the details of a curve are not very determinative. Direction of curvature matters a great deal: degree and rate of curvature, usually less so.)

A similar fixation tends to happen with regular patterns, so these should always be tested against the most irregular version of the same pattern to see what in fact is doing the work.

Irregularity versus regularity, plotted and repeated patterns versus free-form and varying curves—all this raises another issue, this time a purely aesthetic one: the old, grand tension between mathematical optima and repeatability on the one side, and romantic and individual expression on the other. This is rather a large topic to broach just here: entire cultures are defined by where and how they come out on this continuum. I will say only this. Certainly in the animal world, the outline curve is a prime bearer of information about a living form's identity and emotional state; and in

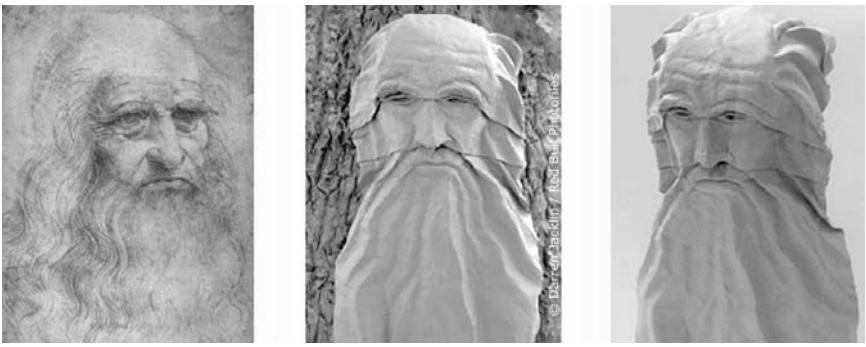

Figure 12. *Triptych of Leonardos.*

the handwriting and drawing of humans, the curve or the flourish is where personality is looked for—and found. It would be a shame if origami's inherent tendency for pattern and repetition should give rise in this new field to mainly a cold and crystalline form of model design, to the calculated rather than the expressive. Curved folds leave a great deal of freedom for the shaping of three-dimensional form: too much freedom, to many folders' tastes. But where there is freedom, there can also be—individuality.

The *Celes* Family of Modular Origami

Miyuki Kawamura

1 Genesis of *Celes*

Sometimes when square paper is cut from a larger sheet, long, slender paper strips remain. I wanted to make origami works with these paper strips and so I designed several models in 2001 and 2002. *Celes* [3], shown in Figure 1, is one of my modular works that is made with paper strips. The basic model is made with 30 strips in the proportions of 1 by 6, but other proportions can be used; 1 by 5 or longer strips are required.

The name *Celes* came from the word *celestial* because the model has 12 stars on the surface. *Celeste* might be the name in English, but the pronunciation of *Celes* is easier for me.

2 Variations of Symmetry

Polyhedral symmetry provides basic and important guidelines for the design and assembly of any modular work. There are basically three different kinds of symmetry, which dictate, among other things, the number of units needed for the structure. Phrases such as "assembled with 6, 12, or 30 modules" might be familiar to modular workers; these numbers, such as 6, 12, or 30, correspond to the number of edges in the underlying regular polyhedron. We can make two different types of models with 12 modules—those based on the cube and the octahedron. There is the same situation for 30-module models too, in which either the dodecahedron or icosahe-

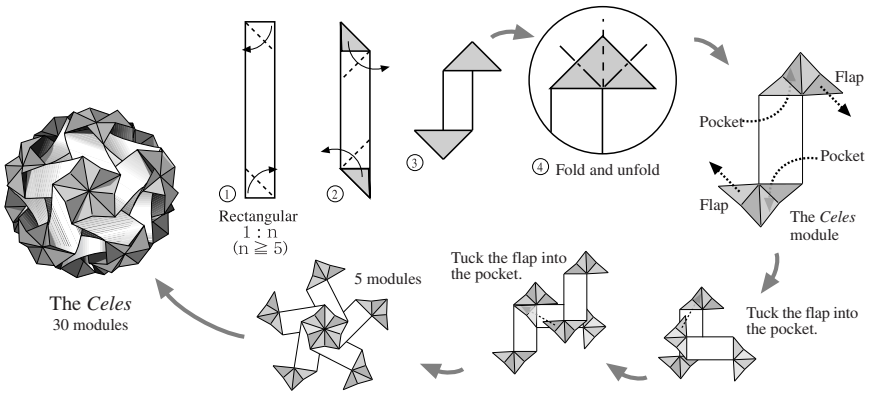

Figure 1. The *Celes* module.

dron is the underlying polyhedron. So, five different models corresponding to the five regular polyhedra can be made with one kind of module. It is possible to make five different models with the basic *Celes* modules, too, but one of the models made with 30 modules is not stable.

Generally, we can also make other, more complex models with larger numbers of modules. For example, polyhedra are possible using 24 units, 60 units, 90 units, and so on. These models correspond to the *semiregular* polyhedra; their symmetry is based, in turn, upon the symmetry of one of the five regular polyhedra. The symmetry of a prism is also available. We can design many variations of modular works by making use of different types of polyhedral symmetry.

3 Variation of Inside Out

The basic *Celes* modules can be assembled as a model turned inside out as well. It is very hard to complete this model because all of the connection parts are inside; the reader is encouraged to try.

4 Changing Angles of Connections

More exciting arrangements can be made by changing the angle of connection of the *Celes* module. The form of the connection of the basic module is a right triangle, as shown in Figure 2. The key angle inside the triangle is denoted by θ in Figure 2 and in the following discussion. This angle θ can be changed by redesigning the connection of module: specifically,

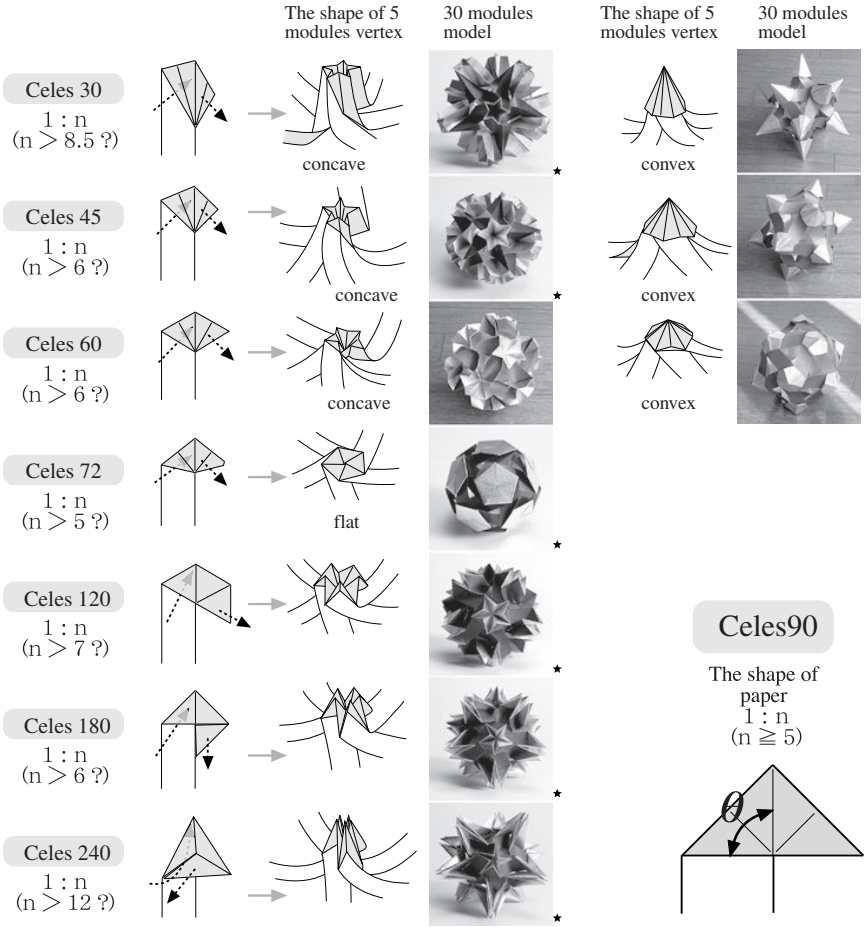

Figure 2. The *Celesθ* family.

by varying the angle at which each end of the strip is folded over. This defines a family of modules, parameterized by the angle θ, and so we call this family *Celesθ*. Individual members are named by replacing θ with the value of the angle; thus, the basic *Celes* module is called *Celes90*. Angle θ can be changed continuously from 0 to 360 degrees, so there are infinite variations of the *Celes* module.

To take just one example, in the complete model of the basic *Celes*90 model, the symmetry is the same as that of the icosahedron. Each star on the surface is made from the ends of five modules. With this symmetry, when the angle θ is smaller than 72 degrees, the curvature of a surface star

is positive and we can make two different types of *Celes*. One has concave stars and the other one has convex stars. When θ is bigger than 72 degrees the star shape is wavy because the interior angles exceed 360 degrees, and when it is just 72 degrees the star is flat. So 72 degrees is the boundary between convex/concave and wavy stars.

When a star on the surface is made from four modules, the boundary angle is 90 degrees, and when a star is made by three modules, the boundary is 120 degrees. The relation between the shape of the star and the connection angle θ is the same as the relation between the form of a curved surface and its local curvature.

5 Bridge

Generally, many origami modules consist of two different and distinct functional regions. One region forms the connections between modules, e.g., pockets, flaps, and other assembly structures. The other part is not used in the connection between modules; instead, it extends from one connection region to another. That part is called the *bridge* [1, 2]. If the connection and the bridge are independent of one other, we can make the bridge any shape without influencing the connection. So there is some level of freedom in their arrangement.

In case of the basic *Celes* module, the two right triangles are the connection and the middle part is the bridge (Figure 3). We can fold the bridge into any shape: crane, flower, beetle, dragon, devil, etc., without affecting the connection. Because of this, there are innumerable variations of the bridge and it is difficult to describe all possible variations.

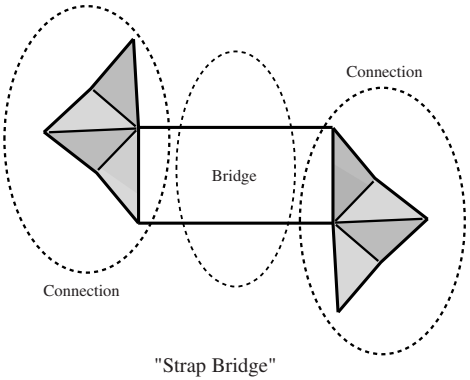

Figure 3. Bridge.

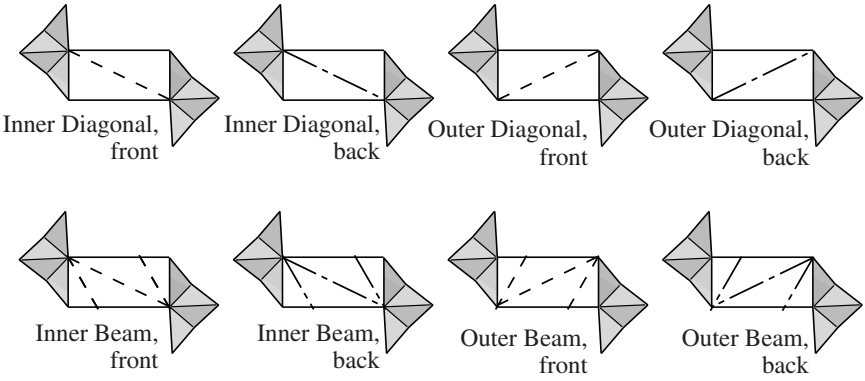

Figure 4. Diagonal and beam bridge.

However, we can begin with the simplest variations of the bridge. When the bridge has no crease line, we call it a *strap bridge*. If it has one crease line along the diagonal of the bridge, we call this the *diagonal bridge* (Figure 4). There are four possibilities for this crease.

As a second example, let's add further creases to the bridge. In this case, the bridge has three creases (Figure 4). This structure is named *beam bridge*. Fold along the diagonal line first, and then wrap each end around the raw edge of paper. As with the diagonal bridge, there are four variations; in each variation, all three creases are of the same type (mountain or valley).

6 Second Bridge

Each connection of the *Celes*90 module is made by two small right triangles. We redesign the module, split the two triangles and make a new bridge between these two (Figure 5). The new bridge is called the *second bridge*, and we rename the original bridge to be the *main bridge*. The complete module is called the *Celes spread module*. We can make the same treatments of the second bridge as on the main bridge, e.g., strap, diagonal, beam, and so forth.

Several examples are shown in Figure 6. All of these models are made from same length strips but the ratio of the lengths of the main bridge and the second bridge is different. The main bridge is shaped as a beam bridge (three diagonal creases) and the second bridges are shaped as strap bridges (no diagonal creases).

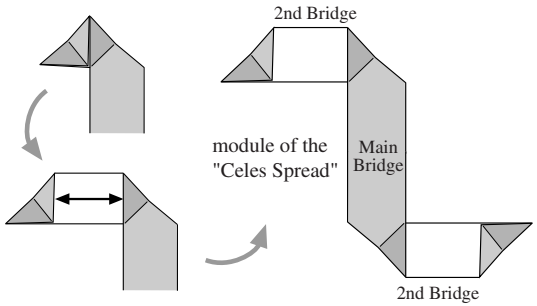

Figure 5. Second bridge.

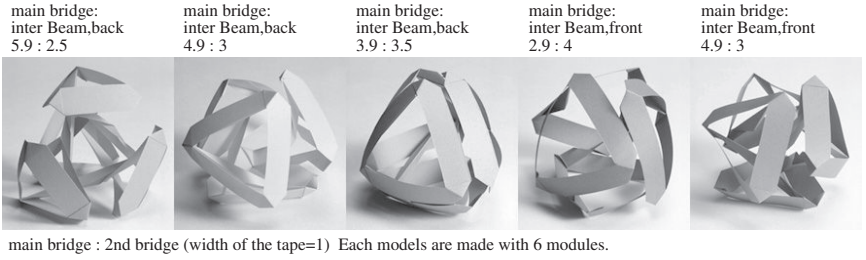

Figure 6. Main and second bridge.

7 Local Uniting Relation

The second bridge has a pocket or a flap on each end (Figure 7). There are two different ways to lay out the flap and pocket. Type 1 is called *basic* and Type 2 is called *twist*. The creases on the flap and the pocket can be independently chosen to be mountain or valley, giving eight kinds of module. One pocket has two slits, one on the front side and the other on the back side. When we choose two modules arbitrarily from the eight possibilities, the pattern to assemble is dictated by the choice of mountain or valley creases on the pocket and the flap, and so only one way of assembling the two is allowed. This property is called the *local uniting relation* of the module. Generally, many kinds of modules have this property, which strongly constrains the assembly and shapes of models made from the modules, and therefore dictates important characteristics of the modular works.

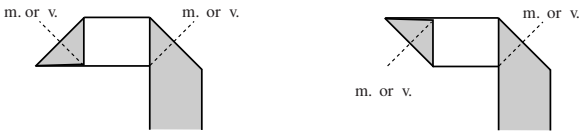

Figure 7. Two types of layout.

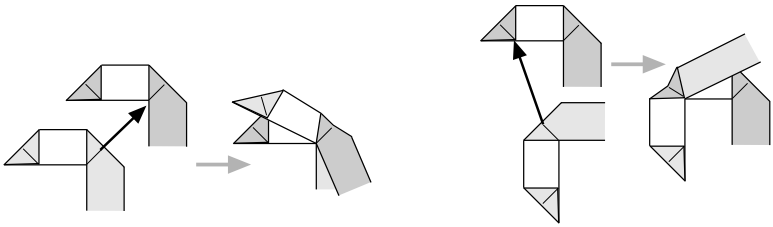

Figure 8. Flap and pocket.

8 Crease Pattern Formula

Here we generalize the module of the basic *Celes*90 and provide a compact notation for describing them. As noted earlier, the arrangement of the positions of the pockets and the flaps can be freely chosen. A flap has the same structure as a pocket, so we can tuck the pocket of one into the pocket of the other, or we can tuck the pocket of one into the flap of the other (Figure 8). Note that the number of pockets of the module need not be two and the shape of a module does not need to be symmetrical. (For that matter, a complete model does not need to be a closed polyhedral form.)

And so a model can be arbitrarily complex by repeatedly adding elements from the simple set of structures along the strip. Figure 9 shows an example of a generalized *Celes*90 module constructed according to this prescription. This module can, in fact, be assembled with copies of itself. The lower diagram in Figure 9 shows the crease pattern of this module.

Here is how we describe the module structure concisely:

- Between each crease, we give an integer that gives the length of the bridge as a multiple of the width of the strip. So, for example, in Figure 9, the numbers $1, 2, 4, 3, 1$ are the lengths of each bridge.
- We use brackets $[\ldots]$ to denote the two ends of the strip.

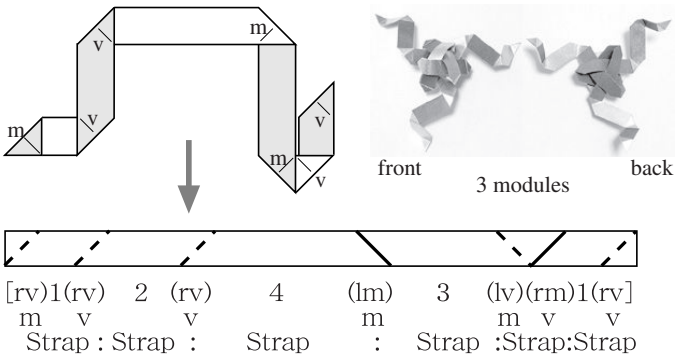

Figure 9. Crease pattern formula.

- We use the letters r and l to denote the slopes of the crease lines; r for a line rising from left to right, l for a line descending from left to right.
- We use the letters m and v to specify whether the fold is mountain or valley.

In general, there are four possible combination of r, l with m, v in each parenthetical pair, i.e., (rm), (rv), (lm), and (lv). Therefore, if a module has N pockets/flaps, the upper limit of the number of the kinds of shapes of the module is 4^N. However, this formula includes duplicates. For the example shown in Figure 9, there are four identical modules with different formulas:

$[rv)1(rv)2(rv)4(lm)3(lv)0(rm)1(rv]$ (original module),
$[rv)1(rm)0(lv)3(lm)4(rv)2(rv)1(rv]$ (right-left reversal),
$[lm)1(lm)2(lm)4(rv)3(rm)0(lv)1(lm]$ (r-l and v-m reversal), and
$[lm)1(lv)0(rm)3(rv)4(lm)2(lm)1(lm]$ (right-left, r-l, and v-m reversal).

With no other forms of duplication, the lower limit of the number of the kinds is 4^{N-1}. But we must also consider the number of forms that does not change with right-left reversal. This number changes with the parity of the module. So, the total number of different kinds of module with N pockets is as follows:

$$4^{N-1} \text{ if } N \text{ is odd,}$$
$$4^{N-1} - 2^{N-1} \text{ if } N \text{ is even.}$$

The m and v in the middle row of the three rows of symbols in Figure 9 indicate mountain or valley fold along the center line of each pocket.

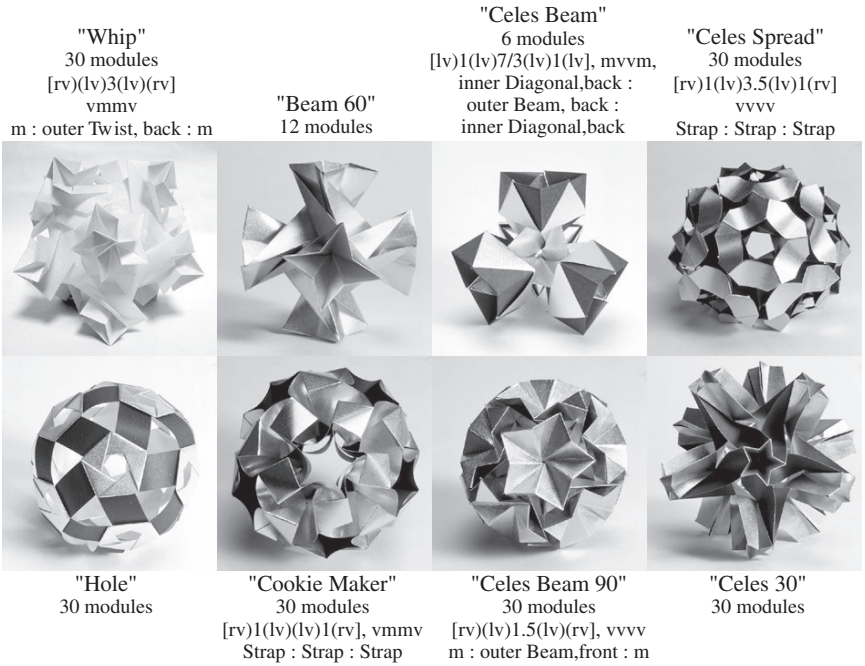

Figure 10. Variations of modular.

When there is no crease through the center line, it is indicated with a ".". The words in the third row indicate the type of each bridge, e.g., strap, diagonal, and beam. A shape of a module that belongs to the *Celes* family is uniquely described by this three-line formula, which we call the *crease pattern formula* for the module.

9 Variations of Modules and Assembly

One of the merits of using this formula is that it leads to automatic design of a module directly from its symbol. Figure 10 shows some models from the *Celes* family, along with the names that I have given them. The diagrams of *Whip* are published [4].

Since the bridge of a *Celes* module has only one layer, it is easy to change the form. A lot of interesting models that have beautiful curves are designed with long bridge modules. Some of these are shown in Figure 11 as well.

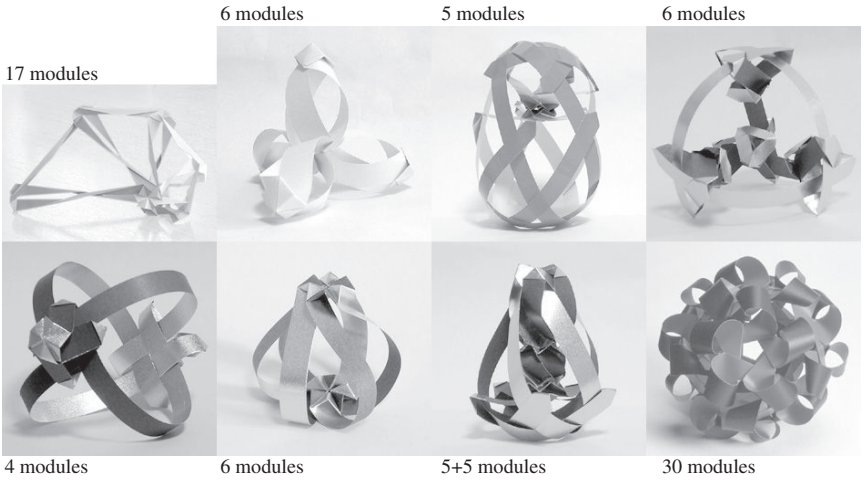

Figure 11. Variations of assembly.

10 Summary

The *Celes* module is very simple, and yet has great potential. In this module, the connection and bridge are separated clearly, so it is easy to construct arrangements of the module. The greatest feature of the *Celes* module is the flexibility to create pockets in arbitrary places within a module. Besides the work described here, many varieties have been made by many people. For example, Dr. Toshikazu Kawasaki has designed some kinds of the *Celes* family. Although the construction method of the *Celes* module is not yet common, it lends itself to a systematic approach for module design, and I expect that many new modular works will appear in the future.

Bibliography

[1] Miyuki Kawamura. "Quick Snap." *Origami Tanteidan Magazine* 60 (2000), 11–13.

[2] Miyuki Kawamura. "The Basic Techniques of Origami Polyhedra 11." *Origami Magazine* 310 (2001), 16.

[3] Miyuki Kawamura. "Celes." In *Origami Tanteidan Convention Book*, Vol. 8, pp. 148–150. Tokyo: Japan Origami Academic Society, 2002.

[4] Miyuki Kawamura. "Whip." In *Origami Tanteidan Convention Book*, Vol. 9, pp. 22–25. Tokyo: Japan Origami Academic Society, 2003.

Fractal Crease Patterns

Ushio Ikegami

1 Redesigning the *Maekawa Pyramid*

Maekawa's pyramid model (Figure 1) is one of the infinite folding models he presented in [4]. By *infinite folding*, we mean that in the limit of infinite iterations, it produces an infinite number of branches in four directions from a finite square. Its crease pattern for any nth iteration consists of two kinds of generators. We can determine the foldability of infinite folding models (not flat foldability but the possibility of infinite iteration) by the existence of such finite generators and their relative arrangement within the crease pattern.

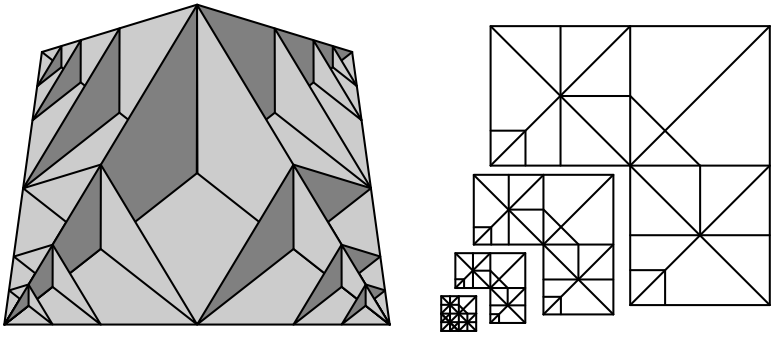

Figure 1. *Maekawa Pyramid.*

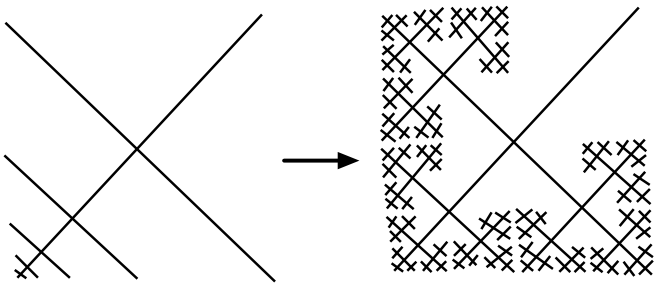

Figure 2. Sketch for the new design.

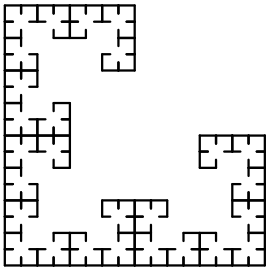

Figure 3. Pyramid curve.

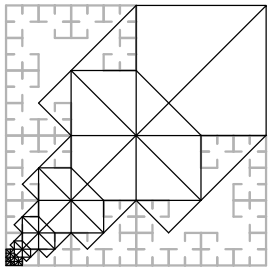

Figure 4. Overlap.

Now, in the *Maekawa Pyramid*, there are four main branches that, in the limit, produce an infinite number of secondary branches. However, each secondary branch doesn't branch any further after it comes off of a main branch. This raises the question: is it possible to fold an infinite number of branches from each secondary branch and subsequent branches as well? Figure 2 shows just such a branch pattern. It is much more complicated than the original pattern and its accumulation points form a curve shown in Figure 3. We will call this the *Pyramid curve*.

Let us use the *Maekawa Pyramid* itself for this new design. The accumulation points of the crease pattern form the same Pyramid curve as the accumulation points of the branch pattern. Furthermore, the curve overlaps the area that becomes the surface of the pyramid (Figure 4). The infinitely folded limit region cannot be made from a smooth surface. Thus, the *Maekawa Pyramid* itself cannot grow further; there is not enough paper. The crease pattern must be modified.

Thus, the Pyramid curve and the smooth surface must be separated within the crease pattern. And the individual contraction of generators shown in Figure 5 separates the curve and the surface because the contraction keeps the accumulation point fixed while the generators become smaller and smaller.

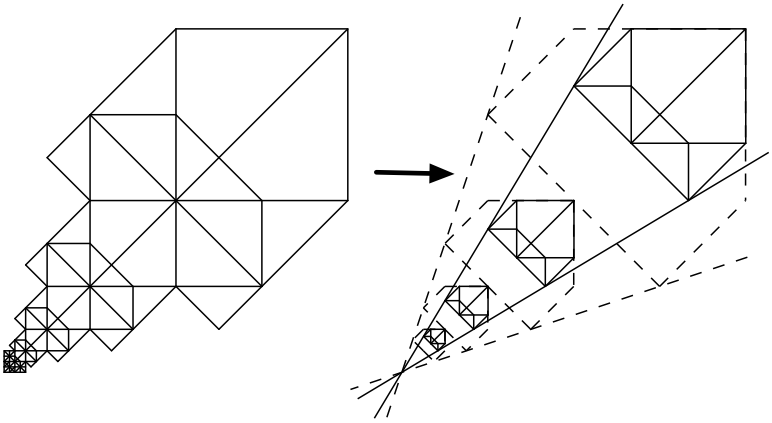

Figure 5. Contraction.

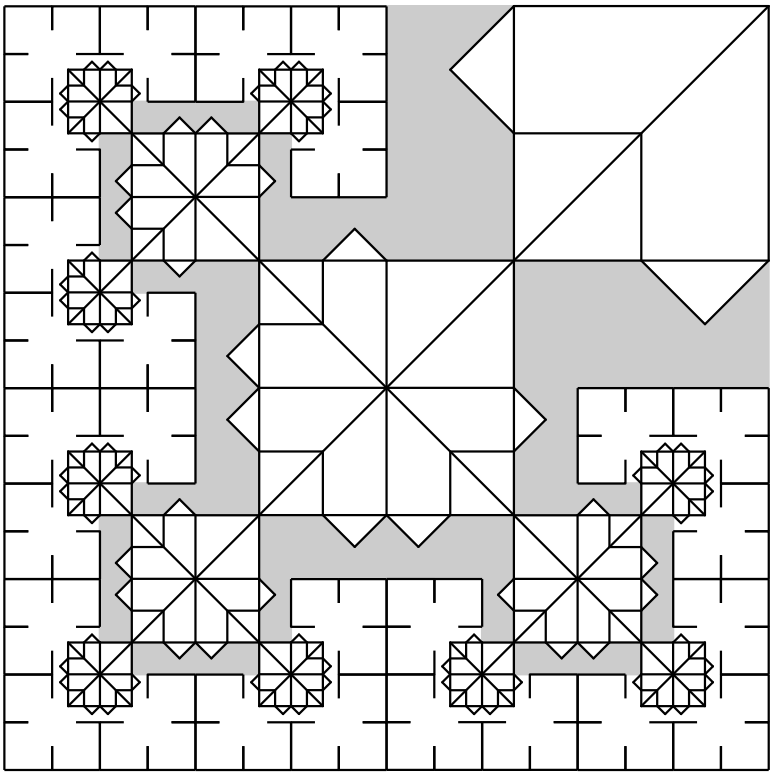

Figure 6. New composition.

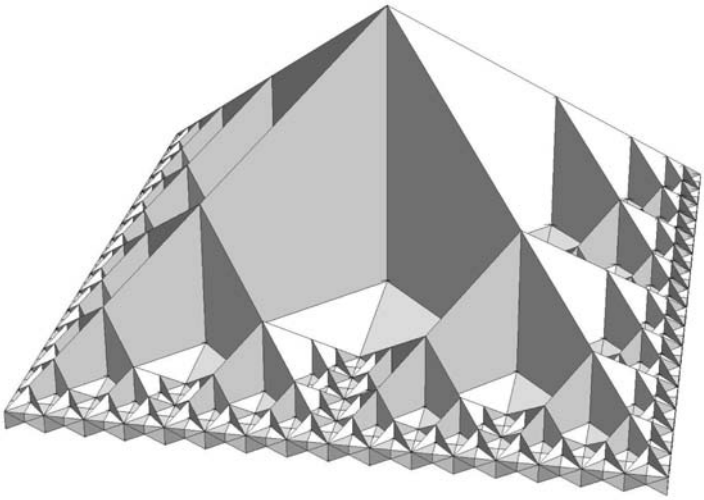

Figure 7. New pyramid.

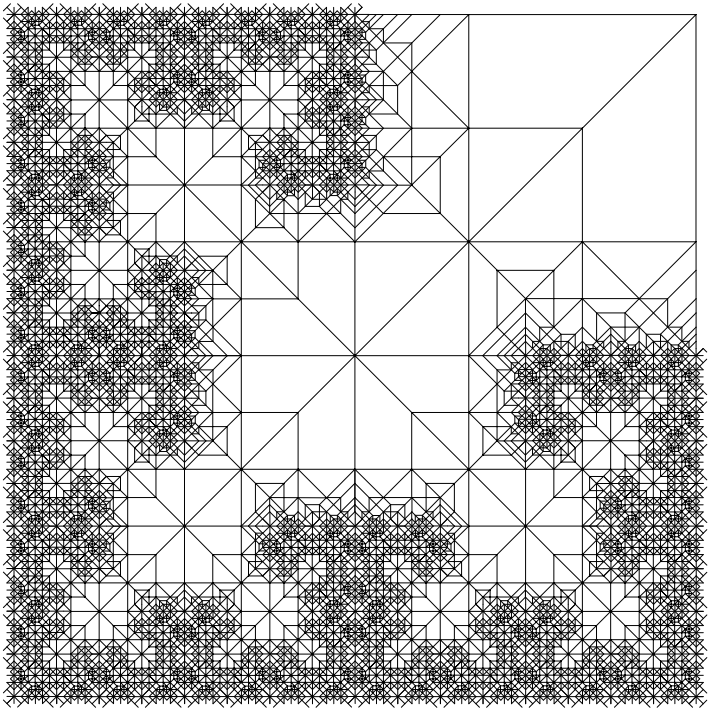

Figure 8. Crease pattern.

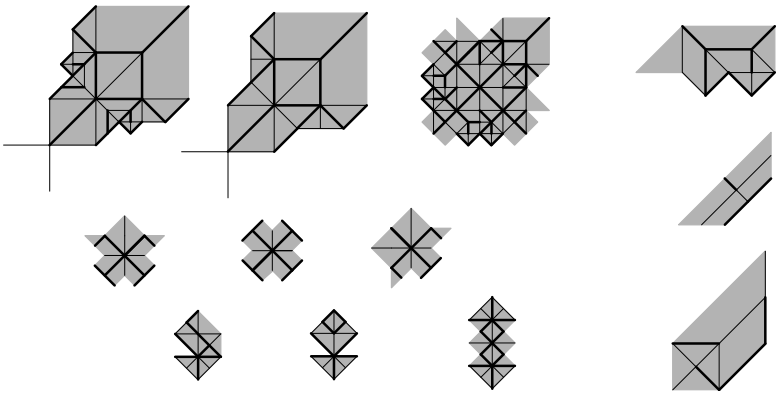

Figure 9. Crease-pattern generators.

Our next task is to fill up the space that was created by the contraction (and is colored gray in Figure 6) using a recursive crease pattern. I found such a crease pattern and resolved it into a finite set of generators. By combining all generators at the appropriate scales, the new pyramid may be completed as shown in Figure 7. Small pyramids protrude on the bottom of the folded structure; they follow the Pyramid curve. They can be folded flat underneath but I left them pointing downward to keep the crease pattern simple.

Figures 8 and 9 show the crease pattern at the fifth iteration and the generators and their representative tiles. Figure 10 illustrates their tiling pattern and thus establishes the foldability of this infinite folding model. My trial and the result of the work described here is also discussed in [2] and [3].

2 Hausdorff Dimension of the Pyramid Curve

The calculation of the Hausdorff dimension dim_H is generally difficult. But in this case, it is relatively easy and the Pyramid curve turns out to be a fractal set. Let C be a Pyramid curve of base length and height 1. C is self-similar, because there exist similarity transformations

$$f(x,y) = \left(\frac{1}{2}x, \frac{1}{2}y\right),\ g(x,y) = \left(1-\frac{1}{2}x, \frac{1}{2}y\right),\ h(x,y) = \left(\frac{1}{2}x, 1-\frac{1}{2}y\right)$$

such that

$$C = f(C) \cup g(C) \cup h(C).$$

Take an open set A as shown in Figure 11.

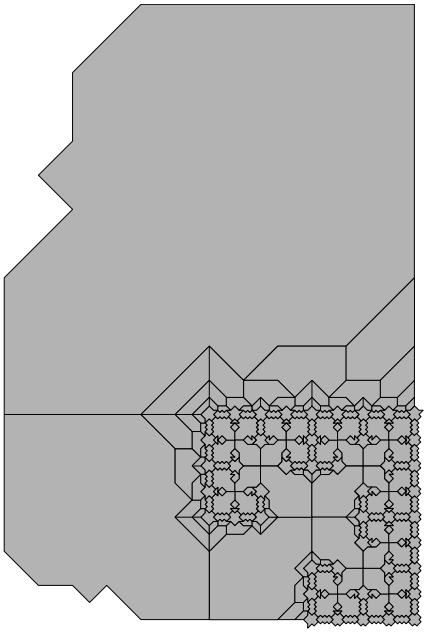

Figure 10. Tiling pattern.

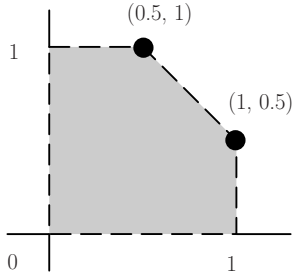

Figure 11. Set A.

Functions f, g, and h satisfy the open set conditions

$$f(A) \subset A,\ g(A) \subset A,\ h(A) \subset A,$$
$$f(A) \cap g(A) = \phi,\ f(A) \cap h(A) = \phi,\ g(A) \cap h(A) = \phi.$$

Hence, $dim_H(C)$ is equal to the similarity dimension of C $dim_S(C)$, which is the solution of $(1/2)^s + (1/2)^s + (1/2)^s = 1$.

Thus, $dim_H(C) = \log 3/\log 2 = 1.58\cdots$, which exceeds its topological dimension of 1. Therefore the Pyramid curve is fractal.

3 The Koch Curve as a Mountain Crease

The famous Koch curve K is defined as the limiting figure of a polygonal curve sequence $\{K_n\}$. Is it possible to use this curve as a flat-foldable crease pattern? (See Figure 12.)

For any given $n \in N$, place one of the curves K_n in the interior of paper as a set of mountain folds. It is obvious that this crease pattern by itself is not foldable. First of all, the Koch curve crease has its end points in the interior of paper. The real question is whether there is some additional crease pattern T_n such that the combination $T_n \cup K_n$ is foldable. As it turns

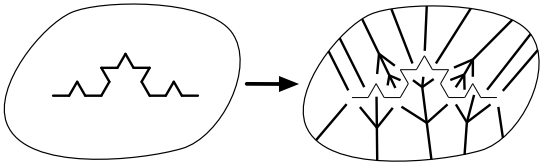

Figure 12. Is the Koch curve foldable?

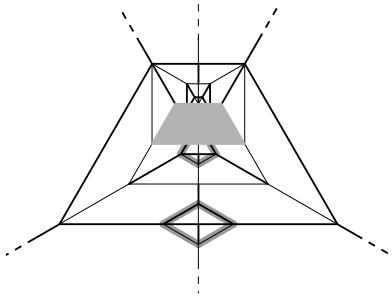

Figure 13. Entire view of the additional crease pattern.

out, there is; I was able to find a concrete example of $\{T_n\}_{n\in N}$, which is shown in Figures 13–17.

Let T be $\lim_{n\to\infty} T_n$. It has a set of accumulation points that correspond to K placed into the middle of it. Moreover, it is gained by open sink-folding at the tip of a single-vertex fold. In other words, the paper doesn't have to be bounded.

However, there is a problem. As you may notice, the highlighted zigzag crease in Figure 14 doesn't appear on the generator that covers the crease.

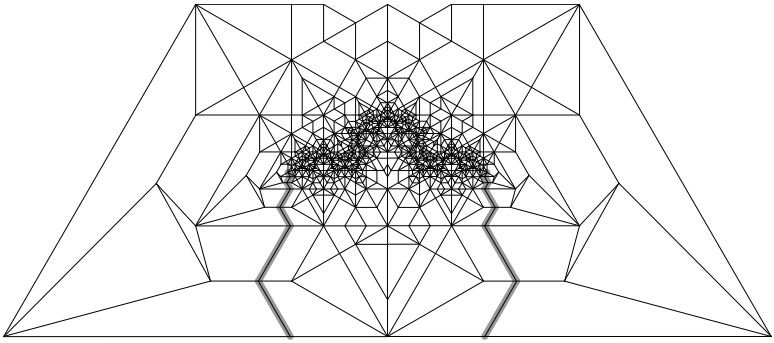

Figure 14. Blow-up of the center part.

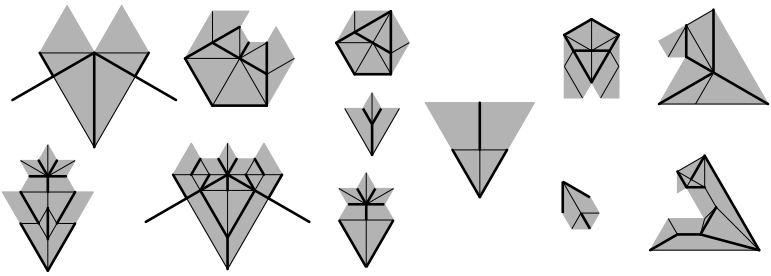

Figure 15. Generators for the center part.

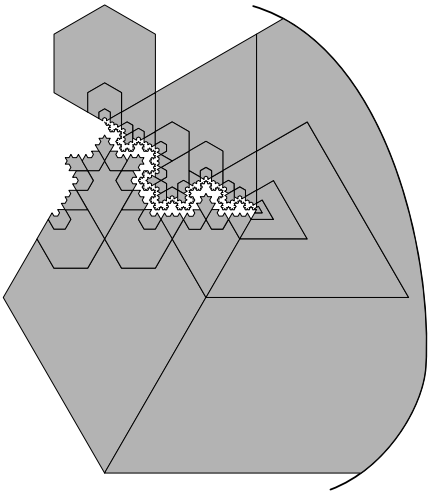

Figure 16. Tiling and Koch crease.

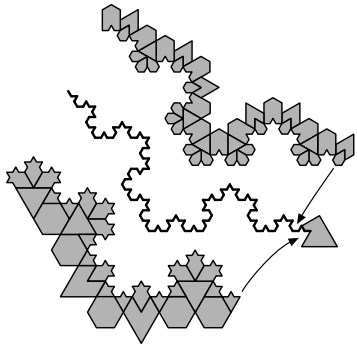

Figure 17. Detail.

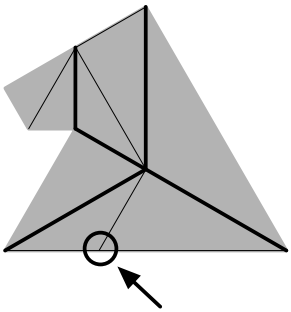

Figure 18. Starting point.

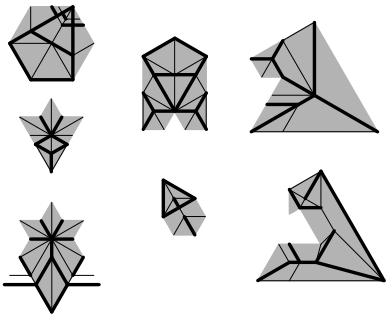

Figure 19. Altered generators.

This is because its location depends on n since its end point connects with the point indicated in Figure 18. Because this part of the pattern varies with the iteration order n, foldability at the limit $T \cup K$ is not yet established; we need to fix this crease on the generator somehow. Figure 19 shows altered generators with the zigzag crease now fixed upon them. In this case, a total of seven generators had to be converted. But by doing so, the foldability of the limit $T \cup K$ now becomes evident.

4 Creating a Snowflake Curve by Folding

We close with an open problem: is it possible to *create* a snowflake curve by folding? This was actually an earlier project for me than the two already described, but it is much more difficult—in fact, it is still open. So far, the trial crease patterns I have tried, including the one in [1], have

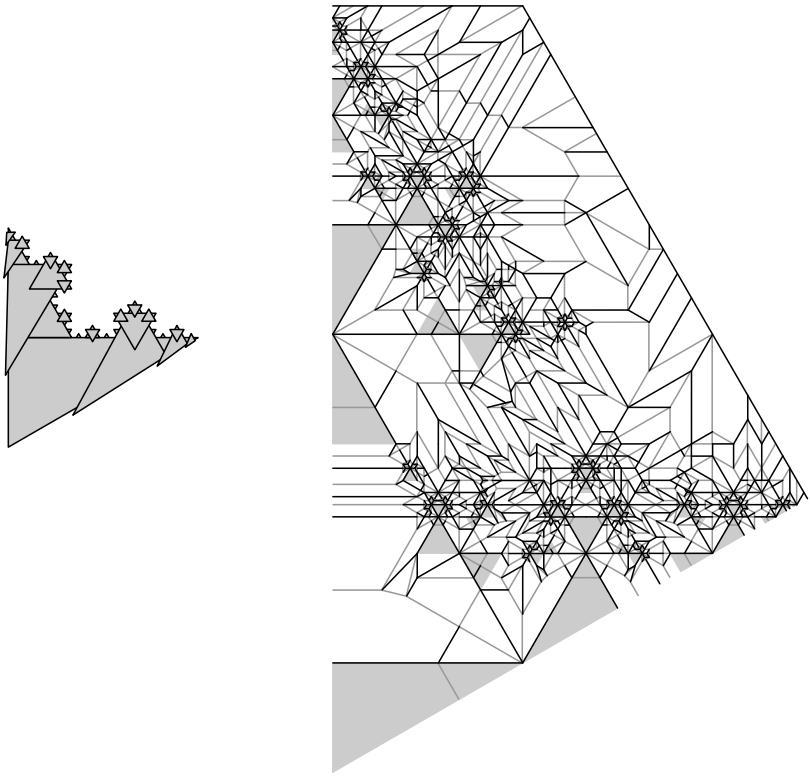

Figure 20. Trial crease pattern that is locally not foldable.

required irregular squash folding. This suggests that an infinite number of different types of generator may be required. As an inspiration to future investigators, I show one possible trial pattern in Figure 20.

Bibliography

[1] U. Ikegami. "Crease Pattern Challenge, Koch's Snowflake Curve." *Origami Tanteidan Magazine* 67 (2001), 34.

[2] U. Ikegami. "Folding Fractal Images." *Origami Tanteidan Magazine* 74 (2002), 11–13.

[3] U. Ikegami. "New Infinite Folding Patterns." *Origami Tanteidan Magazine* 88 (2004), 11–13.

[4] J. Maekawa. "Similarity in Origami." In *Origami Science and Art: Proceedings of the Second International Meeting of Origami Science and Scientific Origami*, edited by K. Miura, pp. 109–118. Shiga, Japan: Seian University of Art and Design, 1997.

Constructing Regular n-gonal Twist Boxes

sarah-marie belcastro and Tamara Veenstra

1 Introduction

Among her one-piece boxes, Tomoko Fuse has a number of polygonal twist boxes [3, 4]. The crease patterns and folding sequences are structurally similar: divide the paper into $(n+1)$ths, fold across these $(n+1)$ths at some height h, fold some angle α emanating from each intersection of the vertical/horizontal folds, overlap the two ends of the paper, and collapse the twist.

Question. Can we generalize one of Fuse's constructions to create an n-gonal twist box for any n? That is, can we construct an n-gonal twist box from a 1×1 (or $1 \times m$) piece of paper by dividing the paper into vertical $(n+1)$ths, marking a horizontal height h, folding diagonals d in the resulting rectangles (formed by the height h fold line, the vertical folds, and the raw edge of the paper), making some folds to form the body of the box, overlapping the ends of the paper, and collapsing the twist? Better yet, can we find a formula for h in terms of n, so that the entire box construction is determined by n?

Answer. Yes! We will show how to construct this box for any n.

More precisely, we discuss the following mathematical considerations involved in proving that such a construction will work for all n. In order

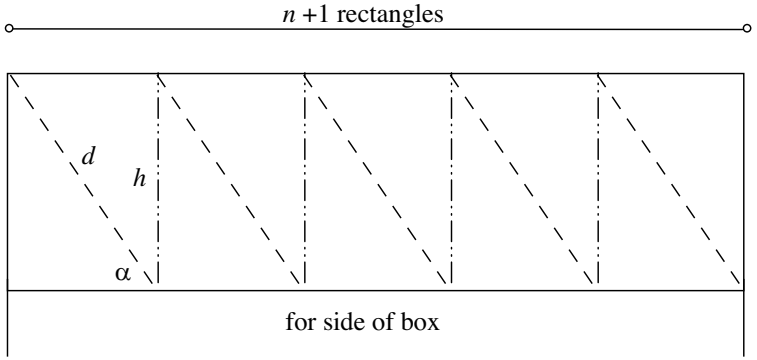

Figure 1. Part of the crease pattern to produce an n-gonal twist box.

for the twist to collapse so that the bottom of the box lies flat and has no hole in the center, the angle α formed by d and the vertical creases must be exact. The height h is determined by the angle α, which is in turn determined by n. We must also examine the paper between the twist center and the raw edge of the paper, and compare the length of d with the diameter of the box body to verify that the raw edges may always be contained within the body of the box. In constructing a folding sequence, we will need to determine a crease for either h or α; thus, we will consider which we can more easily and accurately find. Finally, we will examine the case of large n, give folding instructions for a 17-sided box, and look at the limiting (circular) case.

2 Determining α and h as a Function of n

We will first examine conditions on α in order to construct a regular n-gon. Each (interior) vertex of the rectangles in the crease pattern in Figure 1 has the same arrangement of angles. The sum of the angles around such a vertex before folding is $\pi = \frac{\pi}{2} + (\frac{\pi}{2} - \alpha) + \alpha$, and after folding it must be the interior angle of an n-gon, namely $\pi(n-2)/n$. Recall that the vertical creases h will be mountain folds and the diagonal creases d will be valley folds. The act of folding changes the sign of the angle between the mountain and valley folds, so we obtain

$$\frac{\pi(n-2)}{n} = \frac{\pi}{2} - \left(\frac{\pi}{2} - \alpha\right) + \alpha = 2\alpha.$$

In other words, $\alpha = \pi(n-2)/(2n)$. Since α is half of the interior angle, the diagonal d bisects the interior polygon angle. This means it will cross

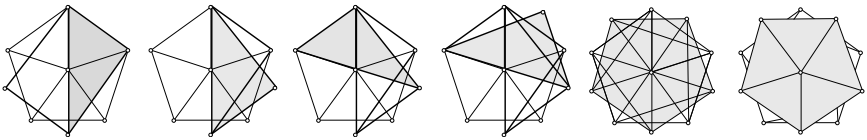

Figure 2. Intermediate folds for the twist of a pentagonal box.

through the polygon center, and thus our completed box will have neither holes nor paper intersections. A visual demonstration of this for $n = 5$ appears in Figure 2, where a sequence of theoretical partial-twist folds is given.

In general, for any n, the cumulative folded angle (for all vertices) is $\max(\frac{\pi}{2}, 2\alpha)$. If $n \geq 4$ then $\alpha \geq \frac{\pi}{4}$ and the cumulative folded angle is 2α. When $n = 3$, we have $\alpha = \frac{\pi}{6}$ so that the cumulative folded angle is $\frac{\pi}{2}$. Figure 3 shows the shape that is formed as a result of using our folding sequence in this case. While we can still construct a triangular box this way, there is some extra paper that must be tucked away.

Now that we have determined α in terms of n, we can construct h. We examine a triangle from the crease pattern for the twist as in Figure 4. The angle α is part of a right triangle with opposite side length h, adjacent side length s, and hypotenuse length d.

This shows that $h = s\tan(\alpha)$, and, given $1 \times m$ paper, $s = 1/(n+1)$. Thus, the formula for h in terms of n is

$$h = \frac{1}{n+1} \tan\left(\frac{\pi(n-2)}{2n}\right).$$

The height h is not particularly easy to approximate in general. In Section 4 we will discuss methods for constructing α and h.

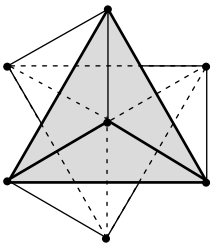

Figure 3. The twisted box when $n = 3$.

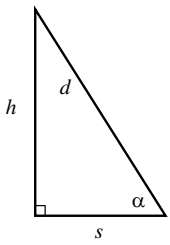

Figure 4. The basic triangle.

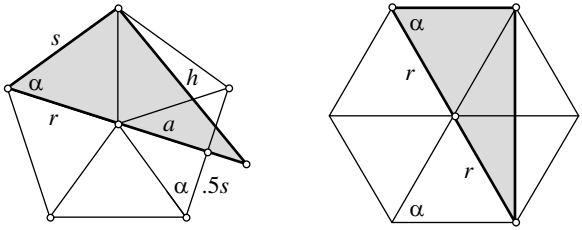

Figure 5. Pentagonal and hexagonal folds.

3 Differences for Even and Odd *n*

When folding the crease pattern from Figure 1, one sees that for $n \geq 4$ the raw edge of the twist will be a regular n-gon either coincident with the bottom of the box or rotated by $\frac{\pi}{n}$. Examples of the two cases are shown in Figure 5. To determine when each of these two cases will happen, we need to examine the placement of the diagonal d after completing the twist. Because d bisects the interior n-gon angle, the point where the diagonal intersects the raw edge of the paper lies at an opposing vertex of the polygon when n is even, and at the midpoint of an opposing edge when n is odd. We would like to compare the length d to the diameter of the n-gon, to see when the paper between the twist center and the raw edge will be contained within the boundary of the n-gon.

Let us consider our n-gon as inscribed in a circle. Radii of the circle partition the n-gon into n isosceles triangles with side lengths r and $s = 1/(n+1)$. Each isosceles triangle has altitude a. When n is even, we compare the length of d to $2r$, and when n is odd, we compare the length of d to $r + a$.

To calculate d we will use two similar right triangles, both with angle α, as in Figure 6. The larger triangle is part of the crease pattern and the smaller triangle is contained in an isosceles triangle of the n-gon. Comparing the hypotenuse and the side adjacent to the angle α, we have

$$\frac{d}{s} = \frac{r}{s/2},$$

so $d = 2r$. This computation may also be done using trigonometry, but the similar-triangles calculations are simpler.

We can now compare d to the length of the diameter of the n-gon. As $d = 2r$ is exactly the diameter of an even n-gon, we see that for even n the raw edge of the twist lines up perfectly with the bottom of the box. For odd n, the diameter of an n-gon is $r + a$. As r is the hypotenuse of the triangle and a is a leg of the triangle, $r + a < 2r$. Thus, the diagonal

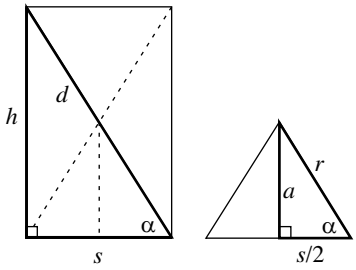

Figure 6. Similar triangles.

does not fit inside the diameter of the n-gon for any odd n. To determine how much excess paper we must fold under (and to ensure that we will always be able to do this), we examine by how much d exceeds $r + a$, i.e. we compute $d - (r + a) = 2r - (r + a) = r - a$. To find a in terms of r we use the triangle in Figure 6 to obtain $\sin(\alpha) = \frac{a}{r}$, so $a = r\sin(\alpha)$. Thus,

$$r - a = r - r\sin(\alpha) = r(1 - \sin(\alpha)).$$

From computing values we see that $r - a$ gets smaller as n gets larger. To verify this, recall that to construct a regular n-gon we have $\alpha = \frac{\pi}{2}((n - 2)/n)$. As n gets bigger, α gets closer to $\frac{\pi}{2}$ since $(n-2)/n$ goes to 1. Thus,

$$\lim_{n\to\infty}(1 - \sin(\alpha)) = 1 - \lim_{n\to\infty}\sin\left(\frac{\pi}{2}\left(\frac{n-2}{n}\right)\right) = 1 - \sin(\frac{\pi}{2}) = 0$$

and the extra paper that we must fold under does, in fact, become much less noticeable for large values of n.

To see that we can tuck away the excess paper toward the center of the box for any odd n, we verify that $r - a < a$. Using the formulas $a = r\sin(\alpha)$ and $r - a = r(1 - \sin(\alpha))$ combined with the fact that $0 \le \alpha \le \frac{\pi}{4}$, we see that $r - a < a$ for all $\alpha \ge \frac{\pi}{6}$. Since $\alpha = \frac{\pi}{2}((n - 2)/n)$, this will hold for all $n \ge 3$. In some cases there are fancier ways to remove the excess, for example, by forming a smaller n-gon with the extra paper. However, these only work for small values of n. Interestingly, Fuse avoids having excess paper in the interior of the box bottom for odd n by shortening h but leaving α the same, thus causing the diagonal creases to miss the corner of the rectangle along the raw edge of the paper.

4 Constructing the Crease Pattern

We have shown that if we are given a crease pattern as in Figure 1, we can use it to make an n-gonal twist box. We now address the question

n	$\tan\alpha$	h	n	$\tan\alpha$	h
4	1	.2	12	3.73	.287
5	1.38	.229	13	4.06	.290
6	1.73	.247	14	4.38	.292
7	2.08	.260	15	4.70	.294
8	2.41	.268	16	5.02	.296
9	2.75	.274	17	5.35	.297
10	3.08	.279	18	5.67	.299
11	3.41	.284	19	5.99	.300

Table 1. Values for computing h.

of how to actually construct this crease pattern. To construct the side s, we divide the paper into $(n+1)$ths. This can be done using the Fujimoto approximation technique (see [2], [1]). Then, we must either construct the angle α or the length h. Constructing $\alpha = \frac{\pi}{2}((n-2)/n)$ is easy for a few values of n such as $n = 3, 4, 6$, but is generally hard. We can adapt the Fujimoto approximation technique to divide angles into $n$ths (see [1]) and use this to divide the angle $\frac{\pi}{2}$ into $n$ths. From this we can construct $\frac{\pi}{2}((n-2)/n)$, so finding the necessary α can always be done, but in general it is rather complicated. It is often easier to compute

$$h = s\tan(\alpha) = \frac{1}{n+1}\tan\left(\frac{\pi(n-2)}{2n}\right).$$

The values of h and $\tan(\alpha)$ in Table 1 will enable us to examine some special cases.

The nicest cases correspond to easy-to-construct values of either $\tan(\alpha)$ or h. For example, when $n = 5$, $\tan\alpha = 1.38 \approx 1\frac{3}{8}$. Thus $h \approx 1\frac{3}{8}s$, which is relatively easy to construct as we can fold a $\frac{\pi}{4}$ angle to mark s, then $2s$ on the side and divide into 8ths. Another simple case is when $n = 7$ as $h \approx 2s$. For an example of easy-to-find h, we see that when $n = 6$, $h \approx \frac{1}{4}$.

Another result seen in the table is that for $n \in \{16, 17, 18, 19\}$, h is approximately $\frac{3}{10}$ths of the paper length. In particular, when $n = 17$, $h \approx .297195973$, which is quite close to $\frac{3}{10}$. (Approximations of $\frac{5}{17}$, $\frac{3}{13}$, and $\frac{7}{23}$ are less close.) This suggests that for a 17-sided box, we could use paper of size $1 \times \frac{1}{2}$ for the lid, so that h will be at the $\frac{3}{5}$ mark. For the body of the box, we might use $1 \times \frac{3}{5}$ paper so that h will be at the $\frac{1}{2}$ mark. This inspired us to create a 17-sided box, for which diagrams appear in Figures 7 and 8.

The other interesting result we see in this table is that h appears to be approaching a limit—in fact, it is approaching $\frac{1}{\pi}$. To verify this curious result, we compute

$$\lim_{n\to\infty} h = \lim_{n\to\infty} \frac{\tan(\alpha)}{n+1}.$$

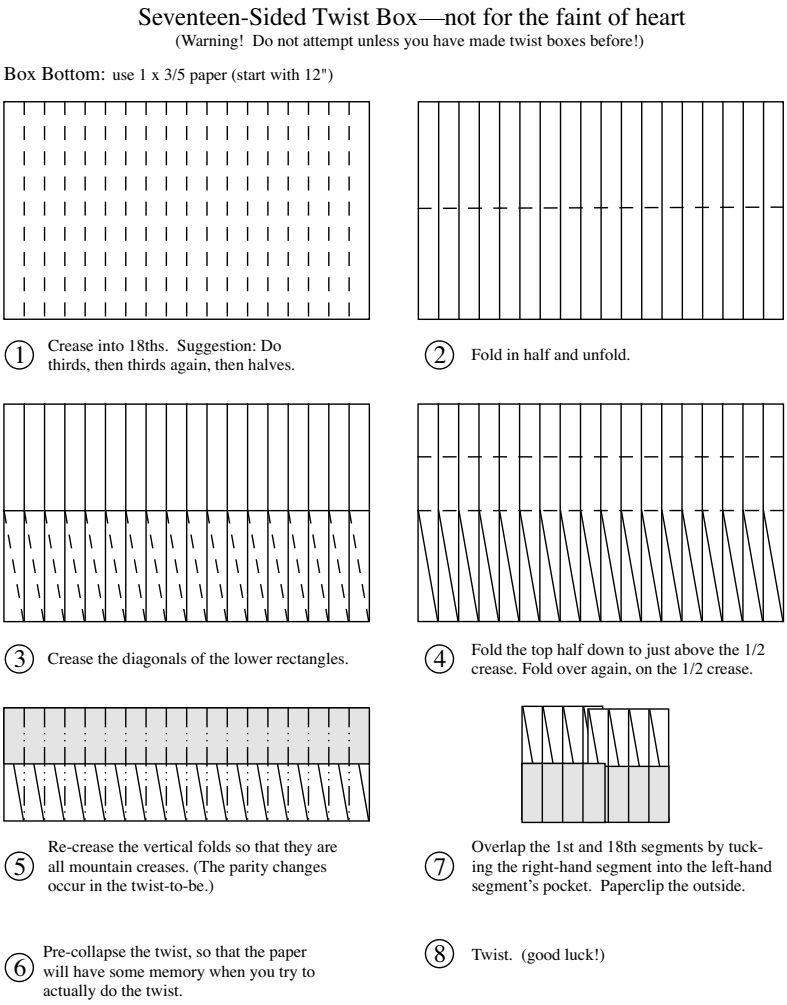

Figure 7. The bottom of a 17-sided box. Even experts find the twist difficult.

In order to more easily apply L'Hôpital to evaluate the limit, we will convert from n to α. Since $\alpha = \frac{\pi}{2}((n-2)/n)$ we have

$$\frac{1}{n+1} = \frac{\pi - 2\alpha}{3\pi - 2\alpha}.$$

Thus,

$$\lim_{n\to\infty} h = \lim_{\alpha\to\pi/2} \frac{(\pi - 2\alpha)\tan(\alpha)}{(3\pi - 2\alpha)} = \lim_{\alpha\to\pi/2} \frac{(\pi - 2\alpha)\sin(\alpha)}{(3\pi - 2\alpha)\cos(\alpha)}.$$

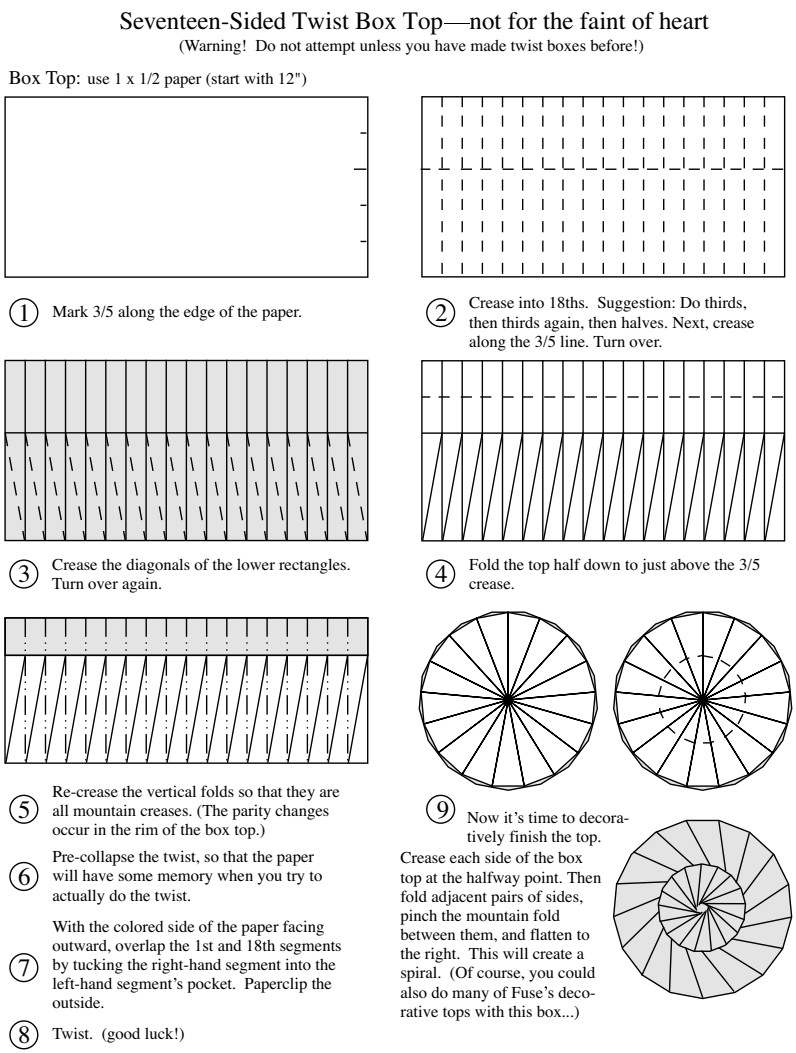

Figure 8. The top of a 17-sided box. Beware the difficulty of the twist.

Both top and bottom of this fraction tend toward 0 as α tends toward $\frac{\pi}{2}$, so we may use L'Hôpital's method from calculus to determine this limit. Thus,

$$\lim_{n\to\infty} h = \lim_{\alpha\to\pi/2} \frac{-2\sin(\alpha) + (\pi - 2\alpha)\cos(\alpha)}{-2\cos(\alpha) - (3\pi - 2\alpha)\sin(\alpha)} = \frac{1}{\pi}.$$

5 Conclusion

In this paper we have shown that for any n, we can construct the crease pattern in Figure 1 and use it to build an n-gonal twist box. Many origami enthusiasts have doubtless wished for easier ways to construct twist boxes with odd numbers of sides. We hope that we have provided one such way, though it is clear from our work that the construction is still far from easy. Some odd values of n are quite challenging, and all require extra folding to account for excess at the raw edge of the twist. However, it is quite interesting that as the value of n increases this becomes less and less of a problem and even more interesting that as n gets larger and larger h approaches a constant value. This means that for large enough n we can use a constant h and the only difference in the crease pattern will be in the number of subdivisions needed for the twist.

As a final note, we mention that our method can be used to create domed box tops. Design details are left to the reader, but the general idea is to make h (and thus α) slightly larger than usual; this could make construction easier for some n, by rounding up to the easiest-approximable rational number for h. Because α is larger, the raw edge of the twist will be rotated an amount other than 0 or $\frac{\pi}{n}$. A master at closed sinks might be able to make the twist flatten against the dome, but mere mortals will want to blintz the raw edge as they close the twist.

Bibliography

[1] James Brunton. "Mathematical Exercises in Paper Folding: I." *Mathematics in School* 2:4 (1973), 25–26.

[2] S. Fujimoto and M. Nishiwaki. *Sōzō Suru Origami Asobi e no Shōtai* (An Invitation to Creative Origami Play, in Japanese). Osaka, Japan: Asahi Culture Center, 1982.

[3] Tomoko Fuse. *Boxes in One Piece* (in Japanese). Tokyo: Chikuma Shobo, 1992.

[4] Tomoko Fuse. *Origami Gift Boxes* (in Japanese). Tokyo: Chikuma Shobo, 2000.

A Brief History of Oribotics

Matthew Gardiner

1 Definition of Oribotics

Oribotics is a hybrid field of research, joining two complex fields of study; origami and technology, specifically bot technology, such as robots, or intelligent computer agents, known as *bots*. The name is broken into two parts: *ori*, which comes from the Japanese verb *oru*, literally means "to fold," and *bot* is the shortened form of the word *robot*. Oribotics is origami that is controlled by robot technology; it is paper or foldable material that will fold and unfold on command.

An *oribot* by definition is a folding robot, therefore any robot that folds, or any device that uses technology and folded actuators together, is an oribot. The definition blurs at the boundaries where origami models, by themselves, exhibit mechanical characteristics. While there may be no robotic component, paper can possesses a programmed memory for movement. Oribotics research looks for rigid and nonrigid crease patterns that have a natural folding motion. Natural folding is found in crease patterns that posses the ability to undergo repetitive shape transformation by mechanical means without compromising their folded form. Forms like the *Miura Ori*, flapping bird, and the oribot *Atom Flower* (see Figure 1) possess this natural folding motion. The idea of natural folding is inspired from the unfolding found in nature, especially that found in leaves and flowers.

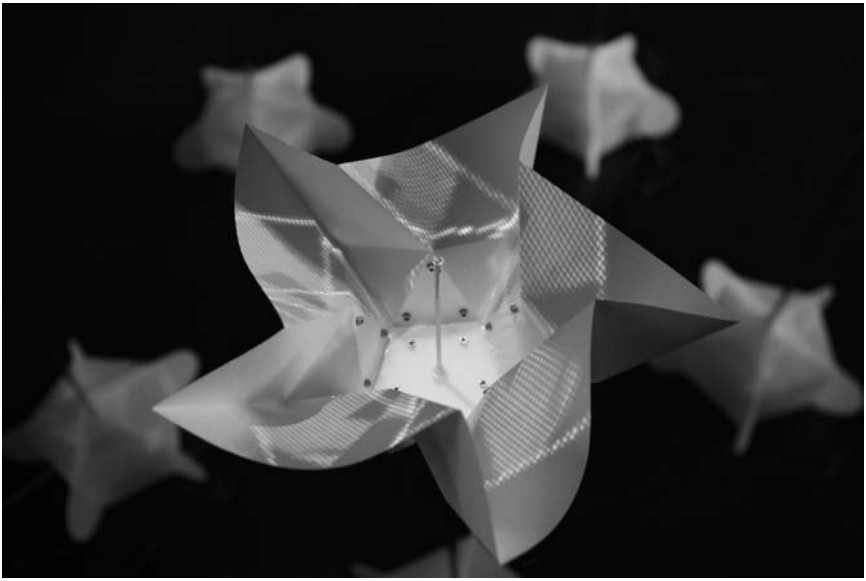

Figure 1. The oribot *Atom Flower*. (Image from the art exhibition Oribotics [Laboratory]; photograph by Yatzek.)

2 The Origin of Oribotics

The origins of oribotics, are not found in fragments of paper, but rather fragments of code. Small snippets of ideas emerged in 2002 when I began making origami animations using Macromedia Flash. I was using Actionscript to make them interactive. *Root 2* was my first interactive work using this theme (see Figure 2). It has two modes, divide and fold. It begins with a set of isosceles triangles (half squares). When divide is active, the mouse recursively makes root 2 divisions of the existing triangles. When fold is active, the mouse makes the triangle animate a fold hinging on one of the shorter edges.

Orimattic takes a step along the same path, adding a tiny bit of artificial intelligence to the mix (see Figure 3). *Orimattic* was a work commissioned in 2002 for the Bed Supper Club in Bangkok, designed to be projected alongside an origami installation that took over the entire club. As such the work needed to change autonomously, creating an ever-changing origami wallpaper. The core of the programming was the bot that controlled the animation. The bot is an origami snake of equilateral triangles, that can only walk on a triangular grid. The work used six base images and six colors that combine randomly at startup. As each bot takes a step, it

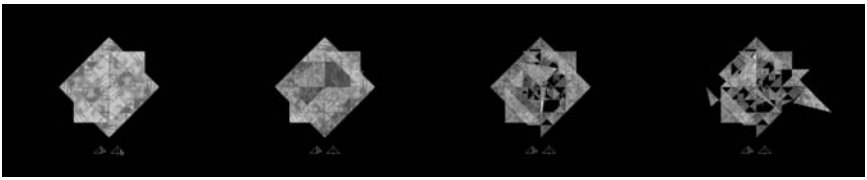

Figure 2. *Root 2* interactive Macromedia Flash animation.

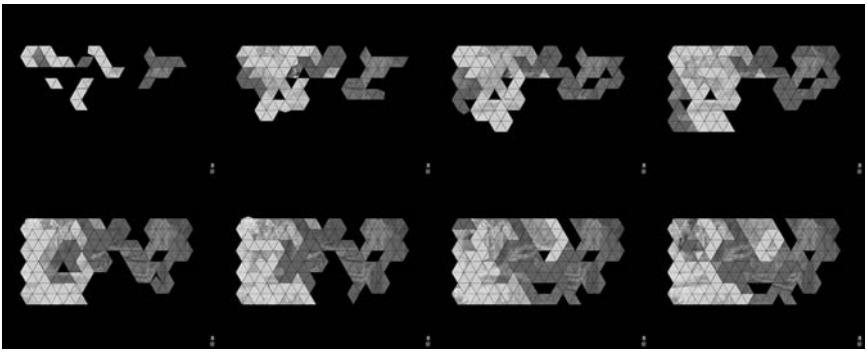

Figure 3. *Orimattic* generative Macromedia Flash animation.

leaves a footprint, and each subsequent step rubs the footprint down in opacity, gradually revealing the image below.

2.1 Tetrabot

Later in 2002, I was granted a residency at the Latrobe Regional Gallery, and during the weeks prior to starting, I was having visions in the morning of *Orimattic* being made as a three-dimensional robot, or as walking tetrahedrons moving on the floor with projected animation. Once my residency began and I started work, I found that it was actually quite tricky to make a folding, walking tetrabot with Legos. In 2005 I read in a *New Scientist* magazine that NASA actually built a successful Tetrabot [2] that walked beautifully. This original idea sparked several others ideas including a mechanized flapping bird.

2.2 Robotic Tato

One of the most promising was a robotic Tato, an idea inspired by Chris Palmer's extensions to the Japanese Tato. My first attempts at pure mechanical construction were conceptually solid, but the practical results were not especially interesting. My mechanical design intended to move in the

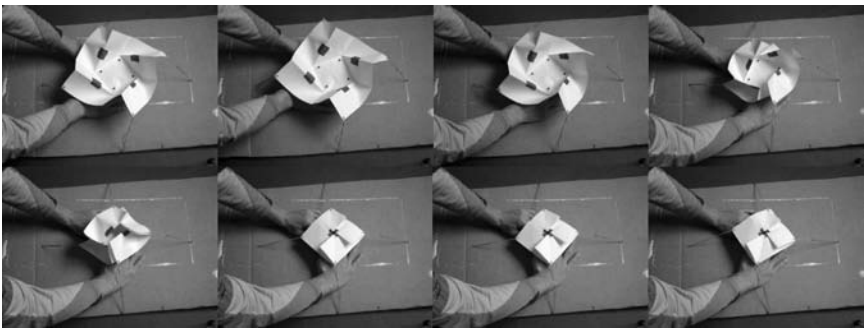

Figure 4. Tato rubber band theory.

same path as the folding paper, however, when I attached the paper, the Lego proved too inaccurate, and just crushed the paper. So instead of using mechanics to push the paper in and out of shape, I began experimenting with pulling the paper. Figure 4 illustrates the low tech, rubber-band-and-cardboard-box approach that I chose to successfully prove this theory.

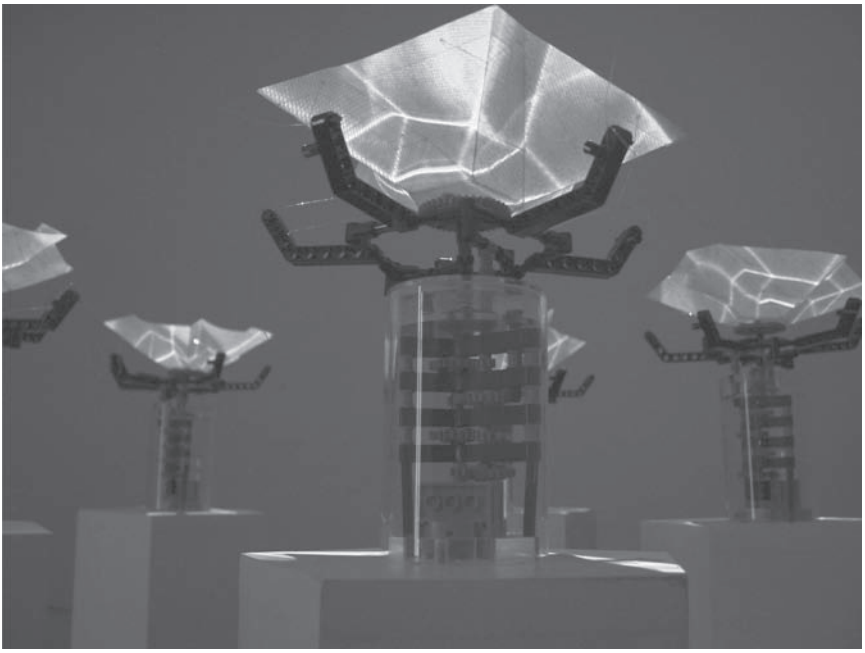

Figure 5. Oribotics 2004, Next Wave Festival, Melbourne.

3 Oribotics 2004

The rubber band proof was enough to inspire me to write an application for a youth arts festival, and led me to dub the work Oribotics. And what followed was a period of prototyping pentagonal designs. Which, with the robotic programming by my father, Ray Gardiner, resulted in the global premiere of Oribotics in 2004 (Figure 5). Many design changes occurred, the most significant being the design of the pentagonal crease pattern, used because of the pentagon's mathematical perfection, its beauty, and its regular occurrence in nature, as signified by the Fibonacci sequence.

3.1 Design Problems with Oribotics 2004

There were several fascinating design problems with Oribotics 2004. It was beautiful, but in terms of design, it was a flawed project. The audience found these problems endearing, as they summed up the fragility and fallibility of technology. The sense of natural entropy was maintained, the flowers bloomed and required some "gardening," and some eventually died. The problems were plentiful, both in the choice of materials and crease pattern design. Most of all, the mechanical design produced considerable stress and therefore required a lot of energy.

3.2 The Corruption and Breakdown of the Crease Pattern

The life of the flowers was initially counted in days. So I worked through a number of paper stocks and plastic sheet reinforcement designs, and I improved the count to weeks, if all was perfect. But any corruption in the crease pattern would cause eventual breakdown of the origami mechanism. My final solution was to use a plastic/fabric lamination, wherein I would cut up plastic sheets, with gaps for folds, and then, using heat, laminate the plastic between the fabric (see Figure 6).

4 Oribotics 2005 [Atom Generation]

In late 2004, I was awarded an Artists Residency in Tokyo 2005 by the Australia Council for the Arts. When I arrived in Tokyo in May 2005, it was my aim to solve these problems and make a better, stronger Oribot. I was full of optimism, high from the energy of a series of talks and exhibitions in Belgium. Mr. Jun Maekawa was a guest of ours at Folding Australia earlier in the year, and he suggested that he could introduce me to a number of people with whom I could speak about oribotics research. Kindly, Mr. Maekawa took me to meet them, and on our travels

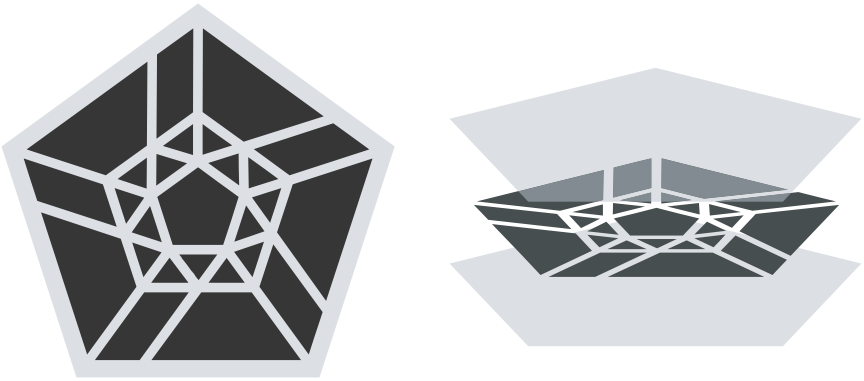

Figure 6. Lamination—the dark gray shows the shape of the plastic parts cut out, and the light gray shows the fabric area. The right-hand image shows the sandwich of materials.

we met with Mr. Shunsuke Ito, the chief robotics engineer at Denso, and Mr. Ohara, an engineer at Kuramae Industries.

At Denso in Nagoya, Aichi, I was introduced to Mr. Ito's masterwork titled Karakuri Maiginu featuring two mechanically folding origami cranes. To my surprise he was not using computers, but elegant mechanical design, with superbly crafted brass hinges, and fabric. A feature of his design for the cranes was the areas of rigidity and flexibility in the crease pattern. I was very inspired to see a work of this caliber.

Mr. Ohara was the head engineer of the origami paper cup project as introduced in 3OSME by Tomoko Fuse et al. [1]. I had many questions for Mr. Ohara regarding his research into industrial folding techniques. I was made aware that the project was still in development, and that the research was still "top secret." So I am unable to share any details, except to state that even by hand it is quite difficult to fold a paper cup, but the result is very strong, and I use a folded cup on my desk as a pen holder.

4.1 Crease Patterns

While looking at the crease pattern for Ito's Karakuri, a few ideas came to me. I realized that the original crease pattern demanded far too much stress on the paper as the folds moved through 180°. So I redesigned the model and introduced a pyramid shape in the middle of the closed flower. (See Figure 7.) The redesign provided faces with more leverage, and less of an angle of movement, thus reducing the stress in the model. After many

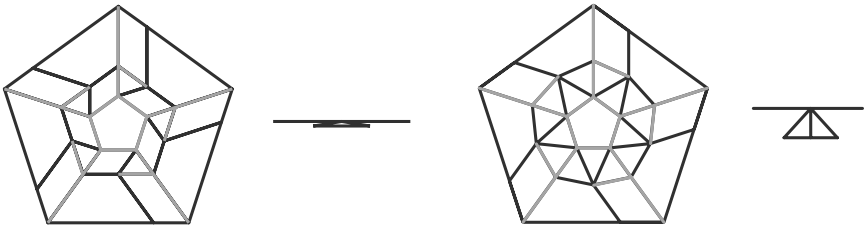

Figure 7. The 2004 crease patternand profile (left), and the 2005 crease pattern and profile (right).

trips to the Japanese craft store Tokyu Hands, and many experiments with paper stocks and mechanical designs, I found the most elegant way to actuate this new crease pattern.

The new crease pattern and mechanical design were taken back from Japan and prototyped in Australia before evolving into the atom generation of oribots.

5 Prototyping

The prototyping process was rather direct, and not as well documented. It focused almost solely on the mechanical and electrical design. The process was to design three-dimensional models, and translate them into two-dimensional planes that could be cut from flat sheets of 3 mm plastic, and assembled back into physical three-dimensional models. (See examples in Figure 8.) The key elements of design were as follows.

5.1 Base

Inside the base are the following main components: the custom-designed printed circuit board with a PIC microprocessor; an LED or two; and a high-quality Servo motor, like the kind used in radio control models. The electronic system was designed and programmed to specification by Ray Gardiner.

5.2 Hand Actuator

The hand actuator constitutes the parts that touch, and are fastened to, the paper. All of the parts are laser cut from 3mm acrylic. When choosing the material, I wanted something that would seem light, and not bulky.

Figure 8. A range of prototype models for Oribotics [Laboratory].

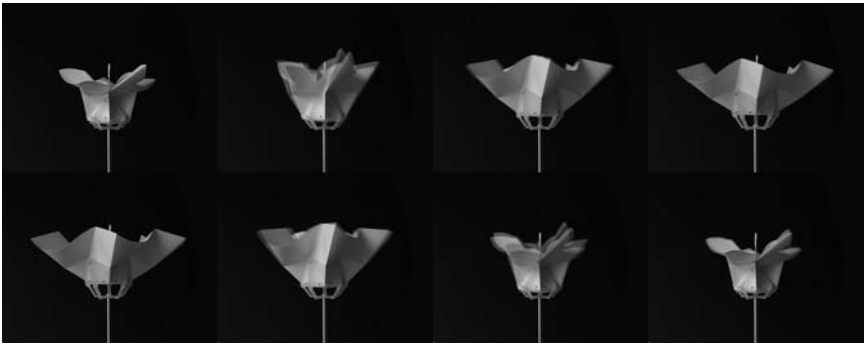

Figure 9. A profile of the hand actuator in motion from closed, to open, and back to closed.

With one single degree of motion, this relatively complex set of folds is actuated, capable of thousands of repetitions. This particular design has shown great resilience, thriving for over nine months of day-in and day-out operation in exhibitions (see Figure 9).

Figure 10. Oribotics [Laboratory], Asialink Centre, Melbourne. (Photograph by Yatzek.)

5.3 Flower

The exhibition flowers use a pearlescent paper to reflect as much light as possible. The paper was carefully scored, folded, punched with holes, and bolted to the hand. Over a period of three years, the only degradation I have seen is wear at the corners, as all of us find when we fold on the same fold over and over again. The commercial versions use a plastic paper and have shown no sign of wear.

5.4 Light Sensor

The only eye of the oribot is a light dependent resistor. A PIC microcontroller brain in the base receives light levels as changes in voltage from the sensor. It has a calibration range, so that in exhibition it opens with a particular level of light and closes at another. Brightness opens the flower and darkness closes it, and so the audience likens it to a real flower.

6 Oribotics [Laboratory]

The final work was premiered at the Asialink Centre at the University of Melbourne, over two nights with four performances. Figure 10 shows a view of the final installation. The installation used digital animation from data projectors to animate light on each of the oribots. During the exhibition there were percussive performances. In the exhibition space there were fifteen oribots, eight speakers, four computers, and two projectors. For the performance there was one projection screen for the score composed by

David Young, and instruments by Rosemary Joy, played by percussionist Eugene Ughetti.

The oribots, sensitive to light, were networked via animation beaming from the data projectors above them. For the audience, the literal connection was that the weather was being projected onto the oribots, and that was making them move. Actually, the arrangement was a little more complex; the animation changed according to the city that the robot was linked to, showing the city's current weather condition as read from a live XML data source. Each weather condition had a corresponding pattern as influenced by origami paper designs.

7 Conclusion

As a field of study, oribotics is a hybrid of science and art that has grown in complexity over the past four years. To date the project has been supported with funding from the New Media Board of the Australia Council for the Arts, Arts Victoria, the City of Melbourne, Aphids, and Ray Gardiner. The next generation of oribots, with the working title Oribotics [Network] was supported by Arts Victoria's Arts Innovation Board and held its premiere in 2007 at Federation Square in Melbourne as part of the Melbourne International Arts Festival.

For more information, and video, see www.oribotics.net.

Acknowledgment. This paper was made possible with the support of ANAT, the Australian Network of Art and Technology Professional Development Fund.

Bibliography

[1] Tomoko Fuse, Akira Nagashima, Yasuhiro Ohara, and Hiroshi Okumura. "Origami Pots." In *Origami^3: Proceedings of the Third International Meeting of Origami Science, Mathematics, and Education*, edited by Thomas Hull, pp. 147–152. Natick, MA: A K Peters, 2002.

[2] Will Knight. "Shape-Shifting Tetrabots Tumble into Action." *New Scientist* 2494 (April 9, 2005), 20.

Graphics Transformation of Origami Models

L. I. Zamiatina

1 Introduction

As an artistic form, every origami model is designed to express an object, idea, or emotion, and is always a product of creative imagination. On the other hand, an origami model is a nontrivial mathematical entity, and often becomes a delightful source of geometric, topological, or algebraic problems. A piece can be appreciated on both levels at once: origami converges the artistic quality of elegance with a measurable mathematical quantity, the efficiency with which the folding process turns paper into form [2].

An origami model is a work of art in and of itself. When used as the "seed-image" for a digital artwork, the model acquires new life and a vast array of possible new artistic meanings. Every origami model is intrinsically a collection of simple geometric shapes, and lends itself naturally to computer modeling as a structured set of polygons, and further transformation into novel images using formal mathematical operations and derived techniques.

2 From Art to Math

> Perceiving as well as representing a thing means finding form in its structure. ... In art as well as in representation in general,

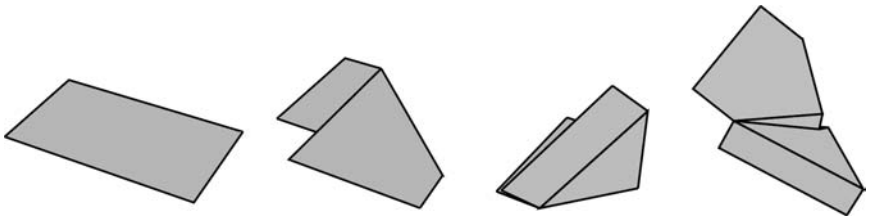

Figure 1. Folding the butterfly model.

> form is an indispensable prerequisite for the perceptual characterization of the content. ... In a work of art, composition has the task of conveying, in structurally most straightforward manner, such form characteristics as carry the desired expression. ... Form interprets environment. [3]

The prerequisite to creating origami-based digital art is modeling the origami in a way computers can work with. To avoid getting bogged down in the potential complexity of this process, the methodology is illustrated below using a simple origami model—a butterfly created from a business card using only three folds, rendered in Mathematica. The graphics sequence in Figure 1 illustrates the steps of folding the model.

The computer model is represented internally using a set of Mathematica graphics primitives, specified by aggregating vertices in Cartesian space into polygons and the polygons into a single three-dimensional shape [5]:

```
butterfly3D =
 {Polygon[{{-2.55,-2.55,0.},{-1.33111,1.64908,-2.62526},
{-0.3825,0.3825,0.}}],
Polygon[{{-2.55,-2.55,0.},{-3.76797,-2.9802,-1.25359},
{-2.54908,1.21889,-3.87885},{-1.33111,1.64908,-2.62526},
{-0.3825,0.3825,0.}}],
Polygon[{{-2.55,-2.55,0.},{-2.70587,-4.04229,0.994366},
{1.14791,-2.47811,3.94592},{1.30379,-0.985816,2.95155},
{-0.146376,0.146376,0.49976}}],
Polygon[{{-2.55,-2.55,0.},{1.30379,-0.985816,2.95155},
{-0.146376,0.146376,0.49976}}],
Polygon[{{-2.55,-2.55,0},{0,0,0},{-0.3825,0.3825,0}}],
Polygon[{{-2.55,-2.55,0},{0,0,0},
{0.146376,0.146376,0.49976}}]}
```

Taking an orthogonal projection of this structure onto a certain plane, and giving each polygon a distinct color results in

```
butterfly2D =
{{Hue[1.875],Polygon[{{-0.815695,12.6035},
  {-5.57857,12.9485},{-2.83232,13.9319}}]},
...
{Hue[6.25],Polygon[{{-0.815695,12.6035},{-2.39093,13.7993},
{-2.37061,14.3053}}]}}
```

Conformal transformations can be used to quickly create a novel incarnation of the butterfly form. First, treat each coordinate of the orthogonal projection as a complex number. Then, apply the following complex variable functions to the flattened model:

```
f[z]=z^2+Log[z]/(z^3)
```

and

```
f[z]=z^2 E^z
```

Before applying the transformations, the function's base projection (the leftmost image in Figure 2) is shifted by a certain vector in order to avoid the singularities of $f[z]$.

Although Mathematica is a high-level programming language that enables the formulation and visualization of problems with programmable graphics primitives [4], the following example illustrates why a transition in the tools used for transformation is desirable at this point in the process. To programmatically specify a simple transformation, even using the specialized `Graphics‘Shapes‘` package, takes the following code at a minimum.

```
Show[
Table[
TranslateShape[
WireFrame[Join[{Thickness[0.001],GrayLevel[0.95]},
AffineShape[Map[# z&, butterfly3D,
{-1}],{9z,10z,11z}]]],
                {100 Sin[Pi z],100 Cos[Pi z],0}],
    {z, 2, 8,.1}],
   PlotRange->All, Boxed->False,
   ViewPoint->{-4.000, -0.050, 1.240},
   AspectRatio->Automatic, Background->GrayLevel[0]]
```

This expression results in the image shown on the left-hand side of Figure 3. For the artistic part of the process, a considerable amount of trial and error is required. To speed up the experimental cycle, the transforma-

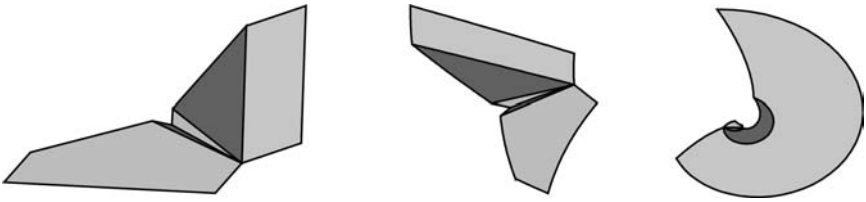

Figure 2. Conformal transformations.

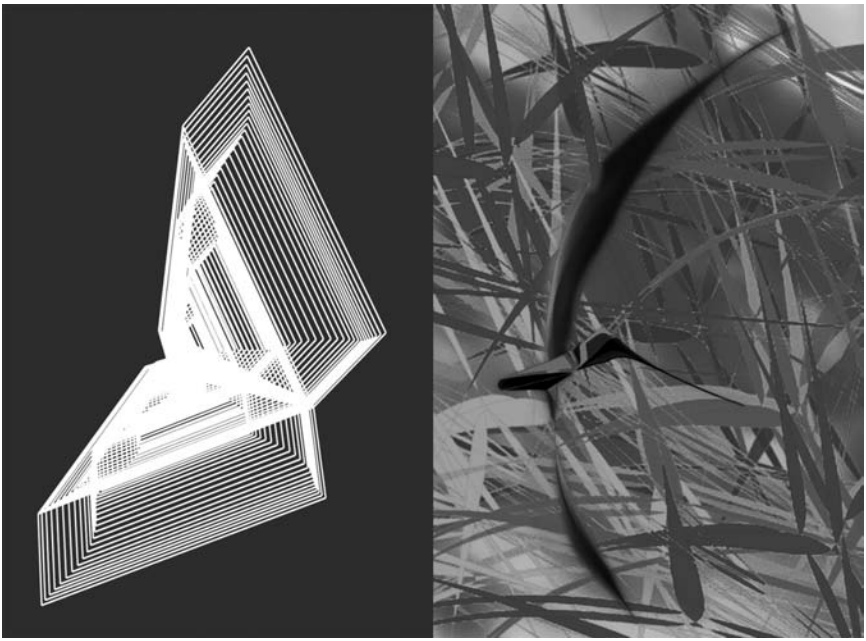

Figure 3. Composition with hummingbird.

tions available in Adobe Illustrator are used. To this end, the next step is to export the model as SVG to bridge the gap between the tools.

```
Export["butterfly3D.svg", butterfly3D, "SVG"]
```

The image in the right half of Figure 3 was created using Adobe Illustrator and Photoshop commands. Although these commands are powered by mathematical algorithms, the nature of these algorithms is less transparent.

Mathematica and Illustrator are thus complementary tools in the artistic process.

Figure 4. Creating the body for the hummingbird.

Figure 5. Creating the wings, the hummingbird, and the grass.

3 Math Back to Art

When the butterfly.svg file was opened in Illustrator, the polygons constituting the model structure were triangulated automatically, and this immediately feeds into subsequent transformations performed to create the right-hand "hummingbird" image in Figure 3. The diversity of forms in this image is achieved by a sequence of steps in Illustrator shown in Figures 4 and 5.

In Figure 3, both parts are composed of transformations of the same origami model, but the image in the left is a still recognizable "crystal butterfly" while the images on the right—the "hummingbird" and the "grass"—are entirely different visual shapes. To create the "hummingbird," the butterfly's triangles were *grouped* and transformed as a single unit, whereas for the "grass," the triangles were *ungrouped* and therefore transformed independently.

4 Methodology

To generalize the process thus described: there are four major steps in creating the artwork by transformation of the folded model.

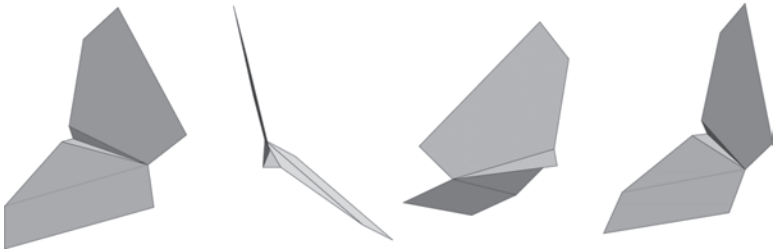

Figure 6. Different views on the model.

4.1 Digital Model Generation

To start a composition we need *a digital three-dimensional model of an origami design* represented as a structured collection of polygons. It is not very important where such a model would come from. The two things that are important: the model should be easily manipulated in a three-dimensional graphics client and various views of it can be exported to vector graphics formats.

Each of the butterfly *views* (see Figure 6) can become a basis for future transformations.

The image in Figure 7 is unusual because one butterfly appears in its unaltered form, while three others are almost unrecognizable. The unaltered initial butterfly is just a particular viewpoint of Mathematica's butterfly model, and is used in the picture as a laptop computer that symbolizes cyberspace. The other three butterfly transformations constitute sky, ocean, and a dolphin.

4.2 Import into Graphics Software

The use of vector graphics is essential because it saves the geometric structure of the model so that its topology is preserved throughout all further transformations. Notably, there are two kinds of transformations: those that keep history of the original shape, and those that do not. Adobe Illustrator calls them effects and filters, respectively. It is preferable to use effects because the parameters of an effect can be altered even after other effects have been applied. The changes propagate to the final result without needing to repeat the subsequent transformations.

Whereas the application of several effects can be treated as a composition of functions on the original image, the use of filters is equivalent to the application of numerical methods to the problem, where the precision, or resolution, of subsequent steps is bounded by the error introduced as a result of using the filter.

Figure 7. The dolphin's way of searching the Internet.

4.3 Model Fragmentation

The crease pattern defines the semantics of the model and can be used as a source of geometric shapes for further artistic interpretation. The leftmost image in Figure 8 shows a digital model; in the next one, eight disjoint polygons comprise the model—these polygons are defined by the intrinsic crease pattern of the origami model; in the third image, further triangulation of the polygons yields 12 separate triangles.

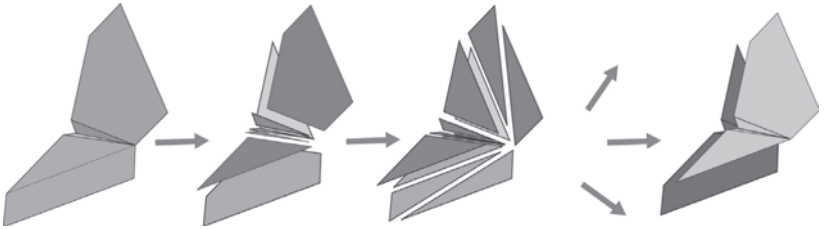

Figure 8. Fragmentation of the butterfly model.

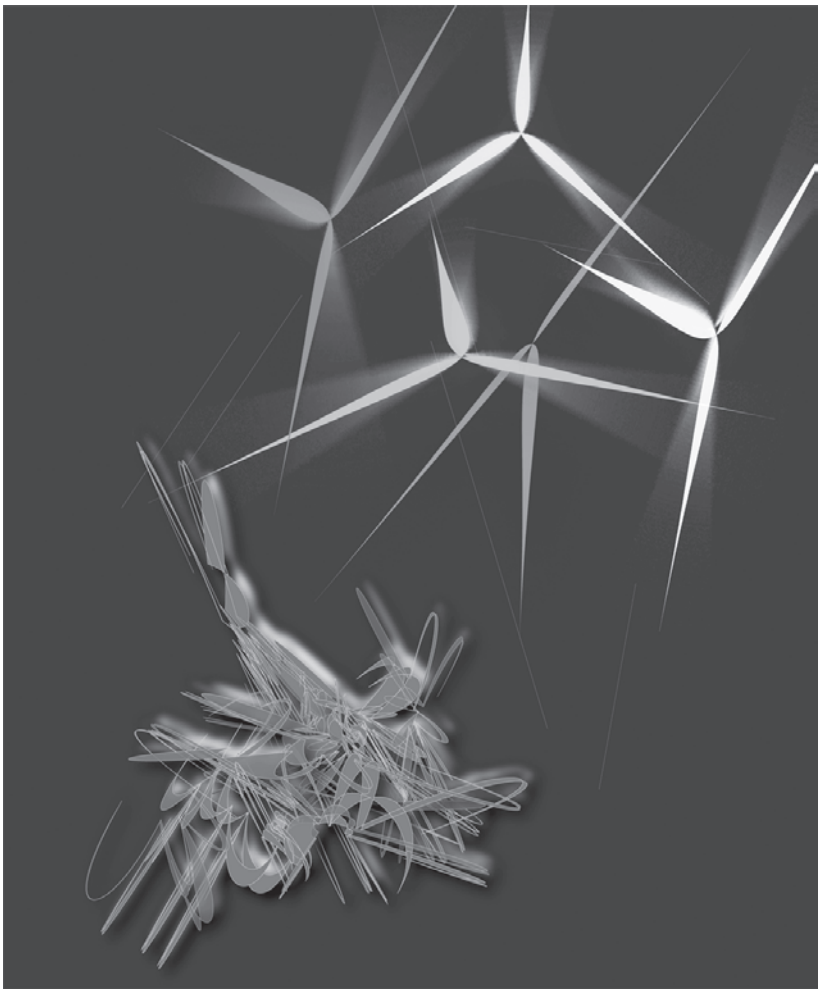

Figure 9. *Don Quixote of La Mancha.*

The rightmost image is an example of reuniting the polygons in a new way to create a novel pattern as the basis for transformation.

4.4 Transformation of the Structure's Polygons

Creating an origami-based artistic image inevitably involves a trial-and-error process of applying transformations to generate the desired effect. The following are some principles that produce images that are aesthetically pleasing in addition to being mathematically interesting.

Be diverse. Ungroup and regroup polygons while applying different transformations to different collections of these elements.

Break symmetry. Perfect symmetry as a rule is not necessarily beautiful—if a picture is too symmetric, consider dropping one or two underlying triangulation elements at random.

In more general terms—randomize. Beauty is to be found in the no-man's land between symmetry and chaos, between the structured and random.

While the geometry of a polygon structure is fragile, its topology is almost indestructible.

For example, Figure 9 contains three polygons distorted into highly eccentric shapes. The image is suggestive of the noble but scattered mind of the ingenious hidalgo Don Quixote of La Mancha. The windmill image comes from the half of same triangulated structure with a relatively moderate warp applied.

5 Case Studies

Figure 10 is an abstract nonrepresentational piece based on the butterfly motif.

Everything in this picture comes from transformations of same simple origami model—the butterfly. Looking at the shapes constituting the picture, the link to their origins may be hard to see. Let us step through the key stages in the transformation. Keep in mind that all the elements of this composition are generated algorithmically—the artist's role in the process is to decide the order and parameterization of the algorithms applied.

The image is a superposition of four layers, all derived from butterflies: background, two intermediate layers, and foreground. The background is made using Illustrator's "Envelope Distortion," with the "Make with Top Object" parameter enabled. The effect basically inscribes a copy of the entire image into each of its triangles. (See Figure 11.) This image is then superimposed onto the original, a "Radiant Blur" effect is applied, and the result is cropped to retain only the center portion.

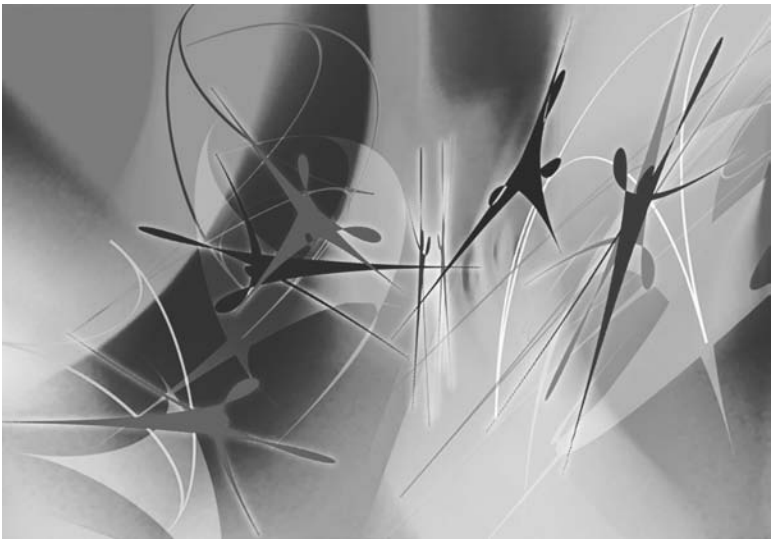

Figure 10. An abstract composition.

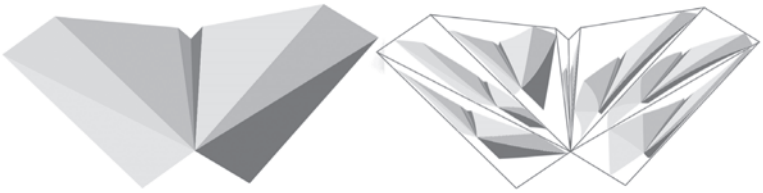

Figure 11. Model transformations for the background.

The foreground layer requires only two transformations—Illustrator's "Bloat" followed by "Pucker." To achieve intermediate layers that are less busy than the other layers, the butterfly's six inner triangles are first removed before any transformations are applied. Next the "Shear Tool" is used, and the "Bloat" and "Pucker" transformations are applied in succession—this time with a very different parameterization than for the foreground layer. Different color schemes are used for the two layers, and one retains only the outlines of its shapes. (See Figure 12.)

Now on to pieces that are not based on the butterfly. Figure 13 is created from two of my original origami teddy bears. The models themselves use an efficient folding process, and the form of each is a reciprocal of the other, with minor modifications. The final ornamental composition is designed to create the illusion that the bears are dancing. The trans-

Figure 12. Model transformations for the foreground and intermediate layers.

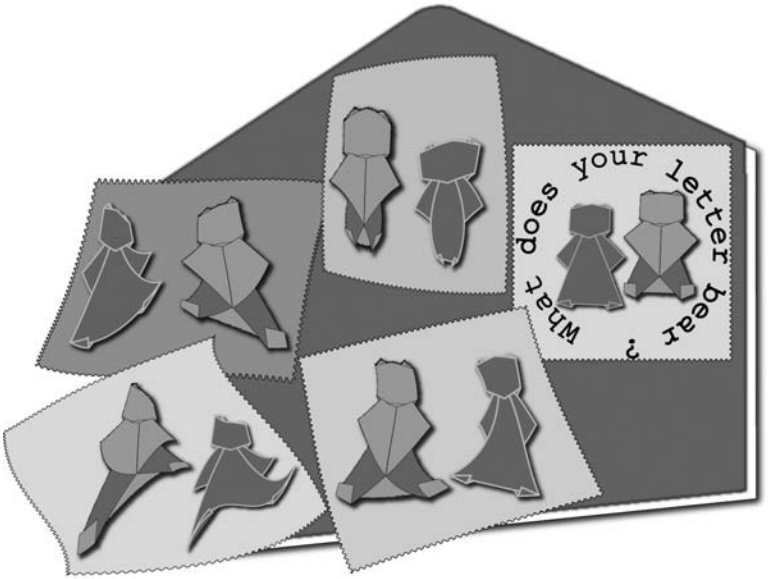

Figure 13. Composition with teddy bears.

formations used to accomplish this are nowhere as extreme as in previous pieces, and differ from each other only in parameterization, which gives the components of the piece a rhythm akin to frames of an animation.

The *Cranes' Cradle* origami design in Figure 14 was created specifically for the composition shown in Figure 15. While a scanned image limits artistic options, in this case it was fruitful because the piece is more directly symbolic than the abstract art depicted in Figure 10.

The process described in the Methodology section is also effective in creating directly symbolic compositions. The "olive branch" piece shown in Figure 16 was created using the methods already described from the digitally rendered butterfly motif. "Indeed the artistic symbol is characterized

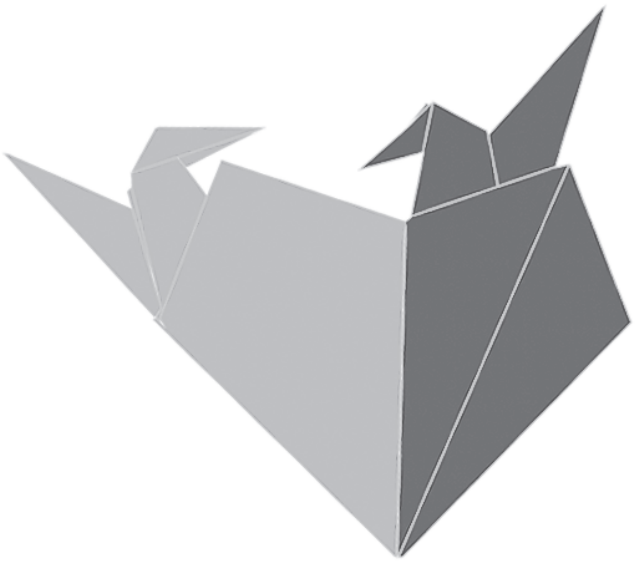

Figure 14. The *Cranes' Cradle* design.

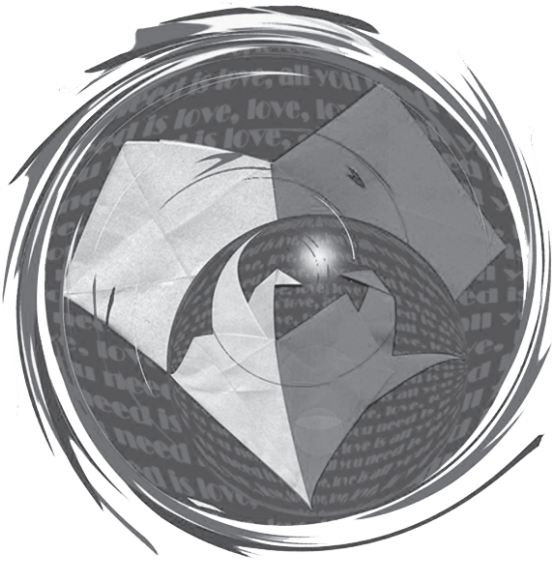

Figure 15. The *Cranes' Cradle* composition.

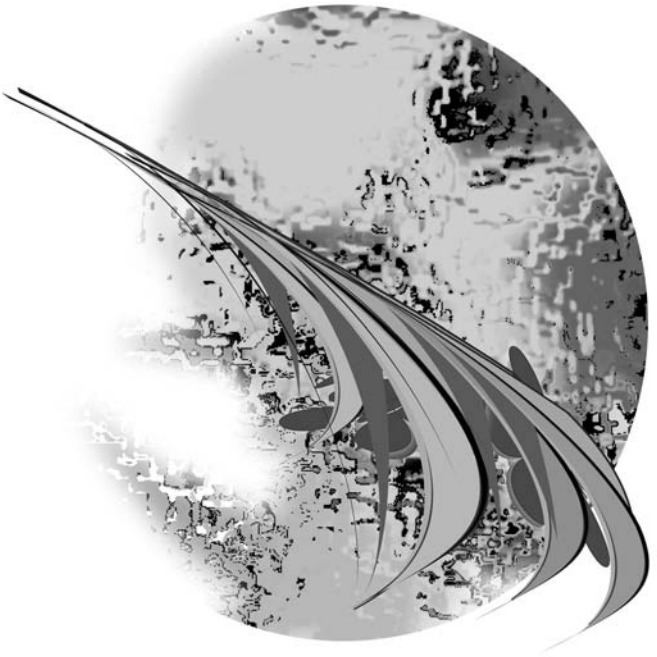

Figure 16. An olive branch.

by certain distinctive properties, generally labeled aesthetic, which pertain to the unity and internal integrity of its parts" [3].

6 Conclusion

Origami-based digital compositions epitomize a closed-circle relationship between art and mathematics. The expression of an art form, an origami figurine, is brought into the realm of pure mathematics by simulating it with a computer to a degree of perfection that cannot be achieved with a physical medium. A human artist then guides its transformation by applying transformations with a strong mathematical basis, but in a direction that only artistic vision can generate. The circle is completed, and the composition returns fully to the artistic realm when the artist deliberately introduces imperfection, imbalance, and entropy to achieve the desired vi-

sual effect. However, provided this last step is not taken to an extreme, the harmony and symmetry of its intermediate geometrically perfect state remain visible to the viewer.

The relationship between mathematical truth and its visual form has been well documented, most notably by the great contemporary mathematician Anatolij Fomenko:

> It happens rather frequently that the proof of one or another mathematical fact can at first be 'seen,' and only after that (and following this visual idea) can we present a logically consistent formulation, which is something a very difficult task requiring serious intellectual efforts. ... Thus, the criterion of beauty of one or another geometric image often serves as a compass for choosing an optimal way of a further formal logical proof. [1]

Hopefully, the methodology I have outlined above will allow mathematical truth to be harnessed for the benefit of visual art.

Acknowledgment. I would like to thank Alexei and John Bocharov for constant inspiration and support during my work on this project and paper.

Bibliography

[1] Anatolij Fomenko. *Visual Geometry and Topology.* Berlin: Springer-Verlag, 1994.

[2] Robert J. Lang. *Origami Design Secrets.* Natick, MA: A K Peters, Ltd., 2003.

[3] Enrique Mallen. *The Visual Grammar of Pablo Picasso*, Berkeley Insights in Linguistics and Semiotics 54. New York: Peter Lang Publishing, Inc., 2003.

[4] Michael Trott. *The Mathematica GuideBook for Graphics.* New York: Springer-Verlag, 2004.

[5] Liudmila I. Zamiatina. "Computer Simulation of Origami." *Mathematica in Education* 3:3 (1994), 23–31.

One-Dimensional Origami: Polyhedral Skeletons in Dance

Karl Schaffer

Recent advances in genetic engineering have included constructions of polyhedra from single strands of DNA, a process sometimes labeled *DNA origami* [5,12], and have generated interest in what might be called *one-dimensional origami*. The author has investigated similar—but simpler—constructions in dances that he and colleagues have choreographed [6,11], in which polyhedral skeletons are formed by dancers carrying identical linked sections of PVC pipe. For example, in one dance four sets of pipes linked by a short length of string at their ends (Figure 1) are used to create a rotating cube, an octahedron, and a pair of tetrahedra.

These might be considered as four identical line segments, each "folded" at two points. This paper will focus on constructions of polyhedral skeletons and other structures by this one-dimensional modular origami, including some mathematical constructions that are too large to be implemented in actual dances under normal circumstances.

The dance company codirected by the author has also utilized loops of rope, string, and bungee cords, as well as "finger geometry" and the dancers' bodies for polyhedral constructions in our dances [7, 8]. If we think of origami as folding a section of a two-dimensional surface such as a square along specific crease lines, then one-dimensional origami could be the imparting of folds at specified points to a one-dimensional line segment. Demaine and Demaine [1] have used the terms *hinges* and *bars* in their discussion of polygonal folding that stays within a plane, and this

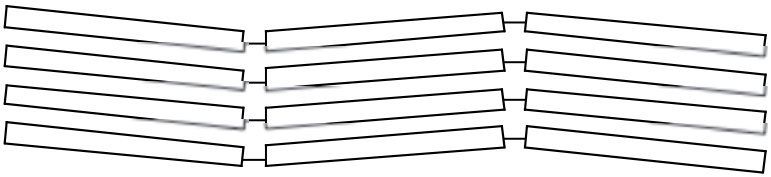

Figure 1. PVC pipe linkages used in dances.

terminology emphasizes that the fold points do not shift, and the segments remain rigid. Rope is continuously deformable, but PVC pipe and fingers may be "folded" in a manner analogous to paper, in that the "fold points" do not shift along the segment. Perhaps a better medium for one-dimensional origami would be pipe cleaners, since they hold the fold with a certain amount of tension, but we have not utilized anything like that in our dances. We will also not be concerned in this paper with polyhedral constructions with loops of rope. Some of these constructions have been presented from the point of view of classroom activities in Schaffer, Stern, and Kim [10], and in a more extended manner in the show, *Through the Loop: In Search of the Perfect Square* [7]. *The Secret Life of Squares* [9] uses a more "normal" origami construction, a tetraflexatube [3] large enough for two dancers to hide in.

Modular origami usually utilizes several sheets of paper folded in an identical manner, often to form the surface of a polyhedron, so modular one-dimensional origami might fold several line segments identically to form a polyhedral "skeleton." Paper modular origami constructions are held together by friction along the paper surface, by the tension at the folds, or by linkages that are part of the design. One-dimensional origami constructions that create three-dimensional forms might maintain their structure by wrapping or hooking the segments around or to each other. However, in our dances, it is the dancers who actively maintain the shape as long as necessary, and then segue to new shapes. The "ligatures" holding the constructions together are thus the dancers' hands, whereas in DNA origami the ligatures are "helper strands" of DNA. We will not be concerned with linkages between modular units in what follows.

The mathematical problems involved in creating dances that include polyhedral constructions include not only deciding what geometric shapes can be made effectively, but also exactly how to construct them, how to create transitions between shapes, and when to establish sequences that might be interesting to the audience. Shapes that involve theatrical or emotive metaphors are as enjoyable as those that are purely geometric, so there is often a give and take between the geometric and nongeometric imagery. The performance problems for the dancers are also significant,

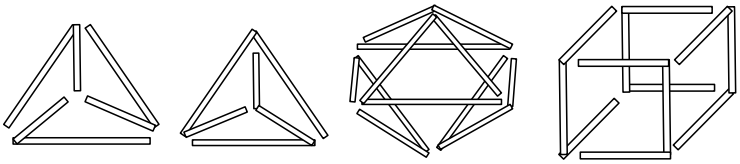

Figure 2. Platonic solids formed during dances from length two and three paths.

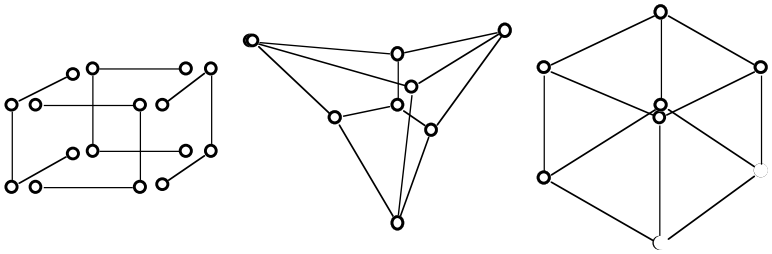

Figure 3. Shapes formed by flexing the cube.

and include deciding how best to hold, manipulate, move with, and link the PVC pipes or other props. Mathematically, we might consider the polyhedra construction problem to be that of determining decompositions of the skeletons of the polyhedra of interest into a uniform set of smaller subgraphs that will coincide at the vertices.

Figure 2 shows PVC pipe constructions utilizing what the dancers call "twosies" and "threesies," or paths of length two and three, to create tetrahedra, an octahedron, and a cube [6].

Notice that the first tetrahedron, the octahedron, and the cube are constructed with a three-, two-, and four-fold rotational symmetry, allowing the dancers to move in unison with those symmetries while forming the shapes. Figure 3 shows how the dancers flex the cube, once formed, into a four-pointed star and a hexagonal wheel. We have noticed that the full-three-dimensionality of these forms are more visible to the audience if they are in motion, so the dancers move in a large circle while forming the various polyhedra. The PVC pipe segments are 40 inches in length and 1.25 inches in diameter, and in one of the dances we have painted the segments with fluorescent paint and utilize black light in the polyhedral section of the dance to focus attention on the pipes rather than the dancers.

The dance "Pipe Dreams," in which the cube and octahedron are constructed, requires four dancers. Because maintaining a performance involving four dancers, who are wont to move off to New York or become real

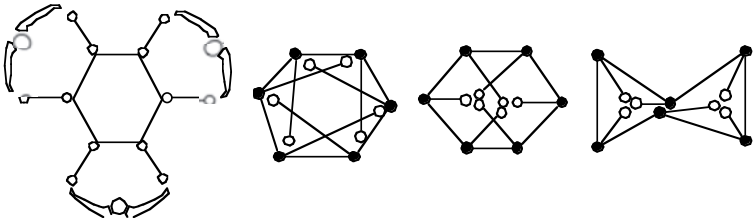

Figure 4. The hexastar folds into the cube, octahedron, or two tetrahedra.

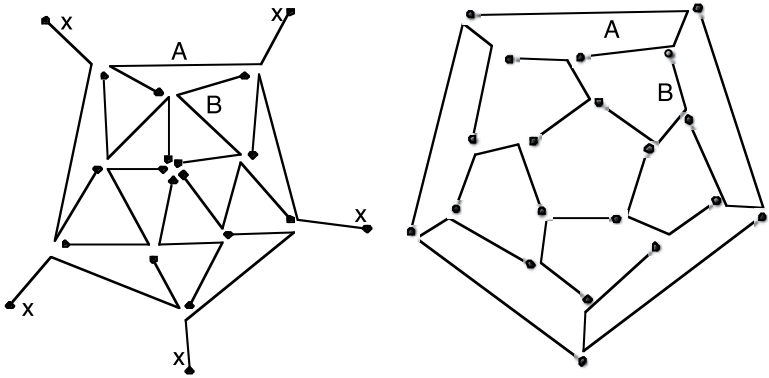

Figure 5. Decompositions of the icosahedron and dodecahedron.

estate agents, is much more difficult than a performance for three dancers, I have lately been recreating the show that includes that dance, for three dancers. Figure 4 shows a winged hexagon or *hexastar*, which itself decomposes into six segments of length two, which can be folded into a cube, an octahedron, or two linked tetrahedra (the black vertices are the vertices of the central hexagon.) The hexastar has recently been used to make these polyhedra in a three-person dance [2].

Similar decompositions of the icosahedron and the dodecahedron exhibit five-fold symmetries (Figure 5) but would involve ten dancers each wielding a length three path, and so have not been tried (In the icosahedron the vertices labeled x are actually "identified" as a single vertex). In one trio we have used three threesies to form a 9-gon, which we then fold into a tetrahedron briefly (Figure 6, [11]). Decompositions of the Platonic solids into paths of length two that have nice symmetries are also possible (the cube and octahedron are shown in Figure 6—there are many possibilities for the dodecahedron and icosahedron). The "twosie" tetrahedron shown in Figure 2 has been used in a dance [6], and this and the cube and

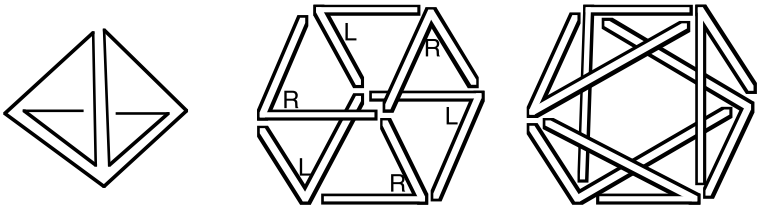

Figure 6. Tetrahedron made with a 9-gon, cube, and octahedron made with six length 2 paths.

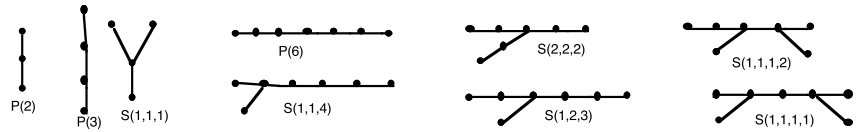

Figure 7. Graphs that are candidates for decomposing the Platonic solids.

octahedron in Figure 6 make entertaining classroom activities in which the length two paths are created by the pointer and middle finger of each hand (right hands labeled R, left L in the cube). There is a transition between the cube and the octahedron, and another from the cube to the wheel shown in Figure 3 and then to another cube in which the right index fingers are on the bottom instead of the top, but these take some practice! A construction devised by Scott Kim uses four hands to form a tetrahedron, with the thumb, pointer, and middle fingers of each hand forming half an edge; this and other similar constructions are shown in Schaffer, Stern, and Kim [10].

These constructions suggest interesting mathematical questions. For example, what is the largest graph that can be used in multiple copies to fold the skeletons of the five Platonic solids? Such a graph would necessarily have a number of edges that is a divisor of the 6, 12, and 30 edges of these five polyhedra, and also cannot have vertices of degree greater than three, since the tetrahedron, cube, and dodecahedron only have degree three vertices. The cube and dodecahedron rule out the use of a three-cycle or six-cycle, since those polyhedra have vertices of odd degree, and each vertex of such a cycle would add two degrees to any of their vertices. Also, any such decomposing graph cannot contain a cycle of length less than five, since that is the smallest cycle in the dodecahedron. This limits the possibilities to the five graphs shown in Figure 7.

For convenience, these graphs have been labeled either as paths $P(n)$ with n edges, or as $S(a, b, c, d)$, where a, b, c, and d indicate the lengths

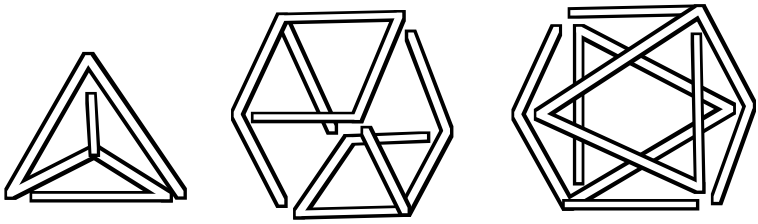

Figure 8. Decompositions by $S(1, 2, 3)$.

of the appendages from degree three vertices. Two copies of the "3-star" $S(1, 1, 1)$ do not fold into the tetrahedron, though this graph does decompose the cube, octahedron, and icosahedron. The decompositions of the cube and octahedron can be nicely modeled using the thumb and the first and second fingers of four hands [10]. The dodecahedron cannot be decomposed into 3-stars, since each pair of adjacent edges must include central vertices from at least two 3-stars, and any pentagon can contain only two 3-stars that do not overlap. We have already mentioned decompositions using $P(2)$ and $P(3)$. $P(6)$ cannot fold into the tetrahedron since it has only two odd degree vertices, and the tetrahedron has four. Similarly, five copies of $P(6)$ provide only 10 odd degree vertices, not enough for either the 12 or 20 odd degree vertices in the dodecahedron and icosahedron. The proofs that $S(2, 2, 2)$, $S(1, 1, 4)$, $S(1, 1, 1, 2)$, and $S(1, 1, 1, 1)$ do not decompose the dodecahedron are too lengthy to include here. $S(1, 2, 3)$ does decompose all five, however. The smaller three decompositions are shown in Figure 8; to decompose the dodecahedron and icosahedron using $S(1, 2, 3)$, in Figure 5 we join each path of type B by its end vertex to the adjacent path of type A. If used in a dance, each of the $S(1, 2, 3)$'s would probably have to be manipulated by two dancers, but we have not yet experimented with it.

The hexastar shown in Figure 4 does not decompose the dodecahedron or icosahedron, since it has 12 edges. However two copies do fold into two other interesting polyhedra, the rhombic dodecahedron and the cuboctahedron (Figure 9).

The hexastar also folds up to tile the plane in a variety of patterns (Figure 10).

Other dancers have explored polyhedra in a number of ways. Rudolf Laban (1879–1958) visualized the moving body within a variety of polyhedra, and developed a series of exercises in which the dancer moves the limbs so as to trace a sequence of edges. His diagrams show, for example, a 12-gon that folds into the edges of the octahedron in the order in which

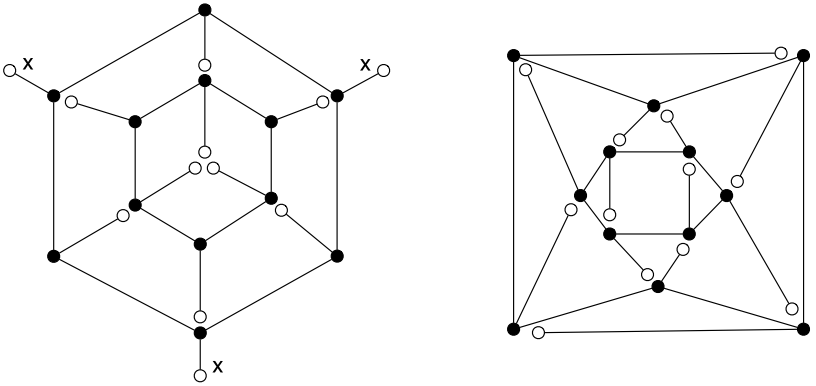

Figure 9. The rhombic dodecahedron (x's identified) and the cuboctahedron, decomposed by hexastars.

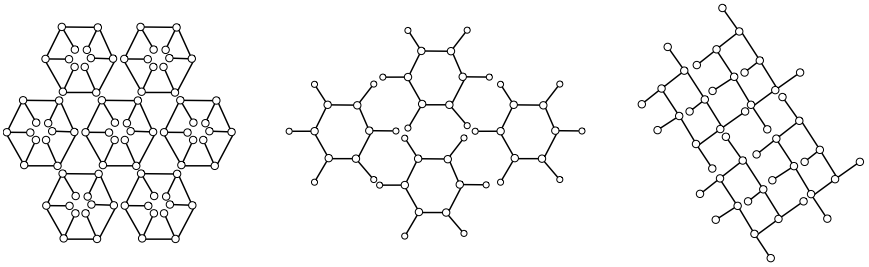

Figure 10. The hexastar tiles the plane in a variety of ways.

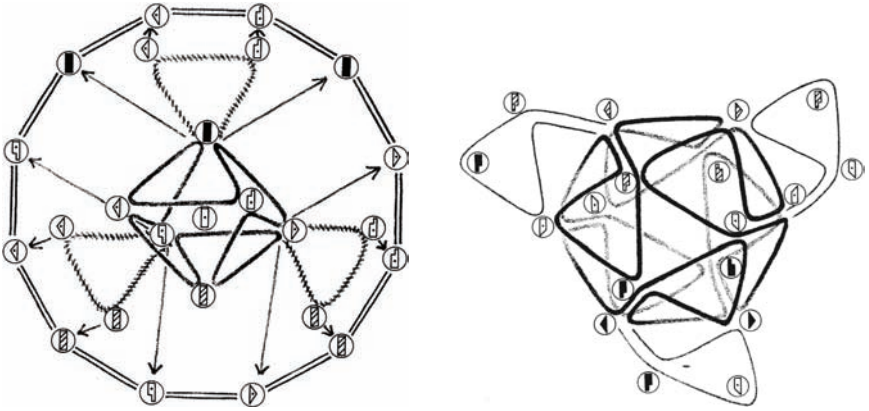

Figure 11. Laban's folding of 12-gon into an octahedron (left) and 36-gon into an icosahedron (right) [4, pp. 116, 117].

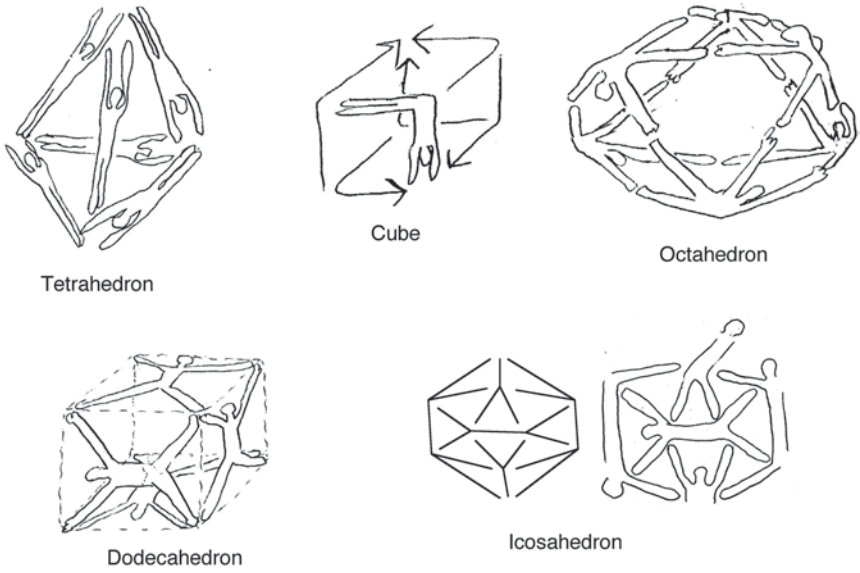

Figure 12. Six dancers "folded" into the Platonic solids.

the dancer moves, and a 36-gon that similarly folds into the icosahedron (Figure 11, [4]).

Finally, we might fold the entire dancer's body in such a way as to create the Platonic solids. Figure 12 shows a series of these polyhedra for six dancers. Note that there is a simple transition from the dodecahedron to the icosahedron, in which each dancer slides feet and hands to the shoulders and hips of the next dancer. We have not attempted these yet either; they would probably need to be performed as an aerial dance with the dancers suspended from ropes, underwater, or in the weightlessness of space!

Bibliography

[1] Erik D. Demaine and Martin L. Demaine. "Recent Results in Computational Origami." In *Origami^3: Proceedings of the Third International Meeting of Origami Science, Mathematics, and Education*, edited by Thomas Hull, pp. 3–16. Natick, MA: A K Peters, Ltd., 2002.

[2] Keith Devlin, Zambra, and Karl Schaffer. *Harmonious Equations*. Premiered December 2008.

[3] Martin Gardner. *The Second Book of Scientific American Mathematical Puzzles and Diversions*. Chicago: University of Chicago Press, 1961.

[4] Rudolf Laban and Lisa Ullman. *The Language of Movement: A Guidebook to Choreutics*. Boston: Plays, Inc., 1974.

[5] Paul W. K. Rothemund. "Folding DNA to Create Nanoscale Shapes and Patterns." *Nature* 440 (March 16, 2006), 297–302.

[6] Karl Schaffer. "Pipe Dreams." Choreographed 1998.

[7] Karl Schaffer, Scott Kim, and Barbara Susco. *Through the Loop: In Search of the Perfect Square*. Text and choreography 1995.

[8] Karl Schaffer and Erik Stern. *The Bounds of Discovery*. Text and choreography 2000.

[9] Karl Schaffer, Erik Stern, and Scott Kim. *The Secret Life of Squares*. Choreography by Schaffer and Stern, text by Kim, 1993.

[10] Karl Schaffer, Erik Stern, and Scott Kim. *Math Dance with Dr. Schaffer and Mr. Stern*, Preliminary Edition. Santa Cruz, CA: MoveSpeakSpin, 2001.

[11] Karl Schaffer, Erik Stern, and Gregg Lizenbery. "Shadowed Flight." Choreographed 1999.

[12] Y. Zhang and N.C. Seeman. "The Construction of a DNA Truncated Octahedron." *Journal of the American Chemical Society* 116 (1994), 1661–1669.

Part II

Origami and Technology

The Science of *Miura-Ori*: A Review

Koryo Miura

1 Introduction

The concave polyhedral surface that is now known as the *Miura-ori*[1] first appeared in a scientific paper of the shell structures society [4]. Since then, its unique geometric structure has become a source of interest to many people. *Miura-ori*—or rather, its surface, depending on one's viewpoint—may be viewed in several ways: as the simplest origami, an origami unchanged by inversion, a symmetry-rich tessellation (tiling), an infinite concave polyhedron, a wrinkle, a deployable structure, and an art piece.

However, the physical properties of this fold have not received much interest until recently. In point of fact, it was discovered as the solution of a physical problem of the behavior of thin elastic plates. In other words, it is not an artificially formed free shape but it is a natural surface fulfilling the principle of minimum potential energy. Therefore, it must inevitably relate to physical principles as well as principles of the geometric essence of folds.

In this paper, I review several studies done from 1970 to 1990, which is when the basic science of this surface was explored. I will then close with some recent relevant studies.

[1] This surface was initially called the developable double corrugation (DDC) surface. The nickname became popular after its application to map design [9] was introduced by the British Origami Society [1].

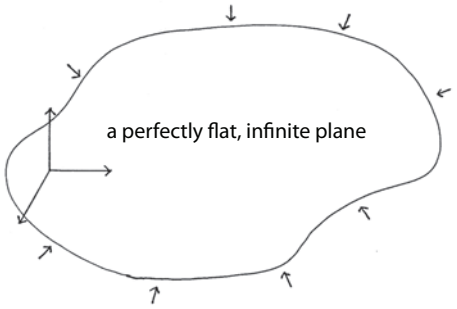

Figure 1. Conceptual drawing of the proposed problem.

2 Problem and Hypothesis

In 1970, the author proposed a problem schematically represented by Figure 1. The problem was to determine the deformation of a perfectly flat, infinite, elastic plate subject to uniform terminal compression or shortening. Necessarily, the plate should be treated as infinitesimally thin due to its infinite extent.

This problem seems to be absurdly simple on the surface, but is in fact quite deep in its essence. The background of this subject is as follows. There is an interesting but dangerous phenomenon that arises in the axial buckling of a thin cylindrical shell. It can happen anywhere: on a soda can, or on a launcher of space shuttles. If you carefully examine a buckled soda can, you can observe diamond patterns here and there on the surface. This is called the *Yoshimura-pattern* in memory of Yoshimura's pioneering work on the subject [11]. The exciting fact he discovered was that the buckled shape is exactly an origami—by which we mean that the transformation from the original cylindrical shell to the polyhedral (origami) shell is implemented purely via bending, i.e., without in-plane (stretching) deformation. Since such deformation can occur with relatively little energy (and therefore unexpectedly), the phenomenon can be dangerous when it occurs.

If the Yoshimura-pattern is the buckling phenomenon characteristic of thin cylindrical structures, then an analogous phenomenon should be observed for thin plate structures that are also two-dimensional (negligible thickness) media. And, most likely, the result of this buckling should emerge as an origami model. The scenario illustrated in Figure 1 is, in a sense, looking for an origami model that satisfies all of the imposed conditions.

Soon after starting the study, the author arrived at a unique periodic, concave polyhedral surface. As shown in Figure 2, it consists of a "feather

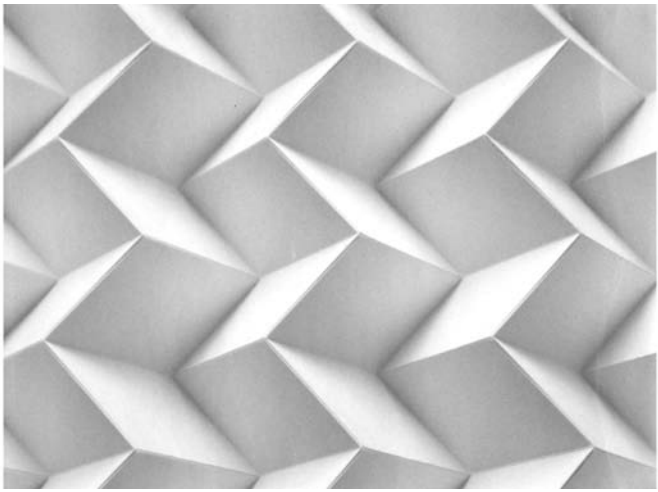

Figure 2. Developable double corrugation (DDC) surface (an exaggerated view).

(of an arrow) pattern" unit that consists of four identical rhomboids. The surface was tentatively named the *developable double corrugation* (DDC) surface. Though it is a simple form, it satisfies perfectly all of the requirements imposed in the original problem. Supported by these observations, the present author made a hypothesis that the DDC surface is one of the solutions of the compressed-thin-plate problem.

3 Hypothesis and Analysis

To *prove* this hypothesis was much more difficult than our expectation, however. An experimental approach analogous to that used for thin cylinders did not work in the case of plates. One of the reasons was that providing a suitable experimental approximation of a perfect infinite flat plate is much more difficult than approximating a perfect circular cylinder. In 1978, we had attacked the problem using an analytical method similar to von Kármán-Tsien-Legget's procedure, which they used for the post-buckling analysis of axially loaded cylindrical shells [10].

Some of these results are shown in the following figures. Because we assumed an infinite plate, only periodic solutions are expected. Figures 3–7 show the deflection of the plate for the fundamental unit (or its equivalent area) using a normalized contour map format. By repeating each figure along the x and y axes, one can construct a larger image of the deflection pattern. Figure 3 shows the deflection occurring just after the first incre-

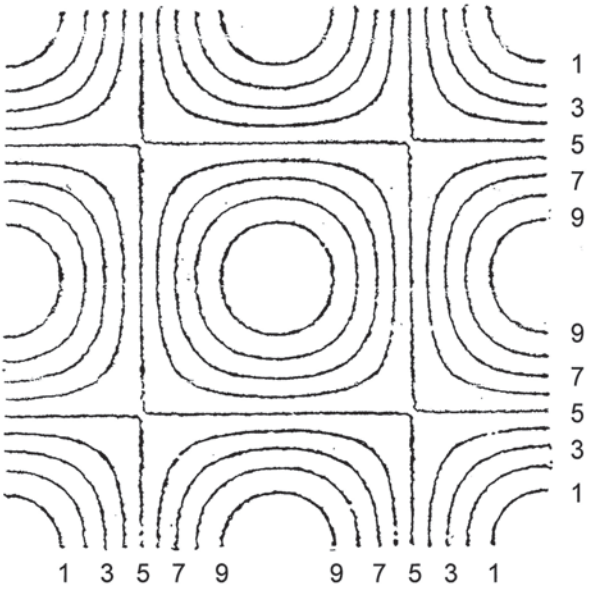

Figure 3. Deflection pattern just after the first buckling.

ment of compression. This type of pattern of "hills and craters" can be expressed as the product of simple sinusoidal functions.

By increasing the shortening or decreasing the thickness, the deflection changes into quite different patterns, as shown in Figures 4–7. These solutions are obtained for the same end-shortening and thickness value. As a matter of fact, there are infinite numbers of solutions. The quantity that distinguishes among these solutions is the total strain energy. The normalized energy index of each solution is shown in the caption.

By inspecting the energy index, one can easily identify the type of deflection pattern that gives a lower strain energy. We found that those configurations expressed by "herringbone" pattern exhibit lower strain energy without exception. Among them all, the pattern of Figure 7 gives the least strain energy. It is clear that when this pattern is replicated periodically (Figure 8), it is exactly the same configuration for the DDC surface shown in Figure 2.

Further important information is shown in Figure 9, which shows the distribution of bending stress for the case of Figure 7. We observe that the bending stress is concentrated along linear features that are the mountain and valley lines of the DDC pattern.

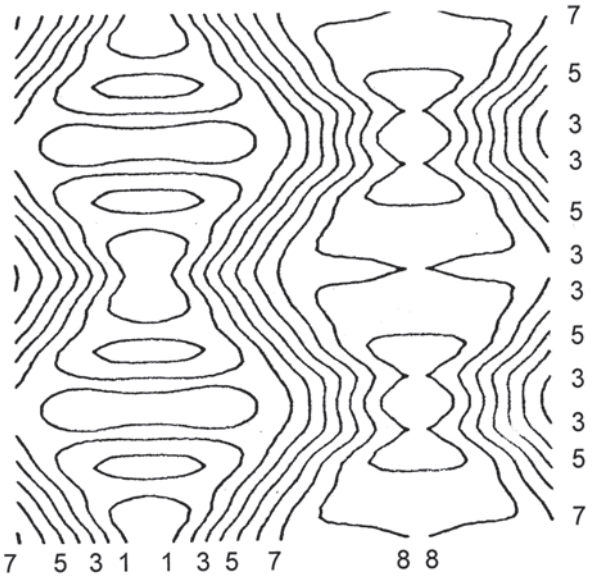

Figure 4. Deflection pattern in post-buckling domain, energy index 36.

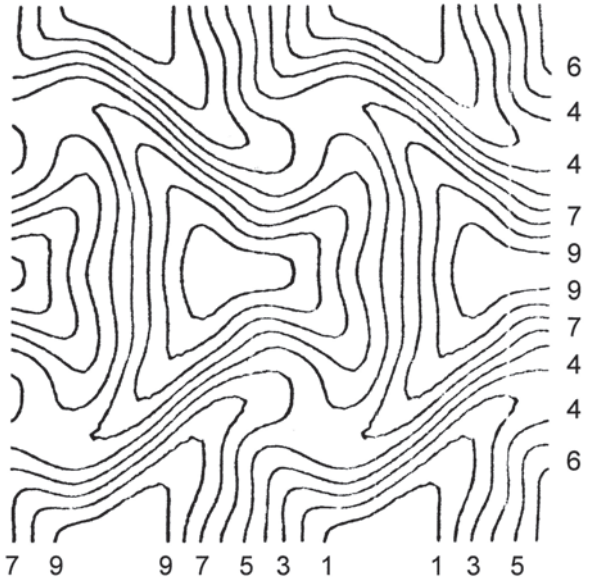

Figure 5. Deflection pattern in post-buckling domain, energy index 37.

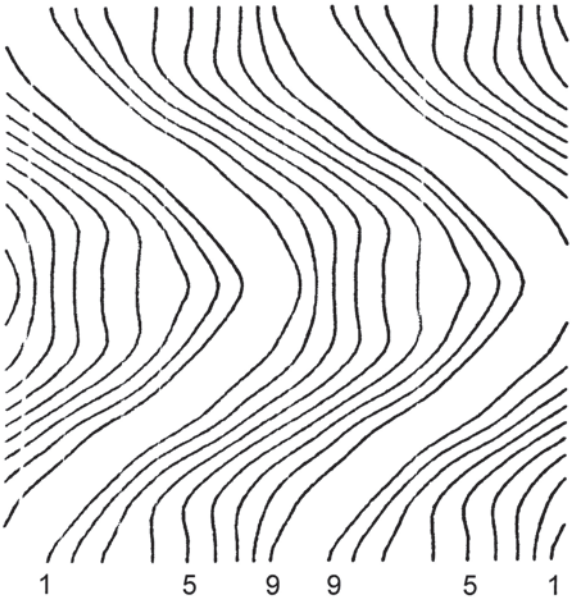

Figure 6. Deflection pattern in post-buckling domain, energy index 6.

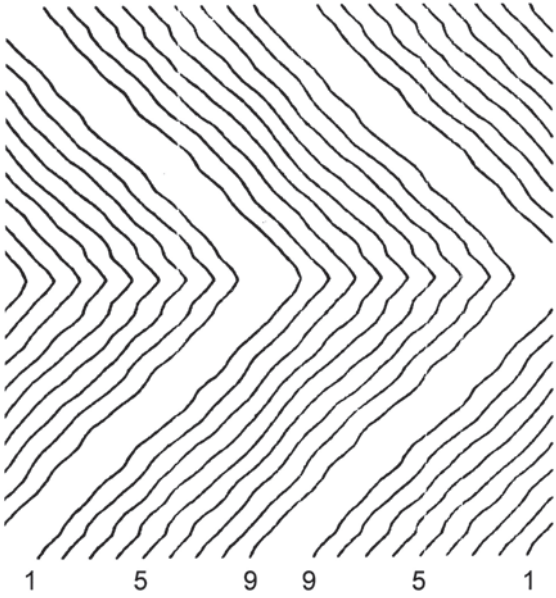

Figure 7. Deflection pattern in post-buckling domain, energy index 5.

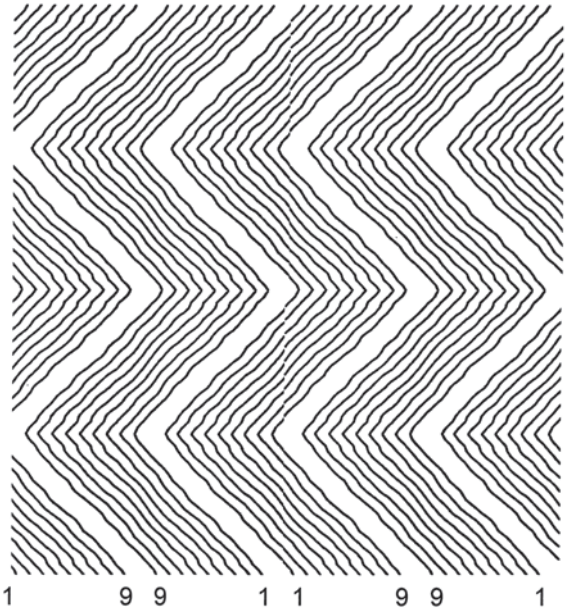

Figure 8. Integration of four units of the pattern in Figure 7.

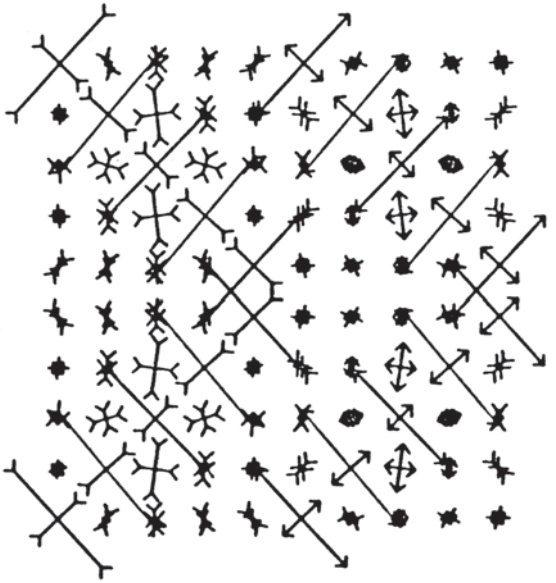

Figure 9. Bending stress distribution for the pattern in Figure 7.

It should be noted that the above computation is based on equations valid only for a finite deformation range. Therefore, the pattern shown in Figure 8 is not as large as that of the three-dimensional image of Figure 2. It is fortunate for the result that the model of that pattern satisfies the rules of a flat origami. Therefore, the result of computation and the origami are connected seamlessly, and the result can be extended to the maximum limit of the flat origami. Conclusively, the hypothesis was verified numerically. This correspondence was also verified by recent experiments [3].

4 *Elastica* and *Miura-ori*

In the *Miura-ori* surface, we are able to observe the essence of deformation of paper that represents a thin two-dimensional elastic media. In the analogously slender one-dimensional elastic medium, the essence of deformation is represented by the so-called elastic curve or *Elastica*, which was first explored by Euler (Figure 10).

Now we may compare similarities and as differences of elastic curves and the *Miura-ori* surface. For comparative purposes, Figure 2 has been modified to Figure 11. We notice that, in spite of the similarity of two problems of elastic media, the resultant configurations are quite different from each other. While the former shows a smooth curve with curvature evenly distributed, the latter shows a rugged surface consisting of flat facets with all curvature concentrated at the straight ridges [7].

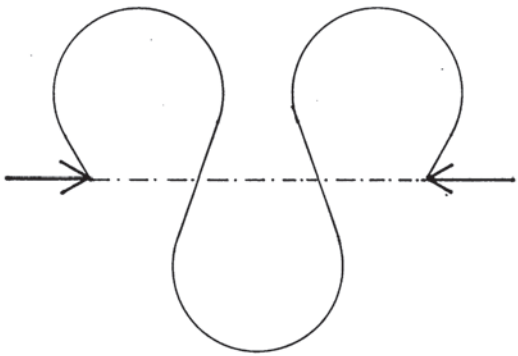

Figure 10. Curve for a slender one-dimensional elastic medium (*Elastica*).

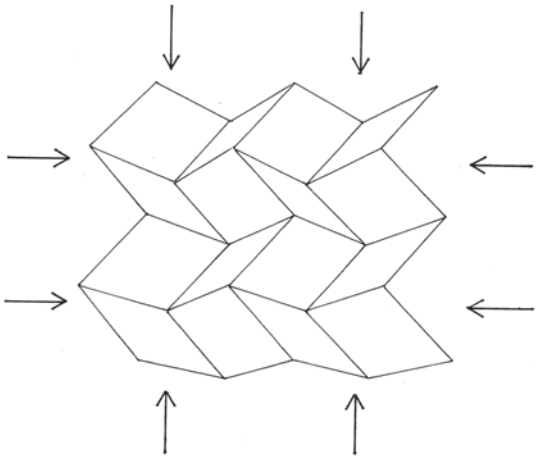

Figure 11. Surface for a thin two-dimensional elastic medium (*Miura-ori*).

5 Deployable Structures

The most unique behavior of the *Miura-ori* is its deployable property. Figure 12 shows a simulation of deployment and retraction of a *Miura-ori*. Its primary features are the following:

- It is deployed simultaneously in orthogonal directions and is homogeneous in each direction.
- It possesses a single degree of freedom of motion no matter how large the array.
- Its deployment and retraction follow the same path.

To demonstrate a practical use for the deployable property of the Miura-ori, it was applied to a foldable map [5].

Figure 13 shows the "Map of Venezia" published as an appendix for *SPAZIO* magazine [5]. To deploy the folded map, pull the map at opposite corners along the diagonal of the rectangle. This will give an equal and simultaneous deformation to all the units along the diagonal.Those folds in their neighborhood expand to cover the main part of the map and the desired deformation can therefore be propagated, without delay, to the rest of the map. The same situation occurs for the case of the refolding process.

A number of future space missions will require ultra-low-mass, large membrane structures. Thus, packaging and deployment of such membrane structures will become more and more important. Many of the deployable

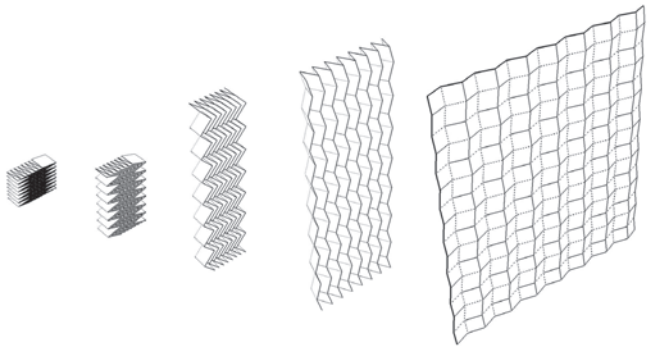

Figure 12. Deployment of *Miura-ori*. (Provided by Tomohiro Tachi.)

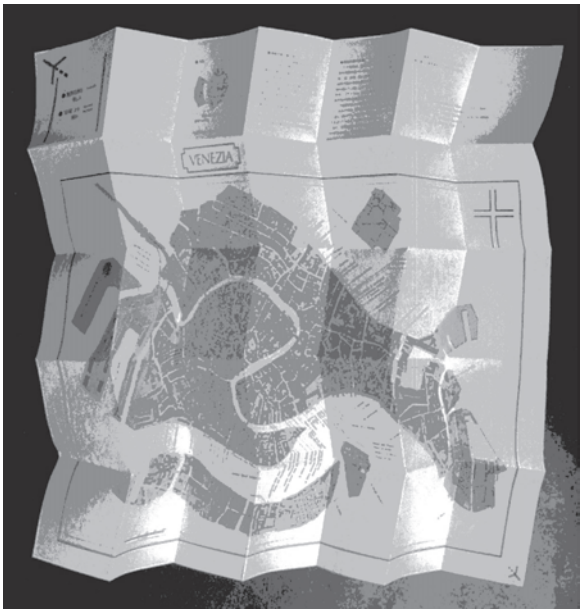

Figure 13. Map of Venezia published in *Miura-ori* form. (Produced by Olivetti Japan in 1978.)

properties of *Miura-ori* seemed to be favorable for such application. In 1980, the author proposed a paper entitled "Method of Packaging and Deployment of Large Membranes in Space" [6].

The first opportunity to test the applicability of *Miura-ori* in space came when Japan planned the Space Flyer Unit, a space platform, in the 1980s.

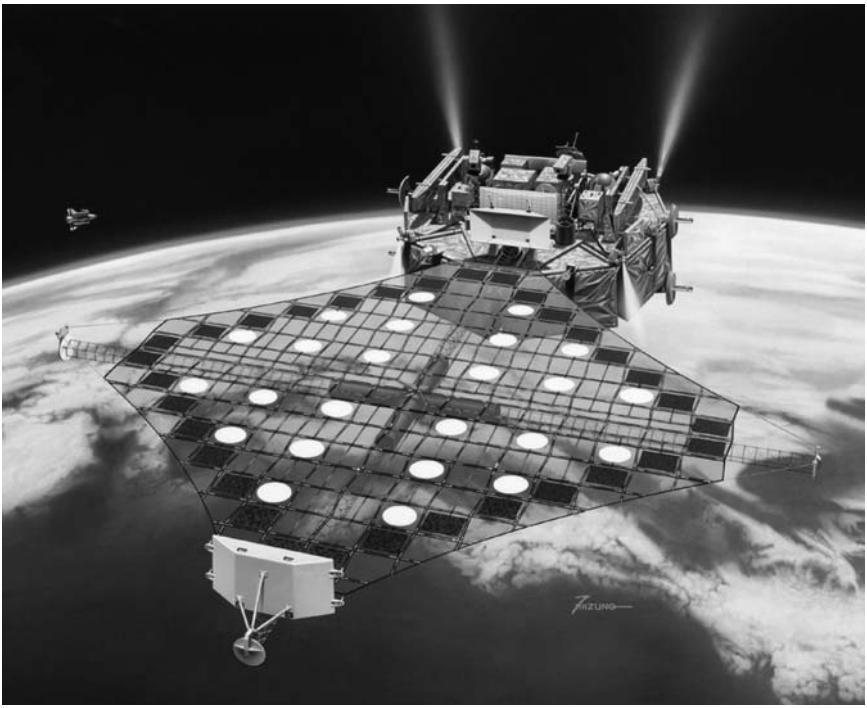

Figure 14. *Miura-ori* solar cell array on Space Flyer Unit (Flight 1994-5).

The two-dimensional array system and experiment mission, which uses a two-dimensionally deployable solar array, was proposed subsequently [8]. The experiment mission was carried out successfully in 1995. Figure 14 shows an illustration of the solar cell array in the deployed state.

6 *Miura-ori* and Biology

We have already seen that the *Miura-ori* surface is a kind of natural solution obtained by an energy-optimization procedure. Therefore it is not surprising that in recent studies, some relations of this surface to the deployable mechanisms of tree leaves have been found. Kobayashi et al. [2] carried out the simulation of deploying leaves using a corrugated model, which is the fundamental structure of *Miura-ori*, as shown in Figure 15.

Most recently, Mahadevan and Rica [3] have also solved experimentally the problem imposed on Figure 1. They produced a zigzag *Miura-ori* pattern in a thin film atop a thick elastic substrate that is compressed biaxially

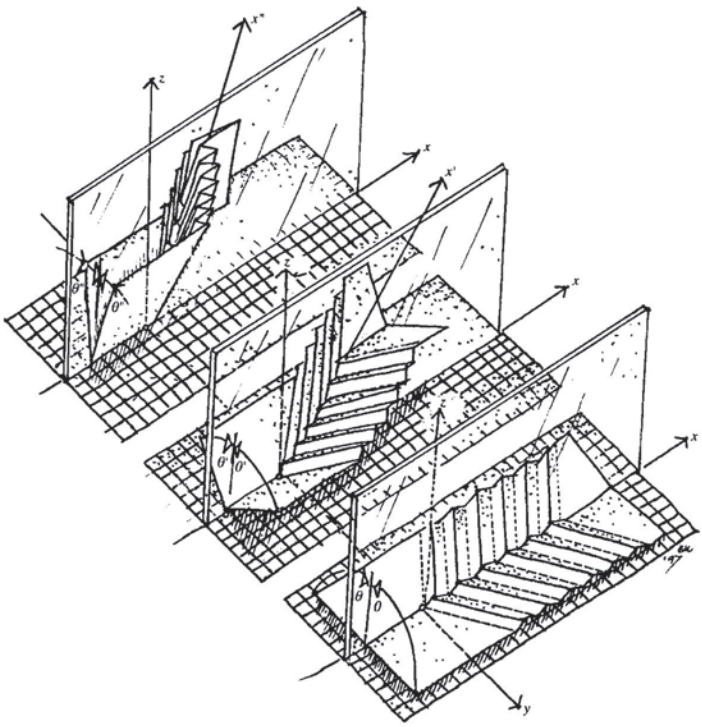

Figure 15. Corrugation model (simple form of *Miura-ori*) for unfolding tree leaves.

manifest in a drying slab of gelatin with a thin skin that forms naturally. This result also supports this author's hypothesis, that the *Miura-ori* is a natural minimum-energy folding pattern that arises in, and has applicability to, many systems.

Bibliography

[1] Anon. "The Miura-ori Map." *British Origami* 88 (1981), 3–5.

[2] H. Kobayashi, B. Kresling, and J. F. V. Vincent. "The Geometry of Unfolding Tree Leaves." *Proc. R. Soc. Lond.* B 265 (1998), 147–154.

[3] L. Mahadevan and S. Rica. "Self-Organized Origami." *Science* 37 (2005), 1740.

[4] K. Miura. "Proposition of Pseudo-Cylindrical Concave Polyhedral Shells." Paper presented at the IASS Symposium on Folded Plates and Prismatic Structures, International Association for Shell Structures, Vienna, Austria, 1970.

[5] K. Miura. "The Fun of Map Folding" (in Japanese and English). *Olivetti Corp. Japan SPAZIO* 19 (1978), 72–83.

[6] K. Miura. "Method of Packaging and Deployment of Large Membranes in Space." Paper presented at the 31st Congress of the International Astronautical Federation, Tokyo, Japan, 1980.

[7] K. Miura. "Folds—Its Physical and Mathematical Principles." In *Origami Science and Art: Proceedings of the Second International Meeting of Origami Science and Scientific Origami*, edited by K. Miura, pp. 41–50. Shiga, Japan: Seian University of Art and Design, 1997.

[8] K. Miura and M. Natori. "2-D Array Experiment on Board a Space Flyer Unit." *Space Solar Power Review* 5 (1985), 345–356.

[9] K. Miura, M. Sakamaki, and K. Suzuki. "A Novel Design of Folded Map." Paper presented at the 10th International Conference of the International Cartographic Association, Tokyo, Japan, 1980.

[10] K. Tanizawa and K. Miura. "Large Displacement Configurations of Bi-Axially Compressed Infinite Plate." *Trans. Japan Society for Aeronautical and Space Sciences* 20 (1978), 177–187.

[11] Y. Yoshimura. "On the Mechanism of a Circular Cylindrical Shell under Axial Compression." Technical report, NACA TM 1390, 1955.

Origami-Inspired Self-Assembly

Galen T. Pickett

1 Introduction

Origami-inspired structures and ideas are increasingly informing the design of state-of-the-art microscopic mechanical devices and molecular assemblies. Mico-electrical-mechanical-systems (MEMS) mirrors have been constructed [13, 44] based on a complex layering of flexible and stiff layers to create specific upward and downward folds [47]. Complex three-dimensional structures [2, 4, 19, 20] have been induced by taking advantage of a strain mismatch in a multilayer structure causing spontaneous curvature and "rolling-up" of a structure into pinchers, enclosures, hinges, nanoscopic capacitors, and other machines. Stress mismatch has been identified, in the guise of a rigid membrane supported by a gently contracting elastic substrate [30], as an explanation for the structure of unfolding botanical leaves [23]. Here, a mechanism controlling the unpacking of an embryonic leaf has been harnessed to engineer a patterned surface, one with a characteristic "herringbone" relief pattern. Paper models guided the understanding of the leaf-unfurling process by referring to patterns of folds that had been discovered in the context of efficiently folding automobile maps [1, 31]. Thus, the origami-design process circulates between folded structures known well to paper-folding artists, toward engineered structures, and finally back to naturally appearing surfaces [49].

Another instance of such a design convergence involves the spontaneous patterns of stress in compressed elastic membranes. These patterns appear in crumpled sheets [29, 52], and in a rather more ordered pattern in the

bucking of thin-walled cylinders [18,32]. A folding pattern inspired by these sorts of self-organized creased sheets is the basis for the construction of a novel arterial stent [25]. A similar effect is behind the discovery of hollow, helical silica tubules, self-folded under specific interior interactions [53]. At a smaller scale, complex, yet flexible molecules have been designed with an origami-flavor, capable of flexibly bending in a number of directions [28], and graphite sheets have been coaxed to behave as nanoscopic paper, forming tubule "peapod" structures [46]. In the end, the packing of a membrane into a specific volume, requiring outward and inward folds in the right places, is a problem nature, artists, and engineers have solved in turn, each for their own specific purposes.

Below, I consider two kinds of origami that I am personally inspired by as a paperfolder, tessellations in Section 2 and modulars in Section 3, in the context of two very different technological challenges.

2 Self-Folded Origami Tessellations

While complex geometries and three-dimensional mechanical functionality are routinely achieved at the meso and macroscale (folded "by hand"), there continues to be a lack of articulated detailed folds at the microscopic and smaller scales. One problem standing in the way of origami methods being more widely applied at smaller length scales is the lack of a reliable method to coax an ordered, thin membrane into adopting a particular three dimensional shape. Here, I offer a geometric method to force a controlled collapse by manipulating self-interactions and gentle external influences. It is my hope that these methods, culled from the origami artistic community, will allow the construction of MEMS machines at unprecedented scales with unprecedented functionalities.

Below, I look at the collapse of a precreased thin membrane. The nature of the creasing is, in this respect, meant to model the actual pattern of polygonal facets of a manufactured sheet, either through scoring and precreasing (for macroscopic papers or metal foils), or through lithographic means (for mesoscopic applications) [13, 25, 44, 47]. The triangular net of freely-bendable joints holding together a network of otherwise rigid polygons has been used as an approximation in the collapse of smoothly elastic sheets [10, 12, 14, 24, 29, 50, 52]. Through the application of local weakly attractive forces, such a triangulated membrane can adopt many interesting geometric phases, from roughly flat, to a fractal crumple, to a compact, collapsed *flat-folded* state. As is well known, the pattern of scores must obey several key properties to allow this flat-folded state to exist. As each polygonal facet in the folded structure must either have its normal parallel or anti-parallel to the same direction, it is natural to assign

Ising-like variables to each cell [14]. Thus, the folded, flattened configuration must be characterized by an *anti-ferromagnetic* state of these spin variables. An *up* domain must be surrounded by *down* domains, or there must be unfolded creases in the system. Thus, the folding pattern must divide the plane into a *two-colorable* map. This is essentially a restating of the Kawasaki Theorem of flat-folding origamis: each vertex in the folded, collapsed state must assign 180° to the up segments at the vertex and 180° to the down segments arriving at the vertex, and the up/down domains have to alternate [22]. Any target structure that is designed to fold flat must obey minimally these restrictions in the crease-pattern design. The problem of self-intersection during the collapse [3,34] introduces more interesting, long-range constraints that enrich the underlying spin model, and dramatically complicate the folding sequence and design.

What is needed for such an origami-inspired construction of useful three-dimensional structures from folded flat sheets is a robust method of driving a possibly disordered, frustrated process towards a robust, efficient collapse. I will study exactly such a collapse in terms of the crease pattern designed by Kuribayashi et al. [25] in response to weak internal interactions, and then in the presence of an externally-applied curvature of the sheet. This external curvature in an indentation experiment [5] gives a depression with a very similar geometry to the indentations designed by Kuribayashi et al. [25], inspired by an architectural application of paper art and architecture [39]. Additionally, it is well known that an intrinsic curvature (in this case enforced by using a toroidal sheet) guides a randomly crumpled sheet into new phases [12]. The application of an external curvature is indeed the method origami artists use to collapse paper sculptures with the same folded structures.

I will describe the dynamic model I employ to investigate the system first, and describe the features of collapse of a stent-like scored sheet in the absence of an applied curvature, then demonstrate the dramatic effect an external curvature can have during the collapse, and offer some conclusions and speculations on the further applications of origami collapses to MEMS technology.

2.1 Model

As I am less interested in the thermodynamic equilibrium of these membranes than their dynamic collapse from an open state, I have implemented a Brownian motion simulation for the sheet [9, 36], rather than attempt to locate the global minimum energy state of the sheet directly [10, 29, 52] or through a Monte Carlo procedure [12,14,24,50]. As I restrict the discussion to relatively weak forces driving the collapse, the sheet is essentially a two-dimensional version of the freely jointed chain model of flexible polymers.

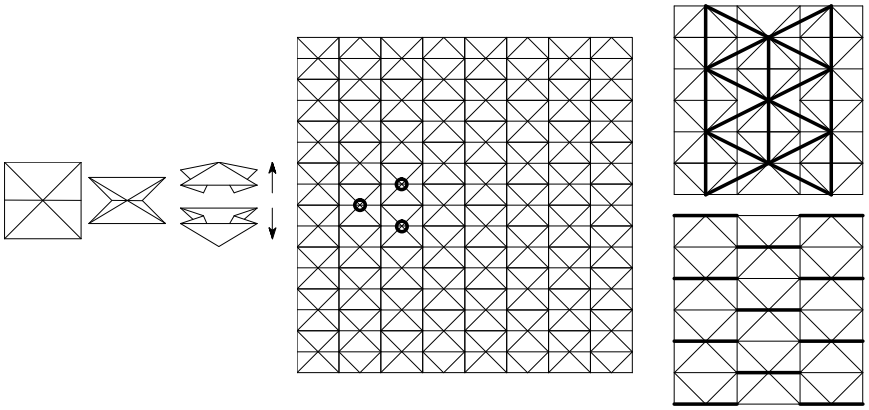

Figure 1. Crease pattern. On the left is the basic shape with its two possible states of collapse. In the middle, a square sheet with edge length of $16D$ has been scored, so that the sheet can flex along any of the lines shown. Three of the "central" vertices controlling the collapse have been indicated by circles. On the right, the two sets of attractive intra-sheet interactions are displayed. Each bold line is a spring with zero rest length.

As in Figure 1, the pattern of connections is composed of triangular domains joined at flexible boundaries. To keep the triangular domains from changing shape, it is sufficient to maintain the distances between all connected vertices. Thus, the model I study below is a *vertex model*. Each vertex obeys an equation of motion:

$$b\frac{d\mathbf{r}_i}{dt} = \sum_{j-conn.} \mathbf{T}_{ij} + \mathbf{F}_i. \tag{1}$$

Here, $\mathbf{r}_i$ is the vector position of the ith vertex in the sheet, b is a drag coefficient, and the $\mathbf{T}_{ij}$ forces are tensile forces responsible for maintaining the initial distance between vertices connected by a flexible joint:

$$\mathbf{T}_{ij} = \begin{cases} -k\hat{\mathbf{r}}_{ij}(r_{ij} - l_{ij}) & \text{when } i \text{ and } j \text{ are connected,} \\ 0 & \text{otherwise.} \end{cases}$$

Here, r_{ij} is the distance between vertices i and j, and l_{ij} is the distance between the vertices in the *unfolded sheet*, and k is the spring constant for fluctuations of the bond lengths. Thus, the in-sheet distances are allowed to fluctuate harmonically around their given initial lengths. A more complex method for ensuring the constant-length constraints exists [9, 36], but as long as all other driving forces are small compared to the elastic restoring

force above, the bond lengths will remain as in the initial sheet. The force $\mathbf{F}_i$ contains all other interactions in the system:

$$\mathbf{F}_i = \xi_i + \text{attractions},$$

where $\xi_\mathbf{i}$ is a Gaussian random noise chosen so that thermally activated extensions and contractions of the bond lengths do not exceed 1% of a bond length during the simulation,

$$\langle \xi_i(t)\xi_k(t')\rangle = 2bk_BTD^2\delta_{ij}\delta(t-t').$$

Here, D is the underlying lattice scale for the crease pattern (as in Figure 1), and the effective temperature k_BT is chosen so that

$$|\xi| \approx 0.01kD,$$

thus choosing a dimensionless noise, $|\xi| \approx 0.01$, and dimensionless spring and lattice constants $D = 1, k = 1$, and the unit of simulation time to be b/k.

The attraction term is a short-ranged restoring force shown schematically in Figure 1 as the bold lines. These lines link various pairs of vertices with elastic attractive forces on the scale of the thermal noise for the flattened sheet. I have modeled two kinds of elastic forces. The first, indicated schematically by the bold lines in the upper-right panel of Figure 1, models the effect of supporting the entire crease pattern with a soft, elastic substrate which is applying an isotropic compressive stress to the membrane (see [30]). The second set of interactions impose weak interactions between spots in the sheet directly opposite the intersection of six crease lines. These vertices, when brought together, will force each square domain of the crease pattern to collapse as in Figure 1 so that the "central vertex" points either up or down. Thus, the substrate-mediated interaction drives each of the central vertices to point in the *same direction as their neighbors* giving an effective Ising interaction between the domains. On the other hand, the purely compressive interaction (bottom panel in Figure 1) gives no such bias, so whatever correlations exist between central vertices are mediated solely by the crease-pattern tensions, $\mathbf{T}_{ij}$. These compressive interactions could be engineered lithographically by decorating the scored sheet with solvent-sensitive electroactive polymer domains.

The equation of motion for each vertex, Equation (1), is numerically integrated over a total simulation time of 30 in dimensionless units. In each case below, 200 runs starting from a flat sheet have been executed, over independent realizations of the thermal noise.

Figure 2. Typical configurations of the collapsed sheet. Two line defects in the overall down configuration are clearly visible in the two left-most configurations.

2.2 Collapse

In Figure 2, I show typical configurations of the collapsed sheet under both types of internal interactions. Large domains of vertices with common alignments are visible, but defects are common. Interestingly, roughly 80 of the generated configurations were basically uncollapsed, as in the right-most configuration in Figure 2. As the interactions themselves are up/down symmetric, and the crease pattern itself has no intrinsic tendency favoring the central vertices to point either up or down, we have a spontaneously broken symmetry. Thus, even a very weak bias in the initial collapse will lead to remarkably ordered behavior of the collapsed membrane. Thus, we have a system that manifestly has a multitude of ground-state configurations (each of the central vertices has a discrete degree of freedom in the collapsed structure), and the disordered, flat state has a relatively long life. In such a case, a quenched external field can serve to break the initial symmetry of the problem, and provide a sure guide to collapsing the membrane in an a priori, designed state.

This is indeed the case. The biasing field in this case is geometric. In Figure 3, I show the main results of this study. In each of the three cases displayed, the initial state of the sheet has been biased by bending the sheet in a particular manner. The upper row of figures show the sheets in their initial configurations. The left figure has the sheet bent upwards in a parabolic arc, the middle panel has a sinusoidal corrugated profile, and the right panels have their initial state as

$$z_{ij} = \epsilon \sin\left(\frac{2\pi i}{L}\right) \sin\left(\frac{2\pi j}{L}\right),$$

where i and j index the position of each vertex and L is the side-length of the sheet (in this case $L = 17$). In each case, the maximum deviation of initial sheet from absolutely flat is small ($\epsilon = 1$ for $L = 17$ in this study). These final configurations are repeatable over *200 different realizations of the thermal noise*. In *each case* the central vertices point *opposite* to the imposed initial local curvature of the sheet. The small initial bias guides the self-folding of the sheet toward a unique final state among the myriad

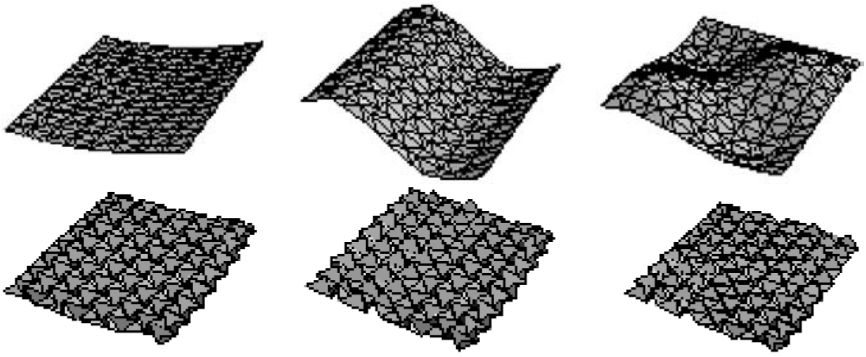

Figure 3. Initial and final configurations of the sheet subject to a bent initial state. The initial profile of the sheet has been exaggerated in this plot by a factor of 10.

of equivalent energy ground states of the system. Thus, the *linear response* of the system to an initial condition is enough to guide the entire future behavior of the system. This property of collapsing origami sheets is well-known to origami artists. A combination of gentle bending and crosswise compression is often sufficient to gain the collapse of a structure in a desired state. Here, I have taken that paper-artist strategy and validated it through these small-scale simulations. Indeed, the buckle pattern for an axially compressed thin-walled cylinder [18] shows the same tendency for inward dimples to appear in an ordered manner.

3 Modular DNA Origami

Today, wonderful control is being exercised over the synthesis of complex polymer molecules in anything from microscopic up to bulk quantity [17]. Orderings of individual monomers on these chains including homopolymer, alternating copolymer, multiblock, multicomponent, branched, grafted, and crosslinked, are all achievable. The investment in ordering the sequences and architectures of single polymers allows the supramolecular self-assembly of environment-sensitive patterns [11, 42]. Generally, the more complex the pattern, and the more complex the needed behavior of the pattern (for instance, how and when will a particle expand or contract), the more complex the needed constituent polymers are, with consequently more stringent tolerances on errors in synthesis. For example, absolute monodispersity is rarely a requirement when designing a material for a desired bulk application, but monodispersity and low error rates are critical to the proper function of naturally occurring enzymes.

When the polymers involved are intended for use in high-precision measurements on model systems, polymers with as closely defined properties as possible are required. Here, I put forward a general method for achieving essentially biologically accurate model materials of various geometries, architectures, and compositions.

The essential strategy is to take advantage of the specific DNA base-pair reaction, where single strands of DNA combine to make the familiar double-helix structure, to create a multitude of specific-interaction "sticker" sites [51] that can be synthesized with relative ease and end-attached to flexible polymers at modest prices. Taking advantage of the self-assembly of complimentary single-strand DNA ligands is generally referred to as the *DNA-origami technique* and has been used to construct self-assembled DNA cubes [6], truncated octahedra [54], two-dimensional crystals [51], designed patterns [40], scaffolds for computing devices [41], walking DNA machines [43], and "dendrimer-like" buckyball encapsulations [27]. The application I envision here is far simpler than that conceived in those works, but uses the DNA-origami technique in polymer synthesis. The design method for these structures resembles the long-sought-after "tinker toy" approach to complex molecule synthesis, but in reality has much more in common with so-called modular origami [15,16], where relatively simple folded structures are designed with clever pocket and tab systems to allow a skillful paper folder to assemble geometric sculptures of incredible subtlety [21]. Here, the units are "folded"—that is synthesized—beforehand and then self-assembled rather than assembled by hand. The basic two-stage synthesis protocol I describe has the aim of doubling the chain molecular weight at each stage. Then, a relatively simple variation on the protocol is described, showing how to create specific copolymers with complex block arrangements and branches. A particularly important example of such a self-assembled, regularly branched molecule is the flexible-chain analogue of the dendrimer molecule [45]. A significantly open question for small-molecule dendrimers concerns whether they have voids or solidly filled cores at their centers [8,26]. The original prediction of the open-core dendrimer was based upon a polymer physicist's toy model in which monodisperse chains are joined regularly at threefold junctions. While there are good reasons to believe that this model in fact requires the cores to be filled [55], experiments on these molecules are lacking. The method stated below could answer definitely a long-standing controversy.

3.1 Monodisperse Homopolymers

Figure 4 shows schematically the basic two-cycle synthesis route that I am proposing. The essential strategy is to use the specific DNA base-pair reaction to drive short, well characterized chain segments to assemble into

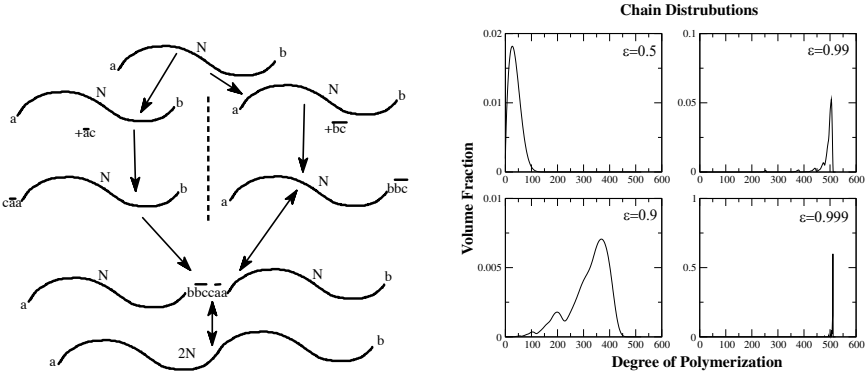

Figure 4. Schematic of the synthesis protocol on the left, and chain-length distributions on the right.

pairs, and then these pairwise joined chains will be joined together to make fourfold chains, and so on.

Let us begin with small-molecular-weight homopolymers, of a well defined molecular weight, N, which have been end-decorated with two distinct (although short) ligands of single-stranded DNA, a and b as in Figure 4. The specific sequences to be chosen for a and for b are arbitrary, but the a sequence of bases should be chosen to not bind well to the b sequence of bases. That is, a and b should not only *not be complimentary base-pair sequences*, they should be chosen so that partial base pairing of a and b should cost free energy. The a sequence has a base-pair complement, $\bar{a}$, likewise the b sequence complement has a structure $\bar{b}$, so that the spontaneous reaction

$$a + \bar{a} \rightarrow a\bar{a}$$

goes to completion.

The system of a, b-end labeled chains is then divided up into two different containers. To the first container, enough single-stranded DNA with the structure $\bar{a}c$ is added to ensure that the reaction

$$aNb + \bar{a}c \rightarrow c\bar{a}aNb \tag{2}$$

goes to completion. The specific molecular weight N, and the energy of the $a\bar{a}$ base-pair reaction, can easily be chosen to drive the equilibrium in Equation (2) to as small a number as desired of unreacted polymer.

Likewise, the ligand $\bar{b}\bar{c}$ can be added to drive

$$aNb + \bar{b}\bar{c} \rightarrow aNb\bar{b}\bar{c}$$

to completion.

When the contents of the two containers are thoroughly mixed together, the base-pair condensation of the c and $\bar{c}$ ligands will produce

$$aNb\bar{b}\bar{c} + c\bar{a}aNb \rightarrow aNb\bar{b}\bar{c}c\bar{a}aNb \equiv aNNb.$$

Here, in the final product of the reaction, I have suppressed the internal structure of the joint between the N-chains to emphasize the fact that two and only two of the homopolymer chains N are in the final product.

The next step of the synthesis is to take the $aNNb$ chains, divide them into two containers, and add the required $\bar{a}c$ and $\bar{b}\bar{c}$ ligands, and finally mix the results together to produce chains with a structure

$$aNNb\bar{b}\bar{c} + c\bar{a}aNNb \rightarrow aNNb\bar{b}\bar{c}c\bar{a}aNNb \equiv aNNNNb.$$

That is, each time the cycle is run, there are one half as many chains, each of which has doubled its molecular weight, a process that can be continued to a desired end-state monodisperse molecular weight.

The above protocol will indeed join chains from the first container to chains of the second container, but the consequences of an incomplete reaction would be to introduce, say, chain fragments with the structure aNb. In fact, the master equation for this two-stage chain growing process is easy enough to write down:

$$\begin{aligned} f_n^0 &= \delta_{n,1} \\ f_n^{i+1} &= \sum_j f_j^i f_{n-j}^i \epsilon + \sum_j f_n^i f_j^i (1-\epsilon), \end{aligned}$$

where ϵ is a measure of the efficiency of the reaction (where I have taken the assumption that the efficiency of each stage of the reaction is exactly the same), and f_n^i is the volume fraction in the ith iteration of the species consisting of n of the homopolymer units. As in Figure 4 (right panel), when each reaction can be counted on to go to 99% completion, the distribution of molecular weights in the finished sample is weighted heavily toward the target molecular weight, but there is a long trail of lower molecular-weight fragments contaminating the system. An interesting point, however, is that molecular weight distribution is peaked at the *largest possible molecular weight* under this scheme.

Here the efficiency of the reaction, ϵ, determines the overall molecular weight distribution at the end of the synthesis. With $\epsilon = 0.5$, there are always plenty of unreacted chain fragments in the solution, and a typical synthetic polymer molecular weight distribution results. When each stage of the reaction is required to go to 99.9% completion, the distribution is essentially monodisperse, with approximately one half of the total volume fraction of chains in the system achieving the target molecular weight.

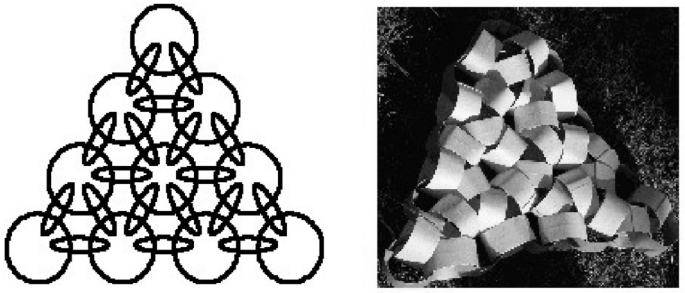

Figure 5. Hexagonal-close-packed olympic membrane, and a paper model.

3.2 Olympic Gels and Membranes

Topological gels (so-called Olympic gels [7] because of their schematic resemblance to the entwined rings of the flag of the Olympic Games) should prove to be interesting materials with unique mechanical properties [48]. Each chain in the gel has been end-reacted with itself to form a physical loop encircling a number of its neighboring, also cyclic, chains.

Simply mixing up a melt of end-reacting polymer is not sufficient to create the Gaussian Olympic gel, however [7]. The process of closing rings competes with end-end reactions between different chains, so that the end product of the reactions is a polydisperse mixture of chains of many molecular weights with several isolated rings interspersed. Indeed, given that a single ideal polymer will encompass $N^{1/2}$ other chain-ends within its swept-out volume, and only one of these will correspond to the ring-closing reaction, we quickly come to the conclusion that some other, clever method will have to be used to create the gel. The original suggestion was to complete the cyclization reaction in solution in several stages [7], and elaborations including a stepwise reaction of large and small rings [38], and slide-ring chain-chain crosslinks [33] have been proposed. Here, I propose a method to achieve an Olympic gel with a controlled n from the melt state in a single-reaction step, taking advantage of the wonderfully specific reaction of sequences of DNA bases. If, for instance, each chain in the melt were decorated with unique DNA ligands and their complimentary ligands, then each chain could *only end-react with itself*, forming loops without the competing chain-growing reaction. While a detailed calculation is certainly possible [35], for our purposes Figure 5 illustrates the idea. As each chain is held closed by a particular pairing of DNA bases, free DNA chain fragments are capable of reopening the rings, thus unraveling the tangled mess of interlocked loops. Thus, in contact with the correct target DNA, an Olympic microgel will disassociate, dumping its constituent polymers at a

desired location. I envision this mechanism, which is in principle biologically specific, to be the basis of a selective, targeted drug delivery system.

4 Conclusion

Here, I have developed two scientific and technological applications of the paper-folding art that I have spent countless hours pursuing. Applications ranging from microscopic machinery, pumps, and armatures, to even smaller membranes and gels with a regular knitted structure, all the way down to self-assembled "modular" molecules are all probable.

It would not have occurred to me to do any of this work, and I presume any further work that I will pursue along these lines, had I not come across a book by Tomoko Fuse [15]. As I continue exploring in my hands the wonder and versatility of folded paper, it is natural for me to continue to explore the connections that I see between beautiful paper objects and scientific and technical questions.

Bibliography

[1] E. M. Arkin, M. A. Bender, E. D. Demaine, M. L. Demaine, J. S. B. Mitchell, S. Sethia, and S. S. Skiena. "When Can You Fold a Map?" *Comp. Geom.* 29 (2004), 23–46.

[2] W. J. Arora, A. J. Nichol, H. I. Smith, and G. Barbastathis. "Membrane Folding to Achieve Three-Dimensional Nanostructures: Nanopatterned Silicon Nitride Folded with Stressed Chromium Hinges." *Applied Phys. Letts.* 88 (2006), 053108.

[3] s.-m. belcastro and T. C. Hull. "Modelling the Folding of Paper into Three Dimensions Using Affine Transformations." *Lin. Algebr. and Appl.* 348 (2002), 273–282.

[4] A. Bernardi, A. R. Goni, M. I. Alonso, F. Alsina, H. Scheel, P. O. Vaccaro, and N. Saito. "Probing Residual Strain in InGaAs/GaAs Micro-origami Tubes by Micro-Raman Spectroscopy." *J. Applied Phys.* 99 (2006), 063512.

[5] A. Boudaoud, P. Patricio, Y. Couder, and M. B. Amar. "Dynamics of Singularities in a Constrained Elastic Plate." *Nature* 407 (2000), 718–720.

[6] J. Chen and N. C. Seeman. "The Synthesis from DNA of a Molecule with the Connectivity of a Cube." *Nature* 350 (1991), 631–633.

[7] P.-G. de Gennes. *Scaling Concepts in Polymer Physics.* Ithica, NY: Cornell University Press, 1979.

[8] P.-G. de Gennes and H. Hervet. "Statistics of 'Starburst' Polymers." *J. Phys. (Paris)* 44 (1983), L351.

[9] J. M. Deutsch. "Theoretical Studies of DNA During Gel Electrophoresis." *Science* 240 (1988), 922–924.

[10] B. A. DiDonna and T. A. Witten. "Anomalous Strength of Membranes with Elastic Ridges." *Phys. Rev. Letts.* 87 (2001), 206105-1.

[11] H. Ding, F. Wu, Y. Huang, Z.-R. Zhang, and Y. Nie. "Synthesis and Characterization of Temperature-Responsive Copolymer of PELGA Modified Poly(N-isopropylacrylamide)." *Polymer* 47 (2006), 1575–1583.

[12] I. Endo and H. Koibuchi. "Phase Transitions of a Tethered Membrane Model on a Torus with Intrinsic Curvature." *Phys. Letts. A* 350 (2006), 11–16.

[13] T. Fleischmann, K. Kubota, P. O. Vaccaro, T.-S. Wang, S. Saravanan, and N. Saito. "Self-Assembling GaAs Mirror with Electrostatic Actuation Using Micro-origami." *Physica E* 24 (2004), 78–81.

[14] P. D. Francesco, E. Guitter, and S. Mori. "Folding of the Triangular Lattice with Quenched Random Bending Rigidity." *Phys. Rev. E* 55 (1997), 237–251.

[15] T. Fuse. *Unit Origami: Multidimensional Transformations.* New York: Japan Publications, 1990.

[16] R. Gurkewitz and B. Arnstein. *Multimodular Origami Polyhedra: Archimedeans, Buckyballs and Duality.* New York: Dover, 2003.

[17] J. Hong, Q. Wang, and Z. Fan. "Synthesis of Multiblock Polymer Containing Narrow Polydispersity Blocks." *Macromol. Rapid Commun.* 27 (2006), 57–62.

[18] G. W. Hunt and I. Ario. "Twist Buckling and the Foldable Cylinder: An Exercise in Origami." *Inter. J. Non-Linear Mech.* 40 (2005), 833–843.

[19] H.J. In, S. Kumar, Y. Shao-Hornand, and G. Barbastathis. "Origami Fabrication of Nanostructured, Three-Dimensional Devices: Electrochemical Capacitors with Carbon Electrodes." *Applied Phys. Letts.* 88 (2006), 083104.

[20] E. Iwase and I. Shimoyama. "A Design Method for Out-of-Plane Structures by Multi-step Magnetic Self-Assembly." *Sensors and Actuators* A127 (2006), 310–315.

[21] Miyuki Kawamura. "Cosmosphere." In *Origamido: The Art of Folded Paper*, edited by M. Lafosse, pp. 88. Beverly, MA: Rockport Publishers, 2000.

[22] T. Kawasaki. "$R(\gamma) = I$." In *Origami Science and Art: Proceedings of the Second International Meeting of Origami Science and Scientific Origami*, edited by K. Miura, pp. 31–40. Shiga, Japan: Seian University of Art and Design, 1997.

[23] H. Kobayashi, B. Kresling, and J. F. V. Vincent. "The Geometry of Unfolding Tree Leaves." *Proc. R. Soc. Lond.* 265 (1998), 147–154.

[24] D.-M. Kroll and G. Gompper. "Floppy Tethered Networks." *J. Phys. I France* 3 (1993), 1131–1140.

[25] K. Kuribayashi, K. Tsuchiya, Z. You, D. Tomus, M. Umemoto, T. Ito, and M. Sasaki. "Self-Deployable Origami Stent Grafts as a Biomedical Application of Ni-rich TiNi Shape Memory Alloy Foil." *Mater. Sci. and Engr.* A419 (2006), 131–137.

[26] R. L. Lescanec and M. Muthukumar. "Configurational Characteristics and Scaling Behavior of Starburst Molecules: A Computational Study." *Macromolecules* 23 (1990), 2280–2288.

[27] Y. G. Li, Y. D. Tseng, S. Y. Kwon, L. D'Espaux, J. S. Bunch, P. L. Mceuen, and D. Luo. "Controlled Assembly of Dendrimer-Like DNA." *Nature Materials* 3 (2004), 38–42.

[28] X. Liu, C. L. Stern, and C. A. Mirkin. "Chemical Origami: Formation of Flexible 52-Membered Tetranuclear Metallacycles via a Molecular Square Formed from a Hemilabile Ligand." *Organomettalics* 21 (2002), 1017–1019.

[29] A. Lobkovsky, S. Gentges, H. Li, D. Morse, and T. A. Witten. "Scaling Properties of Stretching Ridges in a Crumpled Elastic Sheet." *Science* 270 (1995), 1482–1485.

[30] L. Mahadevan and S. Rica. "Self-Organized Origami." *Science* 307:5716 (2005), 1740.

[31] K. Miura. "Concepts of Deployable Space Structures." *J. Space. Struc.* 8 (1993), 3–16.

[32] T. Nojima. "Modeling of Folding Patterns in Flat Membranes and Cylinders by Origami." *JSME-C* 45 (2002), 364–370.

[33] Y. Okumura and K. Ito. "The Polyrotaxane Gel: A Topological Gel by Figure-of-Eight Cross-Links." *Adv. Mater.* 13 (2001), 485–487.

[34] M. Paczuski, M. Kardar, and D. Nelson. "Landau Theory of the Crumpling Transition." *Phys. Rev. Letts.* 60 (1988), 2638–2640.

[35] G. T. Pickett. "DNA-Origami Technique for Olympic Gels." *Europhys. Letts.* 76 (2006), 616–622.

[36] G. T. Pickett, D. Jasnow, and A. C. Balazs. "Simulation of Fracturing Reinforced Polymer Blends." *Phys. Rev. Letts.* 77 (1996), 671–674.

[37] G. T. Pickett, D. Jasnow, and A. C. Balazs. "Brownian Motion Simulation of Chain Pullout: Modeling Fracture in Polymer Blends." *Trends in Polymer Science* 5 (1997), 128–133.

[38] E. Raphael, C. Gay, and P.-G. de Gennes. "Progressive Construction of an 'Olympic' Gel." *J. Stat. Phys.* 89 (1997), 111–118.

[39] R. Resch. "Construction-Element." US Patent no. 4397902, 1983.

[40] P. W. K. Rothemund. "Folding DNA to Create Nanoscale Shapes and Patterns." *Nature* 440 (2006), 297–302.

[41] P. W. K. Rothemund, N. Papadakis, and E. Winfree. "Algorithmic Self-Assembly of DNA Sierpinski Triangles." *PLoS Biol.* 2:1 (2004)2, e424.

[42] C. M. Schilli, M. F. Zhang, E. Rizzardo, S. H. Thang, Y. K. Chong, K. Edwards, G. Karlsson, and A. H. E. Muller. "A New Double-Responsive Block Copolymer Synthesized via RAFT Polymerization: Poly(N-isopropylacrylamide)-block-poly(acrylic acid)." *Macromolecules* 37 (2004), 7861–7866.

[43] W. B. Sherman and N. C. Seeman. "A Precisely Controlled DNA Biped Walking Device." *Nano Letters* 4 (2004), 1203–1207.

[44] T. Tokuda, Y. Sakano, D. Mori, J. Ohta, M. Nunoshita, P. O. Vaccaro, A. K. Vorob'ev, K. Kubota, and N. Saito. "Fabrication and Current-Drive of SiGe/Si 'Micro-Origami' Epitaxial MEMS Device on SOI Substrate." *Electronics Letters* 40:21 (2004), 1333–1334.

[45] D. A. Tomalia, H. Baker, J. Dewald, M. Hall, S. Martin, J. Roeck, J. Ryder, and P. Smith. "New Class of Polymers: Starburst-Dendritic Macromolecules." *Polym. J.* 17 (1985), 117–132.

[46] D. Tomanek. "Mesoscopic Origami with Graphite: Scrolls, Nanotubes, Peapods." *Physica B* 323 (2002), 86–89.

[47] P. O. Vaccaro, K. Kubota, T. Fleischmann, S. Saravanan, and T. Aida. "Valley-Fold and Mountain-Fold in the Micro-origami Technique." *Microelectronics J.* 34 (2003), 447–449.

[48] T. A. Vilgis and M. Otto. "Topological Interactions in Multiply Linked DNA Rings." *Phys. Rev. E.* 56 (1979), R1314.

[49] J. F. V. Vincent. "Smart by Name, Smart by Nature." *Smart Mater. Struct.* 9 (2000), 255–259.

[50] G. A. Vliegenthart and G. Gompper. "Forced Crumpling of Self-Avoiding Elastic Sheets." *Nature Mater.* 5 (2006), 216–221.

[51] E. Winfree, F. R. Liu, L. A. Wenzler, and N. C. Seeman. "Design and Self-Assembly of Two-Dimensional DNA Crystals." *Nature* 394 (1998), 539–544.

[52] T. A. Witten. "Stress Focusing in Elastic Sheets." *Rev. Mod. Phys* 79 (2007), 643–675.

[53] S. M. Yang, I. Sokolov, N. Coombs, C. T. Kresge, and G. A. Ozin. "Formation of Hollow Helicoids in Mesoporous Silica: Supramolecular Origami." *Adv. Mater.* 11 (1999), 1427–1431.

[54] Y.W. Zhang and N. C. Seeman. "Construction of a DNA-Truncated Octahedron." *JACS* 116 (1994), 1661–1669.

[55] T. C. Zook and G. T. Pickett. "'Hollow-Core' Dendrimers Revisited." *Phys. Rev. Letts.* 90 (2003), 015502.

Expandable Tubes with Negative Poisson's Ratio and Their Application in Medicine

Zhong You and Kaori Kuribayashi

1 Introduction

Specially designed materials can exhibit a transverse expansion when stretched. This behavior can be described by a negative Poisson's ratio, commonly defined as the ratio between the negative transverse strain and the longitudinal strain. Some polymers found by Lakes [4] have such property. In a separate paper [5], Lakes showed a two-dimensional version of the micro-structure of the materials consisting of a honeycomb with inverted cells and the possible conversion to a three-dimensional structure with inwardly bulging cells. Here, we report that the same technique can be used in origami to create expandable tubes with a negative Poisson's ratio based on folding patterns for flat paper and their application as deployable stents in medicine.

Many folding patterns for flat paper could lead to an overall negative Poisson's ratio. Typical examples can be found in some of the map folding patterns including the well-known *Miura-ori* in which the folded paper can expand in two orthogonal directions simultaneously through out-of-plane motion.

It has been reported that a number of folding patterns for flat sheets can also be utilized for the folding of cylinders. Fujimoto and Nishiwaki first explored this possibility. In their book published in 1982 [1], they presented

numerous folding patterns for flat sheet and their transformation to tubes by joining together two edges of the paper. Similar concepts have also been reported by other authors [2]. The reported work focuses primarily on the artistic aspect of the folding cylinders. Most of the patterns, including the one based on *Miura-ori*, lead to cylinders which are completely rigid or possess little expansion. Nevertheless, a few patterns do enable the diameter of the tubes to alter. This property makes the compact packaging of tubes possible. More importantly, some of the expandable tubes have an overall negative Poisson's ratio, i.e., both the length and diameter increase during expansion.

Many potential applications involving expandable cylindrical structures exist in medicine simply because the human body is composed of an extensive pipe network. With the advance of minimally invasive surgery, it becomes possible to deliver these structures to the diseased sites to treat certain illnesses, provided that they can be packaged into a very small volume.

A few years ago, we started working on a kind of deployable stent graft called the *origami stent graft*. A *stent graft* is a tubular medical device made of biocompatible materials. Stent grafts are designed for two purposes: to open up a blocked site in the human body caused, for instance, by diseases such as stenosis, arteriosclerosis, or cancer; or to isolate an aneurism caused by disease or weakening of the wall of a blood vessel. Existing stent grafts are in general made of a metallic expandable scaffold (also called stent) to which a membrane or fabric cover is attached. Most manufacturers simply attach a soft cover around an existing stent with the expectation that the expansion of the stent would automatically deploy the cover into the desired shape. However, such approach often leads to geometrical incompatibility between the stent and its cover. The cover has to be attached to the stent at discrete points by bonding or stitches so that the combined structure can be expanded. The cost of manufacturing tends to be very high. Subsequently, the deployment of the stent graft involves the cover sliding with respect to struts of the stent. It is not uncommon that uneven distribution of stresses, rupture, or entanglement occur during expansion of a stent graft.

The origami stent graft concept was developed to deal with the problem of geometrical incompatibility. For the first time, a stent graft has been designed without any reliance on an existing stent structure. The technique of origami has been employed to generate a set of crease patterns enabling the stent graft to be folded up into a small volume for delivery to locations in human bodies in the same way as existing stent grafts. The origami stent graft then expands to form the desired profile and the creases disappear. The crease patterns are optimized to avoid any large geometrical incompatibility between a stent and its cover.

The layout of this paper is as follows. In Section 2, the most common folding pattern for thin-walled cylinders is discussed. The distortion factor, a parameter measuring geometrical incompatibility, is introduced. Through optimization, a crease pattern associated with the minimum geometrical distortion is presented. The concept is then extended by incorporation of helical folds in Section 3, which leads to a synchronized expansion and higher radial stiffness in the fully expanded state. Other possible designs are given and briefly discussed in Section 4, which concludes the paper.

2 Basic Folding Pattern

Stent grafts generally have a tubular profile. For simplicity, consider first of all a developable short thin-walled tube. The cylindrical surface of the tube can be mapped onto a flat sheet. The sheet can consequently be divided into a row of rectangular units; see Figure 1(a). Within each unit, two inclined valley folds and a central mountain fold are introduced to enable them to fold flat; see Figure 1(b). Take l as the length AB, α_1 and α_2 as the angles that define the inclination of the valley folds. The two edges of the sheet, $a_1 - a_2$ and $b_1 - b_2$, are then joined together to form a deployable cylinder. A partially folded cylinder is shown in Figure 1(c). It has rotational symmetry. The angle sustained by a single unit is 2δ, which is a constant determined by the total number of units circumferentially. Figure 1(d) is the projection of the cylinder with locations for the vertices of the folds. It can be found that

$$\delta = \frac{360^\circ}{2m} = \frac{180^\circ}{m},$$

where m is the total number of units in a row.

Figure 2 shows the behavior of a single unit during the expansion of the cylinder. Denote by $\theta = (\angle ABC)/2$ the deployment angle. When the cylinder is fully folded, the central vertex of a unit, O, reaches the projection position of the center of the cylinder O_0. Hence,

$$\theta_0 = \delta,$$

in which θ_0 is the deployment angle when the cylinder is fully folded.

When θ reaches 90° the device opens up to form a polygon, as shown in Figure 2(b). It is interesting to note that from then on the tube actually shrinks a bit radially for the units to fit onto the cylindrical surface. If we take the configuration shown in Figure 2(c) as the final expanded state, then

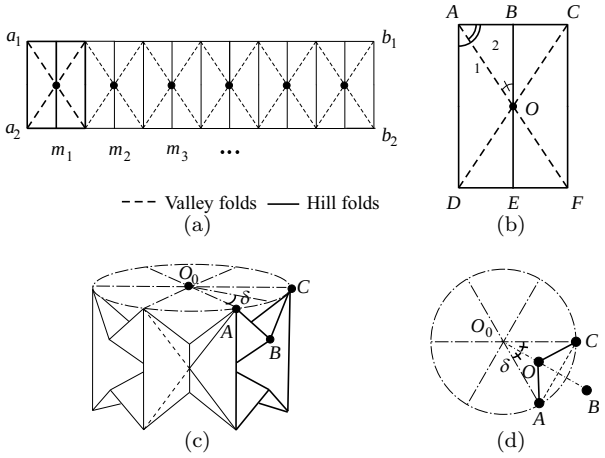

Figure 1. Folding of a short thin-walled cylinder by introduction of a single row of identical rectangular units: (a) a row of units, (b) a single unit, (c) a partially folded cylinder, and (d) projection of the cylinder .

$$\theta_1 = 90^\circ + \frac{\delta}{2}.$$

Obviously θ_0 and θ_1 vary with m.

For long cylinders, a single row of units often lead to very narrow rectangular units. It is therefore more practical to have more than one row of units. However, a close inspection of Figure 1(c) reveals that it is not possible to simply place one row after the other longitudinally because the central vertices in the longitudinally adjacent units, i.e., B or E, move apart when the cylinder is folded. This problem can be solved by rotating one row by half a unit circumferentially; see Figure 3(a). On this occasion, the corner of the unit at the top is connected with the midpoint of the unit below, and vice versa. For example, E_2 and F_2 are connected to A_1 and B_1, respectively. Figure 3(b) shows a partially folded cylinder with two rows. By observation, this seems enough to solve the problem because the second row of units is firmly slotted into the first row. But a more robust proof is required.

Let d be the distortion factor,

$$d = \frac{O_0B - O_0A}{l},$$

in which O_0A and O_0B are the radii of the corners and the midpoint of a unit, respectively. Obviously no distortion exists if and only if d is zero.

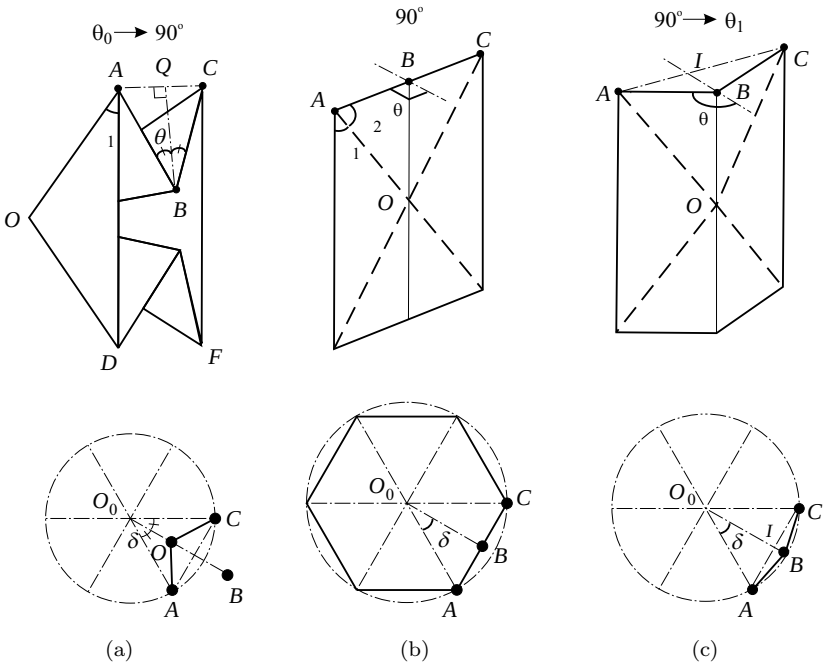

Figure 2. The expansion of a single unit from $\theta = \theta_0$ till $\theta = \theta_1$: folded unit (top) and projection (bottom) for (a) $\theta < 90^\circ$, (b) $\theta = 90^\circ$, and (c) $\theta > 90^\circ$.

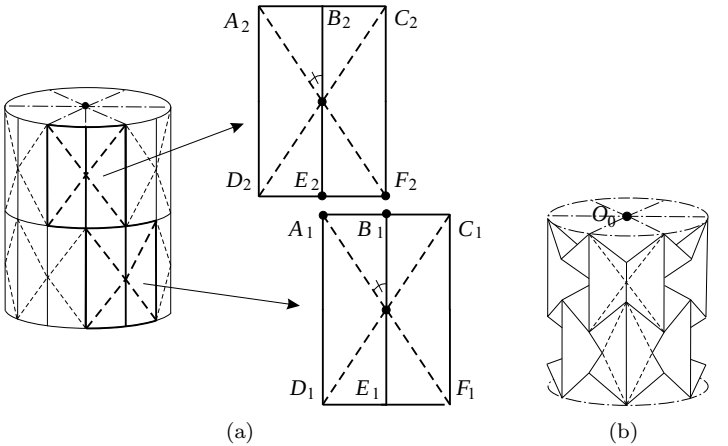

Figure 3. (a) Folding pattern consisting of two rows of units and (b) the folded model.

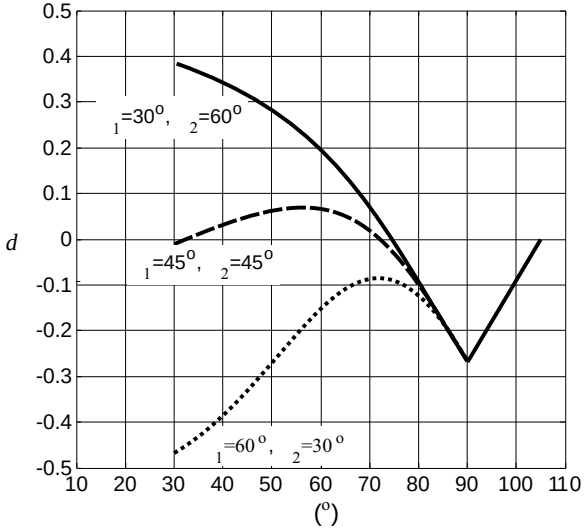

Figure 4. Distortion factor d versus deployment angle θ.

It can be found based on Figure 2(a) that for $\theta \leq 90°$,

$$O_0B = \frac{l \sin\theta}{\tan\delta} + l\cos\theta \frac{\cos^2\alpha_1 - \sin^2\alpha_1 \cos^2\theta}{1 - \sin^2\theta \sin^2\alpha_1}, \tag{1}$$

and

$$O_0A = \frac{l \sin\theta}{\sin\delta}. \tag{2}$$

When $\theta \geq 90°$, using Figure 2(c) we have

$$O_0B = \frac{l \sin\theta}{\tan\delta} - l\cos\theta, \tag{3}$$

and

$$O_0A = \frac{l \sin\theta}{\sin\delta}. \tag{4}$$

With Equations (1)–(4), the variation of distortion factor d with respect to deployment angle θ can be determined.

Figure 4 shows a set of d versus θ curves for given α when $m = 6$. It can be found that there is little or no distortion in the fully folded and expanded states but the distortion is unavoidable during expansion. Moreover, overall d becomes the smallest when angles α_1 and α_2 are equal. Furthermore, when $90° \leq \theta \leq \theta_1$, the distortion remains the same no matter what α_1 and α_2 are.

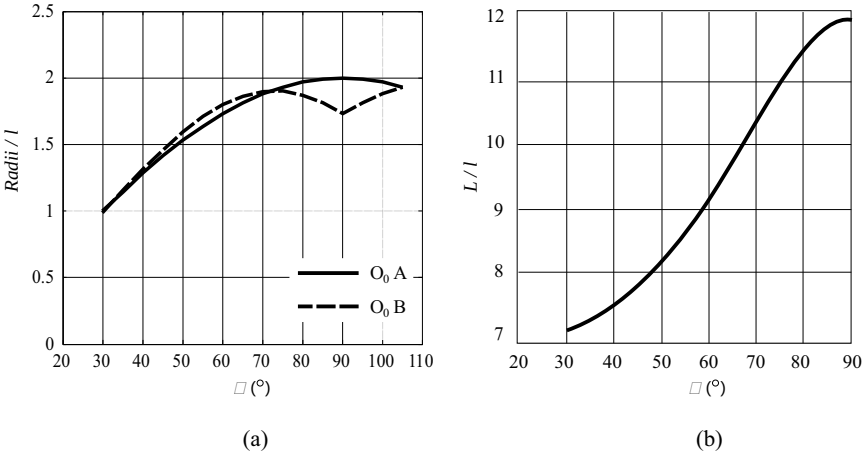

Figure 5. Variation during expansion of (a) radii and (b) overall length. Note that $m = n = 6$, $\alpha_1 = \alpha_2 = 45°$, and L remains constant when $\theta \geq 90°$.

For $\alpha_1 = \alpha_2 = 45°$ and $m = 6$, the variation of the cylinder's radii during expansion is plotted in Figure 5(a).

For longer tubes, more rows of units can be arranged similarly. Assume that there are a total of n row units. The overall length of the tube, L, can be expressed as follows: for $\theta \leq 90°$,

$$L = n\frac{2l}{\tan\alpha_1} - \frac{(n-1)l}{1-\sin^2\theta\sin^2\alpha_1}\left(\sin 2\alpha_1\cos^2\theta + \frac{\cos^2\alpha_1 - \sin^2\alpha_1\cos^2\theta}{\tan(\alpha_1+\alpha_2)}\right)$$

and for $\theta \geq 90°$,

$$L = n\frac{2l}{\tan\alpha_1} - \frac{(n-1)l}{\tan(\alpha_1+\alpha_2)}.$$

Note that L is independent of θ in this case.

The overall length variation with respect to θ is given in Figure 5(b) in which $n = 6$.

Reading the plots in Figure 5 indicates that the foldable tube exhibits a negative Poisson's ratio. This is further verified by a tube model shown in Figure 6. The expanded shape is both larger in diameter and longer in length than the folded one.

3 Helical Folding Pattern

The rotationally symmetric design of the foldable tube described in Section 2 does provide compact folding. However, it has low radial stiffness

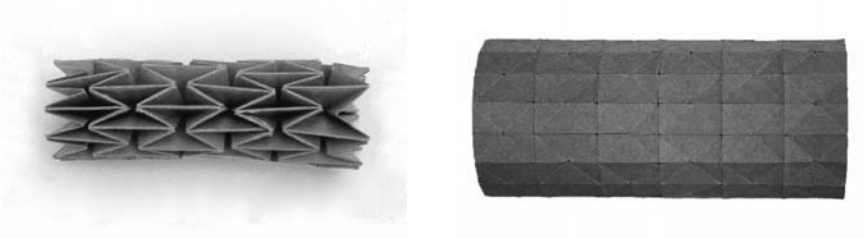

Figure 6. A card model of a foldable tube with $m = n = 6$.

because the longitudinal folds coincide with the hinge lines of the collapse mechanism when the tube is pressurized radially. Moreover, the folding and expansion of the units are, in general, not synchronized. External intervention is often required to keep all of the units expanding uniformly. An approach to overcome these problems is to replace longitudinal folds with helical ones.

Helical folds can be easily introduced by adjusting the joining positions of the left and right edges of a developed cylindrical surface. Figure 7(a) shows the surface of a foldable cylindrical tube with helical folds. It is based on the same rectangular units where $\alpha_1 = \alpha_2 = 45°$. To form a cylindrical tube with helical folds the opposite edges of the sheet, i.e., sections a_2–a_3 and b_1–b_2, etc., are joined together. In this example there are six and one half units in one turn of a helix. Always one half of a unit needs to be added at the end of each full circumference to allow connection of the left and right edges.

The main helical folds are denoted as H_A and H_B. They are orthogonal to one another as shown in Figure 7(a). Figures 7(b) and (c) show perspective views of the cylindrical tube in the unfolded and folded states. H_A is a single long fold that spirals around the circumference of the tube, whereas H_B runs diagonally from one open end of the tube to the other.

The number of H_A- and H_B-type helices may vary. A foldable cylindrical tube with more than one H_A-type helix can be made by adjusting the joining position of the left and right edges of the developed surface. For instance, it is possible to have two helices, in which the opposite edges of the sheet a_3–a_4 and b_1–b_2, etc., are joined together.

Helical folds bring several important advantages. Firstly, as shown in Figure 7(b), H_A-type helices connect all of the elements like ribbons, enabling the folding and expansion processes to be synchronized among the units. Secondly, the helical folds provide far greater resistance to structural collapse in the expanded configuration of the tube because none of the folds coincide with the collapsed hinge lines of the tube under external radial pressure. The tube will be permitted to collapse only under torsion

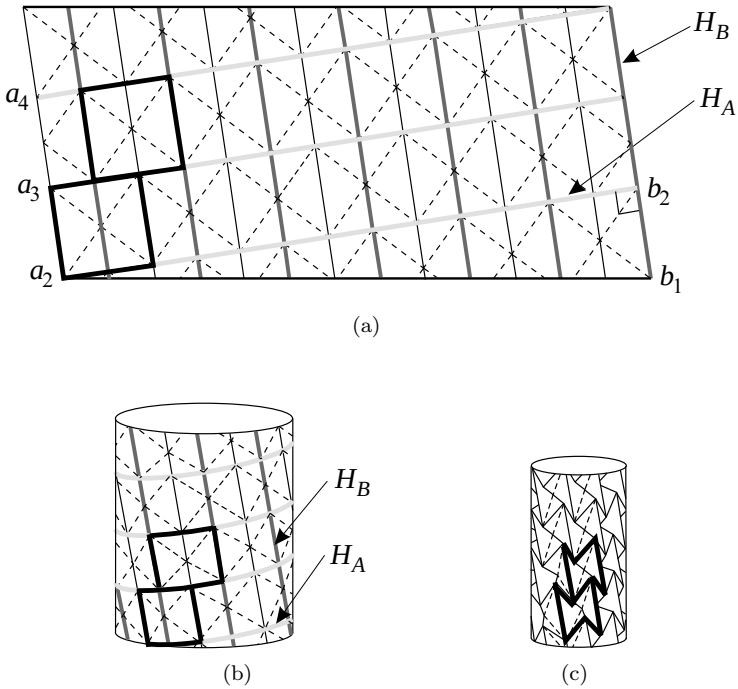

Figure 7. Folding of a tube with helical pattern: (a) folding pattern, (b) unfolded cylinder, and (c) folded cylinder.

at both ends. It will not do so easily in practice since torsional loadings are rare.

Procedures identical to those introduced in Section 2 can be implemented to calculate and minimize geometrical distortion during expansion. Interested readers can refer to [3] for detailed analysis. It was discovered that folding patterns with a single H_A-type fold have more or less the same amount of distortion as that in the rotationally symmetric patterns because the variations of radii and length of the tube are highly comparable. However, the distortions increase dramatically with the introduction of more H_A-type folds.

Figure 8 shows the folding of a thin stainless steel tube. It demonstrates how small the distortion can become considering the stiffness of the material.

The folding with helical patterns exhibits overall negative Poisson's ratio, as well.

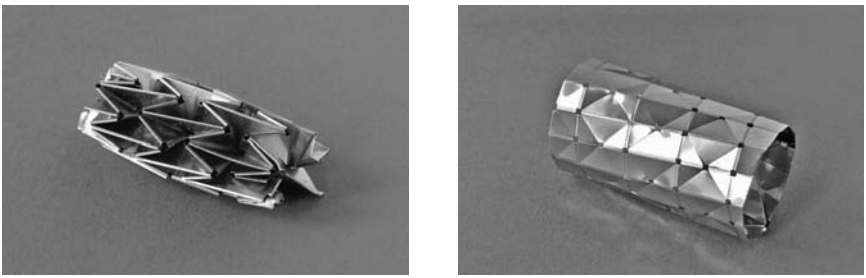

Figure 8. Folding of a thin-walled stainless steel tube with a helical pattern.

4 Final Remarks

In this paper, a study on the geometrical characteristics of foldable cylinders that exhibit negative Poisson's ratio is presented. The basic folding pattern, which was first introduced by Fujimoto and Nishiwaki, has been extended by introduction of helical folds. Although the new folding scheme does not alter the fundamental behavior of the tube, i.e., the overall negative Poisson's ratio is preserved, it has greatly improved both the deployment and mechanical properties of the structure. These improvements make it an ideal concept for medical applications as deployable stent grafts.

The discussion so far has been confined to cylindrical profiles. In other work of the authors, stent grafts with conical and funnel ends were also investigated and suitable folding schemes were proposed accordingly [3]. For example, the pattern shown in Figure 9 can be used for a tube with a conical profile. It can even be combined or mixed with those with cylindrical structure. Whether these hybrid patterns can lead to a reduction of

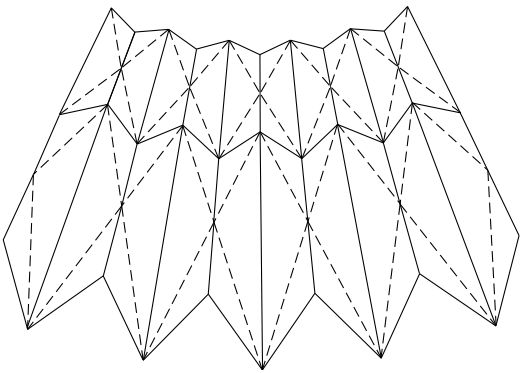

Figure 9. A folding pattern for a tube with a conical opening.

geometrical distortions during expansion is a matter for further investigation.

Acknowledgment. Financial support from the Engineering and Physical Sciences Research Council in the UK (Grant Number EP/C51937X/1) is acknowledged. Zhong You would like to express his gratitude to the Royal Academy of Engineering for giving him a Global Research Award, which enabled this paper to be completed.

Bibliography

[1] S. Fujimoto and M. Nishiwaki. *Sōzō Suru Origami Asobi e no Shōtai* (An Invitation to Creative Origami Play, in Japanese). Osaka, Japan: Asahi Culture Center, 1982.

[2] B. Kresling. "Plant 'Design': Mechanical Simulations of Growth Patterns and Bionics." *Biomimetics* 3:3 (1995), 105–122.

[3] K. Kuribayashi. "A Novel Foldable Stent Graft." PhD dissertation, University of Oxford, 2004.

[4] R. Lakes. "Foam Structures with a Negative Poisson's Ratio." *Science* 235 (1987), 1038–1040.

[5] R. Lakes. "A Broader View of Membranes," *Nature* 414 (2001), 503–504.

Airbag Folding Based on Origami Mathematics

Christoffer Cromvik and Kenneth Eriksson

1 Introduction

Simulating a crash when the crash-test dummy hits the airbag while it is still expanding remains a challenge to the industry. This situation is called out-of-position (OOP), reflecting the fact that the airbag was not designed for occupants that are sitting too close to the airbag or for some other reason hit the airbag before it is fully inflated.

The difficulty with an OOP situation compared to an in-position situation is that the inflation of the folded airbag is much more important. It has to be realistically computed, since it affects the impact of the dummy. Attaining a realistic simulation means starting with a correct geometry of the folded airbag and simulating the inflation with correct gas dynamics. Several commercial software packages exist that can simulate the inflation process of an airbag, e.g., the explicit Finite Element (FE) code `LS-DYNA` [5].

This work aims at developing an algorithm for computing an accurate geometry of the flat folded airbag. Different airbags are folded by different methods and with different numbers and types of foldings. The airbags are often folded by both machines and humans according to a folding scheme. Still, the creases are not entirely deterministically positioned. It is very difficult to control the placement of smaller creases. The folding schemes all assume that the airbag lies flat and stretched in some direction. In this position, different foldings are executed until the dimension of the folded

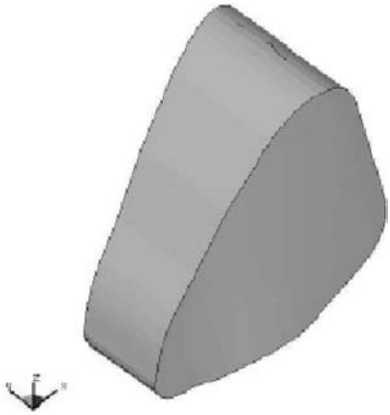

Figure 1. A CAD model of a passenger airbag.

airbag is small enough so that it fits into the airbag compartment. The foldings can be a combination of simple folds, but also roll folds.

Some preprocessors to `LS-DYNA`, for example, `EASi-FOLDER` [4] and `OASYS-PRIMER` [1], contain software for folding a (nearly) flat FE airbag mesh. They are capable of executing the type of foldings that are normally used in production on flat airbags, e.g., roll-fold, z-fold. However, they are not as accurate when folding an airbag in its three-dimensional shape to a flat airbag.

Some airbag models have a simple construction, e.g., the driver model, which is made of two circular layers sewn together. It is essentially two-dimensional. Passenger airbags are often more complicated. They are made of several layers sewn together in a three dimensional shape, with no trivial two-dimensional representation. See Figure 1 for an example.

In the present work, the computation of the geometry of the flat folded airbag is organized into two steps. First, a crease pattern is computed on a polyhedral approximation of the airbag. Second, a nonlinear optimization problem is formed and solved for the purpose of finding the flat geometry. The accuracy of the computed approximation is measured by comparing its area to the area of the inflated model.

2 Crease Pattern

A crease pattern is first designed for a tetrahedron. We present a series of proofs for different types of polyhedra. The proofs are constructive, and their results can be used to design a crease pattern for our application.

Flat foldability, meaning that the polyhedron can be flattened using a fixed crease pattern, is achieved by cutting along the crease lines, folding the resulting object, and then gluing the cut-up faces back according to the correct connections.

Theorem 1. *The tetrahedron can be folded flat.*

Proof: The proof is organized in a sequence of figures shown in Figure 2, each visualizing the cutting and folding. Consider the tetrahedron with vertices A, B, C, D as in the figure. Cut up the triangle BCD of the tetrahedron, with straight cuts from a point E on the face, to the three vertices B, C, D, respectively, as in the figure.

Then open up the tetrahedron by rotating the triangular patches BDE, BCE, and CDE around the axes BD, BC, and CD, respectively, until these triangles become parts of the three planes through ABD, ABC, and ACD, respectively, as in the figure.

Cut the quadrilateral surface with vertices A, B, E', D along a straight cut from E' to A, and then rotate the resulting triangular faces ABE' and $AE'D$ around the axes AB and AD, respectively, until these faces become parts of the two planes ABC and ACD, respectively, as in the figure.

We choose the point E such that the edge BE' after rotation coincides with BE'' and DE' with DE'''. The condition for this is that $\angle ABD + \angle DBE = \angle ABC + \angle CBE$ and $\angle ADB + \angle BDE = \angle ADC + \angle CDE$.

Using this, we may now (partly) restore the surface of the tetrahedron by joining the surfaces ABE'' and $ABE''C$ along the edge BE'', and the surfaces ADE''' and $ADE'''C$ along the edge DE'''.

Finally we rotate the (partly double-layered) surface $ADE'''C$ around the axis AC until it coincides with the plane through A, B and C as in the figure. To conclude the proof of the flat foldability of the tetrahedron we now note that the point E''' after rotation coincides with E''. We may therefore now completely restore the topology of the original tetrahedron by joining the edges AE'' and AE''' (after rotation) and the edges CE'' and CE''' (after rotation). □

Note that the proof is based on cutting and gluing. It does not reveal if there is a continuous deformation to a flat shape.

Remark 1. Concerning the line AE' we remark that the angles $\angle BAE'$ and $\angle DAE'$ satisfy $\angle BAE' + \angle DAE' = \angle BAD$ and $\angle BAC - \angle BAE' = \angle CAD - \angle DAE'$, as in the figure, and are thus independent of the plane BCD. We further note that we may also consider rotating the triangles BDE, BCE, and CDE in the opposite direction, again until they become parts of the planes ABD, ABC, and ACD, respectively, as in the figure. We now choose the point E so that $\angle ABD - \angle DBE = \angle ABC - \angle CBE$

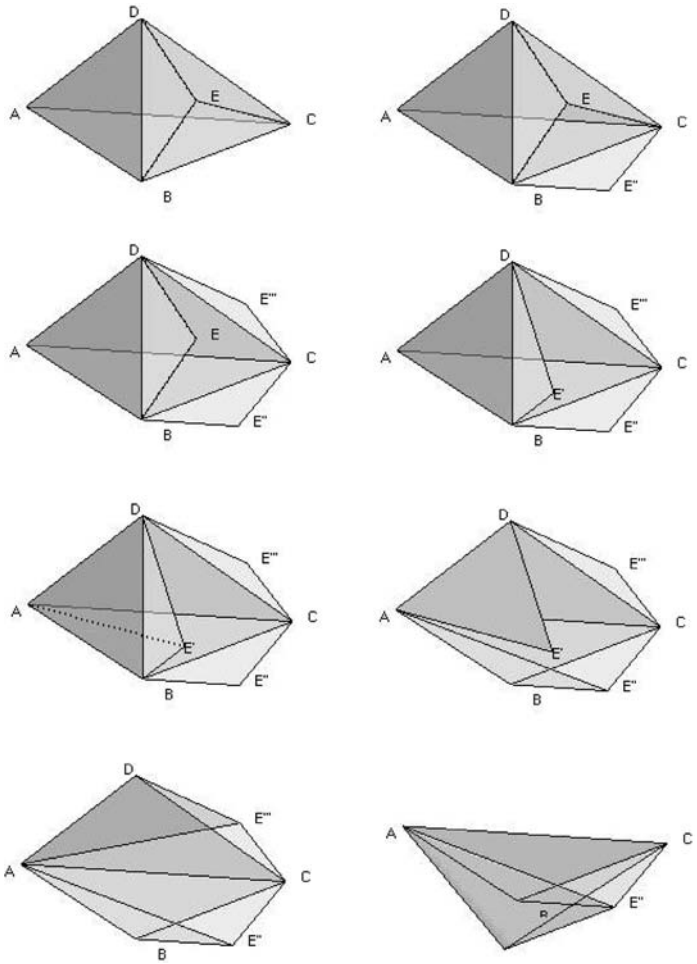

Figure 2. Supporting figure for the proof of Theorem 1. The proof follows the figures from left to right beginning at the top.

and $\angle ADB - \angle BDE = \angle ADC - \angle CDE$. Continuing from the figure we may then again make a straight cut from E' to A (partly double layered). Again, when we now rotate around the axes AB and AD as before the (rotated) point E' will coincide with E'' and E''', respectively, and we can partly restore the tetrahedron by joining along the edges. Finally, after rotation around AC we may completely restore the topology of the surface of the tetrahedron by joining along the edges. Concerning the crease line from A to E'' we note that again the angles $\angle BAE'$ and

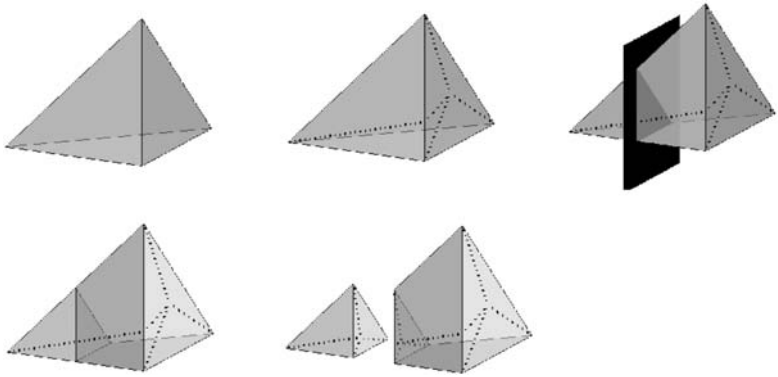

Figure 3. A tetrahedron is cut, and in the cut, two additional interior triangular faces are created. Identical crease patterns are created on both interior faces, and the tetrahedron is separated into two parts: a smaller tetrahedron and a prism. The flat foldability of the prism follows from the foldability of the tetrahedron.

$\angle DAE'$ must satisfy the same equations $\angle BAE' + \angle DAE' = \angle BAD$ and $\angle BAC - \angle BAE' = \angle CAD - \angle DAE'$ as before and therefore must be the same as above. We therefore conclude that this crease line is independent of both direction of rotation of the triangles BCE, BDE, and CDE, and of the position and orientation of the plane BCD (as long as the angles at A are unchanged).

We now proceed by cutting the tetrahedron by a plane; see Figure 3. We call the cut-off tetrahedron a prism-type polyhedron.

Theorem 2. *The prism-type polyhedron can be folded flat.*

Proof: Consider a tetrahedron $ABCD$ with the crease pattern from the proof of Theorem 1. Cut the tetrahedron with a plane; see Figure 3. In the cut, insert two additional triangular surfaces, such that the two cutoff parts are closed, but not separated. The "smaller" cutoff part is a tetrahedron, and the "bigger" part is a prism type polyhedron. Let the vertices of the smaller tetrahedron be a, b, c, d, where $A = a$, b lies on the edge AB, c on AC and d on AD.

Remark 1 shows that the crease line from A to E' (see Figure 2) is independent of how the inserted triangular face of the smaller tetrahedron is folded. Let it be folded to the interior of the smaller tetrahedron. This means that a crease pattern can be constructed that will coincide with the crease pattern of the original tetrahedron, i.e., the crease line that is constructed by drawing a straight line from a to e' will coincide with the

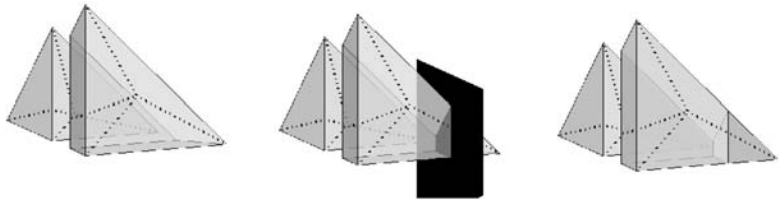

Figure 4. The prism from Figure 3 is cut, and in the cut, an additional interior quadrilateral surface is created. The flat foldability of the box-type polyhedron follows from the foldability of the prism and the tetrahedron.

crease line that was created from the line segment from A to E' in the proof of Theorem 1.

Now, make an identical copy of the crease pattern on the inserted triangular face belonging to the prism. Folding the original tetrahedron with its inserted triangular faces is possible by the construction of the crease pattern. Let the two polyhedra be separated by moving the tetrahedron in the plane. By the foldability of the tetrahedron, both the smaller tetrahedron and the prism can be folded flat. □

Next, we cut the prism-type polyhedron by a plane; see Figure 4. We call the cut-off prism a box-type polyhedron.

Theorem 3. *The box-type polyhedron can be folded flat.*

Proof: Let the prism from the cut-off tetrahedron, with its crease pattern, be cut by a plane; see Figure 4. In the cut, insert one additional quadrilateral surface that is only connected to the prism by its four vertices. Along the inserted surface put a crease line γ. Its position is only determined by the positions of the upper and lower faces of the prism. When the prism (with its cut) and the additional inserted surface are folded, there will be a gap along the sides of the prism; see Figure 5. Let the crease line on the side of the original prism be called ξ. Also, let the point where the crease γ meets ξ unfolded be called p_1; see Figure 5. The gap can be closed by forming two triangles: from a point p (see Figure 5) somewhere along ξ, to the intersection where ξ meets the inserted surface p_2, to B respectively C.

Note that the lengths Cp_1 and Cp_2 are the same, as well as the lengths Bp_1 and Bp_2, and the length Cp is shared by both the gap and the new triangles. Let C_1 and C_2 be positioned according to Figure 5. If the point p is chosen such that $\angle C_1Cp_1 + \angle p_2Cp = \angle C_1CC_2 + \angle C_2Cp$, then the new triangles are an identical match to the gap. By Theorem 2, the prism is foldable, so the full construction is foldable, and since the cut does

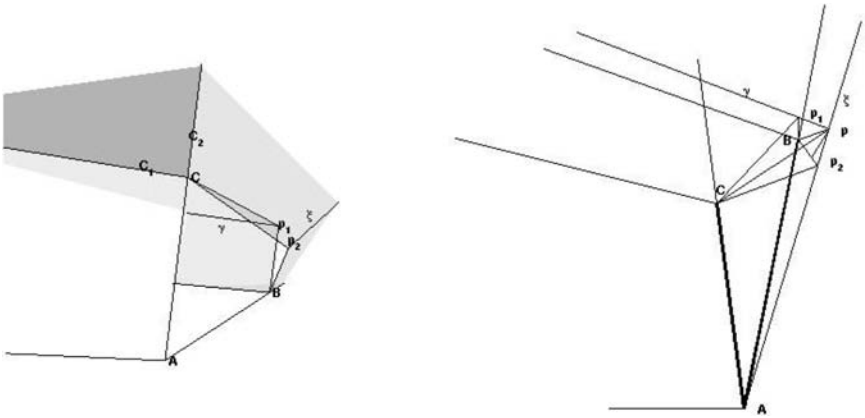

Figure 5. The left figure shows the gap around the inserted additional surface from the cut. The right figure shows the same object from above.

not influence its foldability, and its gap is filled, therefore the box-type polyhedron is flat foldable. □

In the proof of Theorem 3, a prism was cut off the polyhedron. The process of cutting off a prism can be repeated to create other types of polyhedra.

Definition 1. A *quasi-cylindrical polyhedron* is a closed cut-off cylinder with a polygonal cross-section.

Theorem 4. *Convex quasi-cylindrical polyhedra are flat foldable.*

Proof: This follows by the proof of Theorem 3. In each step, cut off a prism from the polyhedron, until the result forms the given shape. □

Airbags are usually quasi-cylindrical. There are cases, e.g., nonconvex polyhedra, for which the technique for generating a crease pattern does not work. These situations might be avoided by slicing the polyhedron, and computing a crease pattern for each part.

Theorem 4 provides an algorithm for designing a crease pattern. Given a quasi-cylindrical polyhedron, we can extend it gradually using prisms until it reaches the shape of a tetrahedron. In each step, we apply the theory for flat foldability, creating a working crease pattern.

3 Folding

For airbags, there are various alternatives for simulating the folding process. This is due to the fact that the problem is artificial in the sense that the folding need not be realistic, e.g., there is no need to introduce the concept of time. The objective is to create a flat geometry that is physically correct, not to fold it in a realistic way.

Our algorithm for folding the polyhedron is based on solving an optimization problem. A program is formulated such that the optimal solution represents a flat geometry. The target function, to be minimized, is a sum of rotational spring potentials, one spring over each crease. The minimal value of a spring potential is found when a fold is completed. The constraints are formulated in order to conserve a physically correct representation of the polyhedron, which means conserving the area and avoiding any self-intersections of the faces of the polyhedron.

The crease pattern over a polyhedron induces a subdivision of polygons called *patches*. In addition, the patches are triangulated, and the interior of the polyhedron is meshed with tetrahedra. Let the nodes of the mesh be $\{x^i\}_{i=1}^{n}$, and let the indices of the surface nodes be I_S. Let the tetrahedra be $\{K_i\}_{i=1}^{n_K}$ and set $I_K = \{1, \ldots, n_K\}$. Let the four indices of the nodes of tetrahedron k be $V_k(i)$, $i = 1, \ldots, 4$. The edges of the triangular faces are denoted $\{E_i\}_{i=1}^{n_E}$, and the indices of the two nodes of edge e are $W_e(i)$, $i = 1, 2$.

Denote the creases $\{C_i\}_{i=1}^{n_C}$. The spring potential over each crease C_i is computed using the scalar product of the normals, n_i^1,n_i^2, of the two neighboring patches. The normals point outward from the polyhedron, and the scalar product is 1 when the two patches are parallel, and -1 when the fold is completed.

The folding process of a polyhedron with n nodes (surface and interior mesh nodes) is formulated as the following nonlinear program with $f : \mathbf{R}^{3n} \to \mathbf{R}$,

$$\min_x f(x),$$

$$\begin{aligned} f(x) &= f_1(x) + f_2(x) + f_3(x) \\ &= k_m \sum_{k=1}^{n_K} \left(\sum_{i=1}^{4} \sum_{j=i+1}^{4} \|x^{V_k(i)} - x^{V_k(j)}\| - d_{V_k(i),V_k(j)} \right)^2 \\ &\quad + \sum_{i=1}^{n_C} n_i^1 \cdot n_i^2 + k_p \sum_{i=1}^{n_E} \left(\|x^{W_i(1)} - x^{W_i(2)}\| - l_{W_i} \right)^2, \end{aligned}$$

$$\begin{aligned} &\text{subject to} \\ &\quad \operatorname{vol}(K_i) \quad \geq \varepsilon_1, \qquad i = 1, \ldots, n_K, \\ &\quad \operatorname{dist}(x^i, K_j) \geq \varepsilon_2, \qquad i \in I_S,\ j \in I_K \setminus p_i, \end{aligned}$$

where d_{ij} is the original distance between node x^i and x^j, l_i is the original length of edge i, and k_m, k_p are penalty parameters. The first constraint function is $\operatorname{vol}(K_i)$, which is the signed volume of the tetrahedron K_i. The second constraint is $\operatorname{dist}(x^i, K_j)$, which is the distance from a surface node x^i to a tetrahedron K_j, and p_i are the tetrahedron indices connected to node x^i. Finally, ε_1 and ε_2 are small positive constants.

The target function f is composed of three parts. The first part, f_1, is a penalty function that strives to keep the tetrahedral mesh uniform. The second part, f_2, is the virtual spring potential that drives the folding. The third part, f_3, is a penalty function that keeps the edges of the triangles stiff. This is used to maintain the shape and surface area of the patches.

4 Numerical Example

In Section 2, a theory for computing a crease pattern was discussed. To demonstrate its practical use, and also to demonstrate the folding algorithm, a numerical experiment is presented here. From a CAD drawing, an airbag-shaped polyhedron was constructed. The surface area of the approximation differs about 0.5% from the original area. An in-house optimization solver was used to solve the optimization problem described in

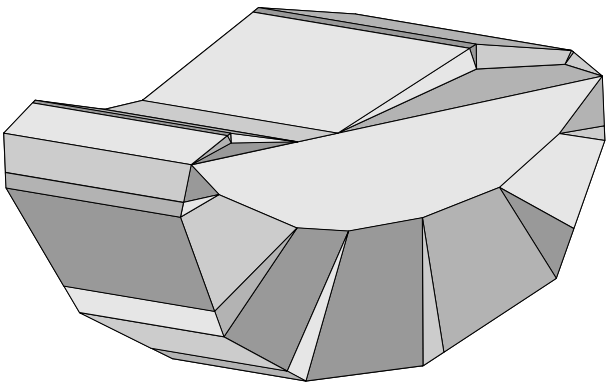

Figure 6. Polyhedral approximation of an airbag model together with a computed crease pattern.

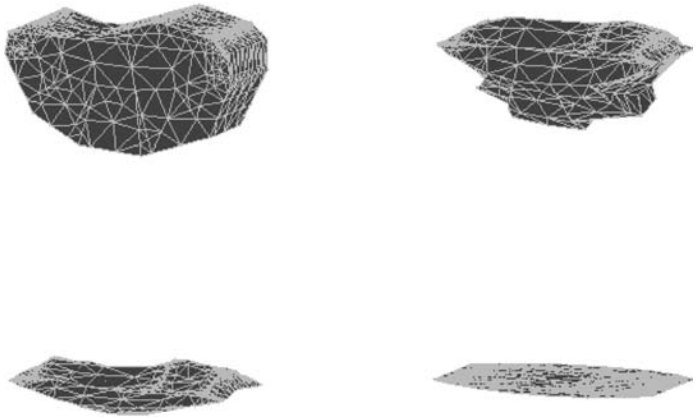

Figure 7. The figures show iteration snapshots from the folding of the polyhedron approximation from Figure 6. The upper left shows the unfolded polyhedron, the upper right: 40 iterations, the lower left: 60 iterations, and the lower right: 200 iterations.

Section 3. It is a Fortran 90 implementation of a low-storage Quasi-Newton SQP method [2, 3, 6], that can handle a few thousand variables and constraints.

The crease pattern was generated by slicing off two upper "bumps" (see Figure 6) from the airbag approximation. The crease patterns for these parts were computed separately from the rest of the polyhedron, and the complete crease pattern was formed by joining the parts.

The polyhedron approximation with its crease pattern was meshed using `TetGen` [7]. The visual result (solution) from the optimization progress is shown in Figure 7 for different iteration snapshots.

It was found that the surface area of the flat folded polyhedron was within 0.5% of the surface area of the unfolded polyhedron.

Acknowledgment. The authors would like to thank Professor S. Larsson and Dr. B. Pipkorn for valuable advice. This work was funded by Autoliv Development AB.

Bibliography

[1] ARUP. *Oasys-PRIMER*. Available at http://www.arup.com, 2009.

[2] D. P. Bertsekas. *Nonlinear Programming*. Nashua, NH: Athena Scientific, 1999.

[3] R. Byrd, R. Schnabel, and J. Nocedal. "Representations of Quasi-Newton Matrices and Their Use in Limited Memory Methods." *Mathematical Programming* 63 (1994), 129–156.

[4] ESI-group. *EASi-FOLDER*. Available at http://www.esi-group.com, 2009.

[5] Livermore Software Technology Corp. *LS-DYNA*. Available at http://www.lstc.com, 2009.

[6] J. Nocedal and S. J. Wright. *Numerical Optimization*. New York: Springer-Verlag, 1999.

[7] Hang Si. "Tetgen: A Quality Tetrahedral Mesh Generator and Three-Dimensional Delaunay Triangulator Version 1.3 User's Manual." Technical report, Weierstrass-Institut für Angewandte Analysis und Stochastik, 2004.

Part III

Computational Origami

Surface Transitions in Curved Origami

Jeannine Mosely

1 Introduction

Most folded paper designs exclusively use straight creases to divide the paper into a collection of planar polygons, giving the result a characteristic "origami" look. More and more artists, however, are designing with curves, either bending a flap of the paper into a curved surface, as in van Goubergen's *Curler* model, or introducing curved creases to create curved surfaces on either side of the fold, as in Jackson's family of one-fold designs [6, 8]. It has long been the practice to add small curved creases in the final stages of shaping a model, to add expression or provide a more three-dimensional appearance. Such curves, however, tend to be ad hoc, placed at random without a true understanding of what is happening to the paper. Such understanding is hard to come by.

It can be shown that for a curved surface to be *unfolded* or *developed* it must have Gaussian curvature equal to 0 everywhere [3]. Such a surface is called *developable* and its mapping into the plane is its *development*. Every point on a developable surface has a straight line through it that lies in the surface. These lines are called the generators of the surface. There are four kinds of developable surfaces: planes, cylinders, cones, and tangent surfaces (see Figure 1). The cones or cylinders are understood to be generalized: their cross sections are smooth but not necessarily circular. A tangent surface is derived from an arbitrary smooth space curve. It contains the curve and the tangent lines to the curve form the generators of the surface.

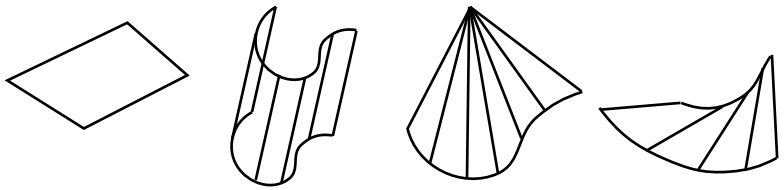

Figure 1. Four kinds of developable surfaces.

Developable surfaces have been studied extensively by automotive, aeronautical, and nautical engineers [1,2,4]. They have important applications in the manufacture of auto bodies, airplane wings and fuselages, and ships' hulls. But most of these studies have limited value to the origamist who wishes to design curved models, because the typical manufacturing application involves the design of a single developable surface, or possibly multiple surfaces that are assembled from separate sheets of material, whereas the paper folder usually desires to create multiple different developable surfaces from a single sheet of paper. Results involving creased developable surfaces are less common [5,7,9].

In designing curved origami models I use two distinct approaches that I call *analysis* and *synthesis*. In analysis you make specific creases (e.g., circular arcs) in a sheet of paper and fold along them, usually subjecting them to additional symmetry constraints. You then analyze the result to discover its shape. In synthesis you decide what shape you would like to fold and then derive the equations for the creases that create your shape. In some cases the approach may be hybrid: you begin with some known creases and constraints, and then analyze the shape that a portion of the paper will form. This shape determines where the rest of the paper must go and you derive the additional creases from that.

The *Orb* model (Figure 2, left) is an example of the first approach and was analyzed in an earlier paper [10]. *Arcturus* (Figure 2, right) is an example of synthesis and its derivation will be sketched below. The *Bud* (Figure 3) is a hybrid model, which I designed by starting with four overlapping half circles forming the four gores of an egg-shaped object. I calculated the equations governing its shape in space and used that to determine where the additional curves must go to allow the rest of the paper to be folded aside.

These models suggest the following problem: given two developable surfaces, how can you fold both of them from a single sheet of paper? If you take their developments and embed them in the same plane with enough space between them, you should be able to fold the excess paper "out of the way" somehow to create the desired surfaces, as in the *Bud*.

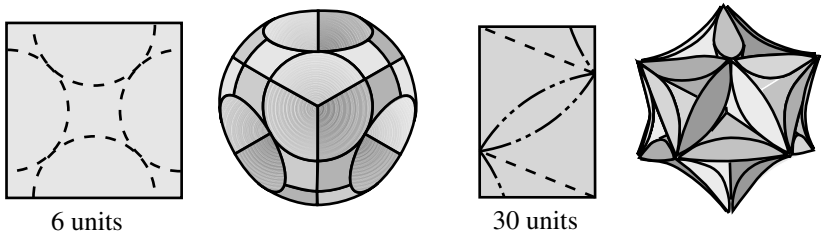

Figure 2. The *Orb* (left) and *Arcturus* (right) and their crease patterns.

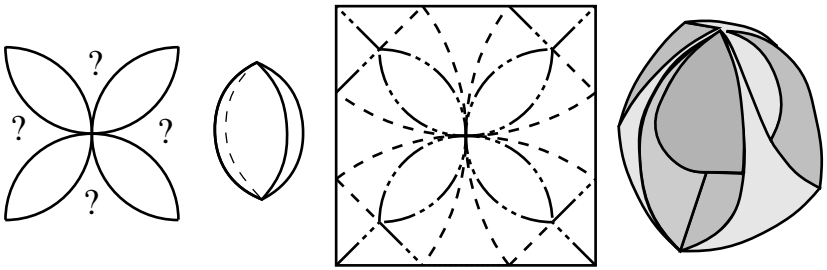

Figure 3. Designing the *Bud*.

But sometimes you want to make the transition directly from one surface to another. For this to work the two surfaces must share a common boundary not only in space, but also when they are developed in the plane. This rarely happens.

It is not hard to see, however, that a given developable surface may be folded along a curved edge to create a surface on the other side that meets certain desired criteria. For example, a cylinder can be folded so that a second cylinder is formed opposite the crease, subject to the constraint that its generators are all parallel to a given vector. In fact, the solution is not even unique, and additional constraints may be imposed. Likewise, a cone may be folded to form a cylinder on the other side of the crease, subject to a similar constraint. A cylinder may be folded to create a cone subject to its containing a particular generator or having a specified apex. (See Figure 4.) In this paper, I do not enumerate all such transitions and the constraints upon them; I merely provide an example of how a typical problem, involving a cone and a cylinder, can be solved.

Suppose that you have a cone defined by its apex $\mathbf{P} = (h, 0, 0)$ and a parametric curve $\mathbf{c}(u)$ lying in the xy-plane, where $\mathbf{c}(u)$ is defined for $0 \leq u \leq 1$. The surface is given by

$$\mathbf{s}(u, v) = v\mathbf{c}(u) + (1 - v)\mathbf{P} \; for \; 0 \leq u, v \leq 1.$$

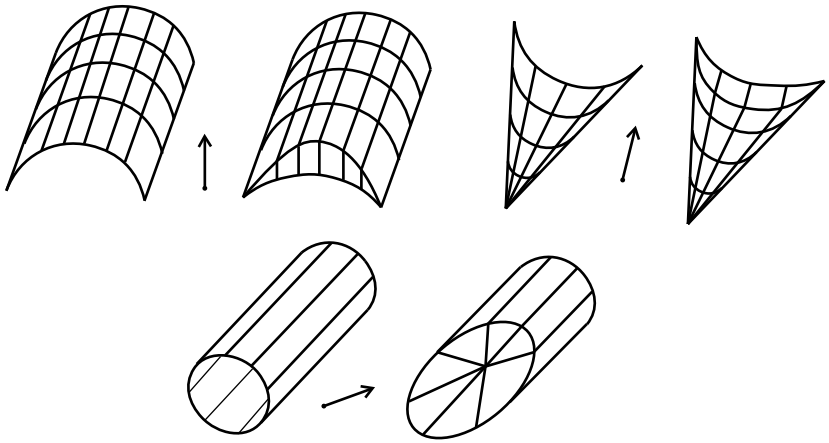

Figure 4. Some cone and cylinder surface transitions.

Further suppose that $\mathbf{c}(u)$ has been chosen such that when $\mathbf{s}(u, v)$ is flattened, the angle subtended by the edges that meet at the apex is $\pi/4$. Now consider a subset of $\mathbf{s}$ such that its development is the right isosceles triangle shown in Figure 5.

We want to find a curve $\mathbf{c}_1$ in the cone $\mathbf{s}$ such that, if we crease along it, the surface formed on the other side is a cylinder with the constraint that its generators are parallel to the y-axis, as shown in Figure 6. The goal here is to be able to fold two mirror image cones back to back from a single sheet of paper, with the cylinder section making the transition between them. For this to work, we additionally require that the line $\mathbf{d}_2$ is the development of $\mathbf{c}_2$, the projection of $\mathbf{c}_1$ onto the xz-plane. Our fold will be along the curve $\mathbf{d}_1$, the development of $\mathbf{c}_1$. Because we are dealing with a cone, it is easiest to express $\mathbf{d}_1(u)$ in polar coordinates $(r(u), \theta(u))$.

First we find the function $\theta(u)$. Note that, for each u_0, the generator $\mathbf{s}(u_0, v) = v\mathbf{c}(u_0) + (1 - v)\mathbf{P}$ maps to the line $\theta = \theta(u_0)$. Let $\mathbf{n}(u) = (\mathbf{c}(u)-\mathbf{P})/\|\mathbf{c}(u)-\mathbf{P}\|$. This curve lies in the cone and has the property that every point on it is at distance 1 from the apex $\mathbf{P}$. Thus, the development of $\mathbf{n}$ is the circular arc of radius 1, as shown in Figure 7, and the angle $\theta(u_0)$ is the arc length of $\mathbf{n}(u)$ from $u = 0$ to $u = u_0$. Hence,

$$\theta(u_0) = \int_0^{u_0} \sqrt{\mathbf{n}'(u) \cdot \mathbf{n}'(u)}\, du.$$

Earlier we supposed that $\mathbf{c}(u)$ was chosen so that its development subtended the angle $\pi/4$ at the cone's apex, without giving any hint as to how

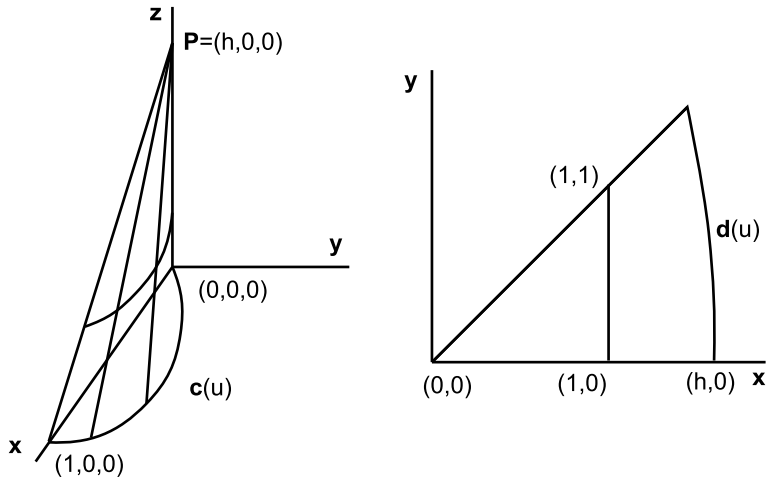

Figure 5. A subset of a cone (left) and its development in the plane (right).

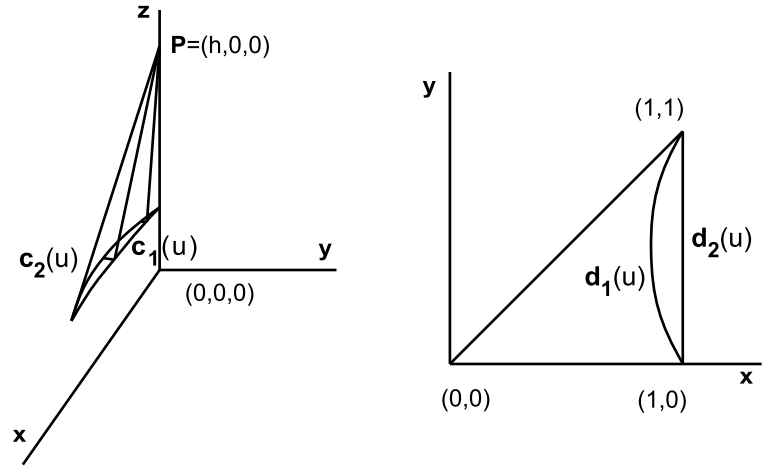

Figure 6. The cone folded through a curved crease (left) and its development in the plane (right).

this might be achieved. That angle is just $\theta(1)$, so if $c(u)$ is chosen from a known family of curves, then some parameters defining the curve (e.g., the coefficients of a polynomial) can be adjusted to produce the desired result.

Consulting Figure 7 again we see that

$$\frac{r(u)}{y} = \frac{\|\mathbf{c}(u) - \mathbf{P}\|}{\mathbf{c}_y(u)}$$

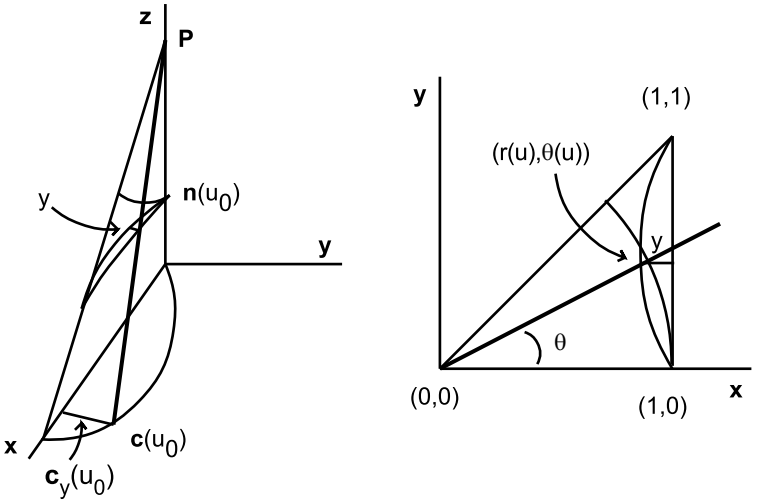

Figure 7. Calculating the crease in polar coordinates.

by similarity of triangles. Furthermore,

$$y = 1 - r(u)\cos(\theta(u)).$$

Solving for r we get

$$r(u) = \frac{1}{\mathbf{c}_y(u)/\|\mathbf{c}(u) - \mathbf{P}\| + cos(\theta(u))},$$

which concludes the derivation of our curved crease $\mathbf{d}_1$.

The *Arcturus* model is derived in much the same way, with some minor differences. The thirty units are arranged with icosahedral symmetry and each is composed of three developable surfaces: two mirror symmetric cone sections connected by a cylinder section. The cone sections must be chosen so that the two edges that meet at the apex subtend the angle $2\tan^{-1}(\phi^{-2})$, where ϕ is the golden ratio, and the dihedral angle between the tangent planes of the two cones at their shared edges is less than or equal to $\pi/5$. These constraints determine our choice of the curve $\mathbf{c}$. Many such curves can be found—any one will do. We see from the crease pattern in Figure 8 that the unit's development is an isosceles triangle, as in our example, but the curved crease lies along the base of the triangle, rather than along one of its legs. Hence, the equations defining $\mathbf{d}_1$ will be a little different.

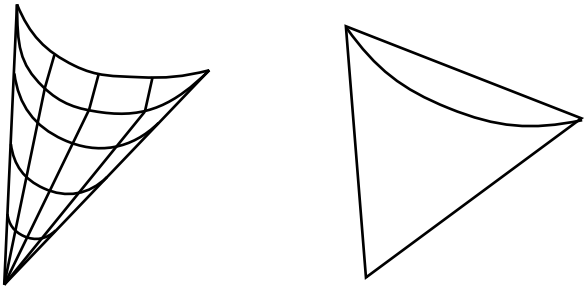

Figure 8. Half of an *Arcturus* unit (left) and its crease pattern (right).

2 Conclusions

At first glance, the task of designing curved origami to produce a desired shape, as opposed to simply making some curved creases and seeing what shape they form, may seem daunting. But as we have seen, some basic techniques from multivariable calculus can be used to solve some interesting design problems. More work needs to be done to determine the range of problems solvable by these methods.

Acknowledgment. This research was funded in part by a grant from the Cookie Jar Fund of the Institute for Figuring (www.theiff.org). Some software used was provided by Steve Wolfram of Wolfram, Inc. (www.wolfram.com).

Bibliography

[1] R. M. C. Bodduluri and B. Ravani. "Design of Developable Surfaces Using Duality between Plane and Point Geometries." *Computer Aided Design* 25:10 (1993), 621–632.

[2] John C. Clements and L. J. Leon. "A Fast, Accurate Algorithm for the Isometric Mapping of a Developable Surface." *SIAM J. Math. Anal.* 18:4 (1987), 966–971.

[3] I. D. Faux and M. J. Pratt. *Computational Geometry for Design and Manufacture*. Chichester, UK: Ellis Horwood Limited, 1979.

[4] L. W. Ferris. "A Standard Series of Developable Surfaces." *Marine Technology* XX (1968), 52–62.

[5] D. Fuchs and Serge Tabachnikov. "More on Paperfolding." *American Mathematical Monthly* 106:1 (1999), 27–35.

[6] Herman van Goubergen. "Curler Units." *British Origami* 205 (2000), 17.

[7] D. A. Huffman. "Curvature and Creases: A Primer on Paper." *IEEE Transactions on Computers* C-25:10 (1976), 1010–1019.

[8] Paul Jackson. *The Encyclopedia of Origami and Papercraft Techniques.* Philadelphia: Running Press, 1991.

[9] Martin Kilian, S. Floery, Z. Chen, N. J. Mitra, A. Sheffer, and H. Pottmann. "Curved Folding." *ACM SIGGRAPH* 27:3 (2008), 75-1–75-9.

[10] J. Mosely. "The Validity of the Orb." In *Origami^3: Proceedings of the Third International Meeting of Origami Science, Mathematics, and Education*, edited by Thomas Hull, pp. 75–82. Natick, MA: A K Peters, 2002.

Folding Curves

Robert Geretschläger

1 Introduction

In this paper, I would like to present some basic results pertaining to the "folding" of curves in origami. Whereas most practical origami consists of linear folding—all creases created by folding are line segments—creating a curved crease is certainly not unheard of. Under most normal circumstances, creating such a curved crease is a mistake, an accidental slip of the hand or paper. It is, however, quite possible to "fold" paper while moving it continuously during the process, creating a planned curved crease.

For the purpose of this paper, I will assume that the folding medium is always finite (generally limited by a square, as is most commonly the case in practical origami) and that both the curve on the flat paper that is to be folded (which I will refer to as the *fold*) as well as the resulting spatial curve (referred to as the *crease*) are continuously differentiable. Folding such curves is, in fact, not at all difficult.

An initial attempt at such a maneuver immediately shows us the first big difference from "normal" linear folding: the paper does not remain flat. In fact, neither part of the paper delineated by the crease can remain flat if a curve is folded. (This intuitively obvious fact follows from Theorem 1 in the next section.) Taking a closer look at such a creased piece of paper immediately suggests several questions. Which curves can be folded and what types of surfaces are created by the paper? What is the relationship between the two curved surfaces delineated by the resulting crease? If a specific plane curve is given as the fold, which surfaces can result? Which

spatial curve (crease) will the fold twist into? As it turns out, the answer to the first question is: most everything, within reason. (Only developable surfaces can result, for instance, but this is obvious.) In fact, much of the theory needed can be readily derived from standard results in differential geometry, as we shall see. Some very nice pictures of certain curved folds can be created using mathematical software. (For this paper, I use Mathematica 3.0 for all three-dimensional graphics.)

2 Simple Sine Curves and Cylinders of Rotation

Example 1. I would like to begin with a folding experiment. Assume a unit folding square as our folding medium and a system of cartesian coordinates (u, v) as shown in Figure 1(a) with origin in the midpoint of one side and the u-axis on the side. We wish to fold the curve represented by the equation

$$f(u) = \frac{1}{\pi} \cdot \cos \pi u,$$

such that the section of the folding square between the curve and the u-axis is transformed into part of a cylinder of rotation as shown in Figure 1(b).

The bottom line AB of the folding square is transformed into a semicircle in the yz-plane with radius $\frac{1}{\pi}$, and the maps of the points $A\left(-\frac{1}{2}, 0\right)$, $M(0,0)$, and $B\left(\frac{1}{2}, 0\right)$ are $A'\left(0, -\frac{1}{\pi}, 0\right)$, $M'\left(0, 0, \frac{1}{\pi}\right)$, and $B'\left(0, \frac{1}{\pi}, 0\right)$, respectively. The point $H\left(0, \frac{1}{\pi}\right)$, in which the fold intersects the v-axis, maps to $H'\left(-\frac{1}{\pi}, 0, \frac{1}{\pi}\right)$ on the crease, since $M'H'$ is a generator (ruling) of the resulting cylinder.

A point $P\left(u, \frac{1}{\pi}\cos \pi u\right)$ on the fold is mapped to the point $P'\left(-\frac{1}{\pi}\cos \pi u\,, \frac{1}{\pi}\sin \pi u, \frac{1}{\pi}\cos \pi u\right)$ on the crease. All such points P' lie in the plane $A'B'H'$: $x + z = 0$, and we see that the resulting crease $\mathbf{c}$ is a plane curve.

Folding the paper in this way yields a shape as shown from two distinct viewpoints in Figure 2.

Taking a closer look at this result, it appears that the larger section of the paper has also been transformed into part of a cylinder. In fact, this must be the case. Since the plane $x + z = 0$ containing the crease $\mathbf{c}$ bisects the angle between the coordinate planes xy and yz, we can also obtain this shape by cutting the original curved paper as shown in Figure 1(b), flipping the rear section, and pasting it to the front as shown in Figure 2. The half ellipse we obtain as a result of the plane section will certainly lie on both cylindrical sections because of the 45° angles between the plane of $\mathbf{c}$ and the coordinate planes.

Obviously, this is a very special case. The type of spatial symmetry we have here will not exist for very many folds. Fortunately, we can also

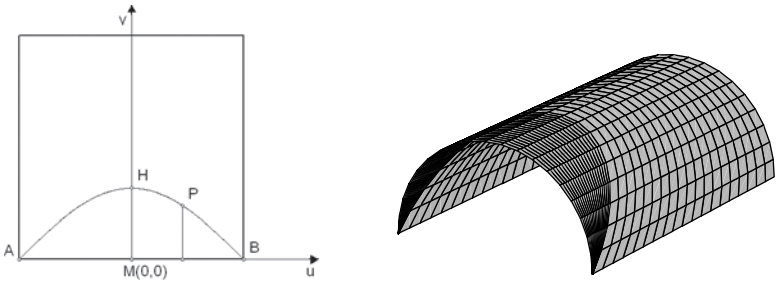

(a) (b)

Figure 1. The cosine curve (a) in the plane and (b) on a half cylinder.

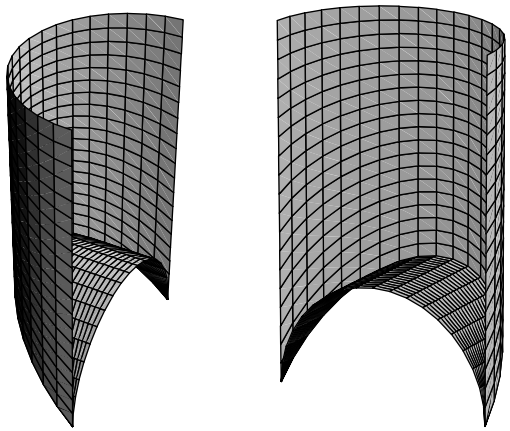

Figure 2. Two views of the folded half cylinder.

consider the result of our experiment in the light of some well-established results of differential geometry. This will give us ideas on how to proceed for other curves and surfaces.

The most important result in the background for all computations to follow is the following:

Theorem 1. *In all points of a crease curve* $\mathbf{c}$ *with parameter* t *in a developable surface, the osculating plane of* $\mathbf{c}$ *in the point* $\mathbf{c}(t)$ *is a bisector plane of the two tangent planes of the surface in the point* $\mathbf{c}(t)$.

A complete proof of this theorem can be found in [2, p. 418].

It is clear that the situation described in Theorem 1 is the result of some curved folding of a plane surface, since a developable surface is precisely

the result of the "bending" of a plane. The spatial curve $\mathbf{c}$ is the result of some mapping of a plane curve c_p, which is used as a template for the crease.

An immediate consequence is the following:

Lemma 1. *If a continuously differentiable finite crease curve* $\mathbf{c}$ *divides a developable surface* S *into two sections* S_1 *and* S_2*, one of which is part of a plane* π*,* $\mathbf{c}$ *is a line segment.*

Proof: If $\mathbf{c}$ is not a line segment, the osculating plane in every point of $\mathbf{c}$ is identical to π. Let S_1 be part of the plane π. By Theorem 1, this means that the tangent planes of S_2 are all symmetric to the tangent plane π of S_1 with respect to the osculating plane of $\mathbf{c} = c_p$ with respect to π, and therefore equal to π. Any such surface must be identical to π. If there is to be a crease at all, S_1 and S_2 must overlap somewhat. If $\mathbf{c}$ has positive curvature in some point of S_1, it must simultaneously have equal negative curvature, since it also lies in S_2. This is impossible, and the curvature of $\mathbf{c}$ must therefore be equal to 0 everywhere, contradicting the assumption that it is not a line segment. □

As a direct consequence of Theorem 1, we see that any curved fold that results in a plane crease $\mathbf{c}$ yields a surface divided into two symmetric sections by the plane in which $\mathbf{c}$ lies, whereby the plane of $\mathbf{c}$ is the plane of symmetry. This follows from the fact that the tangent planes are all symmetric with respect to this plane, and the surface determined as envelope of its tangent planes is unique.

Looking at our experiment once more, we see that the two cylindrical sections determined by folding the curve in question are each sections of cylinders of rotation symmetrical with respect to the plane $x + z = 0$ of $\mathbf{c}$. As soon as one section is bent to form part of such a cylinder, the other part must follow suit.

We can also show this in a much more convoluted way, that will, however, have the advantage of showing us the way to calculate the results of more general curved folds. We assume that one section of our folding paper P as delineated by c_p (we name this section P_1) can be bent to a specific section S_1 of a specific developable surface S. This process maps c_p onto the spatial curve $\mathbf{c}$ on S, and the tangent planes of the developable surface S_2 that results from the section $P_2 := P \backslash P_1$ of the paper can be derived by applying Theorem 1. If $\mathbf{c}(t)$ is a point on $\mathbf{c}$, we can determine both the tangent plane $\tau(t)$ of S in $\mathbf{c}(t)$ and the osculating plane ω_t of $\mathbf{c}$ in $\mathbf{c}(t)$. The tangent plane $\tau_2(t)$ of S_2 in $\mathbf{c}(t)$ is then the plane symmetric to the tangent plane of S in $\mathbf{c}(t)$ with respect to the osculating plane of $\mathbf{c}$ in $\mathbf{c}(t)$.

Letting t vary over the appropriate interval, we obtain S_2 as (a section of) the envelope of all resulting planes $\tau_2(t)$.

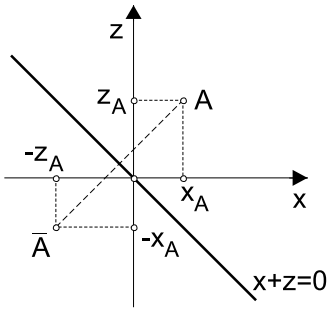

Figure 3. Projection in the direction of the tangent of c.

In this specific case, the osculating plane is always the plane of $\mathbf{c}$, of course. S_1 is the front section of the cylindrical paper. By Theorem 1, the section of the folding square above the curve

$$f(u) = \frac{1}{\pi} \cdot \cos \pi u$$

is transformed into part of the envelope of all planes symmetric to the tangent planes of the cylinder with respect to the plane containing $\mathbf{c}$, and we can calculate S_2 by applying this property.

The tangent plane τ_p of the cylinder in P' is perpendicular to the vector $(0, \sin \pi u, \cos \pi u)$, and is therefore represented by the equation

$$\tau_p : \ (\sin \pi u) \cdot y + (\cos \pi u) \cdot z = \frac{1}{\pi}.$$

We now note that reflecting a point $A(x_A, y_A, z_A)$ with respect to the plane $x + z = 0$ yields the point $\overline{A}(-z_A, y_A, -x_A)$ as shown in Figure 3.

Since reflection of a vector $\overrightarrow{OA}$ with respect to this plane yields $\overrightarrow{O\overline{A}}$, and P' lies in both τ_p and the plane $\overline{\tau_p}$ symmetric to τ_p, we have

$$\overline{\tau_p} : -(\cos \pi u) \cdot x + (\sin \pi u) \cdot y = \frac{1}{\pi}.$$

In order to determine the generators of the envelope of all such planes $\overline{\tau_p}$, we first consider the fact that the generator contained in $\overline{\tau_p}$ is perpendicular to the normal vector $(-\cos \pi u, \sin \pi u, 0)$. Simultaneously, it is almost perpendicular to the normal vector of the nearby plane

$$\overline{\tau_{p;\varepsilon}} : -(\cos \pi(u + \varepsilon)) \cdot x + (\sin \pi(u + \varepsilon)) \cdot y = \frac{1}{\pi}.$$

The vector can therefore be calculated as

$$\lim_{\varepsilon \to 0} (-\cos \pi u, \sin \pi u, 0) \times (-\cos \pi(u + \varepsilon), \sin \pi(u + \varepsilon), 0) = k \cdot (0, 0, 1)\,.$$

(Note that we are ignoring the fact that k in fact tends to 0, as we are only interested in the direction of the vector.) We see that, in this simple case, all generators are vertical, and we have once again shown that the section S_2 of the paper is cylindrical, with vertical generators.

In order to calculate specific creases $\mathbf{c}$ and surfaces S_2 if folds c_p and surfaces S_1 are given, the following theorems are quite useful.

Theorem 2. *Assume that we are given a plane curve c_p and a space curve $\mathbf{c}$ each parameterized with the arc-length parameter such that the absolute value of the curvature of c_p in every point $c_p(u)$ is less than that of $\mathbf{c}$ in the corresponding point $\mathbf{c}(u)$. Then there exist exactly two extensions of the function f mapping $c_p(u)$ to $f(c_p(u)) = \mathbf{c}(u)$ to isometric embeddings of a plane neighborhood of c_p to space.*

It is obvious that this means that essentially any reasonable plane fold can become any crease in space, as long as the relevant curvatures increase for every point of the curve.

A proof can be found in [1]. It is worth noting that the proof essentially relies only on knowledge of the fact that the geodesic curvature κ_g in some point P of a curve $\mathbf{c}$ on a surface S and its curvature κ in P are related by $\kappa_g = \kappa \cdot \cos\alpha$, whereby α is the angle between the tangent plane of S in P and the osculating plane of $\mathbf{c}$ in P. (Recall that, since the curvature is the reciprocal of the curvature radius ρ, this is equivalent to $\rho = \overline{\rho} \cdot \cos\alpha$, whereby ρ is the curvature radius of $\mathbf{c}$, and $\overline{\rho}$ can be thought of as either the curvature radius of the curve resulting from $\mathbf{c}$ on the development of the surface or the curvature radius of the orthogonal projection of $\mathbf{c}$ onto the tangent plane of the surface in P.)

For practical calculations, we will also find the following quite useful:

Theorem 3. *Let S be a developable surface and $\mathbf{c} = P(u)$ be a curve on S with parameter u and points $P(u)$ on S. Further assume that the tangent planes of S in all points $P(u)$ are given by $\vec{n}(u) \cdot \vec{x} = d(u)$, and that all normal vectors $\vec{n}(u)$ are known. Let*

$$\vec{n}(u) = (f(u), g(u), h(u))$$

with f, g, h all continuously differentiable. Then the generator of S in the point $P(u)$ has the direction vector

$$(g'(u)h(u) - g(u)h'(u), h'(u)f(u) - h(u)f'(u), f'(u)g(u) - f(u)g'(u)).$$

Proof: This is, of course, a generalization of the idea presented at the end of Example 1.

Since $\vec{n}(u)$ is perpendicular to the tangent plane in $P(u)$, it is also perpendicular to the generator of S in $P(u)$. The same is true for $\vec{n}(u+\varepsilon)$ in the nearby point $P(u+\varepsilon)$. Since these two generators are arbitrarily close together (assuming that ε is sufficiently small), the direction of the common perpendicular $\vec{n}(u)\times\vec{n}(u+\varepsilon)$ is already quite close to the direction of the generator in $P(u)$, and letting ε tend to zero will yield a vector in the direction of the generator. Calculation yields

$$\begin{aligned}
&(f(u+\varepsilon), g(u+\varepsilon), h(u+\varepsilon)) \times (f(u), g(u), h(u)) \\
&\quad = (g(u+\varepsilon)h(u) - g(u)h(u+\varepsilon), h(u+\varepsilon)f(u) - h(u)f(u+\varepsilon), \\
&\qquad f(u+\varepsilon)g(u) - f(u)g(u+\varepsilon)) \\
&\quad = \varepsilon \cdot \left(\frac{g(u+\varepsilon)h(u) - g(u)h(u+\varepsilon)}{\varepsilon}, \ldots, \frac{f(u+\varepsilon)g(u) - f(u)g(u+\varepsilon)}{\varepsilon} \right).
\end{aligned}$$

The factor ε is irrelevant to the direction of the vector and can therefore be ignored. In the x-coordinate, we see that

$$\begin{aligned}
2 \lim_{\varepsilon\to 0} \frac{g(u+\varepsilon)h(u) - g(u)h(u+\varepsilon)}{\varepsilon} &= h(u) \cdot \lim_{\varepsilon\to 0} \frac{g(u+\varepsilon) - g(u)}{\varepsilon} \\
&\quad + \; g(u) \cdot \lim_{\varepsilon\to 0} \frac{h(u) - h(u+\varepsilon)}{\varepsilon} \\
&= g'(u)h(u) - g(u)h'(u)
\end{aligned}$$

holds, and since the analogous results hold for the other two coordinates, the claim follows. □

Example 2. We are now ready to generalize Example 1 somewhat. Let the paper, the cylinder to which we transform the lower half, and the system of coordinates be as before, with the sole exception that the function f on the folding square is now given by the equation

$$f(u) = p \cdot \cos \pi u, \quad \text{with} \quad 0 < p < 1.$$

Of course, this makes Example 1 the special case for $p = \frac{1}{\pi}$. A, B, and M (and thus A', B', and M') remain unchanged, since they are not dependent on the parameter p. Since their coordinates do depend on the value of p, we now have $H(0,p)$, $P(u, p\cos\pi u)$, $H'\left(-p, 0, \frac{1}{\pi}\right)$, and $P'\left(-p\cos\pi u, \frac{1}{\pi}\sin\pi u, \frac{1}{\pi}\cos\pi u\right)$. All points P' still lie in a common plane ε_p, but now we have

$$\varepsilon_p : \frac{x}{p} + \pi z = 0 \qquad \text{or} \qquad \varepsilon_p : x + p\pi z = 0.$$

Since $\mathbf{c}$ is still a plane curve, S_2 must again be part of the cylinder symmetric to the cylinder on which S_1 lies.

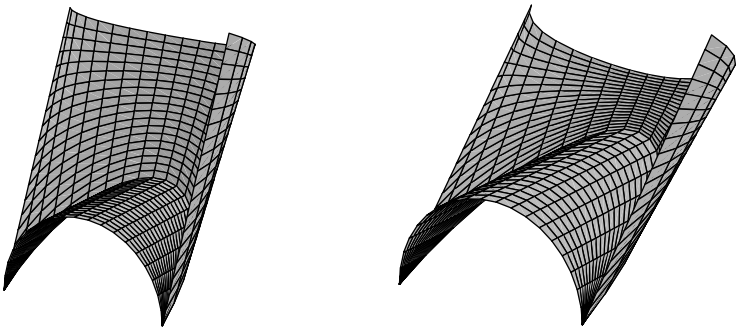

Figure 4. Resulting surfaces for $p = 0.5$ (left) and $p = 0.8$ (right).

Figure 4 shows the resulting surfaces for p equal to 0.5 and 0.8.

Once again, we can also calculate S_2 as the envelope of its tangent planes.

The tangent plane of the cylinder in P' is still

$$\tau_P : (\sin \pi u) \cdot y + (\cos \pi u) \cdot z = \frac{1}{\pi},$$

but these planes must now be reflected with respect to ε_p in order to obtain tangent planes of the upper section S_2 of the folded paper.

In Example 1, we saw that reflecting a point $A(x_A, y_A, z_A)$ with respect to the plane $x + z = 0$ yields the symmetric point $\overline{A}(-z_A, y_A, -x_A)$. A bit of calculation shows us that reflecting A with respect to a plane ε_p : $x + p\pi z = 0$ yields the symmetric point

$$\overline{A}\left(\frac{p^2\pi^2 x_A - x_A - 2p\pi z_A}{p^2\pi^2 + 1}, y_A, \frac{-p^2\pi^2 z_A + z_A - 2p\pi x_A}{p^2\pi^2 + 1}\right).$$

(Note that the special value $p = \frac{1}{\pi}$ yields the simpler values of Example 1.)

As in Example 1, reflection of a vector $\overrightarrow{OA}$ with respect to this plane yields $\overrightarrow{\overline{OA}}$, and since $P'\left(-p\cos\pi u, \frac{1}{\pi}\sin\pi u, \frac{1}{\pi}\cos\pi u\right)$ lies in both τ_P and $\overline{\tau_P}$, the plane $\overline{\tau_P}$ symmetric to τ_P with respect to ε_p is therefore

$$\overline{\tau_P} : -\frac{2p\pi \cdot (\cos \pi u)}{p^2\pi^2 + 1} \cdot x + (\sin \pi u) \cdot y + \frac{(1 - p^2\pi^2) \cdot (\cos \pi u)}{p^2\pi^2 + 1} \cdot z = \frac{1}{\pi}.$$

We are now ready to apply Theorem 2 in order to determine the direction vectors of the generators of S_2 through the points P', and some calculation yields

$$\left(1 - p^4\pi^4, -\frac{1}{2}p\pi(1 - p^2\pi^2)\sin 2\pi u, 2p\pi(1 + p^2\pi^2)\right)$$

as the direction vector of the generator in $P(u)$.

With this in mind, we are ready to try a case in which the crease $\mathbf{c}$ is not a plane curve.

3 General Curves and Cylinders of Rotation

What if we wish to consider a general function $f(u)$ (with some reasonable constraints concerning smoothness, i.e., continuous differentiability, convexity, and so on) as the fold? A point P of the fold is then represented by $P(u, f(u))$. If we once again wish to have S_1 be part of a cylinder of rotation as in Examples 1 and 2, we have

$$P'\left(-f(u), \frac{1}{\pi} \cdot \sin \pi u, \frac{1}{\pi} \cdot \cos \pi u\right),$$

and the tangent plane of the cylinder in P' is still

$$\tau_P : (\sin \pi u) \cdot y + (\cos \pi u) \cdot z = \frac{1}{\pi}.$$

In general, the points P' will not all lie in a common plane, and we must therefore determine the osculating plane of the spatial curve resulting from the curve $v = f(u)$ after bending to form S_1.

This involves a straightforward application of standard methods of differential geometry. Since the curve $\mathbf{c}(u)$ is given by $P'(u) = (-f(u), \frac{1}{\pi} \cdot \sin \pi u, \frac{1}{\pi} \cdot \cos \pi u)$, the vector $\frac{d}{du}P'(u)$ points in the direction of the tangent of $\mathbf{c}(u)$ in $P'(u)$ and the vector $\frac{d^2}{du^2}P'(u)$ points in the direction of the principle normal (first normal) of $\mathbf{c}(u)$ in $P'(u)$, i.e., its direction is in the osculating plane of $\mathbf{c}(u)$ in $P'(u)$ and perpendicular to the tangent. This means that the vector $\frac{d}{du}P'(u) \times \frac{d^2}{du^2}P'(u)$ is a normal vector of the osculating plane of $\mathbf{c}(u)$ in $P'(u)$. Since

$$\frac{d}{du}P'(u) = (-f'(u), \cos \pi u, -\sin \pi u)$$

and

$$\frac{d^2}{du^2}P'(u) = (-f''(u), -\pi \sin \pi u, -\pi \cos \pi u)$$

we obtain

$$\frac{d}{du}P'(u) \times \frac{d^2}{du^2}P'(u) = (-\pi, f''(u) \cdot \sin \pi u - \pi f'(u) \cdot \cos \pi u, \\ \pi f'(u) \cdot \sin \pi u + f''(u) \cdot \cos \pi u).$$

Plugging in the coordinates of P' shows us that the equation of the osculating plane in each point $P'(u)$ is therefore

$$-\pi \cdot x + (f''(u) \cdot \sin \pi u - \pi f'(u) \cdot \cos \pi u) \cdot y \\ + (\pi f'(u) \cdot \sin \pi u + f''(u) \cdot \cos \pi u) \cdot z = \pi f(u) + \frac{1}{\pi} f''(u).$$

With this in mind, we are ready for the following.

Example 3. For this example, we once again let the paper, the cylinder to which P_1 is bent to form S_1, and the systems of coordinates be as before, but the function f is now given by

$$f(u) = -2u^2 + \frac{1}{2}.$$

By choosing the function in this way, the fold passes through the two bottom corners and the midpoint of the square as it did in Example 2 for $p = \frac{1}{2}$. A, B, M, A', B', and M' are still as before, but a point $P\left(u, -2u^2 + \frac{1}{2}\right)$ of the fold maps to $P'\left(2u^2 - \frac{1}{2}, \frac{1}{\pi} \sin \pi u, \frac{1}{\pi} \cos \pi u\right)$, and these points P' do not lie in a common plane for $u \in \left[-\frac{1}{2}, \frac{1}{2}\right]$. We therefore cannot apply any of the methods relating to symmetry with respect to the planes of the crease as in the previous examples, but must use the more general method of reflecting the tangent plane in each point in the osculating plane of the crease in that point, and then determining the envelope of the set of tangent planes of S_2 determined in this way.

The tangent plane in P' is

$$\tau_P : (\sin \pi u) \cdot y + (\cos \pi u) \cdot z = \frac{1}{\pi},$$

as was stated above, and plugging into the formula for the osculating plane yields the expression

$$-\pi \cdot x + (4\pi u \cos \pi u - 4 \sin \pi u) \cdot y \\ + (-4 \cos \pi u - 4\pi u \sin \pi u) \cdot z = -2\pi u^2 + \frac{\pi}{2} - \frac{4}{\pi}$$

as the equation of the osculating plane of the crease $\mathbf{c}$ in P'. Some calculation (best left to the computer, since the expressions involved are quite large) yields the equation of the tangent plane of S_2 in P', and application of Theorem 3 then yields the direction vector of the generator of S_2 in P'.

With these results in hand, we are able to generate a picture of the result of the described fold, and we see such a picture in Figure 5.

Note that this picture is not limited to the part of the resulting surface S_2 that is actually obtained by folding a square. This would only be a

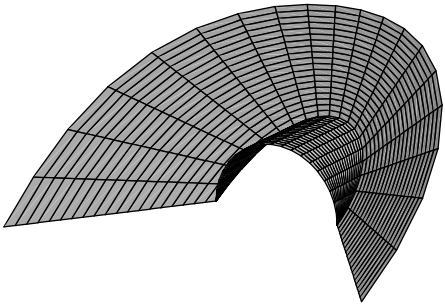

Figure 5. Fold to a half cylinder for $f(u) = -2u^2 + 1/2$.

part of the surface in the picture, but we can see in this picture that the result of the described fold is very similar to that described in Example 2 for $p = \frac{1}{2}$, as we would expect.

4 An Example on a Cone

In the three previous examples, the bottom section P_1 of the surface has always been bent to fit part of a cylinder. For obvious reasons, a cylinder seems to be the easiest type of developable surface for which to develop the calculations in this context. Just as it would seem to be interesting to have a look at bending to some type other than a cylinder of rotation (a parabolic cylinder seems to be a reasonable candidate), it is now also a natural next step to consider something similar for a cone or a tangent surface.

In the following example, a special cone will be used in place of the cylinders of the previous examples.

Example 4. The aim of this example is simply to produce a picture of the result of folding part of a square to a section of a very specific cone with methods as described so far. Assume that a unit square (i.e., the sides are of length 1) is bent (without any folding, for now) to become part of a (finite) right cone, such that two corners of the unit square (endpoints of a common edge) meet and the other two corners come to lie on diametrically opposite points of the base. The cone and bent square will then look something like what we see in Figure 6.

Some relatively straightforward calculation shows us that the radius r of the base is given by $r = \frac{1}{6} \cdot \sqrt{2 + \sqrt{3}}$, the slant height (i.e., the length of the generators of the cone) s is $s = \sqrt{2 + \sqrt{3}}$, and the height h of the

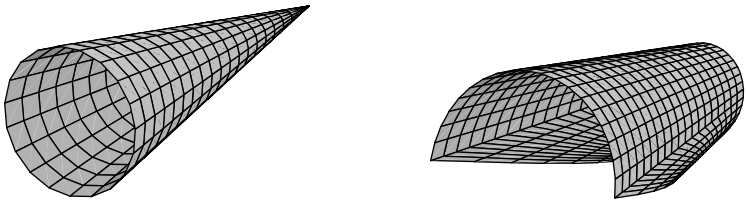

Figure 6. The cone (left) and bent square (right).

cone is therefore $h = \frac{\sqrt{35}}{6} \cdot \sqrt{2+\sqrt{3}}$. Two other views of the resulting bent square are shown in Figure 7.

Especially the right-hand view reminds us of a superhero's cape, giving us an image that might be easier for many to visualize than just a bent square.

A reasonable candidate for a fold on the paper to be bent in this way would now seem to be a curve whose crease would end up as the intersection of the plane $x+z = 0$ with this cone, since we can then use simpler reflection techniques to calculate the result. The algebraic expression for this curve is incredibly complicated, but we can quickly check that the three points

$$\left(0, \pm\frac{1}{6} \cdot \sqrt{2+\sqrt{3}}, 0\right) \quad \text{and} \quad \left(-\frac{1}{7} \cdot \sqrt{2+\sqrt{3}}, 0, \frac{1}{7} \cdot \sqrt{2+\sqrt{3}}\right)$$

all lie both in this plane and on the cone. The result of this fold is shown in Figure 8. (Note that some sections of the paper are shown both in their original position and in the position they go to after reflection, namely, the part of the paper above the xy-coordinate plane before folding. These parts are not actually part of the paper model.)

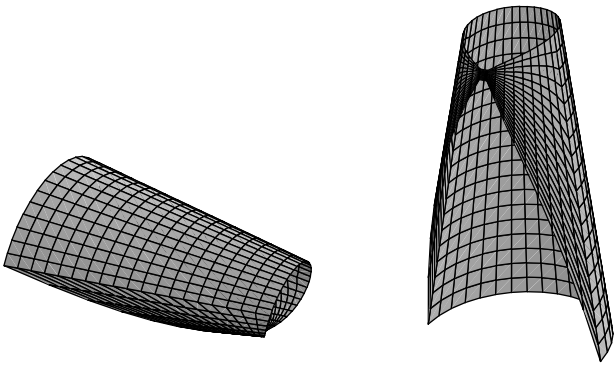

Figure 7. The bent square as a "superhero's cape."

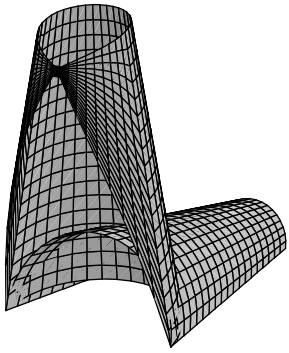

Figure 8. The final result of folding to the cone.

5 Conclusion

In order to fully appreciate these results, it is definitely necessary to do the folds described and compare the paper with the pictures. It is quite interesting to note how much computer power is needed to calculate these graphics; the algebraic expressions involved are quite complex.

One thing that comes to mind from looking at the results of these musings is the idea that curved folds such as those described here could be used much more for the development of concrete origami models. Certainly the "superhero's cape" gives us the impression of an origami model, and it is really just a bent piece of paper, not folded at all. Perhaps this type of calculation could even eventually lead to a whole new class of practical origami models.

Bibliography

[1] Dmitry Fuchs and Serge Tabachnikov. "More on Paperfolding." *The American Mathematical Monthly* 106:1 (1999), 27–35.

[2] Helmut Pottman and Johannes Wallner. *Computational Line Geometry.* Berlin: Springer Verlag, 2001.

The Method for Judging Rigid Foldability

Naohiko Watanabe and Ken-ichi Kawaguchi

1 Introduction

For engineers, the concept of rigid origami is useful in the study of flexible structures. *Rigid origami* is defined as "origami in which each surface surrounded with crease lines neither stretches nor bends," that is, all flexure takes place along well-defined lines. Tom Hull has compared rigid origami to a model of metal plates having hinges instead of creases. The question of rigid foldability is, "can we still fold a given crease pattern, even though each polygon made by crease lines must remain rigid as we fold?"

To formulate and understand a rigid foldable condition, we will compare it with the better-known concepts of *flat foldability* or, equivalently, the *flat foldable condition*. The issue of flat foldability deals with the question "when we can fold a paper flat along the lines of a given diagram, what properties should this diagram have?" or "can we judge whether the crease pattern can fold flat or not from a given diagram?" As two necessary flat foldable conditions, the Kawasaki theorem and the Maekawa theorem are well known. And, the research on flat foldability has expanded by many other people, such as J. Justin, H. Azuma, T. Hull, M. Bern, and B. Hayes [4–8]. Flat foldability deals with the final state of folding. On the other hand, *rigid foldability* deals with the existence (or not) of a continuous route between the first state and the final state.

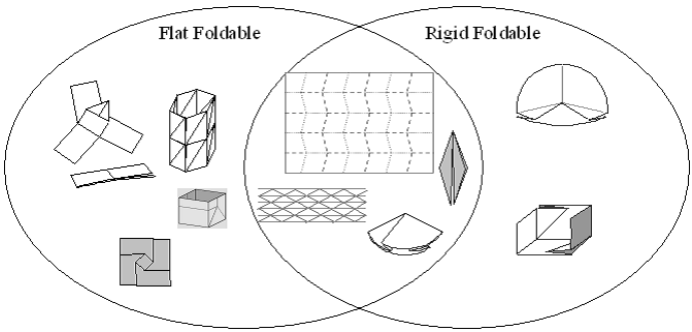

Figure 1. Examples of rigid foldability and flat foldability.

Figure 1 shows specific examples of flat foldable and rigid foldable crease patterns. In many cases, a flat foldable crease pattern is rigid foldable. However, there are several cases that satisfy flat foldable conditions but do not satisfy rigid foldable conditions, for instance, the *twisting fold*. A twisting fold can reach a flat state, but each surface has to be bent during the transition in order to reach the final state. There are many other cases that are rigid foldable but not flat foldable.

Properties of rigid origami have been researched by many as well—D. Huffman [3], K. Miura [9,10], T. Hull, R. Lang [5], and others. Huffman and Miura used Gaussian curvature to study the properties that paper must have to fold in a rigid manner. Lang showed relationships between folding angles in a single vertex of degree 4 using spherical trigonometry.

The rigidity of models made with balls and joints has also been studied as *structural rigidity*. It can be seen as rigid origami in low dimension. The *Maxwell formula* is well known as a property of rigid structures that describes the relationship between a number of balls and joints. But the Maxwell formula, while necessary, is not a *sufficient* condition for structural rigidity. H. Tanaka and H. Hangai have proposed the concepts of *infinitesimal rigidity* and *finite rigidity*, and methods to judge structural rigidity using the matrix constructed from the coordinates and connection of points. They have also proposed a method to find the mode of feasible finite deformations for flexible structures. In this method, Moore-Penrose's generalized inverse matrix is used [2].

R. Connely, E. Demaine, and G. Rote have also researched the question of whether a one-dimensional piece of paper can be folded continuously into a desired folded state without introducing new creases.

However, there is not a general method to judge rigid foldability from a pattern of crease lines assigned mountain-valley status that is analogous to the flat foldable conditions. This paper proposes two practical methods to

judge rigid foldability from an arbitrary pattern of given crease lines. They are the *diagram method* and the *numerical method* and will be explained in this work.

2 Diagram Method

First, we will consider the diagram method and apply it to examples of single-vertex models. We will show how to identify which crease patterns can fold rigidly from parts (a), (d), and (g) in Figure 2 by this diagram method.

Here is the approach. First, replace mountain or valley crease lines with vectors whose directions are, respectively, pointing toward or away from the vertex, as in parts (b), (e), and (h).

Second, proceeding in anticlockwise order around the vertex, connect each vector to the next, head-to-tail, adjusting the lengths of vectors as necessary in order to (if possible) form a closed loop, as shown in parts (c), (f), and (i).

As shown in Figure 2(c), a crease pattern whose vectors cannot make a closed loop cannot fold rigidly. Even if it can form a closed loop, if its oriented area is nonzero as in (i), the crease pattern also cannot fold rigidly. Only when the vectors can make the closed loop, and the vectors' oriented area is zero as in case (f), is the crease pattern one that can fold rigidly. So, in fact, only case (d) is rigid foldable among (a), (d), and (g). This is the diagram method to judge rigid foldability.

3 The Validity of the Diagram Method

The validity of this method is explained with a matrix treatment. Let us consider with an analysis of a single-vertex fold as shown in Figure 3. Here, we suppose that the crease lines on the plane that can fold rigidly are able to make an infinitesimal change of dihedral angle. The crease lines $l_1, l_2, .., l_n$ are enumerated in counterclockwise order beginning from the x-axis. We label each crease line l_i, with a pair of angles (θ_i, ρ_i) where θ_i, ρ_i denotes the plane angle and the supplement of the dihedral angle, respectively.

Let A_i be the matrix corresponding to a rotation in the xy-plane by the plane angle θ_i. Let C_i be the matrix that rotates by the folding angle ρ_i. Now, use $\chi_i = A_i C_i A_i^{-1}$ to denote the counterclockwise rotation of angle ρ_i around the axis corresponding to the crease line l_i in the plane. If a single-vertex crease pattern can fold rigidly, the product of all matrices $\boldsymbol{\chi}_i$

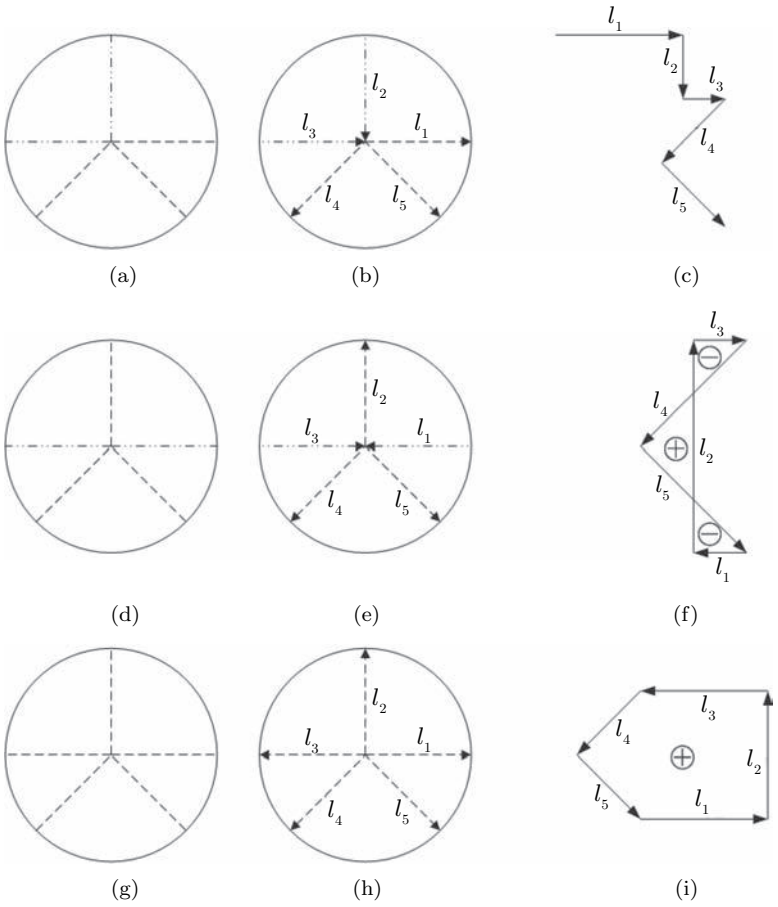

Figure 2. Three examples of the diagram method: crease pattern ((a), (d), (g)), first step ((b), (e), (h)), and second step ((c), (f), (i)).

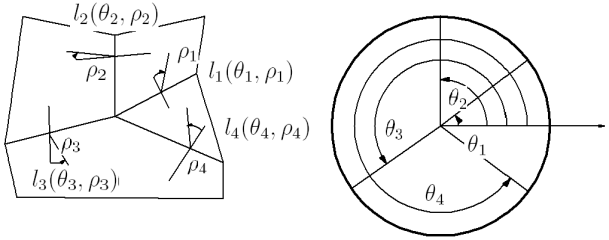

Figure 3. Symbol $l_i(\theta_i, \rho_i)$

must be equal to the identity, $\boldsymbol{I}$. This requirement has been discussed by T. Kawasaki, T. Hull, and s-m. belcastro [1, 7].

Here, specific components of the matrix $\boldsymbol{\chi}_i$ are described as follows:

$$\chi_i = \begin{bmatrix} \cos^2\theta_i + \cos\rho_i \sin^2\theta_i & (1-\cos\rho_i)\sin\theta_i\cos\theta_i & \sin\rho_i\sin\theta_i \\ (1-\cos\rho_i)\sin\theta_i\cos\theta_i & \sin^2\theta_i + \cos\rho_i\cos^2\theta_i & -\sin\theta_i\cos\theta_i \\ -\sin\rho_i\sin\theta_i & \sin\theta_i\cos\theta_i & \cos\rho_i \end{bmatrix}.$$

Now, assume that folding angles ρ are infinitesimal, $\Delta\rho_i$. Then, we can approximate $\cos\Delta\rho_i \simeq 1$ and $\sin\Delta\rho_i \simeq \Delta\rho_i = \epsilon_i$, and so the matrix χ_i is approximately given by

$$\chi_i = \begin{bmatrix} 1 & 0 & \epsilon_i\sin\theta_i \\ 0 & 1 & -\epsilon_i\cos\theta_i \\ -\epsilon_i\sin\theta_i & \epsilon_i\cos\theta_i & 1 \end{bmatrix}.$$

Now, we take the product of the χ_i for $i = 1, 2, \ldots, n$, neglecting the terms of more than second order of ϵ_i. The result of this product of the χ_i can be described as follows:

$$\chi_1\chi_2\cdots\chi_n = \begin{bmatrix} 1-\sum_{\substack{i,j=1\\ i<j}}^{n}\delta_i^s\delta_j^s & \sum_{\substack{i,j=1\\ i<j}}^{n}\delta_i^s\delta_j^c & \sum_{i=1}^{n}\delta_i^s \\ \sum_{\substack{i,j=1\\ i<j}}^{n}\delta_i^c\delta_j^s & 1-\sum_{\substack{i,j=1\\ i<j}}^{n}\delta_i^c\delta_j^c & -\sum_{i=1}^{n}\delta_i^c \\ -\sum_{i=1}^{n}\delta_i^s & \sum_{i=1}^{n}\delta_i^c & 1-\sum_{\substack{i,j=1\\ i<j}}^{n}\delta_i^s\delta_j^s-\sum_{\substack{i,j=1\\ i<j}}^{n}\delta_i^c\delta_j^c \end{bmatrix}.$$

Here, δ_i^s and δ_i^c represent $\epsilon_i\sin\theta_i$ and $\epsilon_i\cos\theta_i$, respectively. Considering that this matrix is equal to the identity $\boldsymbol{I}$, we will consider each component of this matrix.

First, let's note the component of (1,3)(2,3) that includes the term of first order about ϵ_i.

$$\boldsymbol{A\epsilon} = \begin{bmatrix} \cos\theta_1 & \cos\theta_2 & \cdots & \cos\theta_n \\ \sin\theta_1 & \sin\theta_2 & \cdots & \sin\theta_n \end{bmatrix} \begin{bmatrix} \epsilon_1 \\ \epsilon_2 \\ \vdots \\ \epsilon_n \end{bmatrix} = \boldsymbol{0}.$$

This formula corresponds to the requirement that "the vector can draw a closed loop" in the diagram method. We can observe that the terms ϵ_i, which represent infinitesimal folding angles, are vector lengths.

Second, picking out the component (1,1)(1,2)(2,1)(2,2), which includes the terms of second order about ϵ_i, we can make the formula as follows:

$$\boldsymbol{\epsilon}^T\boldsymbol{C\epsilon} = \boldsymbol{0},$$

where $\boldsymbol{C}$ is the matrix

$$\begin{bmatrix} 0 & \cos\theta_1 \sin\theta_2 - \sin\theta_1 \cos\theta_2 & \cos\theta_1 \sin\theta_3 - \sin\theta_1 \cos\theta_3 & \cdots & \cos\theta_1 \sin\theta_n - \sin\theta_1 \cos\theta_n \\ & 0 & \cos\theta_2 \sin\theta_3 - \sin\theta_2 \cos\theta_3 & \cdots & \cos\theta_2 \sin\theta_n - \sin\theta_2 \cos\theta_n \\ & & \vdots & & \\ & sym. & & & 0 \end{bmatrix}$$

This formula corresponds to the requirement that "the directed area drawn by vector is zero." These are necessary conditions for the ϵ_i mode to exist.

4 Numerical Method

We now introduce the numerical method for judging rigid foldability. As we have discussed earlier, if a crease pattern can be folded rigidly,

$$\boldsymbol{A}\boldsymbol{\epsilon} = \boldsymbol{0},$$
$$\boldsymbol{\epsilon}^T \boldsymbol{C}\boldsymbol{\epsilon} = \boldsymbol{0}.$$

Here, $\boldsymbol{A}$ and $\boldsymbol{C}$ are determined by the values of θ_i. The question is whether given values of θ_i and the signs of $\boldsymbol{\epsilon}$ can satisfy these formulae. The signs of $\boldsymbol{\epsilon}$'s mode represent combinations of mountain-valley folds. To solve this question, we use the generalized inverse matrix and the Newton-Raphson method of iteration.

First, the solution of the first formula can be proposed by *orthonormal base in zero-space* as follows:

$$\boldsymbol{\epsilon}' = [I - A^+ A]\boldsymbol{\alpha}.$$

Here, A^+ is the Moore-Penrose generalized inverse matrix of A [2] and $\boldsymbol{\alpha}$ is the combination of mountain-valley given by ± 1. However, this $\boldsymbol{\epsilon}'$ does not, in general, satisfy the second formula. Therefore, using the Newton-Raphson Method, we make $\boldsymbol{\epsilon}$ converged. If $\boldsymbol{\epsilon}$ cannot be converged on a mode with an assumed sign of α_i, this mode of $\boldsymbol{\alpha}$ is not rigidly foldable. On the contrary, if $\boldsymbol{\epsilon}$ can be converged on the same mountain-valley mode as assumed by $\boldsymbol{\alpha}$, this mode is rigid foldable and these components of $\boldsymbol{\epsilon}$ show the feasible mode of infinitesimal folding angles.

5 Multivertex Patterns

Next, let us consider the case of patterns of multiple vertices. In the case of the diagram method, the rigid foldability can be judged from the compatibility of the lengths of vectors. Simple examples are considered in Figure 4;

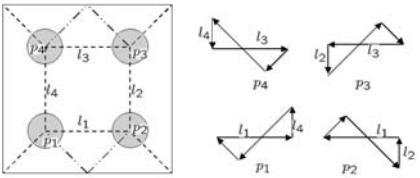

Figure 4. Rigid foldable pattern.

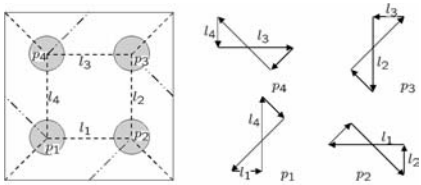

Figure 5. Nonrigid foldable pattern.

in this figure the vector diagrams in each vertex are mutually compatible. By contrast, for each vertex in Figure 5, the vector lengths can be chosen such that each vector diagram can be drawn closed, but, when considering all vertices simultaneously, the relationship of the lengths of vectors are incompatible: we find that $l_1 < l_4$, $l_4 < l_3$, $l_3 < l_2$, and $l_2 < l_1$. In a multivertex pattern, the vectors that represent the same crease line must be the same length. Since this is not possible in Figure 5, this pattern in fact cannot fold without its surface bent.

To apply the numerical method to multivertex patterns, we can judge by considering the formula for each vertex and superposed matrix, as follows:

$$\begin{aligned} \boldsymbol{A}_1\boldsymbol{\epsilon}_1 = 0, \quad & \boldsymbol{\epsilon}_1^T\boldsymbol{C}_1\boldsymbol{\epsilon}_1 = 0, \\ \boldsymbol{A}_2\boldsymbol{\epsilon}_2 = 0, \quad & \boldsymbol{\epsilon}_2^T\boldsymbol{C}_2\boldsymbol{\epsilon}_2 = 0, \\ & \vdots \\ \boldsymbol{A}_n\boldsymbol{\epsilon}_n = 0, \quad & \boldsymbol{\epsilon}_n^T\boldsymbol{C}_n\boldsymbol{\epsilon}_n = 0, \end{aligned}$$

$$[\boldsymbol{A}_{\text{total}}]\{\boldsymbol{\epsilon}_{\text{all}}\} = 0, \qquad \{\boldsymbol{\epsilon}_{\text{all}}\}^T[\boldsymbol{C}_{\text{total}}]\{\boldsymbol{\epsilon}_{\text{all}}\} = 0.$$

These formulas must have a simultaneous solution; if they do not, then the pattern is not rigidly foldable.

6 Application of Numerical Method

The usefulness of the numerical method is shown as follows. For n lines, the number of combinations of possible mountain-valley assignments is 2^n. Using the numerical method, we can identify the rigid foldable pattern (if any) from these total patterns. In this way we can check the validity of the method.

As a first example, consider a single vertex of degree 4 as shown Figure 6. The number of combinations of mountain-valley assignments is 16. In Table 1, the left part shows all combinations of mountain-valley as-

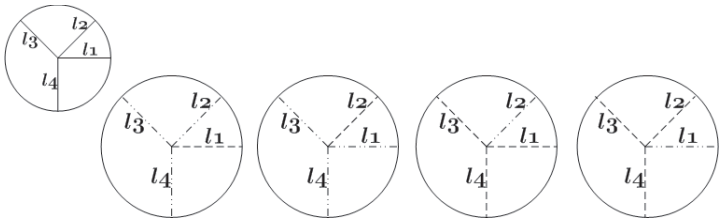

Figure 6. The single vertex having degree 4 (upper left) and four possible mountain-valley assignments.

signments and the supposed mode of $\boldsymbol{\alpha}$. The right part shows the values of converged $\boldsymbol{\epsilon}$. In all combinations, the patterns whose sign of $\boldsymbol{\epsilon}$ agree with $\boldsymbol{\alpha}$ are only the four patterns shown in Figure 6. In fact, the rigidly foldable patterns are only these four patterns. These four patterns also satisfy the flat foldable conditions, which shows that some foldable crease patterns that satisfy the flat foldable condition can also satisfy the rigid foldable condition. And, we can note that $|l_1| = |l_3|$ and $|l_2| = |l_4|$ in absolute value of converged ϵ. This property corresponds to a result shown by Lang [5] (and, implicitly, by Huffman [3]) that opposite dihedral angles of a flat-foldable degree-4 vertex are equal in absolute value.

A second example is a single vertex of degree 5 (Figure 7). From the 2^5 possible patterns, the ten patterns shown are selected as rigid foldable. This example illustrates the fact that a vertex pattern can be rigidly foldable even if it is not flat foldable (since a flat-foldable vertex must have even degree).

pattern No.	Actual Foldability	Input α				Judging Result	Converged ϵ			
		l_1	l_2	l_3	l_4		l_1	l_2	l_3	l_4
1	×	−1	−1	−1	−1	×	−0.007	−0.001	0.000	−0.019
2	✓	1	−1	−1	−1	✓	0.500	−1.207	−0.500	−1.207
3	✓	−1	1	−1	−1	✓	−1.207	0.500	−1.207	−0.500
4	×	1	1	−1	−1	×	−0.013	0.001	0.000	−0.031
5	×	−1	−1	1	−1	×	0.207	−0.500	−0.207	−0.500
6	×	1	−1	1	−1	×	0.019	0.000	0.001	−0.007
7	×	−1	1	1	−1	×	−0.031	0.000	0.001	0.013
8	×	1	1	1	−1	×	0.500	−0.207	0.500	0.207
9	×	−1	−1	−1	1	×	−0.500	0.207	−0.500	−0.207
10	×	1	−1	−1	1	×	0.031	0.000	−0.001	−0.013
11	×	−1	1	−1	1	×	−0.019	0.000	−0.001	0.007
12	×	1	1	−1	1	×	−0.207	0.500	0.207	0.500
13	×	−1	−1	1	1	×	0.013	−0.001	0.000	0.031
14	✓	1	−1	1	1	✓	1.207	−0.500	1.207	0.500
15	✓	−1	1	1	1	✓	−0.500	1.207	0.500	1.207
16	×	1	1	1	1	×	0.007	0.001	0.000	0.019

Table 1. Judging results of a single vertex having degree 4.

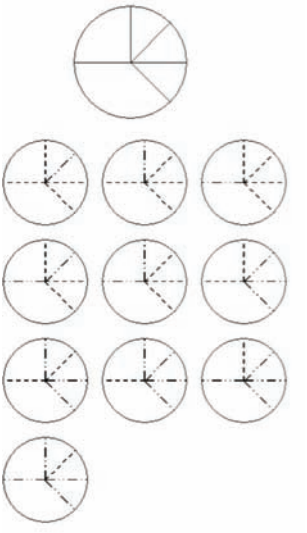

Figure 7. A vertex having degree 5 (top) and the ten rigid-foldable patterns.

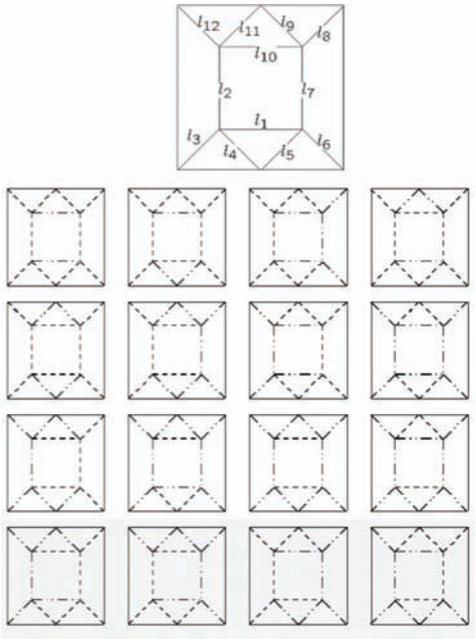

Figure 8. Four-vertices pattern (top) and its flat-foldable patterns.

A third example is the pattern having four vertices of degree four (Figure 8). In this pattern, the mountain-valley combinations satisfying flat foldability total 16. But, the selected patterns that are rigid foldable total only 12 (those not shaded in Figure 8). This means that the other four are patterns that are flat foldable but are not rigidly foldable. In fact, these four patterns cannot be folded without bending some of the surfaces.

7 Conclusion

To summarize, the two methods, diagram method and numerical method, have been presented for judging rigid foldability, and their validity and practicability have been demonstrated by using considerations of infinitesimal deformations. We have illustrated their application with several examples. This system is not complete, however, because we have shown only *necessary* conditions; we have not shown that these conditions are sufficient. We expect that these concepts will be refined further in the future.

Bibliography

[1] s.-m. belcastro and T. C. Hull. "A Mathematical Model for Non-Flat Origami." In *Origami^3: Proceedings of the Third International Meeting of Origami Science, Mathematics, and Education*, edited by Thomas Hull, pp. 39–51. Natick, MA: A K Peters, 2002.

[2] H. Hangai and K. Kawaguchi. *Keitaikaiseki* (Shape Analysis: A Generalized Inverse and Its Applications). Tokyo: Baifukan, 1991.

[3] D. Huffman. "Curvature and Creases: A Primer on Paper." *IEEE Transactions on Computers* C-25:10 (1976), 1010–1019.

[4] T. C. Hull. "The Combinatorics of Flat Folds: A Survey." In *Origami^3: Proceedings of the Third International Meeting of Origami Science, Mathematics, and Education*, edited by Thomas Hull, pp. 29–38. Natick, MA: A K Peters, 2002.

[5] T. C. Hull. *Project Origami*. Wellesley, MA: A K Peters, 2006.

[6] T. Kawasaki. "On High-Dimensional Flat Origamis." In *Proceedings of the First International Meeting of Origami Science and Technology*, edited by H. Huzita, pp. 131–141. Padova, Italy: Dipartimento di Fisica dell'Università di Padova, 1991.

[7] T. Kawasaki. "$R(\gamma) = I$." In *Origami Science and Art: Proceedings of the Second International Meeting of Origami Science and Scientific Origami*, edited by K. Miura, pp. 31–40. Shiga, Japan: Seian University of Art and Design, 1997.

[8] T. Kawasaki. *Rose, Origami and Mathematics*. New York: Kodansha America, 2005. (Originally published in Japanese by Morikita Shuppan, 1998.)

[9] K. Miura. "A Note on Intrinsic Geometry of Origami." In *Proceedings of the First International Meeting of Origami Science and Technology*, edited by H. Huzita, pp. 239–249. Padova, Italy: Dipartimento di Fisica dell'Università di Padova, 1991.

[10] K. Miura. "Fold—Its Physical and Mathematical Principle." In *Origami Science and Art: Proceedings of the Second International Meeting of Origami Science and Scientific Origami*, edited by K. Miura, pp. 41–50. Shiga, Japan: Seian University of Art and Design, 1997.

[11] T. Nojima. "Origami/Harigane Kozo" (Origami/Wire Structure). In *Kozokogaku Handbook* (Structural Engineering Handbook), edited by Yagawa, pp. 819–822, 948–958. Tokyo: Maruzen, 2004.

Simulation of Rigid Origami

Tomohiro Tachi

1 Introduction

Simulation of origami is very important for representing or designing origami via computer. It helps paperfolders to understand the structure of origami models and can be used as a tool for designers to draw diagrams. We propose a system for simulating the folding process from a given crease pattern to the folded base, based on rigid origami simulation (Figure 1).

There have been several approaches for simulating origami. One way is to simulate origami by a sequence of simple folding steps as shown by Miyazaki et al. [5]. Since the final state of an origami model is represented by folding steps, it is easy to reconstruct an animation progressing from a sheet of paper to the finished model. However, the origami models that can be represented in this system are limited by an enforced simplicity of the individual folding steps, and this approach is not suitable for many complex origami models whose folding process cannot be divided into simple folding steps.

Thus, representing origami models by crease patterns seems suitable. ORIPA is a crease pattern editor developed by Mitani [4] that provides an estimation of the folded figure from the crease pattern. The final state with stacking order is estimated, though sometimes the estimation fails. The thickness of paper is included in the representation for better understanding of the structure of the model, but it does not provide intermediate states between the crease pattern and the final shape.

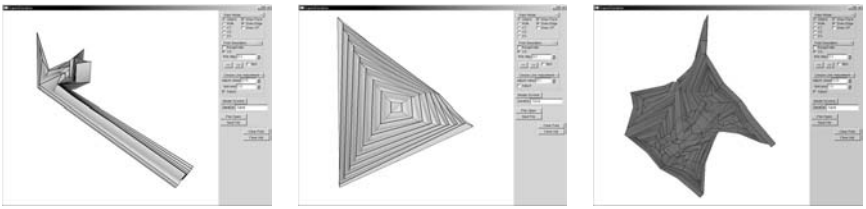

(a) (b) (c)

Figure 1. Screenshots of the simulation program. (a) Base of *Kamehameha Wave* (model by the author). (b) Pleated hypar. (c) Base of *Tachikoma* (model by the author).

It is possible to simulate an intermediate state of folding, by using a rigid origami model, i.e., a model with plates connected by hinges. Resch and Christiansen [6] solved the geometry of a kinematic folded-plate structure based on a combination of elastic analysis and constraints by truss elements. In their method, the configuration is represented by the coordinates of vertices, as opposed to our method representing the configuration with fold angles. Balkcom [1] used a rigid origami model represented by fold angles for origami simulation. His method is based on virtual cutting and a combination of forward and inverse kinematics. The calculation of the trajectory runs fast in this method, but the method was not general enough to provide a system that simulates a folding motion from an arbitrarily given crease pattern.

Our system is based on rigid origami simulation, and uses the crease angles of all fold lines as variables to represent the configuration of an origami model. The simulation method is based on projection onto the constraint space, thus it is possible to use the folding motion of all crease lines as the driving force of folding. This results in a robust overall motion that is not influenced by the degeneracy of vertex coordinates at the flat-folded state or artifacts caused by virtual cutting. Additionally, our system can add flexibility to origami models by adding and adjusting crease lines. With this method, the folding motion of non-rigidly-foldable models can also be simulated.

The system provides a smooth and comprehensible interactive folding animation from a crease pattern to the folded base. This helps users to understand the structure of origami models, and encourages paper folders to fold models from crease patterns. This also indicates the possibility of using crease patterns as a primary medium for publishing origami models.

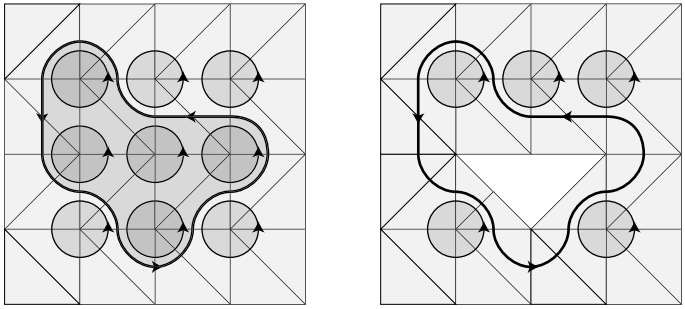

Figure 2. Left: No hole is inside the loop and the constraint is satisfied by the intersection of single-vertex constraints inside. Right: There is a hole inside the paper, around which we need to separately formalize the constraint.

2 Kinematics of Rigid Origami

In our model, an origami configuration is represented by the fold angles of edges (fold lines). Fold angles change according to the mountain-valley assignment of the fold lines when the paper gets folded. These fold lines are connected with facets and form closed loops, and for each closed loop we have a constraint on angle movement. If there is no hole inside the loop, then the constraint is satisfied by the intersection of all constraints by single vertices inside the loop (Figure 2). Our model assumes that the paper has no holes, i.e., is homeomorphic to a disk. The folding motion is numerically calculated using a linear approximation of constraints by single vertices.

Necessary conditions for single-vertex rigid origami shown by belcastro and Hull [2] are used as the constraints of multivertex rigid origami models. Suppose there are n fold lines $\ell_1, \cdots, \ell_n$ connected to the vertex. For a single-vertex origami, the 3×3 matrix constraint function $\mathbf{F}$ of fold angles $\rho_1, \cdots, \rho_n$ is given by

$$\mathbf{F}(\rho_1, \cdots, \rho_n) = \chi_1 \cdots \chi_{n-1} \chi_n = \mathbf{I},$$

where matrices $\chi_1, \cdots, \chi_n$ represent the rotations about fold lines $\ell_1, \cdots, \ell_n$, respectively (Figure 3). Differentiating this equation gives

$$\frac{d\mathbf{F}}{dt} = \frac{\partial \mathbf{F}}{\partial \rho_1}\dot{\rho}_1 + \cdots + \frac{\partial \mathbf{F}}{\partial \rho_i}\dot{\rho}_i + \cdots + \frac{\partial \mathbf{F}}{\partial \rho_n}\dot{\rho}_n = \begin{bmatrix} 0 & 0 & 0 \\ 0 & 0 & 0 \\ 0 & 0 & 0 \end{bmatrix}.$$

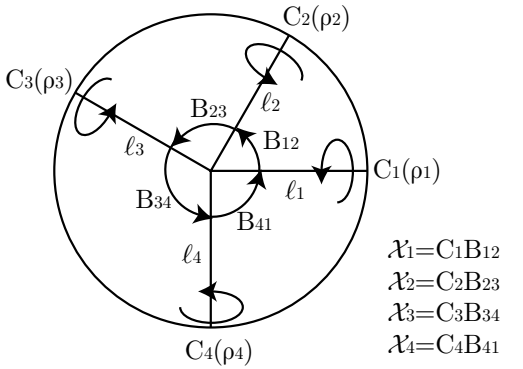

Figure 3. An example of rotation matrices of a single-vertex origami.

We get nine equations (i.e., one for each element of $\mathbf{F}$) for angle movements $\rho_1, \cdots, \rho_n$ represented using a $9 \times n$ matrix:

$$\underbrace{\begin{bmatrix} \frac{\partial \mathbf{F}}{\partial \rho_1}(1,1) & \cdots & \frac{\partial \mathbf{F}}{\partial \rho_n}(1,1) \\ \frac{\partial \mathbf{F}}{\partial \rho_1}(1,2) & \cdots & \frac{\partial \mathbf{F}}{\partial \rho_n}(1,2) \\ \vdots & & \vdots \\ \frac{\partial \mathbf{F}}{\partial \rho_1}(3,3) & \cdots & \frac{\partial \mathbf{F}}{\partial \rho_n}(3,3) \end{bmatrix}}_{9 \times n \text{matrix}} \begin{bmatrix} \dot{\rho_1} \\ \vdots \\ \dot{\rho_n} \end{bmatrix} = \begin{bmatrix} 0 \\ \vdots \\ 0 \end{bmatrix}. \tag{1}$$

However, since $\mathbf{F}$ is a rotation matrix (i.e., orthogonal matrix), the equations are redundant and only three of the nine equations are independent. The partial derivative of an orthogonal matrix $\mathbf{F}$ at $\mathbf{F} = \mathbf{I}$ is a skew-symmetric matrix because

$$\frac{\partial \mathbf{F}}{\partial \rho_i} + \left(\frac{\partial \mathbf{F}}{\partial \rho_i}\right)^{\mathrm{T}}\Bigg|_{\mathbf{F}=\mathbf{I}} = \frac{\partial \mathbf{F}}{\partial \rho_i}\mathbf{F}^{\mathrm{T}} + \mathbf{F}\frac{\partial \mathbf{F}^{\mathrm{T}}}{\partial \rho_i}\Bigg|_{\mathbf{F}=\mathbf{I}} = \frac{\partial}{\partial \rho_i}\left(\mathbf{F}\mathbf{F}^{\mathrm{T}}\right)\Big|_{\mathbf{F}=\mathbf{I}} = \mathbf{0}.$$

The partial derivative of the constraint function is represented in the following form using three independent variables a, b, and c [1]:

$$\frac{\partial \mathbf{F}}{\partial \rho_i} = \begin{bmatrix} 0 & -a & c \\ a & 0 & -b \\ -c & b & 0 \end{bmatrix}.$$

[1] It was later pointed out by Professor Ken'ichi Kawaguchi that a, b, and c are the direction cosines of corresponding fold lines.

We get the following $3 \times n$ matrix instead of the $9 \times n$ matrix shown in Equation (1):

$$\begin{bmatrix} a_1 & \cdots & a_n \\ b_1 & \cdots & b_n \\ c_1 & \cdots & c_n \end{bmatrix} \begin{bmatrix} \dot{\rho_1} \\ \vdots \\ \dot{\rho_n} \end{bmatrix} = \begin{bmatrix} 0 \\ \vdots \\ 0 \end{bmatrix}.$$

Then, we rewrite the matrix using a global edge number to construct a global matrix. Assume that edge i is connected and edge j is not connected to vertex k. Constraint by vertex k is represented by matrix $\mathbf{C}_k$, whose ith column is identical to the column of the previous matrix that corresponds to the edge, and whose jth column is the zero vector.

$$[\mathbf{C}_k] \begin{bmatrix} \dot{\rho_1} \\ \vdots \\ \dot{\rho_N} \end{bmatrix} = \underbrace{\begin{matrix} & & i\text{th} & & j\text{th} & \\ \begin{bmatrix} \cdots & a_{ki} & \cdots & 0 & \cdots \\ \cdots & b_{ki} & \cdots & 0 & \cdots \\ \cdots & c_{ki} & \cdots & 0 & \cdots \end{bmatrix} \end{matrix}}_{3 \times N \text{matrix}} \begin{bmatrix} \dot{\rho_1} \\ \vdots \\ \dot{\rho_i} \\ \vdots \\ \dot{\rho_j} \\ \vdots \\ \dot{\rho_N} \end{bmatrix} = \begin{bmatrix} 0 \\ 0 \\ 0 \end{bmatrix},$$

where N is the number of fold lines. The global constraints by multiple vertices are given by the intersection of the conditions:

$$\mathbf{C}\dot{\boldsymbol{\rho}} = \underbrace{\begin{bmatrix} [\mathbf{C}_1] \\ \vdots \\ [\mathbf{C}_M] \end{bmatrix}}_{3M \times N \text{matrix}} \begin{bmatrix} \dot{\rho_1} \\ \vdots \\ \dot{\rho_N} \end{bmatrix} = \begin{bmatrix} 0 \\ \vdots \\ 0 \end{bmatrix}, \tag{2}$$

where M is the number of vertices inside the paper.

If and only if the rank of matrix $\mathbf{C}$ is less than N, the linear equation has nontrivial solutions. The solution of this linear equation is calculated using the pseudoinverse matrix $\mathbf{C}^+$ of matrix $\mathbf{C}$:

$$\dot{\boldsymbol{\rho}} = \left[\mathbf{I}_N - \mathbf{C}^+\mathbf{C}\right] \dot{\boldsymbol{\rho}}_0,$$

where $\dot{\boldsymbol{\rho}}_0$ is the unconstrained value of the angles' velocity determined from the mountain-valley assignment of the fold lines. The idea is to project unconstrained angle movement into constrained space by using the orthogonal projection matrix $[\mathbf{I}_N - \mathbf{C}^+\mathbf{C}]$. The trajectory can then be calculated by Euler integration as follows:

$$\Delta\boldsymbol{\rho} = \dot{\boldsymbol{\rho}}(t)\Delta t = \left[\mathbf{I}_N - \mathbf{C}^+\mathbf{C}\right] \Delta\boldsymbol{\rho}_0.$$

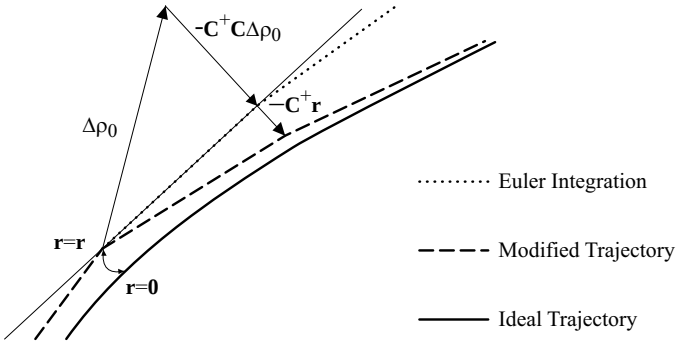

Figure 4. Idea of the trajectory: $\left[\mathbf{I}_N - \mathbf{C}^+\mathbf{C}\right]$ is a projection matrix that projects unconstrained angles movement vector $\Delta\boldsymbol{\rho}_0$ to the constraint linear space. The angles movement vector is further modified to reduce residual.

However, this Euler integration results in the accumulation of numerical error, so we modify Equation (2) using residual vector $\mathbf{r}$:

$$\mathbf{C}\dot{\boldsymbol{\rho}} = -\mathbf{r},$$

where

$$\mathbf{r} = \begin{bmatrix} r_{1a} & r_{1b} & r_{1c} & \cdots & r_{ka} & r_{kb} & r_{kc} & \cdots r_{Ma} & r_{Mb} & r_{Mc} \end{bmatrix}^{\mathrm{T}},$$

and r_{ka}, r_{kb}, and r_{kc} are the residuals of elements of $\mathbf{F}$ corresponding to a_k, b_k, and c_k, respectively.

$$\mathbf{F} = \begin{bmatrix} 1 & 0 - r_a & 0 + r_c \\ 0 + r_a & 1 & 0 - r_b \\ 0 - r_c & 0 + r_b & 1 \end{bmatrix}.$$

The modified solution is as follows (see Figure 4):

$$\Delta\boldsymbol{\rho} = -\mathbf{C}^+\mathbf{r} + \left[\mathbf{I}_N - \mathbf{C}^+\mathbf{C}\right]\Delta\boldsymbol{\rho}_0.$$

The pseudoinverse is calculated as $\mathbf{C}^+ = \mathbf{C}^{\mathrm{T}}\left(\mathbf{C}\mathbf{C}^{\mathrm{T}}\right)^{-1}$ if $\mathbf{C}$ is full rank and $3M < N$. When this condition is satisfied, the linear equation is solved as follows:

$$\begin{aligned} \Delta\boldsymbol{\rho} &= -\mathbf{C}^+\mathbf{r} + \left[\mathbf{I}_N - \mathbf{C}^+\mathbf{C}\right]\Delta\boldsymbol{\rho}_0 \\ &= -\mathbf{C}^{\mathrm{T}}\left(\mathbf{C}\mathbf{C}^{\mathrm{T}}\right)^{-1}\mathbf{r} + \left[\mathbf{I}_N - \mathbf{C}^{\mathrm{T}}\left(\mathbf{C}\mathbf{C}^{\mathrm{T}}\right)^{-1}\mathbf{C}\right]\Delta\boldsymbol{\rho}_0 \\ &= \Delta\boldsymbol{\rho}_0 - \mathbf{C}^{\mathrm{T}}\left\{\left(\mathbf{C}\mathbf{C}^{\mathrm{T}}\right) \setminus \left(\mathbf{r} + \mathbf{C}\Delta\boldsymbol{\rho}_0\right)\right\}. \end{aligned}$$

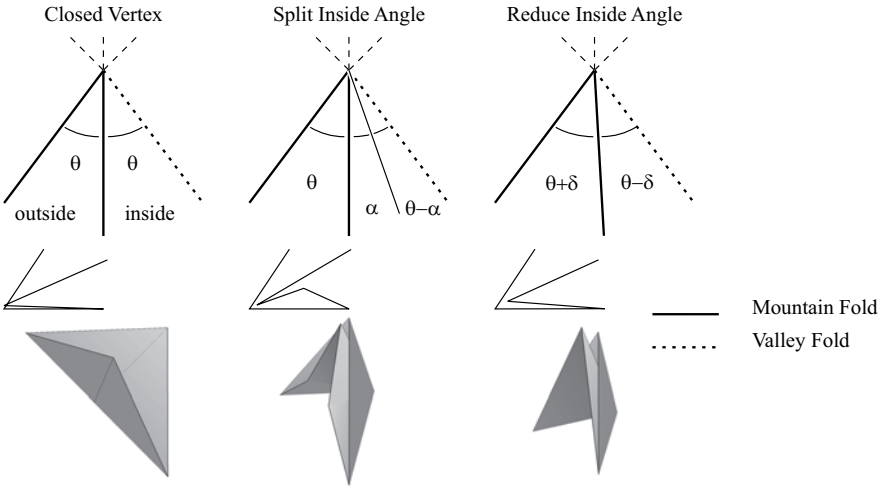

Figure 5. Two ways to avoid a closed vertex.

3 Adding and Adjusting Crease Lines

3.1 Closed Vertex

If we simply fold a paper on an existing fold line, the intersection of a new line and an old line is a vertex with fold lines whose motion is locked by the new fold. We call this kind of a singular vertex a *closed vertex*. In our system, a vertex is detected as a closed vertex if there is a set of three adjacent crease lines connected to the vertex whose outer two are symmetric about the center crease and their mountain-valley assignments are opposite.

There are two ways to avoid closed vertices. One way is to split the *inside angle*, i.e., the angle to be folded inside, by adding crease lines. The other way is to reduce the inside angle (Figure 5).

3.2 Adding Crease Lines by Triangulation

Many rigid origami models with degree-4 vertices are not rigidly foldable because of the lack of sufficient degrees of freedom (DOF). The total number of degrees of freedom of the model is $N-3M$ if the constraint matrix is full rank (i.e., if there is no singularity), where M and N are the number of vertices and edges inside the paper (i.e., not on the perimeter), respectively.

Polygons with more than three vertices are triangulated. By adding $k-3$ crease lines on each polygon, $k-3$ degrees of freedom are added to the model per each k-gon. If all the polygons are triangulated, the

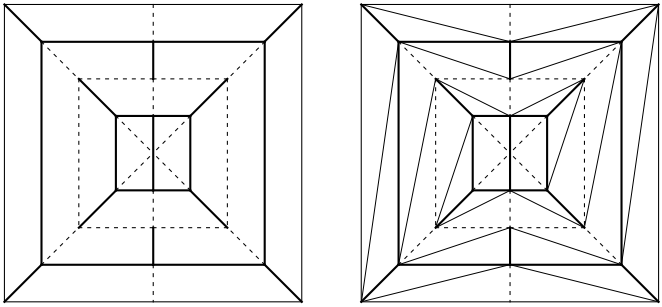

Figure 6. An example of triangulation. Left: Not-triangulated model is overconstrained ($M = 19, N = 42, \mathrm{DOF} = N - 3M < 0$). Right: Triangulated model has three DOF ($M = 19, N = 60, N_0 = 6, \mathrm{DOF} = N - 3M = N_0 - 3 = 3$).

total degrees of freedom of the model is $N_0 - 3$ where N_0 is the number of edges on the perimeter of the paper (Figure 6). There are multiple ways to add crease lines when triangulating polygons. Appropriate crease lines are added so that as many inside angles as possible are split.

3.3 Adjusting Crease Lines

Crease lines are adjusted to avoid singularity arising from closed vertices. The position of each vertex is moved in the direction that reduces the inside angles of closed vertices. The amount of displacement for each vertex is set according to the *angle unevenness* of the vertex, which is defined as $\{\max(\rho_i) - \min(\rho_i)\}$, for better balance of the folding process for fold lines. This reasonably results in no adjustment of the crease pattern when in both the unfolded and completely folded state.

Most origami models have many flat-foldable vertices. Flat-foldable vertices are kept flat foldable during the adjustment of crease lines so that an adjusted model can be folded to the final state. *Kawasaki's theorem* is used to set the constraints on displacement of the vertices [3]. Here is Kawasaki's theorem:

$$\sum_{i:\mathrm{odd}} \theta_{k,i} = \sum_{i:\mathrm{even}} \theta_{k,i} = \pi,$$

where $\theta_{k,i}$ represents the ith angle between the edges around vertex k (Figure 7).

The displacement of the vertices is represented as a $2M_{\mathrm{all}} \times 1$ vector

$$\begin{bmatrix} \Delta\mathbf{X} \\ \Delta\mathbf{Y} \end{bmatrix},$$

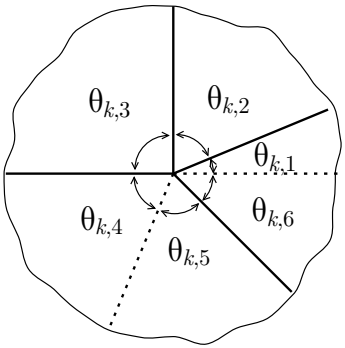

Figure 7. A flat-foldable vertex k.

where M_{all} is the total number of vertices. The constraint for the displacement is represented by a matrix $\mathbf{C}_{\text{adj}}$ as

$$\underbrace{\begin{bmatrix}\dfrac{\partial \mathbf{G}}{\partial \mathbf{X}} & \dfrac{\partial \mathbf{G}}{\partial \mathbf{Y}}\end{bmatrix}}_{[\mathbf{C}_{\text{adj}}]}\begin{bmatrix}\Delta \mathbf{X} \\ \Delta \mathbf{Y}\end{bmatrix} = \mathbf{0},$$

where $\mathbf{G}$ is a $M \times 1$ vector function of $\mathbf{X}$ and $\mathbf{Y}$ whose kth element is

$$\mathbf{G}\left(\mathbf{X}, \mathbf{Y}\right)_k = \sum_{i:\text{odd}} \theta_{k,i} - \sum_{i:\text{even}} \theta_{k,i}.$$

Constrained displacements of the vertices are calculated in the same way as calculating the trajectory of the angles:

$$\begin{bmatrix}\Delta \mathbf{X} \\ \Delta \mathbf{Y}\end{bmatrix} = -\mathbf{C}_{\text{adj}}^{+}\mathbf{r}_g + \left[\mathbf{I}_{2M_{\text{all}}} - \mathbf{C}_{\text{adj}}^{+}\mathbf{C}_{\text{adj}}\right]\begin{bmatrix}\Delta \mathbf{X}_0 \\ \Delta \mathbf{Y}_0\end{bmatrix},$$

where

$$\begin{bmatrix}\Delta \mathbf{X}_0 \\ \Delta \mathbf{Y}_0\end{bmatrix}$$

is the unconstrained vertex displacement and $\mathbf{r}_g$ is the residual vector of function $\mathbf{G}$.

3.4 Result of Adding and Adjusting Crease Lines

Figure 8 shows the results of adjusting crease lines after triangulating the model. Some models become flexible enough to show how the facets are stacked when all the crease lines are simultaneously folded. Other models become possible to fold only when their crease lines have been adjusted. The overall animation of folding from the crease pattern to the final shape is smoother and more comprehensible when the crease lines are adjusted.

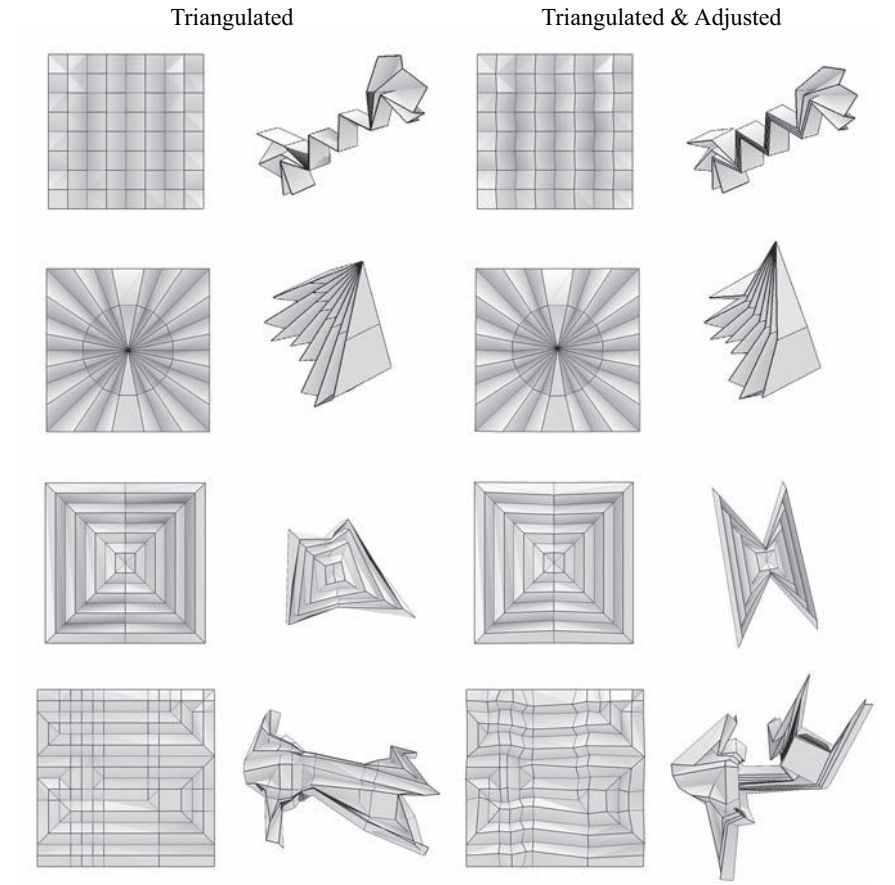

Figure 8. Top two rows: Adjusting crease lines adds flexibility to the model and results in more natural and comprehensible origami representation. Bottom two rows: Some models cannot be folded to the final state without adjustment. (Model in last row is the base of *Tea Time* by the author.)

4 Implementation and Result

The system described above has been implemented as a program written in C using ATLAS and OpenGL. The user can interactively simulate folding and unfolding of origami models, whose crease pattern data is given in DXF format or ORIPA format. A conjugate gradient method was used for solving the linear equation system. The program runs at an interactive

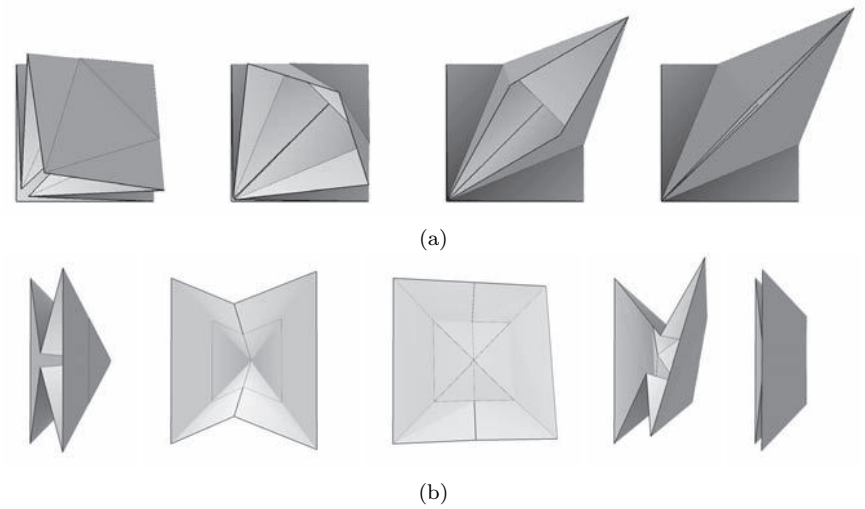

Figure 9. Transition from one folded state to another. (a) Petal fold can be simulated. (b) Simple open sink can be folded, but one needs to unfold all crease lines during the folding process.

speed for many complex origami models (e.g, a 16×16 box-pleated model). Screenshots of the program are shown in Figure 1.

Two types of penalty forces are used to avoid local self-intersection. One limits the fold angles of mountain or valley crease lines to $[-\pi, \pi]$ to prevent two adjacent facets from intersecting each other. The other limits the fold angles of added crease lines according to the fold angles of adjacent crease lines such that three adjacent facets sharing one vertex do not intersect each other. Although this self-intersection avoidance is not sufficient to avoid global or complicated local self-intersection, it is observed that it works in many practical cases.

The system also supports transitions from one folded state to another folded state so that it can be used as a tool for drawing diagrams. The folding process can be controlled by a set of multiple crease patterns. However, it is observed that many origami folding steps are not rigidly foldable. For example, it is impossible to execute sink folds and some reverse folds without unfolding all crease lines (Figure 9).

Many models can be folded to the desired state in this system, although some cannot be so folded. We have observed that the foldability of the model is determined by whether the model has closed folds in the structure rather than by the number of the fold lines in the model. In general, origami models that are easy to open into a sheet of paper in the "real world" can

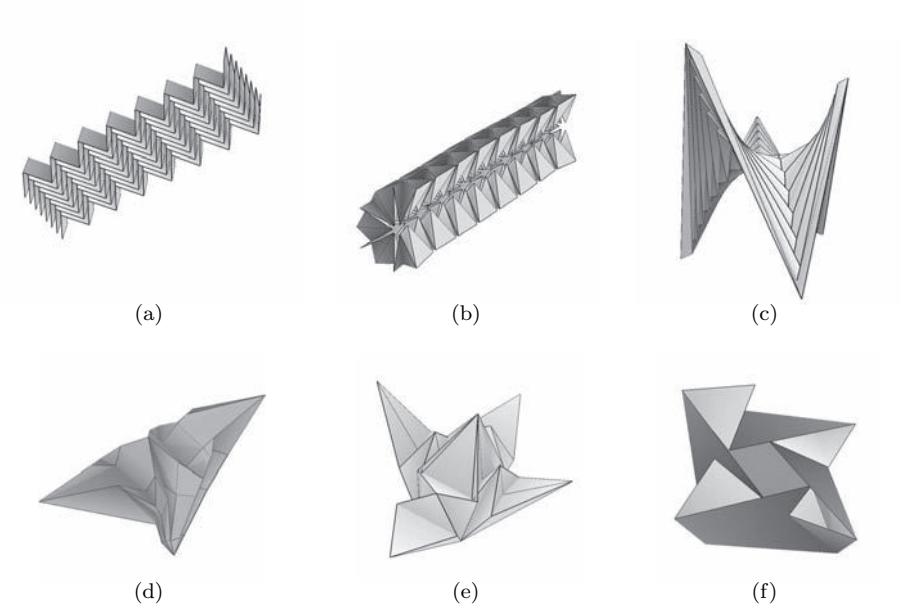

Figure 10. Examples of simulation. (a) *Miura-ori*, (b) waterbomb tessellation, and (c) pleated hypar are foldable; and (d) crane with finishing, (e) four-crane base, and (f) tatou get stuck or intersect themselves before becoming completely folded.

be easily folded and unfolded in the simulation. For example, a *Miura-ori*, a waterbomb tessellation, and a pleated hypar are smoothly folded in the simulation, while a crane with its finishing step (reverse-folding the neck), a four-crane base, or a tatou cannot be folded to the final state (Figure 10).

Rigid Origami Simulator, the simulation program based on the proposed method, is available on the author's website (http://www.tsg.ne.jp/TT/software/), and the resulting images can be seen on Flickr (http://www.flickr.com/photos/tactom/).

5 Conclusions and Future Works

We proposed a system for simulating folding motion of origami by calculating the trajectory via projection to the constrained space based on a rigid origami model. An additional method was proposed for making origami models more flexible by triangulating polygons and adjusting crease lines. Moreover, we investigated local self-intersection avoidance and the transi-

tion from one state to another. As a result, we can get an interactive system with which users can fold and unfold relatively "open" origami models to and from the crease pattern in a robust, smooth, and comprehensible way.

The global self-intersection avoidance problem and the stacking order problem are not solved in this paper and should be the subject of future work. Another work to be done in the future is controlling the surface of high-DOF origami models through user interaction, which is useful for understanding how an origami surface three-dimensionally changes its form.

Bibliography

[1] D. Balkcom. "Robotic Origami Folding." PhD dissertation, Carnegie Mellon University, 2002.

[2] s.-m. belcastro and T. Hull. A mathematical model for non-flat origami. In *Origami^3: Proceedings of the Third International Meeting of Origami Science, Mathematics, and Education*, edited by Thomas Hull, pp. 39–51. Natick, MA: A K Peters, 2002.

[3] T. Kawasaki. "On the Relation between Mountain-Creases and Valley-Creases of a Flat Origami." In *Proceedings of the First International Meeting of Origami Science and Technology*, edited by H. Huzita, pp. 229–237. Padova, Italy: Dipartimento di Fisica dell'Università di Padova, 1991.

[4] J. Mitani. "Oripa: Origami Pattern Editor." Available at http://mitani.cs.tsukuba.ac.jp/pukiwiki-oripa/, 2005.

[5] S. Miyazaki, T. Yasuda S., Yokoi, and J. Toriwaki. "An Origami Playing Simulator in the Virtual Space." *The Journal of Visualization and Computer Animation* 7:1 (1996), 25–42.

[6] R. Resch and H. Christiansen. "Design and Analysis of Kinematic Folded Plate Systems." Paper presented at the IASS Symposium on Folded Plates and Prismatic Structures, Vienna, September 28–30, 2007.

Facet Ordering and Crease Assignment in Uniaxial Bases

Robert J. Lang and Erik D. Demaine

1 Introduction

A renaissance of origami began in the mid-twentieth century as the exposure of the works of Japanese master Akira Yoshizawa inspired a wave of creation of new design that continues unabated today. Beginning in the 1960s with the development of box pleating and through the ensuing decades, the state of complexity and sophistication of origami designs grew steadily, leading to ever-more challenging subjects as origami artists including Elias, Hulme, Engel, and Maekawa developed techniques to design origami shapes with specified features.

By the 1990s, these techniques began to assume mathematical form. At roughly the same time, Toshiyuki Meguro in Japan and one of the authors (Robert Lang) in America devised a set of techniques based on disk packing that allowed an origami artist to design a basic form, called a *base*, with an arbitrary configuration of flaps [8, 9]. These techniques and their subsequent diffusion through the origami communities on both sides of the Pacific led to a wave of new origami creation and an "arms race" (or perhaps a "legs race" is more accurate) of arthropodal invention known informally as the "Bug Wars."

While origami artists were not overly concerned with the mathematical niceties of circle packing so long as it worked in practice, in the mid- to late 1990s, origami began to receive attention from computational geome-

ters, including the other author (Erik Demaine), who began investigating origami design issues from a computational perspective, examining questions of computational complexity, existence, and formal algorithms for the solution of various folding problems.

The first computational geometric description of the *circle packing* design algorithm was provided by Robert Lang in 1996 [9]. We showed that a broad class of origami structure—called *uniaxial bases*—could be designed by solving a nonlinear constrained optimization (NLCO) problem that, under certain conditions, amounted to a disk packing. The construction of the base occurred in two steps. After describing the desired base by a weighted tree graph, one constructed an NLCO from the properties of the tree graph and then solved it for a set of points that ultimately became key vertices of the desired crease pattern. In the second step, the pattern of vertices was filled in with a set of creases utilizing patterns known as *molecules* (a name and concept coined by Meguro). The resulting crease pattern was foldable into a base whose flaps possessed the lengths and connections specified by the original tree graph. We called this algorithm *tree theory*, and incorporated it into a freely available software tool for origami design, TreeMaker [11].

A complete description of a flat folded origami shape requires three things: the locations of the creases; their assignment (mountain or valley); and the stacking order of the folded layers. in our original analysis, we noted that the creases could be classified into four families and that the crease assignments for some of the families were known, and we commented that the remaining crease assignments could *usually* be determined by a bit of experimentation.

However, lack of a complete description of crease assignment (and the related information of stacking order) has remained a hole in tree theory for some ten years. It is by no means assured that the solution to either problem is trivial; in general, finding crease assignment and/or stacking order for a given crease pattern is NP-complete [3]. On the other hand, polynomial-time algorithms for crease assignment and stacking order for closely related problems [2] have been described, giving grounds for hope for the existence of a general algorithm.

In this work, we describe for the first time a relatively simple algorithm for crease assignment in a uniaxial base. The method hinges on the construction of an ordering of the facets, expressed as a digraph, that allows a mountain-valley assignment that satisfies the Justin conditions on layer ordering [5]. Although we defer the proof of the algorithm to a future work due to space limitations, we present it here; this algorithm, plus the NLCO of tree theory, provides a complete computation algorithm for the crease pattern, crease assignment, and stacking order for an arbitrary uniaxial origami base.

2 Tree Theory

2.1 Optimization

We begin with a brief recapitulation of tree theory and relevant terms and concepts.

A *uniaxial base* is a folded shape that can be partitioned into distinct regions, called *flaps*, and for which a particular line can be defined, called the *axis*. Each flap must be incident to the axis and the perpendicular projection of the flap onto the axis must be fully contained within each flap. The connections between flaps are called *hinges*, and the hinges are all perpendicular to the axis. Each flap has a defined *length*, which is simply the length of its projection upon the axis.

The lengths and connections between flaps in a uniaxial base can be described by an edge-weighted graph in which edges represent flaps, edge weights are the flap lengths, and the nodes of the graph represent connections between flaps. Since the paper is simply connected, any shape folded from the paper must be simply connected, and therefore its graph must be as well. We call such a graph the *tree graph* of the base. Given a uniaxial base, constructing its tree graph is simple and straightforward. (See Figure 1.)

Many of the classic bases of origami, and many modern bases of great complexity, are uniaxial bases (although of course many are not). The property of uniaxiality permits a solution of the inverse problem: given a tree graph and a sheet of paper, construct a uniaxial base with the given tree graph (or one that differs by only a proportionality constant), using an algorithm which we call the *TreeMaker algorithm*.

We will present examples in which the sheet of paper is a square, but the algorithm is applicable to any convex polygon P. We first classify nodes and edges within the tree graph: a node of degree 1 is a *leaf node*; all others are *branch nodes*. Similarly, any edge incident to a leaf node is a *leaf edge*; all others are *branch edges*. With each leaf node n_i, we associate a vertex of the crease pattern v_i, which we call a *leaf node vertex*. (Branch nodes do not have unique associated vertices.) The first step of the TreeMaker algorithm is to solve for the positions of the leaf node vertices within the paper P.

Since the tree graph is simply connected, there is a unique shortest path between any two nodes n_i and n_j, called a *tree path*, consisting of an ordered list of nodes and edges. With each such tree path, we associate a *tree length* l_{ij}, which is the sum of the lengths of the edges of the tree path. In our prior work [9], we showed that for any uniaxial base, a necessary condition on the crease pattern was that

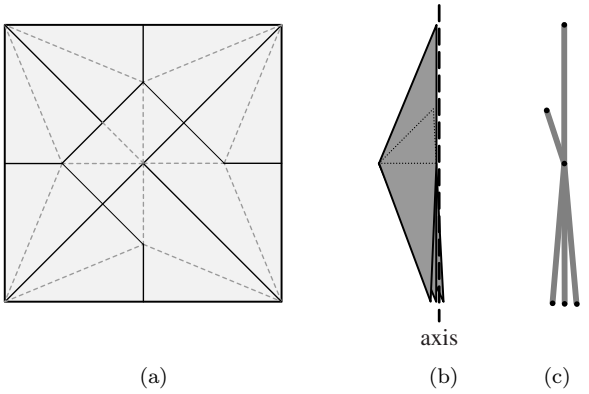

Figure 1. (a) Crease pattern of a uniaxial base. (b) Folded form of the same base, with axis highlighted. (c) Its tree graph. Note that one flap is hidden inside the folded form.

$$|v_i - v_j| \geq l_{ij} \tag{1}$$

for all possible pairs of leaf node vertices.

For an arbitrary tree graph, there is no guarantee that a solution to Equation (1) exists. We therefore introduce a scaling factor m, which is the ratio between the length of an edge of the tree graph and the length of the corresponding flap in the folded form. With this introduction, Equation (1) becomes

$$|v_i - v_j| \geq m l_{ij} \tag{2}$$

for all possible pairs of leaf node vertices.

The scale is a measure of the efficiency of the folded base; a base with a large scale will have a folded form that is relatively large compared to the starting paper. The largest potential base is therefore given by the extremum of the following nonlinear constrained optimization problem:

$$\text{maximize } m \text{ over } \{v_i\} \text{ subject to } |v_i - v_j| \geq m l_{ij}, v_i \in P. \tag{3}$$

A straight line between any two vertices v_i, v_j in the crease pattern is also called a *path* (not to be confused with tree paths, which are defined on the tree graph rather than on the crease pattern). For every tree path between leaf nodes, there is a corresponding path between leaf node vertices on the crease pattern, which we call a *leaf path*. The length of any path in the crease pattern is the Euclidean distance between its endpoints. If the length of a leaf path is equal to its scaled length on the tree graph, corresponding to equality in Equation (2), the path is said to be an *active path*, because its associated constraint in the NLCO is in the active set of constraints. A path that is not active is *inactive*.

A leaf path is a *polygon path* if it is either (a) an active path, or (b) on the convex hull of the leaf node vertices, in which case it is called a *hull path*. If a chain of polygon paths closes on itself, forms a convex polygon, and contains no leaf node vertices in its interior, the enclosed region and boundary is said to be an *active polygon*.

A set of leaf node vertices in a polygon P with convex hull P_H is said to be *well-formed* with respect to a tree graph if it satisfies the following properties:

1. Every point within the convex hull lies within some active polygon.
2. Every active polygon contains at most one inactive hull path.

There is no guarantee that a solution to Equation (3) satisfies these two conditions; it is not uncommon to find a solution with active paths all around the boundary and one or more unconstrained leaf vertices "rattling around" in the interior of the polygon. However, it is usually possible to either add additional edges to the tree graph or to selectively lengthen certain edges of the tree graph to attain the well-formed state—and importantly, this is accomplished without reducing the size of the original graph; the solution to Equation (3) remains an optimum.

2.2 Molecules

Given a well-formed vertex set, we can now construct the crease pattern itself. We first note that any paper outside of the convex hull of the leaf vertices is effectively unused. In practice, it can be folded underneath and the resulting polygon treated as a single sheet of paper; in the interest of brevity, we will ignore it going forward and will assume that the paper P and the convex hull of the leaf node vertices P_H are one and the same.

We now introduce a coordinate system in the folded form: for any point p in the crease pattern, its perpendicular distance from the axis is called the *elevation* e, and its distance along the axis from some fixed reference point (to be defined presently) is called the *depth* d.

The leaf node vertices, by definition, lie on the axis of the base in the folded form, and so have elevation zero. It can be shown that any active path must have constant elevation along its length; thus, every point along an active path between two leaf node vertices has elevation zero and lies on the axis in the folded form. We call such a path an *axial path*. Since all points in the immediate neighborhood of an axial path lie at higher elevation than the axial path, there must be a gradient discontinuity along an axial path in the mapping from the crease pattern to the folded form—in other words, every axial path is folded. We can therefore construct creases along all axial paths in a well-formed vertex set; said creases are *axial creases*. (See Figure 2.)

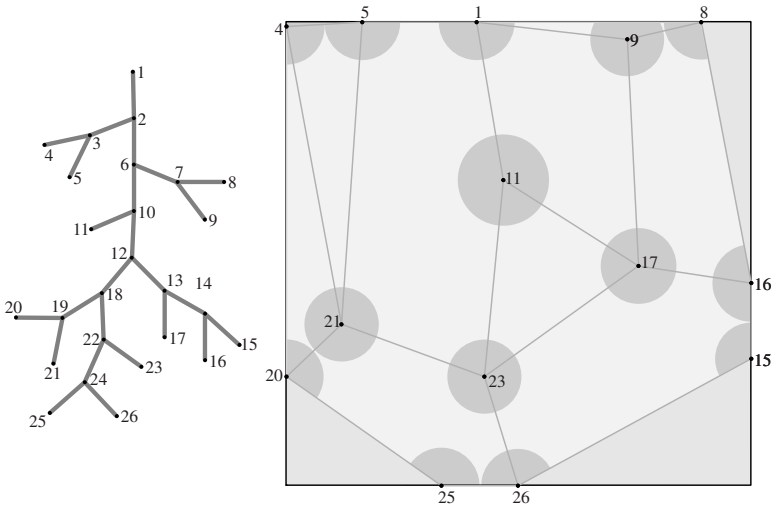

Figure 2. (a) A tree graph. (b) A well-formed vertex set for this tree graph with active and inactive polygon paths highlighted.

We now construct the crease pattern inside of each active polygon. They can be treated independently at this point; we call the crease pattern for any axial-boundary polygon a *molecule*. Inactive polygon paths (which exist only on the boundary of the convex hull) are not forced to be axial paths but we will choose them to be so. Thus, every active polygon has elevation zero on its boundary and, as it turns out, elevation greater than zero everywhere in its interior. The boundary paths of each active polygon are all lines of constant elevation and run parallel to the axis in the folded form. If we inset the boundary by some constant distance h, the resulting smaller polygon must also have a boundary that has constant elevation, but that elevation is now given by h. (See Figure 3.)

The corners of the inset polygon are gradient discontinuities in the mapping from the crease pattern to the folded form, and therefore must be folded points. In other words, there must be creases radiating inward from the corners of the active polygons. We call such creases *ridge creases*. If we denote the vertices of the active polygon by $\{v_i\}$ and the vertices of the inset polygon by $\{v_i'\}$, the inset vertices must obey a set of conditions analogous to the tree conditions, which are

$$|v_i' - v_j'| \geq ml_{ij} - h(\cot\alpha_i + \cot\alpha_j) \tag{4}$$

for all possible pairs of inset vertices, where α_i and α_j are, respectively,

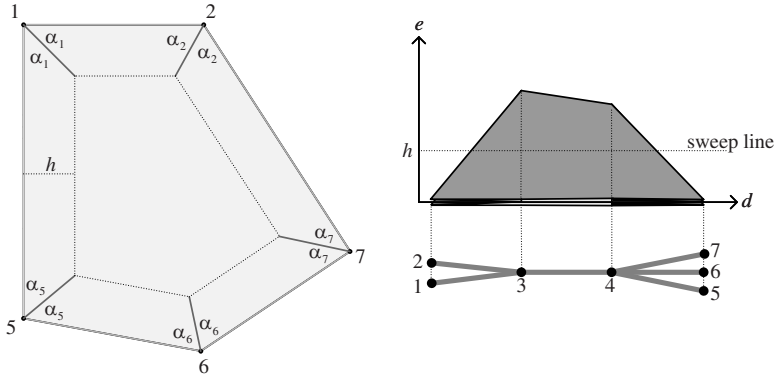

Figure 3. Insetting the boundary of an active polygon produces a polygon with a constant-elevation boundary at higher elevation.

half of the vertex angles at v_i and v_j. The path from v_i' to v_j' is called a *reduced active path*.

As the inset distance h is increased, one of two things happens. Either two inset vertices merge—in which case the polygon degree is reduced—or one (or more) of the reduced active paths becomes active, i.e., the inequality in Equation (4) reaches equality. When this happens, the situation is analogous to an axial path; the reduced path must be a line of constant elevation, the paper on either side of the path lies at higher elevation, and therefore, the path must be a (folded) crease, called a *gusset crease*. The gusset crease(s) divide the reduced polygon into two (or more) separate reduced polygons, each of which has degree lower than the original polygon, and the insetting process continues. Eventually, the ridge creases and vertices merge at a point, and the polygon is filled by a network of ridge and gusset creases, all of which are folded. (See Figure 4.)

These are not the only creases in the crease pattern, however. For a given uniaxial base, the flaps can be positioned in multiple arrangements. As noted earlier, the boundaries between flaps are called hinges; in the crease pattern, hinges are represented by *hinge creases*. A hinge crease can be folded or unfolded, depending on the relative positions of the flaps to either side.

While the tree graph is a discrete structure, we can expand it into a metric space in which a point can be defined anywhere along an edge and characterized by its distance along the edge. We call this space the *metric tree*. If we do this, then along any axial path in the crease pattern, there is a one-to-one mapping between any point on the path and a unique point on the metric tree. In particular, we can identify points

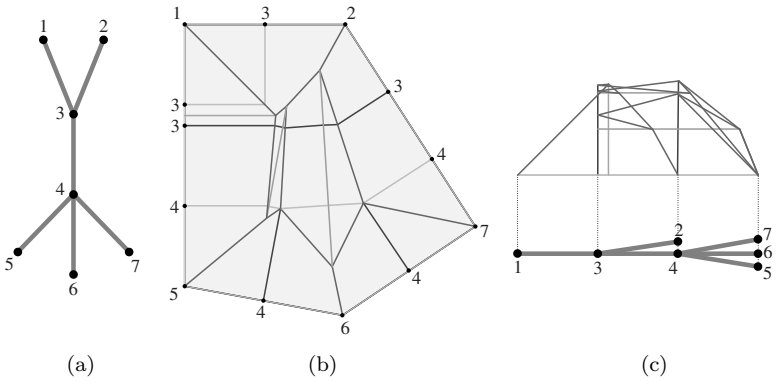

Figure 4. (a) The tree graph. (b) The universal molecule, showing ridge, gusset, folded and unfolded hinge, and pseudohinge creases. (c) The folded form, showing the folded positions of each crease.

on the crease pattern that map to branch nodes on the metric tree. Such points must be incident to hinge creases. And since hinge creases are lines of constant depth (just as axial and gusset creases were lines of constant elevation), we can identify vertices along the axial creases that correspond to the branch nodes along the tree, and then by propagating hinge creases out from them (and reflecting the hinge creases when they hit ridge creases), we can construct all of the hinge creases in the crease pattern (though not, as yet, determine whether they are folded or unfolded).

There is one more type of crease to construct. From every hull path in the crease pattern, there is a chain of ridge creases—called a *ridgeline*—connecting its endpoints. The intermediate vertices along this chain are incident to hinge creases that connect the ridgeline to the hull path, for the most part. However, if the hull path is inactive, there will be at least one vertex formed in the insetting process that is *not* incident to a hinge crease connecting it to the hull. We drop a new crease from each such vertex to the hull path, and call such creases *pseudohinge creases*. Like hinge creases, pseudohinge creases are creases of constant depth. Unlike hinge creases, pseudohinge creases are *always* folded and do not map to branch nodes on the metric tree.

Thus, the crease pattern is composed of creases and vertices that partition each active polygon into regions called *facets*. Each facet is part of a flap that corresponds to an edge of the tree graph; that edge is called the *projection* of the facet. If we take the projection of all of the facets in a molecule, we get a set of tree graph edges that is a subset of the edges of the entire tree graph. This set of edges and their incident nodes form a

subgraph of the tree graph, which is called the *subtree* of the tree graph. A facet that is incident to the boundary of a molecule (and which therefore is incident to an axial crease) is an *axial facet*. A facet that is incident to a pseudohinge crease is a *pseudohinge facet*. Since all pseudohinge creases are incident to axial creases, all pseudohinge facets are also axial facets. A *corridor* is a connected set of facets that belong to the same flap in the folded form. A corridor can (and typically does) extend across multiple molecules.

This completes the construction of the crease pattern. Most of this algorithm has been previously described in [9, 10], although we had not previously made the distinction between hinge and pseudohinge creases. The crease pattern within each polygon is called the *universal molecule*, and the algorithm to construct it, the *universal molecule algorithm*. This algorithm provides all of the folds necessary to create the folded form. However, it does not give the crease assignments, nor even fully specify which of the hinge creases are folded, and it says nothing about the stacking order of the layers. It is well known that given a stacking order, the crease assignment is trivially deduced, while even given a full crease assignment, determining a valid stacking order can be NP-complete. Fortunately, determination of the stacking order and crease assignment in uniaxial bases is *not* NP-complete, as we will show in the next section.

3 Facet Ordering

3.1 Ordering Conditions

For an origami crease pattern to be flat foldable, it must satisfy three sets of conditions. The most famous of these are Maekawa's Theorem on crease directions at a vertex ($|M - V| = 2$) [4] and Kawasaki's Theorem on angles between creases around a vertex ($\sum_{i\ \text{odd}} \phi_i = \sum_{i\ \text{even}} \phi_i = 180°$) [6,7]. Less known are the layer ordering conditions formulated by Jacques Justin [5], which govern the stacking order of overlapping facets in the folded form. In fact, it is these conditions that lead to the computational complexity of many folding problems.

Our crease pattern satisfies Kawasaki's Theorem by design, and Maekawa's Theorem follows automatically if Justin's conditions are satisfied; thus, our focus on determining crease assignment is in fact an attempt to satisfy Justin's conditions. In his original formulation, Justin considered that all creases would be folded. In our crease pattern, we allow for unfolded creases, which necessitates a slight modification of the descriptions of the Justin conditions, of which there are four. (See Figure 5.)

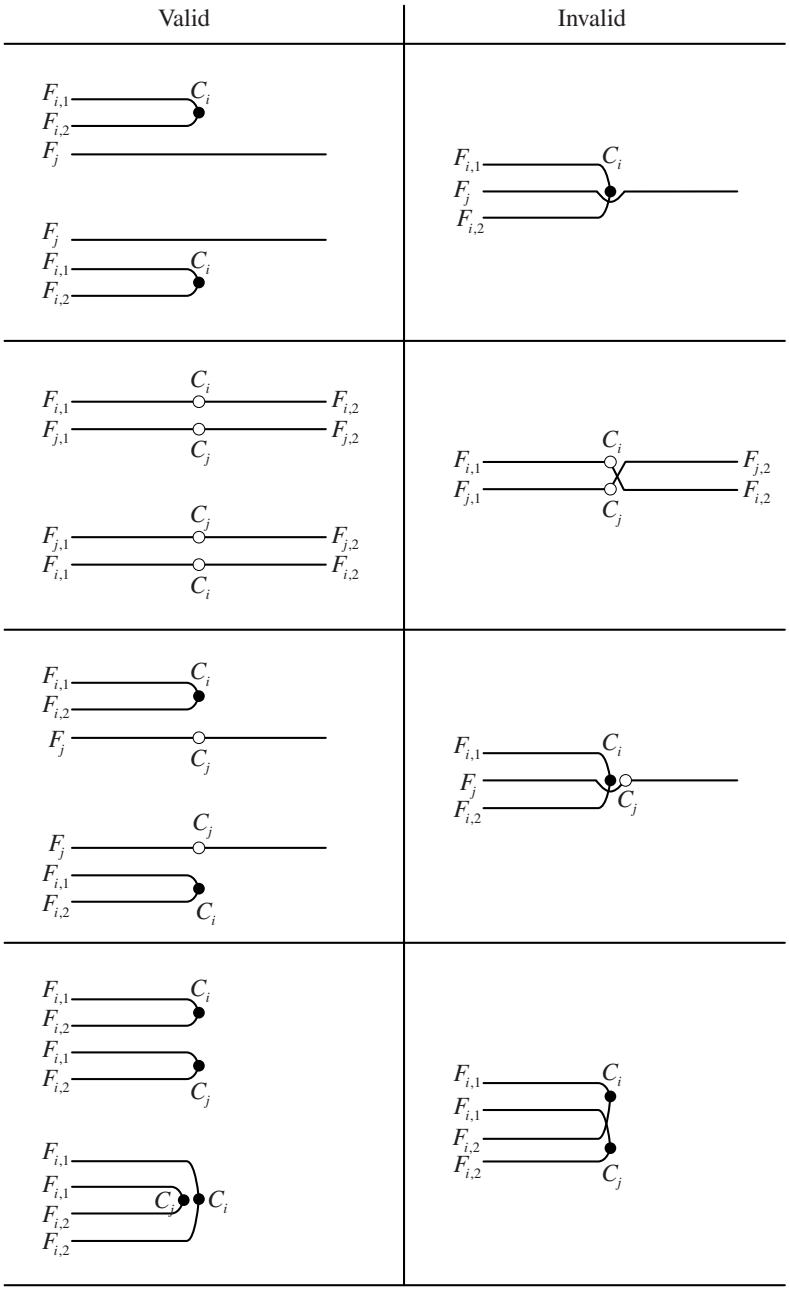

Figure 5. The four Justin conditions, illustrated schematically (edge views of the creases). Both valid and invalid configurations are illustrated.

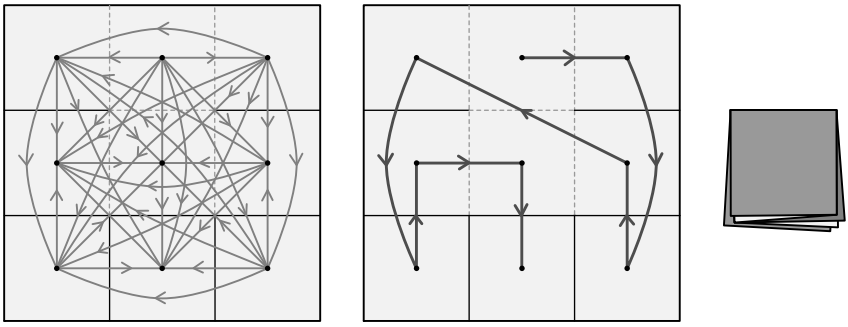

Figure 6. (a) A complete ordering graph. (b) An equivalent ROG. (c) The folded form.

The Justin conditions affect layer ordering among overlapping facets; we therefore must define an ordering relation for any two facets that overlap in the folded form. Such a relationship can readily be described by a directed graph, called an *ordering graph*, or OG, where the nodes of the graph represent the facets of the crease pattern and the directed edges represent order. An edge (F_i, F_j) is in the ordering graph if and only if facet F_i overlaps facet F_j. For convenience, one can draw an embedding of the ordering graph by positioning the nodes at the centroids of their corresponding facets, as shown in Figure 6.

An ordering graph can be fairly complex; for N facets, it can have as many as $N(N-1)/2$ edges (see, e.g., the stamp-folding problem). The Justin conditions apply to edges of the ordering graph that relate facets on either side of creases that overlap in the folded form. The ordering graph is directed, but it need not be simply connected, acyclic, or possessed of any other particular property. However, if an ordering graph *is* acyclic, it can be described by a simpler structure, which we call a *reduced ordering graph*, or ROG. Specifically, one can derived the OG from an ROG; the edge (F_i, F_j) is in an OG if and only if F_i overlaps F_j and there exists a directed path $(F_i, ..., F_j)$ in the ROG.

An ROG can be much simpler—having many fewer edges—than an OG, since in an ROG both edges and paths imply ordering relationships between facets. However, an ROG must necessarily be directed acyclic, leading to a directed acyclic ordering graph, and so not all OGs can be described by an ROG. On the other hand, since ROGs are DAGs (directed acyclic graphs), they are sortable; it is possible to assign an index to every facet such that the ordering relationship between the facets can be inferred simply by comparing the values of the two facet indices.

3.2 Rooted Embedding

As already noted, for a given crease pattern, there are usually several different folded forms with the same tree graph, depending on the arrangement of flaps. In particular, any given flap can be "flipped" about its hinge to point in either the positive or negative depth direction. Not all arrangements are possible, however. For some bases, there are flap directions for which no valid facet ordering exists (or put differently, for which the flaps must intersect one another).

To avoid this problem, we choose a particular flap arrangement that avoids such problems, by assigning depth in a particular way. We pick one node of the tree graph, which we call the *root node*, and assign it a *discrete depth* of zero. We then move out from the root node and assign each node a discrete depth, incrementing the discrete depth counter as we cross each edge. Thus, at the end, every node has a discrete depth that is simply its distance (in hops) from the root node.

We can now assign true depth to every vertex of the base, by setting the difference in depth between any two hinges to be the length of the edge between them, and choosing the sign of the difference in depth from the sign of the difference in their discrete depths. In a physical analogy, this algorithm is equivalent to "picking up the base" by its root node and letting all of the flaps dangle under the force of gravity.

Once the true depth of all hinges and hinge vertices has been assigned, there is sufficient information to assign both depth and elevation to every point in the folded form. This information then allows one to determine which hinge creases are folded; if the depth mapping is smooth across the hinge crease, it is unfolded; if it is gradient discontinuous, the hinge crease is folded.

Within the full tree graph, there is exactly one root node, which has the lowest possible discrete depth, i.e., zero. Each molecule has a subtree associated with it; within each subtree, there is one (or more) nodes with the lowest discrete depth, which may be greater than zero. These nodes are called the *local root nodes* of the subtree associated with the molecule. (To further distinguish the local root node of a subtree from the root node of the tree, we will sometimes call the latter the *global root node*.) The hinge creases associated with the local root nodes are the *local root hinges* of the molecule. The vertices incident to local root hinges are *local root vertices* of the molecule.

3.3 Reduced Ordering Graphs

We are now in a position to construct the ROG for the crease pattern. We begin by constructing directed graphs on each molecule. Each graph is

composed of a set of directed paths, called *chains*, of which there are two types.

A *corridor chain* connects facets in the same corridor and is constructed as follows. It begins from an axial facet. We repeatedly add directed edges from the current facet to the next facet; the next facet in the chain is the facet that lies on the other side of either (a) the highest-elevation ridge crease, (b) the gusset crease, or (c) the pseudohinge crease of the current facet (other than the crease just crossed). Repeatedly following this rule gives a connected chain of facets, all within the same corridor, that eventually terminates on another axial facet. Each of the directed edges created in this fashion is a *corridor link*.

The *axial chain* connects facets in distinct corridors and is constructed as follows. We begin with an axial facet positioned immediately CCW from a local root hinge. if this facet is not an in-link of an existing corridor chain, we launch a new corridor chain from this facet and propagate it until it terminates (on some other axial facet). We then look for the next CCW axial facet that is *not* a pseudohinge facet. If the two facets are in different corridors, we add a directed edge from the current facet to this new facet (skipping over any pseudohinge facets between them) and repeat the process until we have reconnected with the first facet with which we started. Each of the directed edges created in this fashion is an *axial link*.

When this process is completed, the resulting graph, called a *molecular ordering graph* (MOG), will be connected. It may not (yet) be an ROG, because it may contain a cycle (if the local root node was a branch node of the subtree). In this latter case, if you delete any single axial link that crosses a local root hinge crease, the graph becomes an ROG and (while it is beyond the scope of this paper to prove) it is a valid facet ordering for the molecule. (See Figure 7.)

However, we must find a valid ROG for the entire crease pattern. We construct the MOG for each molecule—each of which may contain a cycle. We then merge the MOGs into a single directed graph. Two MOGS can merge at any common vertex that is a local root hinge vertex for one of the molecules. To merge two MOGs at a vertex, we delete the axial links on either side of the vertex and add two links connecting the "cut ends" to each other. In this fashion, we merge all molecules into a single directed graph.

At this point, if the global root node is a leaf node of the tree, the resulting graph is acyclic, constitutes an ROG, and produces a valid facet ordering (again, the proof is beyond the scope of this paper). If the global root node is not a leaf node, then this graph contains a cycle; breaking the cycle by deleting an axial link crossing a hinge crease incident to a global root vertex. The resulting graph is then acyclic, is an ROG, and produces a valid facet ordering.

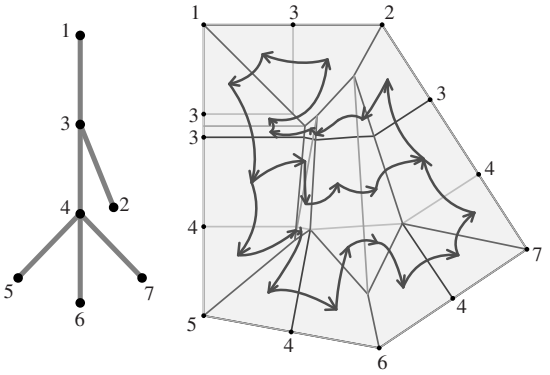

Figure 7. (a) The molecular ordering graph for a single molecule. (b) Deleting the edge crossing the ridge crease incident to node 1 transforms it into a valid ROG.

3.4 Crease Assignment

Once the ROG has been constructed, crease assignment is straightforward. Since the ROG is sortable, each facet can be assigned an index, beginning with the (sole) source facet, such that the relative ordering of the facets implied by the ROG can be deduced by comparing the indices of the two facets. We then two-color the facets as "white-up" (W) and "color-up" (C) so that the facets on either side of every folded crease are of opposite color. (See Figure 8.) Mountain/valley (M/V) assignment of every folded crease can be computed from the two-coloring and the relative ordering of the facets on each side of the crease:

1. $(W \to C) \implies M$.
2. $(C \to M) \implies V$.

Of course, the opposite assignment is equally valid, being equivalent to the interchange of M and V creases. This completes the crease assignment algorithm. (See Figure 9.)

3.5 TreeMaker 5

We have implemented this algorithm in a revised version of our TreeMaker program, in which the optimization, crease construction, and crease assignment algorithms encompass roughly 27,500 lines of code. We have tested the algorithm on a wide range of tree graphs, all producing facet orderings and crease assignments that yield valid folded forms (both mathematically and physically). TreeMaker 5 is cross-platform (Mac, GNU/Linux, and

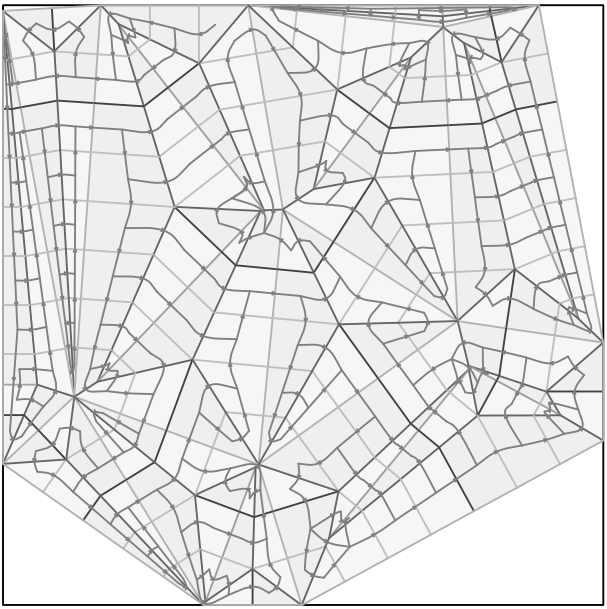

Figure 8. The completed ordering graph and two-coloring.

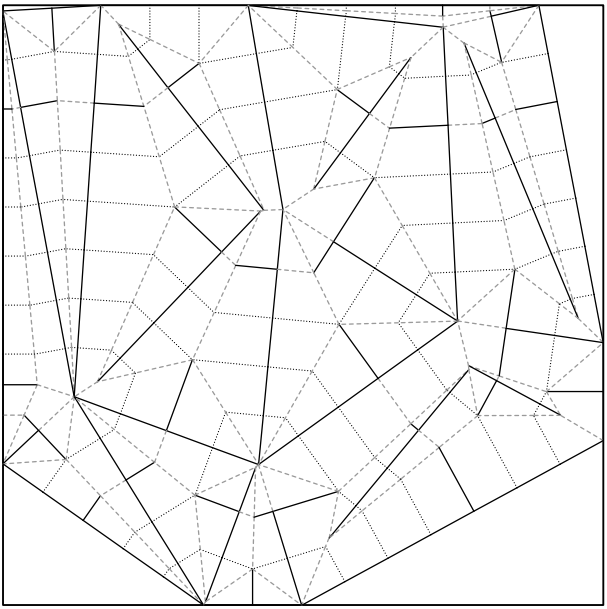

Figure 9. The completed M/V assignment.

Windows), open-source (GPL), and can be downloaded from http://www.langorigami.com.

4 Discussion

This algorithm completes the plan laid out in [9]. Given an arbitrary tree graph, it is now possible to construct the crease pattern, including crease assignment, for a valid base whose projection is the given tree graph. We note that the technique of incrementally constructing ordering graphs and merging them into a single graph is conceptually similar to the technique used in [1]—as is the concept of rooting the folded form. The explicit construction of an ordering graph as we have done here leads to a relatively straightforward computer implementation of the ordering algorithm. It also emphasizes the primacy of the ordering relationship, rather than the crease assignment, as the fundamental mathematical description.

Of course, we have not proven that the ROG satisfies the Justin conditions. To do so requires first, a transformation of the Justin conditions on facets into required properties of the graph, and second, a proof that the constructed graph has those properties. A complete derivation and proof is the subject of ongoing work. We do note, however, that we have tested the algorithm on many individual cases, including intentionally pathological test structures, with success, and so feel that the algorithm may be usefully employed even now. We believe that this approach could be adapted to provide crease assignment and facet ordering for other related folding problems, such as polyhedron flattening (the airbag problem), among others.

Acknowledgment. Both authors would like to acknowledge fruitful discussions with Martin L. Demaine in the course of working on this problem. Robert Lang would like to thank the Massachusetts Institute of Technology for support as a visiting researcher.

Bibliography

[1] Marshall Bern, Erik Demaine, David Eppstein, and Barry Hayes. "A Disk-Packing Algorithm for an Origami Magic Trick." In *Proceedings of the International Conference on Fun with Algorithms, Isola d'Elba, Italy, June 18–20, 1998*, pp. 32–42. Ottawa: Carleton University, 1998.

[2] Marshall Bern, Erik Demaine, David Eppstein, and Barry Hayes. "A Disk-Packing Algorithm for an Origami Magic Trick." In *Origami^3: Proceedings of the Third International Meeting of Origami Science, Mathematics, and*

Education, edited by Thomas Hull, pp. 17–28. Natick, MA: A K Peters, 2002.

[3] Marshall Bern and Barry Hayes. "The Complexity of Flat Origami." In *Proceedings of the Seventh Annual ACM-SIAM Symposium on Discrete Algorithms*, pp. 175–183. Philadelphia: SIAM, 1996.

[4] Thomas Hull. "The Combinatorics of Flat Folds: A Survey." In *Origami^3: Proceedings of the Third International Meeting of Origami Science, Mathematics, and Education*, edited by Thomas Hull, pp. 29–37. Natick, MA: A K Peters, 2002.

[5] Jacques Justin. "Aspects mathematiques du pliage de papier." In *Proceedings of the First International Meeting of Origami Science and Technology*, edited by H. Huzita, pp. 263–277. Padova, Italy: Dipartimento di Fisica dell'Università di Padova, 1991.

[6] Toshikazu Kawasaki. "On High-Dimensional Flat Origamis." In *Proceedings of the First International Meeting of Origami Science and Technology*, edited by H. Huzita, pp. 131–141. Padova, Italy: Dipartimento di Fisica dell'Università di Padova, 1991.

[7] Toshikazu Kawasaki. "On the Relation between Mountain-Creases and Valley-Creases of a Flat Origami." In *Proceedings of the First International Meeting of Origami Science and Technology*, edited by H. Huzita, pp. 229–237. Padova, Italy: Dipartimento di Fisica dell'Università di Padova, 1991.

[8] Robert J. Lang. "Mathematical Algorithms for Origami Design." *Symmetry: Culture and Science* 5:2 (1994), 115–152.

[9] Robert J. Lang. "A Computational Algorithm for Origami Design." In *Proceedings of the Twelfth Annual Symposium on Computational Geometry*, pp. 98–105. New York: ACM Press, 1996.

[10] Robert J. Lang. *Origami Design Secrets: Mathematical Methods for an Ancient Art*. A K Peters, 2003.

[11] Robert J. Lang. "TreeMaker." Available at http://www.langorigami.com/treemaker.htm, 2003.

Integer Programming Models for Flat Origami

Goran Konjevod

1 Introduction

Most traditional and many contemporary origami models fold flat, or at least have flat-foldable crease patterns. Thus, it would be very useful to have a complete mathematical description of flat-foldable origami. This has often been stated as a major open problem in the mathematical foundations of origami. There are three main mathematical properties of an origami model: continuity, piecewise isometry, and noncrossing. Justin [7] proposed a set of noncrossing axioms and claimed their validity was not only necessary but sufficient for flat foldability. His proof, however, is not very formal and the problem of whether the axioms are sufficient has remained open. Recently, E. Demaine [3] announced a positive answer to this question.

However, a mathematical description is of limited practical use unless it is effective, that is, unless it comes with (preferably efficient) procedures for practical manipulation of the objects it describes.

In the case of flat foldability, there are several types of questions an effective model should be able to answer. The simplest is that of deciding flat foldability of a crease pattern[1]: given a set of creases, with their orien-

[1] In this paper, a *crease pattern* includes not only the location of every crease in the model to be folded, but also the information explaining which creases are mountain folds and which are valley folds.

tations (mountain or valley) assigned, is there a flat origami with exactly the given creases taking on exactly the given orientations? Even this problem is unlikely to have an efficient algorithm because it is NP-complete, as shown by Bern and Hayes [1].

More general is the *design problem*: given a certain property required of a flat origami model, for example a given shape, or arrangement of flaps, or, for duo-colored paper, a color-change pattern, is it possible to design such a flat fold? Ideally, in the case of a positive answer, the solution should also include an (efficient) procedure to determine the crease pattern and the arrangement of layers in such a model.

What makes these problems particularly difficult at the current state of mathematical knowledge is that they are at the same time continuous and discrete. There is a continuum of possible creases, and so it is not clear how to model the problem using combinatorial techniques, which have been developed for working with finite sets, and yet at the heart of the foldability problem lies the combinatorial issue of arranging the layers correctly [1].

In order to bring the problem closer to what mathematics can currently deal with, we restrict it to a special case, only considering folds in which all the creases are either vertical, horizontal, or at a ± 45 degree angle, and each crease goes through a point of a fixed square grid (see Figure 1 for an example). Even though the problem now becomes discrete, and may appear simpler, the NP-completeness of flat foldability remains.

We represent a flat origami model by an *integer linear program*[2] (ILP) [10]. The variables of the ILP will model both the creases and the arrangement of layers. If we then set the crease variables to predefined values, we get a specific instance of the ILP whose feasible solutions represent exactly the ways to flat-fold the crease pattern. Thus, flat foldability of a crease pattern reduces to deciding if the corresponding ILP instance has any solutions. We will also show how certain properties (e.g., color-change) of an origami model can be described by linear constraints. In this case, defining additional variables and constraints, and setting them to desired values, gives us an ILP instance whose solutions will provide the necessary values for crease variables and thus an answer to the design problem.

2 Integer Programming Model

2.1 Grids and Creases

Original grid. We begin with a $k \times k$ square grid placed on an uncreased square sheet of paper, and allow folding only on the segments of the grid

[2]The word *program* is here used in the older sense of *planning*, as in *mathematical programming*, and not in the sense of computer programming.

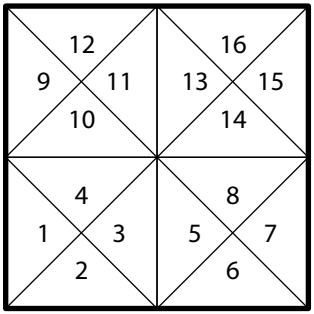

Figure 1. The 2×2 square triangle grid.

and the segments of diagonals of the *grid squares* (Figure 1). Additionally, we allow at most one of the diagonals of each grid square to be folded (this simplifies the model, and leads to no loss of generality).

The two diagonals in each grid square define four *grid triangles*. Due to the restrictions on where creases lie, every grid triangle will be flat and uncreased in the final folded state. We call these triangles the *basic polygons*. Some parts of the ILP model described here depend directly on the fact that the basic polygons are the grid triangles, but other parts of the model would still work even if this were not the case. We use V to denote the set of all basic polygons, and n for the number of elements in V, that is, $|V| = n = 4k^2$.

Creases. For each pair of adjacent basic polygons, the segment separating them may be a crease line. We define a *graph* based on this property, taking V as the set of vertices and adding an edge between two vertices if the basic polygons corresponding to these vertices are adjacent and separated by a potential crease. We label the set of all edges by E.

Folded model. Just like we named the elements of the unfolded sheet of paper by considering the grid of allowed creases, we must name the elements of the folded model. It is not difficult to see that as long as we fold only on the allowed creases, every basic polygon is folded into the location of another basic polygon, possibly lying in a grid that extends beyond the boundaries of the original sheet. This property simplifies the model, and is the main reason to work with this particular triangle-square grid.

We will in general know the area covered by the folded model. For example, if we are interested in figuring out how to fold something, the shape of the folded model is naturally given as a parameter of the problem. On the other hand, if we are testing the foldability of a crease pattern, we can easily infer the location of each basic polygon from the crease pattern.

(Indeed, first we fix one basic polygon to be at a location of our choice in the folded model. Everything else is done relative to this polygon. Then for each other basic polygon we can trace a path along the grid segments from the one fixed polygon, and account for each crease by changing the direction of the path appropriately, until we reach the polygon of interest.)

Thus, we name the set of locations where original basic polygons may lie in the folded model: W, and the set of adjacent pairs of polygons in the folded model: F.

2.2 Crease Variables and Constraints

In order to have a set of numbers describe a fold, we relate them to the features of the fold. The easiest to understand are the crease variables. For each crease segment $e \in E$, we have two variables, f_e^v and f_e^m. In a fold where the segment e is (a part of) a valley fold, we have $f_e^v = 1$. In the case of a mountain fold, $f_e^m = 1$. If the segment e is not folded, then $f_e^v = f_e^m = 0$.

It is clear that the inequality $f_e^v + f_e^m \leq 1$ is always satisfied: if the segment e is folded at all, it is either a mountain or a valley fold, but not both. For each crease segment e we have such an inequality in our model.

2.3 Orientation and Location Constraints

If we are to describe a folded model, we need to know exactly where every basic polygon is located after folding. Folding along a segment flips a part of the sheet about the segment as the axis, turning the folded part of the sheet upside-down and changing the location of every one of its basic polygons. By examining each crease segment and checking whether it is folded, we can figure out exactly where every basic polygon ends up after folding. To describe the location of each polygon, we use *location assignment* variables. Given a basic polygon $v \in V$ of the unfolded grid and a basic polygon $w \in W$ of the folded model, we define $x(v, w)$ to be 1 if v ends up at the same location as w, and 0 otherwise. Since there are no cuts, every basic polygon of the unfolded grid is still present in the folded model, and so it must be true that $\sum_{w \in W} x(v, w) = 1$ for every $v \in V$ (that is, every basic polygon is mapped somewhere).

This is not enough to describe the folded model, however. The basic polygons are isosceles right triangles, and thus symmetric about the line passing through their right angle vertex and dividing the hypothenuse in half. Therefore, a basic polygon can be mapped to the same location in two ways: its original top side may still be at the top after folding, or not. To capture this, we use the variable σ_v for every $v \in V$. If the original top side of v is still its top side, then $\sigma_v = 0$ (otherwise, $\sigma_v = 1$). We refer to σ_v also as the *orientation* of v. Clearly for every v, either $\sigma_v = 1$ or $\sigma_v = 0$.

To understand the following sets of constraints, consider a grid segment e. The orientations of its two defining polygons u and v depend on whether e is folded or not. The next four constraints describe completely the relation between the orientations σ_u, σ_v, and the fold variables $f^m(u,v)$, $f^v(u,v)$:

$$\begin{aligned}
\sigma_u - \sigma_v &\le f^m(u,v) + f^v(u,v),\\
\sigma_v - \sigma_u &\le f^m(u,v) + f^v(u,v),\\
\sigma_u + \sigma_v &\ge f^m(u,v) + f^v(u,v),\\
\sigma_u + \sigma_v &\le 2 - f^m(u,v) - f^v(u,v).
\end{aligned}$$

Location is a little more difficult to characterize. However, the location of a basic polygon is still determined completely by the location of any one of its neighbors and by the value of their common crease variable. Say $v, v' \in V$ are two neighboring basic polygons, sharing the grid segment e. Suppose v' is mapped to the basic polygon w of the folded model, that is, $x(v', w) = 1$. Then stating that v is mapped to w is equivalent to stating that e is folded, in other words, $x(v, w) = f^v(v, v') + f^m(v, v')$. Here we have a condition that says "$x(v', w) = 1$ if and only if this equation holds." Our goal is, of course, to write all this as a linear equation. The key is to notice that if $x(v', w) = 0$, our constraint should require nothing. Here's how to do this:

$$x(v, w) \ge x(v', w) + f^v(v, v') + f^m(v, v') - 1.$$

In other words, if both $x(v', w)$ and one of the fold variables are set to 1, then $x(v, w)$ will be forced to 1 as well. If one of the former is 0, then the constraint will simply say $x(v, w) \ge 0$, which is true anyway.

Of course, it is possible that the segment shared by v and v' is not folded. In that case, v and v' will not be mapped to the same fold polygon, but to adjacent ones—which ones exactly, will depend on their orientation. The constraints are somewhat more complicated for this case, and we will not explain the details here.

2.4 Noncrossing Constraints

The constraints described so far ensure that the locations of points in the fold satisfy two of the three basic properties of flat origami: continuity and isometry (no ripping or stretching of paper). The noncrossing property is the one that actually makes the problem difficult, and will also cause us the most trouble.

Assuming the Justin axioms (see Section 1 for background), there are three types of crossings that a flat-foldable origami avoids, as illustrated in Figure 2: we refer to them by mnemonics W, X, and Y.

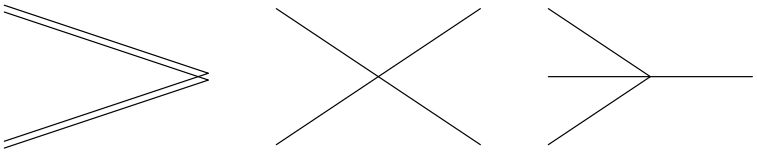

Figure 2. The three crossing types.

In our simplified version, where all folds lie along the square-triangle grid, any imaginable crossing would happen along a grid segment as well, so as with orientation and location, it suffices to enforce noncrossing for pairs of adjacent basic polygons in the grid of the folded model. Consider a flat-folded model. At any point, there may be several layers of paper one below the other. Number them from the bottom, starting from 1. Do this independently for each basic polygon of the fold grid, and we will have for every polygon in the fold an ordering of all the polygons mapped to it by the fold. We next show how to force the integer program to assign layers to basic polygons in the fold grid, and then it will be clear how to complete the constraint set, because it is not difficult to express the noncrossing constraints in terms of layers. (The same idea is used by Jonathan Schneider [9] who calls it *superposition ordering* in order to describe properties of flat-foldable crease patterns.)

For example, suppose w and w' are two neighboring polygons in the fold. Say two neighboring basic polygons, v and v', are mapped to w. They share a grid segment e. Suppose f is the segment of the fold grid to which e is mapped and w' the fold polygon adjacent to w but on the other side of f. If another basic polygon z is mapped to w and lies between v and v' in the fold (that is, it is at a layer between the layers of v and v'), then there will be a noncrossing constraint of type Y that will say that it is impossible for a neighbor of z to be mapped to w'.

Layering constraints. We first make sure that every basic grid polygon is assigned to a layer:

$$\sum_{k \in L} \lambda(v, w, k) = x(v, w),$$

for all $v \in V$ and $w \in W$, where L is the set of all possible layers (that is, the set of numbers $\{1, 2, \ldots, L_{\max}\}$ for some large enough $L_{\max}$). What the constraint really says is that if v is mapped to w by the fold, then it lies at some layer over w. The value of the variable $\lambda(v, w, k)$ is 1 if v lies at layer k over the fold polygon w, and 0 otherwise.

Then we make sure that layers fill up starting from the bottom by requiring that if layer k is empty, then so are all the layers above it:

$$\sum_{v \in V} \lambda(v, w, k) \leq \sum_{v \in V} \lambda(v, w, k-1),$$

for all $w \in W$ and $k > 1$.

Finally, we make sure that at each layer there is at most one polygon:

$$\sum_{v \in V} \lambda(v, w, k) \leq 1,$$

for all k and all $w \in W$.

Now we can compute the layer at which a polygon v lies. First, let $l(v, k) = 1$ if v is at layer k, and $l(v, k) = 0$ otherwise. Then we have

$$\lambda(v, w, k) \leq l(v, k),$$
$$\lambda(v, w, k) \geq x(v, w) + l(v, k) - 1.$$

In order to write constraints that compare layers of different basic polygons, we use the variable ll_v to be the exact layer of the basic polygon v. This value can be expressed directly in terms of l:

$$ll_v = \sum_{k \in L} k \cdot l(v, k).$$

In comparing the layers we do not care about their values, only about the sign of their difference. We use $\alpha(u, v)$ to denote whether the polygon u lies above polygon v (that is, whether $ll_u > ll_v$). First, no polygon can lie above itself:

$$\alpha(v, v) = 0,$$

for all $v \in V$. Then, if u is above v then v cannot be above u:

$$\alpha(u, v) + \alpha(v, u) \leq 1,$$

for all $u, v \in V$. Finally, we define α in terms of ll:

$$\alpha(u, v) \geq \frac{ll_u - ll_v}{L_{\max}}.$$

This suffices to establish an ordering among the polygons mapped to the same location, but additional constraints may be useful. What happens when the model is used to solve a problem is that a complicated algorithm examines many possibilities for assigning the 0-1 values to the variables of the model, and attempts to eliminate inconsistent assignments as efficiently as possible. Additional constraints usually help in such a situation, and therefore in the actual implementation of the model we also enforce other constraints that relate the ordering constraints to orientation and location constraints.

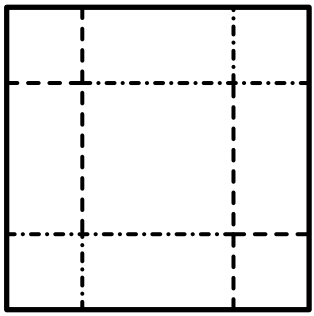

Figure 3. The 2×2 iso-area chessboard crease pattern.

3 Example and Conclusion

Due to limited space, we do not enumerate all the constraints. The complete integer programming model (written in the modeling language AMPL [5]) can be found on the author's webpage.

Figure 4 is a short example showing how the model can be used. The simplest approach is to list additional constraints that are to be enforced in order to model an actual fold. The given example gives the crease pattern illustrated in Figure 3 of the iso-area 2×2 chessboard folded from a 4×4 square.

This example is very simple, however the current version of the model results in a very large integer program even for this small crease pattern, and takes several hours to solve on a reasonably fast computer (an AMD64-based machine). The model can undoubtedly be improved and made more tractable. This is usually done by a careful examination of constraints. Some types of linear constraints (such as the one we used to define a lower bound on $\alpha(u, v)$) are computationally awkward, in that they cause the integer program solver to generate too many cases that all have to be solved. It doesn't seem obvious how to replace these constraints by better ones, but there are very likely additional inequalities that will reduce the search space. Schneider describes several necessary conditions for flat foldability, some of which do not follow immediately from our location and orientation constraints. It may be possible to derive further inequalities based on these conditions and thus make the solver's job easier. A simple improvement for the foldability problem (but not for the design problem) would be to precompute all the point locations and then have the integer program "only" test if there is a valid layering.

This work was motivated by attempts to prove bounds on the size of a $k \times k$ chessboard that can be folded out of a unit square of black-and-white paper. Hulme's chessboard [6] was the first one, giving an 8×8 board from

```
set Valley within E:={(11,13), (16,30), (19,21), (27,29), (35,37),
(36,50), (43,45), (51,53)};

set Mountain within E:={(3,5), (4,18), (8,22), (12,26), (40,54),
(44,58), (48,62), (59,61)};

subject to valleys{(a,b) in E: (a,b) in Valley or (b,a) in Valley}:
  fv[a,b] = 1;

subject to mountains{(a,b) in E: (a,b) in Mountain or (b,a) in
Mountain}:
  fm[a,b] = 1;

subject to ss: s[1] = 1;

subject to flat{(a,b) in E: not((a,b) in Valley union Mountain)
 and not((b,a) in Valley union Mountain)}: fv[a,b] + fm[a,b] = 0;
```

Figure 4. Additional constraints for the 2×2 iso-area board.

a 64×64 square, with a "reduction factor" of 8. Montroll's board [8] uses a 36×36 square, and those of Chen [2] and Dureisseix [4] use a 32×32 square, for a reduction factor of 4. It is conjectured that the latter two are optimal, that is, that an 8×8 board with correctly colored squares cannot be folded from a square smaller than 32×32. (In general, according to this conjecture, a $k \times k$ board would require a reduction factor of $2k$ in the even case.) For now, our work leaves this question open. As far as we can tell, even for folding a 4×4 chessboard, there are no rigorous proofs that our current best designs (out of 8×8 square grid, or 10×10 for a seamless design) are optimal.

Bibliography

[1] Marshall Bern and Barry Hayes. "The Complexity of Flat Origami." In *Proceedings of the Seventh Annual ACM-SIAM Symposium on Discrete Algorithms*, pp. 175–183. Philadelphia: SIAM, 1996.

[2] Sy Chen. "Checkerboard." In *Proceedings of the Annual OrigamiUSA Convention*, pp. 72–75. New York: OrigamiUSA, 2001.

[3] Erik D. Demaine. Personal communication, 2006.

[4] David Dureisseix. "Chessboard." Unpublished diagram, 2001.

[5] Robert Fourer, David M. Gay, and Brian W. Kernighan. "A Modeling Language for Mathematical Programming." *Management Science* 36 (1990), 519–554.

[6] Max Hulme. *BOS Booklet 7: Chess Sets.* Stockport, UK: BOS, 1985.

[7] Jacques Justin. "Towards a Mathematical Theory of Origami." In *Origami Science and Art: Proceedings of the Second International Meeting of Origami Science and Scientific Origami*, edited by K. Miura, pp. 15–29. Shiga, Japan: Seian University of Art and Design, 1997.

[8] John Montroll. *Origami Inside-Out.* New York: Dover, 1993.

[9] Jonathan Schneider. "Flat-Foldability of Origami Crease Patterns." Manuscript, 2005.

[10] Alexander Schrijver. *Theory of Integer and Linear Programming.* New York: Wiley, 1986.

Construction of 3D Virtual Origami Models from Sketches

Hiroshi Shimanuki, Jien Kato, and Toyohide Watanabe

1 Introduction

A large number of origami works are presented by origami creators in origami drill books, webpages, and so on. Traditional origami has usually been studied using diagrams in drill books in which the processes of the simple folding operations were illustrated. Origami creators who are the authors of such books commonly simplify origami models and illustrate the order of folding using detailed step-by-step instructions. However, recently, we often find realistic, modern, and complex origami models that are designed by geometric origami design methods [4]. These origami designers draw line segments (creases) onto a sheet of paper and generate the crease pattern, which is the unfolded state of the paper with creases indicated thereon. In other words, they design a new model fully before they fold it. In these works, designing the models consumes much of the creators' time and energy, because they have to imagine the completion of the crease pattern or actually fold it after designing in order to determine its final appearance.

In this paper, we propose a method for constituting origami models from handwritten sketches and other two-dimensional images. When there is no illustration of a design that users want to fold, origami models may be constituted from images that users input or draw. By this means it becomes possible to create origami models that users seek at any time.

In the past, Uchida et al. [9] have proposed an approach to deduce a folding process from a crease pattern of origami models, but it was based on the premise that the origami models were designed by traditional folding operations. Eisenberg et al. [1,3] have discussed the "folding net problem" for the purpose of transforming three-dimensional virtual objects such as polyhedra into a paper representation of the model as a way of creating a hard copy from virtual environments; this is the opposite of our approach. However, in such scenarios, the faces of the three-dimensional polygon models do not overlap each other. In our approach, constructed models may be inconsistent because of the overlapping faces. This paper proposes a method for constructing consistent origami models from the crease patterns.

2 Overview

The outline of processing is shown in Figure 1. This processing is roughly divided into two phases. The first phase constitutes a crease pattern from a sketch; the second constructs a virtual model from the crease pattern. These are described in further detail below.

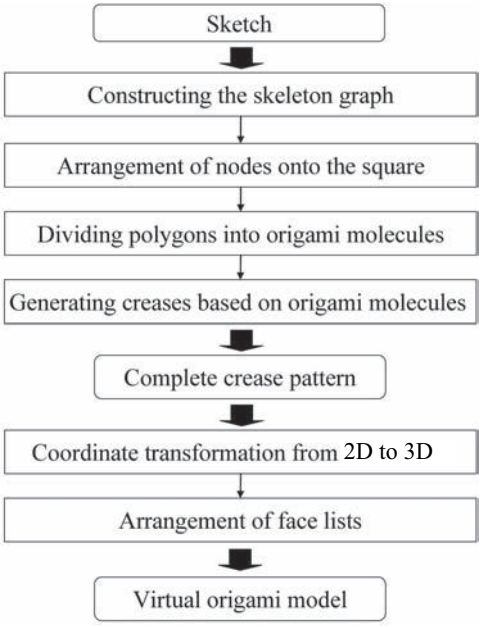

Figure 1. The outline of the process.

2.1 From Sketches to Crease Patterns

The procedure of constituting a crease pattern from sketches is as follows [7]. First, a data structure, called a *skeleton graph*, of an object is extracted from a sketch given as input. Second, the skeleton graph is arranged onto a square, and polygons are constituted in the square. Third, the polygons are divided into origami molecules. Finally, creases are created based on the origami molecules and the complete crease pattern is constituted.

Skeleton graph. Skeleton graphs are constructed by segmenting the skeleton images of the initial sketch. Figure 2 shows an example of extracting a skeleton image from a sketch and constructing a skeleton graph. The skeleton graph is defined as follows:

$$\begin{aligned} SG &= (V, E), \\ V &= \{v_i \mid 1 \leq i \leq \mathcal{N}\}, \\ E &= \{e_{ij} = (v_i, v_j) \mid v_i, v_j \in V\}, \\ X &= \{x_i\}_{v_i \in V}. \end{aligned}$$

In the above, SG represents the skeleton graph, which is a pair that consists of sets of vertices and edges. Moreover, the vertices V have their coordinates X of $\mathcal{N}$ points extracted from the skeleton image. The SG is constituted from the image by thinning the silhouette image, resulting in a tree graph, which is a connected graph without cycles.

Crease pattern. In order to construct three-dimensional virtual paper-made objects from crease patterns, the rotational transformations based on creases using the adjacency relationship among the faces are needed. Therefore, a graph of the crease pattern in which nodes represent faces and edges represent creases is constituted, which can represent the positional relationships among the faces easily (Figure 3). We call this graph the *CP-graph*.

The crease pattern CP consists of the vertex set V, the crease set C and the face set F. A crease $c_{i,j} \in C$ has information on position coordinates and angle $\theta_{i,j}$ between two faces f_i, f_j. If $\theta_{i,j} = \pm\pi$ then the crease means valley or mountain folding in origami. Moreover, as shown in Figure 4, when one of the right-handed-rotation vectors around the face f_i is defined as $\overrightarrow{c_{i,j}}$ which belongs to $c_{i,j}$, the unit vector of $\overrightarrow{c_{i,j}}$ is defined as $\widehat{c_{i,j}}$, and the vector from the origin to the starting point of $\overrightarrow{c_{i,j}}$ is defined as $t_{i,j}$.

Origami design. Origami models are designed based on *origami molecules*. Origami molecules are defined as minimum units that have a certain meaning and a set of faces in origami. Although there are many types of molecules, the most general one is shown in Figure 5. The left figure represents a triangular molecule that has creases of three bisectors of each

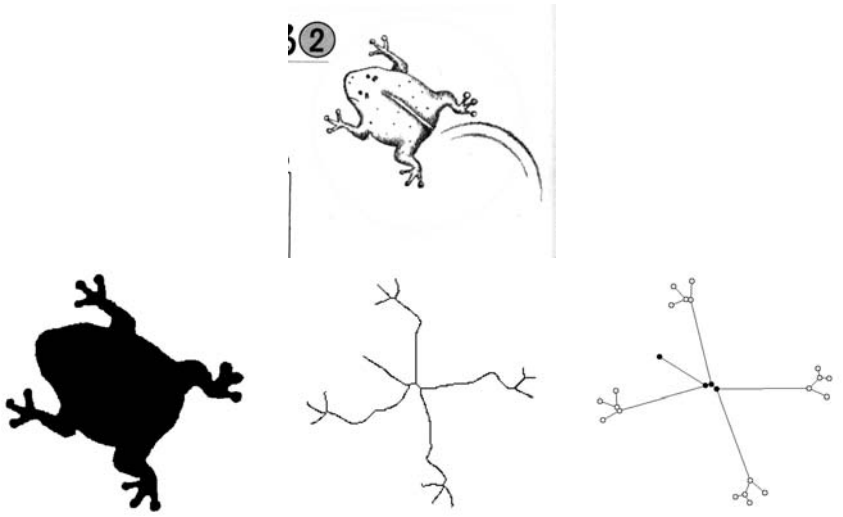

Figure 2. An example of extracting a silhouette, a skeleton, and a skeleton graph.

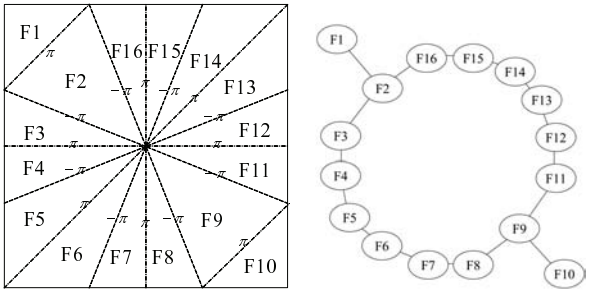

Figure 3. An example of a crease pattern (left), and a face-crease graph of the crease pattern (right).

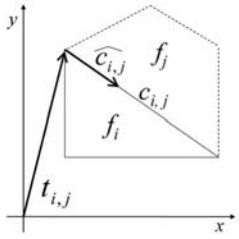

Figure 4. Vectors for a crease.

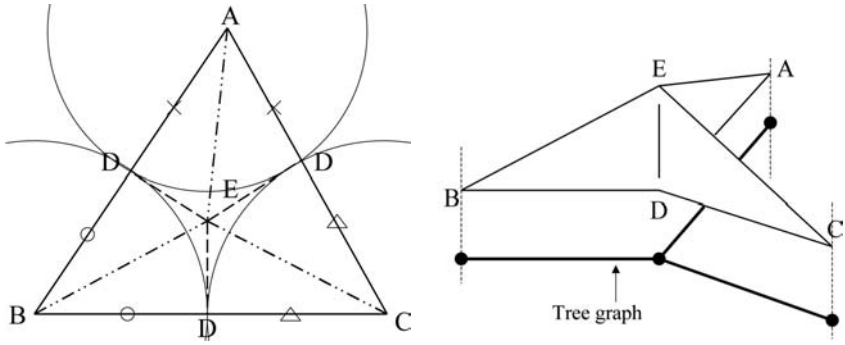

Figure 5. An example of a triangular origami molecule called *rabbit ear*.

corner and perpendiculars from the center of gravity of the triangle to each edge. The right figure is the origami model that is folded from the triangular molecule in practice. A crease pattern is constituted so that the faces in the square are origami molecules.

A *flap* is one of the most important concepts in origami design. We explain this concept using Figure 5. The flap is the part of the origami model that is represented as a circle, and the center of the flap represents the apex of the part (A, B, and C). The circles map out regions that are necessary to constitute each distinct part of origami model. The tree graph is now seen to be the two-dimensional projection of the origami model and the terminal nodes of the tree graph are corresponding to distal points of the flaps. In this paper, the crease pattern is constituted from the skeleton graph when used as the tree graph. The node arrangement optimization method and the method for dividing these polygons into origami molecules proposed by Lang [4] may therefore be used.

2.2 From Crease Patterns to 3D Models

Although international conferences on origami science have been held only four times in recent decades, research related to origami has been ongoing in various fields, including mathematics, engineering, and art. In these fields, especially in the mathematical field, *foldability* was the focus of research. Origami foldability means to decide the following problem: given a crease pattern, does it have a folded state? Bern et al. [2] proved that this decision problem is NP-hard and thus can be computationally intractable. This difficulty arises specifically because computing a valid overlap order of faces that fold to a common portion of the plane is very difficult. In this paper, an approximate algorithm for analyzing the overlap order from the given crease pattern by using *cross sections* of an origami model is proposed [8].

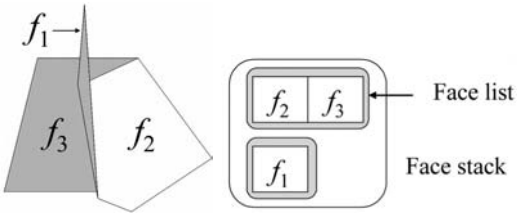

Figure 6. A structure of faces.

Preconditions of the given crease pattern and the structure of the resulting origami models are described in the following subsections.

2.3 3D Origami Model

Miyazaki et al. [5] have previously proposed a data structure for origami that has made it possible to easily represent overlapping faces on the same plane. An example of this structure is shown in Figure 6. The structure groups face on the same plane while face lists hold the order of overlapping between faces, e.g, $f_2 \rightarrow f_3$. Because the orders of overlapping faces are unknown when we try to transform a crease pattern into a three-dimensional origami model, we propose a method for consistently arranging the face lists from the given crease patterns in the following section.

3 Coordinate Transformation

Once an arbitrary face f_0 in a crease pattern has been fixed on the xy-plane, three-dimensional transformations of all other faces can be calculated using the CP-graph as follows. First, a path from the fixed face f_0 to another face f_p is searched. In order to minimize computational complexity, the shortest path (the path length of any edge is regarded as one) is selected. When the obtained path is provided, for example,

$$f_0 \rightarrow \cdots \rightarrow f_q \rightarrow \cdots \rightarrow f_p,$$

the order of edges along this path is defined as

$$c_{0,1} \rightarrow \cdots \rightarrow c_{q-1,q} \rightarrow c_{q,q+1} \rightarrow \cdots \rightarrow c_{p-1,p}.$$

Next, a transformation matrix for each crease $c_{q-1,q}$ is calculated. A rotational matrix through an angle $\theta_{q-1,q}$ for the crease vector $\widehat{c_{q-1,q}}$ is defined as R_q; a parallel translation matrix for the vector $t_{q-1,q}$ is defined as T_q. Then, the transformation matrix X_q for the crease $c_{q-1,q}$ is

$$X_q = T_q R_q T_q^{-1}.$$

Consequently, the 3D transformation matrix Z_p for a face f_p based on the path from the fixed face f_0 is

$$Z_p(x, y, 0, 1) = X_1 ... X_q ... X_p(x, y, 0, 1)^t \quad \text{for } (x, y) \in f_p.$$

By calculating this Z_p for all faces in the crease pattern, it is possible to construct the 3D shape of the paper object.

4 Arrangement of Face Lists

In the previous section, we described how all faces in a crease pattern are transformed into a 3D space. Therefore, the 3D origami model, which is described in Section 2.3, can be constructed by using these faces.

First, all faces are grouped with faces on the same plane. Moreover, each group is able to be defined as a subgraph of the CP-graph and the subgraph consists of the edges of only those creases whose angles θ are $\pm\pi$: those creases correspond to valley/mountain foldings. Such a subgraph can be colored with two colors because the sides of any two faces which share the same folded crease become reversed with respect to one another.

Next, by using the two-colored subgraph, a face list is consistently arranged by considering the positional relationship between two faces in the list. The positional relationship between two faces is defined as follows.

Definition 1. When a face f_i should exist above a face f_j, we write $f_i > f_j$.

Therefore, the face list is ordered (numbered) so that all face pairs in the list satisfy $f_i > f_j$ for $i < j$, where the i-th face and the j-th face in the list are f_i and f_j, respectively. A method for arranging face lists from faces in a crease pattern is proposed in the following subsections. This method first judges the relationships between any two adjacent faces in a crease pattern, and then analyzes overlap order of all faces by using the obtained adjacency relationship.

4.1 Overlap Order of Adjacent Faces

When there are two adjacent faces f_i, f_j that share a crease $c_{i,j}$, the condition for satisfying $f_i > f_j$ is

- the near side of f_i is the front and $\theta_{i,j}$ is $-\pi$, or
- the near side of f_i is the back and $\theta_{i,j}$ is π.

Figure 7 shows an example of two adjacent faces. The near side of face f_1 is the front and the near side of face f_2 is the back. Moreover, the angle $\theta_{i,j}$ of the crease between the faces is $-\pi$, that is, a mountain fold. Therefore, it is certain that the positional relationship between these two faces becomes $f_1 > f_2$.

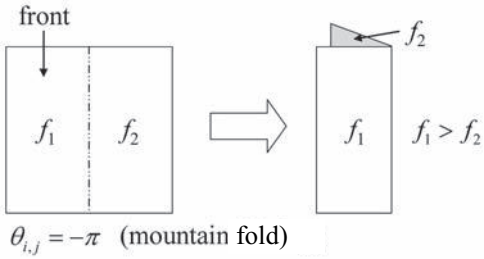

Figure 7. An example of adjacent faces.

4.2 Analyzing Overlap Order of Faces

By using the adjacency relationship, the elements of the face list are sorted and the order is analyzed. However, it is realistically impossible to compute a global solution for the ordering under all circumstances due to the inherent computational complexity of the problem. Therefore, we propose a method for analyzing overlap order based on simulated annealing and consideration of cross sections of the origami model.

Figure 8 shows an example of the cross section that is obtained by cutting an origami model. The obtained cross section consists of a set of segments. A cross section is obtained perpendicular to a face in the face list. Moreover, all nodes of the cross section need to be linearly connected with segments. A method for generating the cross section by drawing line segments in the crease pattern has already been proposed [6]. This method generates the cross sections using the symmetry of the obtained segments. The obtained cross section S that consists of segments is defined as

$$\{s_0, ..., s_i, ..., s_j, ..., s_n\} \in S$$

where S is a simple path or may be a cycle, where $s_0 = s_n$.

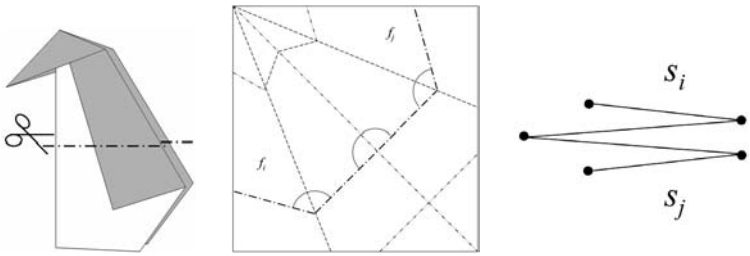

Figure 8. An example of generating a cross section.

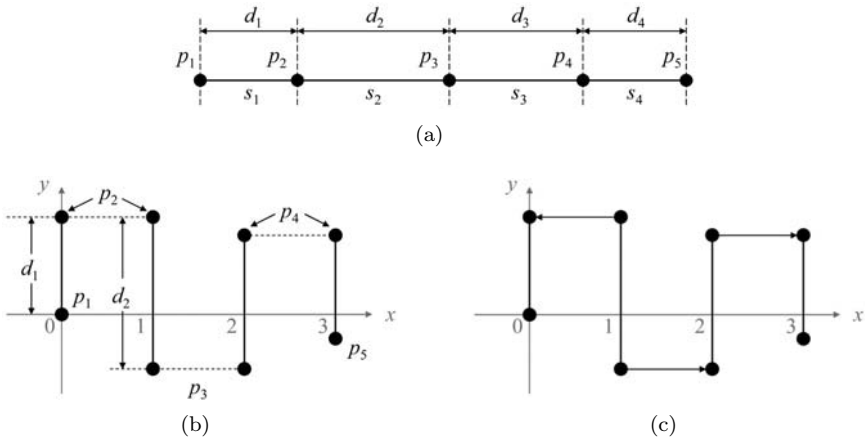

Figure 9. Arrangement of a cross section onto a two-dimesnional plane: (a) A cross section that consists of segments. (b) Arrangement onto two-dimensional plane. (c) The linked vectors.

M cross sections are generated equiangularly around the center of gravity of each face in the crease pattern. In order to analyze relationships among segments of each cross section, the segments are arranged in a two-dimensional plane such as Figure 9. In this figure, there are segments $\{s_1, s_2, s_3, s_4\}$ and the distance between terminal nodes p_i, p_{i+1} of the segments is represented as d_i.

First, the segments are arranged to be parallel with the y-axis in order at a regular interval, and the y-coordinates of the terminal nodes are associated with the same nodes. Next, by using a vector r_i, we link the terminal nodes of pairs of adjacent faces. If $f_i > f_{i+1}$, the direction of r_i is negative about x-axis. If $f_i < f_{i+1}$, the direction of r_i is positive.

When the order of segments satisfies the following conditions, the relationship among segments is consistent:

1. All r_i's are positive directions to the horizontal axis.
2. All r_i's do not cross any segments.

The first condition determines global consistency using local (adjacent) relationships, and the second condition specifies physical feasibility. Figure 10 shows an ordering that satisfies these conditions, using the segments in Figure 9. Only two types of ordering are consistent.

We use a simulated annealing algorithm to obtain consistent overlap order of the cross section. The cost function F is defined by formulating the above conditions:

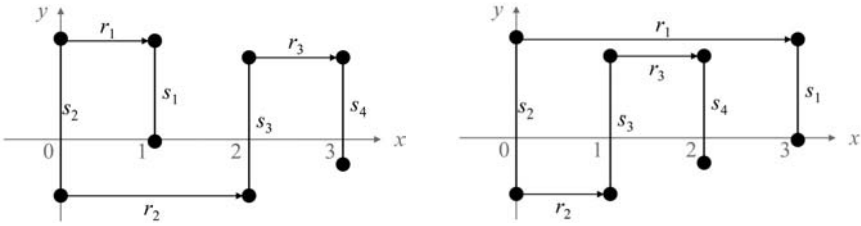

Figure 10. Feasible order of segments in Figure 9.

$$F = \sum_{j=1}^{M} (\alpha \cdot Nd(j) + \beta \cdot Ns(j)) \quad \text{for all } s(j) \in S,$$

where $Nd(j)$ is the number of r_i's in the negative direction (i.e., condition 1), $Ns(j)$ is the number of points at the intersection of r_i with other segments (i.e., condition 2), and α and β are coefficient constants.

5 Experimental Results

We have implemented a prototype system based on the proposed method. The crease pattern is designed using the proposed origami design method from the extracted skeleton. Moreover, the system automatically constructs the three-dimensional paper-made object from the crease pattern. The implementation is tested with some skeletons and the resulting objects are represented in 3D virtual space.

Figure 11 shows the result of constituting the origami model from a sketch that is a real illustration taken from an origami drill book. The nodes are arranged in the optimal position onto a square, polygons are divided into origami molecules and creases are created (Figure 11(e)). Finally, an origami model is actually constituted based on the crease pattern (Figure 11(f)).

Origami models constructed from crease patterns constituted by the proposed method have fundamental 3D forms. However, these crease patterns are confined to constitute each part of objects, and it is infeasible to realize the small details. At any rate, in the field of origami design, final design is dependent upon the aesthetic sense of the designer. As an example, Figure 11(g) shows the result of modifying the origami model in Figure 11(f) by the authors' subjectivity.

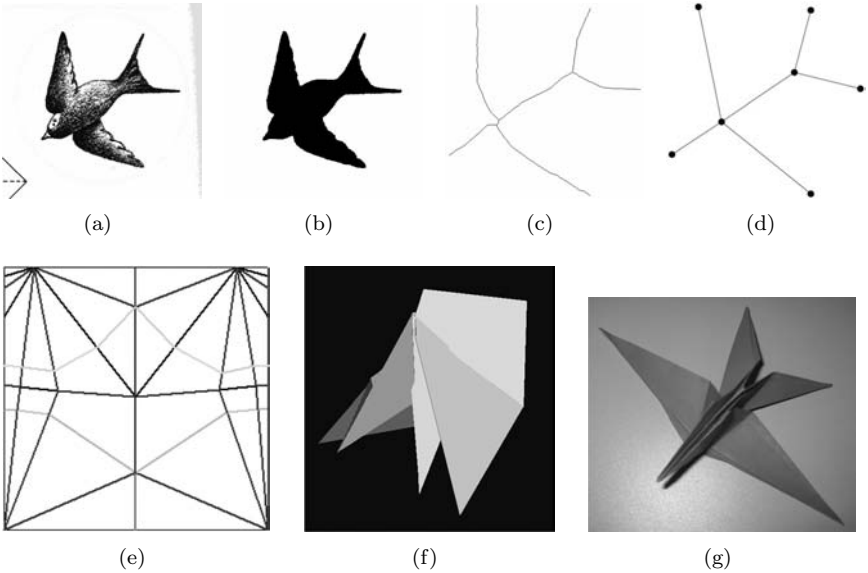

Figure 11. The experimental results: (a) A sketch. (b) The silhouette image. (c) The skeleton image. (d) The skeleton graph. (e) The crease pattern. (f) The virtual model. (g) Modification the "real" origami model in Figure 11(f).

6 Conclusion

This paper proposes and describes a method for constructing 3D paper-made objects by using skeletons obtained from 2D images such as handwriting sketches. The framework that constitutes origami models from the skeleton graph is explained, which makes it possible to constitute crease patterns automatically from sketches. Moreover, the method for constructing 3D paper-made objects from crease patterns is presented. The proposed coordinate transformation makes it possible to represent paper-made objects in 3D virtual space. Furthermore, the proposed analysis method of the positional relationships among faces arranges the faces overlapped on the same plane after the transformation in a consistent order. Experimental results have demonstrated that our current work is able to construct consistent paper-made objects from sketches.

We note that as part of the origami design process, it is necessary to deal with this problem: how to find the "optimal" solution if multiple interpretations for one crease pattern exist. Moreover, in order to animate origami in 3D virtual space, it is necessary to extract folding process or something close to it from given crease patterns. We leave that for future work.

Bibliography

[1] Shaun Bangay. "From Virtual to Physical Reality with Paper Folding." *Computational Geometry: Theory and Applications*, 15:1–3 (2000), 161–174.

[2] Marshall Bern and Barry Hayes. "The Complexity of Flat Origami." In *Proceedings of the Seventh Annual ACM-SIAM Symposium on Discrete Algorithms*, pp. 175–183. Philadelphia: SIAM, 1996.

[3] Michael Eisenberg. "The Thin Glass Line: Designing Interfaces to Algorithms." In *Proceedings of the SIGCHI Conference on Human Factors in Computing Systems*, pp. 181–188. New York: ACM Press, 1996.

[4] Robert J. Lang. A Computational Algorithm for Origami Design. In *Proceedings of the Twelth Annual Symposium on Computational Geometry*, pp, 98–105. New York: ACM Press, 1996.

[5] S. Miyazaki, T. Yasuda, S. Yokoi, and J. Toriwaki. "An ORIGAMI Playing Simulator in the Virtual Space." *The Journal of Visualization and Computer Animation* 7:1 (1996), 25–42.

[6] H. Shimanuki, J. Kato, and T. Watanabe. "Constituting Feasible Folding Operations Using Incomplete Crease Information." In *Proceedings of the IAPR Workshop on Machine Vision Applications (MVA2002)*, pp. 68–71. Nara, Japan: IAPR, 2002.

[7] H. Shimanuki, J. Kato, and T. Watanabe. "Constituting Origami Models from Sketches." In *Proceedings of the 17th International Conference on Pattern Recognition*, pp. 628–631. Washington, DC: IEEE Computer Society, 2004.

[8] H. Shimanuki, J. Kato, and T. Watanabe. "Construction of 3-D Paper-Made Objects from Crease Patterns." In *Proceedings of the IAPR Conference on Machine Vision Applications (MVA2005)*, pp. 35–38. Tsukuba Science City, Japan: IAPR, 2005.

[9] T. Uchida and H. Itoh. "Knowledge Representation of Origami and Its Implementation" (in Japanese). *IPSJ* 32:12 (1991). 1566–1573.

An Excel-Based Solution to the One-Cut Folding Problem

Alexander C. Huang

1 Introduction

Given a planar graph drawn with straight lines on a paper, can the piece of paper be folded so that the entire graph can be mapped to a common line for a straight single cut? In 1998, Erik Demaine, now an MIT professor, approached the question using two different methods. The first method [2,3], the *straight skeleton*, solves the problem for a polygon by shrinking the sides at a given rate and stopping when one side disappears, then continuing the process with the new, smaller polygon. In this way, a hexagon, for example, could be reduced to a pentagon, then a square, then a triangle, then a point. However, in this method there is no guarantee of finiteness of the number of so-called perpendicular creases in the solution. The second method [1], called the *disk packing* method, describes an algorithm that fills up a polygon diagram with different sizes of disks from which a crease pattern is then constructed; this method provides a guaranteed finite solution. The calculation time for filling up the disk packing is on the order of $n(\log n)^2$ with n being the number of disks placed, and they must be placed according to these rules: the disks may not overlap, the edges of the polygon are the union of the radii of the disks, and the gaps between disks have either three or four sides creating both triangles and quadrilaterals. Triangles are filled with the three (intersecting) angle bisectors and perpendiculars from the incenter to the sides. Quadrilaterals are filled by a pattern called the *gusset quad molecule* [1,5].

Although the straight skeleton-based algorithm may in principle result in an infinite number of creases, for many patterns it is not only finite; it is also quite simple to implement. In this work, this famous one-cut problem is revisited with the description of an implementation of the straight skeleton using only angle bisectors and perpendiculars. The new method is simple enough to be implemented in Excel to automate the crease creation process.

2 A New Implementation of the Straight Skeleton

Among all possible folding creases, angle bisectors and perpendiculars are the most important. The angle bisectors allow two adjacent sides of a polygon to be folded into a single line. The perpendiculars, on the other hand, allow a single side to be folded toward itself into a single line. After many experiments it was concluded that the following algorithm, a variation of the straight-skeleton technique, solves the one-cut folding problem:

1. Create angle bisector of the angle created by two adjacent sides; repeat at all other vertices.
2. For bisector A extending from vertex A, find out where it intersects with the two adjacent bisectors.
3. Find the bisector that intersects with bisector A closest to vertex A, dubbed bisector B extending from vertex B.
4. If the intersection of bisectors A and B is also closer to vertex B than the intersection between bisectors B and C, then form crease A and B up to their intersection, now labeled intersection Z.
5. Remove bisectors A and B from the pool and repeat steps 2–4 with all other bisectors and different names. Bisectors left without a determined intersection will be dealt with later.
6. At intersection Z, form perpendicular creases out to the neighboring sides. Repeat with all other intersections.
7. Create a flat vertex fold at intersection Z using bisectors A, B, and one of the perpendicular creases created in step 6. This gives us a new line, bisector $A1$. Repeat with all other intersections.
8. Repeat steps 2–4 with bisectors $A1$, $B1$, etc.
9. Repeat steps 2–8 until the system is finally closed, when the final three angle bisectors meet at the same point (the *in-center*).

It is worthy to note the following:

1. Bisectors A and B can be considered *primary bisectors* because they come from two sides adjacent to each other.

2. Bisectors $A1$ and $B1$ can be considered *secondary bisectors* because they can be envisioned as the angle bisectors from two sides that are not immediately adjacent to each other. The secondary bisector is the result of a flat vertex fold, but it can also be regarded as the angle bisector of sides 1 and 3 while side 2 is sandwiched.

3. Higher-order angle bisectors (for example, $A2$, $B2$, $A3$, $B3$, ...) are needed for more complex polygons. For example, a *tertiary bisector* is the angle bisector of sides 1 and 4 while sides 2 and 3 are sandwiched.

4. The above algorithm was also tested on shapes both convex and non-convex. It was observed that concave vertices obey the same law that convex vertices do. That is, the angle bisectors from concave vertices also intercept with other angle bisectors just like the way angle bisectors from convex vertices do, except that the intersections may lie outside the original polygon.

5. This new algorithm was verified to obey the Maekawa theorem and the Kawasaki theorem [4]. The former states that when creases meet at an intersection, to be a flat origami, there must be two more (or two fewer) mountain folds than valley folds. As a result of the Maekawa theorem, the total number of creases that meet at the intersection must be an even number. The Kawasaki theorem, on the other hand, states that every other angle at the flat vertex fold must add up to 180°.

As an example, the above algorithm is illustrated step-by-step in constructing the folding creases of an irregular hexagon.

1. Start with a hexagon (Figure 1(a)) and draw the angle bisectors (Figure 1(b)).

2. Drawing out the bisectors is like shrinking the sides at a uniform rate (Figure 1(c)). After extending the angle bisectors, two will meet (Figure 1(d)).

3. One side of the shrunken polygon eventually disappears and reduces the hexagon to a pentagon (Figure 1(e)). Two sides of the outer hexagon form an additional vertex outside the original hexagon (Figure 1(f)).

4. The new vertex forms a secondary angle bisector (Figure 1(g)).

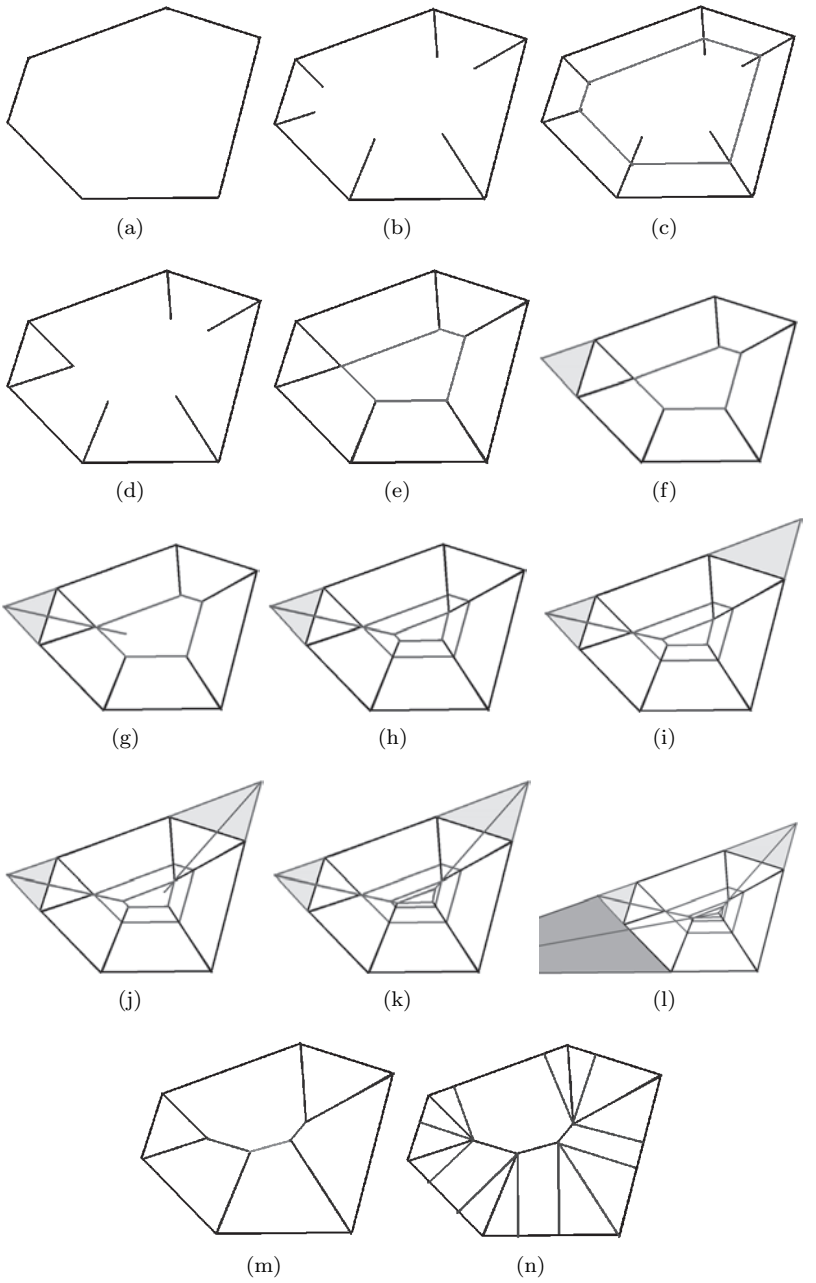

Figure 1. (a)–(m) Step-by-step construction of angle bisectors. (m) Completed bisectors. (n) Perpendicular creases are added further to complete the pattern.

5. The same shrinking process is repeated. Continue until two more bisectors intersect, one more side is further reduced, and the inner polygon is now a quadrilateral (Figure 1(h)).

6. The above reduction has the same effect as extending the sides of the original polygon (Figure 1(i)), and another secondary angle bisector is drawn (Figure 1(j)).

7. Continue shrinking the inner quadrilateral. Two more bisectors touch, creating the final form. The most inner shape is now a triangle (Figure 1(k)).

8. The reduction process results in one big triangle whose bisectors meet at the in-center (Figure 1(l)).

9. After removing the extra lines and returning the original polygon, the solution is shown (Figure 1(m)).

10. Perpendicular lines are added to finalize the overall folding crease construction (Figure 1(n)).

3 Implementation with Excel

As an illustration, an Excel program was written for generalizing the calculation of pentagon creases to the one-cut folding problem. The coordinates of the pentagon's five vertices can be arbitrarily assigned or automated via scroll buttons. The primary and secondary angle bisectors are automatically calculated and displayed. This program, though in its current form dealing with pentagons, can be easily expanded to arbitrary polygons and fold crease-creation. Below is the sequence of our calculations.

1. The computer program starts by calculating the slope and y-intercept of each side.

2. The convexity of each vertex is determined using the vertex coordinates in relation with its neighboring vertices.

3. The interior angle of the vertex is calculated via trigonometric formula.

4. The interior angle of the vertex is halved to form the primary angle bisector's direction. The slope and the y-intercept of the bisector are calculated subsequently.

5. Repeat the calculation of the slopes and intercepts of the primary bisectors of all vertices. This provides the entire set of primary bisector information.

6. Calculate the coordinates of all intersections of bisectors from adjacent vertices. Folding crease line is drawn only from the nearer intersection to the vertex. This completes the drawing of the primary bisectors.

7. Information of the secondary angle bisectors is calculated next. If side 1 and side 2 meet up at vertex 1, side 2 and side 3 intercept at vertex 2, and if vertex 1 and vertex 2 shoot off bisectors meeting at point F, the secondary bisector from point F can be calculated with the angle and vertex formed by side 1 and side 3.

8. Repeat for all vertices. For pentagons, two primary-bisector intersections and two secondary bisectors are calculated.

In the calculations of the secondary bisectors based on three neighboring sides, nine different scenarios of concave/convex combinations were found during the debugging phase of the Excel program. Each scenario was implemented differently such that a secondary angle bisector could be computed by rotating a neighbor side counterclockwise or clockwise.

The screenshot of the Excel program is shown in Figure 2. The A and B columns in Figure 2 store the pentagon's x- and y-coordinates; users can arbitrarily scroll up and down the coordinate numbers. Each time the coordinate changes, the calculation of line equations, inner angles, bisectors, and intersection points is automated, and the crease graph is updated. The graph can then be output to a printer to facilitate manual folding.

4 Summary and Conclusion

In this work, we revisited the famous one-cut folding problem and proposed a variation of the straight-skeleton algorithm to solve it. The method is based on only angle bisectors of adjacent sides (primary bisectors) and nonadjacent sides (higher-order bisectors). The reason that only angle bisectors are involved is because they allow adjacent sides to line up topologically. Adding the perpendiculars allows a single side to fold toward itself. The method is easy enough to be implemented programmatically. Using the algorithm, a computer automation program was developed via Excel. With arbitrarily chosen coordinates of vertices, the program can generate the primary and secondary angle bisectors, which are the folding creases for the one-cut problem.

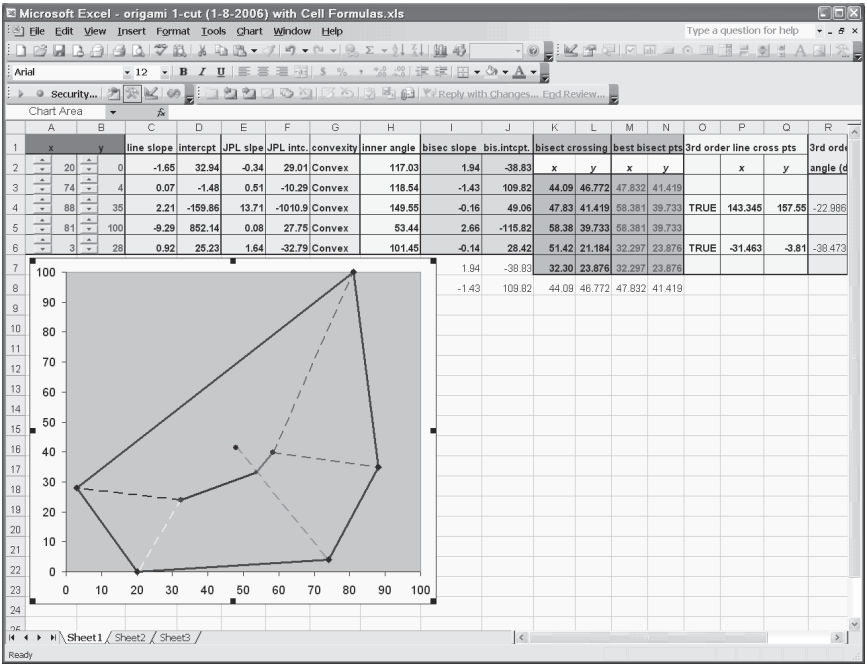

Figure 2. A screenshot of the Excel program demonstrated with pentagons. The five coordinate pairs (x, y) of the pentagon are listed in columns A and B. Each x- and y-coordinate is attached with a simple scroll so the user can easily change the pentagon shape at runtime.

Acknowledgment. The author thanks Dr. Robert J. Lang for corrections and suggestions.

Bibliography

[1] M. Bern, E. D. Demaine, D. Eppstein, and B. Hayes. "A Disk-Packing Algorithm for an Origami Magic Trick." In *Origami^3: Proceedings of the Third International Meeting of Origami Science, Mathematics, and Education*, edited by Thomas Hull, pp. 17–28. Natick, MA: A K Peters, 2002.

[2] E. D. Demaine, M. L. Demaine, and A. Lubiw. "Folding and Cutting Paper." In *Revised Papers from the Japan Conference on Discrete and Computational Geometry*, edited by J. Akiyama, M. Kano, and M. Urabe, pp. 104–117. New York: Springer, 2000.

[3] E. D. Demaine, M. L. Demaine, and A. Lubiw. "Folding and One Straight Cut Suffice." In *Proceedings of the Tenth Annual ACM-SIAM Symposium on Discrete Algorithms*, pp. 891–892. Philadelphia: SIAM, 1999.

[4] K. Kasahara and T. Takahama. *Origami for the Connoisseur*. Tokyo–New York: Japan Publications, 1987.

[5] R. Lang. "A Computational Algorithm for Origami Design." In *Proceedings of the Twelfth Annual Symposium on Computational Geometry*, pp. 98–105. New York: ACM Press, 1996.

Computer Origami Simulation and the Production of Origami Instructions

Tung Ken Lam

1 Introduction

Computer origami simulation has challenged many different researchers. This paper summarizes existing achievements and explores the usability of origami simulation programs.

In particular, it discusses the challenges of automatically producing diagrams for the printed page. The motivation for this work is that the task of making origami diagrams is both difficult and time consuming. Although it is now common for diagrammers to use computers, few authors use programs that are specifically written for origami diagramming.

As part of a research project, the author developed a program that extended S. Miyazaki's origami simulation [22] to automatically produce diagrams. Feedback on the prototype suggested that further work on this approach would be worthwhile.

2 Motivation

Whenever a group of origami enthusiasts gather, it's likely that, sooner or later, they will share the folding of some origami designs, and, sooner or later, someone will ask the question, "Do you have diagrams. . . ?"

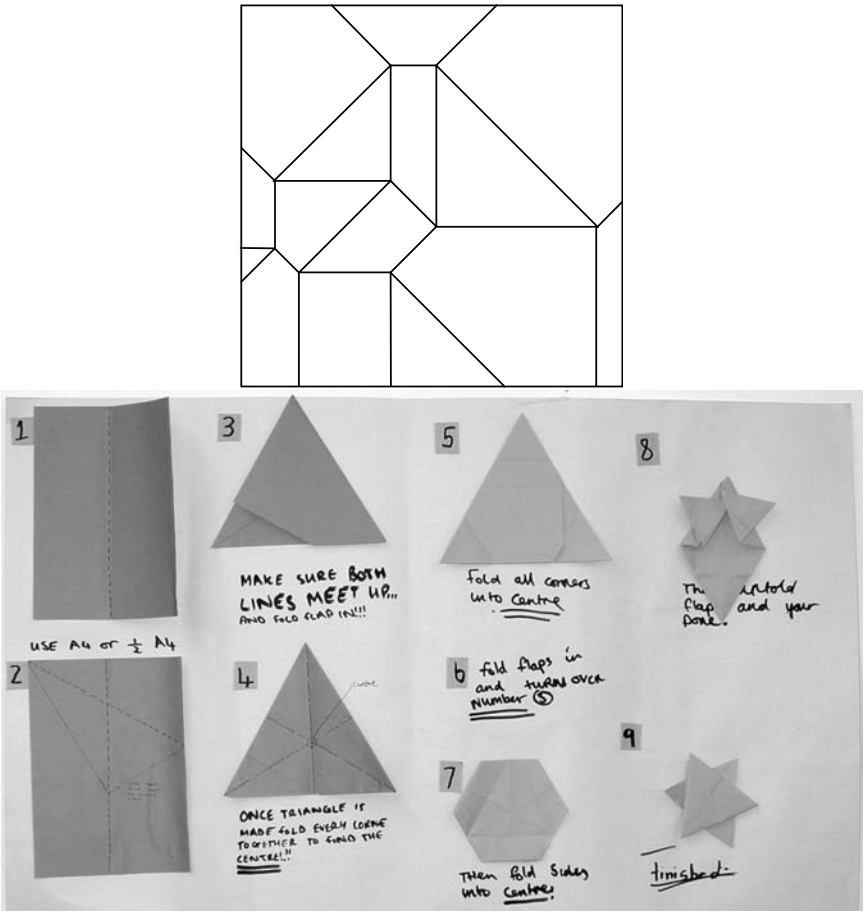

Figure 1. A crease pattern (from [6]) and step folds (by Josh + Ferron 7M).

As Koshak [12] wrote:

> Even though diagrams are the most common way to document origami, the labor involved keeps many model designers from documenting their models ... The major disadvantage to diagramming is that generating them is a tedious, laborious and error prone process.

Diagrams are commonly used because they are relatively easy to view and reproduce. There are a number of alternatives such as video, computer animation, photographs, step folds (Figure 1, bottom), crease patterns

(Figure 1, top), and text. The first four methods are relatively difficult and expensive to create and/or reproduce. Furthermore, the first two are not convenient to view because they require special equipment. For most people the last two methods are not sufficiently detailed.

A further advantage of diagrams is that they are understood by almost all origami enthusiasts. Even if they are written in a foreign language, they can be understood from their use of pictures and standardized symbols.

3 Computers and Origami Diagramming

The use of computers to aid diagramming has been established since the mid 1980s [15]. Typical computer tools include

- bitmap paint programs,
- vector drawing/illustration programs (Figure 2),
- CAD (computer aided design),
- General purpose software, e.g., word processors,
- programming languages (Figure 3).

Although the use of computer tools can help, their usefulness is limited because many are not designed specifically with the task of origami diagramming in mind. From time to time, folders have mooted the use of a tool that simulates origami and automatically produces origami diagrams for the printed page. Therefore a search of previous and related work would establish the feasibility of such a diagramming tool.

4 Existing Origami Simulations

A typical origami enthusiast may be surprised by the number of researchers that simulated origami in the course of their research. The surprise can be partly understood because the research is not about origami *per se*, but origami is used as a *context* for research.

4.1 Origami as a Context for Research

Examples of ways in which origami is used as a context for research include

- simulation of folding and virtual reality [24],
- scene capture [34] and diagram recognition [9, 10, 26, 30],

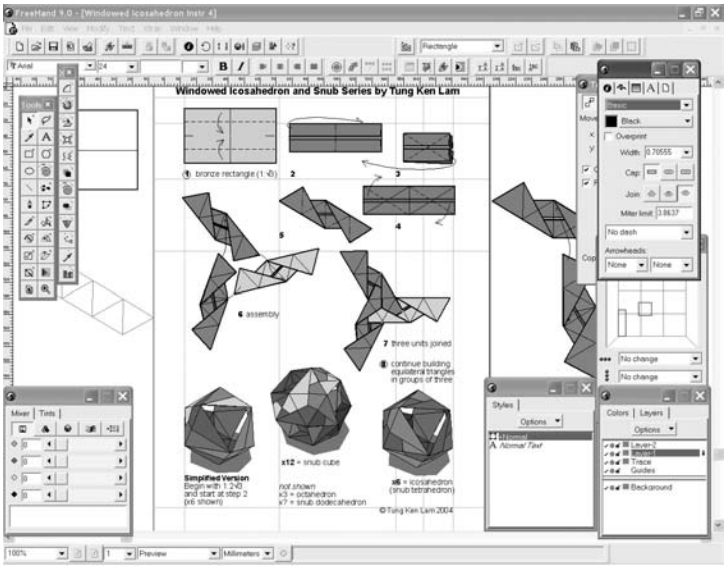

Figure 2. Screenshot of Macromedia Freehand 9.0 showing diagrams in preview mode.

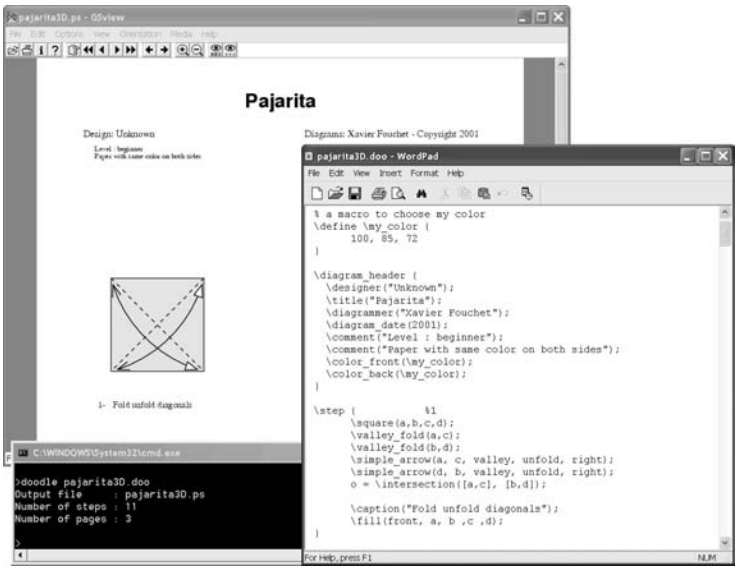

Figure 3. Typical arrangement of windows for working with a Doodle file (Xavier Fouchet's Pajarita).

- investigations of software and teaching and learning [11, 19, 36],
- mathematical modeling and proof [7, 8, 18, 35].

4.2 Origami Specific Software

There are three main categories of software specifically designed for origami.

Tools to assist origami design. These programs simulate particular aspects of origami to fulfill their main purpose.

- Tess is a program that makes crease patterns for origami tessellations and shows their results [1, 2].
- ReferenceFinder determines folding sequences for a specific location, e.g., $(0, \frac{2}{5})$, and produces instructions using diagrams and text [16].
- TreeMaker is a program for designing uniaxial bases [17].
- There is a program that takes a sketch as an input and produces an origami version of the sketched object [27, 28].
- ORIPA is an editor for designing crease patterns and viewing the results [20].

Origami-oriented languages. Examples of this second category are Oridraw [33] and Doodle [5] (Figure 3). They both require the user to construct programs that are compiled into printable PostScript diagrams. Fisher [4] created a system that allowed the user to document a design on-screen using a combination of text and mouse input.

The audience for origami-oriented languages is limited due to the need for programming skills. Although Oridraw and Doodle have features specifically for origami, the user is still required, to a greater or lesser extent, to manage the position of lines, vertices, and polygons by hand.

Direct manipulation and virtual reality origami simulation. *Direct manipulation* is a human-computer interaction style that offers a "natural" input method, offers immediate visual feedback, and allows for rapid, incremental, and reversible actions [29].

There are two types of direct manipulation in this category: in the first type the user *manipulates origami*, whereas in the second type the user *manipulates diagrams*. Examples of the first type are origami simulations by Lang [13] and by Miyazaki [23] and eGami by Fastag [3]. Examples of the second type are Foldinator by Szinger [31] and Java Origami by Nimoy [25]. The type of interaction feels different: the first type attempts

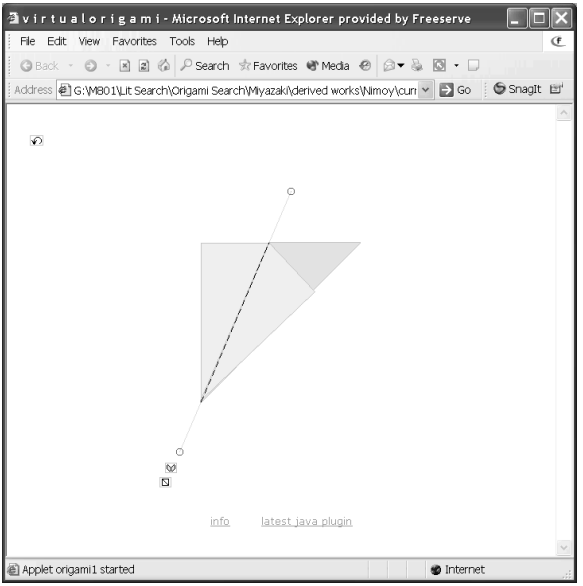

Figure 4. Nimoy's Java origami simulator showing the second step of the traditional cup.

to simulate the feel of folding, but the second requires the user to construct folds by positioning symbols and then executing them (Figure 4).

Manipulating origami is likely to be preferred by novice users because it maps more closely to the familiar domain of folding paper. However, manipulating diagrams could allow more sophisticated users to construct more sophisticated origami and adjust the appearance of the diagrams as they go. The most capable program for manipulating origami currently available is examined in the next section.

5 Extending Miyazaki's Simulation for the Printed Page

5.1 Miyazaki's Simulation

Miyazaki's simulation [22] allows the user to directly manipulate "virtual paper." The user clicks and holds the left mouse button to pick up the paper, drags the mouse to position the paper and then releases the mouse button to put the fold in place.

The simulation is three dimensional and the user can rotate and zoom the camera to better view the origami. Besides valley folds, the user can make (inside) reverse folds. The ability to animate between steps is impressive.

5.2 New Features

The existing simulation is relatively sophisticated, but is limited to screen display. Therefore the program was extended to output PostScript diagrams that can be printed. It used a simple scheme to automatically arrange the diagrams on the page. Each diagram step was meant to have the same camera orientation as the screen view.

Other changes included implementing outside reverse folds, adding menus for controlling viewpoint, adding an extra turn over function, and providing the ability to save/open a folding other than "default.ori" and the ability to load different settings, e.g., paper shape and colors.

5.3 Using the Program

The user interaction is identical to Miyazaki's original program. In folding the crane, the extra turn over fold allows the user to more easily and accurately position the origami. Once the folding has been completed (Figure 5), the user invokes the "Export PostScript Diagrams..." menu item. The program generates diagrams for each step and produces a single PostScript file (Figure 6). This can be viewed in a PostScript viewer and converted to PDF and other vector file formats as required.

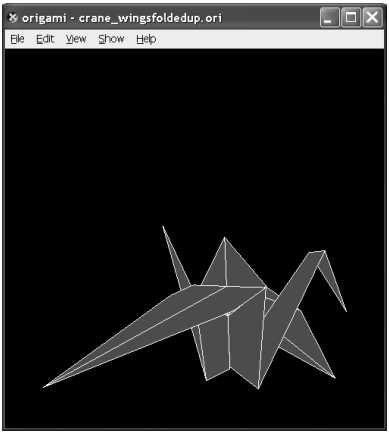

Figure 5. Traditional crane folded in Miyazaki's simulator.

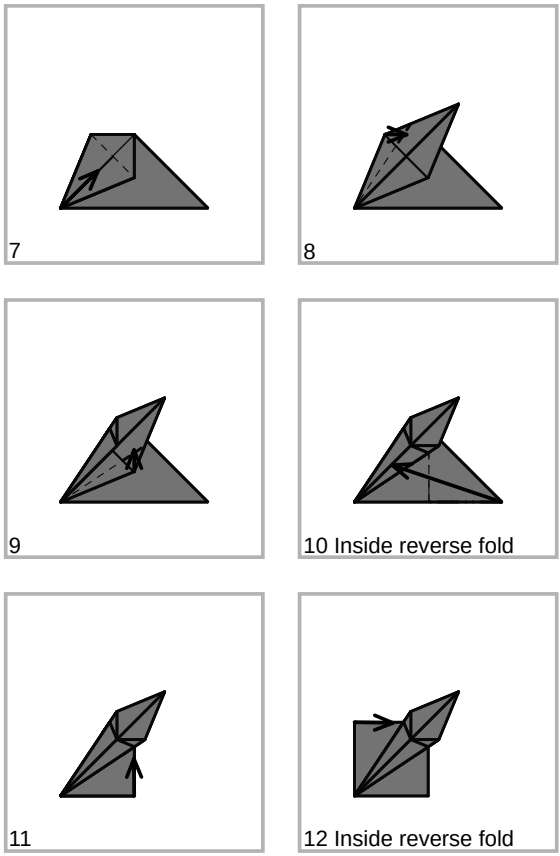

Figure 6. Page 2 of the diagrams automatically produced from the origami in Figure 5.

5.4 Evaluation

Despite the advantages of direct manipulation (namely, "natural" input method, immediate visual feedback, and provision for rapid, incremental, and reversible actions), there are some disadvantages.

The first disadvantage is that the user can only manipulate what he or she can see—if it is not visible, it cannot be manipulated. One manifestation of this problem is that the user cannot distinguish multiple layers, nor can he or she access them.

The second disadvantage is that it is not easy to control "bending" folds. These are folds with flaps that "stick out," i.e., the dihedral angle is not 180°.

The third disadvantage is that the program is mouse intensive. Some users overshoot the mouse and do not get the results they expect. Some have difficulty lining up significant points or lines. The built-in snapping can help, but one user complained that it made the program harder to use.

A survey sent before the development of the program showed that vector drawing programs were considered to be the best type of program for making origami diagrams. A small number of users completed a usability questionnaire for the modified origami simulator. They felt it was more stimulating than vector programs, but vector programs were still better for power and flexibility. These suggest areas for further work, which are discussed in the next section.

6 Future Work

There are several improvements that would immediately increase the appeal and usefulness of the program.

The main criticisms from the usability questionnaire were the prototype's inadequate power and lack of flexibility. The implementation only allows certain kinds of folding, namely valley and inside reverse folds. There are many other types of fold that cannot be done, e.g., all types of rabbit's ear; certain kinds of multiple, overlapping reverse folds; inflation; and stretching. Users needing to make such folds cannot proceed any further. The only option is to continue the diagramming by editing the output in a separate application. Some believe that this is a fatal flaw [14]. Therefore, the usability of the program would be substantially increased by extending the repertoire of folds. Fastag's eGami shows that this is possible.

Improving the visual appearance of the diagrams could be achieved by showing layers and implementing more standard symbols. Layers could be shown by implementing [32] and using "cartoon rendering" [21].

It is unlikely that any program can automatically produce perfect results, so some thought needs to be given to ways to improve the editability of the results. Currently, all lines and polygons are stroked in the PostScript output. This can be confusing as a creased square may have more lines and polygons than the user expects.

Finally, there are a couple of remaining improvements that would not directly increase the functionality of the program, but would make it available to a wider audience with higher expectations than users of a prototype program. Firstly, there are issues with the camera that need to be resolved. Secondly, changes so far have been made to the Windows DirectX version—applying them to the OpenGL could allow Macintosh and Linux users to run the program directly.

If the program's power and flexibility could be increased, then this may improve users' level of satisfaction, ease of use, and enjoyment. The potential of origami simulation for automating origami diagramming may eventually be fully realized.

The program and further information can be found at http://www.angelfire.com/or3/tklorigami0.

Bibliography

[1] A. Bateman. "Computer Tools and Algorithms for Origami Tesselation Design." In *Origami^3: Proceedings of the Third International Meeting of Origami Science, Mathematics, and Education*, edited by Thomas Hull, pp. 121–121. Natick, MA: A K Peters, 2002.

[2] A. Bateman. "Tess: Origami Tessellation Software." Available at http://www.papermosaics.co.uk/software.html, 2005.

[3] J. Fastag. "eGami: Virtual Paperfolding and Diagramming Software." In *Origami^4: Fourth International Meeting of Origami Science, Mathematics, and Education*, edited by Robert J. Lang, pp. 273–283. Natick, MA: A K Peters, 2009.

[4] D. Fisher. *Origami on Computer*. Manuscript, 1994. Available at http://www.mvg-ori.nl/ori-l/articles/thesis.ps.

[5] J. Gout. "Doodle." Available at http://doodle.sourceforge.net/resources.html, 2001.

[6] T. Hull. *Project Origami*. Wellesley, MA: A K Peters, 2006.

[7] T. Ida and B. Buchberger. "Computational Origami: Interaction of Solving, Proving and Computing." In *World Conference on 21st Century Mathematics 2004*, pp. 37–51. Lahore, Pakistan: GC University Press, 2004.

[8] T. Ida, D. Tepeneu, B. Buchberger, and J. Robu. "Proving and Constraint Solving in Computational Origami." In *Artificial Intelligence and Symbolic Computation: 7th International Conference, AISC 2004, Linz, Austria, September 22–24, 2004, Proceedings*, Lecture Notes in Computer Science 3249, pp. 132–142. Berlin: Springer, 2004.

[9] J. Kato, T. Watanabe, and T. Nakayama. (1997) "Recognition of Essential Folding Operations: A Step for Interpreting Illustrated Books of Origami." In *Proceedings of the Fourth International Conference on Document Analysis and Recognition*, Vol. 1, pp. 81–85. Los Alamitos, CA: IEEE Press, 1997.

[10] J. Kato, T. Watanabe, T. Nakayama, L. Guo, and H. Kato. "A Model-Based Approach for Recognizing Folding Process of Origami." In *Proceedings of the Fourteenth International Conference on Pattern Recognition*, Vol. 2, pp. 1808–1811. Washington, DC: IEEE Computer Society, 1998.

[11] N. Kishi and Y. Fujii. "Origami, Folding Paper over the Web." In *Proceedings of the 3rd Asia Pacific Computer Human Interaction*, pp. 337–342. Los Alamitos, CA: IEEE Press, 1998.

[12] R. Koshak. "Automated Crease Pattern Generation: Applying Transdisciplinary Engineering to Software Design." A Master of Engineering Report, Texas Tech University, 2003. Available at http://www.mythsearch.com/Koshak-TTU_Master_of_Engineering_Report.pdf.

[13] R. Lang. (1991) "Because It's There: Idiot Savant." *British Origami* 148 (June 1991), 2–5. Available at http://www.britishorigami.info/practical/highlite/140-49.php#148.

[14] R. Lang. "Re: "Visual/Virtual" diagramming application," *Origami Listserv*. Available at http://dev.origami.com/email/viewmessage.asp?id=163383, May 15, 1996.

[15] R. Lang. "Origami Diagramming Conventions: A Historical Perspective," *Robert J. Lang Origami*. Available at http://www.langorigami.com/info/diagramming_series.pdf, 2000.

[16] R. Lang. "ReferenceFinder," *Robert J. lang Origami*. Available at http://langorigami.com/referencefinder.htm, accessed January 30, 2009.

[17] R. Lang. "TreeMaker," *Robert J. lang Origami*. Available at http://www.langorigami.com/science/treemaker/treemaker5.php4, accessed January 30, 2009.

[18] C. Lavoie. "Axiomatic Origami—or the Mathematical Backbone of Paper Folding." Available at http://cgm.cs.mcgill.ca/~athens/cs507/Projects/2002/ChristianLavoie/maths.html, accessed February 14, 2005.

[19] L. Leventhal. "Tools and Techniques for Interaction: Delivering Instructions for Inherently-3D Construction Tasks: Lessons and Questions for Universal Accessibility." In *Proceedings of the 2001 EC/NSF Workshop on Universal Accessibility of Ubiquitous Computing: Providing for the Elderly*, pp. 51–55. New York: ACM Press, 2001.

[20] J. Mitani. *ORIPA; Origami Pattern Editor*. Available at http://mitani.cs.tsukuba.ac.jp/pukiwiki-oripa/index.php?ORIPA\%3B\%20Origami\%20Pattern\%20Editor, Accessed June 16, 2006.

[21] J. Mitani. "Recognition, Modeling, and Rendering Method for Origami Using 2D Bar Codes." In *Origami^4: Fourth International Meeting of Origami Science, Mathematics, and Education*, edited by Robert J. Lang, pp. 251–258. Natick, MA: A K Peters, 2009.

[22] S. Y. Miyazaki. "Origami Simulation." Available at http://www.om.sist.chukyo-u.ac.jp/old.main/research/origami/index.html, accessed November 15, 2006.

[23] S. Miyazaki, T. Yasuda, S. Yokoi, and J. Toriwaki. "An Interactive Simulation System of Origami Based on Virtual Space Manipulation." In *Proceedings of the IEEE International Workshop on Robot and Human Communication*, pp. 210–215. Los Alamitos, CA: IEEE Press, 1992.

[24] S. Y. Miyazaki, T. Yasuda, S. Yokoi, and J. I. Toriwaki. "An Origami Playing Simulator in the Virtual Space." *Journal of Visualization and Computer Animation* 7:1 (1996), 25–42. Available at http://www.om.sist.chukyo-u.ac.jp/old.main/research/origami/journal/jvca.html.

[25] J. Nimoy. "Making Origami Instructional Symbolics Interactive." Available at http://www.jtnimoy.net/itp/origami/, 2002.

[26] H. Shimanuki, J. Kato, and T. Watanabe. "Recognition of Folding Process from Origami Drill Books." In *Proceedings of the Seventh International Conference on Document Analysis and Recognition*, Vol. 1, pp. 550–554. Washington, DC: IEEE Computer Society, 2003.

[27] H. Shimanuki, J. Kato, and T. Watanabe. "Constituting Origami Models from Sketches." In *Proceedings of the 17th International Conference on Pattern Recognition*, pp. 628–631. Washington, DC: IEEE Computer Society, 2004.

[28] H. Shimanuki, J. Kato, and T. Watanabe. "Construction of 3D Virtual Origami Models from Sketches." In *Origami^4: Fourth International Meeting of Origami Science, Mathematics, and Education*, edited by Robert J. Lang, pp. 217–228. Natick, MA: A K Peters, 2009.

[29] B. Shneiderman and C. Plaisant. *Designing the User Interface: Strategies for Effective Human-Computer Interaction*. Boston: Pearson Addison-Wesley, 2005.

[30] T. Suzuki, J. Kato, and T. Watanabe. "Extraction of Contextual Information Existing among Component Elements of Origami Books." In *Graphics Recognition: Algorithms and Applications*, Lecture Notes in Computer Science 2390, pp. 158–166. New York: Springer, 2002.

[31] J. Szinger. "The Foldinator Modeler and Document Generator." In *Origami^3: Proceedings of the Third International Meeting of Origami Science, Mathematics, and Education*, edited by Thomas Hull, pp. 129–135. Natick, MA: A K Peters, 2002.

[32] T. Terashima, H. Shimanuki, J. Kato, and T. Watanabe. "Method for Representing 3-D Virtual Origami." In *Proceedings of the Eighth International Conference on Document Analysis and Recognition, 2005*, pp. 1211–1215. Los Alamitos, CA: IEEE Press, 2005.

[33] M. van Gelder. "ORIDRAW Package." Available at ftp://ftp.funet.fi/pub/culture/japan/origami/rugcis.rug.nl/programs/oridraw/read.me, 1999.

[34] D. Wilkes and J. K. Tsotsos. "Active Object Recognition." In *Proceedings of the 1992 IEEE Computer Society Conference onComputer Vision and Pattern Recognition*, pp. 136–141. Los Alamitos, CA: IEEE Press, 1992.

[35] L. I. Zamiatina. "Computer Simulations of Origami." *Mathematica in Education* 3:3 (1994), 23–31. Available at http://library.wolfram.com/infocenter/Articles/1786/.

[36] G. Zimmerman, J. Barnes, and L. Leventhal. "A Comparison of the Usability and Effectiveness of Web-Based Delivery of Instructions for Inherently-3D Construction Tasks on Handheld and Desktop Computers." In *Proceedings of the Eighth International Conference on 3D Web Technology*, pp. 49–54. New York: ACM Press, 2003.

Recognition, Modeling, and Rendering Method for Origami Using 2D Bar Codes

Jun Mitani

1 Introduction

The use of computer graphics (CG) to build and display origami models on a PC has been proposed in several studies [1, 3, 4]. Although some useful applications have been developed as the results of these studies, there are still two large problems. The first problem is how to input the data of origami models into a computer. We can use commercial CG software to build a three-dimensional model of origami work, or we can use one of the special origami editors developed in recent studies. But, it is difficult to master such software and much time is needed to build a three-dimensional origami model on a PC using a trial-and error approach. The second problem is how to render (display) the model. Usually, origami models are displayed in a CG image as a set of polygonal faces that do not have thickness (we call a polygonal part of the structure a *face*). When the faces are represented with zero thickness, it is difficult to recognize the origami configuration because multiple faces are typically located at the same (overlapping) position. So far, there have been very few studies addressing this problem.

In this paper, we propose two new methods for origami modeling. One method constructs an origami model on a PC. This method is a unique

technique that uses a digital camera and two-dimensional bar codes for capturing the configuration of an origami model from photographs. The second method renders origami models on a screen. This method is not just a rendering technique; it also perturbs the model geometry to emphasize the origami configuration to make it easier to understand.

We use Miyazaki's data structure [3] to implement the proposed method as an application. One of the benefits of Miyazaki's data structure is that it can hold the face stacking order, which represents the order of faces when they overlap. We can find which face is located above any another face by using this stacking order. In the next section we describe our method to recognize and model the origami configuration. Then, we present our rendering method. Finally, we present our conclusions.

2 Recognizing and Modeling the Origami Configuration

In this section, we describe a method for inputting origami data into a PC. Building an origami model on a PC is a very difficult task. Even though there is a great deal of commercial CG software that implements advanced interfaces, it is still difficult to build an origami model while adhering to origami's restrictions, such as no-stretch, no-penetration, keeping the flatness of facial polygons, and so on.

With our approach, the required task for a user is simply to take pictures of an origami model under construction with a digital camera. Then, the images are used to automatically capture the model in a PC. To do this, we use QR codes. A *QR code*, shown in Figure 1, is a two-dimensional bar code; in other words, the QR code stores information horizontally and

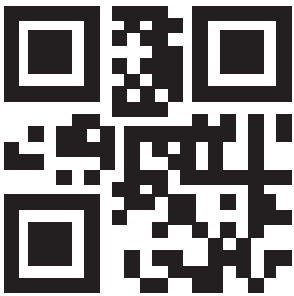

Figure 1. An example of a QR code.

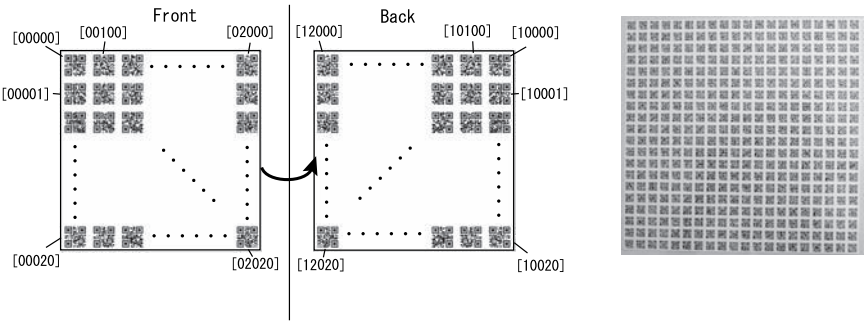

Figure 2. QR code layout and the encoded information.

vertically. Thus, this code can contain hundreds of bytes of information. The size of the data can be set depending on the number of the dots in the square and the code's robustness against noise.

As preparation for our method, QR codes are printed on both sides of the target origami paper in grid form. We put five-digit numbers into each QR code. The first number represents a front/back flag (0 or 1) and the other numbers represent the coordinates of the code (x, y). Figure 2 shows an example of one of our target papers with 20x20 (400) codes on one side. We use a QR-code-capturing application programming interface (API) [5]. With this API, our system recognizes multiple codes at once. Moreover, when the origami is folded flat, rotated codes in the plane are allowed.

Figure 3 shows the flow of our method to capture an origami configuration using a digital camera. First, we prepare an actual square, flat origami (a) and a virtual model (h) in a PC. A user folds the origami paper once (b), then takes a photo of it (d). The system estimates the progression of the folding operation (f) by comparing the photo (d) and the virtual model (h). Then, the system updates the virtual model by adopting the estimated folding operation (i). Capturing one folding operation is composed of these steps. Additional folding operations can be captured by repeating these steps (e.g., (c), (e), (g), and (j)).

We can estimate the location of a folding line as the perpendicular bisector (line l in Figure 4) of the two positions of one QR code before and after folding (positions P and Q, respectively, in Figure 4).

To define the configuration of the folded origami, information about the location of the folding line(s) is not enough. We need further information, such as the type of folding (whether the line is a mountain or a valley (Figure 5, left), and which faces are folded in multiple target faces (Figure 5, right).

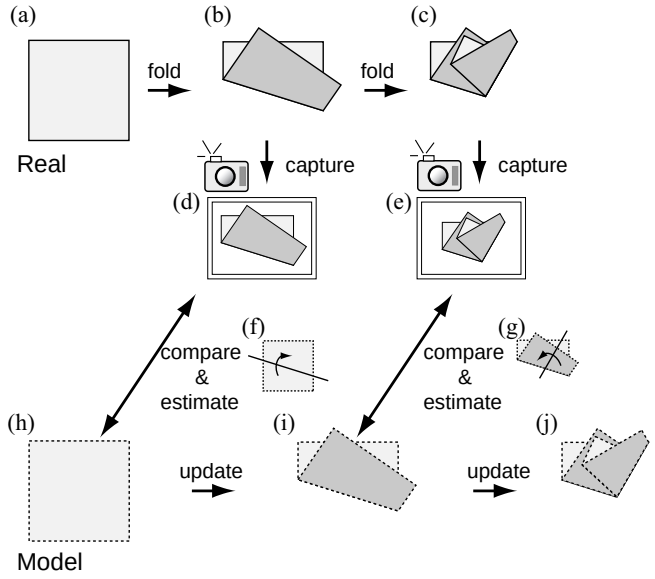

Figure 3. Flow of capturing an origami configuration; see text for details.

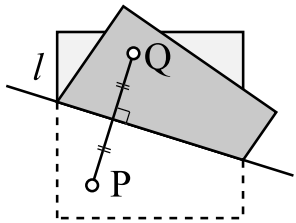

Figure 4. Estimation of folding line location.

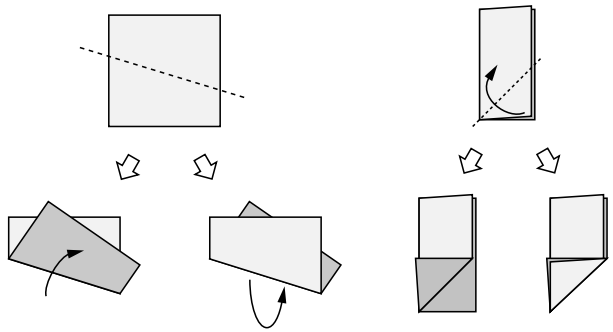

Figure 5. Variation of folding operations for a single folding line.

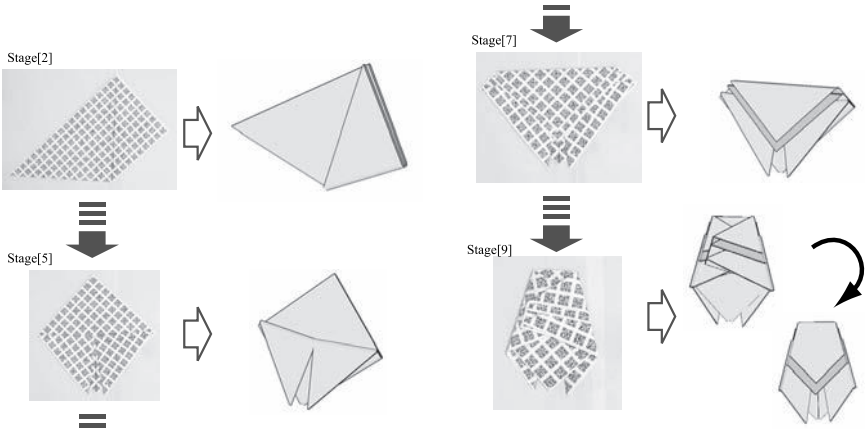

Figure 6. Photos and corresponding CG results of folding a cicada.

To estimate this additional information, we use a brute-force approach. First, the system simulates all possible patterns of foldings. For example, there are two possible cases for the left side of Figure 5 (valley fold or mountain fold), and there are four for the right side of Figure 5 (one-sheet fold or two-sheet fold as well as valley fold or mountain fold). The number of possible patterns may be a few hundred in complicated cases. For each possible case, the system extracts a set of QR codes that can be seen from the user's eye. Then, the QR codes are compared with the QR codes in the photo. By doing this, the best match for folding is extracted as the estimated folding from the set of possible foldings.

Figure 6 shows the result of our method applied to the folding of a cicada model, which is made by nine folding operations. Figure 6 shows four of the nine folding stages. The cicada folding was correctly captured and reproduced in a PC. The data of the model is represented using Miyazaki's model. Consequently, it is possible to play back the folding operation as a three-dimensional CG animation.

3 Rendering

As stated above, one usually uses a flat plane (the thickness is zero) as the model of a sheet of paper on a PC. This is simple and as easy to handle as digital data in a computer. But, when multiple sheets of paper are displayed with zero thickness, the overlapping layers are not represented and we cannot visually recognize the configuration. As Figure 7 shows, displaying the overlapping is very important for understanding the configuration.

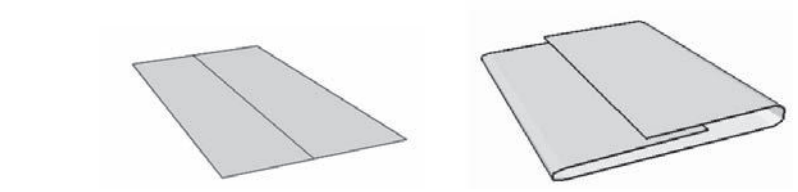

(a) (b)

Figure 7. CG images of the folded paper (a) without and (b) with thickness.

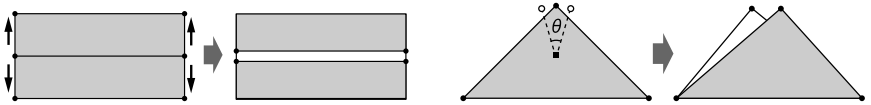

(a) (b)

Figure 8. Sliding vertices when the front face hides the back face. (a) Edges are separated from each other. (b) Vertices rotate to different positions.

To express the overlapping, we shift each polygonal face toward the normal direction according to the stacking order. By doing this, we can see the overlapping relation between the faces. The degree of shifting is based on the position of the face in the face stack of Miyazaki's data structure.

There are still common problems when origami is viewed from the exact front. In this situation, the top face hides the back faces. This makes it difficult to recognize the configuration. To solve this problem, origami drill books commonly perturb the shape of the faces so that the configuration is easier to understand. With this approach, accuracy is not important. So, we add functions to slide the positions of the vertices. There are two ways of sliding. When multiple edges are located at the same position, we can move the vertices so that the edges are separated from each other, as shown in Figure 8(a). Or, as shown in Figure 8(b), we can rotate the vertices so that the vertices rotate to different positions.

After the model geometry is defined, we use cartoon rendering to display the model. Cartoon rendering is not real, but it makes it easier to understand the features of an object [2]. As shown in Figure 9, the boundary edges and silhouette edges are drawn, but the inner edges are not drawn.

Figure 10 shows some examples using our method. We can see from the results located under the top row in Figure 10 that the structures are easy to recognize. These models are three-dimensional models, and so users can rotate and view them from any angle.

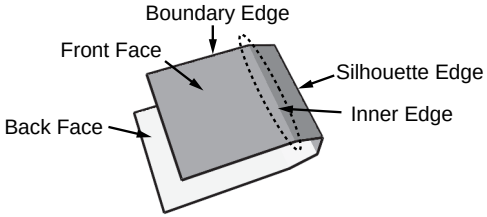

Figure 9. Cartoon rendering.

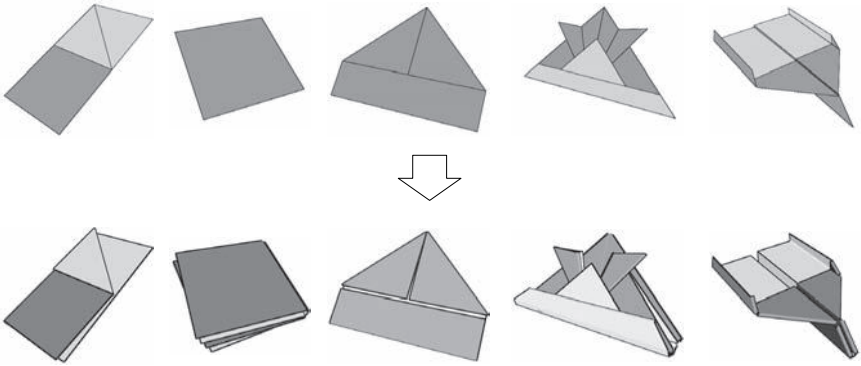

Figure 10. Results using our rendering method.

4 Conclusion

In this paper, a new method for recognizing and configuring an origami model in a PC using QR codes was proposed. The proposed method worked well for simple cases and we could build a cicada model, which has nine folds, from digital images. But, there are drawbacks to this approach. The system cannot handle a "tuck-inside" action (Figure 11) because a digital camera cannot capture the inside of an object from the outside. Also, the

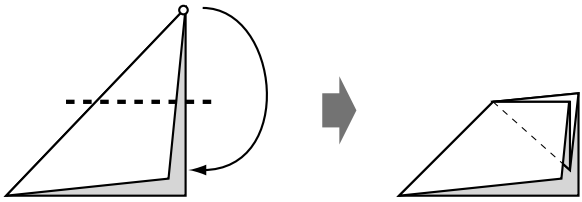

Figure 11. Tuck-inside action.

system can only handle flat folded models. So, more improvements are planned as future work.

Additionally, a new method for rendering (displaying) an origami model was proposed. This method emphasizes the thickness of a sheet of paper by shifting faces according to the paper's position in the face stack, and it slides vertices to make it easier for users to understand the configuration. As a result, we found this approach can generate easily understandable images. In future work we plan to add more advanced visualization features, such as changing the position of vertices depending on the user's eye position in real time.

Bibliography

[1] Y. Furuta, J. Mitani, Y. Fukui. "Virtual ORIGAMI System with Interactive Mouse Manipulation." *IPSJ SIG Technical Reports* 2006:CG-123 (2006), 13–18.

[2] A. Gooch, B. Gooch, P. Shirley, and E. Cohen. "A Non-Photorealistic Lighting Model For Automatic Technical Illustration." In *Proceedings of the 25th Annual Conference on Computer Grahics and Interactive Techniques*, pp. 447–452. New York: ACM Press, 1998.

[3] S. Miyazaki, T. Yasuda, S. Yokoi, and J. Toriwaki. "An Origami Playing Simulator in the Virtual Space." *The Journal of Visualization and Computer Animation* 7:1 (1996), 25–42.

[4] H. Shimanuki, J. Kato, and T. Watanabe. "Construction of 3-D Paper-Made Objects from Crease Patterns." In *Proceedings of the IAPR Conference on Machine Vision Applications (MVA2005)*, pp. 35–38. Tsukuba, Japan: MVA Conference Committee, 2005.

[5] Soft Advance, Inc. "QR Code Reader" (in Japanese). Available at http://www.softadvance.co.jp/qr/index.html, 2007.

3D Origami Design Based on Tucking Molecules

Tomohiro Tachi

1 Introduction

Designing arbitrary three-dimensional surfaces by origami is one of the ultimate objectives of origami design. There are currently several approaches for designing 3D models, but none of them provide methods for designing arbitrary 3D surfaces.

The most popular way of designing a 3D origami model is by shaping a flat-folded uniaxial base with controlled flap lengths. Methods for designing uniaxial bases using circle-packing patterns have been investigated by Toshiyuki Meguro [8, 9], Fumiaki Kawahata [2], and Robert Lang [4–7]. This method works well for organic models such as insects and some animals. However, it is not possible to fully specify the 3D shape, because the only controllable parameters are the lengths of the flaps.

Some origami artists are also engaged in two-dimensional design of origami bases. A practical design method for 2D origami shape based on placing facets has been investigated by Toshiyuki Meguro [10]. Theoretically, Demaine et al. [1] gives a constructive proof for designing the silhouette of an arbitrary 2D polygon. Another method has been proposed by Masahiko Tanaka [12].

The idea for 2D origami design was extended to a 3D origami design method by Demaine et al. [1], who proved that any polyhedron can be folded from a sheet of paper. However, the method used in the proof is

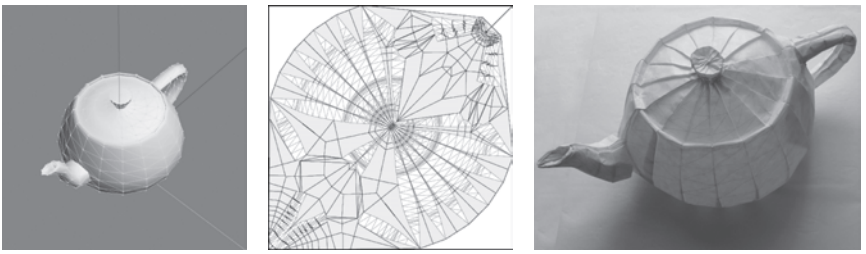

Figure 1. A 3D teapot can be folded (right) from the crease pattern (middle) constructed from the teapot represented by a triangle mesh (left).

based on wrapping a thin strip of paper around a polyhedron, and so it is not a practical method to design a real model.

A few true 3D polyhedral models have been designed in practice. Two such examples—roofs by the author [11] and a frog by Masahiko Tanaka [12]—are constructed by placing facets and inserting symmetric tucks between the facets. However, it is very hard to design a complex model using only symmetric tucks, since the symmetry of the alignment constrains the overall configuration to a very limited range of possibilities.

In this paper, we propose a new approach for designing an arbitrary polyhedral surface, with an example of our method realized as shown in Figure 1. Instead of using symmetric tucks between edges, we propose a general structure, which we call an *edge-tucking molecule*, which can be generated for arbitrarily given alignments of pairs of mating edges (with a few limitations). Edge-tucking molecules are flexible and general enough to enable manual design of complex 3D origami figures using conventional paper craft and drawing software. We further investigate the conditions for 3D foldability represented by several inequalities; these conditions are the key part of 3D origami design.

2 Method Overview

2.1 Tucking Molecules

Our approach is to align facets of the polyhedral surface (surface polygons) onto a convex region of a plane and fill the gap between the surface polygons with edge-tucking molecules and *vertex-tucking molecules*. The purpose of the "molecules" is to "use up" the paper between the surface polygons, thereby bring corresponding pairs of surface polygon edges into alignment. Figure 2 shows an example of how the paper is tessellated into surface polygons and molecules.

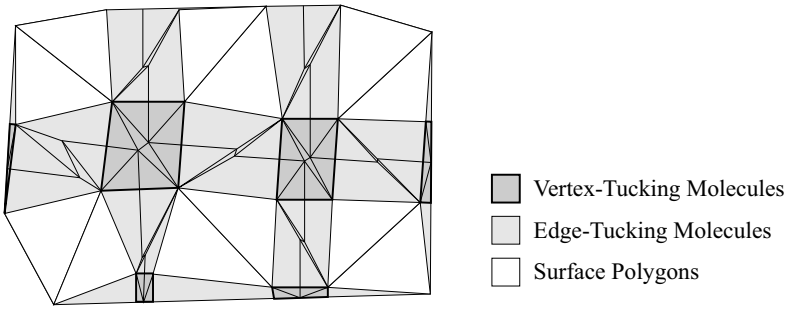

Figure 2. Paper surface tessellated into surface polygons and molecules.

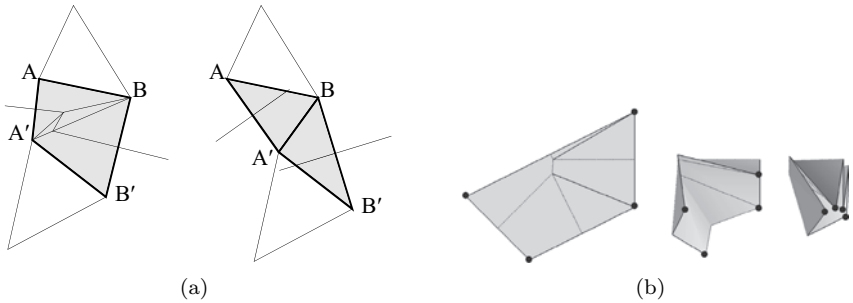

Figure 3. Edge-tucking and vertex-tucking molecules. (a) Edge-tucking molecule maps two segments to an identical position. (b) Vertex-tucking molecule maps vertices to an identical position.

An edge-tucking molecule is inserted between a pair of edges of the surface polygons that have been laid out on the paper. The two edges are mapped to the same position by folding the edge-tucking molecule (Figure 3(a)). A vertex-tucking molecule is inserted between the multiple vertices in the crease pattern that correspond to one vertex of the three-dimensional surface. The vertices are mapped to the same position in the 3D form by folding the vertex-tucking molecule (Figure 3(b)). Hence, the set of edge-tucking molecules and vertex-tucking molecules "paste" together the pairs of edges and the sets of vertices, respectively.

2.2 Conditions

There are two types of conditions for laying out surface polygons and tucking molecules. One is called a *2D condition*, which is primarily related to the possibility of aligning the surface polygons and molecules on the un-

folded paper. The other is called a *3D condition*, which comes from the relationships between the surface polygons and the molecules in the folded state. In the following, Conditions 1 and 2 represent 2D conditions, and Conditions 3 and 4 represent 3D conditions:

Condition 1. *Surface polygons and tucking molecules must properly tessellate a convex planar region of the paper.*

Condition 2. *The crease pattern can be properly generated without intersecting surface polygons.*

Condition 3. *Tucking molecules and surface polygons do not intersect each other in the folded state.*

Condition 4. *Tucking molecules provide adequate angles to obtain the curvature of the required 3D surface in the folded state.*

Since an origami model is designed by placing surface polygons and molecules and generating the crease pattern on a 2D sheet, the 3D conditions must be satisfied by the 2D configuration. We use the idea of a *tuck proxy* (Section 6) to handle the 3D positions of the folded tucking molecules, so that the sufficient conditions of the 3D conditions may be written as angle inequalities that apply to the 2D configuration.

The procedure and the conditions for a proper tessellation are shown in Section 3. The method and the conditions for generating the crease pattern for the edge-tucking molecule for a given pair of edges is shown in Section 4.1 and Section 4.2, respectively. The method and the conditions for generating the crease pattern of the vertex-tucking molecule for a given combination of vertices is shown in Section 5.1 and Section 5.2, respectively. The 3D conditions are then investigated in Section 6. Finally, Section 7 shows examples of the successful application of this method.

3 Tessellation

We begin by cutting the polyhedral surface into one or more groups of connected polygons, i.e., so that each group forms an isometric map from its corresponding portion of the polyhedral surface to the 2D plane. Then, edge-tucking molecules and vertex-tucking molecules are inserted into the surface to connect edges and vertices of the surface polygons to form a 2D composite figure topologically equivalent to a disk. The ordering of vertices around the molecules is set according to the surface orientation in a 3D configuration.

Surface polygons and inserted molecules must be mapped onto a convex region of a plane without intersection of the elements or any change in the

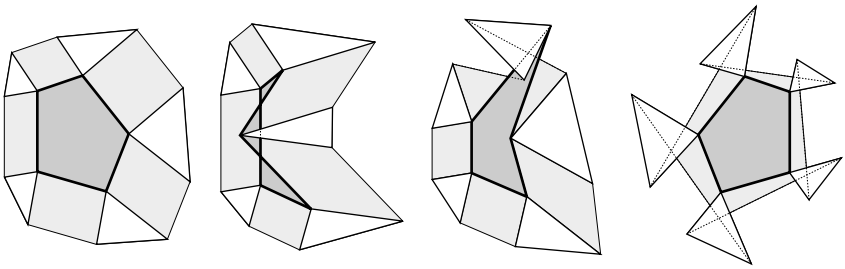

Figure 4. (a) A proper tessellation. (b) The vertex-tucking molecule is crossed. (c) The edge-tucking molecule is crossed. (d) The vertex-tucking molecules and edge-tucking molecules have negative signed area.

connectivity between corresponding pairs of edges and vertices. The surface polygons are kept congruent after the 2D mapping, while the tucking molecules are deformed to conform to the gaps between the aligned surface polygons. The following are the conditions for properly tessellating a planar region by surface polygons and molecules:

Condition 5. *Any mapped tucking molecule may not cross itself.*

Condition 6. *The signed area of any tucking molecule cannot be negative.*

Condition 7. *The mapped boundary of the surface must be convex.*

Figure 4 shows an example of how Conditions 5 and 6 help avoid intersections of molecules.

Once the surface polygons have been mapped and the (empty) edge-tucking molecules and vertex-tucking molecules defined, we then turn to creating the creases inside each polygon that turn it into the appropriate molecule.

4 Edge-Tucking Molecules

4.1 Generating Edge-Tucking Molecule

Figure 5 shows the procedure for generating the creases inside an edge-tucking molecule. An edge-tucking molecule is a quadrilateral ($AA'B'B$) surrounded by a pair of edges of surface polygons (AB and $A'B'$) and two segments that connect corresponding vertices of the paired edges (AA' and BB').

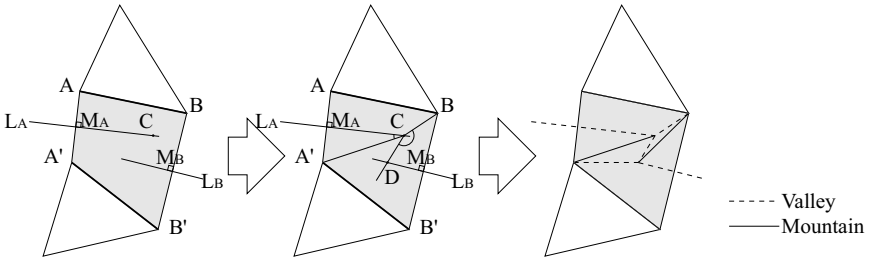

Figure 5. Generating procedure of crease pattern for an edge-tucking molecule. Right image shows the resulting crease pattern.

The basic idea of the edge-tucking molecule is that it contains two valley folds along perpendicular bisectors of AA′ and BB′ so that point A is folded to A′ and B to B′; with this pair of lines as the starting point, we then generate a flat-foldable crease pattern that connects these perpendicular bisectors. The procedure is as follows:

1. Define L_A as the perpendicular bisector of segment AA′ and define L_B as the perpendicular bisector of segment BB′.
2. Let M_A and M_B denote the midpoint of segment AA′ and the midpoint of segment BB′, respectively.
3. If AB′ = A′B, then L_A is on L_B and the crease pattern can be obtained by drawing a valley crease on segment M_AM_B. Otherwise, we assume without loss of generality that A′B < AB′.
4. Arbitrarily define point C on L_A inside quad AA′B′B.
5. Define point D on L_B such that $\angle M_ACA' + \angle DCB = \pi$.
6. The necessary vertices are defined; draw the crease pattern shown in the right image of Figure 5 with mountain and valley folds defined as shown.

In Step 5, Kawasaki's theorem [3] is used to ensure the flat-foldability of vertex C. Note that Kawasaki's theorem is satisfied also in vertex D. Although we do not provide the detailed proof here, this condition is always satisfied if and only if you can locate point D on L_B.

4.2 Conditions for Generating Edge-Tucking Molecule

The following are the two conditions for a quadrilateral to be a valid edge-tucking molecule:

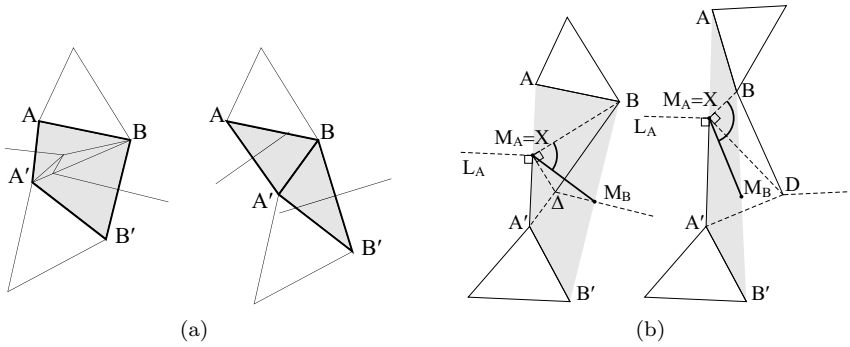

Figure 6. Conditions for an edge-tucking molecule. (a) The condition to generate the crease pattern: on the left, $AB' \geq AB$ and $A'B \geq AB$, but on the right, $A'B < AB$. (b) The condition for ensuring that the crease pattern is contained inside the molecule: on the left, CP is inside; on the right, CP is outside.

Condition 8. *A crease pattern can be generated for each edge-tucking molecule.*

Condition 9. *The generated crease patterns do not intersect each other.*

The necessary and sufficient condition for Condition 8 can be written as follows:

Condition 10. *The perpendicular bisectors of* AA' *and* BB' *do not intersect the surface polygons adjacent to the edge-tucking molecule.*

Figure 6(a) shows an example of this situation. Condition 8 can be represented as

$$AB' \geq AB \quad \text{and} \quad A'B \geq AB(= A'B').$$

Instead of Condition 9, we can use the following sufficient condition, which is more useful because it can be determined only from the shape of each molecule.

Condition 11. *The generated crease pattern lies entirely inside the quadrilateral of the molecule.*

Condition 11 can be represented by an angle inequality (Figure 6(b)). Assume that we put point C (a point on L_A from which the new crease line is generated) on M_A, which is the most favorable position to put the crease pattern inside the quadrilateral. The condition is satisfied if and only if point D lies inside the quadrilateral $AA'B'B$, which is the case as long as

$$\angle BM_AM_B \leq \angle BM_AD.$$

Since point D is defined by flat-foldability around vertex C,

$$\angle \mathrm{BM_A D} = \pi - \angle \mathrm{L_A M_A A} = \frac{\pi}{2}.$$

Therefore, Condition 11 can be represented as

$$\angle \mathrm{BM_A M_B} \leq \frac{\pi}{2}.$$

5 Vertex-Tucking Molecules

5.1 Generating Vertex-Tucking Molecule

Next, we construct the vertex-tucking molecules. Figure 7 shows how the crease pattern for a vertex-tucking molecule is generated. The procedure is as follows:

1. Draw the Voronoi diagram of the vertex-tucking-molecule polygon using valley creases and using the vertices of the molecule as the generating points.

2. Connect the vertices of each Voronoi polygon to the generating points with mountain creases.

3. Crimp fold or rabbit-ear fold any triangles that do not connect to adjacent edge-tucking molecules.

Step 3 ensures that the folded shape of the molecule is connected to one axis (Figure 10), to enable an easy calculation of the 3D conditions as shown in Section 6. However, this procedure can be omitted in the practical design.

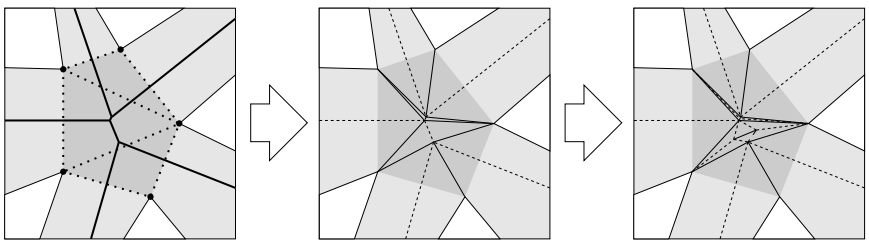

Figure 7. Generating procedure of the crease pattern for a vertex-tucking molecule.

Note that this type of molecule based on the Voronoi diagram has been used previously for some origami designs; Robert Lang showed the same molecule used for the connection of strip grafts [7, p.152], and Toshiyuki Meguro [10] has proposed essentially an identical molecule as a "generalized twist fold."

5.2 Conditions for Generating Vertex-Tucking Molecule

The following are the two conditions necessary for generating valid vertex-tucking molecules:

Condition 12. *A crease pattern can be generated for each vertex-tucking molecule.*

Condition 13. *The generated crease patterns do not intersect each other.*

Condition 12 may be represented as follows:

Condition 14. *The boundary of the vertex-tucking molecule is composed of a subset of the edges of the Delaunay triangles that are dual to the generated Voronoi diagram.*

Figure 8(a) shows how this condition works. If a segment on the boundary does not lie on the edges of the Delaunay triangles, an edge-tucking molecule cannot connect to the segment because the perpendicular bisector does not cross the segment.

Instead of Condition 13, we can use the following sufficient condition:

Condition 15. *The generated crease pattern is wholly inside the molecule.*

This condition can be written in the following way: for every edge $\mathrm{V_iV_j}$ on the boundary of the molecule and for every vertex $\mathrm{V_k}(k \neq i, j)$ of the molecule,

$$\angle \mathrm{V_jV_kV_i} \leq \frac{\pi}{2}. \tag{1}$$

Note that Equation (1) is also a sufficient condition for Condition 14, as well as for Condition 13. Figure 8(b) shows an example of this condition. In the right image, $\angle \mathrm{V_1V_2V_0} > \pi/2$, and the crease pattern crosses segment $\mathrm{V_1V_0}$.

6 3D Conditions

The 3D conditions are conditions that must be met in the folded state, presented earlier as Conditions 3 and 4. These necessary and sufficient conditions for 3D foldability are difficult to test using characteristics of

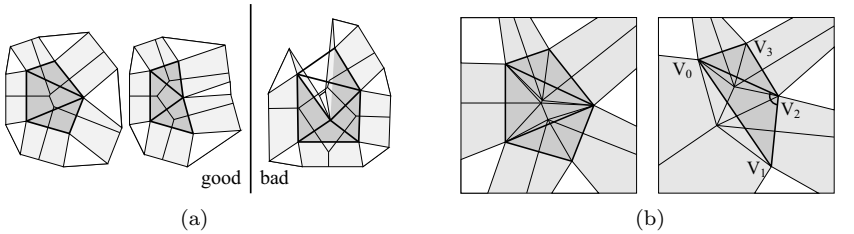

Figure 8. Conditions for a vertex-tucking molecule. (a) The condition to generate the crease pattern: on the left, the condition is valid, but on the right, the boundary is not on the edges of Delaunay triangles. (b) The condition for ensuring that the crease pattern is contained inside the molecule: on the left, CP is inside; on the right, CP is outside.

the crease pattern because the three-dimensional configuration changes not only by the crease pattern, but also by the folding angles of the non-flat-folded crease lines.

Thus we assume that the tucks, i.e., the folded tucking molecules, lie on a predefined surface, which we call the *tuck proxy*, so that Condition 4 can be tested and satisfied with respect to parameters of the crease pattern, i.e., by angle inequalities, while keeping Condition 3 satisfied.

6.1 Generating the Tuck Proxy

The tuck proxy is an imaginary surface that must contain all of the folded tucking molecules and that extends toward the inside of the 3D polyhedron (so that the folded tucking molecules are hidden inside the folded model). The distance that the tuck proxy extends away from the surface is what we will call its *width*. We initially set the width of the tuck proxy as large as possible, as long as it does not intersect with surface polygons or with other parts of the tuck proxy, since it defines the range in which tucking molecules can exist; if the tuck proxy does not exhibit improper intersections, then that guarantees that the tucking molecules will not exhibit improper intersections in 3D.

Here is an example procedure for generating a tuck proxy (Figure 9):

1. Define a segment from each vertex to the direction opposite to the surface orientation (e.g., with the direction chosen as some average of the surface normals at the vertex). The length of the segment is initially chosen such that the segment does not intersect any surface polygons.

2. Connect adjacent segments with strips of two triangles and define the union of all such strips as the tuck proxy.

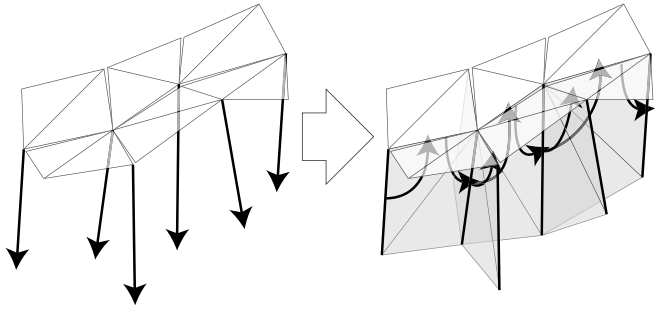

Figure 9. Generating procedure of the tuck proxy.

3. If the strips intersect with other strips, then shorten the segment length and redo the procedure from Step 1. Otherwise end the procedure.

As we assume that folded tucking molecules will conform to the tuck proxy, the width of the folded tuck must be less than or equal to the width of the tuck proxy. Because of the use of bisectors in their construction, half of the distance between the corresponding vertices of the tucking molecules can be used for calculating the width of the folded tucks.

6.2 Angle Inequality

A sufficient condition for Condition 4 to be satisfied can be provided by inequalities between angles of the folded molecules and angles between edges along the tuck proxy.

The relation between the angle along the unfolded paper and the angle along the folded molecule is shown in Figure 10. In this example, which satisfies $\angle \mathrm{ABB}' < \angle \mathrm{A}'\mathrm{B}'\mathrm{B}$, $\angle \mathrm{ABB}'$ keeps its angle in the folded state. The general equation is as follows:

$$\min\left(\angle \mathrm{ABB}', \angle \mathrm{A}'\mathrm{B}'\mathrm{B}\right) + \angle \mathrm{O_B BB}'|_{\text{in 2D}} = \angle \mathrm{ABO_B}|_{\text{in 3D}}\,. \tag{2}$$

We name this angle (i.e., $\angle \mathrm{ABO_B}|_{\text{in 3D}}$) the *tuck angle* and denote it by $\theta_{i,k}$ for edge i connecting to vertex k.

Folded tucking molecules are easily folded to conform to the tuck proxy and are crimped to adjust the tuck angles of each edge (Figure 11). Note that the joint axis (i.e., the axis along which the tucks are connected) can move by folding the tucks so that one of the tuck angles is increased. The

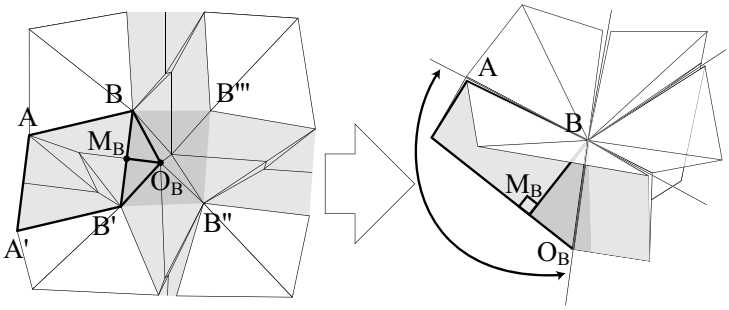

Figure 10. Angles on unfolded paper and on folded molecules.

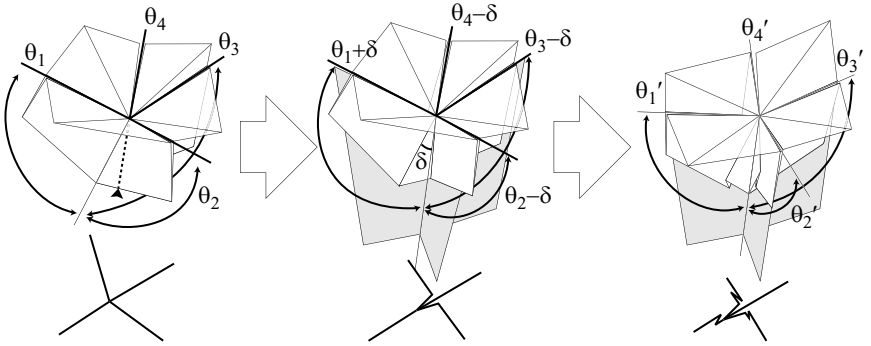

Figure 11. Adjusting tuck angles. Left to middle: One of the tuck angles is increased by moving the joint axis. Middle to right: Any other tuck angle can be reduced by crimping.

necessary and sufficient condition for making such adjustment possible for vertex k is as follows: for every edge i and j $(i \neq j)$ connected to vertex k,

$$\theta_{i,k} + \theta_{j,k} \geq \theta'_{i,k} + \theta'_{j,k},$$

where $\theta_{i,k}$ is the original tuck angle calculated from Equation (2), and $\theta'_{i,k}$ is the desired tuck angle along the tuck proxy.

7 Application

We show two useful applications of our design method. Figure 12 shows the two examples.

First, by applying the proposed method to an entire 3D surface, a complex, three-dimensionally defined model can be folded from a single uncut

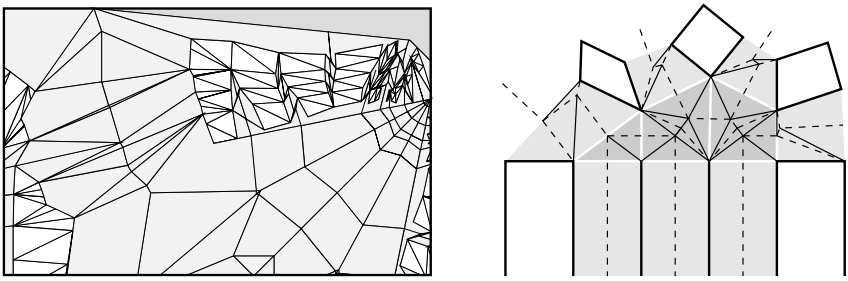

(a) (b)

Figure 12. Examples of applications of the tucking molecule design algorithms: (a) Zoom view of the crease pattern for the *Teapot*. See Figure 1 for the whole crease pattern and the folded model. (b) Connecting a 3D design (top) to a regular box pleating pattern (bottom).

sheet of paper. It is possible to follow the procedure manually, because there is no constraint represented by any equality conditions. Figure 12(a) shows a small part of the crease pattern for the model *Teapot*, whose complete crease pattern and a photograph of the folded model were shown in Figure 1.

This method is also useful for designing selected parts of a 3D model and for connecting it to other parts that might have been designed with other methods. As shown in Figure 12(b), the connection portion of the crease pattern can be flexibly and efficiently designed using tucking molecules. This approach should help designers to locally add 3D high-resolution details to any desired part of their model.

8 Conclusions

In summary, we proposed a method for designing origami renditions of arbitrary 3D polyhedral surfaces using tucking molecules. The procedures for generating vertex-tucking molecules and edge-tucking molecules were shown. We investigated the conditions for generating the crease pattern (2D conditions) and for constructing desired 3D configuration (3D conditions).

The proposed method is easily implemented and can be used for designing complicated three-dimensional models and also for improving other origami designing methods. As a practical implementation of these concepts, Origamizer, a software tool based on a method that further extends the concepts presented here, is available on the author's website (http://www.tsg.ne.jp/TT/software/).

Bibliography

[1] Erik D. Demaine, Martin L. Demaine, and Joseph S. B. Mitchell. "Folding Flat Silhouettes and Wrapping Polyhedral Packages : New Results in Computational Origami." *Computational Geometry: Theory and Applications* 16:1 (2000), 3–2.

[2] Fumiaki Kawahata. "The Technique to Fold Free Flaps of Formative Art 'Origami.'" In *Origami Science and Art: Proceedings of the Second International Meeting of Origami Science and Scientific Origami*, edited by K. Miura, pp. 63–72. Shiga, Japan: Seian University of Art and Design, 1997.

[3] Toshikazu Kawasaki. "On the Relation between Mountain-Creases and Valley-Creases of a Flat Origami." In *Proceedings of the First International Meeting of Origami Science and Technology*, edited by H. Huzita, pp. 229–237. Padova, Italy: Dipartimento di Fisica dell'Università di Padova, 1991.

[4] Robert J. Lang. "Mathematical Algorithms for Origami Design." *Symmetry: Culture and Science* 5:2 (1994), 115–152.

[5] Robert J. Lang. "A Computational Algorithm for Origami Design." In *Proceedings of the 12th Annual ACM Symposium on Computational Geometry*, pp. 98–105. New York: ACM Press, 1996.

[6] Robert J. Lang. "The Tree Method of Origami Design." In *Origami Science and Art: Proceedings of the Second International Meeting of Origami Science and Scientific Origami*, edited by K. Miura, pp. 73–82. Shiga, Japan: Seian University of Art and Design, 1997.

[7] Robert J. Lang. *Origami Design Secrets: Mathematical Methods for an Ancient Art*. Natick, MA: A K Peters, 2003.

[8] Toshiyuki Meguro. "Jitsuyou origami sekkeihou No. 4" (The Method to Design Origami No. 4, in Japanese). *Origami Tanteidan Newspaper*, October 5, 1991, 1.

[9] Toshiyuki Meguro. "Tobu kuwagatamushi-to ryoikienbunshihou" (Flying Stag Beetle and the Circular Area Molecule Method, in Japanese). In *Oru*, pp. 92–95. Saitama, Japan: Sojusha, 1994.

[10] Toshiyuki Meguro. "Design by Facet Placing Method" (in Japanese). Available at http://www.geocities.co.jp/HeartLand-Oak/5487/, 2006.

[11] Tomohiro Tachi. "Japanese Roofs (kiridzuma, koshiore, irimoya)." *Origami Tanteidan Magazine* 14:4 (2003), 30–31.

[12] Masahiko Tanaka. "Possibility and Constructive Proof through Origami." *Hyogo University Journal* 11 (2006), 75–82.

eGami: Virtual Paperfolding and Diagramming Software

Jack Fastag

1 Introduction and Goals

eGami is a computer software application that simulates the sequential folding of flat origami models in real time, using an intuitive interface designed to suggest the experience of folding an actual piece of physical paper. As the model is "folded" or manipulated on-screen by the user, its folding sequence diagram is automatically generated, complete with arrows, symbols, and basic verbal instructions commonly seen in traditional origami diagrams.

Every origami designer has his or her favorite drawing program to publish their diagrams, but there's no specialized package specifically designed for origami diagramming. eGami can be used as an alternative to hand-drawing or to replace the use of illustration software to create origami diagrams quickly and efficiently.

Computational origami is a relatively recent field, whose goal is to find algorithms and solutions for a variety of paper-folding problems. Demaine and Demaine [3] classify these into *origami design* and *origami foldability* problems, and offer a good overview of existing results. The current work belongs to the foldability type, given that we are attempting to prove that the folded state reached after each manipulation of the model is a "valid" one, as defined and further discussed below. Origami design applications are covered in [3] and elsewhere.

Previous computer implementations of origami model and/or diagram manipulation include: Jack Fastag and Robert Lang's simulators [7], working simultaneously in the late 1980s, on PC and Mac applications, respectively; Miyazaki et al. [9]; John Szinger's Foldinator [11]; Josh Nimoy's web-based Java applet [10]; and Tung Ken Lam's simulator and diagrammer [6], also presented at 4OSME.

The goals that the author established when eGami development began were: (a) the simulation must be in real time; (b) manipulation of the model must have a natural "grab-and-pull" feel that resembles real-life paper folding; (c) automatic diagram generation must be fully customizable and printable; and (d) animated step-by-step folding tutorials should be created.

2 Program Features and Use

eGami is designed to follow the standard Windows interface, with intuitive menus, toolbars, and tool panels. The interface allows multiple models to be open at once, which is useful when designing models with multiple parts, such as modulars.

To create a new model, we begin the same way we do in real life, by choosing the piece of paper that we wish to use. Selecting the "File > New" menu item, or pressing the corresponding button on the toolbar, presents the user with a dialog box, where the paper shape, size, and colors can be selected (Figure 1). Many traditional paper shapes are predefined (square, common and custom rectangles, money bills, triangles and other polygons, etc.) or new ones can be defined. The model's name, author, and optional comments can also be entered in this screen.

The selected piece of paper is then presented in the Editor's window, as shown in Figure 2. This is the place where the model is displayed and manipulated by the various tools. As the model is folded, new steps are generated, one for each folding operation, although multiple operations per step are also allowed (such as folding all four corners to the center of a square in a single blintz-fold step). At the bottom of this window there are buttons that let us navigate along our folding sequence.

There are several views available in the Editor window that can be selected either through toolbar or menu options: (a) the "Flat" view, which displays the folded model in mathematically perfect alignment; (b) the "Model" view, which shows underlying layers of the model by skewing vertices slightly, as is customary in published origami diagrams; (c) the "Diagram" view, where the full diagram, complete with fold lines, arrows, instructions, and other symbols is displayed; and (d) the "Crease Pattern" view, which shows, as its name implies, the crease pattern of the flat piece

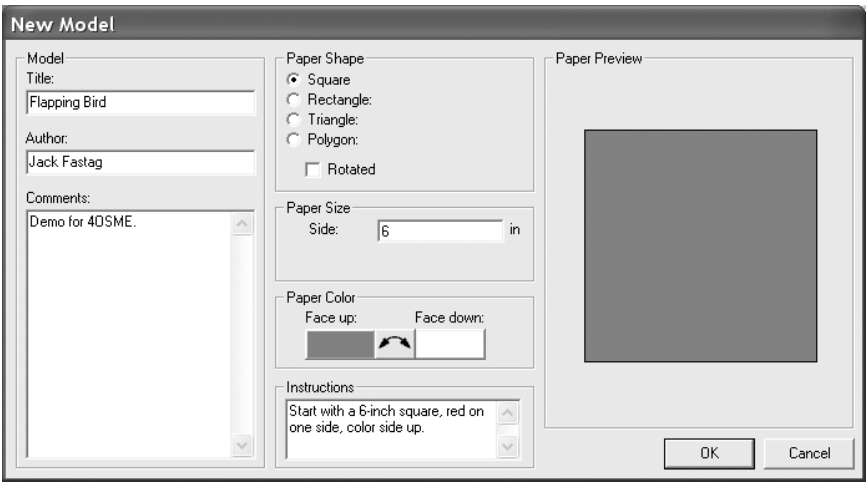

Figure 1. New Model dialog box.

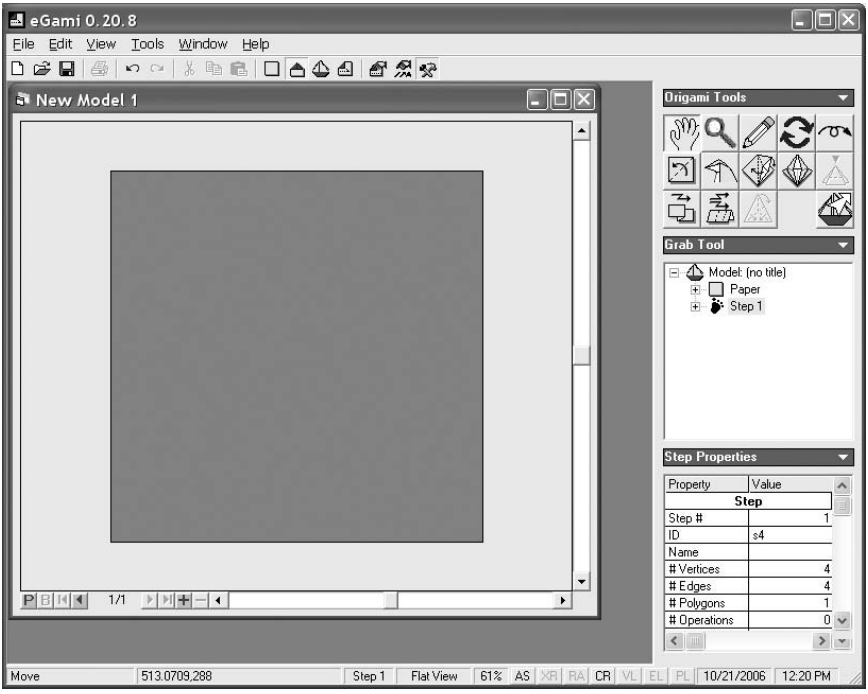

Figure 2. Main screen.

General Tools:

- Grab: select, move, resize
- Zoom: in, out, actual-size, to-fit, %, custom
- Rotate: 1/4 turn clockwise, 1/4 turn counter-clockwise, 1/2 turn, custom angle
- Flip: side-to-side, top-to-bottom
- Diagram: draw line, arrow, circle, rectangle, or text box
- Delete: delete diagram item, delete step
- Duplicate: duplicate diagram item, duplicate step

Folding Tools:

- Fold: valley, mountain, valley-under, mountain-under, crease
- Reverse: inside, outside, asymmetric-inside*, asymmetric-outside*
- Squash: symmetric, asymmetric*
- Petal: symmetric, asymmetric*, swivel-fold*
- Rabbit Ear*
- Sink*
- Pleat: parallel over, parallel under, radial over, radial under
- Fan Fold: parallel over, parallel under, radial over, radial under, parallel crease, radial crease, fold over-and-over
- Crimp: parallel inside, parallel outside, radial inside, radial outside
- Unfold: unfold all, unfold flap*

* Feature under development

Table 1. eGami Tools.

of paper for the current step, with all creases, mountain folds, and valley folds indicated. The ability to view multiple steps on a single page still remains to be implemented, as well as printing and exporting functions.

On the right side of the main window is the Tool Panel, where the various tools can be selected and their properties set. The folding tools reflect the language and procedures traditionally found in modern origami books and diagrams. Table 1 lists the tools that the application currently provides, as well as several that are still under development.

To use the folding tools, the mouse cursor is shown as a hand ready to "grab" the model, which is then folded by clicking and dragging. Figure 3 illustrates a valley fold in progress.

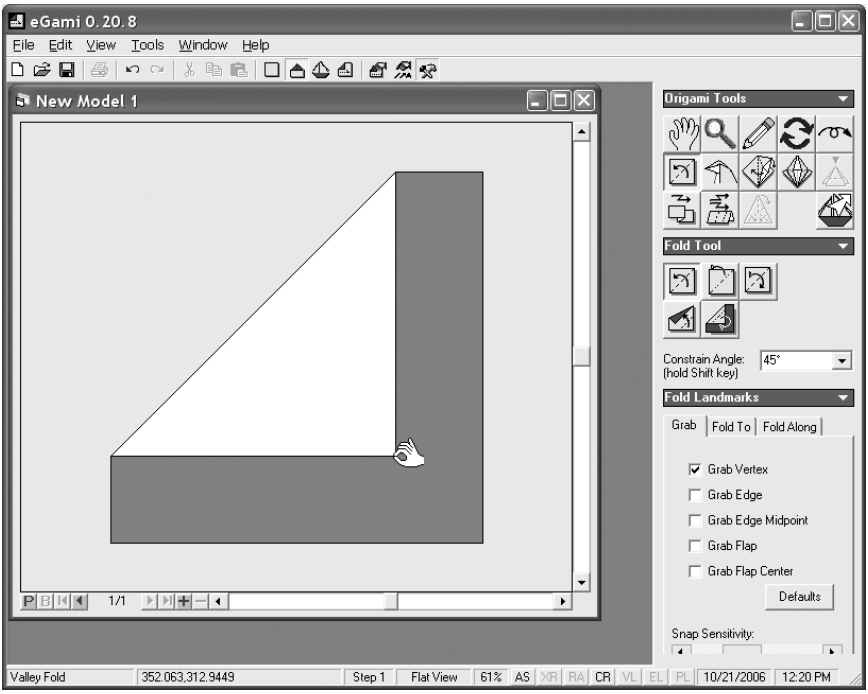

Figure 3. Valley fold in progress.

To help increase fold precision, holding the shift key during folding restricts the movement to a user-specified angle. And as an additional aid during folding, the application defines user-selectable *landmarks* that the cursor can "snap" to. Available landmarks include visible vertices, edges, and flaps, as well as edge midpoints, flap centers, angle bisectors, and the intersection of two edges. The Landmarks panel, also visible in Figure 3, allows us to specify which of these landmarks can be "grabbed," the landmark we want to fold to, and/or landmarks we want to "fold along." Together, the various options in this panel offer the ability to perform most of the operations defined by the Huzita-Hatori Axioms [8].

After one or more folds have been carried out, switching to the "Diagram" view shows the diagram created for each step, with its corresponding fold lines, arrows, and other symbols, as well as automatically generated verbal instructions. An example showing the step before a petal fold was performed can be seen in Figure 4.

The default instructions describe the operation that was performed, including references to any landmarks affected. The program also allows the naming of any landmark, which aids in more readable instructions. For ex-

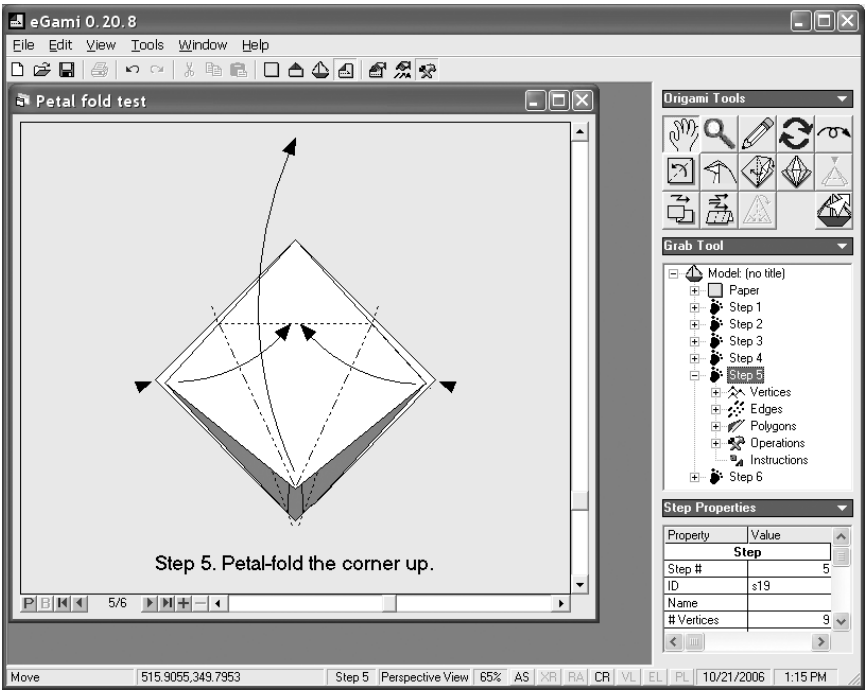

Figure 4. Diagram view.

ample, if we know that a certain vertex will be the model's "head," labeling it as such would generate instructions such as "Inside reverse-fold the head towards the lower right." Of course, program-generated instructions can be turned off, edited, or completely rewritten if desired.

All graphic items in the diagram can be selected individually with the mouse, and moved, resized, or reformatted to fine-tune the illustration or to suit the diagrammer's taste. Furthermore, global *styles* are defined for each diagram object type, which are sets of formatting characteristics that apply to all objects of that type. For instance, some authors prefer using arrows with filled arrowheads for valley folds, while others prefer unfilled arrowheads; defining the basic valley-fold arrow style applies the chosen format to all valley-fold arrows in the diagram. Styles can be defined for lines, arrows, fills, and text boxes. Moreover, the style of any individual object in the diagram can be overridden by custom formatting at any time. This functionality will be quite familiar to users of traditional illustration software.

In addition to all the familiar commands to Open, Save, and Close model files, the File menu also offers an option to "Save As Base. . . ," which

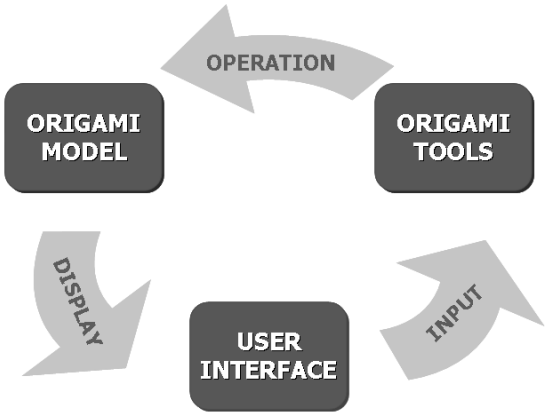

Figure 5. Program structure and data flow.

saves the current model as an origami base that can be used as the starting point for other models. This allows us to create a *library* of origami bases, both traditional and novel.

3 Data and Program Structure

Figure 5 illustrates eGami's general program structure and data pipeline. Its data classes can be grouped into three main sections: (a) classes defining the origami model; (b) those that are part of the user interface; and (c) the origami tools' classes.

3.1 Origami Model

Each step in the sequence of an origami model is a paper configuration that can be considered a *state* of a polygon mesh with strict consistency and other constraints. In eGami, this polygon mesh is defined by a modified winged-edge boundary representation (*b-rep*), common in computer graphics applications that require describing objects in terms of their surface boundaries [4]. This *b-rep* is defined by an interconnected collection of vertices, edges, and polygons, as exemplified in Figure 6.

The consistency of this mesh must be insured at all times, by following these constraints: (a) all polygons are closed; (b) all edges are used by not more than two polygons; (c) each vertex is referenced by at least two edges and at least one polygon; and (d) the mesh is completely connected, topologically planar and has no holes (i.e., one boundary only).

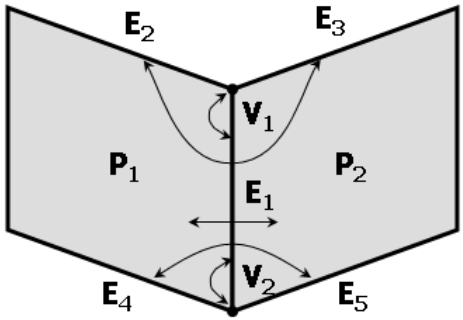

Figure 6. Winged-edge boundary representation.

Our mesh data model must include additional constraints that reflect the properties of the paper: (e) vertices on the raw edge of the paper must be connected to exactly two "raw" edges; (f) vertices inside the paper must satisfy Maekawa's Theorem [5]; (g) paper does not stretch, which means vertex positions are fixed and edge lengths are constant; (h) paper faces are flat, which means that each polygon's vertices are coplanar and implies that only rigid folds are allowed; and (i) no rips or holes.

Finally, some constraints related to the folding itself: (j) paper is infinitely thin, implying that paper "creep" is not taken into account; (k) only flat folds are allowed, meaning each vertex inside the paper must satisfy Kawasaki's Theorem [5]; and (l) paper does not intersect itself. It has been noted in [1], [2], and elsewhere that these last two constraints are the hardest to satisfy and thus implement, and they will be discussed further below.

3.2 User Interface

The heart of the user interface is the "Editor" control, whose main function is to display the origami model, as defined by the *b-rep* mesh described above. This module also manages the collection of landmarks explained in the Program Features section, as well as the various views, sequence navigation, diagram formatting, etc.

The Editor control also handles mouse and keyboard inputs, which are sent to the origami Tools for processing, as was shown in Figure 5.

3.3 Origami Tools

eGami "Tools" are defined as modular program classes with a standard implementation interface, making it relatively easy to add new ones. All

tools are collected in a "Toolbox" object that receives its input from the Editor control and forwards it to the currently active tool.

Instead of manipulating the origami model directly, tools are designed to be *operation-driven*. This means that tools perform their action(s) by creating one or more discrete *operations* (themselves a data class), which contain a full description of the manipulations to be performed. The result is that it is then very easy to maintain a full history of all operations performed and to implement Undo/Redo capability. One could theoretically reproduce the entire folding sequence simply from the starting paper configuration and the history of operations, although this is not how it is implemented in practice.

3.4 Validity Testing

Whenever a tool executes its operation(s) and makes changes to the model, all the constraints defined above must be tested to ensure the consistency of the mesh. This happens to be the most critical step in the pipeline, as well as the hardest. In fact, a full answer to the question whether a given crease pattern can be folded flat has been proven to be an NP-hard problem [2].

This becomes apparent when we test that the model folds flat without intersecting itself, which requires assessing the relationship between each polygon and every other polygon. eGami takes a few shortcuts, but it still remains that the order of complexity is not polynomial but factorial. The practical result is that as the model becomes more elaborate, the simulation becomes noticeably slower. It is unlikely that eGami (or any other origami computer simulation for that matter) would be practical for truly complex models, at least not until nondeterministic computers are invented!

4 Limitations and Future Development

Besides the complexity issue outlined above, the computer interface itself raises some limitations. One limitation is that the mouse is a single-control-point input device that can be equated to "folding with one hand," with the other hand limited to holding the paper down. Many real-life origami operations are defined by multiple points or landmarks, which would require preselecting additional landmarks ahead of time. This still remains to be implemented in eGami.

Another interface-related limitation is the difficulty of selecting which layers are affected in operations that involve multiple layers with alternative outcomes. An example of this is a reverse fold where the "split" can occur

anywhere in between a number of different layers. A way of showing and choosing where this split should occur has yet to be developed.

At this time, all tools fold across single or overlapping fold lines, so reverse folds, squashes, and petal folds all result in symmetrical folds. The ability to fold across multiple nonoverlapping fold lines is a feature that is already under development, and would allow us to create *asymmetrical* as well as swivel folds.

The goal of creating animated step-by-step tutorials mentioned earlier also remains to be implemented. Since eGami stores the full folding sequence of a model, animating that sequence would be relatively straightforward, and would be useful for teaching purposes. Libraries of models could be easily built and distributed with the application, and it is even conceivable that authors may perhaps someday distribute eGami versions of their creations.

In spite of its limitations, eGami so far promises to have practical uses in the origami community. Feedback has been positive and further development is certainly warranted.

Bibliography

[1] s.-m. belcastro and T. C. Hull. "A Mathematical Model for Non-Flat Origami." In *Origami^3: Proceedings of the Third International Meeting of Origami Science, Mathematics, and Education*, edited by Thomas Hull, pp. 39–51. Natick, MA: A K Peters, 2002.

[2] M. Bern and B. Hayes. "The Complexity of Flat Origami." In *Proceedings of the Seventh Annual ACM-SIAM Symposium on Discrete Algorithms*, pp. 175–183. Philadelphia: SIAM, 1996.

[3] E. Demaine and M. Demaine. "Recent Results in Computational Origami." In *Origami^3: Proceedings of the Third International Meeting of Origami Science, Mathematics, and Education*, edited by Thomas Hull, pp. 3–16. Natick, MA: A K Peters, 2002.

[4] J. D. Foley. *Computer Graphics: Principles and Practice*, Second edition. Reading, MA: Addison-Wesley, 1990.

[5] T. C. Hull. "On the Mathematics of Flat Origami." *Congressus Numerantium* 100 (1994), 215–224.

[6] T. K. Lam. "Origami Simulator and Diagrammer." Available at http://www.angelfire.com/or3/tklorigami0/, 2006.

[7] R. Lang. "Because It's There: Idiot Savant." *Highlights from British Origami 140–149*. Available at http://www.britishorigami.info/practical/highlite/140-49.php#148, 1991.

[8] R. J. Lang. "Origami and Geometric Constructions," *Robert J. Lang Origami*. Available at http://www.langorigami.com/science/hha/origami_constructions.pdf, 2003.

[9] S. Miyazaki, T. Yasuda, S. Yokoi, and J. Toriwaki. "An Interactive Simulation System of Origami Based on Virtual Space Manipulation." In *Proceedings of the IEEE International Workshop on Robot and Human Communication*, pp. 210–215. Los Alamitos, CA: IEEE Press, 1992.

[10] J. Nimoy. "Making Origami Instructional Symbolics Interactive." Available at http://www.jtnimoy.net/itp/origami/, 2002.

[11] J. Szinger. "The Foldinator Modeler and Document Generator." In *Origami^3: Proceedings of the Third International Meeting of Origami Science, Mathematics, and Education*, edited by Thomas Hull, pp. 129–135. Natick, MA: A K Peters, 2002.

Computational Origami System Eos

Tetsuo Ida, Hidekazu Takahashi, Mircea Marin,
Asem Kasem, and Fadoua Ghourabi

1 Introduction

In this paper we describe a software environment for computational origami [1, 4] called E-origami system, abbreviated to Eos. We have been developing Eos since 2002 as part of our research in constraint solving and theorem proving. Using Eos we can create an origami on the screen of a computer, as if we had folded it by hand with a piece of paper. Eos is intended to be an integrated tool for constructing and reasoning about origami. So far our emphasis in the design of Eos is on mathematical rigor. This means that we consider origami as an art and also as a science of geometrical shapes, which enables us to reason about them. For this reason, we implemented most of Eos in Mathematica [6], a language for symbolic computation. Mathematica facilitates the manipulation of shapes constituting an origami form both symbolically and numerically. Representing the internal data structures of origami figures symbolically is the first step toward manipulation and visualization of origami. We found that symbolic representation of the internal data structures is important for advanced processing of origami works and for reasoning about them.

The paper is organized as follows. In Section 2, we will give an overview of Eos. In Sections 3 and 4, we explain the use of Eos with illustrative examples. In Section 5, we will explain the use of Eos for proving the correctness of the construction. In Section 6, we explain webOrigami, which interfaces Eos to the web. We summarize our results in Section 7.

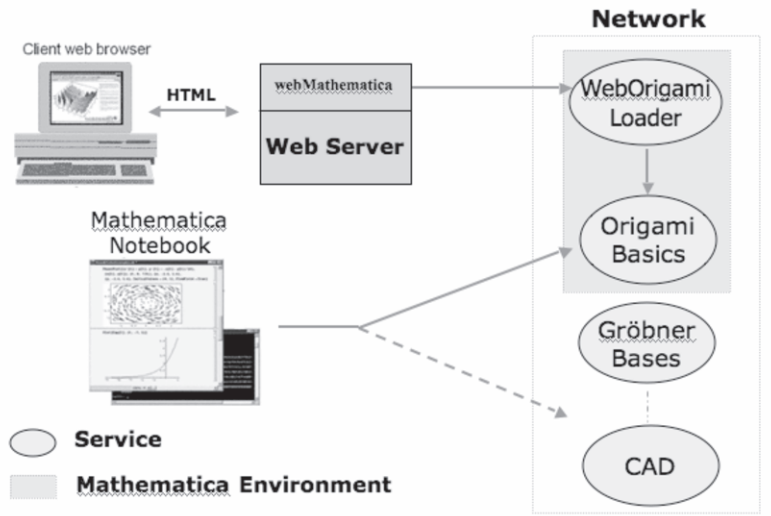

Figure 1. Overview of Eos.

2 Overview of Eos

Figure 1 shows the software architecture of Eos. Eos consists of two modules: OrigamiBasics and webOrigami. OrigamiBasics is a Mathematica package, which implements the algorithms of origami-specific geometrical computation as well as visualization. The Mathematica notebook is the user's interface to OrigamiBasics.

The module webOrigami interfaces OrigamiBasics with a web browser. It consists of a collection of HTML and JSP pages, and a package called webOrigamiLoader. Some functionality of OrigamiBasics is thereby made accessible to users via a web browser.

Eos provides two methods for folding: *mathematical fold* and *artistic fold*. The former fold method is based on the axiomatic definition of origami folds proposed by Huzita [3]. The latter is the classical artistic method of folding, which is typically used for constructing origami art pieces.

We have performed a complete implementation of Huzita's six axioms and the seventh axiom added by Hatori [2]. Those axioms are declarative statements about the existence of lines along which we can make a fold. We transform those axioms into algorithmic statements, which are amenable for computation by Mathematica. We provide each fold method that corresponds to each axiom as a Mathematica function. Table 1 summarizes the function invocations corresponding to each axiom.

Function Call	Corresponding Axiom
`Fold[A,Along→ PQ]`	Fold along the line passing through points P and Q, moving point A.
`Fold[P,Q]`	Fold to bring point P to point Q.
`Fold[PQ,EF]`	Fold to superpose lines PQ and EF.
`Fold[A, AlongPerpendicular→ {P,EF}]`	Fold along the line perpendicular to EF and passing through P (moving point A).
`Fold[P,EF,Through→ Q]`	Fold to superpose point P and line EF along the line passing through point Q.
`Fold[P,EF,Q,GH]`	Fold to superpose point P and line EF, and point Q and line GH, simultaneously.
`Fold[P,EF, AlongPerpendicular→ GH]`	Fold to superpose point P and line EF along the line perpendicular to line GH.

Table 1. Function invocations corresponding to Huzita's axioms.

We will explain the usage of these functions in Section 3, where we construct a regular heptagon.

As for the artistic fold method, we have implemented the mountain fold, valley fold, inside-reverse fold, outside-reverse fold, and squash fold, each of which is realized by functions `MountainFold`, `ValleyFold`, `InsideReverseFold`, `OutsideReverseFold`, and `SquashFold`, respectively. The usage of these functions is discussed in Section 4.

3 Construction of a Regular Heptagon

In this section, we present a stepwise construction of a regular heptagon by Eos. We start the construction by calling function `BeginOrigami`. The following function call creates the initial origami shape and visualizes it as shown in Figure 2(a):

$$\texttt{BeginOrigami}[\,\{10, \texttt{MarkPoints} \rightarrow \{\texttt{"A"}, \texttt{"B"}, \texttt{"C"}, \texttt{"D"}\}\},\\ \texttt{FaceColor} \rightarrow \{\texttt{Hue}[.5], \texttt{Hue}[.17]\}];$$

Actual construction begins with the following call:

$$\texttt{Fold}[\texttt{A},\texttt{D}, \texttt{MarkPointOn} \rightarrow \texttt{True}];$$

This command performs the fold of the origami to bring point A to point D. Note also that the `MarkPointOn` option tells the system to mark the intersection points with the fold line. To make a single unfold of the current origami, we call `Unfold`. Figure 2(b) shows the corresponding result.

We proceed by repeated applications of `Fold` and `Unfold` and obtain the origami shape shown in Figure 2(c). We mark the center of the intended

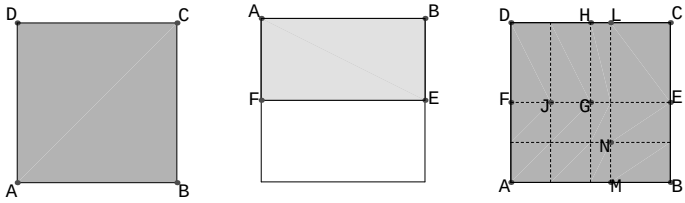

Figure 2. Initial sequence of origami folding steps for heptagon construction: (a) Initial position. (b) After a single fold. (c) After a series of folds and unfolds.

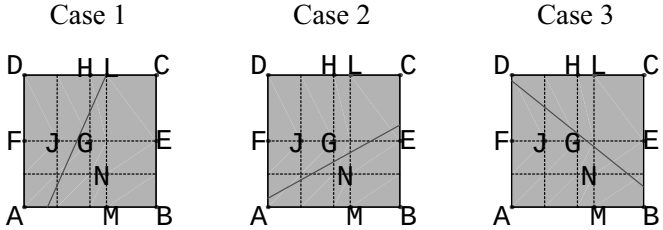

Figure 3. Multiple folding choices.

regular heptagon by point G, and its first vertex by point H. After that, we make a fold to superpose point J and line GH, and point N and line GE, respectively, by:

```
Fold[J, GH, N, GE];
```

For this folding action, we have three cases (see Figure 3). Since we want the third case, we perform again the same call with the additional parameter `Case` → `3`.

```
Fold[J, GH, N, GE, Case → 3];
```

Next, we duplicate point J on other faces in order to keep its projection point P, and then unfold the origami. This produces the origami shown in Figure 4(a).

```
DupPoint["J"]; Unfold[ ];
```

```
Fold[H, PT, Through → G];
Fold[H,  PT, Through → G, Case → 1];
DupPoint["H"];   Unfold[];
```

The second vertex of the regular heptagon lies on the perpendicular of line GH passing through P. So we make this fold by calling:

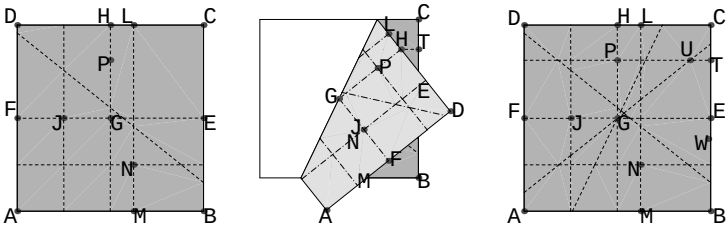

Figure 4. Intermediate construction steps: (a) P, the reflection of J. (b) Fold for the second vertex. (c) U, the second vertex.

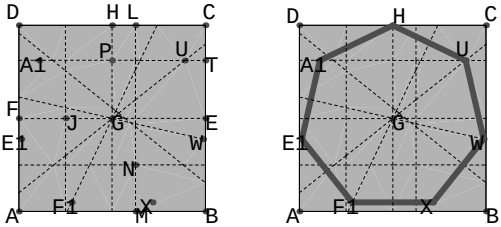

Figure 5. Final origami (left) and final origami displayed using special viewing options (right).

```
Fold[H,AlongPerpendicular→{P,HG},MarkPointOn →BC]; Unfold[];
```

To obtain the second vertex, we make a fold along a line passing through G such that H and line PT are superposed. Since two folds are possible, we choose the first one. Then, we duplicate point H on line PT to obtain the second vertex U. Figures 4(b) and (c) show some output of the subsequent constructions.

The remaining vertices can be obtained by simple folds using the symmetric nature of the problem. Points W, X, F1, E1, and A1 are constructed by the following commands:

```
Fold[H, Along → UG];   DupPoint["H"];   Unfold[];
Fold[U, Along → WG];   DupPoint["U"];   Unfold[];
Fold[B, Along → HG];   DupPoint[{"U", "W", "X"}];   Unfold[];
```

The final origami contains the heptagon HUWXF1E1A1 shown in Figure 5.

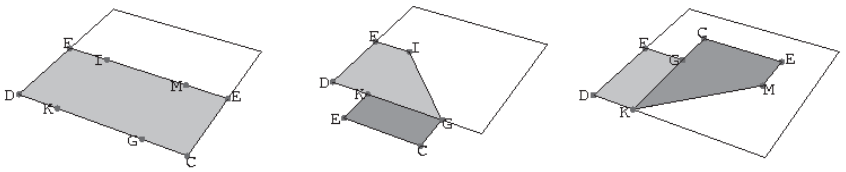

Figure 6. `InsideReverseFold`$[\{2,3\}, \mathrm{GI}]$ and `OutsideReverseFold`$[\mathrm{KM}]$.

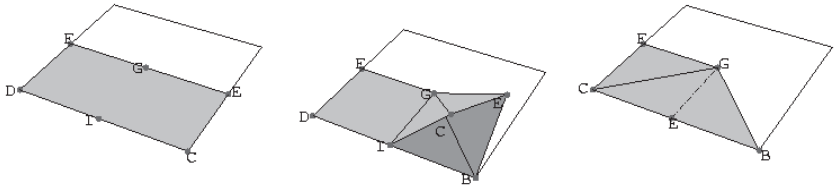

Figure 7. `SquashFold`$[\{2,3\}, \{\mathrm{GB}, \mathrm{GI}\}, \frac{\pi}{4}]$ and `SquashFold`$[\{2,3\}, \{\mathrm{GB}, \mathrm{GI}\}, \pi]$.

4 Artistic Fold Method

In classical artistic origami, mountain and valley folds are the basic actions used to create the work. Functions `ValleyFold`$[seg, \theta]$ and `MountainFold`$[seg, \theta]$ perform valley and mountain folds, respectively, where seg is the segment along which the fold is made and θ is the angle of rotation of the paper about the fold line. Usually (and in flat origami), the angle of rotation θ is π.

`InsideReverseFold`$[\{bottom, top\}, seg]$ performs the inside-reverse fold, which makes a tuck by folding along the segment seg. The pair $\{bottom, top\}$ indicates the bottom and top of the faces that are to be folded.

`OutsideReverseFold`$[seg]$ performs the outside-reverse fold such that the faces are folded along the segment seg in an opposite direction to wrap themselves (see Figure 6).

`SquashFold`$[\{bottom, top\}, \{seg1, seg2\}, \theta]$ performs a squash fold. The pair of faces $\{bottom, top\}$ are the bottom and top of the faces to be folded. The top face is folded along the segment $seg2$ by the angle θ, and the bottom face is folded along the segment $seg1$ (see Figure 7).

Figure 8 shows the construction of a traditional crane. The construction uses `ValleyFold`, `InsideReverseFold`, and `SquashFold`.

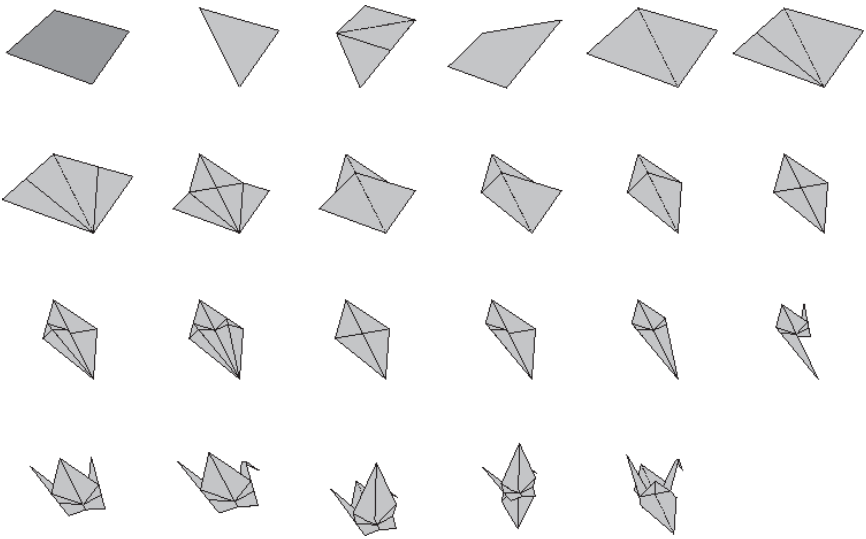

Figure 8. Construction of a crane.

5 Automated Proof of Correctness

After constructing an origami shape with Eos, we can proceed to prove the correctness of the construction. The automated proof of the correctness of the construction by Eos proceeds in the following steps:

1. We extract the geometrical properties of the construction and transform them into a system of polynomial equalities and inequalities.

2. We model and represent the conclusion to be proved also as a system of polynomial equalities and/or inequalities.

3. We form the logical implication *premise* $\Longrightarrow$ *conclusion*. This is the theorem to be proved. The theorem means that under the *premise* (which is true since we constructed the object by origami folds) the *conclusion* holds, which we want to know. We send this formula to a theorem prover. When the formula contains only equalities and disequalities, we can use the Gröbner bases method. When the formula contains inequalities, we need more powerful methods. We use Mathematica implementation of cylindrical algebraic decomposition.

4. Depending on the theorem provers that are used, we obtain the proof result in a human-readable form or in a form that may need further processing for easy interpretation.

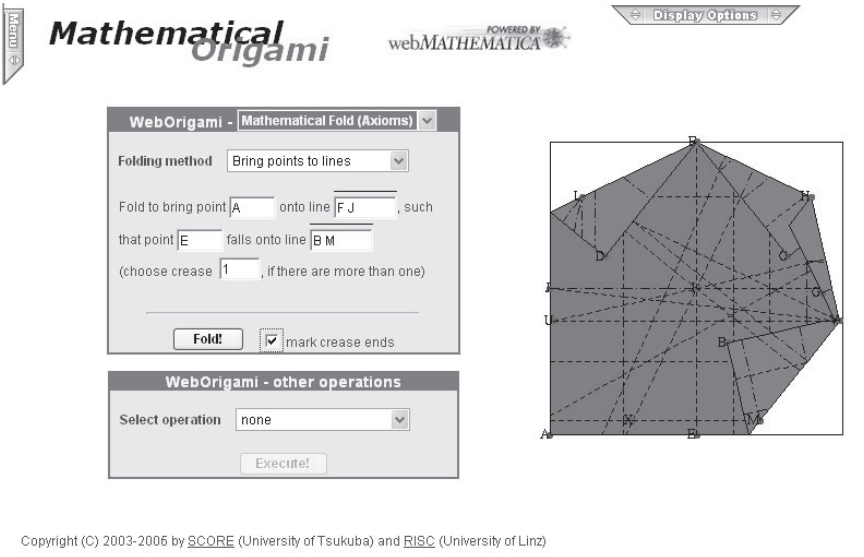

Figure 9. Webpage of webOrigami.

6 webOrigami

The idea of webOrigami is to enable origamists all over the world to have access to part of Eos functionalities without requiring Eos packages and Mathematica installation. We envisage that using a standard web browser, an origamist can access the system and enjoy creating origami pieces.

Figure 9 shows a snapshot of a webOrigami dynamic page that we can create by visiting the URL http://webeos.score.cs.tsukuba.ac.jp.

webOrigami has a collection of special web pages that contain Mathematica programs to be executed by a computing server. The programs in the webpage are executed in the computing server after obtaining the necessary parameter input created by the user of the web browser. These programs call functions defined in OrigamiBasics that run on the computing server. The program part of the web page is replaced by the result of the computation. The web page newly created in this way is then sent to the web browser, which renders the page. To enable this interaction, we use webMathematica [5].

webOrigami offers the following functionalities to users of a web browser for constructing origami pieces: color selection for both faces of an origami; choice between classical artistic origami and mathematical origami; three-dimensional image view of the constructed origami; LiveGraphics3D that generates origami as a three-dimensional Java object; save/restore of user's

session work; save of the construction as Mathematica notebook; a set of useful functions such as duplicating and deleting points, unfolding and flipping of an origami, and rolling back to a previous step; and other viewing options and useful information that can be configured during construction steps.

7 Conclusion

We have presented the computational origami system Eos, which not only simulates origami folds, but also proves geometric properties of the construction. We have also explained webOrigami and its features.

Bibliography

[1] E. D. Demaine and Martin L. Demaine. "Recent Results in Computational Origami." In *Origami^3: Proceedings of the Third International Meeting of Origami Science, Mathematics, and Education*, edited by Thomas Hull, pp. 3–16. Natick, MA: A K Peters, 2002.

[2] K. Hatori. "K's Origami: Origami Construction." Available at http://origami.ousaan.com/library/conste.html, 2006.

[3] H. Huzita. "Axiomatic Development of Origami Geometry." In *Proceedings of the First International Meeting of Origami Science and Technology*, edited by H. Huzita, pp. 143–158. Padova, Italy: Dipartimento di Fisica dell'Università di Padova, 1991.

[4] T. Ida, D. Tepeneu, B. Buchberger, and J. Robu. "Proving and Constraint Solving in Computational Origami." In *Artificial Intelligence and Symbolic Computation: 7th International Conference, AISC 2004, Linz, Austria, September 22–24, 2004, Proceedings*, Lecture Notes in Computer Science 3249, pp. 132–142. Berlin: Springer, 2004.

[5] Wolfram Research. "webMathematica 2." Available at http://www.wolfram.com/products/webmathematica, 2006.

[6] S. Wolfram. *The Mathematica Book*, Fifth edition. Champaign, IL: Wolfram Media, 2003.

Computational Complexity of a Pop-Up Book

Ryuhei Uehara and Sachio Teramoto

1 Introduction

Origami is the centuries-old art of folding paper. Recently, some mathematicians and computer scientists have started to study origami. As one example, a geometric approach to origami design has been taken, resulting in the TreeMaker program by Lang [8]. As another example, *global flat foldability* of an origami has been considered, with the result being a proof that the general problem to find an appropriate overlap order to fold a given origami flat is NP-hard [1]. Many other generalizations of origami and related problems (e.g., map folding) are possible; the reader can find a comprehensive survey of the complexity of folding an origami and related results due to Demaine and Demaine [3] and Demaine and O'Rourke [4].

Another hundred-years-old art of folding paper is the pop-up book. While often considered something primarily for children, contemporary pop-up book artists have invented many sculptures of great beauty and intricacy (see, e.g., [9]).

A pop-up book has two major differences from origami: first, it has two rigid surfaces connected by a hinge (the pages of the book), and the essential movement of the mechanism depends solely on these two surfaces. Hence the movement is strongly restricted (see, e.g., [2,7] for possible movements). Second, a pop-up book form must be functional in both the closed (or folded) and opened (or unfolded) positions. For a pop-up book designer,

then, the problem is to design sculptures using paper that lies between two covers, and to make the book so that it can be opened and closed.

A further constraint arises because to see a page of the book, we usually open or close the page exactly once. That is, we do not repeat the movements of opening and closing to see a page in the book; the form must be created based on a single opening motion of the pages. From the viewpoint of the "computation" of the movement, this point also strongly restricts the designer.

In this paper, we first give a model for the pop-up book design problem. Next, we show that both the opening book problem and the closing book problem are NP-hard. We note that our results do not use the overlap order technique used in [1] to show the NP-hardness of the foldability problem of an origami.

2 Definitions

An input of the problem is a paper sculpture contained within a book structure. That is, a book consists of two *(surface) covers* that are joined by a *hinge*, and some *paper objects* that are fixed between the covers. A paper object between the covers consists of *faces* and *creases*. In our model, creases are given as a part of the input, that is, we are not allowed to create a new crease as part of the opening/closing action. An input crease can be folded in both directions; it is also allowed to be not folded, i.e., flat.

A given input will be the (possible) design of a pop-up book, which consists of two surface covers with a fixed fold angle between them, say θ_0, and our objective will be the opening or closing of the book. More precisely, for a given angle θ_1, we aim to make the angle of the book vary continuously from θ_0 to θ_1 without making a new crease or introducing a penetration of one layer by another.

Now, we denote by $\textsc{Pop}(\theta_0, \theta_1)$ the problem of whether a given pop-up book with two covers of fold angle θ_0 can be opened or closed to fold angle θ_1 without making a new crease. The *size* of an input (or a pop-up book) is defined by the summation of the number of lines (or edges of papers), the number of (predefined) creases, and the number of corners. In this paper, all borders (and creases) of a paper consist of straight lines. That is, we do not deal with the case in which the border of a paper makes a curve.

3 Closing a Pop-Up Book

In this section, we show NP-hardness of the closing of a pop-up book. More precisely, the main theorem in this section is the following:

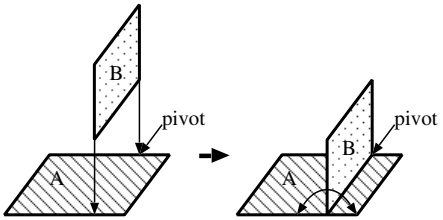

Figure 1. REVSTOP gadget.

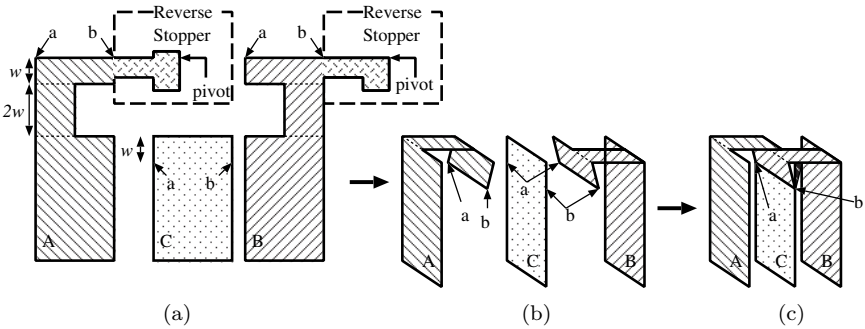

Figure 2. CLAUSE$_c$ gadget: (a) The three parts. (b)–(c) Composition of the parts (reverse stoppers are omitted).

Theorem 1. *The problem* POP(θ_0, θ_1) *is NP-hard for any* $\theta_0 > \theta_1 \geq 0$.

We reduce from a well-known NP-complete problem, NAE3SAT, defined as follows [5, LO3]:

Input: A formula F consists of m clauses $c_1, c_2, \ldots, c_m$ of three literals with n variables $x_1, x_2, \ldots, x_n$.

Output: "Yes" if there is a truth assignment such that each clause has at least one true literal and at least one false literal.

To reduce the problem, we make three kinds of gadgets called REVSTOP, CLAUSE$_c$, and VARIABLE$_c$ from paper.

The REVSTOP gadget is illustrated in Figure 1; for face A, face B can be flipped from degree 0 to degree 180 centered at the line *pivot*.

The CLAUSE$_c$ gadget is illustrated in Figure 2. A CLAUSE$_c$ consists of three parts (Figure 2(a)). On the papers A and B, the right upper parts form REVSTOP. For clarity, they are omitted in Figure 2(b) and (c). Figure 2(c) is the final form of the CLAUSE$_c$ (with REVSTOP).

The VARIABLE$_c$ gadget is illustrated in Figure 3; two bottom lines will be glued to two surface covers, respectively. The neutral position is depicted

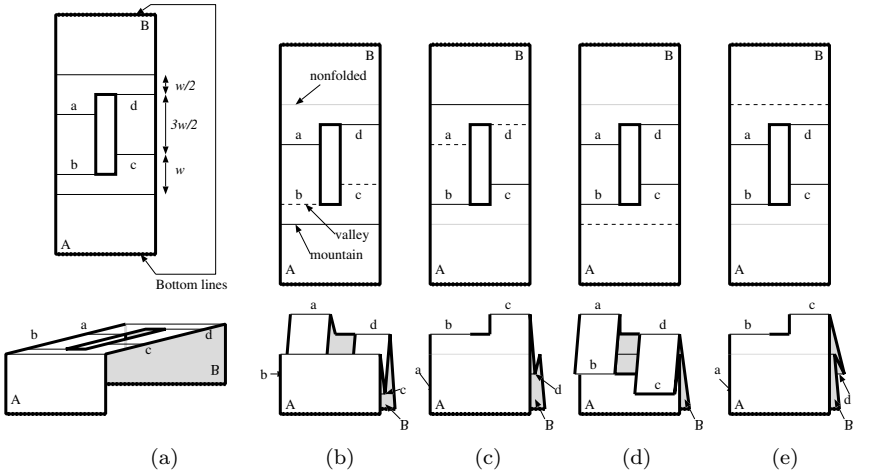

Figure 3. VARIABLE$_c$ gadget. (a) Neutral position. (b) True assignment. (c) False assignment. (d) Illegal position. (e) Another illegal position.

in Figure 3(a). Since the bottom lines have the same height, we have four possible cases to fold the VARIABLE$_c$ flat shown in Figure 3(b)–(e). Among these four cases, the cases (d) and (e) will be inhibited by other gadgets. Hence, we will represent the true and false assignments by the forms (b) and (c), respectively. We call two lines labeled by a and c in the gadget *ridges*. When two foldings (b) and (c) are exchanged, the heights of the two ridges (ex)change $2w$.

Now we show how to construct a paper sculpture, that is, the structure of a pop-up book, from a given formula F (Figure 4). For each $i = 1, 2, \ldots, n$, the VARIABLE$_c$ X_i for x_i are glued to the two covers at the bottom lines. Initially, each VARIABLE$_c$ is in a neutral position; its two ridges are at the same height.

For a clause $c_j = (\ell_{i_1}, \ell_{i_2}, \ell_{i_3})$ with $\ell_i = x_i$ or $\ell_i = \bar{x_i}$, the CLAUSE$_c$ C_j is connected to VARIABLE$_c$ X_{i_1}, X_{i_2}, and X_{i_3} as follows: If $\ell_{i_1} = x_{i_1}$, the bottom line of A in Figure 2 is connected to the right ridge of the VARIABLE$_c$ X_{i_1}. If $\ell_{i_2} = \bar{x_{i_2}}$, the bottom line of C in Figure 2 is connected to the left ridge of the VARIABLE$_c$ X_{i_2}. The bottom line of B in Figure 2 is connected to the ridge of the VARIABLE$_c$ X_{i_3} similarly. The connections are done in a natural way; see Figure 4 for the clause $c_j = (x_1, x_2, \bar{x_n})$. In Figure 4, the ridges imply x_1 is true, x_2 is false, and x_n is true. We note that each VARIABLE$_c$ is in a neutral position, and all ridges have the same height. Thus, each CLAUSE$_c$ is also in a neutral position as in Figure 2(c). We do not glue the gadgets to the covers except along the bottom lines of VARIABLE$_c$s. After connecting CLAUSE$_c$s and VARIABLE$_c$s, each VARIABLE$_c$ cannot be folded in the

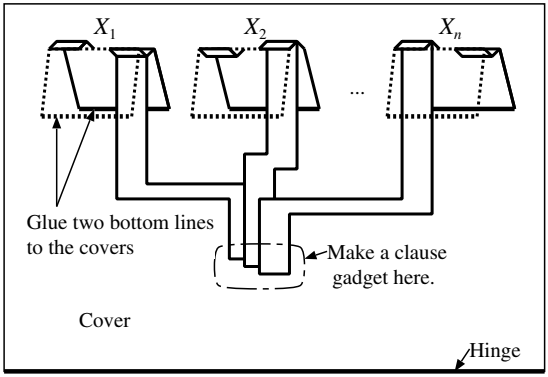

Figure 4. Construction from F.

form in Figure 3(d) and (e) without making a new crease. This reduction can clearly be done in a time that is polynomial in the size of F.

Now we are ready to show the key lemma:

Lemma 1. *The pop-up book constructed above can be closed completely if and only if there is a truth assignment of F such that each clause has at least one true literal and at least one false literal.*

Proof: Each ridge of a $\texttt{VARIABLE}_c$ can be *high* when it is on the top of the mountain, and *low* when it is on the bottom of the valley. To fold each $\texttt{VARIABLE}_c$ flat, one of two ridges is high and the other ridge is low. Hence the parts A, C, B of a $\texttt{CLAUSE}_c$ can take only two states, say, high and low.

We first show feasible cases for a $\texttt{CLAUSE}_c$. When B and C correspond to the same height, and A corresponds to a different height, C can come near to B, and then A can be moved up or down $2w$ height to fold them flat (Figure 5(a)). On the other hand, when A and B correspond to the same height and C takes a different height, A and B can go farther to both sides, and then C can be moved up or down $2w$ height to fold them flat (Figure 5(b)). Using the symmetric way, a $\texttt{CLAUSE}_c$ can be folded flat when one of A, B, and C is high and one of them is low.

The other ways to fold them flat can be classified in two cases. The first case is three different heights; from the form in Figure 5(b), we can fold A, C, and B flat with three different heights in this order or vice versa. However, this case is impossible since the three parts can take either high or low from the restriction by the $\texttt{VARIABLE}_c$s.

The last case is the case that A, B, and C have the same height. This folding can be done if A and B are folded symmetrically as shown in Figure 5(c) where the face A, which forms a symmetric shape of B, is omitted for clarity.

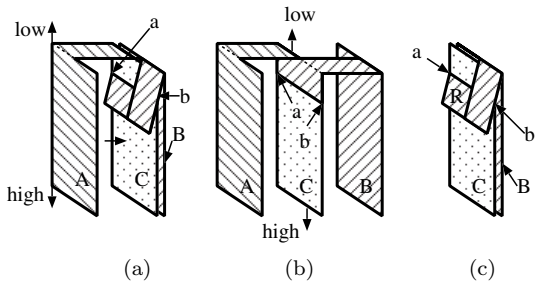

Figure 5. Foldable and unfoldable cases in proof of Lemma 1: face A is omitted in (c) for clarity; see text for details.

However, this case is also impossible. In this case, two symmetric faces, marked by R in Figure 5(c), of A and B have to make a 360 degree rotation. However, the "reverse" movement is inhibited by the REVSTOP in Figure 2(a).

Therefore, the CLAUSE$_c$ C_j can be folded flat if and only if one variable takes the different value from the other two variables. Hence, the pop-up book can be closed if and only if F is a yes instance of NAE3SAT. □

Proof (of Theorem 1): Now we prove the main theorem in this section. In Lemma 1, making the gadgets small enough, we can prove the theorem if θ_0 is small enough and $\theta_1 = 0$. When $\theta_1 > 0$ and θ_0 is close enough to θ_1, we make the gadgets between two inner covers, and put some stable stands between the inner covers and surface covers. On the other hand, when θ_1 is large, we join the inner covers and surface covers by a long paper ribbon with one crease. It is easy to adjust the length of them to fit for given θ_1 and θ_0. This completes the proof of Theorem 1. □

4 Opening a Pop-Up Book

In this section, we show NP-hardness of the opening of a pop-up book. More precisely, the main theorem in this section is the following:

Theorem 2. *The problem* POP(θ_0, θ_1) *is NP-hard for any* $\theta_1 > \theta_0 \geq 0$.

We reduce from the 3SAT, a well-known NP-complete problem [5]. Let F be an instance of 3SAT, which consists of m clauses $c_1, c_2, \ldots, c_m$ of three literals with n variables $x_1, x_2, \ldots, x_n$. To reduce F, we make two kinds of gadgets called VARIABLE$_o$ and CLAUSE$_o$ by paper.

The VARIABLE$_o$ is described in Figure 6; that consists of three thick rectangles and six thin rectangles. Two edges of the same label are glued as in Figure 6. We note that the resultant gadget is completely flat. Let

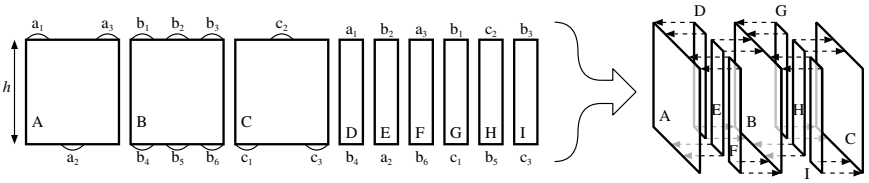

Figure 6. VARIABLE$_o$ gadget.

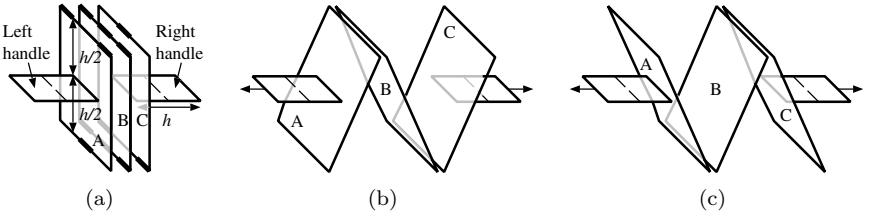

Figure 7. Handles with VARIABLE$_o$ gadget: (a) Two handles are glued. (b) True case. (c) False case.

h be the common height of the rectangles. Next, two handles are glued to the VARIABLE$_o$ at height $h/2$ as in Figure 7(a). (Two handles can be folded flat at the center creases.) Then, there are only two ways to make two handles $2h$ move apart as shown in Figure 7(b) and (c). (Note that this has the same structure as an old Asian wooden toy that consists of several boards banded like Figure 6, which can be continuously flipped by twisting a handle.) We call the case (b) *true* and case (c) *false*. Now, we attach two kinds of arms in Figure 8 to the VARIABLE$_o$. (The number of arms will be described later.) The labeled edges are glued to the corresponding edges in Figure 6. (To be precise, the left arm is between A and F at a_3, and the right arm is between B and I at b_3.) The joints for adjustment are folded flat as in Figure 8.

Now, from the completely closed VARIABLE$_o$, when we make two handles a distance $2h$ apart as in Figure 7(b), the left arm can go down at most $h/2$ since it is free except at the edge a_3, but the right arm has to go up $h/2$ since it is caught by B and C, and pulled up. Hence, the bottom line of the left arm can go down h by unfolding the joint, and the bottom line of the right arm cannot go down from the initial position. We note that, in this case, the left arm can choose to stay at the initial position by using the joint. Similarly, when we make two handles $2h$ apart as in Figure 7(c), the right arm can go down h, and the left arm cannot go down at all.

The CLAUSE$_o$ is described in Figure 9. A CLAUSE$_o$ consists of three ribbons P, Q, and R. The ribbon R has length $6h$, and both sides are glued to the

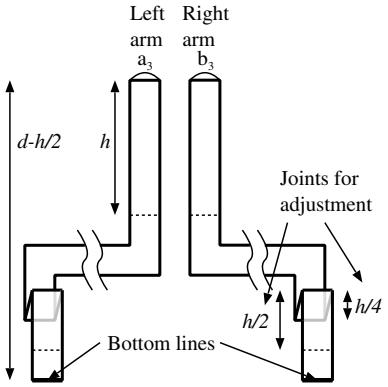

Figure 8. Arms for VARIABLE$_o$ gadget.

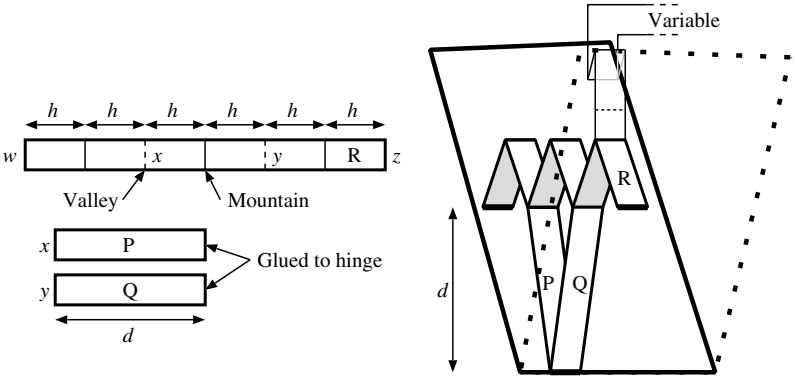

Figure 9. CLAUSE$_o$ gadget.

covers at distance d from the hinge. The ribbon P joins the hinge and one of the valley on R, and the ribbon Q joins the hinge and another valley on R.

Now, we can construct a paper sculpture that is the design of a pop-up book from a given formula F. For each $i = 1, 2, \ldots, n$, the VARIABLE$_o$ X_i for x_i are glued to two covers by two handles at distance $2d$ from the hinge.

For a clause $c_j = (\ell_{i_1}, \ell_{i_2}, \ell_{i_3})$ with $\ell_i = x_i$ or $\ell_i = \bar{x_i}$, the CLAUSE$_o$ C_j is connected to VARIABLE$_o$ X_{i_1}, X_{i_2}, and X_{i_3} as follows: If $\ell_{i_1} = x_{i_1}$, one of three mountains on the ribbon R of C_j is connected to the bottom line of the left arm of X_{i_1}. If $\ell_{i_2} = \bar{x_{i_2}}$, another mountain on R is connected to the bottom line of the right arm of X_{i_2}. The last mountain of R is connected to X_{i_3} similarly.

Hence, X_i has l_i left arms and r_i right arms, where l_i and r_i are the number of occurrences of x_i and $\bar{x_i}$ in F, respectively.

We note that, with suitable choice of h and d, all gadgets can be folded flat, and the resultant pop-up book can be closed completely. The reduction can be done in a time polynomial in the size of F.

Now we are ready to show the key lemma of this section:

Lemma 2. *The pop-up book constructed above can be opened if and only if there is a truth assignment of F such that each clause has at least one true literal.*

Proof: We try to open the book with the assignment for each $\textsf{VARIABLE}_o$. For each clause c_j, if at least one of three literals is true, the corresponding arm comes down to C_j, and hence it can be opened to θ with $d \sin\theta = h$. However, if none of them are true, no arms come close to C_j, and hence it cannot be opened. Hence F is satisfiable if and only if the pop-up book can be opened to θ. □

Proof (of Theorem 2): Now we prove the main theorem. In Lemma 2, letting $d \gg h$, we have the theorem for $\textsf{POP}(0, \theta_1)$ for small $\theta_1 > 0$. We use the same trick in Section 3 for the other cases. This completes the proof of Theorem 2. □

5 Concluding Remarks

For the problems for an origami and a pop-up book, while we have shown that they are NP-hard, we did not show that they are in NP. In fact, the problems might be PSPACE-hard in some models, since the underlying motions seem to be similar to the movement problems for two-dimensional linkages, which is known to be PSPACE-hard due to Hopcroft, Joseph, and Whitesides [6].

Bibliography

[1] M. Bern and B. Hayes. "The Complexity of Flat Origami." In *Proceedings of the Seventh Annual ACM-SIAM Symposium on Discrete Algorithms*, pp. 175–183. Philadelphia: SIAM, 1996.

[2] D. A. Carter and J. Diaz. *The Elements of Pop Up: A Pop-Up Book for Aspiring Paper Engineers*. New York: Little Simon, 1999.

[3] E. D. Demaine and M. L. Demaine. "Recent Results in Computational Origami." In *Origami^3: Proceedings of the Third International Meeting of*

Origami Science, Mathematics, and Education, edited by Thomas Hull, pp. 3–16. Natick, MA: A K Peters, 2002.

[4] E. D. Demaine and J. O'Rourke. "A Survey of Folding and Unfolding in Computational Geometry." In *Combinatorial and Computational Geometry*, Mathematical Sciences Research Institute Publications 52, edited by J. E. Goodman, J. Pach, and E. Welzl, pp. 167–211. Cambridge, UK: Cambridge University Press, 2005.

[5] M. R. Garey and D. S. Johnson. *Computers and Intractability—A Guide to the Theory of NP-Completeness*. New York: W. H. Freeman, 1979.

[6] J. E. Hopcroft, D. A. Joseph, and S. H. Whitesides. "Movement Problems for 2-Dimensional Linkages." *SIAM J. Comput.* 13 (1984),610–629.

[7] P. Jackson. *The Pop-Up Book*. New York: Owl Books, 1993.

[8] R. J. Lang. *Origami Design Secrets*. Natick, MA: A K Peters, 2003.

[9] R. Sabuda. *Winter's Tale: An Original Pop-Up Journey*. New York: Little Simon, 2005.

Concepts and Modeling of a Tessellated Molecule Surface

Elias Halloran

1 Background

The use of repeating folding patterns has produced polyhedral surfaces with remarkable geometric properties. These surfaces have both flat-folded states and three-dimensional folded states and provide solutions to packaging problems where large surfaces must be deployed from small areas.

Moreover, folding polyhedral surfaces have a variety of uses. For example, Miura made use of one such surface in his design of maps and atlases [5] and Z. You made use of another such surface in his design of an expandable heart stent [4, 7]. In fact, such surfaces have also been found operating in nature. In a paper on leaf forms, H. Kobayashi and others [3] discussed how leaves of Carpinus Betulus and Fagus Sylvaticus deployed similarly to a polyhedral surface called *Miura-ori* [6].

This paper will focus on the surface associated with You's expandable origami stent. The design of this surface has a history: although there may have been several, if not many, independent discoveries of the crease pattern for this surface (see Figure 1), the first published appearance of the crease pattern was in 1982 by Fujimoto [2], who used it to make rigid cylinders. However, this rigidity was not too pronounced. You showed that although Fujimoto's cylinder was rigid, it deployed with small deformations [4, 7] and could function as a stent when made with semirigid materials. With that said, this type of cylinder rigidity will not be discussed in this paper;

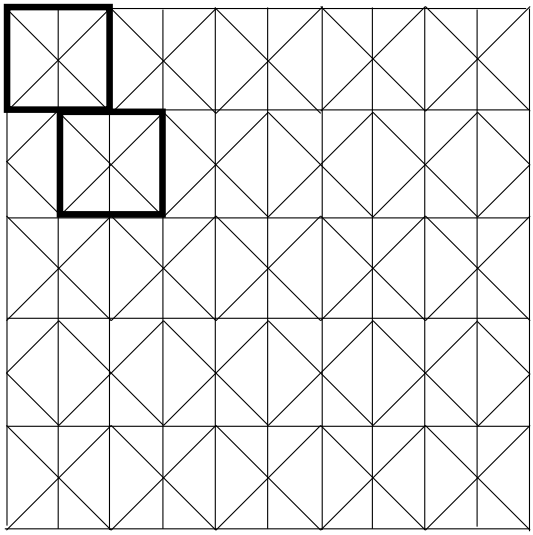

Figure 1. The crease pattern of a tessellated waterbomb.

while the crease pattern shown in Figure 1 was studied by You with a cylindrical connection [7], this paper will explore the same crease pattern and corresponding polyhedral surface without the cylindrical connection.

2 Introduction

Many polyhedral surfaces using repeating folding patterns work on a common principle. By tessellating origami molecules in a crease pattern, basic origami folds produce complete surfaces. Our goal in this paper is to discuss one of these surfaces called a tessellated waterbomb surface.

Definition 1. A *tessellated waterbomb surface* or *tessellated waterbomb* for short is a polyhedral surface consisting of interlocking waterbomb molecules whose crease pattern is arranged as shown in Figure 1.

Such tessellated waterbomb surfaces have many folded states and as they change shape they morph between these folded states. For example, Figure 2 shows a basic empirical result: elongating the highlighted region of a closed model as shown deploys the tessellated waterbomb, giving it a cylindrical shape. As we will show, this highlighted region in Figure 2, called a line of latitude, controls that action.

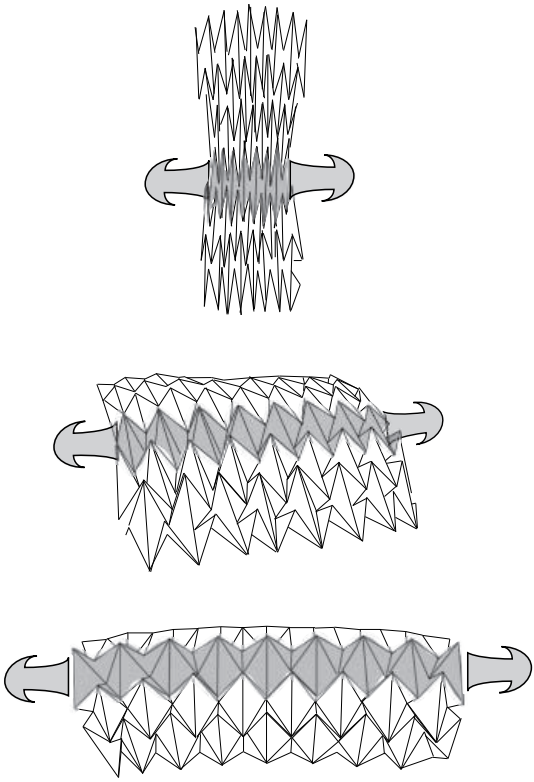

Figure 2. Deploying a tessellated waterbomb.

Definition 2. A *line of latitude* or *latitude* for short is a string of waterbomb molecules connected laterally along axial lines as highlighted in Figure 2.

The pertinence of this naming scheme is shown within another experimental tessellated waterbomb in Figure 3: when placed in a circular shape the many lines of latitude of a tessellated waterbomb appear to shrink and expand with some similarity to the latitudinal lines around the earth.

The body of this paper will be devoted to further discussing the relationship between a latitude and the regions around it. In order to show that a line of latitude controls the action shown in Figure 2, we will assume a line of latitude has been put in a rigid folded state in which all vertex points along that latitude have been fixed in space. Then we will show that fixing these points fixes an entire region, called a *rigid neighborhood*, around that latitude. Thus, if a latitude is put into a rigid folded state, then a neighborhood around that latitude must also be rigid.

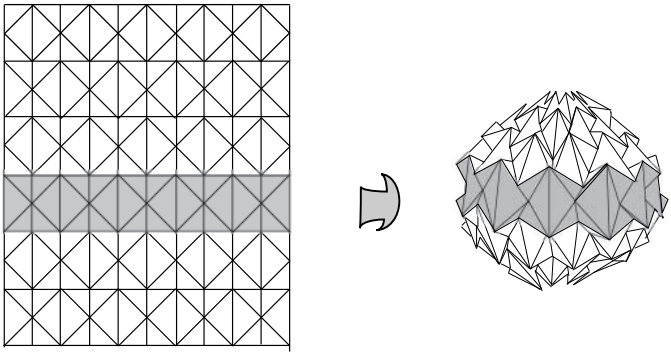

Figure 3. Justification of latitude nomenclature.

3 Surface Analysis

3.1 Rigidity and Hinges

Definition 3. Every crease in a three-dimensional folded structure connects two faces, and together a crease and the two faces it borders make a *hinge*.

A selection of three types of hinges found within the tessellated waterbomb surface, labeled as **R**, **G**, and **B**, are shown in Figure 4. With the exception of a special class of exceptional cases for the **B** hinge, these three hinges are in a rigid folded state when the position of their base segments ($\vec{A}, \vec{C}$ in Figure 4) defined by three points ($\vec{a}, \vec{b}, \vec{c}$ in Figure 4) are fixed in space.

Because of this relationship, we may define functions that output the missing tip of hinges given the input values of three specific points for each of **R**, **G**, and **B**. These functions, called R, G, and B, are defined in Equations (1)–(3), respectively, with labels shown in Figure 4:

$$G(\vec{a}, \vec{b}, \vec{c}) = \vec{b} + \vec{K}, \tag{1}$$

$$R(\vec{a}, \vec{b}, \vec{c}) = \vec{b} + \vec{Q}, \tag{2}$$

$$B(\vec{a}, \vec{b}, \vec{c}) = \vec{b} + \vec{M}. \tag{3}$$

Each of functions R, G, and B, respectively, operates on three domain points on the tessellated waterbomb (one point on each side of a hinge crease, one point on the hinge crease) and give the position in space of a fourth range point on the hinge crease.

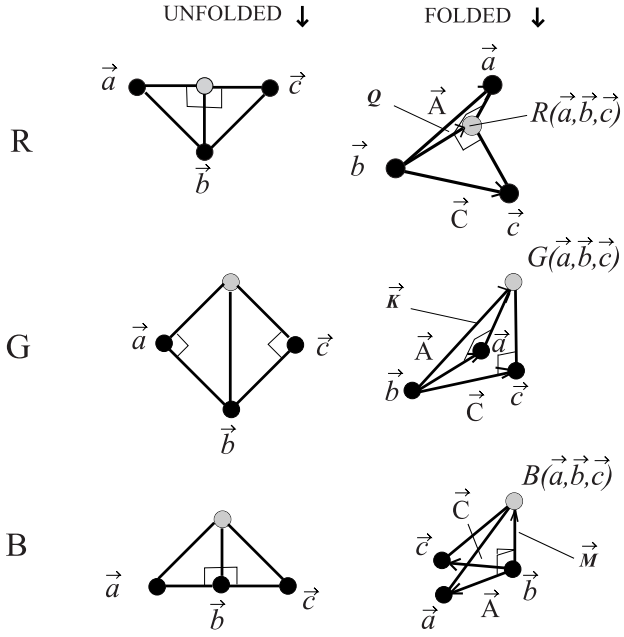

Figure 4. Hinge functions R, G, and B.

As an aside: for the course of this paper, the explicit definition of functions R, G, and B are less important than the observation that they exist. However, since the explicit definitions of these functions do exist, are not too complicated, and would be useful for calculating the curvature and position of points within rigid neighborhoods in a practical setting, it is worth mentioning that in all but a few exceptional cases vectors $\vec{Q}$, $\vec{M}$, and $\vec{K}$ can be written in the form $e(\vec{C}+\vec{A})+f(\vec{C}\times\vec{A})$, where e and f take on varying scalar values. For example, suppose we wanted to calculate the value of $\vec{M}$ that is associated with our B hinge; we would first define $\vec{C}=\vec{c}-\vec{b}$ and $\vec{A}=\vec{a}-\vec{b}$ to form the base vectors of the hinge, then let $\vec{M}=\|\vec{C}\times\vec{A}\|\,|\vec{A}|$, since $\vec{M}$ has the same magnitude as its base segments and is perpendicular to them. Thus, for our B hinge, we would have $e=0$ and $f=|\vec{A}|/|\vec{C}\times\vec{A}|$.

What is most important is that these hinges and their functions, R, G, and B, fully tessellate the crease pattern plane in a variety of useful ways (for example, see the tessellation in Figure 5, which will be put to work in Figure 6) and may therefore be used to show (as planned) that rigidity extends from one latitude to a neighborhood of higher and lower lines of latitude.

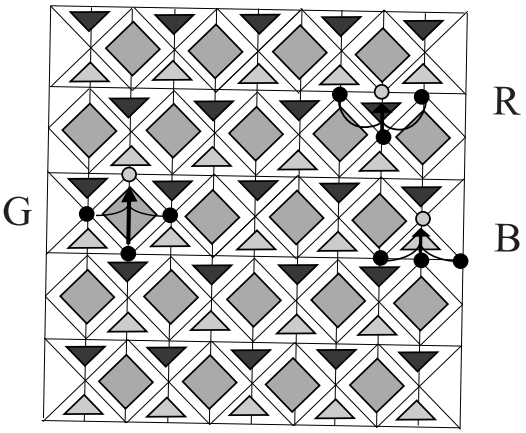

Figure 5. Tessellation of hinge functions.

3.2 Rigidity Neighborhood of a Latitude

Suppose a latitude has been given a fixed position in space. Iterative use of functions R, G, and B can extend what is known to be rigid from just that latitude to a neighborhood around it.

A snapshot is shown in Figure 6: beginning with a line of latitude, R, G, and B are applied wherever possible so that larger and larger portions of our given tessellated waterbomb surface are fixed in space, stopping only when there are no domain points that R, G, and B can operate on.

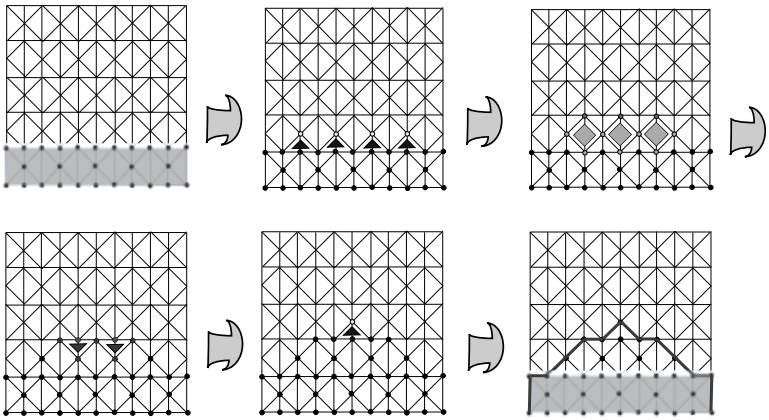

Figure 6. Iterative use of R, G, and B.

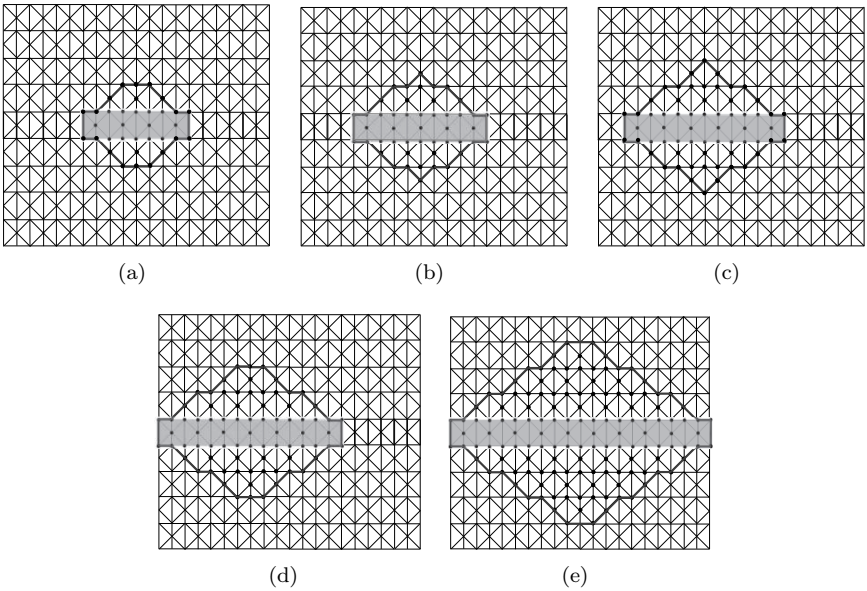

Figure 7. Rigid neighborhoods of several latitudes: (a) 4, (b) 5, (c) 6, (d) 7, and (e) 10.

Definition 4. A *latitude of size* n is a line of latitude consisting of a string of n waterbomb molecules.

The more general result is shown in Figures 7(a)–(e): if we highlight latitudes of several different sizes, then find the rigid neighborhoods around them using compositions of R, G, and B, we get Figures 7(a)–(e), which show the rigid neighborhoods around latitudes of size 4, 5, 6, 7, and 10, respectively.

Definition 5. A *rigid neighborhood* of a latitude is a region of a tessellated waterbomb surface that is fixed in space whenever a given latitude is fixed in space.

Note that these rigid neighborhoods can be shown in three-space. For example, the rigid neighborhood of a latitude of size 4 shown in Figure 7(a) corresponds to the region highlighted in Figure 8 when its latitude is put in the appropriate shape.

3.3 Analysis of Rigid Neighborhoods

Figure 7 shows the rigid neighborhoods of several different sizes of latitudes. This section will provide an informal argument as to why these

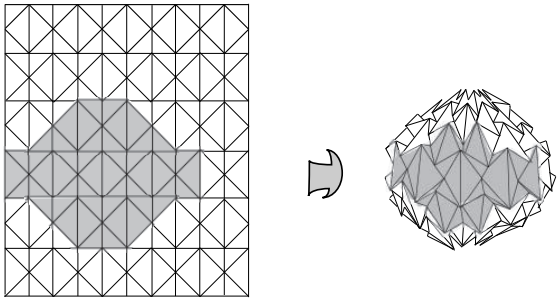

Figure 8. A rigid neighborhood in three-space.

rigid neighborhoods are the largest rigid neighborhoods fixed in place by their latitudes. The argument relies on two considerations—a certain count of creases emanating from the vertex points along the boundary of rigid neighborhoods, and a previous result discussed by Balkom [1].

Definition 6. The *exterior count* of a vertex on the boundary of a rigid neighborhood **W** is the number of creases emanating from that vertex that are both outside of **W** and off the boundary of **W**.

An illustration of an exterior count of the many vertex points of **W** is shown in Figure 9 where Figure 7(a) has been redrawn with circles where counts are made. Here, identical to all the other rigid neighborhoods found in Figure 7, the exterior count of each vertex on the boundary of **W** has a value of 2 or greater.

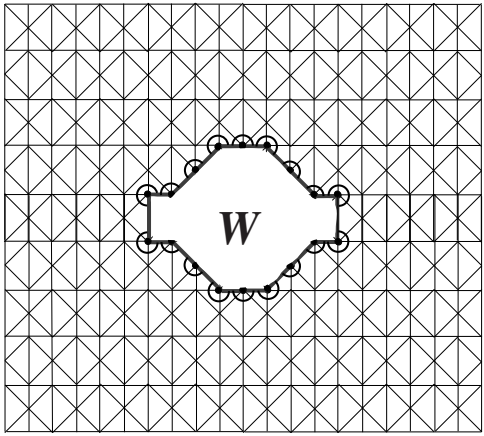

Figure 9. The boundary of a rigidity neighborhood.

If the exterior count of each vertex along the boundary of **W** is 2 or greater, then each counted vertex has at least four dihedral angles that are not fixed to any definite value. This implies that the region around **W** is physically flexible and not rigid since the mobility of a vertex with m creases is $m - 3$ [1].

In other words, if the exterior count of vertex points along **W** were 1 then there would be hinge functions that could extend rigidity, but since the exterior count of each vertex along the boundary of **W** is respectively 2 or greater—assuming that rigidity must come from somewhere already rigid—each of the neighborhoods in Figure 7 is the largest neighborhood fixed by its corresponding latitudes.

4 Conclusions and Future Research

The purpose of this research was to investigate a latitude as a means for controlling the shape of a tessellated waterbomb surface. After assuming the latitude was in a fixed folded state, three types of hinges and their associated functions were used to find what area around the latitude was also fixed in place. Consequently, we have shown that a latitude does in fact control the shape of a tessellated waterbomb surface, though not the entire tessellated waterbomb surface, and we provided some justification as to why this is the case.

Our findings suggest a variety of future results. There are two that could presumably be shown using the methodology within this paper. First, the correspondence between latitudes and their rigid neighborhoods can be extended to tessellated molecule surfaces with some generality, for example, try a *tessellated fish base surface*. Second, the position of points within more general rigid neighborhoods may be defined quantitatively. Thus, the applications of tessellated molecule surfaces may be further studied and properties such as localized curvature fully defined.

Acknowledgment. I would like to thank Dr. Thomas Hull and Dr. Robert J. Lang for their input and advice which helped me refine this paper. I would also like to thank Dr. Matthew Auth for his continued feedback on this project, and Dr. Jim Belk and Dr. Maria Belk for their comments.

Bibliography

[1] Devin Balkcom. "Robotic Origami Folding." PhD dissertation, Carnegie Mellon University, 2004. Available at www.cs.dartmouth.edu/~robotics/papers/thesis.pdf.

[2] S. Fujimoto and M. Nishiwaki. *Sōzō Suru Origami Asobi e no Shōtai* (An Invitation to Creative Origami Play, in Japanese). Osaka, Japan: Asahi Culture Center, 1982.

[3] H. Kobayashi, B. Kresling, and J. F. V. Vincent. "The Geometry of Unfolding Tree Leaves." *Proc. R. Soc. Lond. B* 265:1391 (1998), pp. 147–154.

[4] K. Kuribayashi and Z. You. "Development of a Novel Type of Oesophageal Stent Based on Deployable Tubular Structures." Paper presented at the 4th World Congress of Biomechanics, Calgary, Canada, August 3–8, 2002.

[5] Koryo Miura. "The Application of Origami Science to Map and Atlas Design." In *Origami^3: Proceedings of the Third International Meeting of Origami Science, Mathematics, and Education*, edited by Thomas Hull, pp. 137–145. Natick, MA: A K Peters, 2002.

[6] Koryo Miura. "The Science of *Miura-Ori*: A Review." In *Origami^4: Fourth International Meeting of Origami Science, Mathematics, and Education*, edited by Robert J. Lang, pp. 87–99. Natick, MA: A K Peters, 2009.

[7] Zhong You and Kaori Kuribayashi. "Expandable Tubes with Negative Poisson's Ratio and Their Application in Medicine." In *Origami^4: Fourth International Meeting of Origami Science, Mathematics, and Education*, edited by Robert J. Lang, pp. 117–127. Natick, MA: A K Peters, 2009.

Folding Paper Shopping Bags

Devin J. Balkcom, Erik D. Demaine, Martin L. Demaine,
John A. Ochsendorf, and Zhong You

1 Introduction

In grocery stores around the world, people fold and unfold countless paper bags every day. The rectangular-bottomed paper bags that we know today are manufactured in their three-dimensional shape, then folded flat for shipping and storage, and later unfolded for use. This process was revolutionized by Margaret Knight (1838–1914), who designed a machine in 1867 for automatically gluing and folding rectangular-bottomed paper bags [12]. Before then, paper bags were cut, glued, and folded by hand. Knight's machine effectively demolished the working-class profession of "paper folder."

Our work questions whether paper bags can be truly (mathematically) folded and unfolded in the way that happens many times daily in reality. More precisely, we consider foldings that use a finite number of creases, between which the paper must stay rigid and flat, as if the paper were made of plastic or metal plates connected by hinges. Such foldings are sometimes called *rigid origami*, being more restrictive than general origami foldings, which allow continuous bending and curving of the paper and thus effectively uncountably infinite "creasing." It is known that essentially everything can be folded by a continuous origami folding [7], but that this is not the case for rigid origami.

We prove that the rectangular-bottomed paper bag cannot be folded flat or unfolded from its flat state using the usual set of creases that are

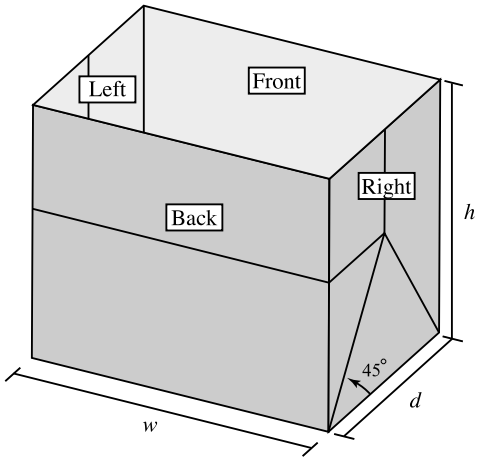

Figure 1. A shopping bag with the traditional crease pattern.

so common in reality—in fact, the bag cannot move at all from either its folded or unfolded state.

The difficulty with folding can be removed by shortening the bag—for example, by making a horizontal cut all the way around the bag at a height of $d/2$, with dimensions as shown in Figure 1. The pattern of creases on the shortened bag resembles that of cardboard boxes department stores use to pack sweaters or collared shirts.

One way to understand the difference between short bags and tall bags is to make a vertical cut along the edge between the right and back sides of the bag, and another along the edge between the left and back sides. As the cut bag is folded, the cut sides separate from each other by as much as 22°. Adding additional paper between the cut edges might therefore allow the bag to be folded.

Finally, we prove that rigid folding is possible without adding paper. If all of the dimensions of the bag are equal, then the pattern of diagonal creases shown in Figure 10(b) can be used to "twist" the bag flat. If the dimensions are not equal, a sequence of "telescoping" folds, as shown in Figure 12, shortens the bag until it can be collapsed. (These are discussed in more detail later.)

2 Related Work

In the mathematical literature, the closest work to rigid folding is *rigidity*. The famous Bellows Theorem of Connelly, Sabitov, and Walz [5] says

that any polyhedral piece of paper forming a closed surface preserves its volume when folded according to a finite number of creases. In contrast, as suggested by the existence of bellows in the real world, it is possible to change the volume using origami folding. Even more fundamental are Cauchy's rigidity theorem, Aleksandrov's extension, and Connelly's extension [3], which all establish an inability to fold a convex polyhedron using a finite number of creases. (In Cauchy's case, the creases must be precisely the edges of the polyhedron; in Connelly's case, any finite set of additional creases can be placed; Aleksandrov's theorem is somewhere in between.) Another result found by Connelly[1] is that a positive-curvature *corner* (the cycle of facets surrounding a vertex in a convex polyhedron) cannot be turned "inside-out" no matter how we place finitely many additional creases; this result answers a problem of Gardner [8]. In contrast, a paper bag can be turned inside-out with an origami folding (and in real life) [4].

Few papers discuss rigid origami directly. Demaine and Demaine [6] present a family of origami "bases" that can be folded rigidly. Streinu and Whiteley [15] proved that any single-vertex crease pattern can be folded rigidly—up to but not including the moment at which multiple layers of paper coincide. Balkcom and Mason [1] demonstrate how some classes of origami can be rigidly folded by a robot.

Huffman [10] and McCarthy [13] derive equations describing the relationship between angles of four creases that meet at a vertex. Hull and belcastro [2] describe the relationship for vertices where several creases intersect using a product of rotation matrices; we solve these equations explicitly to compute three dependent crease angles as a function of the other crease angles.

If a rigid folding is possible, the equations relating crease angles must have a solution along the entire folding trajectory. The connectedness of the space of solutions has been analyzed by Kapovich and Millson [11]; our approach is based on work on planar closed chains by Milgram and Trinkle [14].

3 Model and Definitions

We take a simple polyhedral model of the shopping bag. The facets are rigid and infinitely thin; facets may become coplanar during folding, but are not permitted to pass through one another. Creases are assumed to be line segments, and their positions relative to the facets that they bound are fixed.

[1] Personal communication, 1998.

Several creases may meet at a vertex; we will call the angles between adjacent creases meeting at a vertex *sector angles*, and the angles between adjacent facets across a crease *dihedral angles*. The sector angles depend on the design of the bag, which we will call the *crease pattern*, while the dihedral angles describe the current configuration of the bag.

4 Nonfoldability of the Traditional Crease Pattern

Figure 1 shows the traditional crease pattern for a shopping bag. The height of the bag is h, the width is w, and the depth is d. We assume that $h > d/2$; this ensures that the diagonal creases on the right and left sides of the bag meet.

We can distinguish three types of vertices; see Figure 2. The vertices in the middle of each of the right and left sides of the bag have sector angles of $(90°, 135°, 90°, 45°)$. There is a vertex along each of the two of the upright edges of the bag, with sector angles $(90°, 90°, 90°, 90°)$. There are vertices at the corners of the bag with sector angles $(90°, 90°, 45°, 45°)$.

Some pairs of vertices share a crease; Figure 3 shows how vertices of each type are connected to one another.

The sequence of sector angles around a vertex determines a relationship between the dihedral angles at creases around the vertex. Huffman [10] derives a relationship between opposite dihedral angles m and n for a degree-four vertex,

$$1 - \cos n = \frac{\sin A \sin B}{\sin C \sin D}(1 - \cos m), \tag{1}$$

where A, B, C, and D are sector angles, as shown in Figure 4.

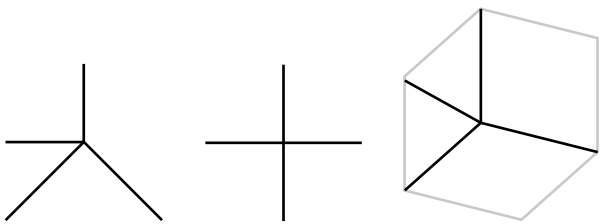

Figure 2. The three types of vertices found in a shopping bag: (a) Side vertex. (b) Edge vertex. (c) Corner vertex.

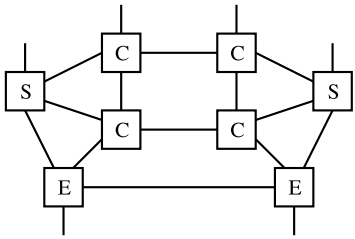

Figure 3. The vertex graph for a shopping bag. The nodes represent edge, side, and corner vertices, and the edges represent creases that connect vertices.

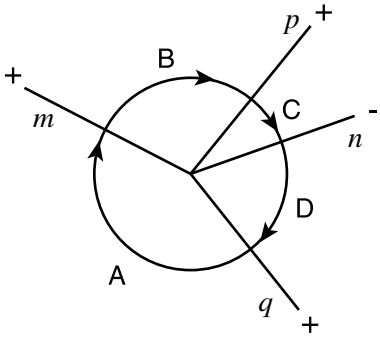

Figure 4. Huffman's notation for the relationship between four creases. A, B, C, and D are sector angles; m, n, p, and q are dihedral angles.

For both *side* and *edge* vertices, $A + C = 180°$, and $B + D = 180°$. Equation (1) can be simplified:

$$\cos n = \cos m.$$

We can use this relationship between dihedral angles to show that a shopping bag with the traditional crease pattern cannot be rigidly folded.

Theorem 1. *A shopping bag with the traditional crease pattern cannot be rigidly folded.*

Proof: Consider an edge vertex. The two vertical creases that meet at this vertex have crease angles that are equal in magnitude; if the magnitude is not 0 or π, then the two horizontal creases from this vertex must be one of $\{0, \pi\}$. Choose a crease that is 0 or π, and connected to another vertex. Walk the crease network; each of the left and right sides is flat (open or folded), and each of the corners is either fully open or collapsed. □

5 Folding Short Bags

On each of the left and right sides of the traditional shopping bag, there are two creases that make a 45° angle with the bottom edge. If $h \leq d/2$, then the creases on each side do not intersect on the interior of the facet; we say the bag is *short*.

Short bags, unlike tall bags with the traditional crease pattern, can be rigidly folded flat. The proof has three components. First, we conjecture a solution: a continuous trajectory of dihedral angles that starts with the open configuration and ends at a flat configuration. We then show that the solution is topologically consistent—i.e., that all configurations along the trajectory satisfy the constraints among crease angles imposed by the geometry of the paper and the crease pattern. Finally, we show that the paper does not pass through itself at any point along the trajectory.

5.1 Configuration-Space Topology

The configuration of a rigid origami mechanism is completely determined by the dihedral angles, but not all choices of dihedral angles satisfy the constraints imposed by the geometry of the paper and the crease pattern.

Finding a trajectory from start to goal that satisfies the constraints can be difficult. The space of configurations may have multiple components, or sections of the configuration space may be joined only at specific regions along their boundaries. For the tall shopping bag described, the possible configurations are *fully open* and *fully closed*; the configuration space is a pair of isolated points.

In this section, we describe a geometric method for analyzing the connectedness of the configuration space for a single vertex at the intersection of four creases; this method is based on work by Trinkle and Milgram [16]. If the configuration space has only one component, then there exists a topologically consistent path between every pair of start and goal configurations.

The technique can also be used to determine whether a given path is topologically consistent. For the purposes of this analysis, we allow paper to pass through itself; we deal with self-intersections separately in the foldability proofs below.

Figure 5 shows an example. We first cut the paper along one of the creases, as shown. If the crease angles were known for creases 1 and 2, then the configuration of the mechanism would be completely determined. However, there is an additional constraint—that the crease angles of the uncut creases be such that the edges of the cut crease "line up." We will therefore analyze the behavior of a point on the cut crease (points A and B in the figure), and see how it restricts motion of the other creases.

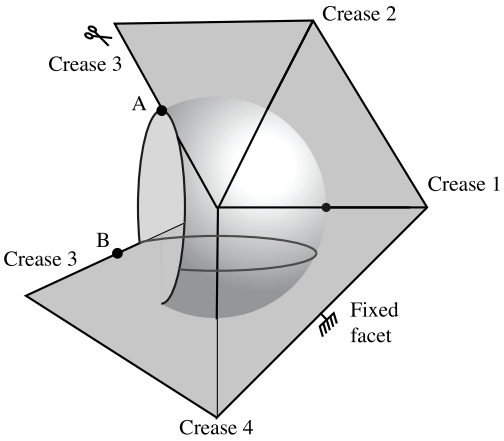

Figure 5. A degree-four vertex, cut along crease 3.

We label the creases as shown in Figure 5, cut crease 3, and rigidly attach the facet between creases 1 and 4 to the ground. Consider the motion of the point A as the paper is allowed to fold along creases 1 and 2. Point A is a fixed distance from the central vertex, and can move on the surface of a sphere. Its motion is also bounded on the left by a plane normal to crease 1, and containing point A. There are two configurations of crease angles 1 and 2 that allow point A to reach most locations on the sphere: crease 2 may be convex, or concave. There are some locations that can only be reached in one way: those that fall on the plane normal to crease 1 and containing point A. There is also one point that can be reached in an infinite number of ways, at the intersection of crease 1 and the sphere.

Now consider point B, that rotates around crease 4. The reachable locations form a circle that lies in a plane perpendicular to crease 4.

If the cut is removed, point A and point B must touch; we will call this point AB. AB must move on the intersection of the sphere cut by a plane that A moves on, and the circle that B moves on. The locations that AB can reach therefore form an arc of a circle.

We can describe the space of possible configurations of the paper by the ways in which point AB can reach each point on the arc. There are two configurations that reach each point on the interior of the arc (crease 2 may be either concave or convex). There is only one way in which each of the endpoints of the arc can be reached—crease 2 is flat at each endpoint.

Each point on the arc corresponds to a slice of the space of configurations of the paper, described by crease angles 1 and 2. Starting at one endpoint of the arc, the slice is a single configuration. Moving continuously

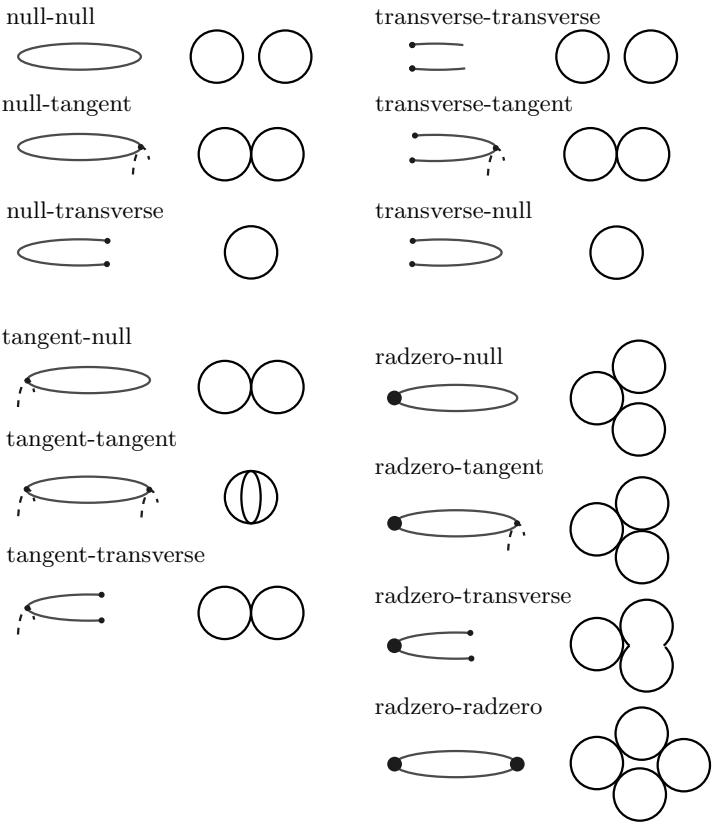

Figure 6. Thirteen of the sixteen possible ways a circle can intersect the workspace of an open three-bar spherical chain. For each class, the ellipses on the left show the workspace; the circles on the right show the configuration space (the preimage of the workspace). There are seven distinct topological classes of configuration space.

along the arc, each new slice corresponds to two configurations. At the final slice (at the other endpoint of the arc), there is only one configuration. The topology of this shape, and thus of the configuration space, is a circle—a one-dimensional manifold with one component.

In general, the set of reachable locations of point A is a sphere bounded by two planes perpendicular to crease 1. The intersection of this surface with the circle reachable by point B can be a circle, an arc of a circle, or two arcs of a circle. Depending on the shape of this workspace, and the ways in which point AB can reach each point on the workspace, the configuration space may have one of several different structures, as shown in Figure 6 and described as follows:

- *Null intersection.* One side of the circle may be completely contained in the workspace. The pre-image of an arc completely contained within the workspace is two arcs.

- *Transverse intersection.* One side of the circle may be cut by the bounding plane at two points. The pre-image of an arc touching the bounding plane is an arc.

- *Tangent intersection.* The circle just touches a bounding circle of nonzero radius. The pre-image of an arc tangent to the bounding circle is a pair of arcs touching at a single interior point.

- *Radius-zero intersection.* The circle touches the bounding plane at one of the poles of the sphere on the x axis. The pre-image of this point is a circle of configurations corresponding to spinning links about the x axis; the pre-image of an arc through this point is two arcs connected by a circle.

We ignore the case where the circle is completely contained within the boundary of the open workspace.

5.2 Proof of Foldability

Theorem 2. *Every short shopping bag can be rigidly collapsed.*

Proof: Consider a corner vertex. If we ignore self-intersections, we can see that the configuration space is a single connected component as follows. Let the links be numbered as shown in Figure 7, and anchor link 1. The workspace of the endpoint of link 3 is the portion of the sphere bounded by two halfplanes; $|x| < \sqrt{2}/2$. The workspace of the endpoint of link 4 is a circle of radius $\sqrt{2}/2$, centered at the point $(0, -1)$. The pre-image of the intersection of these two workspaces is a pair of circles connected at two points. (These points correspond to two collapsed configurations.)

We choose the collapsed configuration in which all dihedral angles are π, and choose a trajectory that moves to this configuration directly (i.e., without passing through the other collapsed trajectory). We let θ_1 increase monotonically from $\pi/2$ to π. From Equation (1), $\theta_2 = \pm\theta_4$; for the trajectory we have chosen, $\theta_2 = \theta_4$. θ_1 also increases monotonically from $\pi/2$ to π for this trajectory.

Adjacent facets can only collide if the angle between them is zero or π; no crease angles are 0 or π except at the start and end of the trajectory. Intersections between facets 1 and 3 must first occur when the θ_2 or θ_3 axis touches the $z = 0$ plane; since θ_1 and θ_4 are positive except at the end of the trajectory, there are no intersections. The case of intersection between facets 2 and 4 is symmetric.

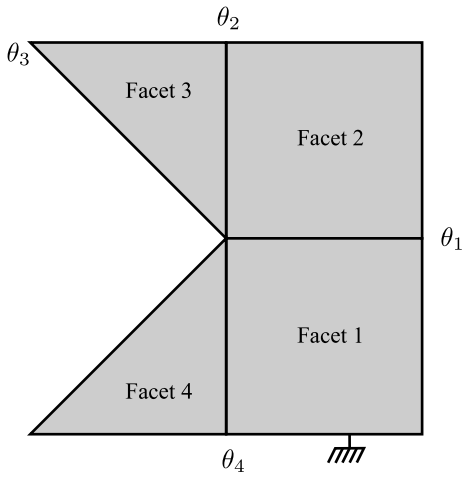

Figure 7. A corner of the short bag, cut between two facets and anchored to the ground.

The four corners of the bag are connected by creases along the bottom of the bag, and all four corners fold simultaneously and symmetrically; the condition that $h \leq d/2$ is sufficient to ensure that no facets that do not share a vertex can intersect. □

6 Folding Tall Bags

Short bags can be folded; this suggests several techniques for folding taller bags. We consider adding new paper between creases, and adding more creases.

6.1 Folding by Adding Material

Figure 8(a) shows a bag whose height is greater than $d/2$. Three horizontal creases have been added at a height of $d/2$, forming a complete rectangle of creases that circumscribe the bag. Experimenting with a card model reveals that the edges of the bag turn to split open during the folding. In other words, gaps, as those shown in Figure 8(b), appear during the folding process. We can compute the size of the gaps.

Consider a tall bag with edges above height $d/2$ being cut open. Figure 8 shows a partially folded bag. A set of vectors, a_3, a_4, a_5, and a_6, are introduced to present the creases and the edges of panels that are slit open. We choose a right-handed Cartesian coordinate system as shown,

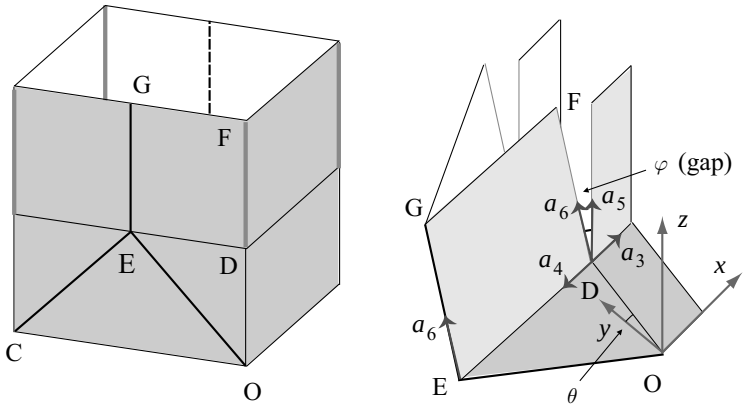

Figure 8. A tall bag. (a) The crease pattern. (b) Partially folded bag when some of the edges are cut open.

with origin at vertex O, the x axis along the bottom front edge, and the y axis in the plane of the bottom of the bag. This can be expressed as follows:

$$a_3 = (1, 0, 0),$$
$$a_4 = \frac{OE - OD}{|OE - OD|} = (-\cos\delta, 1 - \cos\theta, \sin\delta - \sin\theta).$$

Since the slit edges are perpendicular to both FD and DH, $a_3 \cdot a_5 = 0$, and $a_4 \cdot a_6 = 0$. Therefore,

$$a_5 = (0, \cos\omega, \sin\omega),$$
$$a_6 = \left(\frac{\sin\delta - \sin\theta}{\sqrt{1 - 4\sin^4\theta/2}}, 0, -\frac{\cos\delta}{\sqrt{1 - 4\sin^4\theta/2}}\right),$$

where ω is a variable describing the rotation between the portions of the side panel above and below DH. Denote by φ the angle between a_5 and a_6. Since $\cos\varphi = a_5 \cdot a_6$,

$$\cos\varphi = \frac{\sin\omega\cos\delta}{\sqrt{1 - 4\sin^4\theta/2}} = \frac{\sin\omega\sqrt{1 - \tan^2\theta/2}}{\sqrt{1 - 4\sin^4\theta/2}}. \tag{2}$$

While folding the bag with slit edges, it is always possible to adjust ω so that a_5 and a_6 become the closest, or φ is minimum. It is obvious from

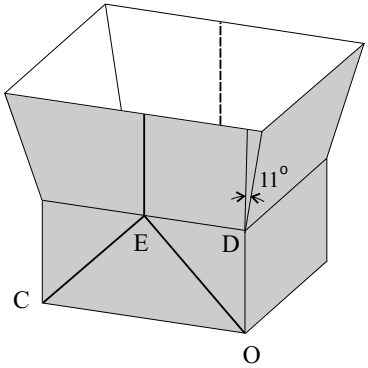

Figure 9. A tall shopping bag with material added to allow folding.

Equation (2) that the minimum is obtained when $\omega = \pi/2$:

$$\cos\varphi_{\min} = \frac{\sqrt{1-\tan^2\theta/2}}{\sqrt{1-\sin^4\theta/2}}.$$

Plotting this curve, we find that the maximum gap angle during folding is about 22°. This solution indicates that the box can be folded rigidly provided that additional material can be found to fill the gap; Figure 9 shows a conjectured solution.

6.2 Folding Cubical Bags by Twisting

In the special case that $d = h = w$, a *twist* folding scheme can be applied. The crease pattern is shown in Figure 10(a) and a card model is displayed in Figure 10(b).

The scheme is not applicable to taller bags with a square base—during the fold, corner and midpoints on the top edges of the bag are not coplanar

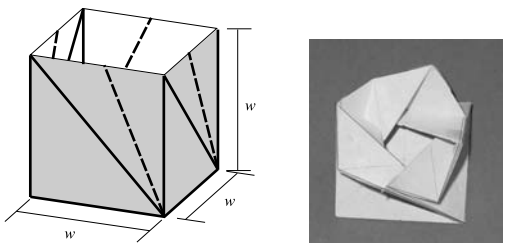

Figure 10. The twist folding of a cubical bag. (a) Crease pattern. (b) Card model.

in spite of the fact that they become coplanar in the fully folded and fully open states. This makes it difficult to join two neighboring portions of the bag when the same folding scheme applies to both portions. The twist folding scheme is not applicable to bags with a rectangular base due to lack of rotational symmetry.

6.3 Folding by Telescoping

We have considered a few special cases; in this section we show that any tall shopping bag can be collapsed with the addition of a finite number of fixed creases. Theorem 3 will show the procedure. In order to verify the procedure, it is necessary to show that facets do not collide during folding; the primary method for showing this will be to consider the volumes that might be swept by each facet during folding, and to show that these volumes do not intersect.

Theorem 3. *A tall shopping bag can be collapsed with the addition of a finite number of creases.*

Proof: The approach is to shorten the box, by adding creases that allow the top to be rolled inside the box. Once the box is short, Theorem 2 allows the box to be collapsed. We consider a single edge of the box, with crease pattern shown in Figure 11.

The crease between facets 1 and 2 is fixed at 90°. The fold takes place in three steps. During step 1, we fix crease 5, and drive crease 3 from 180° to 0°, choosing the solution such that crease angle 1 is positive, crease angle 2 is negative, and crease angle 4 is positive. During step 2, we fix crease 3 at 0°, and drive crease 1 to 180°. Crease angles 2 and 4 do not change sign, and crease angle 5 becomes positive. During step 3, we fix crease 1 at 180°, and drive crease 3 to −180. Crease angles 2 and 4 return to 0°, and crease angle 5 reaches 180°. Table 1 summarizes the crease angles after each step.

Ignoring self-intersection, the existence of a trajectory of this form can be verified using the graphical method for determining the topology of a degree-four spherical linkage, since each of the steps fixes two of the six creases (the crease between facets 1 and 2, and one other).

	θ_1	θ_2	θ_3	θ_4	θ_5
Start	0°	0°	90°	0°	0°
After step 1	$+, < 180°$	$-, > -180°$	0°	$+, < 180°$	0°
After step 2	180°	$-, > -180°$	0°	$+, < 180°$	$+, < 180°$
After step 3	180°	0°	−180°	$+, < 180°$	0°

Table 1. A trajectory for shortening an edge of a shopping bag.

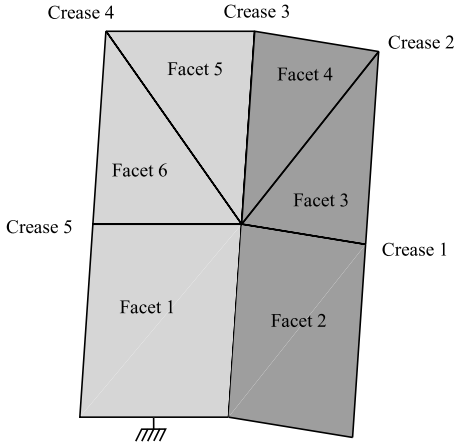

Figure 11. An edge of the shopping bag with creases added to allow folding. Facets 1 and 2 are rigidly connected; there are joints (creases) between all other pairs of adjacent facets.

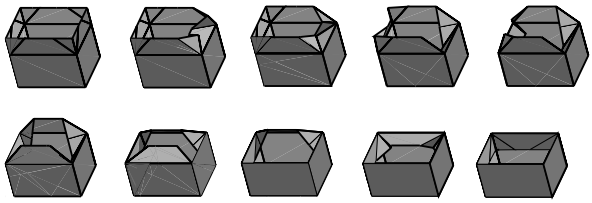

Figure 12. Procedure for shortening a rectangular tube.

To prove that self-intersection does not occur, consider pairwise intersections of facets. No two adjacent facets can collide unless the angle of the crease between them crosses 180°; this never happens for our choice of trajectory. Table 2 summarizes the analysis of collision possibilities for nonadjacent facets.

A single edge can be rolled inside the box using the procedure above; to shorten the box, place symmetric crease patterns at each edge. Figure 12 shows an animation. For a tall box, or a box with dissimilar length and width, it may be necessary to perform a number of shortenings before collapsing the box. Note that the height removed during a shortening can be as small as desired, so it is possible to shorten the box to any desired height. □

	facet(s)	vs. facet(s)	Don't intersect because:
Step 1	3	1, 6	Workspace of 3 is a right circular cone that intersects plane of facets 1, 6 only at origin.
	3	5	Workspaces of 3, 5 right circular cones, sep. $\geq 90°$.
	4	1, 2, 6	Facet 4 is bounded by two creases. Crease 2 is inside the box for $\theta_1 \geq 0$, and crease 3 is as well for $\theta_5 = 0, \theta_4 \geq 0$.
	5	2	Workspace of 5 is a right circular cone that intersects plane of facet 2 only at origin.
	5	6	Facet 6 is coplanar with facet 1.
Step 2	4, 5	1, 2	Crease 2 and crease 4 are inside the box for $\theta_1 \geq 0$ and $\theta_5 \geq 0$.
	3	1	Cone workspace vs. plane; intersection is origin.
	3	6	Right circular cone workspaces sep. $\geq 90°$.
	6	2	Cone workspace vs. plane; intersection is origin.
Step 3	6	2, 3	Cone workspace vs. plane.
	6	4	Right circular cone workspaces sep. $\geq 90°$.
	5	1, 2, 3	Creases 3, 4 inside the box for range of θ_2, θ_5.
	4	1	Cone workspace vs. plane.
	4	6	Right circular cone workspaces sep. $\geq 90°$.

Table 2. Summary of collision possibilities for nonadjacent facets while shortening the tall shopping bag.

7 Relationships Among Crease Angles for Degree-*n* Vertices

Huffman gives a relationship between opposite dihedral angles for a degree-four vertex, and we have described a graphical method for analyzing the connectedness of the space of configurations for vertices, assuming that self-intersection of the paper is ignored.

In order to permit simulation and analysis of more complicated origami mechanisms, we expect it to be useful to be able to determine the relationship between dihedral angles around vertices of higher degree. This section presents a parameterization of the configurations of the paper around a vertex; this parameterization was used to build a simulator for rigid origami, which was used to generate the frames shown in Figure 12.

We choose $n-3$ arbitrary independent crease angles as input, and solve for the remaining crease angles. (In the special case where the dependent

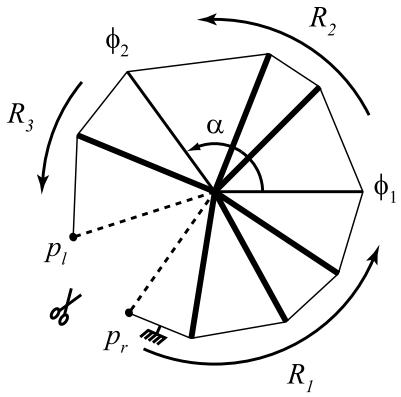

Figure 13. Solving for three dependent crease angles.

crease angles are sequential, a simpler solution is possible using the inverse kinematics approach described in [9].)

Figure 13 shows the procedure; φ_1, φ_2, and φ_3 are the crease angles to be solved for. First cut the crease corresponding to φ_3, and flatten the paper. For any valid configuration of the paper, the two cut edges must line up in such a way that they could be reglued together. Let p_l and p_r be points along these edges a unit distance from the vertex.

Anchor the facet clockwise from the φ_3 crease, and choose a coordinate system with origin at the vertex and with the x-axis along the φ_1 crease. The point p_r lies at a fixed position within the $z = 0$ plane in this coordinate system.

If p_l were permitted to move, then its location would be given by a sequence of rotations about each of the creases. Let R_x and R_z be matrices describing rotation about the x- and z-axes respectively. Let R_1, R_2, and R_3 be matrices corresponding to rotations about the independent crease angles, as shown in Figure 13.

The closure constraint can now be written as

$$R_1 R_x(\varphi_1) R_2 R_z(\alpha) R_x(\varphi_2) R_z(-\alpha) R_3 p_l = p_r. \tag{3}$$

Our goal is to solve for φ_1 and φ_2, given R_1, R_2, and R_3, which may be easily computed from the independent crease angles and the geometry of the paper. Rewrite Equation (3):

$$R_x(\varphi_1) Z R_x(\varphi_2) a = b, \tag{4}$$

where Z, a, and b may be computed as

$$\begin{aligned} Z &= R_2 R_z(\alpha), \\ a &= R_z(-\alpha) R_3 p_l, \\ b &= R_1^T p_r. \end{aligned}$$

Multiplying out Equation (4) gives three equations, the first of which is

$$k_3 = k_1 \cos\varphi_2 + k_2 \sin\varphi_2, \tag{5}$$

with k_1, k_2, and k_3 computed to be

$$\begin{aligned} k_1 &= z_{12} a_2 + z_{13} a_3, \\ k_2 &= z_{13} a_2 - z_{12} a_3, \\ k_3 &= b_1 - z_{11} a_1. \end{aligned}$$

If $k_1 = k_2 = 0$, then Equation (5) implies that φ_2 can take on any value. Otherwise, Equation (5) has the solution(s)

$$\varphi_2 = \operatorname{atan}(k_2, k_1) \pm \operatorname{acos}\left(\frac{k_3}{\sqrt{k_1^2 + k_2^2}} \right).$$

There may be zero, one, two, or infinitely many solutions for φ_2. For each value of φ_2, the remaining two rows of Equation (4) can be used to solve for φ_1, which either has a unique value or is unconstrained. The value of φ_3 is uniquely determined by the angle between the normals to the facets at either end of the cut chain.

8 Open Problems

We conjecture that it is possible to unfold a paper bag from its flat state if it was already folded using the usual set of creases (by an adversary equipped with techniques from origami or reality).

Acknowledgment. Z. You is grateful to the Royal Academy of Engineering from whom he received a Global Research Award that enabled him to work on this most exciting problem.

The idea of gluing two shopping bags together along their tops is due to Robert Lang.

Bibliography

[1] D. J. Balkcom and M. T. Mason. Introducing robotic origami folding. In *Proceedings of the 2004 IEEE International Conference on Robotics and Automation*, Vol. 4, pp. 3245–3250. Los Alamitos, CA: IEEE Press, 2004.

[2] sarah-marie belcastro and T. C. Hull. "Modelling the Folding of Paper into Three Dimensions Using Affine Transformations." *Linear Algebra and its Applications* 348 (2002), 273–282.

[3] R. Connelly. "The Rigidity of Certain Cabled Frameworks and the Second-Order Rigidity of Arbitrarily Triangulated Convex Surfaces." *Advances in Mathematics* 37:3 (1980), 272–299.

[4] R. Connelly. "Rigidity." In *Handbook of Convex Geometry*, Vol. A, edited by P. M. Gruber and J. M. Wills, pp. 223–271. Amsterdam: North-Holland, 1993.

[5] R. Connelly, I. Sabitov, and A. Walz. "The Bellows Conjecture." *Beiträge zur Algebra und Geometrie (Contributions to Algebra and Geometry)*, 38:1 (1997), 1–10.

[6] E. D. Demaine and M. L. Demaine. "Computing Extreme Origami Bases." Technical Report CS-97-22, Department of Computer Science, University of Waterloo, 1997.

[7] E. D. Demaine, S. L. Devadoss, J. S. B. Mitchell, and J. O'Rourke. "Continuous Foldability of Polygonal Paper." In *Proceedings of the 16th Canadian Conference on Computational Geometry*, pp. 64–67. Availavle at http://www.cccg.ca/proceedings/2004/55.pdf, 2004.

[8] M. Gardner. "Tetraflexagons." Chapter 2 of *The Second Scientific American Book of Mathematical Puzzles & Diversions*, pp. 24–31. Chicago: University of Chicago Press, 1987.

[9] L. Han and N. M. Amato. "A Kinematics-Based Probabalistic Roadmap Method for Closed Chain Systems." In *Algorithmic and Computational Robotics: Teh Fourth Workshop on the Algorithmic Foundations of Robotics*, edited by B. R. Donald, K. M. Lynch, and D. Rus, pp. 233–246. Natick, MA: A K Peters, 2000.

[10] D. Huffman. "Curvature and Creases: A Primer on Paper." *IEEE Transactions on Computers* C-25:10 (1976), 1010–1019.

[11] M. Kapovich and J. Millson. "On the Moduli Space of Polygons in the Euclidean Plane." *Journal of Differential Geometry* 42:1 (1995), 133–164.

[12] M. E. Knight. "Paper Bag Machine." Patent no. 116,842, 1871.

[13] J. M. McCarthy. *Geometric Design of Linkages*, Interdisciplinary Applied Mathematics (Systems and Control) 11. New York: Springer-Verlag, 1995.

[14] R. J. Milgram and J. Trinkle. "The Geometry of Configurations Spaces for Closed Chains in Two and Three Dimensions." *Homology, Homotopy, and Applications* 6:1 (2004), 237–267.

[15] I. Streinu and W. Whiteley. "The Spherical Carpenter's Rule Problem and Conical Origami Folds." Paper presented at the 11th Annual Fall Workshop on Computational Geometry, Brooklyn, NY, November, 2–3, 2001.

[16] J. Trinkle and R. J. Milgram. "Complete Path Planning for Closed Kinematic Chains with Spherical Joints." *International Journal of Robotics Research* 21:9 (2002), 773–789.

Origamic Architecture in the Cartesian Coordinate System

Chew Min Cheong, Hajijubok Zainodin,
and Hiromasa Suzuki

1 Introduction

Origamic architecture (OA) is a relatively new concept of making paper models of buildings that was introduced by Masahiro Chatani [1]. In this paper, we attempt to study the mathematical elements connecting two-dimensional patterns and three-dimensional models in OA. We concentrate on the coordinate conversion for points between OA pattern in the 2D plane and those of the OA model in 3D space using the Cartesian coordinate system. Our result generalizes results previously proposed by Mitani and Suzuki [2]. From a single pop-up layer, we have further developed the equations that provide the coordinates of every individual point for up to multiple (n-th) pop-up layers. This is applicable for points located on surfaces or at a folded edge, be it a mountain fold or a valley fold, with angle ranging $0° < \theta \leq 180°$ when being folded and unfolded.

Section 2 describes some of the conditions and definitions for the OA model as well as assumptions made in order to identify the coordinates of points in 2D and 3D. The formulation for relating coordinates of points between the OA pattern and the OA model is illustrated in Section 3. The primary results of this paper can be found specifically in Section 3.4. Section 4 further describes issues relating to coordinate identification for points located on edges or boundaries. Section 5 then identifies the coordinate conversion from 3D to 2D.

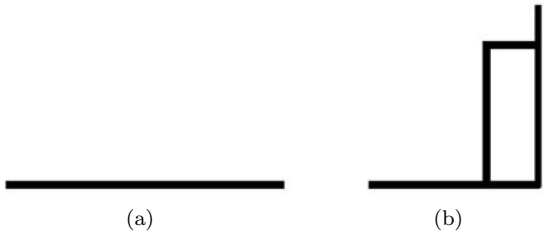

Figure 1. (a) OA pattern at 180°. (b) OA model at 90°.

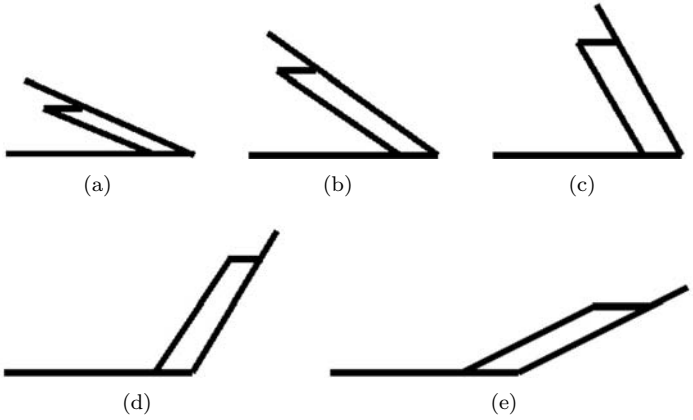

Figure 2. (a) OA model at 30°. (b) OA model at 45°. (c) OA model at 60°. (d) OA model at 120°. (e) OA model at 150°.

2 Cartesian System in OA

The coordinate systems for 2D patterns and 3D models in OA are called the *pattern* coordinates and the *model* coordinates, respectively [2]. We utilize Cartesian coordinates throughout this study. To represent a 2D pattern coordinate, we shall refer to the x-axis and y-axis and describe the coordinate by an ordered pair (x, y). To describe a model coordinate, however, we refer to the mutually perpendicular x-, y-, and z-axes, and describe the coordinate as the ordered triple (x, y, z).

In order to fully describe the coordinates of a point, first of all we need to specify the model coordinate at 90°, corresponding to its pattern coordinate at 180°, as illustrated by Figure 1. Only with both values will it be possible to obtain further coordinates at arbitrary angles (see Figure 2) from a specified model coordinate.

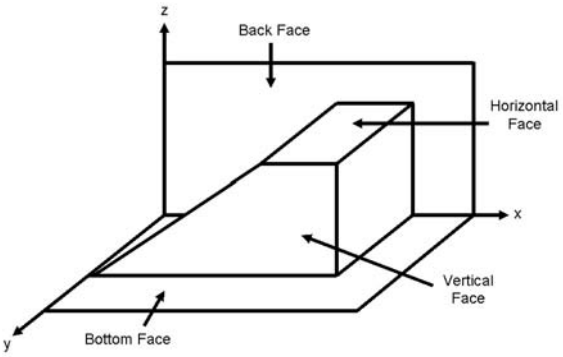

Figure 3. Different faces of OA model.

2.1 Definitions

To begin, we define the various types of faces in an OA model. These faces can be classified as one of the following: *back face*, *vertical face*, *bottom face*, and *horizontal face*, as illustrated in Figure 3. Both the vertical and back faces are perpendicular to the horizon, while the horizontal and bottom faces are parallel to the horizon.

We will compute the coordinates of points located on a vertical face and points on a horizontal face separately, as the pop-up distances may not be the same for both of them, as shown in Figure 5. We denote the distance between the back face and the vertical face as t_v, while denoting the distance between the bottom face and the horizontal face as t_h.

2.2 Assumptions

There are three assumptions made for the formulation in this paper. First, we need to reverse the sign of values for the y-axis in the 2D pattern, so that values for the y-coordinate would be negative in the first quadrant and positive in the fourth quadrant (see Figure 4).

Second, the x-, y-, and z-axes of our OA model will follow the left-hand rule for ease of recognition (compare Figure 5(a) with Figure 4). That is, the model is just the laterally inverted image of its counterpart on the same axes following the conventional right-hand rule (see Figure 5(b)).

Finally, we assume nonzero thickness of paper, that is, the pattern cannot fully close, but can *nearly* close. From 180° in a 2D plane, an OA pattern can be folded to almost 0°. Hence, angle θ ranges within $0° < \theta \leq 180°$, whereby $\theta \neq 0°$.

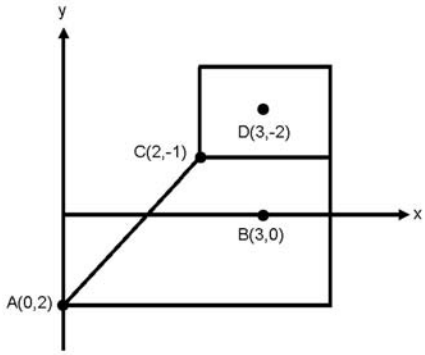

Figure 4. Coordinates of points in a 2D pattern with sign shifted in y-axis.

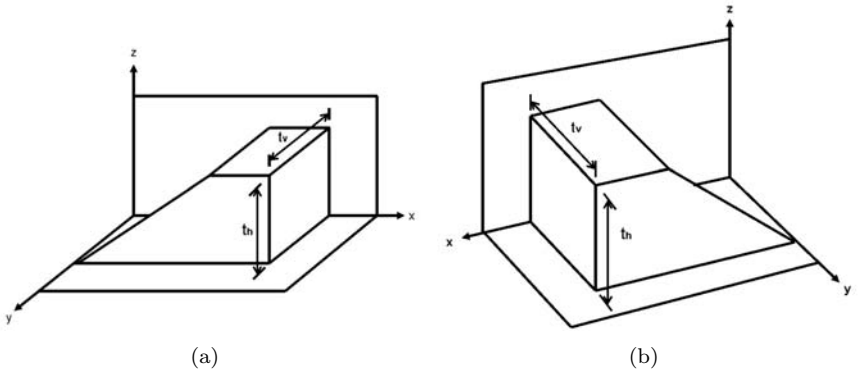

Figure 5. (a) A 3D OA model following the left-hand rule. (b) A 3D OA model following the right-hand rule.

3 Transformation of Coordinates from 2D to 3D

In this section, we proceed to examine the transformation from pattern coordinates to model coordinates.

As described in Section 2, we must first identify the coordinate of points from $\theta = 180°$ in 2D to $\theta = 90°$ in 3D. The equations for vertical and horizontal faces at $\theta = 90°$ are first calculated. Then, the equations for vertical and horizontal faces at θ other than 90° can be identified. Note that the x-coordinates remain unaltered from 2D to 3D, and vice versa at any angle.

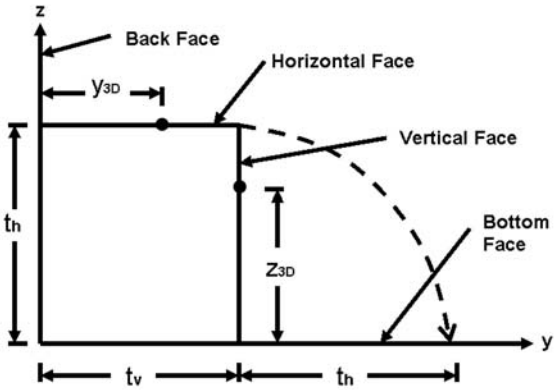

Figure 6. Relationship between y_{3D} with t_v and z_{3D} with t_h at 90°.

3.1 Single Pop-Up Layer

Any point located on a vertical face can either be found within a face or on an edge. Hence, if we represent the height of a given point as z_{3D}, then $z_{3D} \leq t_h$, whereby $z_{3D} = t_h$ if the point is located at the protruding edge (see Figure 6). Similarly, for a point located on the horizontal face, we have that $y_{3D} = t_v$. The formulas for the transformation of coordinates of points located on a vertical face and horizontal face are shown in Equations (1) and (2), respectively:

$$\begin{aligned} x_{3D} &= x_{2D}, \\ y_{3D} &= t_v, \\ z_{3D} &= t_v - y_{2D}; \end{aligned} \tag{1}$$

$$\begin{aligned} x_{3D} &= x_{2D}, \\ y_{3D} &= y_{2D} + t_h, \\ z_{3D} &= t_h. \end{aligned} \tag{2}$$

As the OA model is being folded at an angle other than 90°, we use the values of x_{3D}, y_{3D}, and z_{3D} obtained from these equations to calculate the new coordinates. For a point located on a vertical face, the coordinate will vary with the changes in angle θ, as depicted in Figure 7 (as the vertical face now becomes the hypotenuse of a triangle). The new coordinate can be calculated by Equation (3). Similarly, we can also calculate the new coordinate for a point located on a horizontal face by using Equation (4), where the changes are illustrated by Figure 8.

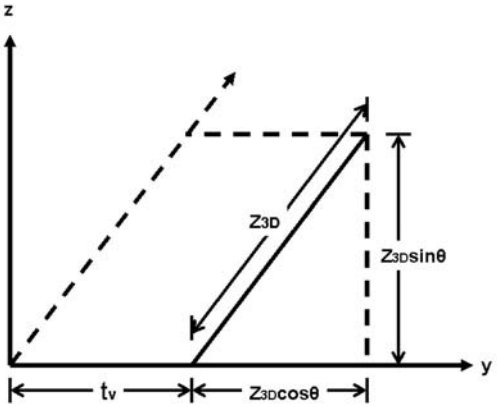

Figure 7. Side view of OA model for identifying vertical face coordinates.

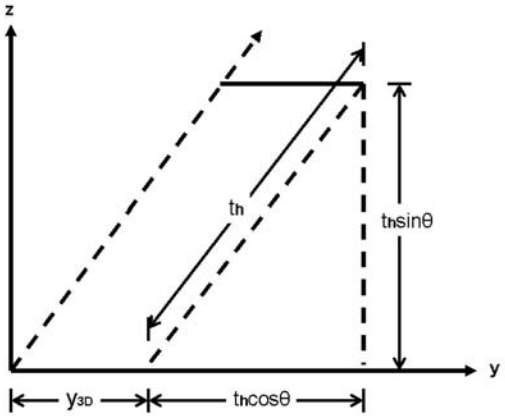

Figure 8. Side view of OA model for identifying horizontal face coordinates.

$$\begin{aligned} x &= x_{3\mathrm{D}}, \\ y &= z_{3\mathrm{D}} \cos\theta + t_v, \\ z &= z_{3\mathrm{D}} \sin\theta; \end{aligned} \tag{3}$$

$$\begin{aligned} x &= x_{3\mathrm{D}}, \\ y &= y_{3\mathrm{D}} + t_h \cos\theta, \\ z &= t_h \sin\theta. \end{aligned} \tag{4}$$

Figure 9 shows the computer-generated output of the OA model folded at various angles by using the coordinate formulas given above. The coordi-

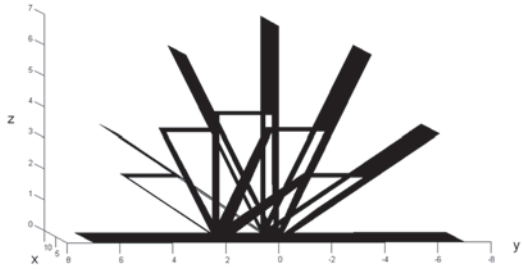

Figure 9. Side view of single pop-up layer OA model at angles 0°, 30°, 60°, 90°, 120°, 150°, and 180°.

nates for points located on the back face and bottom face can be calculated straightforwardly by using sine or cosine as required.

3.2 Double Pop-Up Layers

We now consider double pop-up layers, for which the OA model has additional distances of t_{h2} and t_{v2} for the second pop-up layers as depicted in Figure 10. For transformation of coordinates from 2D to 3D, the formula for the first layer would be the same as that given in Section 3.1, whereas for the second layer, the coordinates could be identified by using Equation (5) for a vertical face and Equation (6) for a horizontal face:

$$\begin{aligned} x_{3\mathrm{D}} &= x_{2\mathrm{D}}, \\ y_{3\mathrm{D}} &= t_{v2}, \\ z_{3\mathrm{D}} &= t_{v2} - y_{2\mathrm{D}}; \end{aligned} \tag{5}$$

$$\begin{aligned} x_{3\mathrm{D}} &= x_{2\mathrm{D}}, \\ y_{3\mathrm{D}} &= y_{2\mathrm{D}} + (t_{h1} + t_{h2}), \\ z_{3\mathrm{D}} &= t_{h1} + t_{h2}. \end{aligned} \tag{6}$$

When the OA model is being folded at angles other than 90° as shown in Figure 11, a similar trigonometric concept may be applied as explained in the previous section. The new coordinates for the second layer can be obtained from Equations (7) and (8) for the second vertical and horizontal faces, respectively:

$$\begin{aligned} x &= x_{3\mathrm{D}}, \\ y &= z_{3\mathrm{D}} \cos\theta + t_{v2}, \\ z &= z_{3\mathrm{D}} \sin\theta; \end{aligned} \tag{7}$$

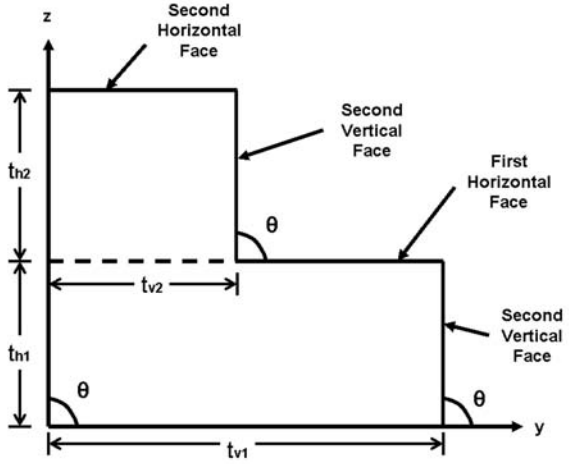

Figure 10. Double pop-up layer OA model at 90°.

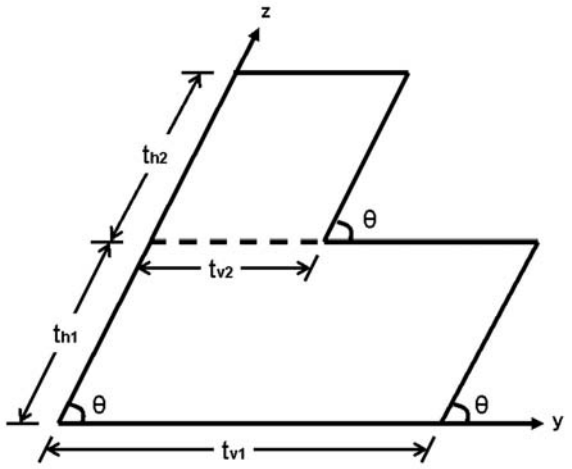

Figure 11. Double pop-up layer OA model when $\theta \neq 90°$.

$$\begin{aligned} x &= x_{3\mathrm{D}}, \\ y &= y_{3\mathrm{D}} + (t_{h1} + t_{h2}) \cos\theta, \\ z &= (t_{h1} + t_{h2}) \sin\theta. \end{aligned} \tag{8}$$

Figure 12 shows the image of a double pop-up OA model being folded and unfolded at various angles.

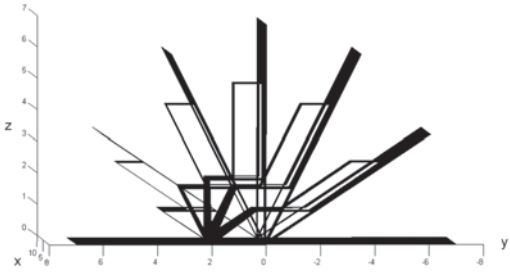

Figure 12. Side view of double pop-up layer OA model at angles 0°, 30°, 60°, 90°, 120°, 150°, and 180°.

3.3 Triple Pop-Up Layers

We continue on to examine the pattern of changes in coordinates for a third pop-up layer in this section. The coordinates for the first and second layers have been discussed in the previous two sections. With t_{v3} and t_{h3} introduced to represent the third vertical and horizontal faces, respectively, as shown in Figure 13, we can use Equations (9) and (10) to compute the coordinates of points when the OA model is folded at 90°:

$$\begin{aligned} x_{3\mathrm{D}} &= x_{2\mathrm{D}}, \\ y_{3\mathrm{D}} &= t_{v3}, \\ z_{3\mathrm{D}} &= t_{v3} - y_{2\mathrm{D}}; \end{aligned} \tag{9}$$

$$\begin{aligned} x_{3\mathrm{D}} &= x_{2\mathrm{D}}, \\ y_{3\mathrm{D}} &= y_{2\mathrm{D}} + (t_{h1} + t_{h2} + t_{h3}), \\ z_{3\mathrm{D}} &= t_{h1} + t_{h2} + t_{h3}. \end{aligned} \tag{10}$$

As for folding angles other than 90°, we may use equations (11) and (12) to locate the new coordinate of points on vertical and horizontal face respectively:

$$\begin{aligned} x &= x_{3\mathrm{D}}, \\ y &= z_{3\mathrm{D}} \cos\theta + t_{v3}, \\ z &= z_{3\mathrm{D}} \sin\theta; \end{aligned} \tag{11}$$

$$\begin{aligned} x &= x_{3\mathrm{D}}, \\ y &= y_{3\mathrm{D}} + (t_{h1} + t_{h2} + t_{h3}) \cos\theta, \\ z &= (t_{h1} + t_{h2} + t_{h3}) \sin\theta. \end{aligned} \tag{12}$$

Figure 14 shows the computer-generated output for a triple layer OA model being folded and unfolded at various angles.

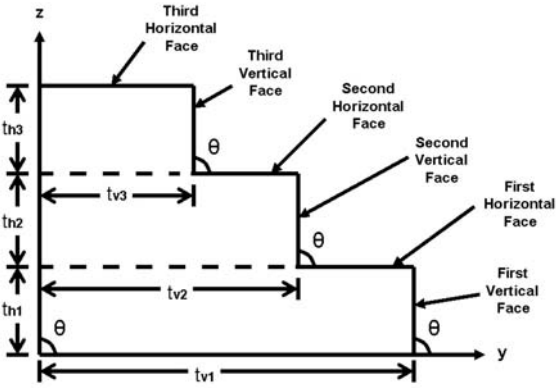

Figure 13. Triple pop-up layer OA model at 90°.

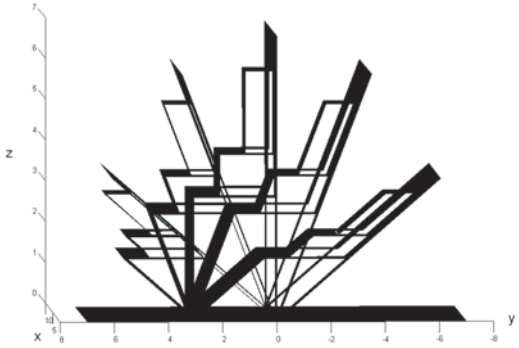

Figure 14. Side view of triple pop-up layer OA model at angles 0°, 30°, 60°, 90°, 120°, 150°, and 180°.

3.4 Generalization of Multiple Pop-Up Layers

Based on the pattern of changes in Equations (1)–(12), we can generalize for any additional layers that build up on the previous base layers and the equations for identifying the coordinates of any points on those layers can be constructed similarly. Thus, the coordinates for any point on the nth vertical face can be calculated by using Equations (13)–(16):

$$\begin{aligned} x_{3D} &= x_{2D}, \\ y_{3D} &= t_{vn}, \\ z_{3D} &= t_{vn} - y_{2D}; \end{aligned} \tag{13}$$

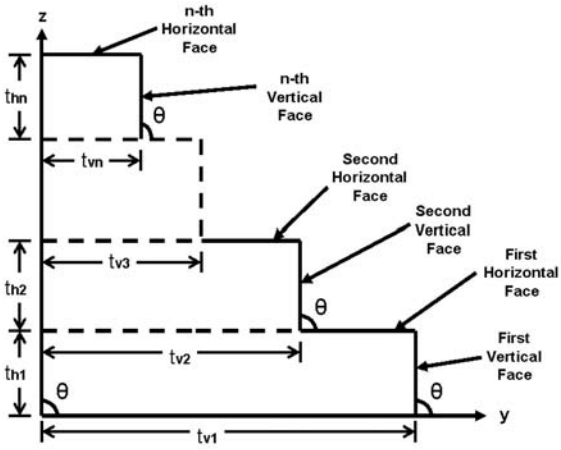

Figure 15. Multiple pop-up layer OA model at 90°.

$$\begin{aligned} x_{3\mathrm{D}} &= x_{2\mathrm{D}}, \\ y_{3\mathrm{D}} &= y_{2\mathrm{D}} + (t_{h1} + t_{h2} + \ldots + t_{hn}), \\ z_{3\mathrm{D}} &= t_{h1} + t_{h2} + \ldots + t_{hn}; \end{aligned} \tag{14}$$

$$\begin{aligned} x &= x_{3\mathrm{D}}, \\ y &= z_{3\mathrm{D}} \cos\theta + t_{vn}, \\ z &= z_{3\mathrm{D}} \sin\theta; \end{aligned} \tag{15}$$

$$\begin{aligned} x &= x_{3\mathrm{D}}, \\ y &= y_{3\mathrm{D}} + (t_{h1} + t_{h2} + \ldots + t_{hn}) \cos\theta, \\ z &= (t_{h1} + t_{h2} + \ldots + t_{hn}) \sin\theta; \end{aligned} \tag{16}$$

where $n = 1, 2, 3, \ldots$. See Figure 15.

4 Coordinates of Points on Edges or at Boundaries

For points located on edges or at boundaries, their coordinates can be computed depending on which layer and surface the points are located. For instance, by referring to Figure 16, the changes of coordinates of P_1 as the OA model is being folded and unfolded can only be calculated by using the first vertical face formulas. However, for point P_2, the coordinates can be obtained in two ways: by using the formulas for the first vertical or the first horizontal face. P_3 can be considered as a point located on the first horizontal face or the second vertical face, while P_5 can be treated as either

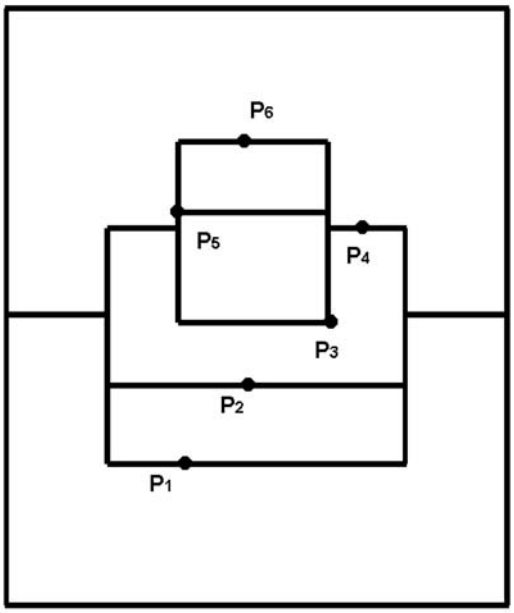

Figure 16. Points located on edges or at boundaries.

a point on the second vertical or second horizontal face. P_4, being on the boundary of the moving parts, can only be considered a point located on the first horizontal face, while P_6, also on the boundary, would be computed as a point on the second horizontal face.

5 Transformation of Coordinates from 3D to 2D

While the formulas for the transformation of coordinates of points from 2D to 3D can be complicated, the formula for the transformation of coordinates from 3D to 2D is simple. When the OA pattern is being opened flat at 180°, the z-axis will be eliminated by setting $z = 0$. We only refer to x- and y-axis to obtain the coordinates of any point as an ordered pair (x, y) by using Equation (17):

$$\begin{aligned} x_{2\mathrm{D}} &= x_{3\mathrm{D}}, \\ y_{2\mathrm{D}} &= y_{3\mathrm{D}} - z_{3\mathrm{D}}. \end{aligned} \tag{17}$$

6 Conclusion and Future Work

In this study, we developed formulas for the coordinates of points in origamic architecture using the Cartesian coordinate system. We may, however, be able to compute the conversion of coordinates of points in OA patterns and OA models by using other coordinate systems, e.g., by use of the vector.

Acknowledgment. We would like to express our highest gratitude to Dr. Lionel G. Ripley from University of Sussex, Brighton for proofreading this paper.

Bibliography

[1] M. Chatani. *Paper Magic: Pop-Up Paper Craft.* Tokyo: Ondorisha Publishers, Ltd., 1988.

[2] J. Mitani and H. Suzuki. "Computer Aided Design for Origamic Architecture Models with Polygonal Representation." In *Proceedings of the Computer Graphics International*, pp. 93–99. Washington, DC: IEEE Computer Society, 2004.

Part IV

Origami Mathematics

How Many Ways Can You Edge-Color a Cube?

Charlene Morrow

1 Introduction

My investigation of this problem began several years ago as I folded one of my favorite origami cubes designed by Tomoko Fuse [2, pp. 34–35]. This is a skeletal model made with 12 pieces of paper where the units are pleated and folded so that they interlock in triples at the vertices of the cube. (See Figure 1 for a picture of several of these cubes.) I have a favorite color scheme for this cube: using four colors, three of each color, I connect the units so that each *vertex* has three different colors and each *face* has all four colors. This construction results in obtaining at the vertices all possible combinations of four colors taken three at a time, with each combination appearing exactly twice on vertices diagonally opposite to each other and with opposite rotations of the colors. That result is so satisfying that it took a long time for me to look beyond this construction. However, one day I innocently asked, "How many different ways could I arrange my favorite set of colors (fours colors, three of each) on a cube?" That is, how many distinctly different results could be achieved—meaning that no matter how I oriented the cubes, no two of them could be made to look the same with color taken into account. This question led to some interesting investigations at the nexus of geometry, symmetry groups, and combinatorics, summarized below. It is written with an "education flavor," that is, with an orientation toward investigations that can be done by students and that

Figure 1. Edge-colored origami cubes using 12 units.

have been field tested with my own students. (An expanded version of the investigations is available.)

2 Defining the Question

Consider a cube: it has six faces, eight vertices, and twelve edges. For this exploration, we will be focusing on the edges and using an origami model that is made of twelve pieces of paper where each piece of paper forms an edge of the cube. This allows us to color each edge independently.

Our question is, given a set of 12 edges with a specific color assigned to each edge (call this the *edge set*), how many distinctly different colorings (taking rotations into account) are there? The number of possible edge sets is very large, and each edge set requires a separate analysis. Some examples of edge sets are six red edges and six black edges; three green, three blue, three red, and three aqua edges; four green, four purple, and four white edges; or seven pink and five orange edges.

Ultimately we will use the Pólya-Burnside Theorem (also referred to as Burnside's Theorem, Burnside's Lemma, or the Pólya-Burnside Counting Lemma) [7] to find a numerical answer, but in order to use the formula produced by this theorem, a number of different investigations are required.

The Pólya-Burnside Theorem produces the following formula, essential to our exploration:

$$\frac{\sum (\text{fix}[g_n])}{|G|} = \text{number of distinct colorings.}$$

where fix$[g_n]$ is the number of color symmetries for group element g_n and $|G|$ is the order of the group.

In group theory terms, this formula deals with the sorting of the colorings of the cube into orbits (mutually exclusive categories with the colorings in each category merely rotations of each other). It is not my intention here to discuss this material in depth, but there are interesting investigations beyond the scope of this paper, including study of the proof of the Pólya-Burnside Theorem.

Note that an advanced mathematical background is *not* needed in order to follow the investigations described below. The "big" question has been broken down into four smaller investigations, outlined below. Each investigation provides information that is essential in order to answer the question about the number of distinct colorings.

3 Investigations

3.1 Find the Colorings of a Cube in a Fixed Position

We want to find the number of different colorings with the cube in a fixed position (i.e., rotations not considered) using combinatorial methods. Our method involves "placing" edges on the cube, so you need to know how to calculate the number of possibilities for placing, for example, two red edges, given twelve possibilities. This expression is referred to as "12 choose 2" and is given by the expression 12!/(2!10!). More generally for a two-colored cube, where a is the number of edges of one color, the number of fixed colorings (i.e., without rotation) is "12 choose a" or

$$\frac{12!}{a!(12-a)!}.$$

This formula takes into account the duplications (permutations) that would not count as different colorings, even when the cube is not rotated. (Note that "12 choose 2" and "12 choose 10" are equal.)

The analysis becomes a bit more complicated when more than two colors are involved. Consider a cube with five red edges, four black edges, and three white edges. Here is the process for getting the number of static colorings: First consider the possibilities for placing the red edges. As described above, this would be 12!/(5!7!). We have colored five of the edges of the cube; we have seven edges open. We repeat our process with the seven open spots, placing the four black edges, which gives 7!/(4!3!). Now we are done because the remaining three open spots will be white, and there is only one way to do this. Thus we have $(12!/(5!7!)) \cdot (7!/(4!3!)) = 27,720$ fixed colorings, without rotation, for a cube with five red edges, four black

edges, and three white edges. But this is equivalent to computing the number of fixed colorings more simply as 12!/(5!4!3!). You can find the number of fixed colorings for any edge set in a similar way, expressed as

$$\frac{12!}{c_1!c_2!\cdots c_n!},$$

where c_i is the number of edges of the ith color.

In group theory terms, the number of colorings wanted here are the fixed colorings (or color symmetries) for the identity in the rotational symmetry group of the cube.

3.2 Categorize the Rotational Symmetries of the Cube

This investigation is prerequisite to finding the color symmetries of a cube with a specific edge set. The cube has 24 rotational symmetries, i.e., 24 ways that it can be rotated so that it looks exactly the same before and after rotation. What is helpful here is to think about the 24 symmetries as falling into several categories according to *type*. Consider a 90° rotational symmetry on an axis that passes through the center of two opposite faces of the cube. We then notice that there are two other axes of symmetry that are "like" this one, although they pass through two different pairs of faces. Our categorization according to type of symmetry is designed for the eventual analysis of color symmetry: the number of colorings that are determined to be "fixed" or color symmetric for a 90° rotation about one axis of symmetry as above, will be equal to the number of fixed colorings for each of the other two "like" axes. Note that we consider a 180° rotation on an axis to be of a different type than a 90° rotation on this same axis.

The task here is to understand each of the different axes of rotation and degrees of rotation around these axes that will produce a symmetry of the cube [1,6]. Finding an "undetectable motion" is an effective way to think about a rotational symmetry. That is, hold the cube in a particular orientation, clearly marked as the starting point, and find a way that the cube can be rotated on an axis so that it looks exactly the same at the end of the rotation as it did at the starting point. For this investigation it is best to use a cube that has solid faces and is all one color, since here we are not considering color in our analysis of symmetry. Table 1 has the 24 rotational symmetries of the cube categorized according to type of symmetry as discussed above.

3.3 Find the Color Symmetries of a Cube with a Specific Edge Set

If you ultimately want to know the number of distinctly different colorings you can get, taking rotations into account, you quickly realize that for any

		Edge Set = 4 Colors, 3 of Each		Edge Set = 2 Colors, 6 of Each		Edge Set = 2 Colors, 10 of One + 2 of Another	
s_n Type of Symmetry Group Element (i.e., axis of rotation)	$\lvert s_n \rvert$ # of Axes of This Type	fix[n] # of Fixed Colorings for One Axis of Type s_n	$\lvert s_n \rvert \cdot$ fix[n]	fix[n] # of Fixed Colorings for One Axis of Type s_n	$\lvert s_n \rvert \cdot$ fix[n]	fix[n] # of Fixed Colorings for One Axis of Type s_n	$\lvert s_n \rvert \cdot$ fix[n]
90° rotation about the midpoint of a face	3	0	0	0	0	0	0
180° rotation about the midpoint of a face	3	0	0	20	60	6	18
270° rotation about the midpoint of a face	3	0	0	0	0	0	0
120° rotation about a diagonal axis from corner to corner	4	24	96	6	24	0	0
240° rotation about a diagonal axis from corner to corner	4	24	96	6	24	0	0
180° rotation about an axis through midpoints of diagonally opposite edges	6	90	540	20	120	6	36
Identity	1	369,600	369,600	924	924	66	66
TOTAL	24		369,792		1152		120
What each total represents	$\lvert G \rvert$		$\Sigma(\lvert s_n \rvert \cdot \text{fix}[n])$		$\Sigma(\lvert s_n \rvert \cdot \text{fix}[n])$		$\Sigma(\lvert s_n \rvert \cdot \text{fix}[n])$

Table 1. Analysis for computation of distinct edge-colorings of a cube for three edge sets.

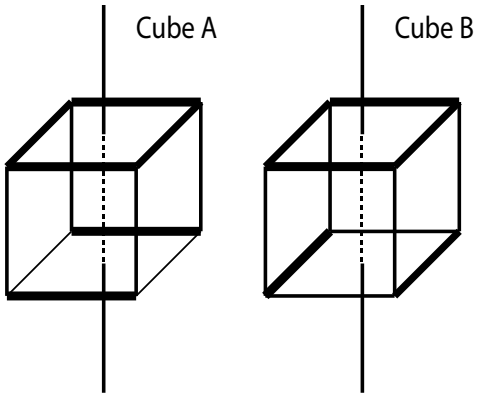

Figure 2. Example of a coloring that looks identical upon 90° rotation on the axis shown. Cubes A and B look different to us from this point of view, but if we rotate Cube A 90° on the axis shown, it will look exactly like Cube B. We really do not want to count these cubes as different. Note that neither cube has color symmetry for this rotation.

given edge set and the distinct static colorings found in Section 3.1, there will be many colorings that are identical upon rotation. That is, many colorings look different while static, but are identical when rotated, as in Figure 2.

In Section 3.1, we found the fixed colorings for the identity, one of the 24 elements in the rotational symmetry group of the cube. Now we need to find the rest of the fixed colorings. Note that this analysis is unique to each particular edge set.

One effective way to approach this task is to first notice how edges interchange within the types of symmetry group elements. For instance, when looking at either type of 180° rotation, we see that edges interchange in pairs when the rotation is performed. Thus if the edge set cannot be divided into pairs *within every color represented*, there will be no color symmetries for any 180° rotation.[1] For a second example look at an axis that goes through diagonally opposite corners with a 120° rotation. Here the edges interchange in triples, thus, if the edge set does not divide into

[1]One might wonder why we have divided the 180° rotations into two types. There is a subtle difference between them: for the axes going through the midpoints of diagonally opposite edges, only ten edges exchange in pairs. The other two edges stay fixed (i.e., do not interchange with another edge). Thus there exists an edge set that produces color symmetries, but that does not divide into pairs within colors. Consider the following edge set: ten black edges, one red edge, one green edge. For an axis of the type described above, there are six color symmetries. For the other type of 180° rotational symmetry (axes going through midpoints of opposite faces), no color symmetries will be produced by this edge set because *all* edges interchange in pairs.

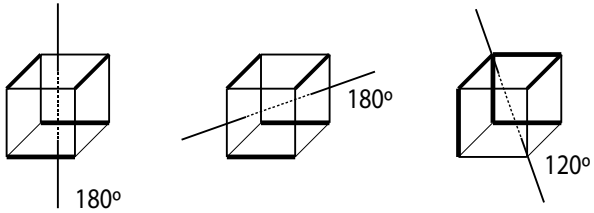

Figure 3. Examples of color symmetries. Each of these cubes will look exactly the same, including color, when rotated the specified amount on the given axis, thus each has color symmetry for the given rotation.

sets of three within each color, there will be no color symmetries for these two symmetries of the cube. Examples of color symmetry for each of three cubes are shown in Figure 3.

Once we see how subsets of edges interchange, we can effectively use a combinatorial approach to find color symmetries for each element of the rotational symmetry group acting on the cube. (See Table 1.)

This investigation is very challenging and requires the use of spatial and combinatorial reasoning [8]. Start with a very simple edge set to begin building understanding and intuition. Keep track of findings so that generalizations can be made and shortcuts can be discovered. You should especially ask how edges *interchange* for each rotational symmetry, i.e., do the edges interchange in pairs, in triples, or sets of four, and how does this help us analyze the color symmetric properties of the specific cube in hand? Record results. You will begin to see that some edge sets cannot produce any color symmetries for particular rotations. For example, if you are looking at a 90° rotation about an axis through the midpoints of two opposite faces, there will be color symmetry only for cubes that have edge sets that can be divided into sets of four within each color.

3.4 Use the Pólya-Burnside Theorem to Compute the Number of Distinctly Different Colorings

The main result of this theorem tells us that the number of distinct colorings (i.e., orbits) for a cube with a specific edge set is found by adding up the number of fixed colorings (or color symmetries) for each rotational symmetry (or group element) of the cube and dividing by the total number of rotational symmetries ($|G|$). Thus, we can deal with duplicate colorings without actually having to identify them—a very powerful result! Using the appropriate numbers, gathered in the investigations above, and the formula given at the beginning of this paper, we find the number of distinct colorings for a cube with a given edge set. Analyses of three cubes with dif-

Edge Set = 4 Colors, 3 of Each	Edge Set = 2 Colors, 6 of Each	Edge Set = 2 Colors, 10 of One + 2 of Another
$\frac{\sum (\lvert s_n \rvert \cdot \text{fix}[n])}{\lvert G \rvert} = \frac{360{,}792}{24}$ =15,408	$\frac{\sum (\lvert s_n \rvert \cdot \text{fix}[n])}{\lvert G \rvert} = \frac{1{,}152}{24} = 48$	$\frac{\sum (\lvert s_n \rvert \cdot \text{fix}[n])}{\lvert G \rvert} = 5$

Table 2. Use of the Pólya-Burnside Theorem to give the number of distinct colorings (i.e., orbits) for three edge sets.

ferent edge sets, including the resulting number of distinct colorings using the Pólya-Burnside Theorem, are given in Table 2.

4 Materials and Pedagogy

Three-dimensional models greatly facilitate these investigations. Some would even say they are essential. Since this paper was written for a conference focusing on origami, facility with origami models is assumed. For the investigations in Sections 3.1 and 3.3, you need origami cubes that are made with 12 pieces of paper, thus giving the possibility for edges to be colored independently. It is useful to begin with a simply colored cube with, for example, ten black edges and two red edges. A cube with six red edges and six black edges would make for a more challenging investigation. For the investigation in Section 3.2, it is best to use a one-color model. An origami cube (e.g., a Sonobe cube) can work well, or you can even glue together a cube made from six sturdy squares of paper or cardboard. Long wooden skewers (easily and cheaply purchased in a grocery store) serve very well as axes of rotation.

There are several origami cube models appropriate for these investigations, including the one I mainly use [2, pp. 34–35], variations of that unit [2, pp. 30–33], *Open Frame I: Bowtie Cube* and *Open Frame II: Plain Cube* [3, pp. 62–66], the PhiZZ unit[2] [4, pp. 125–138], and models presented by Simon et al. [9].[3]

Origami does require some investment in learning how to fold and assemble the models. It is a particularly good choice if you are trying to motivate students through the use of aesthetics.

For all investigations, you will gain the most if you take the time to do hands-on explorations. Discussion of approaches and preliminary results

[2] For exploring edge coloring on dodecahedron and larger polyhedra.

[3] See page 24 for an interesting pleated cube, though slightly more complicated for modeling edge coloring, and page 51 for a unit that can be used to explore vertex coloring on a dodecahedron.

followed by further exploratory work is very useful [5]. The investigations have been designed to be approachable by students with a wide variety of backgrounds. Note that for any of the investigations described, one can revert to an analogous two-dimensional analysis, with the edges of a square, for example. This will be simpler to understand and may provide a needed basis for expanding to the three-dimensional analyses described here.

5 A Question for Further Investigation

A question in which I have now become very interested is, if we wanted to build all of the differently colored cubes for a particular edge set, how could we keep track of the colorings so that we do not produce any duplicates? Although, through conversations with colleagues, I have two or three possible ideas about how to approach this problem, I have not yet solved it. I have been carrying out my explorations with the edge set of six black and six red edges because there are "only" 48 possible colorings for this edge set. This context seems hard enough to be illuminating, but still within reach for actually making cubes representing all of the possible colorings.

Bibliography

[1] Peter R. Cromwell. *Polyhedra*. Cambridge, UK: Cambridge University Press, 1999.

[2] Tomoko Fuse. *Let's Make Three-Dimensional Objects: Unit Origami*. Tokyo: Seibundo Shinko-sha, 2000.

[3] Tomoko Fuse. *Unit Origami*. New York: Japan Publications, 1990.

[4] Thomas Hull. *Project Origami*. Wellesley, MA: A K Peters, 2006.

[5] Charlene Morrow. "Using Graphs to Color Origami Polyhedra." In *Origami^3: Proceedings of the Third International Meeting of Origami Science, Mathematics, and Education*, edited by Thomas Hull, pp. 269–282. Natick, MA: A K Peters, 2002.

[6] Phillip Schultz. "Part 3: Symmetries of the Cube," *Groups and Symmetry*. Available at http://www.maths.uwa.edu.au/~schultz/3P5.2000/3P5.2,3SquareCube.html, 2000.

[7] Phillip Schultz. "Part 12: Actions Count!" *Groups and Symmetry*. Available at http://www.maths.uwa.edu.au/~schultz/3P5.2000/3P5.12Actions.html, 2000.

[8] Marjorie Senechal. "Coloring Symmetric Objects Symmetrically." *Mathematics Magazine* 56:1 (1983), 3–16.

[9] Lewis Simon, Bennett Arnstein, and Rona Gurkewitz. *Modular Origami Polyhedra.* Mineola, NY: Dover Publications, 1999.

Configuration Spaces for Flat Vertex Folds

Thomas C. Hull

1 Introduction

Flat vertex folds are crease patterns with a single vertex that lie in the plane when collapsed. Two well-known results about flat vertex folds are the Kawasaki-Justin Theorem, which states that a vertex will fold flat if and only if the sum of every other angle between the creases equals π, and the Maekawa-Justin Theorem, which states that the difference between the number of mountain and valley creases must always be two at a flat vertex fold. (See [3], [4], and [1] for details and other results.)

In this paper, we focus on more combinatorial issues. Given a single-vertex crease pattern v with specified crease angles but no mountain-valley (MV) assignment, we may count the number of possible valid (physically realizable) MV assignments. This total, denoted $C(v)$, can be determined in linear time [1,2]. If we know only the number of creases, say $2n$, but not the crease angles, we can still obtain sharp bounds on $C(v)$:

$$2^n \leq C(v) \leq 2\binom{2n}{n-1}. \tag{1}$$

We know that $C(v)$ is always even, as the MV parity of the creases can always be flipped. But can $C(v)$ achieve all even values between the bounds in Equation (1)? The answer turns out to be "no," which immediately

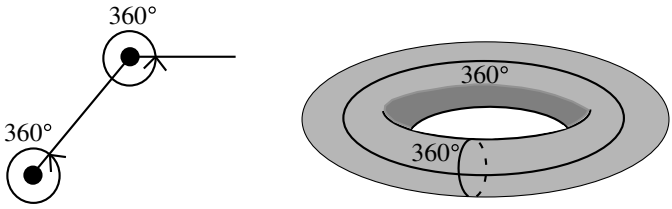

Figure 1. The configuration space for a two-joint robot arm is a torus.

makes us wonder whether we could predict or classify the various values of $C(v)$.

We will approach this question by describing a *configuration space* for flat vertex folds. A configuration space is, typically, a geometric object that is used to visualize the range of possibilities for a physical or mathematical situation. This is done by quantifying the essential variables of the situation and letting these be parameters along different coordinate axes; the combination of these forms the configuration space. One classic example is studying the range of movement for a robot arm with two joints, as illustrated in Figure 1. If each joint has a planar 360° range of rotation, then each joint can be a variable ranging from 0 to 2π, and thus the configuration space is the square $[0, 2\pi] \times [0, 2\pi]$. However, the points 0 and 2π should be identified for each variable, which makes the square "wrap around" and form a torus. Each point on the surface of this torus represents a specific configuration of the robot arm.

Our goal in this paper is to describe the configuration space for a flat vertex fold of degree $2n$.

2 The Degree-4 Case

We begin by examining the $n = 2$ case in which our flat vertex fold has four crease lines. Let $\alpha_1, ..., \alpha_4$ be the angles, in order, between the creases of our vertex v. The Kawasaki-Justin Theorem tells us that $\alpha_3 = \pi - \alpha_1$ and $\alpha_4 = \pi - \alpha_2$. All four angles are determined by α_1 and α_2, so α_1 and α_2 can be the parameters of our configuration space.

Assign α_1 to our first coordinate and α_2 to our second coordinate. Notice that the range for these parameters is $0 < \alpha_1, \alpha_2 < \pi$, since if either were zero, we wouldn't have four creases, and if either were π then one of α_3, α_4 would be zero. Furthermore, if we pick any α_1 and α_2 between 0 and π, we can let $\alpha_3 = \pi - \alpha_1$ and $\alpha_4 = \pi - \alpha_2$ to obtain angles for a degree four flat vertex fold, showing that (α_1, α_2) must be in our configuration space. Therefore the configuration space for degree four flat vertex folds,

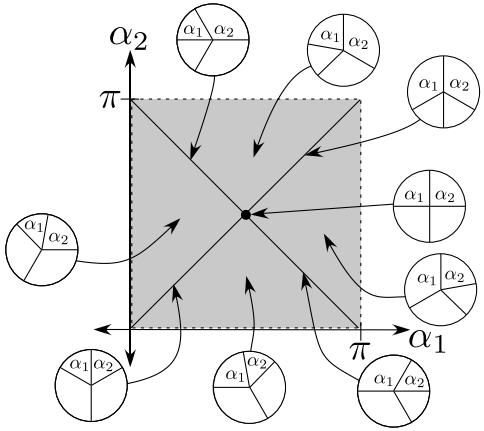

Figure 2. Decomposing P_4 into $C(v)$ subsets.

which we'll denote P_4, is the open square (see Figure 2)

$$P_4 = (0, \pi) \times (0, \pi).$$

Now, within P_4 there exist subsets for the different values of $C(v)$. The maximal $C(v)$ is 8, which corresponds to all the angles being equal. This is the point $(\pi/2, \pi/2)$ in P_4.

Next is $C(v) = 6$, and this occurs when two adjacent angles are equal and different from the other pair. For example, we could have $\alpha_1 = \alpha_2$ (which implies that $\alpha_3 = \alpha_4$). This corresponds to the line $y = x$ in P_4, for $0 < x < \pi/2$ and $\pi/2 < x < \pi$. Or we could have $\alpha_2 = \alpha_3$, which implies that $\alpha_2 = \pi - \alpha_1$ (which forces $\alpha_1 = \alpha_4$) and gives us the line $y = \pi - x$ in P_4 for $0 < x < \pi/2$ and $\pi/2 < x < \pi$.

The remaining regions of P_4 are open right triangles, and these correspond to $C(v) = 4$ cases. For example, the region bounded by the y-axis, $y = x$ and $y = \pi - x$ has $\alpha_1 < \alpha_2$, $\alpha_1 < \pi/2$, and $\alpha_2 < \pi - \alpha_1$. Kawasaki-Justin then gives us that $\alpha_3 > \pi/2$ and $\alpha_1 < \alpha_4$. In other words, α_1 is the unique smallest angle. Therefore, the creases surrounding α_1 must have different MV parity. (If they were the same, then in the folded model we would have two large angles covering a smaller angle on the same side of the paper, forcing a self-intersection.) Thus there are two ways to assign Ms and Vs to those creases, and then the others must either both be M or both be V to satisfy the Maekawa-Justin Theorem, yielding $C(v) = 4$. The analysis is similar for the other three triangular regions.

This decomposition of P_4 into subsets gives us complete classifications of all the possibilities for $C(v)$. This is summarized in Figure 2.

3 Higher Dimensions

The configuration spaces P_{2n} quickly become very difficult to visualize for $n > 2$, as they are bounded, open sets in $\mathbb{R}^{2n-2}$.

Example 1. Consider $n = 3$. Letting $\alpha_1, ..., \alpha_6$ be the angles, we can express α_5 and α_6 in terms of the other angles (using Kawasaki-Justin), and thus we may parameterize P_6 by the angles $\alpha_1, ..., \alpha_4$. That is, $P_6 \subset \mathbb{R}^4$. Our reasoning from the $n = 2$ case as well as the Kawasaki-Justin conditions $\alpha_1 + \alpha_3 + \alpha_5 = \alpha_2 + \alpha_4 + \alpha_6 = \pi$ give us the following restrictions on the angles:

$$0 < \alpha_i < \pi \text{ for all } i,\ 0 < \alpha_1 + \alpha_3 < \pi, \text{ and } 0 < \alpha_2 + \alpha_4 < \pi. \quad (2)$$

This means that the two-dimensional cross section of P_6 along the $\alpha_1\alpha_2$-coordinate plane will be an open square, as in the $n = 2$ case. However, the two-dimensional cross section along the $\alpha_1\alpha_3$-plane will be an open triangle bounded by $\alpha_1 > 0$, $\alpha_3 > 0$, and $\alpha_3 < \pi - \alpha_1$. See Figure 3.

In fact, any point $(\alpha_1, \alpha_2, \alpha_3, \alpha_4)$ satisfying Equation (2) will be part of a viable degree-6 flat vertex fold (along with the proper angles α_5 and α_6 given by Kawasaki-Justin) and thus be in P_6. That is, P_6 is an open set. The closure of this set, $\overline{P_6}$, will have as extreme points (vertices) all angle configurations that give equality for Equation (2) and that are the most degenerate, where one of the angles α_1, α_3, α_5 equals π, one of the angles α_2, α_4, α_6 equals π, and the rest are zero. Thus $\overline{P_6}$ is the polytope formed by the convex hull of the points

$$(0,0,0,0), (\pi,0,0,0), (0,\pi,0,0), (0,0,\pi,0), (0,0,0,\pi),$$

$$(\pi,\pi,0,0), (\pi,0,0,\pi), (0,\pi,\pi,0), (0,0,\pi,\pi).$$

(This can also be seen by viewing the inequalities in Equation (2) as defining the supporting hyperplanes for the polytope $\overline{P_6}$.)

The bounds from Equation (1) give us that $8 \leq C(v) \leq 30$. Examining all the possible cases for six angles around a vertex (which is doable, if somewhat arduous) and using the recursive equations in [2] shows that we have

$$C(v) \in \{8, 12, 16, 18, 20, 24, 30\}.$$

Thus we see that $C(v)$ does not take on all possible values between the bounds in Equation (1). Nonetheless, each of these values should correspond to a subset of P_6.

Rather than focusing on small cases, let us say what we can about the arbitrary-dimension case and then return to P_6.

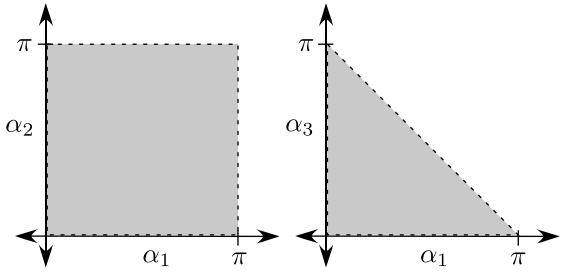

Figure 3. $\alpha_1\alpha_2$-plane and $\alpha_1\alpha_3$-plane slices of P_6.

Let P_{2n} be the configuration space for flat vertex folds of degree $2n$. If our angles are, in order $\alpha_1, ..., \alpha_{2n}$, we know by Kawasaki-Justin that the space can be parameterized by $\alpha_1, ..., \alpha_{2n-2}$. In other words, $P_{2n} \subset \mathbb{R}^{2n-2}$.

We say that a point $x = (\alpha_1, ..., \alpha_{2n-2}) \in \mathbb{R}^{2n-2}$, where $\alpha_i \geq 0$, *corresponds to a set of angles* if there exists $\alpha_{2n-1}, \alpha_{2n} \geq 0$ such that $(\alpha_1, ..., \alpha_{2n})$ satisfy the Kawasaki-Justin conditions. (That is, if $\alpha_{2n-1} = \pi - (\alpha_1 + \alpha_3 + \cdots + \alpha_{2n-3})$ and $\alpha_{2n} = \pi - (\alpha_2 + \alpha_4 + \cdots + \alpha_{2n-2})$.) Note that this corresponding set of angles might not be a degree-$2n$ flat vertex fold, since the definition allows some of the angles to be zero or π.

Theorem 1. *P_{2n} is an open set. Furthermore, if $x \in \overline{P_{2n}} - P_{2n}$ (the boundary of P_{2n}), then x corresponds to a degenerate set of angles where at least one of the angles α_i equals 0 or π.*

Proof: The fact that all angles in a degree-$2n$ flat vertex fold must be nonzero and less than π, together with the Kawasaki-Justin conditions, give us that every point in P_{2n} must satisfy the inequalities

$$0 < \alpha_i < \pi \text{ for all } i,\ 0 < \alpha_1 + \alpha_3 + \cdots + \alpha_{2n-3} < \pi,$$
$$\text{and } 0 < \alpha_2 + \alpha_4 + \cdots + \alpha_{2n-2} < \pi. \tag{3}$$

Furthermore, any point satisfying these equations must be in P_{2n}, which proves that P_{2n} is open. Any point x on the boundary of P_{2n} must also satisfy Equation (3) but have at least one of the inequalities being an equality. Thus x corresponds to a set of angles $\alpha_1, ..., \alpha_{2n}$ where either at least one of the α_i is 0 or π for some $1 \leq i \leq 2n-2$ (in which case, we're done) or $\alpha_1 + \alpha_3 + \cdots + \alpha_{2n-3}$ equals 0 or π or $\alpha_2 + \alpha_4 + \cdots + \alpha_{2n-2}$ equals 0 or π. These latter two cases imply that either α_{2n-1} or α_{2n} equals 0 or π. Thus every case results in x corresponding to a set of angles where at least one of the α_i equals 0 or π. □

We can use Theorem 1 to examine more carefully the faces of $\overline{P_{2n}}$. The vertices of $\overline{P_{2n}}$, for example, will correspond to the most extreme degenerate

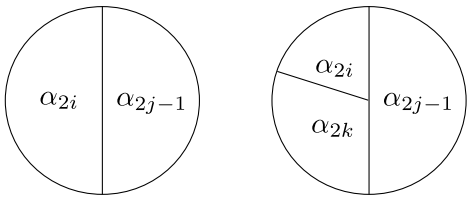

Figure 4. Degenerate angle configurations for a vertex (left) and an edge (right) of $\overline{P_{2n}}$.

degree-$2n$ flat vertex folds, where two angles are equal to π and the rest are equal to zero. In order for such a case to satisfy Kawasaki-Justin one of the π angles must be an even-indexed angle and the other an odd-indexed angle. This is illustrated in the left side of Figure 4.

Thus we have that $\overline{P_{2n}}$ has n^2 vertices whose coordinates are $(\alpha_1, \ldots, \alpha_{2n-2})$ where at most one of the $\alpha_{2i} = \pi$, at most one of the $\alpha_{2i+1} = \pi$, and the remaining $\alpha_i = 0$. (If all the $\alpha_i = 0$ then we have $\alpha_{2n-1} = \alpha_{2n} = \pi$ in the corresponding set of angles.)

An edge (1-face) of $\overline{P_{2n}}$ will be a line segment of points $E(u, v) = \{\lambda u + (1 - \lambda)v : 0 \leq \lambda \leq 1\}$ connecting two vertices u and v where the points of $E(u, v)$, aside from the endpoints, correspond to slightly-less-extreme degenerate degree-$2n$ flat vertex folds than those of the vertices. That is, instead of having an even-indexed angle and an odd-indexed angle equaling π as we did for the vertices, each point in the relative interior of $E(u, v)$ will correspond to a set of angles with either one even-indexed angle equaling π and two odd-indexed angles adding to π, or vice versa (one odd-indexed angle is π and two even-indexed angles sum to π). All the other angles would have to be zero; see the right side of Figure 4. Thus, if the nonzero corresponding set of angles for the vertex u are at coordinate positions $2i$ and $2j - 1$ and those for v are at coordinate positions $2s$ and $2t - 1$, then either $i = s$ or $j = t$ must be true in order for $E(u, v)$ to be an edge of $\overline{P_{2n}}$. That is, u and v must have a π in a common coordinate so that their other π coordinates can switch places as we travel along the edge $E(u, v)$.

The number of edges of $\overline{P_{2n}}$ will therefore be $\binom{n}{1}\binom{n}{2} + \binom{n}{2}\binom{n}{1}$, because in the corresponding set of angles $(\alpha_1, ..., \alpha_{2n})$ we could choose one of the n even-indexed angles to be π, two of the n odd-indexed angles to sum to π, and the rest to be 0, or we could pick two even-indexed angles to sum to π, one of the odd-indexed angles to be π, and the rest to be 0.

The 2-faces of $\overline{P_{2n}}$ follow similarly. In the corresponding set of angles for any point of a 2-face we could have one even-indexed angle $\alpha_{2i} = \pi$ (and the rest = 0) and three odd-indexed angles $\alpha_{2j-1}, \alpha_{2k-1}$, and α_{2l-1}

being nonzero but adding up to π (and the rest equal 0). This gives us two parameters (say α_{2j-1} and α_{2k-1}, which then determine α_{2l-1}) and thus will span a 2-face. Or we could have chosen two even-indexed angles and two odd, or three even-indexed angles and one odd. Thus, there are $\binom{n}{1}\binom{n}{3} + \binom{n}{2}\binom{n}{2} + \binom{n}{3}\binom{n}{1}$ 2-faces total.

Thus we obtain the following:

Theorem 2. *The number of k-cells in $\overline{P_{2n}}$ is*

$$f_k = \sum_{i=0}^{k} \binom{n}{i+1}\binom{n}{k-i+1} = \binom{2n}{k+2} - 2\binom{n}{k+2}.$$

Proof: The previous arguments illustrate how we obtain the summation, and the summation identity can be obtained via standard combinatorial methods such as generating functions. We also offer a different combinatorial reasoning: to count f_k we want to pick $k+2$ angles from the $2n$ corresponding angles to be nonzero in order to create our degenerate flat vertex fold. But we don't want all of the angles to be even-indexed or all odd-indexed, so we subtract the $2\binom{n}{k+2}$ ways in which this can happen. The result is all the ways to have all angles zero except for $k+2$ of them, where some are even-indexed and some odd-indexed. The even-indexed angles must sum to π, and so must the odd-indexed angles. This means that to parameterize these degenerate cases we don't need all of the $k+2$ angles; we can eliminate one of the even-indexed angles and one of the odd-indexed angles, leaving us with k parameter coordinates for this face, thus creating a k-face. □

The arguments given for Theorem 2 provide everything needed to calculate the coordinates for the vertices, edges, etc. of $\overline{P_{2n}}$, which can then be generated using Mathematica or other visualization software.

Figure 5 shows a projection of $\overline{P_6}$. We can try to compare our general calculations with the intuition developed earlier for the degree six flat vertex fold case. For example, the right side of Figure 3 shows how slicing P_6 along the $\alpha_1\alpha_3$-plane gives a right triangle. To make such a slice a 2-face of $\overline{P_6}$, we would need the other angles (the even-indexed ones) to be extreme, either 0 or π, while still obeying Kawasaki-Justin. So we could have

$$\begin{aligned}
&(\alpha_1, 0, \alpha_3, 0) \quad \text{where } 0 \le \alpha_1 + \alpha_3 \le \pi \text{ and } \alpha_6 = \pi,\\
&(\alpha_1, \pi, \alpha_3, 0) \quad \text{where } 0 \le \alpha_1 + \alpha_3 \le \pi \text{ and } \alpha_6 = 0,\\
&(\alpha_1, 0, \alpha_3, \pi) \quad \text{where } 0 \le \alpha_1 + \alpha_3 \le \pi \text{ and } \alpha_6 = 0.
\end{aligned}$$

The same reasoning applies to slices along the $\alpha_2\alpha_4$-plane, giving $\overline{P_6}$ six faces that will be 45° right triangles. Careful examination of Figure 5 reveals these faces.

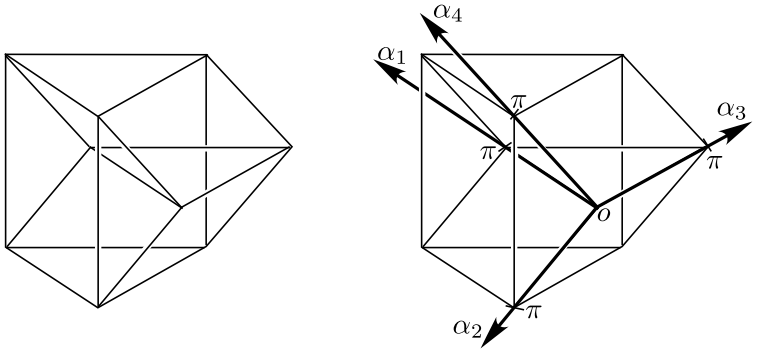

Figure 5. A projection of the four-dimensional polytope $\overline{P_6}$.

In fact, going back to the general case, we can be more specific about the structure of $\overline{P_{2n}}$. Let $e_i \in \mathbb{R}^{2n-2}$ be the point with 0 for every coordinate except the ith, which is π. Let o denote the origin. We denote the convex hull of a finite set of points x_i by $\text{conv}(x_1, ...x_n) = \{\lambda_1 x_1 + \cdots + \lambda_n x_n : \lambda_i \geq 0, \sum_{i=1}^{n} \lambda_i = 1\}$. Define

$$EP_{2n} = \text{conv}(o, e_2, e_4, ..., e_{2n-2}) \text{ and } OP_{2n} = \text{conv}(o, e_1, e_3, ..., e_{2n-3}).$$

Then EP_{2n} and OP_{2n} are both $(n-1)$-simplices in $\mathbb{R}^{2n-2}$.

Lemma 1. *$x \in EP_{2n}$ (resp. OP_{2n}) if and only if $x = \lambda_1 e_2 + \lambda_2 e_4 + \cdots + \lambda_{n-1} e_{2n-2}$ (resp. $x = \lambda_1 e_1 + \lambda_2 e_3 + \cdots + \lambda_{n-1} e_{2n-3}$) where $\lambda_i \geq 0$ and $\sum_{i=1}^{n-1} \lambda_i \leq 1$.*

Proof: If $x \in EP_{2n}$ or OP_{2n} then certainly x can be written as described in the lemma, since $\lambda_0 o$ is just the zero vector. For the other direction, if we write $x = \lambda_0 o + \lambda_1 e_2 + \cdots + \lambda_{n-1} e_{2n-2}$ where $\lambda_0 = 1 - \sum_{i=1}^{n-1} \lambda_i$ then we have that $x \in EP_{2n}$. The same argument with the points e_{2i} switched to e_{2i-1} handles the OP_{2n} case. □

Recall that if A and B are sets of points then their *Minkowski sum* is $A + B = \{x + y : x \in A, y \in B\}$.

Theorem 3. *$\overline{P_{2n}} = OP_{2n} + EP_{2n}$.*

Proof: Note that $x = (\alpha_1, ..., \alpha_{2n-2}) \in \overline{P_{2n}}$ if and only if

$$\begin{aligned} x &= \frac{\alpha_1}{\pi} e_1 + \frac{\alpha_2}{\pi} e_2 + \cdots + \frac{\alpha_{2n-2}}{\pi} e_{2n-2} \\ &= \left(\frac{\alpha_1}{\pi} e_1 + \frac{\alpha_3}{\pi} e_3 + \cdots + \frac{\alpha_{2n-3}}{\pi} e_{2n-3}\right) \\ &+ \left(\frac{\alpha_2}{\pi} e_2 + \frac{\alpha_4}{\pi} e_4 + \cdots + \frac{\alpha_{2n-2}}{\pi} e_{2n-2}\right), \end{aligned}$$

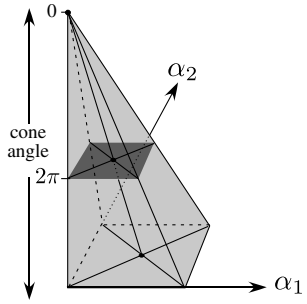

Figure 6. P_4 extended to include the cone angle.

where $0 \leq \alpha_i \leq \pi$ for all i and the coordinates of x correspond to a set of angles that satisfy the Kawasaki-Justin Theorem. These conditions on x are satisfied if and only if $0 \leq \alpha_i/\pi \leq 1$, $\sum_{i=1}^{n-1} \alpha_{2i-1} \leq \pi$ and $\sum_{i=1}^{n-1} \alpha_{2i} \leq \pi$, i.e.,

$$\frac{\alpha_1}{\pi} + \frac{\alpha_3}{\pi} + \cdots \frac{\alpha_{2n-3}}{\pi} \leq \frac{\pi}{\pi} = 1 \text{ and } \frac{\alpha_2}{\pi} + \frac{\alpha_4}{\pi} + \cdots \frac{\alpha_{2n-2}}{\pi} \leq \frac{\pi}{\pi} = 1.$$

Thus by Lemma 1 we have that $x \in \overline{P_{2n}}$ if and only if $x \in OP_{2n} + EP_{2n}$.□

In other words, $\overline{P_{2n}}$ is the sum of two $(n-1)$-simplices.

4 Generalizations and Future Work

Flat vertex folds do not need to be restricted to geometrically flat paper. If we place the vertex of our fold at the tip of a cone-shaped piece of paper, then we can consider folding it up. As described in [1] and [2], the Kawasaki-Justin and Maekawa-Justin Theorems still hold (with some modifications) for folding cones. For example, instead of $0 < \alpha_i < \pi$ for each angle, we have, if ρ is the cone angle of the cone, that $0 < \alpha_i < \rho/2$. Also, the Kawasaki-Justin conditions become: the sum of every other angle around the vertex $= \rho/2$.

Therefore we could extend the configuration space P_{2n} by adding an axis to parameterize the cone angle of the paper. Because changing the cone angle restricts the angles α_i, this effectively turns our configuration space into an infinite cone. The case $n = 2$ is illustrated in Figure 6.

There is one caveat to this cone angle generalization: if the cone angle is $> 2\pi$ then a different kind of flat folding can be done, one where the vertex is neither convex nor concave but flat, with the excess paper layered radially around it. The configuration space described here does not include such cases.

Additional work needs to be done to see whether or not our descriptions of the spaces P_{2n} can determine what values $C(v)$ can attain and the subsets to which they correspond.

Acknowledgment. The author would like to thank sarah-marie belcastro and Günter Rote for valuable comments and corrections.

Bibliography

[1] T. Hull. "The Combinatorics of Flat Folds: A Survey." In *Origami^3: Proceedings of the Third International Meeting of Origami Science, Mathematics, and Education*, edited by Thomas Hull, pp. 29–38. Natick, MA: A K Peters, 2002.

[2] T. Hull. "Counting Mountain-Valley Assignments for Flat Folds." *Ars Combinatoria* 67 (2003), 175–188.

[3] J. Justin. "Mathematics of Origami, Part 9." *British Origami* 118 (June 1986), 28–30.

[4] T. Kawasaki. "On the Relation between Mountain-Creases and Valley-Creases of a Flat Origami" (in Japanese). *Sasebo College of Technology Reports* 27 (1990), 55–80.

One-, Two-, and Multi-Fold Origami Axioms

Roger C. Alperin and Robert J. Lang

1 Introduction

In 1989 [17], Huzita introduced the six origami operations that have now become know as the *Huzita Axioms* (HAs). The HAs, shown in Figure 1, constitute six distinct ways of defining a single fold by bringing together combinations of preexisting points (e.g., crease intersections) and preexisting lines (creases and/or the fold line itself).

It has been shown that all of the standard compass-and-straightedge constructions of Euclidean geometry can be constructed using the original six axioms. In fact, working independently, Martin [25, pp. 145–159] showed that the operation equivalent to Huzita's O6 (plus the definition of a point as a crease intersection) was, by itself, sufficient for the construction of all figures constructible by the full six axioms and that this included all compass-and-straightedge constructions. Conversely, Auckly and Cleveland [5, 15], unaware of O5 and O6, showed that without O5 and O6 the field of numbers constructible by the other four HAs was smaller than the field of numbers constructible by compass and straightedge. An analysis of the hierarchy of fields that can be constructed using different axioms systems has been detailed [2, 4].

We note that since the other five of the six HAs can be constructed using only O6, the derived operations should perhaps be called something other than axioms. However, we will bow to 20 years of established usage and continue to call them axioms.

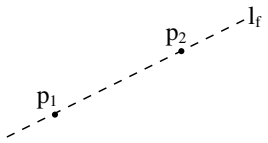

(O1) Given two points p_1 and p_2, we can fold a line connecting them.

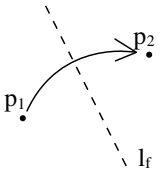

(O2) Given two points p_1 and p_2, we can fold p_1 onto p_2.

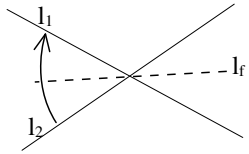

(O3) Given two lines l_1 and l_2, we can fold line l_1 onto l_2.

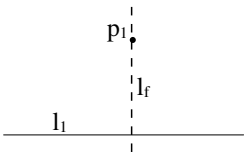

(O4) Given a point p_1 and a line l_1, we can make a fold perpendicular to l_1 passing through the point p_1.

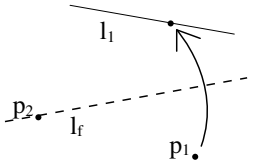

(O5) Given two points p_1 and p_2 and a line l_1, we can make a fold that places p_1 onto l_1 and passes through the point p_2.

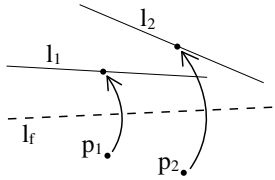

(O6) Given two points p_1 and p_2 and two lines l_1 and l_2, we can make a fold that places p_1 onto line l_1 and places p_2 onto line l_2.

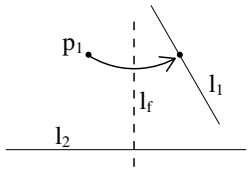

(O7) Given a point p_1 and two lines l_1 and l_2, we can make a fold perpendicular to l_2 that places p_1 onto line l_1.

Figure 1. O1–O6 are the six Huzita Axioms. O7 is Justin's (Hatori's) seventh axiom.

In the same proceedings that Huzita's original listing appeared, Justin [22] presented a list of *seven* distinct operations—which Justin credited, in part, to Peter Messer—including one that had been overlooked by Huzita. (A shorter list of five operations was also presented by Huzita and Scimemi [20].) Justin's longer listing has been somewhat overlooked, but in 2001,

Hatori [14] rediscovered Justin's seventh operation, also shown in Figure 1. While similar to the six HAs, it was not equivalent to any one of them. However, it did not expand the field of origami-constructible numbers beyond the field of the original six HAs. The set of all seven operations might be called the *Huzita-Justin Axioms* (HJAs). Hatori's rediscovery raised an interesting question implied by Justin's original list: are the seven axioms complete, or are there other undiscovered single-fold axioms to be found?

Over the years, various workers have shown many elegant constructions possible with the HJAs, including constructions not possible with compass-and-straightedge such as angle trisection [1, 8, 19, 21], cube doubling [26], and various regular polygons [10–13]. However, there remain constructions that are not possible with the HJAs, such as angle quintisection, the regular 11-gon (the smallest regular polygon not possible with the HJAs), or solution of the general quintic equation.

One of us [23] recently demonstrated an angle quintisection obtained by folding alone. However, this construction lies outside of the field of HJA constructions in that at one step it requires making two simultaneous creases, while all of the HJAs involve making only a single crease. As a consequence of well-known results from field theory [27, p. 170; 9, p. 450], this leads to a construction of a regular polygon with 11 sides. More generally, *any* n-sided regular polygon with value $\varphi(n)$ of Euler's totient function divisible by only 2, 3, or 5 can be constructed using folding operations involving the HJA constructions or the multiple crease quintisection.

This raises the question: if we consider making two, three, or more simultaneous creases, what types of construction are possible? The angle quintisection demonstrates that at least one irreducible quintic equation can be solved by two-fold operations; what higher orders are possible?

In this work, we investigate both one- and two-fold operations. We first show that all of the HJAs can be described as a combination of one or two more fundamental conditions, which we call *alignments*. We identify all possible alignments, and then, by exhaustive enumeration, show that the seven HJAs include all possible combinations of such alignments. In a previous work, one of us [24] noted that the completeness of the HJAs could be shown, and private copies of the proof have been circulated; Hull [16] recently presented a summary of the proof. However, this is, to our knowledge, the first public detailed presentation.

We then turn our attention to two-fold alignments and axioms. We identify a unique set of 17 alignments that may be combined to define two simultaneous creases. We then show how an exhaustive (computer-aided) enumeration of all possible alignment combinations leads to 489 distinct operations analogous to the seven HJAs, but that define two simultaneous creases. We show that the previously demonstrated angle quintisection utilizes one of these two-fold "axioms." We close by showing that three

simultaneous folds leads to a solution of the general quintic equation and that, in general, $n-2$ simultaneous folds are sufficient to solve the general nth-degree equation.

2 Origami Axioms

In Huzita's original work [17], the HAs were given as literal axioms. In order to prove completeness, we must describe them in terms of more fundamental concepts.

Definition 1 (Point). A *point* (x, y) is the ordered pair where x and y are the Cartesian coordinates of the point.

Observe that a point has two degrees of freedom (DOF), i.e., it is defined by two numbers—namely, its coordinates.

A line can be described in many ways: slope and intercept, angle and distance from the origin, etc. The following representation offers algebraic simplicity.

Definition 2 (Line). A *line* (X, Y) is the set of points (x, y) that satisfy the equation $Xx + Yy + 1 = 0$.

This definition has the desirable property that every describable line has a unique representation. However, lines passing through the origin cannot be so described. We can deal with this problem in practice by translating any system of points and lines so that no line passes through the origin.

Since both points and lines are represented by ordered pairs, we will adopt the convention that point coordinates are identified with lower-case letters and line coordinates with upper-case letters.

We can now define the *folded image* of a point or line to be the reflection of the point or line through the fold line. A little algebra gives the following.

Definition 3 (Folded Point). The *folded image* $F_{L_F}(P)$ of a point $P = (x, y)$ in a fold line $L_F = (X_F, Y_F)$ is the reflection of the point in the fold line.

In our representation, the folded image of a point is given by

$$F_{L_F}(P) = \left(\frac{x(Y_F^2 - X_F^2) - 2X_F(1 + yY_F)}{X_F^2 + Y_F^2}, \frac{y(X_F^2 - Y_F^2) - 2Y_F(1 + xX_F)}{X_F^2 + Y_F^2} \right). \tag{1}$$

Definition 4 (Folded Line). The *folded image* $F_{L_F}(L)$ of a line $L = (X, Y)$ in a fold line $L_F = (X_F, Y_F)$ is the reflection of the line in the fold line.

In our representation, the folded image of a line is given by

$$F_{L_F}(L) = \left(\frac{x(X_F^2 - Y_F^2) + 2X_F Y Y_F}{X_F^2 - 2XX_F - 2YY_F + Y_F^2}, \frac{y(X_F^2 - Y_F^2) - 2XX_F Y_F}{X_F^2 - 2XX_F - 2YY_F + Y_F^2} \right). \tag{2}$$

Note that for both points and lines, folding, being the reflection operator, is its own inverse. For any point $P = (x, y)$, line $L = (X, Y)$, and fold line $L_F = (X_F, Y_F)$, it is easily verified that $F_{L_F}(F_{L_F}(P)) = P$ and $F_{L_F}(F_{L_F}(L)) = L$. Thus, for any pair of points or lines A and B, $F_{L_F}(A) = B \iff F_{L_F}(B) = A$.

Each of the HJAs specifies one or more incidences between points, lines, and the folded images of points and/or lines. We call such an incidence an *alignment*. We denote (co)incidence between two objects A and B by the notation $A \leftrightarrow B$. There are three possible types of alignment:

Definition 5 (Point-Point Alignment). Given two points $P_1 = (x_1, y_1)$ and $P_2 = (x_2, y_2)$, the alignment $P_1 \leftrightarrow P_2$ is satisfied if and only if $x_1 = x_2$ and $y_1 = y_2$.

Definition 6 (Line-Line Alignment). Given two lines $L_1 = (X_1, Y_1)$ and $L_2 = (X_2, Y_2)$, the alignment $L_1 \leftrightarrow L_2$ is satisfied if and only if $X_1 = X_2$ and $Y_1 = Y_2$.

Definition 7 (Point-Line Alignment). Given a point $P = (x, y)$ and a line $L = (X, Y)$, the alignment $P \leftrightarrow L$ is satisfied if and only if $xX + yY + 1 = 0$.

As an aside, we note that there is one other incidence-type relation that could be considered: a line can be oriented such that it is *not* incident to a given line—meaning that it is parallel to a given line. While mathematically sound, in practice, this relationship can only be verified with infinite paper, and we will restrict our attentions to alignments that can be verified within a finite region of the paper.

Each of the HJAs can be viewed as a combination of one or more alignments. This leads naturally to the following definition:

Definition 8 (One-Fold Axiom). A *one-fold axiom* (1FA) is a minimal set of alignments that define a single fold line on a finite region of the Euclidean plane with a finite number of solutions.

We stipulate a *minimal* set to exclude redundant alignments that don't do anything. We stipulate a finite number of solutions because some combinations of alignments have multiple solutions. And we stipulate a finite region of the plane to exclude alignments that require infinite paper to verify.

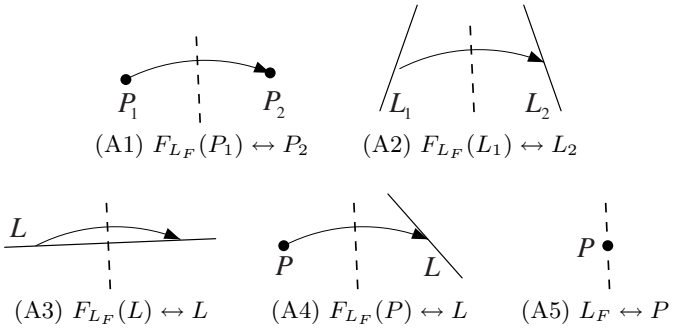

Figure 2. The five one-fold alignments. A1 and A2 define two equations each; A3–A5 define one equation each.

With this definition, each of the HJAs can be seen to be a one-fold origami axiom, and the question of completeness can now be precisely phrased: are there other 1FAs?

To set a condition on a fold line, one side of an alignment must be the folded image of a point or line. There are five possibilities with the three types of alignments for a single fold line L_F; each alignment defines one or two equations. These five *one-fold alignments*, denoted by A1–A5, are shown in Figure 2.

Note that A5—aligning a point to the fold line—is equivalent to requiring that the folded image of a point be aligned to itself. That is, we could write $L_F \leftrightarrow P$ equivalently as $F_{L_F}(P) \leftrightarrow P$ (as was done in [22]).

The case of a line folded onto itself is distinct from a line folded onto another line in that only a single equation need be satisfied in the former.

Folding a point to a line ($F_{L_F}(P) \leftrightarrow L$)) is equivalent to folding a line to a point ($F_{L_F}(L) \leftrightarrow P$)) since they result in the same equations. We therefore consider the alignments $F_{L_F}(P) \leftrightarrow L$) and $F_{L_F}(L) \leftrightarrow P$) to be *equivalent under folding*.

Also, we do not consider the relationship of a line incident to the fold line since the goal is to define a fold line that does not already exist.

The fold line $L_F \equiv (X_F, Y_F)$ is defined by its two parameters and therefore has two degrees of freedom. Therefore, any combination of folds that specifies the fold line must consist of some combination of alignments that specifies exactly two equations.

Each of the first two alignments in Figure 2 results in two equations that must be satisfied; thus, each in and of itself is sufficient to specify the fold line. And indeed, the alignment $F_{L_F}(P_1) \leftrightarrow P_2$ is equivalent to O2, while alignment $F_{L_F}(L_1) \leftrightarrow L_2$ is equivalent to O3.

	$F_{L_F}(L_1) \leftrightarrow L_1$	$F_{L_F}(P_1) \leftrightarrow L_1$	$L_F \leftrightarrow P_1$
$F_{L_F}(L_2) \leftrightarrow L_2$	N/A	O7	O4
$F_{L_F}(P_2) \leftrightarrow L_2$	O7	O6	O5
$L_F \leftrightarrow P_2$	O4	O5	O1

Table 1. All possible pairs of single-equation alignments.

The other three alignments only specify a single equation, which means that we require two such alignments to fully specify the two degrees of freedom of the fold line. We consider all possible pairs of the single-equation alignments in Table 1. The points and lines (other than the fold lines) in each row and column are assumed to be distinct.

The top left combination (folding two different lines onto themselves) cannot be part of a valid axiom; if the two lines are nonparallel, then the equations are inconsistent, whereas if the lines are parallel, the equations are redundant and cannot be part of a minimal set. All other combinations correspond to existing HJAs—and we note that Justin/Hatori's seventh axiom is among them. Thus, Justin/Hatori's axiom can be defined in exactly the same way as the other six axioms. And, since we have considered all possible combinations of alignments, we have proved completeness; there are no more one-fold axioms to be found.

3 Solving Equations with One-Fold Axioms Using Lill's Method

There is a classical method (Lill, 1867 [28]) of using reflections to create the solutions to real polynomial equations. To solve the equation $x^n + a_{n-1}x^{n-1} + ... + a_0$ by Lill's method, you form a right-angle path from the origin (point O) to a terminus (point T) in which the lengths and directions of the segments are given by the coefficients of the equation, starting with the leading coefficient of 1, ending with a_0, and at each junction, turning left or right depending on the sign of each coefficient (left = positive, right = negative). You then launch a line from O at some angle that makes a right-angled turn at each successive line toward the next line, adjusting the initial slope until the final turn strikes point T. When that condition is satisfied, the first intersection point gives the desired solution. Lill's method works for arbitrarily high degree and lends itself nicely to equation solving via origami. Depending on the degree of the equation, we can use origami axioms to determine the correct bouncing strategy.

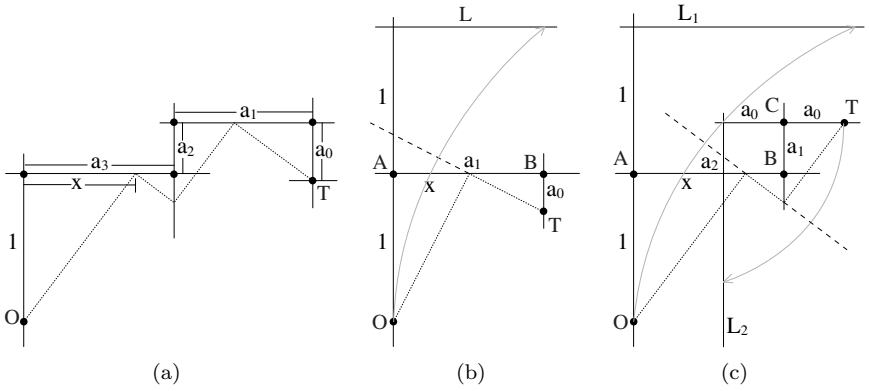

Figure 3. (a) Lill diagram for the quartic equation $x^4 - a_3x^3 + a_2x^2 - a_1x - a_0 = 0$. (b) Lill diagram and fold lines for solving the quadratic equation $x^2 - a_1x - a_0 = 0$ using O5. (c) Lill diagram and fold lines for solving the cubic equation $x^3 - a_2x^2 + a_1x - a_0 = 0$ using O6.

3.1 Quadratics

We are given three signed lengths determined from the polynomial: OA, AB, BT, each segment at right angles to the next, as in Figure 3(b). Construct an auxiliary line L parallel to AB on the opposite side to AB from O and of distance OA. Now use O5 to fold O to L so that the crease passes through T.

3.2 Cubics

Using the diagram in Figure 3(c) made from arcs OA, AB, BC, CT, each at right angles, we construct auxiliary lines: L_1, parallel to AB and opposite O but of distance OA; and L_2, parallel to BC and on the opposite side to T but of distance CT. Using O6, we simultaneously fold O to L_1 and T to L_2. This crease, together with the perpendiculars to O and T, gives the desired bouncing strategy.

We note that a distinct method for producing $\sqrt[3]{2}$ was presented by Messer [26] that, while also relying on O6, uses a somewhat different construction. By applying the method of Figure 3(c) to the cubic $x^3 - a$ it is possible to take arbitrary cube roots, as well as solving a general cubic. This method of solving the general cubic was discovered and described by Beloch [6] in 1936.

We return to this method in Section 5 for solving higher degree equations with two or more folds.

4 Two-Fold Axioms

We now consider two-fold axioms: combinations of alignments that specify two simultaneous fold lines. We proceed in the same way as we did in the previous section. We consider the possible alignments between points, lines, fold lines, and their folded images. We then construct all possible combinations that specify two fold lines.

Definition 9 (Two-Fold Axiom). A *two-fold origami axiom* (2FA) is a minimal set of alignments that defines two simultaneous fold lines on a finite region of the Euclidean plane with a finite number of solutions.

There are a few complications when we consider two (or more) fold lines. First is a practical matter; physically creating a two-fold alignment requires that one smoothly varies the position of both folds until the various alignments are satisfied. With two simultaneous folds, any two nonparallel folds will eventually intersect and in the real world, intersecting folds bind at their intersection and cannot be smoothly varied in both position and angle. We will ignore this practical limitation for the moment.

Next, the number of possible alignments and combinations of alignments grows explosively with number of simultaneous folds (as we will see). In order to minimize the number of combinations to count, we will adopt several rules for equivalence and validity.

Definition 10 (Separability). A two-fold axiom is *separable* if and only if its alignments can be partitioned into two sets, each of which is a one-fold axiom.

For example, the trisection axiom afforded by Abe's method is given as a two-fold separable alignment combining O2 and O6: given points P and Q and a line l through P, we can fold line L_1, which reflects P onto Q, and line L_2, which reflects Q onto l and P onto L_1 [4].

Definition 11 (Equivalence Under Permutation). Two two-fold axioms are *equivalent under permutation* if their alignments are equivalent under permutation of their points, lines, and/or fold lines.

Definition 12 (Equivalence Under Folding). Two two-fold axioms are *equivalent under folding* if their alignments can be paired such that applying $F_{L_{F1}}$ or $F_{L_{F2}}$ to both sides of one or more alignments makes them equivalent under permutation. Two axioms that are not equivalent under folding are *distinct*.

We will restrict our attention to enumerating nonseparable distinct two-fold axioms. To do this, we enumerate the distinct nonseparable two-fold

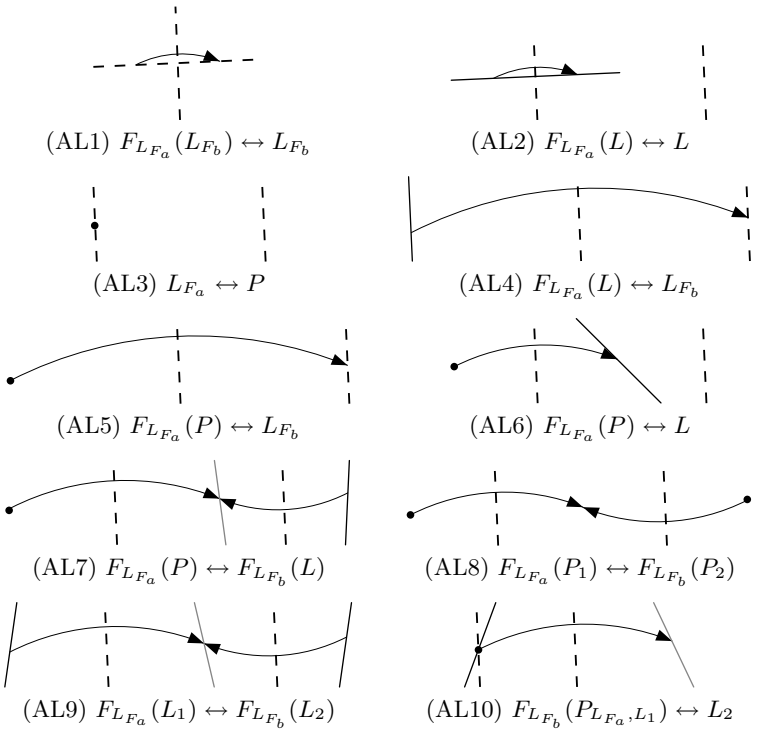

Figure 4. The ten distinct two-fold alignments.

alignments, analogous to A1–A5 as defined in Figure 2. Figure 4 shows them all. For brevity, we name them AL1–AL10.

We include here only the alignments that lead to nonseparable combinations. Any combination in which a single alignment fully specifies one of the fold lines will be separable.

Our ordering is chosen in roughly increasing degree of the underlying equations. If we denote the two fold lines by F_a and F_b, the equations resulting from alignments AL1, AL8, and AL9 are symmetric under interchange of fold line while the equations resulting from alignments AL2, AL3, AL4, AL5, AL6, AL7, and AL10 are not. In forming combinations of the nonsymmetric alignments, we will append the letter a or b to distinguish the two forms. Thus, for example, AL2a is the alignment shown in Figure 4; AL2b would act on the second fold line. We note that the potential alignment $F_{L_a}(L) \leftrightarrow F_{L_b}(L)$ results in the same equations as AL2a + AL2b, so we do not count it in our listing.

Alignment AL10 (which comes in both a and b varieties) is a bit unusual. All points appearing in other alignments are preexisting points, but the

point $P_{L_{F_a},L_1}$ appearing in AL10 is a *virtual point*, the intersection of the first fold line F_{L_a} with the existing line L_1. AL10 aligns this point with a second line L_2; if the two lines are the same ($L_1 = L_2$), then this alignment forces the intersection of the two fold lines with each other to lie on the given line. Alignment $F_{L_{F_b}}(P_{L_{F_a},L_1}) \leftrightarrow P_1$ is not listed because it can be decomposed into $F_{L_{F_b}}(L_{F_a}) \leftrightarrow P_1$ and $F_{L_{F_b}}(L_1) \leftrightarrow P_1$.

Each of these alignments leads to either one or two equations on the four degrees of freedom of the two fold lines, which implies that a valid two-fold axiom will consist of two, three, or four of these alignments. Including both a and b forms of the nonsymmetric alignments gives a total of 17 possible alignments for each element of a combination. That, in turn, gives $17{\times}17{\times}18{\times}18 = 93,636$ possible combinations to consider. However, those combinations include combinations that are over- and under-determined and combinations that are equivalent under permutation or folding. We constructed a computer-assisted enumeration using Mathematica, following this procedure:

1. Construct all possible combinations of two, three, or four of the two-fold alignments.
2. Eliminate duplicates equivalent under permutation or folding.
3. Construct symbolic equations for each remaining combination of alignments.
4. Eliminate combinations that did not lead to exactly four equations.
5. Construct the Jacobian for each set of four equations at a solution; eliminate combinations that did not have four singular values (indicating an inconsistent or under-determined set of equations).

We did this both with and without alignment AL10. Including AL10 gave 489 distinct combinations; leaving it out gave 203 combinations. Each combination is a distinct nonseparable two-fold alignment, equivalent to the HJAs. To identify concisely a particular 2FA, we adopt the following notation for a given combination of alignments. Begin with *AL*. Append the number of each alignment, including its a/b suffix, in numerical order (but without repeating AL). If an alignment appears more than once in combination, only the suffix is repeated. (This only happens with a/b alignments.) Thus, for example, the 2FA denoted by AL6ab8 consists of alignments AL6a, AL6b, and AL8 and involves folding one point to a line using the first fold line, folding a point to a line using the second fold line, and bringing the image of the third and fourth points together using both fold lines. This 2FA and two others that also involve four points and two lines are shown in Figure 5.

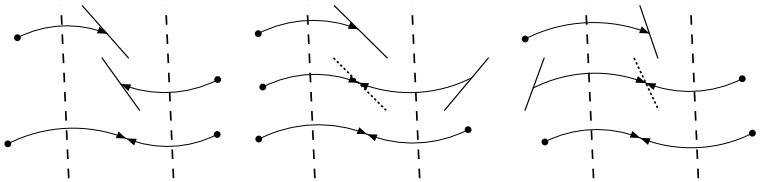

Figure 5. Three of the two-fold axioms.

Space does not permit a complete pictorial listing of the 489 2FAs here, but using our compact notation, we can provide a complete listing by symbol.

AL110aaa, AL110aab, AL12a10aa, AL12a10ab, AL12a10bb, AL12a3b10a, AL12a3b10b, AL12a3b7a, AL12a3b7b, AL12a6b10a, AL12a6b10b, AL12a6b7a, AL12a6b7b, AL12a7a10a, AL12a7a10b, AL12a7aa, AL12a7ab, AL12a7b10a, AL12a7b10b, AL12a7bb, AL13a10aa, AL13a10ab, AL13a10bb, AL13ab10a, AL13ab7a, AL13a6b10a, AL13a6b10b, AL13a6b7a, AL13a6b7b, AL13a7a10a, AL13a7a10b, AL13a7aa, AL13a7ab, AL13a7b10a, AL13a7b10b, AL13a7bb, AL16a10aa, AL16a10ab, AL16a10bb, AL16ab10a, AL16ab7a, AL16a7a10a, AL16a7a10b, AL16a7aa, AL16a7ab, AL16a7b10a, AL16a7b10b, AL16a7bb, AL17a10aa, AL17a10ab, AL17a10bb, AL17aa10a, AL17aa10b, AL17ab10a, AL810aa, AL810ab, AL910aa, AL910ab, AL10aaaa, AL10aaab, AL10aabb, AL2a810a, AL2a810b, AL2a910a, AL2a910b, AL2a10aaa, AL2a10aab, AL2a10abb, AL2a10bbb, AL2ab10aa, AL2ab10ab, AL2ab5a10a, AL2ab5a10b, AL2ab5ab, AL2ab5a7a, AL2ab5a7b, AL2ab7a10a, AL2ab7a10b, AL2ab7aa, AL2ab7ab, AL2a3b8, AL2a3b9, AL2a3b10aa, AL2a3b10ab, AL2a3b10bb, AL2a3b4a, AL2a3b4b, AL2a3b5a10a, AL2a3b5a10b, AL2a3b5aa, AL2a3b5ab, AL2a3b5a7a, AL2a3b5a7b, AL2a3b5b10a, AL2a3b5b10b, AL2a3b5bb, AL2a3b5b7a, AL2a3b5b7b, AL2a3b7a10a, AL2a3b7a10b, AL2a3b7aa, AL2a3b7ab, AL2a3b7b10a, AL2a3b7b10b, AL2a3b7bb, AL2a4a10a, AL2a4a10b, AL2a4a5b, AL2a4a6b, AL2a4a7a, AL2a4a7b, AL2a4b10a, AL2a4b10b, AL2a4b5a, AL2a4b6b, AL2a4b7a, AL2a4b7b, AL2a5a8, AL2a5a9, AL2a5a10aa, AL2a5a10ab, AL2a5a10bb, AL2a5aa10a, AL2a5aa10b, AL2a5aab, AL2a5aa6b, AL2a5aa7a, AL2a5aa7b, AL2a5ab10a, AL2a5ab10b, AL2a5abb, AL2a5ab6b, AL2a5ab7a, AL2a5ab7b, AL2a5a6b10a, AL2a5a6b10b, AL2a5a6b7a, AL2a5a6b7b, AL2a5a7a10a, AL2a5a7a10b, AL2a5a7aa, AL2a5a7ab, AL2a5a7b10a, AL2a5a7b10b, AL2a5a7bb, AL2a5b8, AL2a5b9, AL2a5b10aa, AL2a5b10ab, AL2a5b10bb, AL2a5bb10a, AL2a5bb10b, AL2a5bb6b, AL2a5bb7a, AL2a5bb7b, AL2a5b6b10a, AL2a5b6b10b, AL2a5b6b7a, AL2a5b6b7b, AL2a5b7a10a, AL2a5b7a10b, AL2a5b7aa, AL2a5b7ab, AL2a5b7b10a, AL2a5b7b10b, AL2a5b7bb, AL2a6b8, AL2a6b9, AL2a6b10aa, AL2a6b10ab, AL2a6b10bb, AL2a6b7a10a, AL2a6b7a10b, AL2a6b7aa, AL2a6b7ab, AL2a6b7b10a, AL2a6b7b10b, AL2a6b7bb, AL2a7a10aa, AL2a7a10ab, AL2a7a10bb, AL2a7aa10a, AL2a7aa10b, AL2a7aaa, AL2a7aab, AL2a7ab10a, AL2a7ab10b, AL2a7abb, AL2a7b10aa, AL2a7b10ab, AL2a7b10bb, AL2a7bb10a, AL2a7bb10b, AL2a7bbb, AL3a810a, AL3a810b, AL3a910a, AL3a910b, AL3a10aaa, AL3a10aab, AL3a10abb, AL3a10bbb, AL3ab8, AL3ab9, AL3ab10aa, AL3ab10ab, AL3ab4a, AL3ab5a10a, AL3ab5a10b, AL3ab5aa, AL3ab5ab, AL3ab5a7a, AL3ab5a7b, AL3ab7a10a, AL3ab7a10b, AL3ab7aa, AL3ab7ab, AL3a4a10a, AL3a4a10b, AL3a4a5b, AL3a4a6b, AL3a4a7a, AL3a4a7b, AL3a4b10a, AL3a4b10b, AL3a4b5a, AL3a4b6b, AL3a4b7a, AL3a4b7b, AL3a5a8, AL3a5a9, AL3a5a10aa, AL3a5a10ab, AL3a5a10bb, AL3a5aa10a, AL3a5aa10b, AL3a5aab, AL3a5aa6b, AL3a5aa7a, AL3a5aa7b, AL3a5ab10a, AL3a5ab10b, AL3a5abb, AL3a5ab6b, AL3a5ab7a, AL3a5ab7b, AL3a5a6b10a, AL3a5a6b10b, AL3a5a6b7a, AL3a5a6b7b, AL3a5a7a10a,

AL3a5a7a10b, AL3a5a7aa, AL3a5a7ab, AL3a5a7b10a, AL3a5a7b10b, AL3a5a7bb, AL3a5b8, AL3a5b9, AL3a5b10aa, AL3a5b10ab, AL3a5b10bb, AL3a5bb10a, AL3a5bb10b, AL3a5bb6b, AL3a5bb7a, AL3a5bb7b, AL3a5b6b10a, AL3a5b6b10b, AL3a5b6b7a, AL3a5b6b7b, AL3a5b7a10a, AL3a5b7a10b, AL3a5b7aa, AL3a5b7ab, AL3a5b7b10a, AL3a5b7b10b, AL3a5b7bb, AL3a6b8, AL3a6b9, AL3a6b10aa, AL3a6b10ab, AL3a6b10bb, AL3a6b7a10a, AL3a6b7a10b, AL3a6b7aa, AL3a6b7ab, AL3a6b7b10a, AL3a6b7b10b, AL3a6b7bb, AL3a7a8, AL3a7a9, AL3a7a10aa, AL3a7a10ab, AL3a7a10bb, AL3a7aa10a, AL3a7aa10b, AL3a7aaa, AL3a7aab, AL3a7ab10a, AL3a7ab10b, AL3a7abb, AL3a7b8, AL3a7b9, AL3a7b10aa, AL3a7b10ab, AL3a7b10bb, AL3a7bb10a, AL3a7bb10b, AL3a7bbb, AL4a8, AL4a9, AL4a10aa, AL4a10ab, AL4a10bb, AL4ab, AL4a5b10a, AL4a5b10b, AL4a5bb, AL4a5b6a, AL4a5b6b, AL4a5b7a, AL4a5b7b, AL4a6a10a, AL4a6a10b, AL4a6ab, AL4a6a7a, AL4a6a7b, AL4a6b10a, AL4a6b10b, AL4a6b7a, AL4a6b7b, AL4a7a10a, AL4a7a10b, AL4a7aa, AL4a7ab, AL4a7b10a, AL4a7b10b, AL4a7bb, AL5a810a, AL5a810b, AL5a910a, AL5a910b, AL5a10aaa, AL5a10aab, AL5a10abb, AL5a10bbb, AL5aa8, AL5aa9, AL5aa10aa, AL5aa10ab, AL5aa10bb, AL5aab10a, AL5aab10b, AL5aabb, AL5aab6a, AL5aab6b, AL5aab7a, AL5aab7b, AL5aa6a10a, AL5aa6a10b, AL5aa6ab, AL5aa6a7a, AL5aa6a7b, AL5aa6b10a, AL5aa6b10b, AL5aa6b7a, AL5aa6b7b, AL5aa7a10a, AL5aa7a10b, AL5aa7aa, AL5aa7ab, AL5aa7b10a, AL5aa7b10b, AL5aa7bb, AL5ab8, AL5ab9, AL5ab10aa, AL5ab10ab, AL5ab6a10a, AL5ab6a10b, AL5ab6ab, AL5ab6a7a, AL5ab6a7b, AL5ab7a10a, AL5ab7a10b, AL5ab7aa, AL5ab7ab, AL5a6a8, AL5a6a9, AL5a6a10aa, AL5a6a10ab, AL5a6a10bb, AL5a6ab10a, AL5a6ab10b, AL5a6ab7a, AL5a6ab7b, AL5a6a7a10a, AL5a6a7a10b, AL5a6a7aa, AL5a6a7ab, AL5a6a7b10a, AL5a6a7b10b, AL5a6a7bb, AL5a6b8, AL5a6b9, AL5a6b10aa, AL5a6b10ab, AL5a6b10bb, AL5a6b7a10a, AL5a6b7a10b, AL5a6b7aa, AL5a6b7ab, AL5a6b7b10a, AL5a6b7b10b, AL5a6b7bb, AL5a7a8, AL5a7a9, AL5a7a10aa, AL5a7a10ab, AL5a7a10bb, AL5a7aa10a, AL5a7aa10b, AL5a7aaa, AL5a7aab, AL5a7ab10a, AL5a7ab10b, AL5a7abb, AL5a7b8, AL5a7b9, AL5a7b10aa, AL5a7b10ab, AL5a7b10bb, AL5a7bb10a, AL5a7bb10b, AL5a7bbb, AL6a810a, AL6a810b, AL6a910a, AL6a910b, AL6a10aaa, AL6a10aab, AL6a10abb, AL6a10bbb, AL6ab8, AL6ab9, AL6ab10aa, AL6ab10ab, AL6ab7a10a, AL6ab7a10b, AL6ab7aa, AL6ab7ab, AL6a7a8, AL6a7a9, AL6a7a10aa, AL6a7a10ab, AL6a7a10bb, AL6a7aa10a, AL6a7aa10b, AL6a7aaa, AL6a7aab, AL6a7ab10a, AL6a7ab10b, AL6a7abb, AL6a7b8, AL6a7b9, AL6a7b10aa, AL6a7b10ab, AL6a7b10bb, AL6a7bb10a, AL6a7bb10b, AL6a7bbb, AL7a810a, AL7a810b, AL7a910a, AL7a910b, AL7a10aaa, AL7a10aab, AL7a10abb, AL7a10bbb, AL7aa10aa, AL7aa10ab, AL7aa10bb, AL7aaa10a, AL7aaa10b, AL7aab10a, AL7aab10b, AL7ab10aa, AL7ab10ab

This leads naturally to the question: what good are these? The most complex of the HJAs, axiom O6, imposes a cubic equation on the parameterization of the fold line; this condition enables the solution of the general cubic equation and various related problems. Folding a 2FA imposes higher-order equations on the parameterizations of the fold lines; thus, a 2FA can potentially be used to solve higher-order polynomial equations.

We note that the previously mentioned angle quintisection [23] requires a two-fold alignment at one step. Specifically, the required 2FA is AL3a5b6b7b. Performing an angle quintisection requires the solution of a particular irreducible quintic equation; thus, this 2FA (and others) allows the solution of at least some quintic polynomials by origami. The question of which 2FAs allow this solution, and which still higher-order equations could be addressed by 2FAs, is the topic of the next section.

5 Solving Equations with Two-Fold Axioms

In order to fix a line it needs to be specified by two conditions; so two folds need four conditions to determine the alignment. Each two-fold alignment yields a system of four equations in four variables with each equation of degree at most 4.

Of the first 310 2FAs, 303 of them contain at least one equation of degree 1 in two variables (ending with AL3a7bbb); by eliminating a variable we can reduce the system to three equations of degree at most 4 in three variables. Of these, 85 systems involve two equations of degree 1 so by further elimination we are led to two equations in two unknowns; the solutions to each of these equations is a curve in the plane and the simultaneous solutions give the coordinates for the two fold lines. By Bezout's theorem the product of the two degrees is the number of (complex) solutions counted with multiplicity.

Considering all systems, the number of solutions is much less than the theoretical upper bound of 192 (the product of degrees); we obtain at most 21 solutions in the worst case using Gröbner basis calculations (see, e.g., [30]) in the program Magma.

In our equations, the first fold is (X, Y) and the second fold is (Z, W). The coefficients of our equations belong to the ring A of rational functions in variables determined by the generic points and lines given by the data of the alignment conditions. The fold conditions give an ideal

$$\langle a(X, Y, Z, W), b(X, Y, Z, W), c(X, Y, Z, W), d(X, Y, Z, W)\rangle$$

in $A[X, Y, Z, W]$, which describes an affine variety of dimension 0 (as a consequence of the non-singularity of the Jacobian of a, b, c, d). We apply Gröbner basis methods (after specializing the point and line coordinates in A to rational values). The Gröbner basis method gives another set of ideal generators of the following form

$$\langle f_0(W), X - f_1(W), Y - f_2(W), Z - f_3(W)\rangle.$$

The degree of f_0 is called the *complexity*, denoted cx. The degrees of the other polynomial generators in this ideal are smaller than cx. The complexity is our measure of the number of different crease patterns that fulfill the given alignment conditions. For different choices of given points and lines in the two-fold alignment we get different polynomials; for AL3ab9 the polynomial f_0 is of degree 4, but not all polynomials of degree 4 can arise in this way.

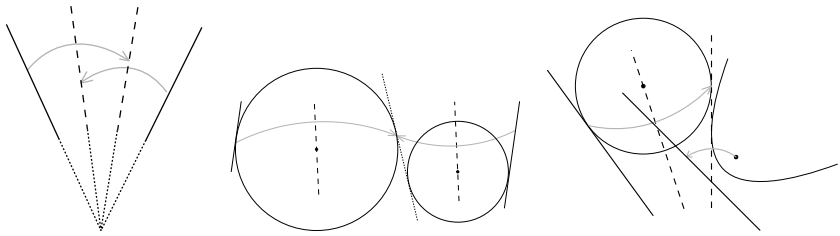

Figure 6. Three 2FAs. AL3ab9 and AL3a4a6b are shown with their associated conic sections.

6 Geometry Examples

We explore some of the geometry involved in selected two-fold alignments and their complexity.

6.1 Trisection

AL4ab, $cx = 3$. For nonparallel given lines, this alignment gives the trisections of the angle between the given lines as one of the creases and the other crease is the bisector of the first crease with the remote line, as shown in Figure 6 (left). For parallel given lines, the alignment gives the folds for the trisection of the segment perpendicular to the given lines.

6.2 Conics

Two circles: AL3ab*—17 two-folds, AL3ab9, $cx = 4$. The fold line and point for AL3a or AL3b can be viewed as a diameter and center of a circle. The folds reflect given lines to other tangents of the circles. Thus, this folds the (at most) four common tangents to two circles, as shown in Figure 6 (middle).

The other alignments of this type have complexity at most eight; the basis polynomial f_0 for AL3ab7ab factors as a quadratic and sextic; others of this type have small complexity.

Circle and parabola: AL3a6b—29 two-folds, AL3a4a6b, $cx = 4$. The second crease can be viewed as a tangent to a parabola with the point and line of AL6b as its focus and directrix; the first crease is a diameter to a circle. The given line is folded to a tangent to a circle and is a tangent of the parabola, as shown in Figure 6 (right); thus alignment creates the (at most) four tangents to a circle and parabola. A method for solving certain quartic polynomials by folding the common tangents to a circle and parabola has

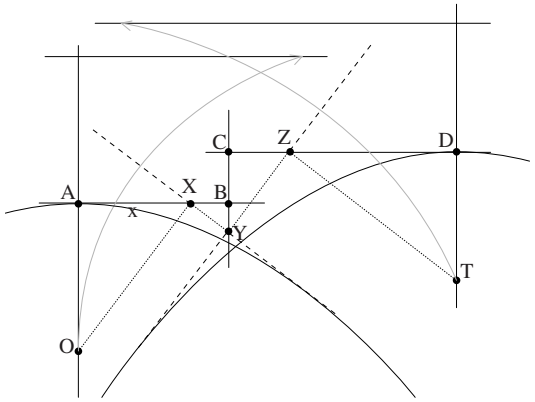

Figure 7. Solving a quartic equation by origami and Lill's method. The two associated parabolas are also shown.

been discussed in [7]. The method discussed there however does not use a two-fold.

The alignments of this type have complexity at most 12. The highest degree factor of f_0 by the Gröbner basis calculations yield: AL3a6b4b of degree 3; AL3a6b5aa of degree 4; AL3a6b5ab of degree 6; AL3a6b5a7a of degree 6;AL3a6b5a7b of degree 8;AL3a6b5bb of degree 3; AL3a6b5b7a of degree 8; AL3a6b5b7b of degree 7; AL3a6b8 of degree 4; AL3a6b9 of degree 6; AL3a6b7aa of degree 10; AL3a6b7ab of degree 10; AL3a6b7bb of degree 8; AL3a6b5a10a of degree 8; AL3a6b7a10b of degree 10.

Two parabolas: AL6ab* and solving quartics. The nine alignments involving AL6a and AL6b have a complexity at most 18. However, the highest degree factor of f_0 by the Gröbner basis calculations yield: AL6ab4a of degree 5; AL6ab5aa of degree 5; AL6ab5ab of degree 10; AL6ab5a7a of degree 10; AL6ab5a7b of degree 12; AL6ab9 of degree 8; AL6ab7aa of degree 11; AL6ab7ab of degree 15; AL6ab7a10a of degree 14.

The alignment AL6ab9 has the highest factor of the polynomial f_0 with Galois group of order 1152 in general. By using a repeated line we reduce the complexity to four and can then solve the general quartic by using Lill's method. We can create this construction using alignment AL6ab9 with the two parabolas and the (repeated) line BC as shown in Figure 7. Using OA, AB, BC, CD, DT we consider two parallel parabolas with vertices at A and D and foci at O and T, respectively. The two directrices of the parabolas are easily constructed atop the Lill path. We then fold points O and T onto their respective directrices so that the two fold lines intersect at a point on line BC. The two creases give two reflections, which is a

rotation; since we use the same line in the alignment the creases must be perpendicular and meet on BC. Thus OX, XY, YZ, ZT is the sequence of right-angled bounces with X and Z on the lines AB and CD, respectively, and on the respective creases. The distance from point A to point X is the desired solution.

Notice that if two folds are perpendicular and meet at P and a line L passes through P, then the reflection of L in the first and the reflection of L in the second are the same line; conversely, if L reflects in two folds to the same line, then the folds are perpendicular and meet at a point on the line L.

We note in passing that the two fold lines meet at right angles (which could be enforced by AL1) and the intersection of the fold lines lies on line BC (which could be enforced by AL10); this particular construction could be equivalently created by AL16ab10a.

7 Higher Origami: Examples of Degrees 5–8

7.1 Origami Cubic Curve

Reflect a point S in the tangents to a parabola; the locus created is the *origami cubic curve*. It is singular at S and is circular, i.e., the cubic part of its equation is $(x^2 + y^2)(ax + by)$ when the directrix of the parabola has equation $ax + by = c$. An example is shown in Figure 8.

In the one-fold axiom O7 we fold a common tangent to two parabolas. Call the foci F and S and the directrix of the first is L; the directrix of the second is M. We can think of this as reflecting S across the tangents of the parabola so as to land on M. In other words, we are intersecting M with the origami cubic curve and getting three intersections [3].

Septics and quintics—AL6ab8. The two-fold alignment AL6ab8 means that we are given two parabolas by foci and directrix F_a, L_a, F_b, L_b and two other points S_a, S_b that reflect across the parabola tangents so as to be coincident. That is the same as locating the intersection of two origami cubics J_a determined by F_a, L_a, S_a and J_b determined by F_b, L_b, S_b. Two cubics will meet in general in nine points but here both cubics are circular so they already meet at the two circular points. Therefore, there are generally seven other intersections; that is, the complexity is seven.

If we enforce other coincidences, like the singular point S_a also lies on J_b, then there will be a common singular point counting for a double intersection, so the complexity is reduced to five.

In this way we can, by taking the intersection of the two cubic curves, obtain a quintic f_0 that can be solved by means of AL6ab8. It is not

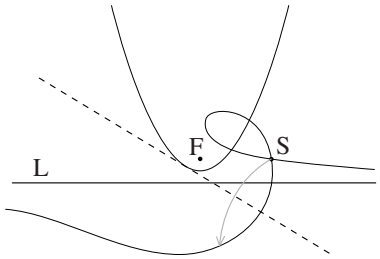

Figure 8. The image of a point S across all fold lines that are tangents to a parabola defined by focus F and directrix L traces out an origami cubic curve.

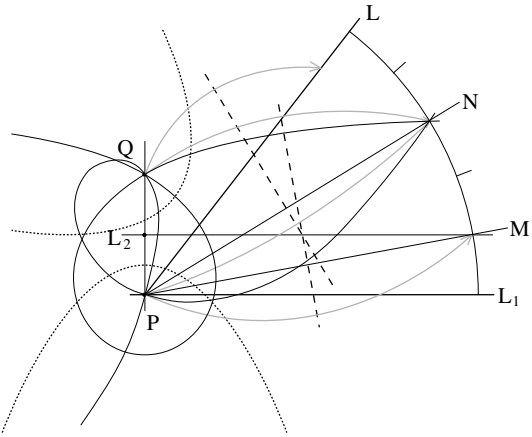

Figure 9. Quintisection by AL6ab8.

known whether all field extensions of the rational numbers of degree 5 can be generated by a root of such an f_0; however by various choices of points and lines we can arrange for both solvable and nonsolvable Galois groups. One of the solvable cases gives a second method for quintisection.

Quintisection. Here we are given lines L_1 and L. We want to fold an intermediate angle determined by N and its trisection by M so that the reflection of M across N lands on L. This is the same as the use of Maclaurin's trisectrix (Abe's origami trisection) and a simultaneous Archimedes trisection (by neusis). We do both to get a quintisection. It amounts to an intersection of two origami cubics as described above. In Figure 9 the angle between L and L_1 is quintisected using the intersection of two cubics. The cubic with singularity at Q is the trisectrix. The cubic with singularity at P is a focal cubic. The angle between N and L_1 is trisected by M using

properties of the trisectrix; N is the bisector of L and M using properties of focal cubics.

7.2 Origami Cubic Line Curve

An analogue of the origami cubic curve is obtained by reflecting a line in the tangents to a parabola and then dualizing this line in a parabola or other relevant conic; this yields a singular cubic curve that we call an *origami line cubic curve*.

AL4a6ab, $cx = 5$. Here we want the reflection of given line L_2 using the focus directrix $P_1 - L_1$ of AL6a to land on the fold made by $Q_1 - M_1$ using AL6b. Let $\mathcal{K}$ be the parabola made by the focus-directrix $Q_1 - M_1$. We dualize the origami line cubic made by P_1, L_1, L_2 in $\mathcal{K}$. The intersections of this singular cubic with $\mathcal{K}$ are precisely those places where reflections of L_2 give tangents to $\mathcal{K}$. Thus, the six possible intersections of the conic $\mathcal{K}$ and the origami line curve give the possible two-folds. Since the point at infinity on the conic is one of the common points the solutions are given by a quintic.

AL6ab9, $cx = 8$. In this construction we create two line curves by reflections of lines L_2 and M_2 in the tangents of $P_1 - L_1$ and $Q_1 - M_1$. We are looking for the coincidences of the two line curves. If we dualize these in the same parabola $\mathcal{K}$ then the two cubics will meet in at most nine points; thus, there are at most nine possible configurations for a given set of data of lines and points. However, there is a common point at infinity (the parabolas) for these two cubics, so there are only eight distinct points of intersection and thus eight possible two-fold configurations.

8 Three Folds and More

8.1 Solving the General Quintic by Lill's Method

While selected quintics can be solved by 2FAs, we have not yet found a solution to the general quintic. However, the general solution is possible using *three* simultaneous folds. Using sides OA, AB, BC, CD, DE, ET at right angles we create the Lill solution OX, XY, YZ, ZW, WT at right angles with X, Y, Z, W on the sides of the diagram (Figure 10).

Fold O to L_1 on F_a where L_1 is parallel to AB passing through the reflection of O in AB; this is AL6a. This fold line meets AB at X and BC at Y. Fold T to L_2 on F_b where L_2 is parallel to DE passing through the reflection of T in DE; this is AL6b. The intersection with DE is W and the intersection with CD is Z.

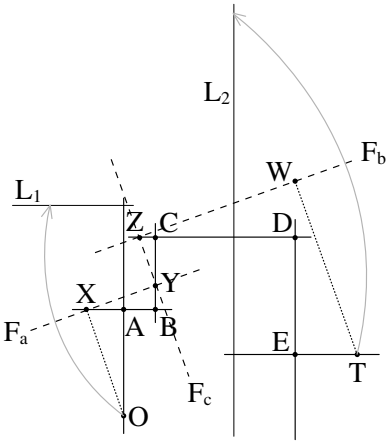

Figure 10. Solving the quintic with three-fold.

At the same time form a third fold F_c that is perpendicular to F_a (AL1) so that the fold intersection lies on CD (AL10) and is perpendicular to F_b (AL1), so that the fold intersection lies on BC (AL10). Lines OX and WT, plus segments of the three fold lines, complete the Lill path and give a solution to the general quintic.

8.2 More Folds, Higher-Degree Equations

Before proceeding, we note that the concept can be more broadly generalized:

Definition 13 (N-Fold Axiom). An *N-fold axiom* is a minimal set of alignments between sets of points, lines, and their folded images that defines a finite number of sets of N fold lines on a finite region of the Euclidean plane.

More generally, this technique can be used to solve an arbitrary polynomial equation using Lill's method. An nth-degree equation has a Lill diagram for which the solution path consists of n segments with $n-1$ turns. As in the preceding example, we use AL6 for the first and last segments of the path and $n-2$ folds for the intermediate segments, applying alignments AL1 and AL10 to enforce right-angle turns and turns lying on specified lines, respectively, for the $n-3$ intermediate turns. The number of equations to be satisfied are $2 \times (n-3) + 2 = 2(n-2)$, matching the available DOF of $n-2$-folds. This brings us to the following theorem:

Theorem 1. *Every polynomial equation of degree n with real solutions can be solved by $n-2$ simultaneous folds.*

The proof follows from the argument in the preceding paragraph. It would be interesting to know if equations of degree n that can be solved by radicals can be solved in general using less than $n-2$-folds. This is certainly true for $n=4$ and unknown for $n=5$.

Bibliography

[1] Hisashi Abe, described in Jacques Justin, "The Mathematics of Origami," *British Origami* 108 (1984), 9.

[2] R. C. Alperin. " A Mathematical Theory of Origami Constructions and Numbers." *New York J. Math.* 6 (2000), 119–133. Available at http://nyjm.albany.edu.

[3] R. C. Alperin. "A Grand Tour of Pedals of Conics." *Forum Geometricorum* 4 (2004), 143–151.

[4] R. C. Alperin. "Trisections and Totally Real Origami." *American Math. Monthly* 112:3 (2005), 200–211.

[5] David Auckly and John Cleveland. "Totally Real Origami and Impossible Paper Folding." *American Math. Monthly* 102:3 (1995), 215–226.

[6] M. P. Beloch. "Sul metodo del ripiegamento della carta per la risoluzione dei problemi geometrici." *Periodico di Mathematiche* Ser. IV, Vol. XVI (1936), 104–108.

[7] B. Carter Edwards and Jerry Shurman. "Folding Quartic Roots." *Mathematics Magazine* 74:1 (2004), 19–25.

[8] Koji Fusimi. "Trisection of Angle by Abe." *Saiensu supplement* (October 1980), 8.

[9] C. F. Gauss. *Disquisitiones Arithmeticae*. Leipzig: Fleischer, 1801. Translated from the Latin by A. A. Clarke. New Haven, CT: Yale University Press, 1965.

[10] Robert Geretschläger. "Euclidean Constructions and the Geometry of Origami." *Mathematics Magazine* 68:5 (1995), 357–71.

[11] Robert Geretschläger. "Folding the Regular Triskaidekagon." Paper presented at AMS Joint Mathematics Meeting, Baltimore, MD, January 9, 1998.

[12] Robert Geretschläger. "Folding the Regular 19-gon." Paper presented at AMS Joint Mathematics Meeting, Baltimore, MD, January 9, 1998.

[13] Robert Geretschläger. "Solving Quartic Equations in Origami." Paper presented at AMS Joint Mathematics Meeting, Baltimore, MD, January 9, 1998.

[14] Koshiro Hatori. "K's Origami: Origami Construction." Available at http://www.jade.dti.ne.jp/~hatori/library/conste.html, 2002.

[15] Thomas Hull. "A Note on 'Impossible' Paperfolding." *The American Mathematical Monthly* 103:3 (1996), 240–241.

[16] Thomas Hull. "Origametry Part 6: Basic Origami Operations." *Origami Tanteidan Magazine* 90 (2005), 14–15.

[17] Humiaki Huzita. "Axiomatic Development of Origami Geometry." In *Proceedings of the First International Meeting of Origami Science and Technology*, edited by H. Huzita, pp. 143–158. Padova, Italy: Dipartimento di Fisica dell'Università di Padova, 1991.

[18] Humiaki Huzita. "A Possible Example of System Expansion in Origami Geometry." In *Proceedings of the First International Meeting of Origami Science and Technology*, edited by H. Huzita, pp. 53–70. Padova, Italy: Dipartimento di Fisica dell'Università di Padova, 1991.

[19] Humiaki Huzita. "The Trisection of a Given Angle Solved by the Geometry of Origami." In *Proceedings of the First International Meeting of Origami Science and Technology*, edited by H. Huzita, pp. 195–214. Padova, Italy: Dipartimento di Fisica dell'Università di Padova, 1991.

[20] Humiaki Huzita and Benedetto Scimemi. "The Algebra of Paper-Folding (Origami)." In *Proceedings of the First International Meeting of Origami Science and Technology*, edited by H. Huzita, pp. 215–222. Padova, Italy: Dipartimento di Fisica dell'Università di Padova, 1991.

[21] Jacques Justin. "The Mathematics of Origami." *British Origami* 107 (1984), 14–15.

[22] Jacques Justin. "Resolution par le pliage de l'equation du troisieme degre et applications geometriques." In *Proceedings of the First International Meeting of Origami Science and Technology*, edited by H. Huzita, pp. 251–261. Padova, Italy: Dipartimento di Fisica dell'Università di Padova, 1991.

[23] Robert J. Lang. "Angle Quintisetion," *Robert J. Lang Origami*. Available at http://www.langorigami.com/science/quintisection/quintisection.php4, 2004.

[24] Robert J. Lang. "Origami Approximate Geometric Constructions." In *Tribute to a Mathemagician*, edited by Barry Cipra, Erik D. Demaine, Martin L. Demaine, and Tom Rodgers, pp. 223–239. Wellesley, MA: A K Peters, 2004.

[25] George E. Martin. *Geometric Constructions*. New York: Springer, 1998.

[26] Peter Messer. "Problem 1054." *Crux Mathematicorum* 12:10 (1986), 284–285.

[27] F. Morley and F. V. Morley. *Inversive Geometry*. New York: Chelsea Publishing, 1954.

[28] M. Riaz. "Geometric Solutions of Algebraic Equations." *American Math. Monthly* 69:7 (1962), 654–658.

[29] B. Scimemi. "Draw of a Regular Heptagon by the Folding." In *Proceedings of the First International Meeting of Origami Science and Technology*, edited by H. Huzita, pp. 71–78. Padova, Italy: Dipartimento di Fisica dell'Università di Padova, 1991.

[30] B. Sturmfels. *Solving Systems of Polynomial Equations*, CBMS Regional Conference Series 97. Providence, RI: American Mathematical Society, 2002.

The Power of Multifolds: Folding the Algebraic Closure of the Rational Numbers

Timothy Y. Chow and C. Kenneth Fan

1 Introduction

Robert Lang described how to quintisect an arbitrary angle using techniques of origami.

How can this be? Is it not well known that angle quintisection is impossible using the Huzita-Hatori axioms[1]? Lang quintisected using a secret weapon: the multifold. In "Angle Quintisection" [5], Lang explains that quintisection is impossible if only one fold is allowed at a time. However, if one allows simultaneous folds in a single origami maneuver, quintisection can be achieved.

The question naturally arises: how large is the new set of constructible numbers if one allows multifolds?

In this paper, we show that the answer is the entire algebraic closure[2] of the rational numbers. In a sense, this means that the set of origami constructible numbers is as large as possible, although we suggest a further expansion in the last section.

[1] We assume the reader is familiar with the Huzita-Hatori axioms. For a good introduction see [4]. Also see [1] for more origami constructions.

[2] We assume the reader has a basic familiarity with field theory. For information on the algebraic theory involved, see any introduction to abstract algebra, such as [3] or [6].

2 Multifolds

A multifold is a single origami maneuver that can simultaneously involve the creation of more than one crease. A multifold is made by forming a sequence of folds and then "rolling" these folds along until a desired shape is attained at which point, all creases are made sharp. The various configurations of the creases involved in the multifold can be parameterized by some variables. As the creases are rolled along, a path is traced in the parameter space.

In other words, a multifold consists of a sequence of folds $F_1, F_2, F_3, \ldots, F_N$. Of course, not any sequence of folds will do! First, the fold F_k must be specifiable in terms of alignments[3] using some combination of preexisting references, references created by prior folds in the sequence and some finite number of parameters. These parameters will typically correspond to measurable features of the model, such as an angle or distance. Second, it must be possible to actually execute these folds. For instance, it's no good if at some point in the fold sequence, a fold is called for in some part of the paper that is completely inaccessible! Finally, these folds should lend themselves to being rolled along continuously in the parameters.

The last condition makes any unfolding in the sequence risky. If, for example, the folding sequence involves unfolding a fold and refolding along a crease that intersects the unfolded crease, it is no longer possible to manipulate the model continuously: to alter the first crease, the model would have to be refolded along a discrete new location as opposed to having the new crease achieved by "rolling" the original crease to a new position.

In the context of origami constructions, only certain multifolds are useful: the multifold must satisfy some kind of alignment condition involving existing references (including references created by the folds in the folding sequence) that fixes and enables explicit computation of the value of at least one parameter that is related to a measurable feature of the origami model. When this occurs, the parameters that get fixed are effectively constructed. When an alignment condition depends on n parameters to fix the value of the desired parameters, we refer to such a multifold as an *n-parameter multifold*.

For example, let F_1 be defined by a fold parallel to a fixed edge of a square sheet of origami paper and a parameter d that gives the distance of the crease from that edge. Every d that specifies a crease within the origami square yields a one-parameter multifold (albeit, a degenerate one because only one crease is formed). However, most of these multifolds are useless for origami constructions because most do not enable computation of d. In this example, the book fold, which is specified by an appropriate

[3] For more details on alignments, see [2,4].

alignment condition, does give a constructive multifold because it fixes d to be half the width of the origami square.

There is a distinct practical advantage to using one-parameter multifolds. In a one-parameter multifold, one is guaranteed to discover the alignment condition, assuming it can be achieved, by rolling the creases. However, in multiparameter multifolds, one could fiddle endlessly with the paper in a desperate search for the alignment condition.

The good news is that one-parameter multifolds suffice because the algebraic closure of the rational numbers can be constructed using one-parameter multifolds alone:

Theorem 1. *Suppose that the complex number z is a root of a polynomial with rational coefficients. Then the real and imaginary parts of z can be constructed using one-parameter multifolds.*

The next six sections are devoted to proving this result.

3 Getting Real

Our construction only directly finds real roots of polynomials. However, we can construct the complex algebraic number a by constructing its real and imaginary parts. This is because the algebraic closure of the rational numbers is a field closed under complex conjugation (see any book on field theory), so the formulas

$$\Re a = \frac{a + \overline{a}}{2} \quad \text{and} \quad \Im a = \frac{a - \overline{a}}{2i}$$

show that the real and imaginary parts of any algebraic number are algebraic. (Note that i is algebraic because it is a root of $x^2 + 1 = 0$.)

The above shows that being able to find real roots of any polynomial with rational coefficients allows us to construct the algebraic closure of the rationals. However, we can do better. Given an algebraic number z and a polynomial with rational coefficients p with $p(z) = 0$, we can construct polynomials with rational coefficients with the real and imaginary parts of z among their roots. This not only enables us to construct the algebraic closure of the rational numbers in the abstract, but also enables us to *solve* for the roots of any given polynomial with rational coefficients.

To see this, let r_k, $k = 1, \ldots, n$ be the roots of p. Let $q_{jk} = (r_j + r_k)/2$, where $1 \leq j, k \leq n$. Let

$$f(x) = \prod_{j,k=1,\ldots,n} (x - q_{jk}).$$

Because nonreal roots of p come in conjugate pairs, the real part of r_k, for any $1 \leq k \leq n$, is a root of f. The coefficients of f are elementary symmetric polynomials in the q_{jk}. By construction, the coefficients are therefore symmetric polynomials in the r_k. Rational symmetric polynomials in the r_k are rational polynomials in the elementary symmetric polynomials of r_k [3, p. 139]. Hence, the coefficients of $f(x)$ are rational and can be directly computed from the coefficients of $p(x)$.

To get the imaginary parts, use the polynomial

$$h(x) = \prod_{j \neq k} \left(x^2 + \left(\frac{r_j - r_k}{2} \right)^2 \right)$$

and apply a similar argument to see that its coefficients are rational and directly computable from the coefficients of $p(x)$.

4 The Set Up

So, in accordance with Section 3, we are given a polynomial $p(x) = a_n x^n + a_{n-1}x^{n-1} + \ldots + a_1 x + a_0$ with rational coefficients and we need to construct its real roots.

Our approach is to use standard constructions for addition and multiplication to construct $p(x)$ from the single parameter x. Then, by varying x, we find a root when the constructed $p(x)$ is 0. However, care must be taken to ensure that the construction of $p(x)$ varies continuously with x and does not involve unfolding and refolding or some other obstruction.

To describe the method of construction, it helps to forget about origami for a moment. Instead, let us imagine that we are working with an unlimited supply of rectangular sheets of paper that can come with any dimensions that we desire. We will show how to find a real root of p using these sheets of paper and later show how to turn this into an origami multifold.

When we speak of using "large" or "long" sheets, what we mean is that some finite sized sheets will work and if you try the construction and discover that you ran out of paper, it means you just have to try again with larger or longer sheets!

So take a large square sheet and make a book fold through it. Unfold and orient it so that the resulting crease is vertical. We will refer to this as the *zero crease*. Please refer to Figure 1.

Now, fold and unfold another sharp crease parallel to and one unit to the right of the zero crease. Call this new crease the *one crease*.

We shall assume that the polynomial is given to us by having rectangular strips with lengths equal to the absolute value of the coefficients. If

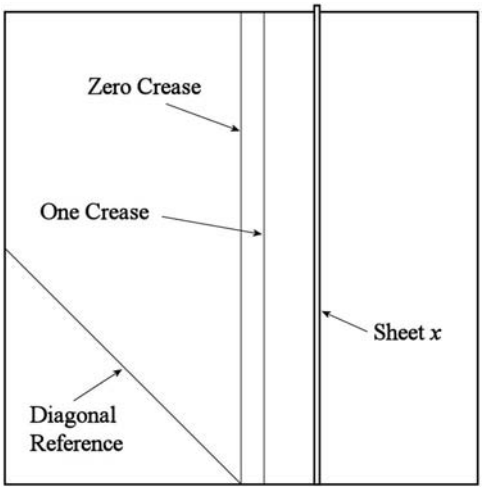

Figure 1. The preliminary setup.

you really want to, you can encode the sign of the coefficient by using one color for positive and another color for negative.

Next, fold the lower left corner of the square to the center to create a 45° crease in the lower left quadrant. Unfold. Call this crease the *diagonal reference*.

Finally, take a very long thin rectangular sheet and place it on top of the square sheet parallel to the zero and one creases. Call this *sheet* x.

Our multifold will be parameterized by the horizontal distance between the zero crease and the left edge of sheet x. We shall also use x to refer to this distance.

In the construction, we will often refer to horizontally, vertically, or diagonally aligned rectangles. Use the edges of the square or the diagonal reference to fix these orientations.

5 Overview of the Construction

The idea behind our construction is to define a sequence of folds that depend on the single parameter x. Performing the folds ultimately results in a pair of edges separated by the distance $p(x)$. This sequence gives rise to a one-parameter multifold defined by the alignment condition that this pair of edges overlap, that is, by the condition that $p(x) = 0$.

Start by writing

$$p(x) = x(x(\ldots(x(xa_n + a_{n-1}) + a_{n-2}) + \ldots) + a_1) + a_0.$$

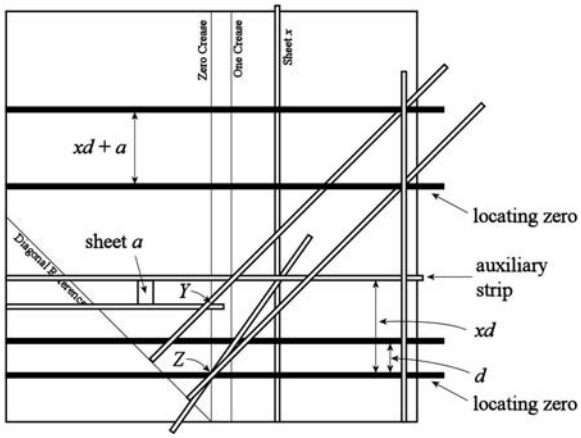

Figure 2. The input and output pairs of horizontal strips are solid black.

We devise a special sequence of folds that takes as input a pair of edges separated by the distance d and outputs a pair of edges separated by the distance $xd + a$, where a is a given constant. Using this special folding sequence, we can achieve a pair of edges separated by the distance $p(x)$ by working outward from the innermost embedded expression $xa_n + a_{n-1}$.

In the next section, we shall describe this special sequence of folds.

6 The Heart of the Construction

Our construction will be achieved by repeated application of the following folding sequence. Please refer to Figure 2.

We assume that we are given a quantity d encoded as the distance between the inner edges of two long, thin horizontal strips situated on the square sheet (the lower pair of black horizontal strips in Figure 2). If the quantity is positive, think of the lower strip as *locating zero*, otherwise, think of the upper strip as locating zero. When we refer to the *inner edge* of one of these long, thin horizontal strips, we shall mean *inner* in the context of the two strips forming a pair. Let Z denote the point of intersection of the inner edge of the strip locating zero and the zero crease.

We aim to produce a new pair of long, thin horizontal strips that encode, in the same manner, the quantity $xd + a$ where a is a real number given to us as the length of a rectangle that we will call *sheet* a (just as the coefficients of the polynomial are given to us).

To do this, note that the inner edges of the horizontal strips together with the zero and one creases form the edges of a rectangle. Place the edge

of a long, thin rectangular strip along the diagonal of this rectangle so that it passes through Z. Follow the edge of this rectangular strip to where it intersects the left edge of sheet x and mark this intersection point by placing the top or bottom (whichever is easier to see) edge of an auxiliary long, thin horizontal strip through the intersection. The vertical distance between the relevant edge of this auxiliary strip and the inner edge of the given horizontal strip locating zero is xd. The relevant edge of the auxiliary strip will be above or below the given horizontal strip locating zero depending on whether $xd > 0$ or $xd < 0$.

Situate sheet a vertically above or below (depending on whether $a > 0$ or $a < 0$) the relevant edge of the auxiliary strip. Pick a place where sheet a will not obscure any important existing intersections. Place another long, thin horizontal sheet so that its top edge is flush with the side of sheet a opposite the auxiliary strip. Let Y denote the intersection of the top edge of this last horizontal sheet and the zero crease.

Points Z and Y are on the zero crease and are separated by a distance of $xd+a$. We want to encode this distance as the separation between a new pair of long, thin horizontal strips in the same way that we were given d. To do this, take a pair of long, thin parallel rectangular strips so that their inner edges pass through Z and Y. Use the diagonal reference to orient these strips at a 45° angle. Place a vertical strip across this pair of diagonal strips in a location where, looking horizontally from the intersections, you have a clean part of the square sheet in which to work. (If you have to go too far, it means that you did not start with a big enough square sheet.)

Finally, place a pair of thin, long horizontal strips so that their inner edges pass through the intersections of the inner edges of the pair of diagonal strips with the vertical strip. Take note of which horizontal strip traces back to point Z and regard this strip as the one that is locating zero.

7 The Construction

As indicated in Section 5, to complete the construction, we iterate the procedure explained in the previous section n times. Begin the process by sandwiching the sheet representing the coefficient a_n between two long, thin horizontal strips.

Now imagine sliding sheet x left or right to vary x. As this is done, the entire contraption of horizontal, vertical, and diagonal sheets move in tandem according to the prescription of alignments given for the construction. Undoubtedly, it would help to have a lot of people working as a team to do this! (A word of advice: put your fastest sprinters on the strips that encode $p(x)$.) The upshot is that the final pair of horizontal strips will

widen and narrow representing the values of $p(x)$. When their inner edges touch, x is a root of $p(x)$.

Our setup is slightly more amenable to computing positive real roots of polynomials, but this does not present any difficulty because one can always replace the polynomial $p(x)$ by $p(-x)$.

8 Returning to Origami Land

Given a polynomial, there are well-known bounds on the size of its real roots. This enables us to find sufficiently large, yet finite sheets to perform the massive procedure outlined in Sections 5–7.

Although our multifold uses several auxiliary parameters, the alignment $p(x) = 0$ depends only on the parameter x, so this is considered a one-parameter multifold. Also, by carefully following the procedure with all its recommendations, there will be no operational concerns such as having some important intersections or sheets blocked from access. Furthermore, the entire construction of $p(x)$ involves no unfolding, so we do not have to concern ourselves with the possibility of such unfolding causing a violation of the last condition for the folding sequence of a multifold.

All that remains then, is to show how the whole contraption can be made from a single sheet of square origami paper!

This can be done by connecting all sheets involved by an ultrathin strip of paper. When making these connections, attach the ultrathin strips to unimportant locations around the edges of the sheets used in the apparatus. Use plenty of slack in these connections so that the whole apparatus can be manipulated without obstructions. Now, purchase a really, really, really long, ultrathin strip of paper and fold it, using standard techniques (see Figure 3), into this massive contraption of connected sheets. Finally, if you are truly determined to use a square sheet of origami paper, purchase a gigantic square of origami paper with side length equal to the length of the super long ultrathin strip and fold it over and over along parallel creases until it has the exact dimensions of said super long ultrathin strip.

This completes the proof of our theorem.

A related, but geometrically different, construction for the real roots of a polynomial was discovered by Lill in 1867 and is described in [7]. However, it should be possible to use Lill's method[4] to create an alternative origami construction. In our construction, we took care to avoid paper obstructing the view of the folder, and some care would have to be taken to avoid this in adapting Lill's method to origami.

[4]The authors thank the referee for pointing out this method.

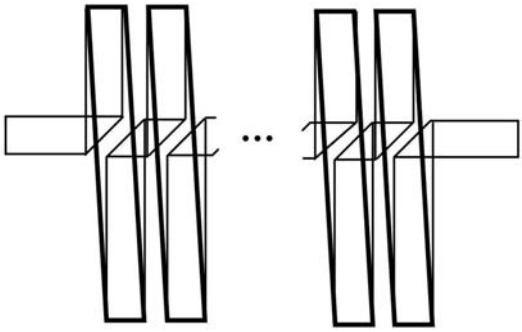

Figure 3. A schematic showing how to turn a strip into a rectangle. In actuality, all intersecting lines make 45° or 90° angles. In order to show all the folds clearly, we drew the folds askew to avoid overlaps. With minor alterations, the dimensions of the rectangle can be changed and the places where the strip enters and exits the rectangle can be relocated.

9 Multifolds and Beyond

The introduction of multifolds into origami constructibility fuels questions of practicality. Typically, multifolds are not easy to perform in the traditional way in which origami is practiced: by a lone folder. Indeed, the multifold introduced in this paper to construct $p(x)$ from x would be impossible to fold by any normal human being! However, keep in mind that ours is a *general* construction that, in principle, could even be applied to polynomials of degree one googol and one, something you couldn't even solve numerically with a supercomputer!

Finally, we ask, can the world of origami constructible numbers be further extended? Can nonalgebraic numbers like π be constructed as well?

Because alignments are specified by algebraic conditions, transcendental numbers would only be possible if the toolbox of allowable origami maneuvers is expanded.

To this end, one could introduce a mathematical model of an ideal sheet of paper that includes a description of how paper behaves in all three dimensions. Such a model would consider not only folds but also how paper curves in space. For example, one might consider continuous, path-length-preserving maps from the square into space with the property that any region of the image that does not involve creases has zero curvature and satisfies certain physical conditions on tension. An allowable procedure would then be to specify a boundary condition in terms of existing references and to extract lengths between reference points in the result-

ing structure where possible. This would bring analysis into the world of origami constructible numbers and pi would likely be attainable (for example, by making a cylinder, measuring off the diameter, and then taking a reciprocal).

Bibliography

[1] Roger C. Alperin. "A Mathematical Theory of Origami Constructions and Numbers." *New York Journal of Mathematics* 6 (2000), 119–133.

[2] Roger C. Alperin and Robert J. Lang. "One-, Two-, and Multi-Fold Origami Axioms." In *Origami^4: Fourth International Meeting of Origami Science, Mathematics, and Education*, edited by Robert J. Lang, pp. 371–393. Wellesley, MA: A K Peters, 2009.

[3] Nathan Jacobson. *Basic Algebra I*. New York: W. H. Freeman and Co., 1985.

[4] Robert J. Lang. "Origami and Geometric Constructions," *Robert j. Lang Origami*. Available at http://www.langorigami.com/science/hha/origami_constructions.pdf, 1996–2003.

[5] Robert J. Lang. "Angle Quintisection," *Robert j. Lang Origami*. Available at http://www.langorigami.com/science/quintisection/quintisection.php4, 2004.

[6] Serge Lang. *Algebra*, Third edition. New York: Springer, 2005.

[7] M. Riaz. "Geometric Solutions of Algebraic Equations." *American Mathematical Monthly* 69:7 (1962), 654–658.

Fujimoto, Number Theory, and a New Folding Technique

Tamara B. Veenstra

1 Introduction

The standard method to fold a piece of paper into fifths, sevenths, or, generally, $n$ths was developed independently by Fujimoto [2] and Brunton [1] in the 1970s. This method, usually referred to as the Fujimoto approximation technique, is a recursive process that finds a better and better approximation to $1/n$th of the paper, eventually reaching this value as precisely as the dynamics of folding paper will allow. During this process, numerous crease marks are made along the paper. In addition to eventually finding $1/n$th of the paper, sometimes these crease lines will also mark all multiples of $1/n$ but sometimes they will mark only certain multiples. This paper discusses results that classify which values of n completely divide the paper into $n$ths in this manner from two different viewpoints: one using modular arithmetic and another using binary representations. As a consequence, there are some interesting connections between these two methods of classifying n that lead to a generalization of the Fujimoto technique that provides an alternate way to find $1/n$th of the paper.

2 The Fujimoto Approximation Technique

The general algorithm for the Fujimoto approximation technique for any odd n works by first placing a pinch mark at a rough approximation for $1/n$th of the paper. A sequence of folds is then made recursively using the current pinch mark to locate the next pinch mark. More precisely, at any stage in the process, the location of the crease line can be viewed as a fraction of the paper, either from the left-hand side or the right-hand side. Since n is odd, exactly one of these fractions will have an even numerator. To get the next crease line, fold in half from the current crease line to the edge of the paper corresponding to the even numerator. Eventually, there will be a pinch mark that provides a new, more accurate approximation for $1/n$th of the paper, since the error is reduced by half every time the paper is folded in half. One can repeat the process until there is no noticeable difference in the successive pinch marks for $1/n$, at which point $1/n$th is found as accurately as possible. At this time, the pinch marks may be extended to crease lines all the way through the paper.

For example, to fold a piece of paper into fifths, the first pinch mark guesses $\frac{1}{5}$ from the left and $\frac{4}{5}$ from the right. Since the numerator of $\frac{4}{5}$ is even, we fold halfway from the right-hand side to the first pinch mark. This gives us a new pinch mark that is $\frac{3}{5}$ from the left and $\frac{2}{5}$ from the right. Again, the numerator on the right-hand side is even, so we fold that side in half. We proceed similarly until we produce a new pinch mark for $\frac{1}{5}$ from the left. We see that by the time we return to the pinch mark for $\frac{1}{5}$ from the left we have made pinch marks at $\frac{1}{5}$, $\frac{3}{5}$, $\frac{4}{5}$, and $\frac{2}{5}$ where these represent, in order, the pinch marks made as a fraction of the paper from the left side. Thus, for this value of n, we have produced pinch marks at all multiples of $\frac{1}{5}$. Thus, after we have found 1/5th accurately and made all the crease lines, we will have completely divided the paper into fifths. This property does not hold for all n. For example, if we apply the Fujimoto approximation technique to $n = 7$, then there are only three crease lines produced at $\frac{1}{7}$, $\frac{2}{7}$, and $\frac{4}{7}$, and the paper is not completely divided into sevenths. To study this property we introduce the following definition:

Definition 1. For odd n, *n has a complete Fujimoto division* if the Fujimoto algorithm for finding $1/n$th of the paper also produces crease lines at all multiples of $1/n$.

There are many examples of n that have a complete Fujimoto division and many examples of n that do not. For example, $n = 3$, 5, 11, 13, and 19 all have a complete Fujimoto division, while $n = 7$, 9, 15, 17, 21, and 23 do not. In the next section, we summarize results that answer the question of which n have a complete Fujimoto division by finding formulas to compute the number of crease lines for any n in two different ways.

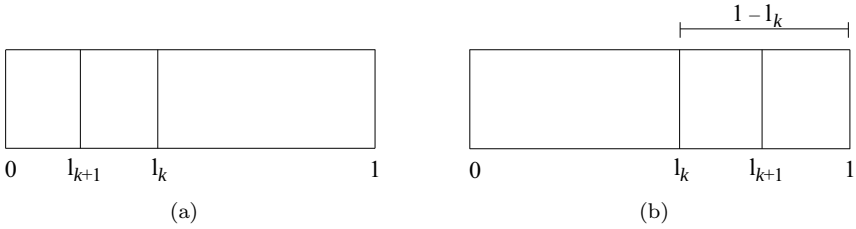

Figure 1. Finding l_{k+1} in terms of l_k. (a) Folding the left side of the paper to l_k. (b) Folding the right side of the paper to l_k.

3 The Number of Crease Lines

Since we are only interested in where the crease lines occur, we will assume that we have already found $1/n$th exactly and are just going through the algorithm the last time to make the creases all the way down the paper. To keep track of the location of these crease lines, we introduce the following notation:

Definition 2. Let $l_k(n)$ denote the fraction of the paper that is to the left of the pinch mark at the kth step in the Fujimoto approximation for finding $1/n$th of the paper.

We will always assume that we start with a pinch mark $1/n$th from the left so $l_1(n) = \frac{1}{n}$. In most instances we will simply write l_k unless it is necessary to specify the n.

To understand where the crease lines fall we first construct algebraic formulas for the l_k. Because the instructions for Fujimoto use the current crease line, l_k, to determine the placement of the next crease line, l_{k+1}, we end up with a recursive function. There are two cases, depending on whether we are folding the left or the right side in half. Note that with our notation, the left-hand side of the paper corresponds to a value of 0 and the right-hand side of the paper corresponds to 1. If we are folding the left side of the paper in half we have $l_{k+1} = l_k/2$ while folding the right side in half gives

$$l_{k+1} = 1 - \frac{1 - l_k}{2} = \frac{l_k + 1}{2}$$

as in Figure 1.

We summarize in Equation (1) below. For l_k as in Definition 2 we have $l_1 = \frac{1}{n}$ and

$$l_{k+1} = \frac{1}{2}\left(l_k + c_k\right), \text{ where } c_k = \begin{cases} 0 & \text{if } nl_k \text{ is even,} \\ 1 & \text{if } nl_k \text{ is odd.} \end{cases} \tag{1}$$

To verify that nl_k really is the numerator of l_k, we state some facts that are proved in a generalized case in Corollary 1. First, $l_k = \frac{a}{n}$ for some integer a with $1 \leq a \leq n-1$. Second, $\gcd(a, n) = 1$ so the fraction $\frac{a}{n}$ cannot be reduced. Thus, Equation (1) does indeed correspond to the directions for the Fujimoto approximation technique.

These facts already give us some insight into which n can have a complete Fujimoto division. For example, if $n = 9$ then $l_k \neq \frac{3}{9}$ for any k since $\gcd(3, 9) = 3$. This means there will be no crease mark at $\frac{3}{9}$, so that 9 does not have a complete Fujimoto division. Thus, if n is a composite number it will not have a complete Fujimoto division. The converse is not true, however, as many prime n, such as $n = 7$, also do not have a complete Fujimoto division. To answer the question about which primes have a complete Fujimoto division we state the following theorem from [6]:

Theorem 1. *Let n be odd. The number of crease marks produced in the Fujimoto approximation technique is the (multiplicative) order of* $2 \mod n$. *Moreover, n has a complete Fujimoto division if and only if n is a prime where* $n \equiv \pm 3 \mod 8$ *and* $|2| = n - 1$.

From this theorem, we see that it is relatively rare for n to have a complete Fujimoto division. We next describe a different way to find a formula for the number of crease lines produced in the Fujimoto technique. This uses the binary representation of $\frac{1}{n}$ and is based on independent work by Robert Lang [4, 5] and James Brunton [1]. Their ideas can be stated as the following theorem.

Theorem 2. *Let n be odd. The Fujimoto approximation technique for $\frac{1}{n}$ produces r crease lines if and only if $\frac{1}{n} = (.\overline{a_1 \cdots a_r})_2$. Moreover, n has a complete Fujimoto division if and only if $r = n - 1$.*

As an example of applying this theorem, we examine the binary representations for $\frac{1}{5} = (.\overline{0011})_2$ and $\frac{1}{7} = (.\overline{001})_2$. We see that Theorem 2 confirms that the Fujimoto algorithm produces four crease lines for $n = 5$ and only three crease lines for $n = 7$.

The idea underlying the proof of this theorem is that $a_i = 0$ or 1 corresponds to folding the left- or right-hand side (respectively) in half. However, it does not refer to what happens at the ith step as the correspondence uses the coefficients in reverse order. To clarify how this works (and to help us generalize later) we use the Fujimoto approximation technique for $n = 7$ to construct the binary representation for $\frac{1}{7}$. Applying Equation (1) converts the folding algorithm into the algebraic algorithm with $l_1 = \frac{1}{7}$, $l_2 = \frac{1}{2}(l_1 + 1)$, $l_3 = \frac{1}{2}(l_2)$, and $l_4 = \frac{1}{2}(l_3)$. To produce a

binary expansion we start with l_4 and recursively substitute in the above formulas:

$$l_4 = \frac{1}{2}(l_3) = \frac{1}{2}\left(\frac{1}{2}(l_2)\right) = \frac{1}{2^2}(l_2) = \frac{1}{2^2}\left(\frac{1}{2}(l_1+1)\right) = \frac{l_1}{2^3} + \frac{1}{2^3}.$$

If we plug in $l_1 = \frac{1}{7}$ we see that $l_4 = \frac{1}{7}$. This is where the Fujimoto algorithm starts repeating since it only produces three distinct crease lines for $n = 7$. Plugging in $1/7$ for both l_1 and l_4 in the above equation and then solving for it yields

$$\frac{1}{7} = \frac{1}{2^3}\left(\frac{1}{1-\frac{1}{2^3}}\right) = \frac{1}{2^3}\left(1 + \frac{1}{2^3} + \frac{1}{2^6} + \cdots\right) = (.\overline{001})_2.$$

Because we substituted the l_k in reverse we see why the coefficients of the binary expansion determine the folding in reverse order. We will prove this always happens for a generalized case in the next section.

4 Consequences and Generalizations

We now have two ways to determine the number of crease lines produced in the Fujimoto approximation technique. Thus, we must have the following connection:

Theorem 3. *Let n be odd. The fraction $\frac{1}{n}$ has a binary expansion $\frac{1}{n} = (.\overline{a_1 a_2 \cdots a_r})_2$ if and only if r is the order of* $2 \mod n$.

We know this theorem is true by combining Theorems 2 and 1, hence we can just say proof by origami! While Theorem 3 emerged naturally out of connections to origami, it does not actually depend on using a base 2 representation (see, e.g., [3, p.112]); that is, we have the following well-known generalization:

Theorem 4. *The fraction $\frac{m}{n}$ has a base b representation as $\frac{m}{n} = (.\overline{a_1 a_2 \cdots a_r})_b$ if and only if the* $\gcd(n, b) = 1$ *and r equals the order of $b \mod n$.*

A natural question arising from this generalization is whether expressing $\frac{1}{n}$ in other bases corresponds to an alternate folding technique for finding $1/n$th of the paper. The theorem forces $\gcd(n, b) = 1$ but with that condition we can, in fact, use a base b representation to produce an interesting folding algorithm, albeit with some added complications.

For motivation on how to turn a base b representation for $\frac{1}{n}$ into a folding algorithm we recall the steps for the binary case. We first translated the folding algorithm into an algebraic algorithm with the l_k. Then we used

these recursive formulas to construct the binary representation. For the base b case, we will go through these steps in the opposite order. That is, we will use the base b representation to construct an algebraic algorithm; then we will translate the algebraic algorithm into a folding algorithm.

To convert the base b representation into a recursive algebraic algorithm, we have the following theorem.

Theorem 5. *Let l_k be a recursively defined set of formulas with $l_{k+1} = \frac{1}{b}(l_k + c_k)$ where the c_k are integers such that $0 \leq c_k < b$. Then $l_{r+1} = l_1$ if and only if $l_1 = (.\overline{c_r \cdots c_1})_b$.*

Proof: We first assume that $l_{r+1} = l_1$. Applying the definition of the l_k recursively we have:

$$\begin{aligned} l_{r+1} &= \frac{1}{b}(l_r + c_r) = \frac{1}{b}(l_r) + \frac{c_r}{b} \\ &= \frac{1}{b}\left(\frac{1}{b}(l_{r-1} + c_{r-1})\right) + \frac{c_r}{b} = \frac{1}{b^2}(l_{r-1}) + \frac{c_{r-1}}{b^2} + \frac{c_r}{b} \\ &\vdots \\ &= \frac{l_k}{b^{r-k+1}} + \frac{c_k}{b^{r-k+1}} + \cdots + \frac{c_r}{b} \\ &\vdots \\ &= \frac{1}{b^r} l_1 + \frac{c_1}{b^r} + \cdots + \frac{c_{r-1}}{b^2} + \frac{c_r}{b}. \end{aligned}$$

Now substituting $l_{r+1} = l_1$ and solving for l_1 yields

$$l_1 = \left(\frac{c_1}{b^r} + \cdots + \frac{c_r}{b}\right)\left(\frac{1}{1 - \frac{1}{b^r}}\right).$$

To convert l_1 into an infinite repeating base b representation we recognize $1/(1 - (1/b^r))$ as the sum of a geometric series. Thus, we have

$$\begin{aligned} l_1 &= \left(\frac{c_1}{b^r} + \cdots + \frac{c_r}{b}\right)\left(1 + \frac{1}{b^r} + \frac{1}{b^{2r}} + \cdots\right) \\ &= \left(\frac{c_r}{b} + \cdots + \frac{c_1}{b^r}\right) + \left(\frac{c_r}{b^{r+1}} + \cdots \frac{c_1}{b^{2r}}\right) + \cdots = (.\overline{c_r \cdots c_1})_b. \end{aligned}$$

For the other direction, essentially we work through all the above steps in reverse. □

To see how Theorem 5 translates a ternary representation into an algebraic algorithm we examine $\frac{1}{5} = (.\overline{0121})_3$. We first define $l_1 = (.\overline{0121})_3 = \frac{1}{5}$.

Now, since the length of the repeated pattern is 4 the formulas will start repeating with $l_5 = l_1$. Applying the coefficients of $(.\overline{0121})_3$ in the reverse order we have

$$l_2 = \frac{1}{3}(l_1 + 1) = \frac{1}{3}\left(\frac{1}{5} + 1\right) = \frac{2}{5},$$

$$l_3 = \frac{1}{3}(l_2 + 2) = \frac{1}{3}\left(\frac{2}{5} + 2\right) = \frac{4}{5},$$

$$l_4 = \frac{1}{3}(l_3 + 1) = \left(\frac{4}{5} + 1\right) = \frac{3}{5},$$

$$l_5 = \frac{1}{3}(l_4 + 0) = \frac{1}{5}.$$

From this example we see where the crease lines should fall in a Fujimoto-like algorithm, but it is not at all obvious how to construct a folding method for obtaining these crease lines in general. We do notice that all the crease lines are multiples of $\frac{1}{n}$. This will always be true, as we see in the following corollary.

Corollary 1. *Let* $\gcd(n, b) = 1$, $l_1 = (.\overline{c_r \cdots c_1})_b$, *and* $l_{k+1} = \frac{1}{b}(l_k + c_k)$. *If* $l_1 = \frac{1}{n}$, *then for all* k, $l_k = \frac{L_k}{n}$ *where* L_k *is an integer such that* $0 \leq L_k < n$ *and* $\gcd(L_k, n) = 1$. *Moreover,* $L_k \equiv (b^{-1})^{k-1} \mod n$ *so it can be completely specified in terms of powers of* $b \mod n$.

Proof: Let the l_k be defined as above with $l_1 = \frac{1}{n}$. By Theorem 5, $l_{r+1} = l_1 = \frac{1}{n}$. Combining this with an intermediate step in the proof of Theorem 5 for $k \leq r$ we have

$$\frac{1}{n} = l_{r+1} = \frac{l_k}{b^{r-k+1}} + \frac{c_k}{b^{r-k+1}} + \cdots \frac{c_r}{b}.$$

Multiplying by nb^{r-k+1} and solving for nl_k gives

$$nl_k = b^{r-k+1} - n(c_k + \cdots + b^{r-k}c_r).$$

All terms except l_k are integers, so nl_k is an integer. Thus, we let $L_k = nl_k$ and prove the remaining properties of L_k. Reducing mod n yields $L_k \equiv b^{r-k+1} \equiv (b^{-1})^{k-1} \mod n$ since r is the order of $b \mod n$ by Theorem 4.

To see that $0 \leq L_k < n$, let

$$M_k = \frac{L_k}{nb^{r-k+1}} = \frac{1}{n} - \left(\frac{c_r}{b} + \cdots \frac{c_k}{b^{r-k+1}}\right).$$

Thus,

$$M_k = (.\overline{c_r \cdots c_1})_b - \left(\frac{c_r}{b} + \cdots \frac{c_k}{b^{r-k+1}}\right) = \frac{c_{k-1}}{b^{r-k+2}} + \frac{c_{k-2}}{b^{r-k+3}} + \cdots.$$

Clearly $M_k \geq 0$. By construction of binary coefficients we must have $M_k < 1/b^{r-k+1}$. Thus, $0 \leq M_k < 1/b^{r-k+1}$ and $0 \leq L_k < n$.

To show that $\gcd(L_k, n) = 1$ we use induction. Since $l_1 = \frac{1}{n}$ we have $L_1 = 1$ so clearly $\gcd(L_1, n) = 1$. We next assume that $\gcd(L_k, n) = 1$. From equation 1 we have $L_{k+1} = L_k + nc_k$. From properties of greatest common denominators, $\gcd(L_k + nc_k, n) = \gcd(L_k, n) = 1$. Thus by induction, $\gcd(L_k, n) = 1$ for all k. □

Now that we have the base b representation for $\frac{1}{n}$ translated into an algebraic equation we are ready to turn this into a folding algorithm. There are two parts to this process: we first need to understand what the formula $l_{k+1} = \frac{1}{b}(l_k + c_k)$ corresponds to in terms of a folding action. Then we need to specify the folding algorithm independently from the base b representation for $\frac{1}{n}$.

We first examine how $l_{k+1} = \frac{1}{b}(l_k + c_k)$ corresponds to a folding action. Multiplying by $1/b$ corresponds to folding $1/b$th of the way between two points, just like multiplying by $1/2$ corresponded to folding halfway between two points in the binary case. Thus, we already see one difficulty of this method as, in general, folding into $b$ths already requires some work. We must also figure out which two points to fold between. As in the binary case, one of the points is always the current crease line l_k. The other is determined by the coefficient c_k. In binary the c_k take only two values, 0 or 1, and these correspond to points at the left and right ends of the paper. For base b we will need b different points since there are b different values for the c_k.

For an example, consider $b = 3$. The formulas for the l_k are of the form $l_{k+1} = \frac{1}{3}(l_k + c_k)$ with $c_k = 0$, 1 or 2. Two of these values for c_k correspond to straightforward generalizations of the binary case where we folded the left side or the right side in half. If $c_k = 0$ then folding $l_{k+1} = l_k/3$ corresponds to folding $1/3$ of the way from the left edge of the paper (denoted as 0) to the crease line l_k. If $l_{k+1} = \frac{1}{3}(l_k + 2) = 1-(1-l_k)/3$ then we fold $1/3$ of the way from the right edge of the paper (denoted as 1) to the crease line l_k.

The case where $c_k = 1$ is not at all similar to the binary case. The formula $l_{k+1} = \frac{1}{3}(l_k + 1)$ still corresponds to folding $1/3$ of the way from a point A to l_k, but A does not fall at either end of the paper. To see what the point A corresponds to, we examine the action of folding $1/3$ of the way from an arbitrary point A to the current crease line l_k as in Figure 2.

This folding corresponds to $l_{k+1} = A - \frac{1}{3}(A - l_k)$. While l_k need not be to the left of A, the formula will be the same. To find A in the case where $l_{k+1} = \frac{1}{3}(l_k + c_k)$ we solve $\frac{1}{3}(l_k + 1) = A - \frac{1}{3}(A - l_k)$ yielding $A = 1/2$. Alternatively, one can think of $A = 1/2$ as the fixed point of the

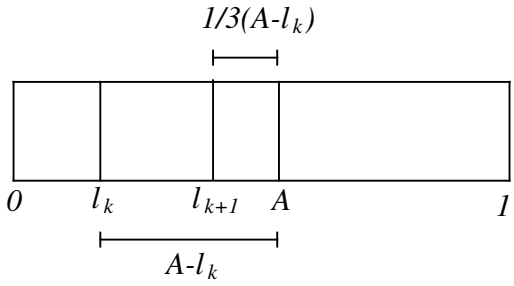

Figure 2. Folding the second crease line

transformation $T(x) = \frac{1}{3}(x+1)$. Thus, this case represents folding 1/3 of the way from the point at 1/2 of the paper to the crease line, l_k.

For an arbitrary base b, if

$$l_{k+1} = \frac{1}{b}(l_k + c_k) = \frac{c_k}{b-1} - \frac{1}{b}\left(\frac{c_k}{b-1} - l_k\right),$$

the folding algorithm is to fold $1/b$th of the way from $A_k = c_k/(b-1)$ to l_k. As a consequence, using this method requires being able to fold $1/b$ and $1/(b-1)$.

Our last step is to construct a folding algorithm that does not require the base b representation of $\frac{1}{n}$ to determine the c_k. Recall that the instructions for the Fujimoto approximation technique specify which way to fold based on the parity of nl_k, or equivalently, $c_k \equiv nl_k \mod 2$. In the general case, we're hoping for a similar condition on the numerator $L_k = nl_k$, presumably mod b, to specify the folding action. From Equation (1) we have $bL_{k+1} = L_k + nc_k$. All terms in this equation are integers, so we may reduce mod b to obtain $L_k \equiv -nc_k \mod b$ and $c_k \equiv (-n)^{-1}L_k \mod b$ since $\gcd(n,b) = 1$. Moreover, since $0 \le c_k < b$, c_k is exactly equal to $(-n)^{-1}L_k$ reduced mod b.

Thus, if $\gcd(n,b) = 1$, the generalized algorithm for folding $1/n$th of the paper using a base b technique is as follows:

1. Guess where $1/n$th of the paper is and make a pinch mark there.
2. Find the fold point by computing $c_k \equiv (-n)^{-1}L_k \mod b$ and mark $A_k = c_k/(b-1)$.
3. Fold $1/b$th of the way from A_k to l_k.
4. Repeat Steps 2 and 3 until return to $l_k = \frac{1}{n}$.
5. Repeat Steps 2–4 until there is no noticeable difference in the approximation for $\frac{1}{n}$.

k	$L_k = nl_k$	$c_k = L_k \mod 3$	$A_k = \frac{c_k}{2}$	$l_{k+1} = \frac{1}{b}(l_k + c_k)$
1	1	$1 \mod 3 = 1$	$1/2$	$\frac{2}{5}$
2	2	$2 \mod 3 = 2$	$2/2 = 1 = \text{RHS}$	$\frac{4}{5}$
3	4	$4 \mod 3 = 1$	$1/2$	$\frac{3}{5}$
4	3	$3 \mod 3 = 0$	$0/2 = 0 = \text{LHS}$	$\frac{1}{5}$

Table 1. Finding the fold points.

Note that Step 2 and Step 3 may require an additional folding algorithm such as the Fujimoto approximation technique. We illustrate with $\frac{1}{5}$ to clarify. Since $(-n)^{-1} \mod b = (-5)^{-1} \mod 3 = 1$, we have $c_k \equiv L_k \mod b$. First, as in the binary case, we make a guess pinch mark for $\frac{1}{5} = l_1$. In Table 1 we show the necessary calculations to compute the fold points for the rest of the algorithm. To get the second crease we fold 1/3 of the way from a point at 1/2 of the paper to $\frac{1}{5}$. This produces a crease line at $l_2 = \frac{2}{5}$. To form the third crease line we fold 1/3 of the way between the right side of the paper and l_2 since $A_2 = 1$. For the fourth crease line we fold 1/3 of the way from $A_3 = \frac{1}{2}$ to the third crease line l_3. For the fifth crease line we fold 1/3 of the way from the left side of the paper ($A_4 = 0$) to l_4. At this point we will have a new more accurate pinch mark for $\frac{1}{n} = l_1$, and the process can be repeated as necessary. The error decreases even faster than in the Fujimoto approximation technique since, assuming we can fold into $b$ths accurately, the error will decrease by a factor of $\frac{1}{b}$ each time we fold into $b$ths.

5 Conclusion

It is quite a bit easier to fully divide a piece of paper into $n$ths when the Fujimoto approximation technique produces crease lines at all multiples of n. Many origami fans have probably wondered why this does or doesn't work for their favorite n. We now have several different viewpoints from which to examine n to see if there will be a complete Fujimoto division. The modular arithmetic method may be an easier way for many people to understand how this algorithm works mathematically and to determine the number of crease lines that will be produced for any odd n. The connection between this new modular arithmetic analysis and previous binary analysis led to a generalized Fujimoto technique. There are cases where this new technique will work better for completely dividing a paper into $n$ths. For example, if $n = 7$, the standard Fujimoto technique did not produce crease lines at all multiples of n. However, if we use the base 3 method instead

it will produce crease lines at all multiples of n since powers of 3 generate all elements mod 7. It requires adding a pinch mark at 1/2 of the paper, folding in thirds instead of halves, and performing some mod 3 calculations along the way, but it is still possible that this may be a useful folding algorithm in some cases. At the very least the mathematical algorithm is quite intriguing and provides an interesting application for expressing numbers in alternate bases.

Bibliography

[1] J. Brunton. "Mathematical Exercises in Paper Folding: I." *Mathematics in School* 2:4 (1973), 25–26.

[2] S. Fujimoto and M. Nishiwaki. *Sōzō Suru Origami Asobi e no Shōtai* (An Invitation to Creative Origami Play, in Japanese). Osaka, Japan: Asahi Culture Center, 1982.

[3] G. H. Hardy and E. M. Wright. *The Theory of Numbers*, Third edition. Oxford, UK: Oxford University Press, 1956.

[4] R. J. Lang. "Four Problems III." *British Origami* 132 (1988), 7–11.

[5] R. J. Lang. "Origami Approximate Geometric Constructions." In *Tribute to a Mathemagician*, edited by Barry Cipra, Erik D. Demaine, Martin L. Demaine, and Tom Rodgers, pp. 223–239. Wellesley, MA: A K Peters, 2004.

[6] T. Veenstra. "Can Origami Compute the Order of Elements mod n?" Preprint, 2009.

On the Fish Base Crease Pattern and Its Flat Foldable Property

Hideaki Azuma

1 Introduction

This is an introductory approach to apply conic sections—in particular, ellipses—to the composition of flat foldable origami crease patterns. Although many studies have been reported on origami bases (see, e.g., [5]), it seems that few articles treat objects using the methods of projective geometry. So we hope that this short article will provide a little hint for people studying or teaching the mathematical aspects of origami.

Mathematical terms, definitions, and several fundamental propositions or theorems without proof in this article are primarily quoted from two books: one by Honsberger [4] (its cover illustration in fact displays the property of isogonal conjugates in a triangle) and another edited by Iwata [6] (in Japanese—the work by Coxeter-Greitzer [2] is a good alternative in English). Technical terms on the topological graph theory are those used in the monograph by Gross-Tucker [3]. In addition, the website *MathWorld* [8] will be useful for looking up mathematical terms used in this article.

In this paper, the phrase *(generalized) fish base crease pattern* will denote not only the well-known traditional fish base but also the pattern that is composed of segments on an appropriate quadrilateral domain that is topologically equivalent to the traditional base as a *planar graph*. Figure 1 shows three examples of such a fish base crease pattern: the traditional crease pattern (left), its flat foldable deformation (center), and a non-flat foldable one (right); each of these is defined on a square domain.

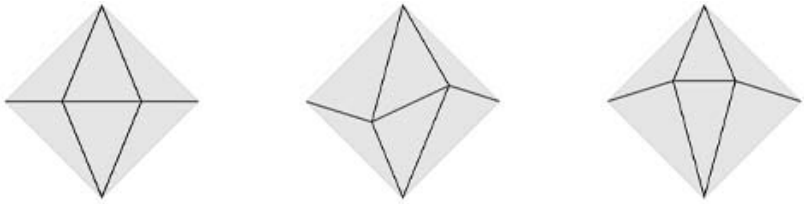

Figure 1. Three equivalent graphs of the fish base crease pattern.

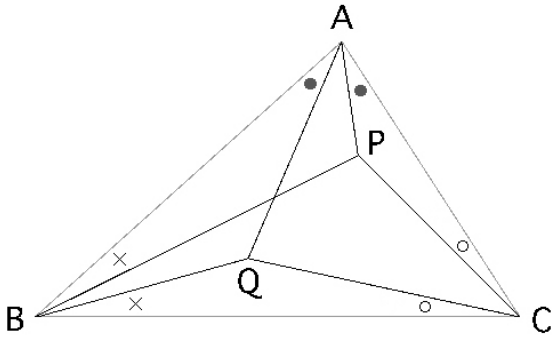

Figure 2. Isogonal conjugates P and Q in $\triangle ABC$.

2 Basic Facts and Results

2.1 Isogonal Conjugates

For any triangle ABC, the following statement is satisfied:

> If lines through A, B, and C are concurrent at P, then the isogonal lines are concurrent at a point Q. [4, p. 53]

The two points P and Q so defined are called *isogonal conjugates* (Figure 2). The angular relations with isogonal conjugates P and Q in $\triangle ABC$ are as follows:

$$\angle PAC = \angle QAB, \quad \angle PBA = \angle QBC, \quad \angle PCA = \angle QCB.$$

2.2 Inellipse of a Triangle

A key relation between isogonal conjugates and conic sections within a triangle is the following:

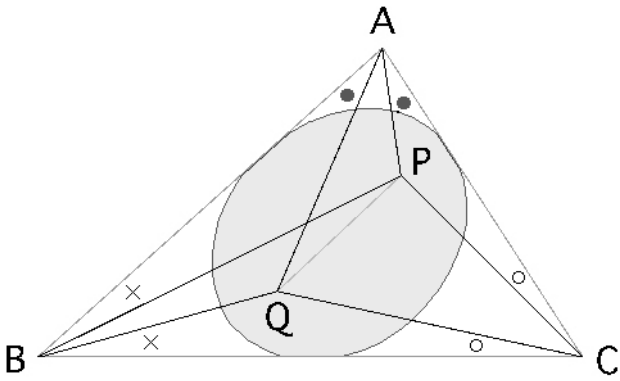

Figure 3. Isogonal conjugates P and Q are foci of an inellipse.

> Two isogonal conjugate points of any $\triangle ABC$ are the two foci of a central conic inscribing $\triangle ABC$ [6, p. 391]

(translated from the original Japanese). See Figure 3.

The *central conic* must be an *ellipse* or a *hyperbola* [8]. Notice that every triangle has inellipses for which the foci are found inside the triangle, and note that any triangle can be regarded as a degenerate hexagon whose three diagonals are concurrent, so that *Brianchon's theorem*—which guarantees the existence of (infinitely many) ellipses inscribing the triangle—will be applicable to it [2, pp. 77–79].

2.3 Apollonius' Result on Conic Sections

Apollonius' theorem for central conics provides angular relations between segments/rays concurrent at those respective foci:

> Let P be a point outside of a fixed central conic, and draw two tangents PT and PT' (i.e., thus T and T' are tangential points on the conic), and let F and F' be the two foci of the central conic. Then, the angle formed by PT and PF is equal to the angle formed by PT' and PF': $\angle TPF = \angle T'PF'$. Moreover, PF bisects $\angle TFT'$ and PF' bisects $\angle TF'T'$ [6, p. 391]

(translated from the original Japanese). See Figure 4. Consider a triangle ABC and let P and Q be foci of its inellipse (so that these are isogonal conjugates of $\triangle ABC$). Denote the three tangential points on the circumscribing $\triangle ABC$ by D, E, and F as in Figure 5. Three angular equations

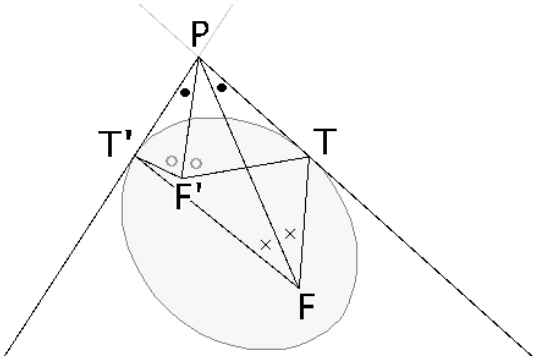

Figure 4. In the case of the ellipse.

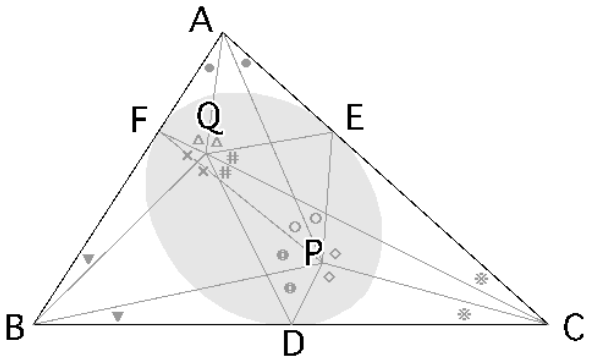

Figure 5. Angular relations with isogonal conjugates.

given by Apollonius' theorem for the six segments: PA, PF, PB, PD, PC, and PE at P are as follows:

$$\angle APF = \angle APE, \quad \angle BPF = \angle BPD, \quad \angle CPD = \angle CPE.$$

Since $\angle APF + \angle BPF + \angle BPD + \angle CPD + \angle CPE + \angle APE = 2\pi$, the equations

$$\angle APF + \angle BPD + \angle CPE = \angle APE + \angle BPF + \angle CPD = \pi$$

are obtained. Namely, the six concurrent segments PA, PF, PB, PD, PC, and PE satisfy *Kawasaki's flat foldable conditions* [7] at P.

In the same way, three angular equations for the six segments QA, QF, QB, QD, QC, and QE at Q may be written as

$$\angle AQF = \angle AQE, \quad \angle BQF = \angle BQD, \quad \angle CQD = \angle CQE.$$

Also those segments satisfy Kawasaki's flat foldable conditions at Q:

$$\angle AQF + \angle BQD + \angle CQE = \angle AQE + \angle BQF + \angle CQD = \pi.$$

Because of the arrangement of these six angles around each focus, the following flat foldable conditions, each applying to four segments/rays, are satisfied at P:

$$\angle APE + \angle BPC = \angle APB + \angle CPE = \pi \text{ with } AP, BP, CP, EP,$$
$$\angle APF + \angle BPC = \angle APC + \angle BPF = \pi \text{ with } AP, BP, CP, FP,$$
$$\angle BPD + \angle CPA = \angle CPD + \angle APB = \pi \text{ with } AP, BP, CP, DP,$$

and at Q:

$$\angle AQE + \angle BQC = \angle AQB + \angle CQE = \pi \text{ with } AQ, BQ, CQ, EQ,$$
$$\angle AQF + \angle BQC = \angle AQC + \angle BQF = \pi \text{ with } AQ, BQ, CQ, EQ,$$
$$\angle BQD + \angle CQA = \angle CQD + \angle AQB = \pi \text{ with } AQ, BQ, CQ, EQ.$$

Each of these angular relations with its crease pattern indicated by symbols/characters in Figure 5 can be applied to determine a flat foldable crease pattern on a symmetrical quadrilateral domain $ABCB'$ as shown in Figure 6: namely, a generalized fish base crease pattern.

The angular equations that relate to the segments/rays that are concurrent at P or Q in Figure 6 describe vertex-wise flat foldability and give rise to total flat foldability on the entire figure, thanks to the shapes of the defined domain and its crease pattern(s).

The flat foldable condition at P with the four segments PA, PB, PC, and PQ' is given by

$$\angle APB + \angle CPQ' = \angle APQ' + \angle BPC = \pi,$$

while the condition at Q' with the segments $Q'A$, $Q'B'$, $Q'C$, and $Q'P$ is

$$\angle AQ'B' + \angle CQ'P = \angle AQ'P + \angle B'Q'C = \pi.$$

Hence, the crease pattern we have composed here satisfies flat foldability at both P and Q simultaneously. Three local systems of the pattern each consists of two segments at respective vertices A $(= A')$, B $(= B')$, and C $(= C')$; those systems, formed in the folding at the same time, are also flat

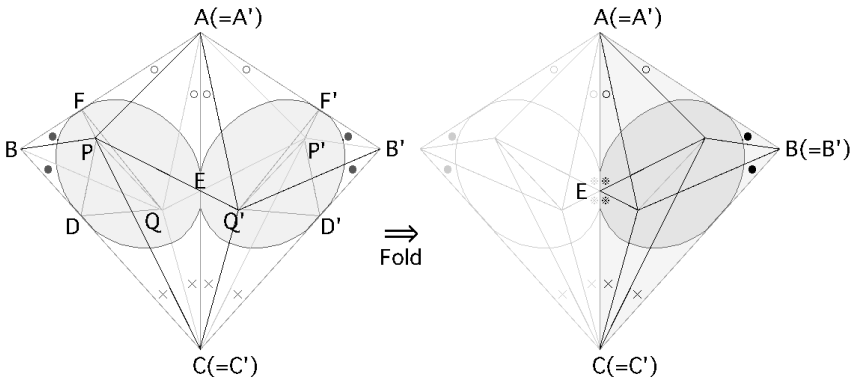

Figure 6. A kite $ABCB'$ consists of two triangles: $\triangle ABC \equiv \triangle A'B'C'$.

foldable. Therefore, thanks to the isogonal conjugate relations at vertices, the generalized fish base pattern is totally flat foldable.

The other crease pattern is also totally flat foldable, since its structure, as mentioned above, is given by the reflection of the flat foldable pattern in the diagonal AC (see Figure 6).

Thus we can sum up these arguments as follows:

Proposition 1. *A generalized fish base crease pattern defined on a quadrilateral domain is flat foldable if and only if the following two conditions hold:*

1. *Its quadrilateral domain is mirror symmetric, so that one of its diagonals is the axis of symmetry itself (that is, the quadrilateral is divided into two congruent triangles that are symmetric about one of its diagonals; see the quadrilateral on the left side of Figure 6).*

2. *When the symmetrical quadrilateral is folded in a triangle along that diagonal, its axis of symmetry, then two vertices of degree 4 in the generalized fish base defined on the quadrilateral will coincide with isogonal conjugates (i.e., the foci of an appropriate inellipse of the triangle; see the inellipsed triangle on the right side of Figure 6).*

We may call such a quadrilateral with an axis of mirror symmetry a *kite*, for simplicity.

If both vertices of degree 4 coincide with the same point of the triangle as those that are folded in, then that point must be the incenter of the triangle. Also the vertices must be respective incenters of two mirror-symmetric triangles that compose the quadrilateral domain. An example of this case, called *Incenter-Incenter*, is shown on the left in Figure 7.

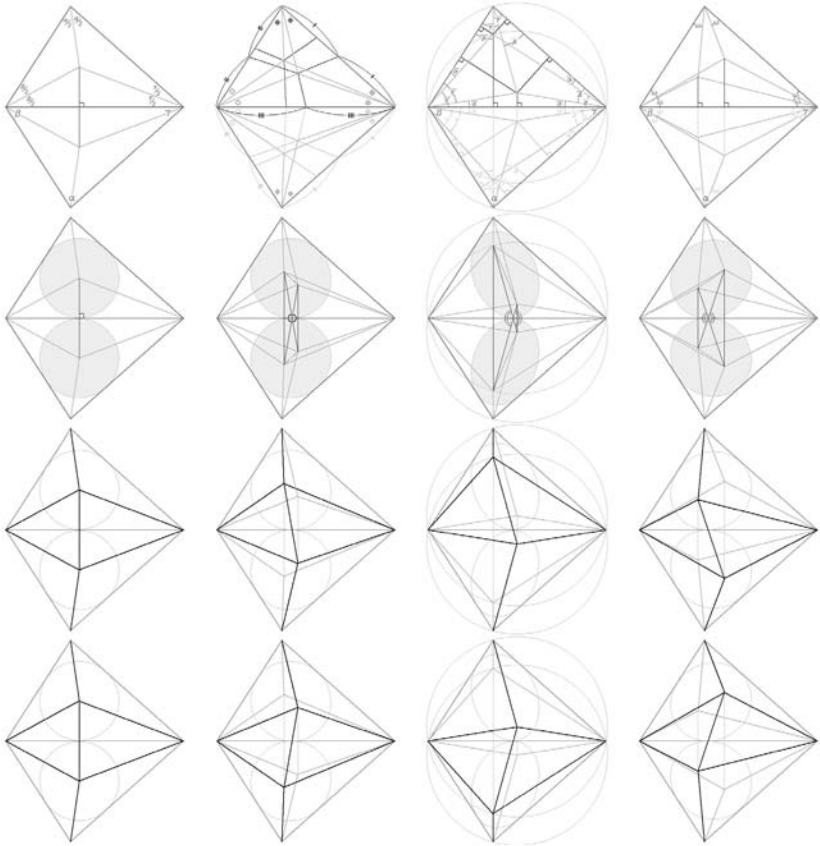

Figure 7. Triangle centers in isogonal conjugates.

Proposition 2. *For any flat foldable generalized fish base crease pattern and its quadrilateral domain, it is possible to deform the given crease pattern smoothly and continuously over the domain while maintaining its flat foldability.*

Both of these propositions demonstrate that the flat foldability of the crease pattern that we have introduced here is an invariant characteristic property in projective geometry. A deformation of an ellipse and its circumscribing polygon by a nondegenerate linear transformation of the two-dimensional Euclidean plane does not always preserve those shapes or values of angles, but the angular relations as described in Apollonius' theorem—which was introduced at the beginning of this section—will be preserved for corresponding foci, vertices, edges, and segments.

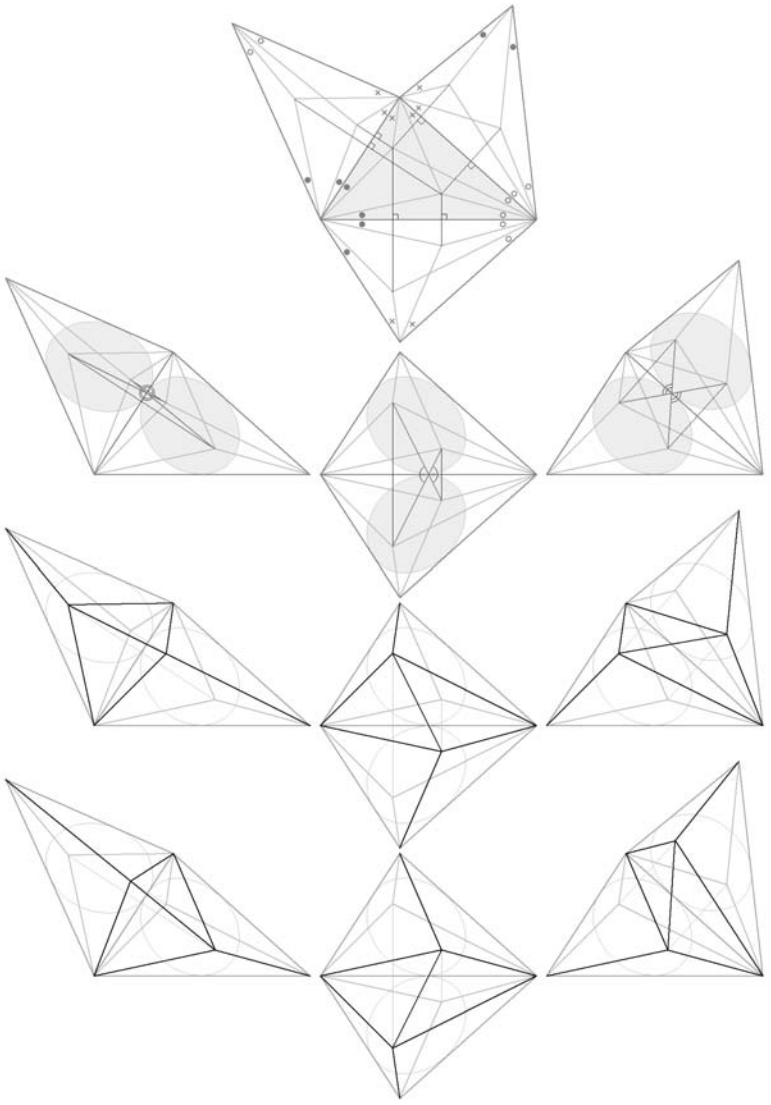

Figure 8. Three arrangements into kites.

3 In Variations

3.1 Three Kites in Composition

Three convex and symmetrical quadrilaterals consisting of the same pair of acute triangles in different arrangements are displayed in Figure 8. Usu-

ally, each admits two generalized flat foldable fish base crease patterns; both crease patterns are defined on a quadrilateral and can be turned over each other by reflection in the symmetrical axis of the quadrilateral (which is one of its diagonals). The discussion about such crease patterns can be developed into further results by systematic approaches: other cases (e.g., with nonconvex/concave symmetrical quadrilaterals, variations on a generalized bird base) will be found in the articles at [1].

3.2 Four Patterns Composed from Triangle Centers

Four generalized fish base crease patterns with different isogonal conjugate relations on the congruent convex quadrilaterals are shown in Figure 7. Each of those will be flat foldable via the traditional paper-folding process. Basic crease patterns with characters/symbols for indicating geometric relations are at the top; inellipsed crease patterns are next; then the two flat foldable patterns of creases, each determined by the corresponding basic pattern, are presented in the bottom two rows. Pairs of isogonal conjugate points may be identified as follows: from left to right, *Incenter-Incenter* (this type corresponds to the traditional fish base and is composed by bisecting angles), *Triangle Centroid-Symmedian* [4, Chapter 7], *Orthocenter-Circumcenter*, and *Brocard Points* [4, Chapter 10].

Acknowledgment. The author gratefully thanks Robert J. Lang for helpful suggestions on the manuscript.

Bibliography

[1] Hideaki Azuma. *Many Folds in Variety.* Available at http://fine.ap.teacup.com/foldings/, 2008.

[2] H. S. M. Coxeter and S. L. Greitzer. *Geometry Revisited.* Washington, DC: Mathematical Association of America, 1967.

[3] J. L. Gross and T. W. Tucker. *Topological Graph Theory.* New York: John Wiley & Sons, Inc., 1987.

[4] R. Honsberger. *Episodes in Nineteenth and Twentieth Century Euclidean Geometry.* Washington, DC: Mathematical Association of America, 1995.

[5] T. Hull (ed.). *Origami^3: Proceedings of the Third International Meeting of Origami Science, Mathematics, and Education.* Natick, MA: A K Peters, 2002.

[6] S. Iwata (ed.). *Kikagaku Daijiten* (Encyclopedia of Geometry, in Japanese), Vol. 1. Tokyo: Maki Shoten, 1971.

[7] T. Kawasaki. "On Relation between Mountain-Creases and Valley-Creases of a Flat Origami." In *Proceedings of the First International Meeting of Origami Science and Technology*, edited by H. Huzita, pp. 229–237. Padova, Italy: Dipartimento di Fisica dell'Università di Padova, 1991.

[8] Wolfram Research. *MathWorld*. Available at http://mathworld.wolfram.com/, 2009.

Orizuru Deformation Theory for Unbounded Quadrilaterals

Toshikazu Kawasaki and Hidefumi Kawasaki

1 Introduction

We usually fold an *orizuru* (the traditional origami crane) from square paper, but square paper is not strictly required. It is also easy to fold an orizuru from any *kite shape*, i.e., a quadrilateral with reflection symmetry about one of the diagonals. However, if in such a kite shape, we choose point O as in Figure 1 as the center of the orizuru (where *the center of orizuru* means the vertex on the orizuru's back), then we get a nonsymmetric orizuru.

Husimi [1] found a method to fold a symmetric orizuru from any kite shape. He took point H in Figure 1 as the center of orizuru. Point H is the point of incidence of two circles tangent to the edges of the quadrilateral and to the line of symmetry.

Justin [2] extended the Husimi deformation to apply to non-reflection-symmetric quadrilaterals. He proved that one can fold a head-wing interchangeable orizuru (see Definition 1) from a quadrilateral if and only if the quadrilateral has an inscribed circle. He chose the intersection of two hyperbolas as the center of orizuru, as shown in Figure 2. One passes through points A and C with foci B and D. The other passes through B and D with foci A and C. Point J exists if and only if the quadrilateral has an inscribed circle. If it does, we call point J the *center of the quadrilateral*.

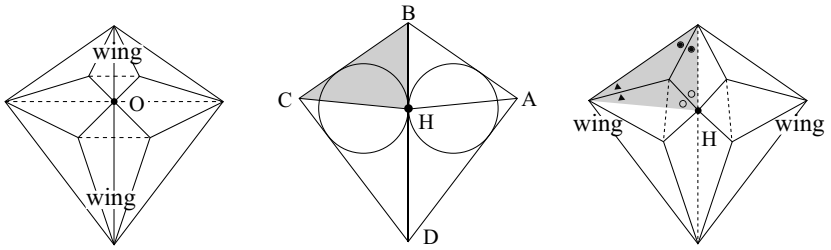

Figure 1. The Husimi deformation.

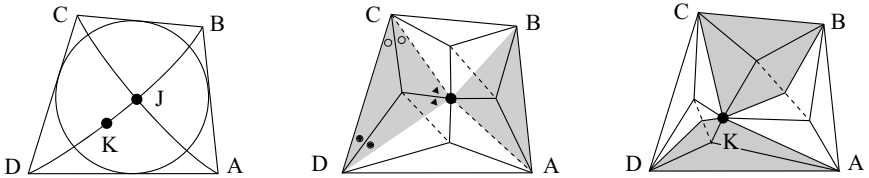

Figure 2. The Justin deformation (middle) and the Kawasaki deformation (right) of a starting position (left).

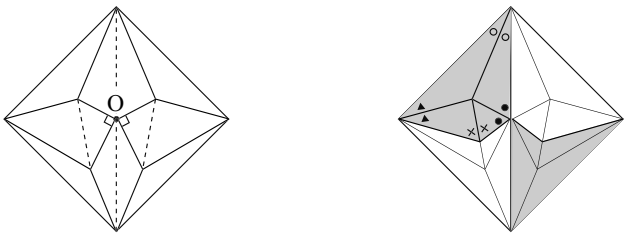

Figure 3. The Maekawa deformation.

Maekawa found a still new type of orizuru; see Figure 3. Even if we apply the Maekawa deformation to the square, it is different from Justin's construction, because Justin's theory is based on triangulation of the paper, while the Maekawa deformation creates a quadrilateral partition—compare the shaded regions in Figures 2 and 3.

One of the authors [4,5] proposed an orizuru deformation theory based on a quadrilateral partitioning that includes the Maekawa deformation. Moreover, it can deal with head-wing noninterchangeable orizurus. He proved that one can fold a not-necessarily-head-wing-interchangeable orizuru from a quadrilateral if and only if it has an inscribed circle. Further, he proved that it is enough to take any point on either of two hyperbolas as the center of the orizuru.

The aims of this paper are to extend the orizuru deformation theory to *unbounded* quadrilaterals and to show that we need other conic sections—namely, parabolas and ellipses—to define the center.

This paper is organized as follows. In Section 2, we describe our notations and definitions. In Section 3, we illustrate an unbounded orizuru from an unbounded kite shape. Section 4 is devoted to one-sided open quadrilaterals. In Section 5, we deal with the other four cases of unbounded quadrilaterals. In Section 6, we discuss foldability and head-wing interchangeability of an unbounded bird base.

2 Preliminaries

In this paper, a *fold* refers to any folded paper object. For any (finite-length) edge e, line e refers to the (unbounded) line including edge e. For any points $F,\ G \in \mathbb{R}^2$, $p \in \mathbb{R}$, and a line λ, we define the following sets:

$$\begin{aligned} E(F,G;p) &:= \{X \in \mathbb{R}^2 \mid FX + GX = p\}, \\ P(F;\lambda) &:= \{X \in \mathbb{R}^2 \mid FX = d(X,\lambda)\}, \text{ and} \\ H(F,G;p) &:= \{X \in \mathbb{R}^2 \mid FX - GX = p\}, \end{aligned}$$

in which, for example, FX denotes the distance between points F and X and $d(X,\lambda)$ denotes the distance from point X to a line λ. These sets are, respectively, an ellipse with foci F and G, a parabola with focus F and directrix λ, and a hyperbola with foci F and G. We remark that $H(F,G;0)$ becomes a line.

Definition 1. We define four terms:

- If the crease pattern in Figure 4 (middle) is flat folded such that the four edges and point K lay on a line in the fold, then we call the fold a *bird base*.
- We say that a bird base is *foldable* from $ABCD$, if there exists a crease pattern satisfying these conditions.
- We call point K and the line the *center* and the *axis* of the bird base, respectively.
- Further, we say that a bird base is *head-wing interchangeable* if it can be folded from the center crease pattern in Figure 4 and another bird base can be folded from the right one with the positions of the vertices unchanged.

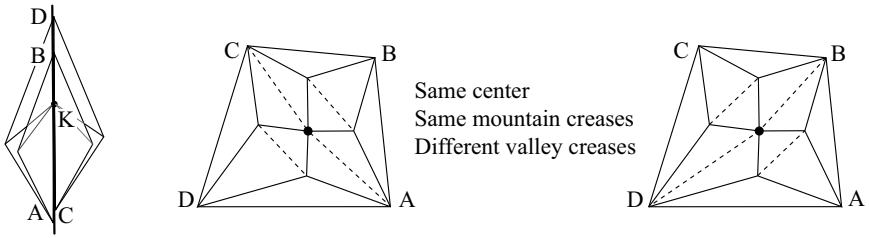

Figure 4. The center and the axis of a bird base (left), and head-wing interchangeability (middle and right).

Lemma 1. [4] *For any not necessarily convex quadrilateral, the following conditions are equivalent to each other. Further, the center of the radical creases in (a) coincides with the point in (b) and the center of the circle in (c):*

(a) The quadrilateral can be flat folded by four radial creases, one from each of the four vertices, so that the four edges of the quadrilateral lie on a common line.

(b) The bisectors of the four vertices of the quadrilateral meet at one point.

(c) The quadrilateral has an inscribed circle.

(d) The alternating sum of the lengths of the four edges taken cyclically equal zero, i.e., $l_1 - l_2 + l_3 - l_4 = 0$ *where* $l_1 \dots l_4$ *are the lengths of the four edges.*

(e) $B,\ D \in H(A, C; p)$ *for some* $p \in \mathbb{R}$.

(f) $A,\ C \in H(B, D; q)$ *for some* $q \in \mathbb{R}$.

Lemma 2. [4] *If two bounded quadrilaterals having an inscribed circle are joined along adjacent edges as in Figure 5, then the result also has an inscribed circle. Conversely, when a quadrilateral having an inscribed circle is divided into two quadrilaterals along adjacent edges, the following conditions are equivalent to each other:*

(a) The left quadrilateral has an inscribed circle.

(b) The right quadrilateral has an inscribed circle.

(c) $A,\ C,\ E \in H(B, D; p)$ *for some* $p \in \mathbb{R}$.

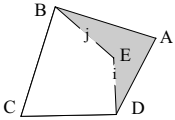

Figure 5. Join and division of quadrilaterals.

3 An Orizuru from an Unbounded Kite Shape

As was mentioned earlier, we can fold a bird base from any finite kite shape. However, we can extend this concept to unbounded shapes. The left image in Figure 6 shows an unbounded kite shape, taken as the limit of a finite shape as one of the vertices moves arbitrarily far away.

Husimi's concept works in this case. Indeed, we get a symmetric bird base having a long tail from the center crease pattern of Figure 6 and another bird base having a long wing from the right crease pattern.

We now consider the generalization of other methods of forming an orizuru. In the following sections, we have to consider five cases of unbounded quadrilaterals; see Figure 7. For brevity, we will give proofs only for case 1 in Figure 7. The proofs for the other cases follow similarly, so in the other cases, we only describe the conclusion in Section 5.

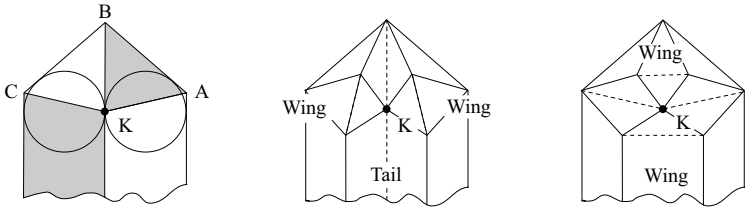

Figure 6. Two crease patterns (middle and left) for the unbounded kite shape (right).

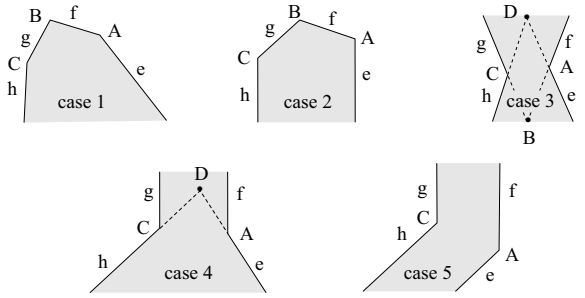

Figure 7. Five patterns of unbounded quadrilaterals.

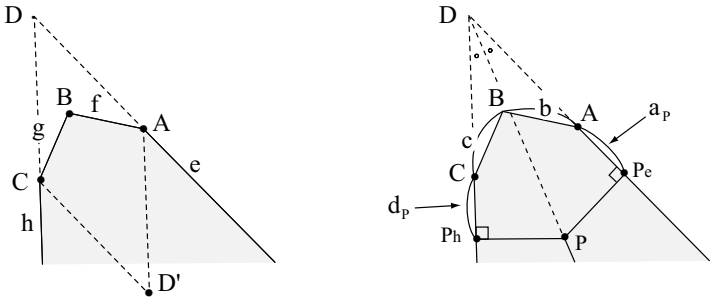

Figure 8. Constructed lines and points that define substitute edge lengths participating in the alternating sum of edge lengths.

4 One-Sided Open Quadrilaterals

The aim of this section is to extend Lemmas 1 and 2 to one-sided open quadrilaterals in which semiinfinite lines e and h have an intersection, as illustrated in Figure 8 (left), which we regard as a fourth vertex D. We define point D' so that $ADCD'$ is a parallelogram. Further, since one-sided open quadrilaterals have two edges of infinite length, we introduce a substitute for the edge length in order to extend condition (d) of Lemma 1.

Definition 2. For any point P on the bisector of D, we denote by P_e and P_h the feet of perpendiculars from P to e and h, respectively. Then, we call $a_P - b + c - d_P$ the alternating sum of edge lengths.

These new points are illustrated in Figure 8.

By suitable identification of new vertices and edges, we can show that exactly the same conditions apply as in Lemma 1.

Lemma 3. *For any one-sided open quadrilateral with nonparallel edges e and h, the following conditions are equivalent to each other. Further, the center of the radical creases in (a) coincides with the point in (b) and the center of the circle in (c):*

(a) The quadrilateral can be flat folded by four radial creases, one from each of four vertices, so that the four edges of the quadrilateral lie on a common line.

(b) Four bisectors of the four vertices meet at one point.

(c) There exists a circle that contacts four lines e, f, g, and h.

(d) The alternating sum of edge lengths equals zero.

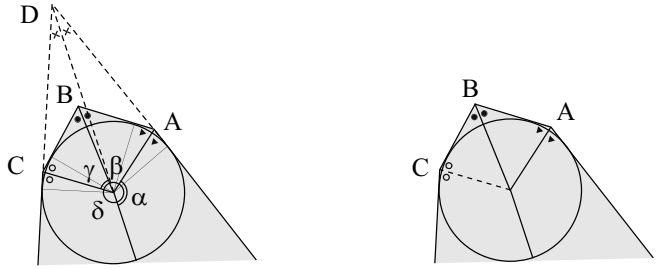

Figure 9. If four bisectors meet at one point, then $\alpha - \beta + \gamma - \delta = 0$. Hence, the quadrilateral can be flat folded by the right crease pattern.

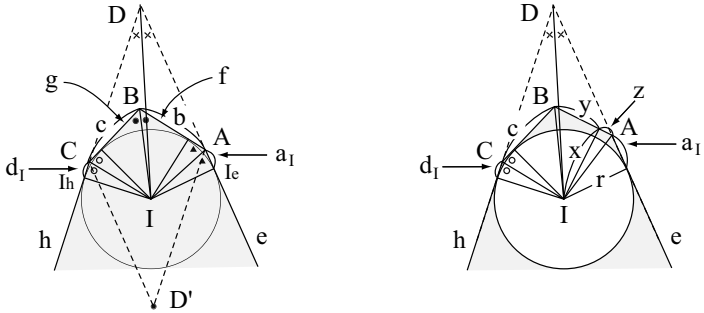

Figure 10. The existence of the inscribed circle is equivalent so that the alternating sum of edge lengths is zero.

(e) $A,\ C \in E(B, D; p)$ *for some* $p > 0$.

(f) $B,\ D' \in H(A, C; q)$ *for some* $q \in \mathbb{R}$.

Proof: (a)⇒(b) is trivial. (b)⇒(a): if four bisectors meet at one point, then, with respect to Figure 9, $\alpha - \beta + \gamma - \delta = 0$. That is, the local flat foldable condition [3] is satisfied at the point. Hence, the quadrilateral can be flat folded.

(b)⇔(c)⇒(d) are evident from Figure 10 (left) and the definition of the alternating sum of edge lengths.

(d)⇔(e)⇔(f): the alternating sum of edge lengths is zero if and only if $(I_eD - AD) - AB + BC - (I_hD - CD) = 0$. Since $I_eD = I_hD$, the latter is equivalent to $AD + AB = CB + CD$, which implies (e). Further (e) is expressed as $BA - BC = DC - DA = D'A - D'C$, where the second equality follows from the definition of D', which implies (f). (d)⇒(c): we may assume that a circle contacts e, g, and h without loss of generality.

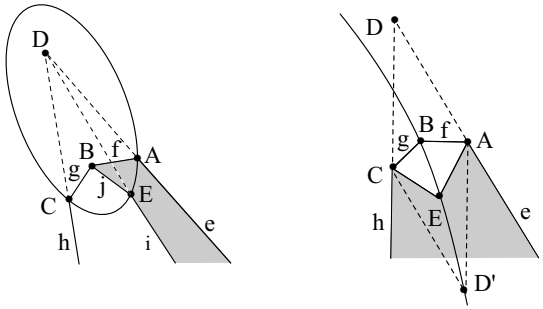

Figure 11. Vertical and horizontal joins and divisions.

Define x, y, z, and r as in Figure 10 (right). Then, by the Pythagorean theorem, $x^2+y^2 = r^2+(c-d_I)^2$, $x^2+z^2 = r^2+(a_I)^2$, and $y+z = b$. Solving these equation, we get $x = r$. Therefore, the circle contacts edge f. □

Lemma 4 (Vertical join and division). *If two one-sided open quadrilaterals having an inscribed circle are joined along two adjacent edges i and j as in Figure 11 (left), where lines e, h, and i are assumed to meet at a point, then the result also has an inscribed circle. Conversely, when a one-sided open quadrilateral $efgh$ having an inscribed circle is divided into two quadrilaterals along two edges i and j, where line i is assumed to pass through point D, the following conditions are equivalent to each other:*

(a) The left quadrilateral has an inscribed circle.

(b) The right quadrilateral has an inscribed circle.

(c) A, C, $E \in E(B, D; p)$ for some $p > 0$.

Proof: Since quadrilateral $efgh$ has an inscribed circle, A, $C \in E(B, D; p)$ for some $p > 0$ by Lemma 3. Also by Lemma 3, condition (a) is equivalent to C, $E \in E(B, D; q)$ for some $q > 0$. Condition (b) is equivalent to E, $A \in E(B, D; r)$ for some $r > 0$. Hence when either (a) or (b) holds, we get $p = q = r$ and the other two conditions immediately follow. □

Lemma 5 (Horizontal join and division). *If two quadrilaterals having an inscribed circle, one being bounded and the other being one-sided open, are joined along two adjacent edges i and j as in Figure 11 (right), then the result also has an inscribed circle. Conversely, when a one-sided open quadrilateral $efgh$ having an inscribed circle is divided into two quadrilaterals along two edges i and j as in Figure 11 (right), then the following conditions are equivalent to each other:*

pattern	parallel edges	vertical	horizontal
bounded	none	$A, C, E \in H(B, D; p)$	$B, D, E \in H(A, C; q)$
case 1	none	$A, C, E \in E(B, D; p)$	$B, D', E \in H(A, C; q)$
case 2	one pair	$A, C, E \in P(B, \lambda)$	$B, D, E \in H(A, C; q)$
case 3	none	$A, C, E \in H(B, D; p)$	$B', D', E \in H(A, C; q)$
case 4	one pair	$A, C, E \in P(D, \lambda)$	$D', E \in H(A, C; q)$
case 5	two pairs	$A, C, E \in$ line	$E \in H(A, C; q)$

Table 1. This table summarizes lemmas corresponding to Lemmas 3–5 in the bounded case and five unbounded patterns.

(a) The upper bounded quadrilateral has an inscribed circle.

(b) The lower one-sided open quadrilateral has an inscribed circle.

(c) B, D', $E \in H(A, C; p)$ *for some* $p \in \mathbb{R}$.

Proof: By Lemma 3, the whole quadrilateral has an inscribed circle if and only if B, $D' \in H(A, C; p)$ for some $p \in \mathbb{R}$, and the lower one has an inscribed circle if and only if D', $E \in H(A, C; q)$ for some $q \in \mathbb{R}$. By Lemma 1, the upper quadrilateral has an inscribed circle if and only if B, $E \in H(A, C; r)$ for some $r \in \mathbb{R}$. Our assertions follow. □

5 The Other Four Patterns

In this section, we deal with cases 2–5 in Figure 7. When the quadrilateral has a pair of parallel edges, we regard the center line between them as a bisector, and define the alternating sum of edge lengths as well as the equivalent of Definition 2.

Table 1 summarizes Lemmas 3–5 in the bounded case and five unbounded patterns. For example, by replacing "A, C, $E \in E(B, D; p)$" with the condition of the third column, we obtain the lemma corresponding to Lemma 4.

6 Foldability

We now expand on some items previously defined in Definition 1.

Definition 3. We say that a bird base is *foldable* from a given unbounded quadrilateral if the following three conditions are all satisfied:

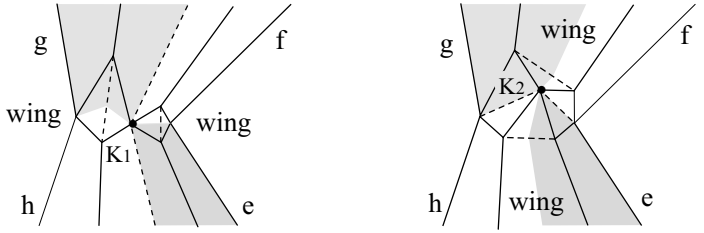

Figure 12. Two kinds of unbounded crease patterns.

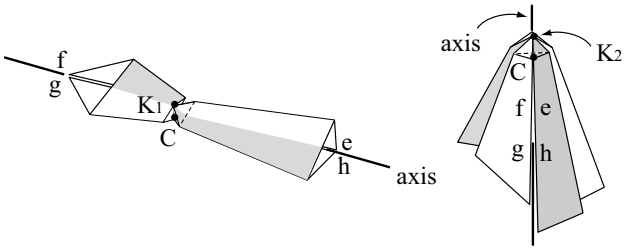

Figure 13. Two kinds of unbounded bird bases.

- The quadrilateral is divided into four quadrilaterals as in Figure 12.
- Either of the crease patterns in Figure 12 is flat folded.
- All edges of four quadrilaterals lie on a line when folded as in Figure 13.

Then we call the fold a *bird base*, point K_i $(i = 1, 2)$ the *center*, and the line the *axis*. When $K_1 = K_2$ and we can fold a bird base from both crease patterns in Figure 12, we say that each bird base is *head-wing interchangeable*.

Definition 4. For any quadrilateral having an inscribed circle, we call the intersection of the quadratic curves in the third and fourth columns of Table 1 the *center* of the quadrilateral. For example, in case 1, the center is the intersection of the ellipse and the hyperbola.

Theorem 1. *A bird base is foldable from a given quadrilateral if and only if it has an inscribed circle. Then the center of the bird base lies on the quadratic curve specified in Table 1. Furthermore, if we choose the center of the quadrilateral as the center of the bird base, then we get a head-wing interchangeable bird base.*

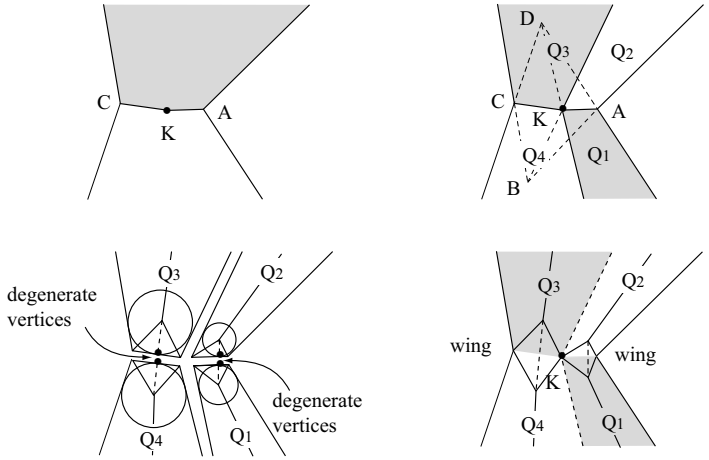

Figure 14. A procedure to design a crease pattern of a bird base.

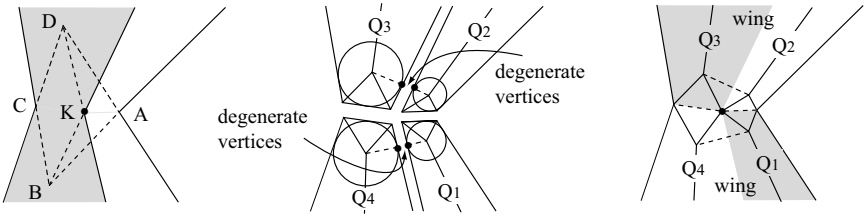

Figure 15. A head-wing interchangeable bird base.

Proof: We give a proof only for case 3. Assume that the quadrilateral has an inscribed circle. Take any point K on the quadratic curve in the fourth column of Table 1 as the center of the bird base. Next, horizontally divide the quadrilateral along polygonal line AKC as in Figure 14 (upper left). Then both quadrilaterals also have an inscribed circle. Further, divide each quadrilateral along line KB and KD, respectively, as in Figure 14 (upper right). Then the four results $Q_i\,(i = 1, 2, 3, 4)$ also each have an inscribed circle. Hence each Q_i is flat folded by its four bisector creases, and its edges lie on a line (see Figure 14, lower left), where we note that each Q_i has a degenerate vertex whose angle is π, so that its bisector is perpendicular to the edge. Joining these four folds along the axis, we get a bird base. Since the converse is easily proved, we omit the proof.

When we take as the center of the bird base the center of the quadrilateral, starting with vertical division in Figure 15 (left), we similarly get four quadrilaterals having an inscribed circle. Then we obtain another

crease pattern, Figure 15 (right). Therefore, the bird base is head-wing interchangeable. □

The proofs of the remaining cases follow similarly.

Bibliography

[1] K. Husimi and M. Husimi. *Geometry of Origami* (in Japanese). Tokyo: Nippon Hyoronsha, 1979.

[2] J. Justin. "Mathematical Remarks about Origami Bases." *Symmetry: Culture and Science* 5:2 (1994), 153–165.

[3] K. Kasahara. *Top Origami* (in Japanese). Tokyo: Sanrio, 1985.

[4] T. Kawasaki. "Expansion and Their Applications of Systematic Compositions of Cell Decompositions of Flat Origami—Theory of Deformations of Orizuru." *Research Report of Sasebo College of Technology* 32 (1995), 29–58.

[5] T. Kawasaki. *Roses, Origami, and Mathematics* (in Japanese). Tokyo: Morikita Publishers, 1998.

A Crystal Map of the Orizuru World

Toshikazu Kawasaki

1 Introduction

We usually fold the *orizuru* (traditional Japanese origami crane) from square paper. However, it is possible to fold orizurus from many kinds of quadrilaterals [1–7]. It is known that an orizuru is foldable from a quadrilateral if and only if the quadrilateral has an inscribed circle (see previous paper). So we may regard the set of quadrilaterals with an inscribed circle as the *orizuru world* (the set of orizurus). The aim of this paper is to present a map of the orizuru world, which, rather pleasingly, takes the form of a crystal.

2 Notation

We denote by $\mathbf{O}$, $\mathbf{Q}$, $\mathbf{R}^3$, and $\mathbf{R}^4$, respectively, the set of all deformed orizurus (see Figure 1), the set of all quadrilaterals with inscribed unit circles (Figure 2), the three-dimensional real space, and the four-dimensional real space. Since the deformed orizurus *must* be folded from quadrilaterals with inscribed circles, we identify $\mathbf{Q}$ with $\mathbf{O}$.

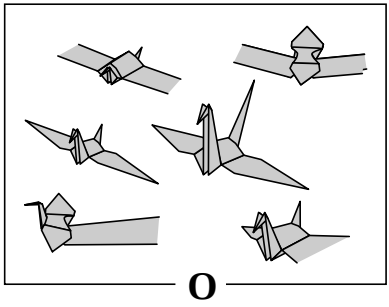

Figure 1. Some representative deformed orizurus. **O** is the set of all such deformed orizurus.

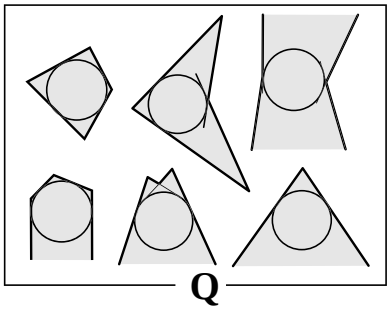

Figure 2. Some representative quadrilaterals with inscribed unit circles.

3 Representation

First of all, we represent a quadrilateral with an inscribed circle as a point in $\mathbf{R}^4$.

Definition 1. For any quadrilaterals $\mathbf{q}$, we let a_1, a_2, a_3, a_4 be the center angles of $\mathbf{q}$ and let T_i be the midpoint of the ith side of the quadrilateral where the circle touches it. We define a mapping $\mathbf{r} : \mathbf{Q} \to \mathbf{R}^4; \mathbf{r}(\mathbf{q}) = (a_1, a_2, a_3, a_4)$, as shown in Figure 3, and call it the *representation mapping*. Furthermore, we call the image $\mathbf{r}(\mathbf{q})$ the *representation* of $\mathbf{q}$.

The examples in Figure 4 show the relation between corner shape and center angle, also shown schematically in Figure 5.

Representation $\mathbf{r}(\mathbf{q}) = (a_1, a_2, a_3, a_4)$ must satisfy some conditions. Since the sum of the exterior angle for any polygon is 360, we have the first condition:

$$a_1 + a_2 + a_3 + a_4 = 360. \tag{1}$$

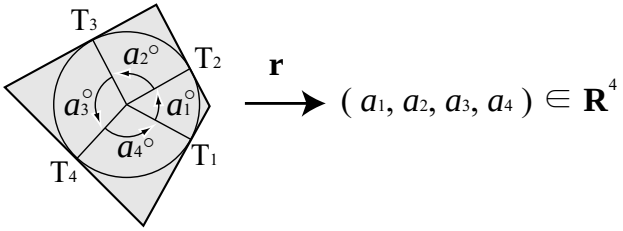

Figure 3. We define the representation mapping in this way.

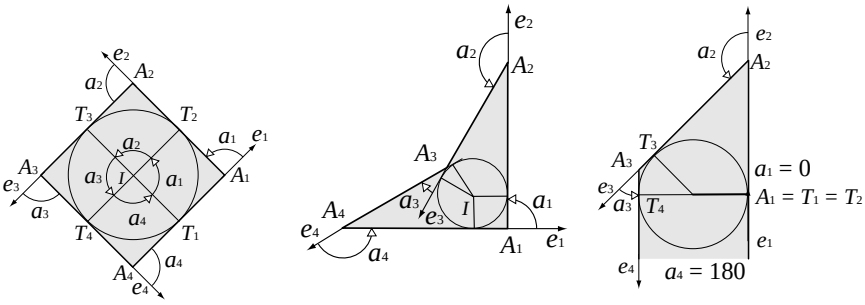

Figure 4. Illustration that the center angle is equal to the exterior angle. (a) Representation of the regular square is $(90, 90, 90, 90)$. (b) A concave quadrilateral with negative angle a_3. (c) Here, two sides of the figure are parallel and the inner angle of the vertex A_1 is 180°. Thus center angles $a_1 = 0$ and $a_4 = 180$.

Now, with respect to Figure 6(a), if the angle a_1 is not larger than -180, then the edge e_1 passes through the edge e_2. Figure 6(b) illustrates an inequality $a_1 < 360$. So we have the second condition:

$$-180 < a_i < 360. \tag{2}$$

In Figure 6(c), dotted half lines depict bisectors. Since their intersection is the center of the inscribed circle, they meet in the quadrilateral. Thus we have the third condition, that the sum of the adjacent angles a_i and a_{i+1} is positive, i.e.,

$$a_i + a_{i+1} > 0. \tag{3}$$

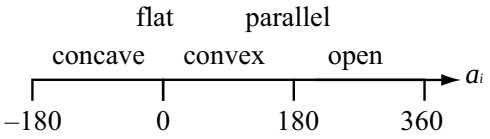

Figure 5. Relation between corner shape and center angle.

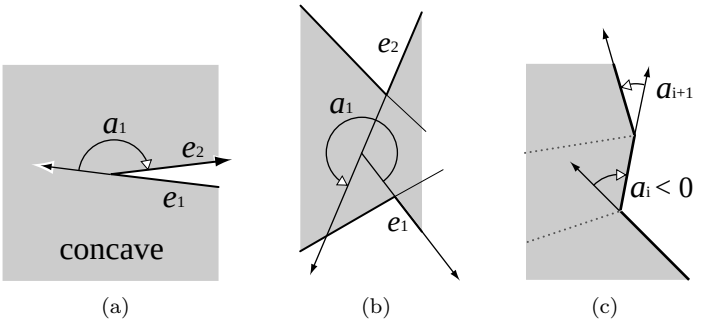

Figure 6. (a) A concave quadrilateral. (b) The angle from side e_1 to side e_2 is less than 360. (c) If $a_i + a_{i+1}$ is 0 or negative, then bisectors do not meet in the quadrilateral. Thus, $a_i + a_{i+1} > 0$.

4 Normalization

Definition 2. Normalization $\mathbf{n}$ is an affine mapping $\mathbf{n} : \mathbf{R}^4 \to \mathbf{R}^4; b_i = a_i/270 - 1/3$ and $\mathbf{n}(a_1, a_2, a_3, a_4) = (b_1, b_2, b_3, b_4)$.

Theorem 1. *The three conditions in Equations (1)–(3) and Figure 5 are transformed by normalization* $\boldsymbol{n}$ *to*

$$b_1 + b_2 + b_3 + b_4 = 0, \tag{4}$$

$$-1 < b_i < 1, \tag{5}$$

$$-2/3 < b_i + b_{i+1} < 2/3, \text{ and} \tag{6}$$

Figure 7.

Proof:

$$\begin{aligned} b_1 + b_2 + b_3 + b_4 &= (a_1 + a_2 + a_3 + a_4)/270 - 1/3 \\ &= 360/270 - 4/3 \\ &= 4/3 - 4/3 \\ &= 0. \end{aligned}$$

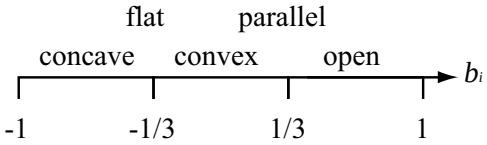

Figure 7. Relation between corner shape and center angle after normalization.

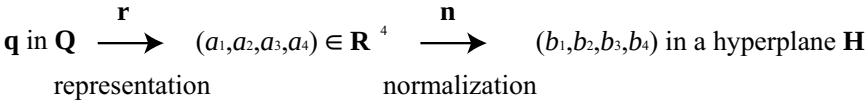

Figure 8. Transformation of a representation of a deformed orizuru into a normalized hyperplane.

$$\begin{aligned}\mathbf{n}(-180) &= -80/270 - 1/3\\ &= -2/3 - 1/3\\ &= -1.\end{aligned}$$

$$\begin{aligned}\mathbf{n}(360) &= 360/270 - 1/3\\ &= 4/3 - 1/3\\ &= 1.\end{aligned}$$

$$\begin{aligned}b_i + b_{i+1} &= a_i/270 - 1/3 + a_i/270 - 1/3\\ &= a_i + a_{i+1} - 2/3\\ &> -2/3.\end{aligned}$$

$$\mathbf{n}(-180) = -1, \quad \mathbf{n}(0) = -1/3, \quad \mathbf{n}(180) = 1/3, \quad \text{and} \quad \mathbf{n}(360) = 1.$$

Thus we have the relationship shown in Figure 7. □

Equation (4) implies that image $\mathbf{n}(\mathbf{r}(\mathbf{Q}))$ is a subset of a hyperplane in $\mathbf{R}^4$. We denote it $\mathbf{H}$. Equation (5) implies that $\mathbf{n}(\mathbf{r}(\mathbf{Q}))$ is a subset of a four-dimensional cube. (See Figure 8.)

5 Embedding

Definition 3. An *embedding* is the linear mapping

$$\mathbf{e} : \mathbf{R}^4 \to \mathbf{R}^3; \mathbf{e}(b_1, b_2, b_3, b_4) = b_1\mathbf{v}_1 + b_2\mathbf{v}_2 + b_3\mathbf{v}_3 + b_4\mathbf{v}_4,$$

where $\mathbf{v}_1 = (3/4, -3/4, -3, 4)$, $\mathbf{v}_2 = (-3/4, 3/4, -3, 4)$, $\mathbf{v}_3 = (-3/4, -3/4, 3, 4)$, and $\mathbf{v}_4 = (3/4, 3/4, 3, 4)$.

Theorem 2. *Embedding* $\boldsymbol{e}$ *restricted in* $\boldsymbol{H}$ *is injective.*

Proof: Since $\mathbf{v}_1 + \mathbf{v}_2 + \mathbf{v}_3 + \mathbf{v}_4 = (3/4, -3/4, -3/4) + (-3/4, 3/4, -3/4) + (-3/4, -3/4, 3/4) + (3/4, 3/4, 3/4) = 0$, we have that $\mathbf{v}_4 = -(\mathbf{v}_1 + \mathbf{v}_2 + \mathbf{v}_3)$. If $\mathbf{e}(b_1, b_2, b_3, b_4) = \mathbf{0}$ for (b_1, b_2, b_3, b_4) in a hyperplane $\mathbf{H}$, then $b_1\mathbf{v}_1 + b_2\mathbf{v}_2 + b_3\mathbf{v}_3 + b_4\mathbf{v}_4 = \mathbf{0}$. Thus we have

$$b_1\mathbf{v}_1 + b_2\mathbf{v}_2 + b_3\mathbf{v}_3 - b_4(\mathbf{v}_1 + \mathbf{v}_2 + \mathbf{v}_3) = \mathbf{0},$$
$$(b_1 - b_4)\mathbf{v}_1 + (b_2 - b_4)\mathbf{v}_2 + (b_3 - b_4)\mathbf{v}_3 = \mathbf{0}.$$

Since $\{\mathbf{v}_1, \mathbf{v}_2, \mathbf{v}_3\}$ are linearly independent, the coefficients $b_1 - b_4$, $b_2 - b_4$, and $b_3 - b_4$ are all 0. So we have

$$b_1 = b_2 = b_3 = b_4. \tag{7}$$

$$b_1 + b_2 + b_3 + b_4 = 0 \text{ for} (b_1, b_2, b_3, b_4) \in \mathbf{H}. \tag{8}$$

Combining Equations (7) and (8), we obtain

$$b_1 = b_2 = b_3 = b_4 = 0.$$

Thus, the restricted embedding $\mathbf{e}|_H$ is injective. □

6 Reverse Mapping

Theorem 2 allows us now to consider the reverse mapping $\mathbf{f}$ of embedding $\mathbf{e}$ (See Figure 9). For this reverse mapping, we have that

$$\begin{aligned}(x, y, z) &= \mathbf{e}(b_1, b_2, b_3, b_4)\\ &= b_1\mathbf{v}_1 + b2\mathbf{v}_2 + b3\mathbf{v}_3 + b4\mathbf{v}_4\\ &= b_1(3/4, -3/4, -3, 4) + b_2(-3/4, 3/4, -3/4)\\ &\quad + b_3(-3/4, -3/4, 3/4) + b_4(3/4, 3/4, 3/4)\\ &= 3(b_1 - b_2 - b_3 + b_4, -b_1 + b_2 - b_3 + b_4, -b_1 - b_2 + b_3 + b_4)/4.\end{aligned}$$

Since $b_1 + b_2 + b_3 + b_4 = 0$, we have the following:

Theorem 3. *For any* $\boldsymbol{e}(b_1, b_2, b_3, b_4) \in \boldsymbol{H}$,

$$(x, y, z) = \boldsymbol{e}(b_1, b_2, b_3, b_4) = -3(b_2 + b_3, b_1 + b_3, b_1 + b_2)/2. \tag{9}$$

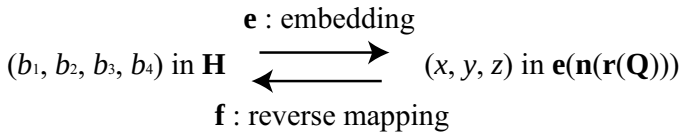

Figure 9. Embedding **e** and its reverse **f**.

Continuing on, for any point $(x, y, z) \in \mathbf{e}(\mathbf{n}(\mathbf{r}(\mathbf{Q})))$,

$$(b_1, b_2, b_3, b_4) = \mathbf{f}(x, y, z) = (x-y-z, -x+y-z, -x-y+z, x+y+z)/3. \quad (10)$$

Theorem 3 converts Theorem 2 to the following:

Theorem 4. *For any* $(x, y, z) \in \boldsymbol{e}(\boldsymbol{n}(\boldsymbol{r}(\boldsymbol{Q})))$*, each of the following is true:*

$$-3 < x - y - z < 3, \quad (11)$$
$$-3 < -x + y - z < 3, \quad (12)$$
$$-3 < -x - y + z < 3, \quad (13)$$
$$-3 < x + y + z < 3, \quad (14)$$
$$-1 < x < 1, \quad (15)$$
$$-1 < z < 1. \quad (16)$$

Proof: The proof follows from direct substitution. □

7 Crystal Map of the Orizuru World

Equations (11)–(16) determine a solid with 12 faces. We denote it **C**. Each point within **C** represents a deformed orizuru. Equations (15) and (16) imply that **C** is a subset of a quadratic prism. Inequality (11) determines a domain that lies between parallel planes. The other inequalities are similar to (11). So, we end up with the solid shown in Figure 10. It looks like a crystal. We call it the *crystal map of the orizuru world* **C**.

Where do we find the traditional orizuru within **C**? The traditional orizuru is folded from a regular square and maps to the point $\mathbf{e}(\mathbf{n}(90, 90, 90, 90)) = \mathbf{e}(0, 0, 0, 0) = (0, 0, 0) = \mathbf{0}$. So, we find that it maps to the origin O in $\mathbf{R}^3$.

Recall that the set of all quadrilaterals with inscribed circles, **Q**, contains various quadrilaterals—rhombuses, kite shapes, concave squares, one-sided open quadrilaterals, and two-sided open quadrilaterals. Where are these to be found in **C**, the crystal world? What shape do they form? In order to know that, we prepare the following:

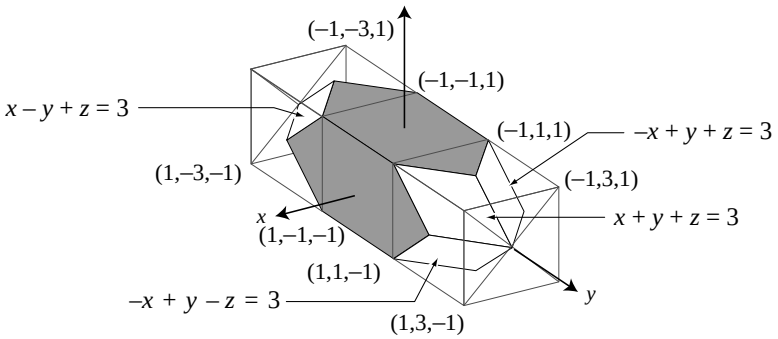

Figure 10. The crystal map. White faces are defined by equations $x-y-z=\pm 3$, $-x+y-z=\pm 3$, $-x-y+z=\pm 3$, and $x+y+z=\pm 3$. Dark faces are defined by equations $x=\pm 1$ and $z=\pm 1$.

Theorem 5. *For any* $\boldsymbol{q} \in \boldsymbol{Q}$ *and its image* $\boldsymbol{e}(\boldsymbol{n}(\boldsymbol{r}(\boldsymbol{q}))) = (x, y, z)$*, the following are true:*

$$\begin{aligned} \boldsymbol{q} \textit{ is bounded } \Leftrightarrow -3 < x-y-z < 1, -3 < -x+y-z < 1, \\ -3 < -x-y+z < 1, \textit{ and } -3 < \quad x+y+z < 1. \end{aligned} \tag{17}$$

$$\begin{aligned} \boldsymbol{q} \textit{ is convex } \Leftrightarrow -1 < x-y-z < 3, -1 < -x+y-z < 3, \\ -1 < -x-y+z < 3, \textit{ and } -1 < \quad x+y+z < 3. \end{aligned} \tag{18}$$

$$\begin{aligned} \boldsymbol{q} \textit{ is convex and bounded } \Leftrightarrow -1 < x-y-z < 1, -1 < -x+y-z < 1, \\ -1 < -x-y+z < 1, \textit{ and } -1 < x+y+z < 1. \end{aligned} \tag{19}$$

Proof: See Figure 7. Quadrilateral $\mathbf{q}$ is bounded if and only if $\mathbf{q}$ has no open corner, which is the case if and only if $b_i < 1/3$. Substituting this into Equation (9), we find that

$$x-y-z<1, -x+y-z<1, -x-y+z<1 \text{ and } x+y+z<1. \tag{20}$$

Now, $\mathbf{q}$ is convex if and only if $a_i > 0$. So $b_i > -1/3$. Substituting this into Equation (9) gives that

$$-1<x-y-z, -1<-x+y-z, -1<-x-y+z, \text{ and } -1<x+y+z. \tag{21}$$

The lower bound -3 in Equation (17) and the upper bound 3 in Equation (18) result from Equations (11)–(14). So these satisfy Equations (17) and (18). Equations (20) and (21) in turn, give (19). □

Inequalities (20) define a regular tetrahedron, as shown in Figure 11. It shows the bounded orizuru world. Inequalities (21) define another regular

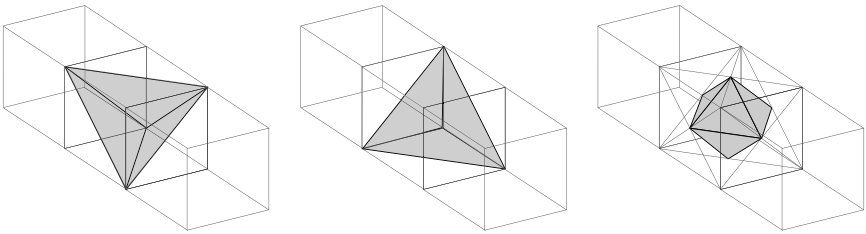

Figure 11. (a) Bounded quadrilateral orizuru world. (b) Convex quadrilateral orizuru world that includes unbounded quadrilateral orizurus. (c) Bounded and convex quadrilateral orizuru world.

tetrahedron (Figure 11(b)). It shows the world of orizurus folded from convex quadrilaterals. The intersection of the two tetrahedra forms a regular octahedron (Figure 11(c)), which is the bounded and convex orizuru world.

We continue to analyze the orizuru world. Next we consider the diamond (rhombus) shape. What shape is the rhombus quadrilateral part of the orizuru world? For any rhombus $\mathbf{q} \in \mathbf{Q}$,

$$a_{i+2} = a_i (i = 1, 2). \tag{22}$$

Normalization $\mathbf{n}$ transforms Equation (22) to

$$b_{i+2} = b_i (i = 1, 2). \tag{23}$$

This results in two equations: $x - y - z = -x - y + z$ and $-x + y - z = x + y + z$ according to Equation (10). Reducing these gives

$$z = x, \quad z = -x,$$

and so

$$x = z = 0.$$

This is a segment of the y-axis. For any kite shape $\mathbf{q} \in \mathbf{Q}$, Equation (23) is satisfied for $i = 1, 2$. Thus, the kite shape quadrilateral region of the orizuru world is the set $\{(x, y, z) \in \mathbf{C} | \quad z = x \text{ or } z = -x\}$.

How about the unbounded quadrilateral orizuru world? For any two-sided open quadrilateral $\mathbf{q} \in \mathbf{Q}$, according to Figure 7,

$$(b_1 > 1/3 \text{ and } b_3 > 1/3) \text{ or } (b_2 > 1/3 \text{ and } b_4 > 1/3).$$

In the former case, since $y = 3(b_1 + b_3)/2$, $y > 3(1/3 + 1/3)/2 = 1$. In the latter case, $b_1 + b_2 + b_3 + b_4 = 0$ gives $b_1 + b_3 < -2/3$. So $y < -1$.

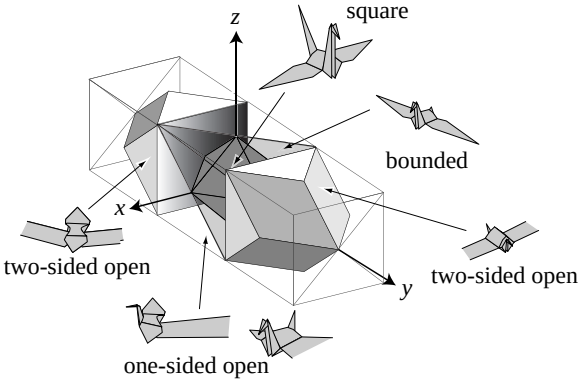

Figure 12. Structure of a crystal map of the orizuru world **C**.

This completes our description of the structure of the crystal map of orizuru world **C**. A full picture with representative examples of the various types of orizuru is shown in Figure 12.

Bibliography

[1] K. Husimi and M. Husimi. *The Geometry of Origami*. Tokyo: Nihon Hyouronsha, 1979.

[2] H. Huzita (ed.). *Proceedings of the First International Meeting of Origami Science and Technology*. Padova, Italy: Dipartimento di Fisica dell'Università di Padova, 1991.

[3] J. Justin. "Mathematical Remarks and Origami Bases." *Symmetry: Culture and Science* 5:2 (1994), 153–165.

[4] K. Kasahara and J. Maekawa. *Viva! Origami*. Tokyo: Sanrio, 1983.

[5] T. Kawasaki. "Expansion and Their Applications of Systematic Compositions of Cell Decompositions of Flat Origami—Theory of Deformations of Orizuru." *Research Report of Sasebo College of Technology* 32 (1995), 29–58.

[6] T. Kawasaki. "The Geometry of Orizuru." In *Origami^3: Proceedings of the Third International Meeting of Origami Science, Mathematics, and Education*, edited by Thomas Hull, pp. 61–73. Natick, MA: A K Peters, 2002.

[7] T. Kawasaki. *Rose, Origami and Math*. New York: Japan Publications, 2004.

A Geometrical Tree of Fortune Cookies

Jun Maekawa

1 Introduction

Cookies with strips of paper on which various oracles are written, called fortune cookies, are served after a meal at many Chinese restaurants in the United States. This is not a Chinese traditional custom, but an American one started in the twentieth century. I personally learned of the custom of fortune cookies in the US, but subsequently found their relatives in Japan. To my surprise, it turned out that fortune cookies originated in Japan [2, 6]. I have become more interested in the fact that the shapes of Japanese cookies are slightly different than those of American ones.

The fortune cookie is a kind of origami that has the following characteristics:

1. It is folded from one circular sheet.
2. It is homeomorphic with a sphere: one side becomes the inside and the other the outside, without overlapping.
3. It is a *developable surface*: the sheet does not stretch or shrink.
4. It contains no curved folds. (In fact, most fortune cookies do not have any curved folds despite the fact that they are formed from curved surfaces.)

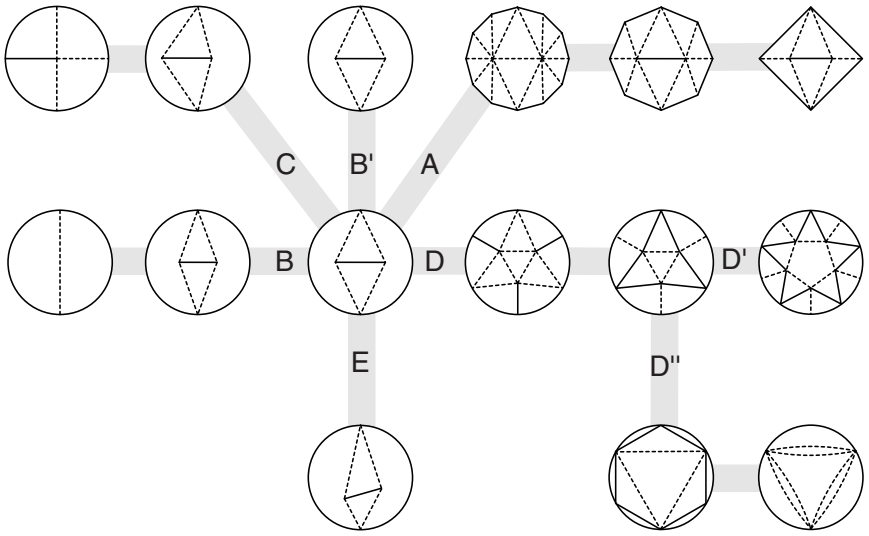

Figure 1. The "genealogical" tree of fortune cookies.

Various shapes that have all of these features are used as fortune cookies or other cookies of the same kind. Their different shapes enumerate the geometric possibilities. They also resemble diverse life forms that have been evolving in their environment—that environment being restaurants. I have made a unified list of them as a tree, which is shown in Figure 1. In this paper, I will explain this tree in detail.

2 Developable Surface

First, I will confirm that a fortune cookie is truly a developable surface. Developable surfaces are certain types of ruled surfaces, or curved surfaces formed from a combination of straight lines. There are only four basic types of developable surface:

1. plane,
2. cylindrical surface,
3. conical surface,
4. tangent surface.

The first three are well known. Tangent surfaces may not be familiar. One example is the helical convolute surface, which is formed from tangents of a helix curve. Any fortune cookie is a developable combination of

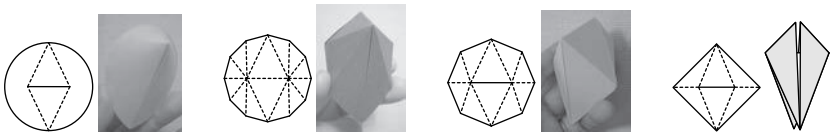

Figure 2. Transformation of fortune cookies to polyhedra (branch A of Figure 1): (a) circle, (b) regular dodecagon, (c) regular octagon, and (d) square (fish base).

planes and conical surfaces, meaning that it can be decomposed into some combination of planes and conical surfaces.

To understand this intuitively, think of the curved surface as the limit of a polyhedron formed from triangles, and the circle from which it is folded as the limit of a polygon that can be folded into the corresponding polyhedron. Observe that two edges of each face of the polyhedron should be equal to the ruling lines of the corresponding curved surface, and that the ruling lines must not be skew lines. Keeping this in mind, look at approximations by polygons, shown in Figure 2.

Figure 2(a) is a model of *tsujiura-senbei*, a Japanese traditional fortune cookie made from a circle. Figure 2(b) has the same structure but is made from a regular dodecagon. Figure 2(c) shows a cookie that is made from a regular octagon. Such transformation is possible with other even-gons, such as a regular decagon or duodecagon. And a square is the most interesting. As shown in Figure 2(d), folding this structure from a square makes the fish base, a well-known pattern in origami. Therefore, we can say a fortune cookie is a fish base folded from a circular sheet.

Such transformations are represented as branch A of the fortune cookie tree (Figure 1). Though they are not used in real fortune cookies, I modified one from a regular octagon to design a fortune-cookie-style stable package folded from square paper.

3 Volume Measurement and Spiral

Now, look at the branches B and B′ in Figure 1. Here I examine the relationship between the shape and the length of the central straight part, normalized to the radius of the circle. Figure 3 is a graph describing the relationship between the length of the central straight line and the volume of the resulting solid. Though the curve looks simple, the relationship is quite difficult to solve analytically. This graph is a result of numerical calculation using a 10,000-gon. The one whose central straight line is about 0.406 units long has the largest volume. Its overall shape is two triangles facing each other with some gap. Interestingly, the shape is very close to

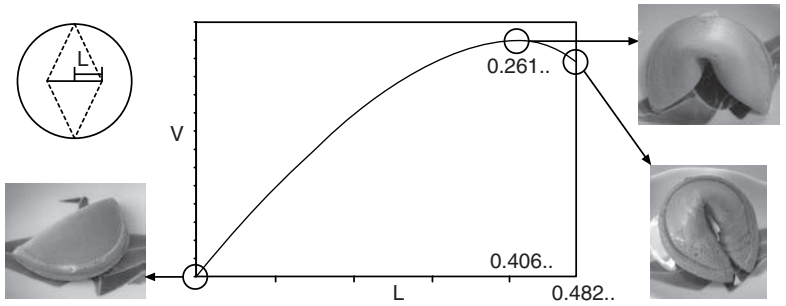

Figure 3. Relationship between fortune cookies' volume and the length of the central straight lines (branch B of Figure 1).

that of typical American fortune cookies. If we consider fortune cookies to be a type of container, fortune cookies that have large volume are desirable. Is this a view of American pragmatism?

On the other hand, typical Japanese tsujiura-senbei have the longest straight line, which is about 0.482 units long, which results in the two triangular faces contacting each other, as shown at the lower right of Figure 3. This type can also be seen in the US, whereas the version that has the largest volume is not seen in Japan. In Japan, some cookies have no volume. I show one in the picture, though it is not a fortune cookie since it has no strip. A tsujiura-senbei of the same shape is depicted in a publication that was printed around 150 years ago [2] .

Now, why is the limiting length of the straight section about 0.482? If the only condition is that the opposite points of the circular sheet should meet each other, the limit is half of the radius, that is, 0.5. If the length exceeds this value, the faces do not close. In practice, however, there is a obstacle to reach 0.5. Two trianglular faces start to interfere with each other when the length gets close to 0.5.

Let us consider what happens if surfaces are allowed to intersect one another. The result is shown in Figure 4 as the length of the straight section approaches the maximum length of 0.5. Figure 4(a) resembles a cardioid curve, and Figure 4(d) a trochoid curve, but these are stranger functions. In Figure 4(f), two triangular surfaces again interfere with each other. And it goes further. In fact, the two surfaces must rotate an infinite number of times for the length to reach 0.5. The final shape, shown in Figure 4(h), somewhat resembles a logarithmic spiral, though it is not the same. But the shape is very similar to that of structures of some shells such as those of Fragum unedo (Figure 4(i)). It is an interesting coincidence, though it does not appear that they are based on the same principle (the latter is based on a growth pattern that is roughly logarithmic).

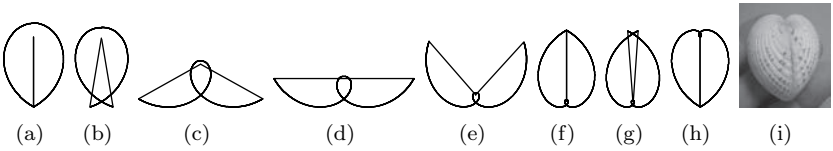

Figure 4. Allowing intersection of the faces brings spirals (branch B′ of Figure 1): (a)–(h) Various possibilities for intersections. (i) Fragum unedo (a species of shellfish).

4 Asymmetrical Transformation

I have previously examined asymmetrical transformation of the bird base before [3, 5]. The same type of transformation can be applied to fortune cookies, which is illustrated in Figure 5. At the limit of the transformation, two valley folds disappear and another valley fold appears. The result is a simple two-fold. Its volume is 0, of course. There are cookies of this type in Japan, though they are not fortune cookies because they do not contain strips of paper. (They have a strange brand name, which translates to "The Hardest Senbei in Japan.") Figure 6 shows a contour map representing the volumes of asymmetrical structures folded from a square, where I have plotted volume against the lengths of segments P and Q. We can see that the symmetrical cookies ($P = Q$) has the largest volume. These shapes correspond to branch C in Figure 1.

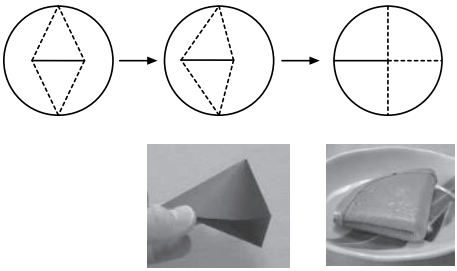

Figure 5. Asymmetrical transformation of fortune cookies (branch C of Figure 1).

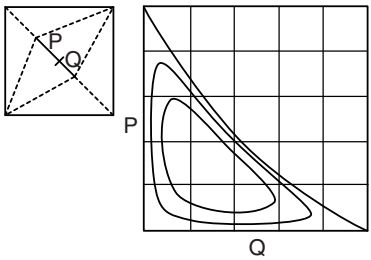

Figure 6. Relationship between the volume and the length of the straight lines in asymmetrical transformation of fortune cookies.

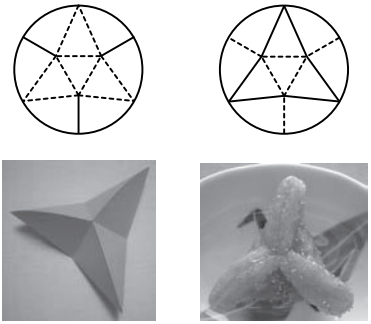

Figure 7. Structure of fortune cookies with three projections (branch D of Figure 1).

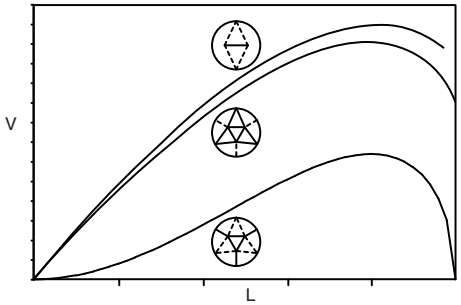

Figure 8. Relationship between fortune cookies' volume and size of the central polygons.

5 Multiprojections

Thus far, we have considered structures that have exactly two projections. But they can have more than two projections. Figure 7 shows two kinds of shapes that have three projections. Although they look similar to one another, these two are actually quite different. The left one in Figure 7 has curved surfaces, while the right one is formed from only planes. In the limit of a large number of projections, however, the central polygons of both become circles, and they come to have the same structure. A Japanese traditional sweet, *yubeshi*, has a similar shape, though it is not a fortune cookie, either.

In Figure 8, we plot the volume versions of the side L of the interior polygon for the two shapes of Figure 7 and a conventional fortune cookie as described earlier. As can be seen, the volume decreases with increasing number of projections, so that those that have two projections have the largest volumes.

Figure 9 shows a fortune cookie that has five projections. This type of cookie is only available in the year-end and new-year seasons from a long-established confectionery at Kanazawa, an old city in Japan.

The right figure of Figure 7 becomes the center one of Figure 10 at the limit of a maximum-size central polygon. Its volume is 0. There is a fortune cookie that has this structure with some curved folds and slight overlapping. It is called *Karakara-senbei* and contains a small toy instead of an oracle. These are represented in branch D of Figure 1.

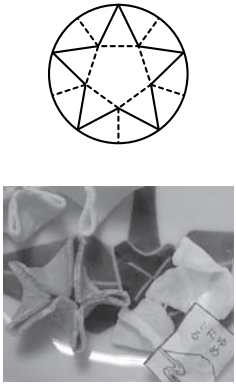

Figure 9. A fortune cookie with five projections (branch D′ of Figure 1).

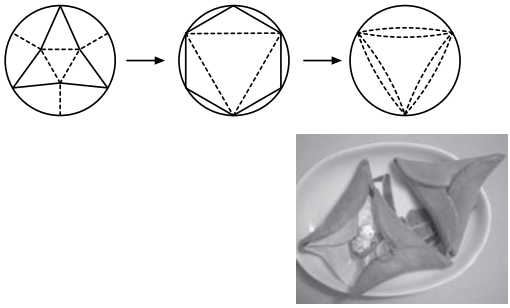

Figure 10. Further transformation of fortune cookies with three projections (branch D″ of Figure 1).

6 Summary and Further Research

We have already discussed asymmetrical transformation in the branch C of Figure 1, but we can generalize it further. One example is the branch E. Those that have more than two projections have many more degrees of freedom. If they have three projections, they have eight parameters. In making a unified list, I considered creating a parameter space. But, because of the large number of degrees of freedom (and other reasons) I abandoned the parameter space and made it a tree. The number of degrees of freedom is too large to illustrate that extended parameter space in an intuitive way.

Lastly, I mention some topics for further research. First, there is the problem of the largest volume: what is the solid of largest volume folded from a circular sheet? I have suggested that one type of American fortune cookies has the largest volume, but I have not been able to prove it yet. The similar largest volume problem, in which the sheet is square and the shape is a convex polyhedron, has been solved by Alexander, Dyson, and O'Rourke [1]. I have been dealing with this problem with my own approach, but I have hit a wall because I consider curved folds. One of the reasons why O'Rourke at al. dealt with only convex polyhedra is that they wanted to exclude curved folds. Though no convex polyhedron with any volume can be made from a circular sheet, excluding curved folds would simplify the problem.

The presentation of crease patterns creates a new theme derived from this study. How can crease patterns represent structures that have curved surfaces such as fortune cookies? Conventional origami crease patterns use

lines for sharp folds but do not represent the smooth curvature of surfaces. I have tried to color each ruling line according to its curvature and have succeeded to some degree, but there still remain some issues, such as how to represent the dihedral angle of a fold when the curvature is infinite (i.e., a sharp fold).

Aside from the geometry, the history of fortune cookies, which I have described briefly in the introduction, is itself an interesting theme. It relates to the history of Japanese Americans and Chinese Americans. Fortune cookies also relate to robot technology, since many of them are made by machines. Some machines can make two or three fortune cookies a second when fed with materials [4]. But, as far as I have seen, machine-made fortune cookies tend to be of lower-quality than human-made ones, having distorted shapes or multiple strips. It is difficult to automate origami even with such simple structures as fortune cookies.

Acknowledgment. I would like to thank Hatori Koshiro for helping me to translate this paper into English.

Bibliography

[1] R. Alexander, H. Dyson, and J. O'Rourke. "The Foldings of a Square to Convex Polyhedora."In *Discrete and Computational Geometry: Japanese Conference, JCDCG 2002, Tokyo, Japan, December 6–9, 2002, Revised Papers*, Lecture Notes in Computer Science 2886, pp. 38–50. New York: Springer, 2003.

[2] H. Aoki. *Tsujiura-gashi ga Tanjo suru made: Uranai, Yakuyoke, Kaiun-gashi* (An Early History of (Japanese) Fortune Cookies: Confectionery for Fortune, Talisman, and Good Luck, in Japanese). Exhibition booklet, Toraya Confectionery Co., Ltd., 2004.

[3] T. Kawasaki. "The Geometry of Orizuru." In *Origami^3: Proceedings of the Third International Meeting of Origami Science, Mathematics, and Education*, edited by Thomas Hull, pp. 61–73. Natick, MA: A K Peters, 2002.

[4] Kitamura Co., Ltd. *Kitamura Automatic Confectionery Baking Machine.* Available at www.kitamura-fcm.co.jp, 2006.

[5] J. Maekawa and K. Kasahara. *Viva! Origami.* Tokyo: Sanrio, 1983.

[6] Y. Nakamachi. "Kyokai kara Sekai he Ekkyou suru Uranai-gashi" (Fortune Confectionery Became Global from the Marginal Field, in Japanese). In *Ikai Mangekyo* (Kaleidoscaope of Different Worlds), exhibition booklet, National Museum of Japanese History, 2001.

Part V

Origami in Education

Origametria: A Program to Teach Geometry and to Develop Learning Skills Using the Art of Origami

Miri Golan and Paul Jackson

1 Background

The name *Origametria* is made from the words *origami* and *geometry*. The term was created by the Israeli Origami Center (IOC) to describe its innovative program to teach curriculum geometry through origami.

In Israel, the Origametria program is taught in 70 Jewish, Arab, and Christian schools. The IOC has a team of 40 teachers who are trained to teach the program. Thus, each week, about 10,000 school students around the country study Origametria as part of their curriculum. In 2008, after several years of scrutiny, the Israeli Ministry of Education formally approved the program. Soon, a pilot course of Origametria will begin in a college of teacher training. If successful, courses will be made more widely available. At present, the program is taught to elementary school students (grades one through six), but there are plans to expand it into high schools.

1.1 Origins of the Program

In 1992, the IOC began to teach an origami program with the purpose of developing learning skills. The program was designed to enhance self-esteem and a sense of accomplishment, while developing learning skills such as motor skills, spatial perception, logical and sequential thinking, hand-eye coordination, focusing and concentration, aesthetics, three-dimensional perception, and principles of basic geometry.

1.2 Why the Program Changed to Origametria

Although the Origami as a Learning Tool program was successful, with the number of schools in which it was taught increasing each year, it became apparent that the natural long-term home for origami was not as a special learning tool class, but rather, as a class integrated into a particular subject of the school curriculum. Specifically, it was felt that origami should be integrated into the geometry curriculum.

After a year-long pilot, we found that Origametria was indeed an important tool and a powerful way to improve students' knowledge of geometry. The transition was not easy at first. When the system was introduced into schools that already had participated in our old program, we encountered some problems with the program's teachers; since those teachers came from a predominantly arts background and not a mathematics background, they had difficulty teaching geometry. Additionally, teachers who were familiar with the old program did not easily adapt to concepts of the new program.

Therefore, in 2002, we replaced almost all of our teachers. Each teacher we trained was required to have a background in mathematics. This, among other factors, greatly added to the success of our program. While the basic concepts, ideas, and didactic methods of the previous program remained in the new program, the class structure, goals, and subjects had changed. Without these adaptations, the program could not have succeeded.

The main decision to change the principal IOC program from Origami as a Learning Tool to Origametria was made after meeting the director of Ha'Achim School in Kiryat Malaachi. During the discussion, a mathematics teacher described how she taught two third-grade classes and had noticed a significant difference in the spatial perception and understanding of geometry between the students of the two classes. Evidently, the IOC course was taught in only one of the classes—the class in which the level of understanding was higher. This realization gave the IOC the confidence to begin expanding the Origametria program.

2 Origametria in the Classroom

2.1 Lesson Structure

Before a lesson can begin, a specific topic of geometry must be chosen for teaching. This is often done in consultation with the mathematics teachers at the school. The choice of topic depends on the requirements of the national curriculum for each grade.

Once a topic is chosen, an origami model is found which, in its sequence, focuses on that topic: for example, a model that may consist of

many different triangles, or specifically isosceles triangles, or polygons, or bisections.

During the folding of the model by the class, the teacher will stop after each new step to check if new examples of the chosen topic could be identified, and if they are the same or different from earlier examples. The process of identification can be summarized as follows:

- *Geometric insight*: This term denotes the understanding of the topic using folds.
- *Exploration*: This refers to the continuous search throughout the folding process.
- *Properties and context*: This refers to the studying of the topic in various ways using the folded paper or while folding. Importantly, each year we repeat topics taught in the previous year, in cooperation with the school's mathematics staff and the standard geometry curriculum.
- *Lesson summary*: At the end of the lesson we check if each student has acquired the geometric knowledge taught in that particular class. We specifically verify that the weaker students have understood the concepts. Significantly, after every lesson the students leave with a folded model, which serves as a motivational tool for future learning.

2.2 The Method of Teaching

Here are some of the principles that define the Origametria program:

1. *The way it is taught*: We do not use negative terms during our classes. For example, we will not use a phrase such as: "this isn't correct." Rather, we will say: "this is beautiful; now, open this and fold ...." We do not criticize a student's folding. This ensures that even weaker students can fold like all other students. Indeed, everyone receives positive feedback.
2. *We never check the accuracy of folding*: We stress that accuracy is important, although "accuracy" is a relative term that changes from student to student. When a student asks the teacher if a fold is accurate, the teacher returns the question to the student, asking if he thinks it is the most accurate fold that he can make. This obliges students to inspect their work and to fold as accurately as they possibly can. Such an approach both improves the students' accuracy and prevents disappointment.

3. *Our teachers never touch a student's model*: A teacher will show a step using her own paper again and again. This gives students a stronger sense of ownership and accomplishment, as their work is entirely their own, folded by themselves without any assistance.

4. *The choice of models*: We carefully select the models and improve their folding sequences, so that the teachers can explain the folding procedure once and the students should be able to follow easily.

5. *Positive reinforcement*: After each step, the teacher inspects a student's folds and gives her positive encouragement in Japanese, such as "*Ichiban sugoi!*" ("This is excellent!")

6. *The model is never named while being folded*: Throughout the folding, the identity of the final model is never revealed. This has the double effect of focusing students' attention on the geometry of the current step instead of seeing it as a "leg" (or whatever) and also of opening students' imaginations. It also gives control of the subject of the model to the teacher and concludes the lesson with a surprise.

3 The Advantages of Teaching Origametria

In Origametria, the specific model being taught is of little importance. More important is *the way* the model is taught.

Most of the success stems from a process the student undergoes while folding. For the student, the main goal is to create a finished model of an animal, a toy, or any other form. For the teacher, this is a secondary goal. The main aim of the program (and of the teacher) is to improve a student's knowledge of the geometric topic selected for the class, and to develop learning skills by exploring and studying the topic *while folding the model.*

The strength of using origami for this is that the geometry is inherent in the folding process—one needs only a quick look at any folding sequence to identify geometric topics in abundance. For example, in the lesson in which we teach diagonals, we will look for diagonals while folding, check whether various folding lines are diagonals, and explore the properties of the diagonal until we finally complete the model.

The students find the lessons fascinating. For many, it is their favorite lesson of the week. They are excited to fold a model, and enjoy exploring the topic with the teacher. For them, it is a game that uses several senses and provides a positive experience. This deepens their knowledge and motivates them to learn more. This way, the students will remember a topic, even after several years.

3.1 Reasons for the Success of the Program

There seem to be a number of reasons why the Origametria program is successful, and why it continues to expand:

- We employ rigorous didactic principles in our classes.
- We focus on a single geometric subject in each lesson.
- We use special methods of teaching origami to ensure a student's success and satisfaction with the folding.
- There is close coordination between the IOC's Origametria teacher and the school's mathematics teacher(s), so that new topics are taught in parallel. A student who has just learned the concepts of angles in Origametria, for example, will have the chance to use his newfound knowledge in the regular geometry lesson. If this is a weaker student, his self-esteem will improve and he will be perceived by others as having a greater self-confidence.
- The IOC teachers are trained continuously. Once a month, they attend a special training session with senior IOC Supervisors. We also visit the various school classes to observe in detail the teaching of each teacher, and to suggest how to improve their skills. The IOC's teachers and I introduce innovations and interesting, new ideas from our own experiences.

The success of Origametria can be described and measured at three levels:

1. *cognitive:*
   - developing spatial perception,
   - developing logical thinking,
   - developing visual perception,
   - improving use of imagination,
   - building knowledge;
2. *emotional:*
   - building self-esteem,
   - enhancing feelings of success;
3. *motoric:*
   - developing motor ability,
   - improving hand-eye coordination.

4 Kindergarten Origametria

Here, we explore the experiences of the first author.

4.1 The Origametria Pilot in Broshim Special School

The Broshim Special Education School in Tel Aviv admits students from first to twelfth grades for a period of three or four years with the explicit purpose of enabling their rehabilitation into the school system. It has a special origami room to which the students come for origami lessons in small groups, or one-to-one with the teacher.

I have been teaching origami in the school for 15 years. While piloting the Origametria program, I taught it to first graders and also to the older students. It was apparent that the younger students found it easier to understand geometric concepts and terms after just a single lesson, whereas the older students required extra lessons. Regardless, all the classes in which I had taught Origametria had distinctly better retention of the topics. Even pupils who at first showed resistance to the program enjoyed visualizing the concepts being taught while folding a model.

The program in Broshim is dynamic. With each lesson we find more insights and discover other ways to enhance it.

4.2 Origametria in Kindergartens

The IOC has been teaching in kindergartens for 14 years, but we have always advised that children under the age of five should not be taught origami since their motor skills are not mature enough.

However, following my experiences with first-grade students at Broshim School, I have developed a series of origami models that do not require accurate folding. This ensures that any child folding a model succeeds at doing so, even if the model is made inaccurately.

These models have opened a new approach to teaching basic geometric concepts to preschoolers, and to improving important abilities such as motor skills, hand-eye coordination, and spatial awareness. The didactic principles are similar to those of Origametria, whereby we emphasize improving the self-esteem of children by ensuring that they succeed in the folding, and by providing positive reinforcement.

It is my belief that the window of opportunity to acquire basic knowledge is between the ages of three to nine, because it is during these years that a child's imagination is at its most active stage. It is during this time that children can most quickly and surely grasp the concepts of geometry. Consequently, Origametria is a powerful tool to provide children with an

understanding of these concepts. As students mature, they find it more difficult to use imagination to understand three-dimensional and abstract concepts. Therefore, I believe that the earlier we can teach Origametria to children, the better we can utilize the resource of imagination to teach geometry.

5 The Future of Origametria

Many schools provide very positive informal feedback on the successes of Origametria. However, we understand the necessity of a scientific analysis of this success, and we are planning to conduct a special study in which the effects of Origametria as a tool to learn geometry will be systematically measured.

We believe passionately in the validity of Origametria as a method to teach geometry, one that additionally (and importantly) uses origami as a tool to develop learning skills. Origametria makes the traditionally dry, abstract, and remote subject of geometry not only fun to learn but also empowering. Furthermore, its hands-on approach to learning makes it an effective tool for students with learning problems. While it makes geometry easier to teach, its effective use requires skills in the teaching of origami and of the specific Origametria method.

The program continues to expand within Israel and it seems likely to be adopted by schools overseas. In time, we would like to see it adopted as one of the accepted ways to introduce basic geometric topics as an alternative and/or an addition to the traditional ruler-and-straight-edge or chalkboard methods.

We conclude with a story. A school in Hod HaSharon introduced the Origametria program but, due to a funding crisis, had to cancel it in mid-semester. Such was their enthusiasm for the program that the affected students staged a placard demonstration outside the school, demanding the reinstatement of their Origametria class. Astonished by the students' enthusiasm for their geometry class, the school reinstated the program. The studens won.

6 Origametria: An Example

Here is an example of a model, taught according to the principles of Origametria.

Polygon Heart by Paul Jackson

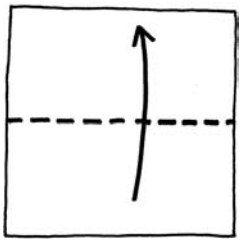

1. Fold to make a rectangle

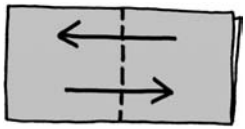

2. Fold as shown, then completely unfold

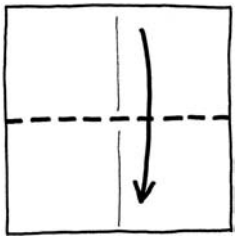

3. Fold a rectangle

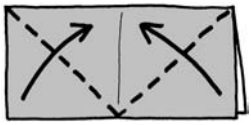

4. Fold in only one corner on each side

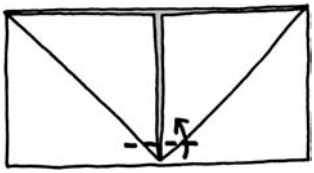

5. Fold up the tip

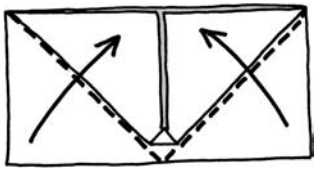

6. Fold the remaining corners over the top to look like the next step

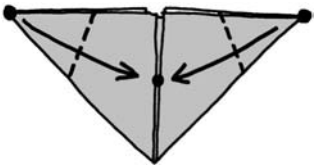

7. Fold the corners to the centre line to look like the next step

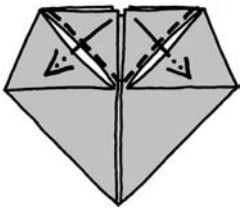

8. Fold the small triangles into the pockets

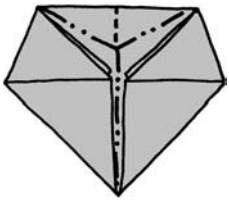

9. Fold as shown

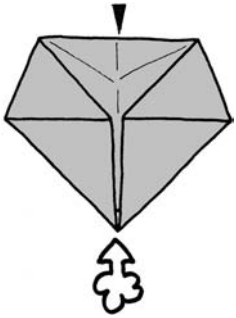

10. Inflate. Push down on the top edge

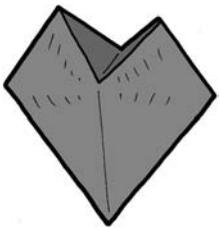

11. Open the Heart as shown, making it hollow in the middle

7 Origametria Commentary

7.1 Main Topic: Polygons

Topic of lesson. First and second grades—identify polygons by counting the number of edges. Third through sixth grades—identify and describe polygons found during the folding.

Purpose of lesson. To develop abstract thinking and to identify and describe all major polygons.

Definition of a polygon. A closed figure made from three or more straight line segments.

Definition of a square. A four-sided polygon having four equal sides and four angles of 90 degrees.

7.2 Sample Questions

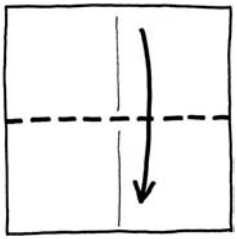

Step 3. How many squares are in the paper?

4

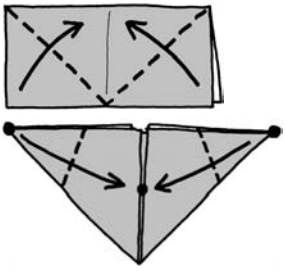

7

6

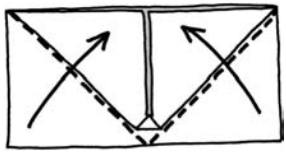

Steps 4, 6, and 7. How many triangles are found in the paper? Are triangles also polygons?

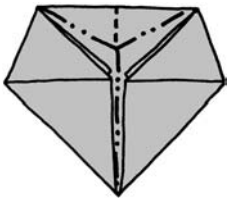

Step 9. What is the largest polygon?

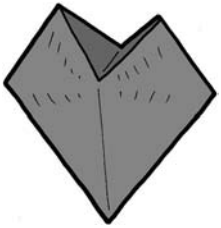

Step 11. After the *Polygon Heart* is inflated, what polyhedron is made?

Acknowledgment. The authors gratefully acknowledge the advice of Professor Yoav Vardi and Dr. Dina Vardi and the translation of this article by Boaz Shuval.

An eight-minute movie about Origametria can be downloaded from the Green Fuse Films website, www.greenfusefilms.com/origametria.html.

The Impact of Origami-Mathematics Lessons on Achievement and Spatial Ability of Middle-School Students

Norma J. Boakes

1 Introduction

Origami has become a popular instructional method in the mathematics classroom. Numerous books and practitioner articles cite origami as a useful way to teach mathematics concepts, especially as it relates to geometry and spatial concepts [6, 16, 22, 27]. In addition, the National Council of Teachers of Mathematics (NCTM) [20], in its *Principles and Standards of School Mathematics*, supports the use of such methods, suggesting that students engage in active exploration that allows students to study the construction and deconstruction of two- and three-dimensional figures. An examination of literature regarding origami as an instructional tool, however, reveals a lack of studies focusing on the impact of origami instruction within the mathematics classroom. With a continued need to find effective instructional methods in mathematics and the substantial support for origami as such a method, this study was designed and implemented to explore origami and its effect on student understanding.

2 Research Questions

In exploring the impact of origami in the mathematics classroom, the following research questions were formulated:

1. How did students who participated in origami-mathematics lessons integrate into a traditionally instructed geometry unit compared to students who were instructed solely through traditional instruction in terms of (a) spatial visualization skills and (b) mathematical achievement level?

2. Do the effects of origami-mathematics lessons differ by gender? [3]

3 Spatial Visualization and Related Research

Named within the major topics areas in the K-12 mathematics curriculum is the study of geometry. A key component within geometry is the development of spatial thought [29]. Generally speaking, spatial thought deals with a student's ability to visualize, describe, and critically analyze spatial aspects of the real world. NCTM recognizes the importance and need to assist students in developing this ability, often referred to as *spatial ability*. Within this capability is the concept of *spatial visualization*. Though definitions vary from author to author, this term refers generally to the visualization and mental manipulation of figures in two- and three-dimensions [21]. Spatial visualization, beyond its importance to geometry, also has direct connections to defining and quantifying human intelligence and, more specifically, mathematics ability. As a result, a great deal of research links to this skill and its development in children.

Research reviewed concerning spatial ability and its attainment fall into three areas: the connection of spatial ability to gender and age, the connection between spatial ability and overall mathematics ability, and the potential of improving spatial ability through training. Clearly important after a review of gender- and age-based research is the awareness that males and females may differ in terms of spatial ability. Though in some cases females outperformed males on spatial tasks [17], generally researchers conclude that a difference persists, with males' scores superior to females' on spatial tests [5,30]. In terms of age, males and females both improve their spatial abilities as they mature [18]. However, as children reach middle- and high-school age, improvements are not necessarily equal, with male gains often greater than females [18,19].

Many studies sought to research the connection between spatial ability and mathematics achievement. According to a review of educational research from 1910 to the late 1950s, spatial ability did play a critical role

in evaluating mathematical ability [23]. However, more recent publications are not necessarily in agreement. While there are those that found spatial ability to be a predictor of performance [1, 5, 11, 12], a meta-analysis by Friedman questions the claim, noting that "the bulk of correlational evidence casts doubt on the conjecture that spatial skill is pervasive in mathematics as mathematics is taught and tested today" [15, p. 29].

A final area reviewed dealt with studies seeking to improve spatial ability through specialized instruction. Training came in many forms from computer software [8, 9] to a variety of hands-on methods [1, 2, 24]. Many of these studies found that, in some fashion, students made improvements in their performance as a result of training [2, 4, 8].

Though research is not fully in agreement, there are general themes that were important to this study. For one, gender and age are both factors that could have some effect on performance. There is also the possibility that there is a direct correlation between spatial ability and mathematics achievement. A final conclusion is that training does have the potential to improve student performance. Though these are more themes than absolute truths, they are valuable in studying the influence of origami instruction on students' abilities.

4 Procedures

A quasi-experimental pre-test/post-test design with a control and treatment group was used for this study. A convenience sample of 56 seventh-grade students with the same mathematics instructor from a southern New Jersey middle school served as participants. Of these, 31 (based on class assignment) made up the control group and received strictly traditional textbook-based instruction during experimentation. The remaining 25 students (also based on class assignment) served as the experimental group receiving treatment. Treatment consisted of 12 origami lessons, taught by the researcher, interspersed within traditional instruction over a one-month geometry unit. To determine how this setup impacted performance, a 2×2 factorial design was used. Independent variables included gender and the method of instruction. For dependent variables, mathematics achievement level and spatial ability were selected.

To determine the mathematics achievement level of students, a 27-question multiple-choice test was created using released items from the National Assessment of Educational Progress [20]. All items were from the geometry/spatial skill strand of the NAEP and geared for middle-school-age students. A report reviewing a sample of mathematics questions from NAEP mathematics assessments between the years of 1973 and 1996 calculated weighted alpha reliability levels of .87 and .85 for middle-school-age children, establishing fairly strong reliability for NAEP items [28].

According to NCTM, spatial visualization refers to a student's ability to "[build] and [manipulate] mental representations of two- and three-dimensional objects and [perceive] an object from different perspectives" [21, p. 40]. With the close tie spatial visualization has to geometry [1] and to the act of paper-folding [14, 26], three spatial ability tests were also selected as instrumentation for this study. Based on a review of existing research on spatial ability and appropriateness for the age of participants, the Paper Folding, Surface Development, and Card Rotation Tests were chosen from the Kit of Factor-Referenced Cognitive Tests [10]. Each of these tests consisted of two parts and took between three and six minutes to complete. Due to time constraints, one part from each test was used. Reliability was established based on a study conducted by Fleishman and Dusek, who reported test-retest reliability values ranging from .76 to .92 for spatial-based tests [13].

At the start of the study, all students were pre-tested using the selected mathematics achievement and spatial ability tests. The regular classroom teacher then began the unit on geometry. During this time, the treatment group participated in origami instruction three times a week. Each of these origami lessons was conducted by the researcher with no involvement by the regular classroom teacher. While modeling each step to produce the origami figure, the researcher interspersed relevant mathematics terminology and encouraged dialogue with students regarding mathematics concepts and terminology identifiable within the folding process. (See the appendix for sample dialogue used with the instruction of an origami model.)

During the one-month time period, three days of instruction were randomly selected and videotaped. This was done to assure that the only difference in instruction between the control and treatment groups was the addition of the origami lessons within the treatment group. Three readers (including the researcher) reviewed the videotapes using a researcher-designed checklist to track what objectives and terminology were covered during each session as well as what teaching delivery method was utilized. Accumulated information revealed that the regular classroom teacher maintained the same instructional methods and covered very similar material in all classes.

When the one-month unit was complete, students were again given the mathematics achievement and spatial ability tests. Data was then gathered and analyzed using a statistical analysis software package. Analysis of Covariance (ANCOVA) was used to determine if significant differences occurred between adjusted mean post-test scores, with the pre-test score serving as the covariate (to control for initial differences that may have existed between groups).

Instrument	Group	Gender (N)	Pre-test Mean	SD	Post-test Mean	SD
Card Rotation Test	Experimental	Male (14)	62.69	17.14	69.00	13.45
		Female (11)	49.27	15.65	48.64	11.87
		Total (25)	56.56	17.46	60.04	16.22
	Control	Male (11)	49.45	14.44	55.82	13.38
		Female (20)	53.85	15.21	62.30	13.37
		Total (31)	52.29	14.85	60.00	13.52
Paper-Folding Test	Experimental	Male (14)	4.14	2.25	5.36	1.69
		Female (11)	3.91	2.55	4.55	2.62
		Total (25)	4.04	2.34	5.00	2.14
	Control	Male (11)	3.00	1.18	3.36	2.01
		Female (20)	3.95	1.67	4.85	1.63
		Total (31)	3.61	1.56	4.32	1.89
Surface Development Test	Experimental	Male (14)	10.50	8.30	15.57	9.75
		Female (11)	9.36	5.16	12.64	6.07
		Total (25)	10.00	6.98	14.28	8.30
	Control	Male (11)	5.73	2.83	9.91	6.76
		Female (20)	12.60	7.64	16.00	8.01
		Total (31)	10.16	7.13	13.84	8.04
Mathematical Achievement Test	Experimental	Male (14)	14.50	3.80	17.00	3.68
		Female (11)	13.36	5.14	16.09	4.30
		Total (25)	14.00	4.38	16.60	3.91
	Control	Male (11)	15.55	3.70	15.91	4.30
		Female (20)	14.65	4.00	15.55	3.87
		Total (31)	14.97	3.86	15.68	3.96

Table 1. Descriptive statistics for all instruments.

5 Results

Descriptive statistics for all pre- and post-tests administered are given in Table 1. Results are further broken down by group and gender.

A 2×2 between-groups ANCOVA was conducted for each of the spatial ability tests. For the first of three spatial tests, the Card Rotation Test, values calculated revealed a significant interaction effect between group and gender ($F(1, 51) = 9.09$, $p < .005$) with a small effect size ($\partial\eta^2 = .15$), while neither of the main effects were statistically significant (group: $F(1, 51) = .78$, $p = .381$; gender: $F(1, 51) = 2.69$, $p = .107$). For the Paper-Folding Test, calculated ANCOVA values approached significance for the

Group	Gender (N)	Adjusted Mean	Combined
Experimental	Male (14)	64.62	57.96
	Female (11)	51.30	
Control	Male (11)	58.39	60.44
	Female (20)	62.49	
Combined	Male (25)	61.50	
	Female (31)	56.90	

Table 2. Adjusted means for Card Rotation post-test scores.

interaction between group and gender ($F(1, 51) = 3.59$, $p = .064$). For main effects, no significance was found (group: $F(1, 51) = 1.39$, $p = .244$; gender: $F(1, 51) = .05$, $p = .830$). The ANCOVA completed for the final of three spatial tests, the Surface Development Test, revealed no significant interaction effect ($F(1, 51) = .38$, $p = .540$) as well as no main effects by group or gender (group: $F(1, 51) = .10$, $p = .750$; gender: $F(1, 51) = .45$, $p = .504$). An ANCOVA was also completed for the NAEP Mathematics Achievement Test. Calculations revealed no significant interaction effect between group and gender ($F(1, 51) = .05$, $p = .817$). Similarly, for the main effects, neither produced significant values (group: $F(1, 51) = 2.96$, $p = .091$; gender: $F(1, 51) = .00$, $p = .977$).

One of the four tests utilized in the study resulted in statistical significance. For this test, the Card Rotation Test, further analysis was completed by reviewing the adjusted means shown in Table 2. Males who received treatment maintained a higher adjusted mean than females within the same group. Males in the experimental group also scored higher than males in the control group while females' adjusted mean scores within the control group surpassed their female counterparts experiencing treatment.

6 Conclusions

In terms of spatial ability, analysis of pre- and post-tests reveals that origami did have some impact on students' spatial visualization skills. The Card Rotation Test, selected to evaluate students' ability to mentally rotate two-dimensional figures, produced interesting results with males and females responding differently dependent upon the instructional method experienced. Based on results of the ANCOVA, males seemed to respond best to origami instruction while females seemed to flourish within a traditional structure. Additionally, for the Paper Folding Test, interaction effects approached significance, indicating again that group (experimental or control) and gender had some bearing on mean scores received. The Paper-Folding Test also dealt with students' two-dimensional visualization abili-

ties. The final of these tests, the Surface Development Test, was selected to determine students' ability to visualize in both two- and three-dimensions. Results from this test reveal no significance and seem to indicate that the instructional method had little to no bearing on mean scores earned by participants. Clearly the lesson to be learned here, of course within the limitations of this study, is that males and females can respond differently to origami instruction.

In considering why such gender differences occurred, one must take into account what might have inadvertently impacted the results found in this study. For instance, many spatial ability tests have been found to be predisposed to gender differences due to the nature of the test questions [19, 30]. Social and environmental factors such as out-of-school activities and hobbies may also cause males and females to benefit differently from such a spatially-based instruction technique [2, 11]. Though the cause of the results found here cannot be identified with certainty, future studies should consider gender and factors influencing performance on spatially-related tasks.

A set of samples from the geometry/spatial sense strand of the NAEP assessment was used to determine students' mathematical achievement level. Based on results presented, mathematics achievement gains were similar regardless of gender or the type of instruction experienced. This leads one to conclude that both methods were equally beneficial. Though this is limited by the confines of this study, this result implies that origami lessons integrated within mathematics instruction can be a valuable experience for students. A further convincing factor is the fact that by adding origami instruction into traditional instruction, 20 to 30 minutes of instructional time was lost within each meeting. Although the treatment group spent less time under traditional instruction by the regular classroom teacher, students still did as well as those within the control group. This finding stands then to substantiate the numerous claims that origami is an effective instructional tool in mathematics.

As is always the case, there are factors that may have contributed to the results found for mathematical achievement. For one, multiple-choice tests such as the NAEP are quite common and are something students are comfortable taking. In addition, the specific NAEP questions selected for use in the assessment may have had some influence. Though each was chosen because of their relationship to geometry and spatial ability, they may not have accurately captured the specific skills and concepts gained from the unit on geometry [24]. A final factor may be the text used by the instructor. Most mathematics texts now recognize the importance of the national mathematics standards and include material to fulfill them. With the classroom instructor in this study using such a text, it may be that geometry instruction was already geared to develop students' geometry

knowledge and understanding, dampening the effect origami might have had on students' skills.

In all, the intent of this study was to determine the impact origami lessons integrated into a mathematics classroom would have on students' abilities. Though spatial visualization and mathematics achievement results differed, it can be said that origami can be beneficial to students. It is important, though, that others continue to study origami's true impact on students. There is little formal research currently reported in this field. Future studies should seek to substantiate other possible benefits of origami and for a variety of age levels. It is in this way that the mathematical community can realize the full potential of origami as an instructional tool.

7 Appendix: Sample Dialogue for Instruction of an Origami Model

The following presents key questions that could accompany the instructions for the *Leaping Frog* origami model (Figure 1). Note that in the following text, *italics* indicates answers expected to teacher-initiated questions.

1. Before you fold your card, what mathematical terms could you use to describe it? [*Rectangle or plane.*] Once you make the creases using adjacent corners of the card, what kind of line segments were formed? [*Perpendicular line segments.*] What kind of angles are formed then? [*Right angles.*] What could you say about the measure of two adjacent right angles? [*They're supplementary.*]

2. Once you mountain fold you form a third line segment. Do you recognize any of the angles formed here? [*There are right and acute angles formed.*] Can you find a set that are supplementary? [*Have student show where they are.*] Could you find the exact measures of the angles without a protractor? [*Yes, since the last line cut them in half, the angles are 45 degrees and 90 degrees.*]

3. Once you do the squash fold, what kind of shapes are formed? [*Right triangle and a rectangle.*] Can you identify the angle measures of each of them? [*Yes, the rectangle has all 90 degree angles and the right triangle has two 45 degree angles and one 90 degree angle.*] Is there a more specific name you can give to the triangle? [*Yes, it's isosceles right!*] What special terms are associated with an isosceles triangle? [*Vertex angle, base angles, legs, and base.*]

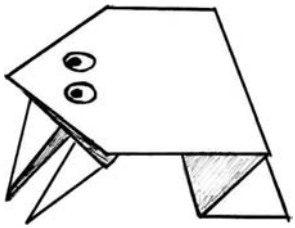

Figure 1. Accompanying model: *Leaping Frog* [25].

4. When you fold the base angles of the isosceles right triangle up, what have you formed? [*Two new, smaller triangles.*] What can you say about them? [*There are four of them that are all congruent. They're all isosceles right like the other larger one.*] How does the area of the small triangles compare to the one from the previous step? [*It's exactly a fourth of the original one.*]

5. When you fold the sides into the middle, what new shapes do you have? [*Trapezoids.*] How do they compare in size? [*They're congruent.*] If you ignore all the folds and look at the figure as a whole, what is it? [*It's a pentagon.*]

6. When you're all done with your frog, what kind of mathematical terms can you identify with it? [*Pentagon, triangles, rectangle, parallel lines, perpendicular lines, ...*]

Bibliography

[1] M. J. Battista, G. H. Wheatley, and G. Talsma, "The Importance of Spatial Visualization and Cognitive Development for Geometry Learning in Preservice Elementary Teachers." *Journal for Research in Mathematics Education* 13 (1982), 332–340.

[2] D. Ben-Chaim, G. Lappan, and R. Houang. "The Effect of Instruction on Spatial Visualization Skills of Middle School Boys and Girls." *American Educational Research Journal* 25 (1988), 51–71.

[3] N. Boakes. "Origami Instruction in the Mathematics Classroom: Its Impact on Spatial Visualization and Achievement of Students." Preprint, 2006.

[4] E. Brinkmann. "Programed Instruction as a Technique for Improving Spatial Visualization." *Journal of Applied Psychology* 50 (1966), 179–184.

[5] M. Casey, R. Nuttall, and E. Pezaris. (2001). Spatial-mechanical reasoning skills versus mathematics self-confidence as mediators of gender differences on mathematics subtests using cross-national gender-based items. *Journal for Research in Mathematics Education, 32*(1), 28–57.

[6] B. Cipoletti and N. Wilson. "Turning Origami into the Language of Mathematics." *Mathematics Teaching in the Middle School* 10:1 (2004), 26–31.

[7] D. Clements and M. Battista. "Geometry and Spatial Reasoning." In *Handbook of Research on Mathematics Teaching and Learning*, edited by D. A. Grouws, pp. 420–464. New York: MacMillan Publication Company, 1992.

[8] J. Dixon. "Computer Use and Visualization in Students' Construction of Reflection and Rotation Concepts." *School Science and Mathematics* 97:7 (1997), 352–359.

[9] N. Drickey. "A Comparison of Virtual and Physical Manipulatives in Teaching Visualization and Spatial Reasoning to Middle School Mathematics Students." PhD dissertation, Utah State University, 2000.

[10] R. Ekstrom, J. French, H. Harman, and D. Derman. *Kit of Factor-Referenced Cognitive Tests*. Princeton, NJ: Educational Testing Service, 1976.

[11] E. Fennema and J. Sherman. "Sex-Related Differences in Mathematics Achievement, Spatial Visualization and Affective Factors." *American Educational Research Journal* 14:1 (1977), 51–71.

[12] E. Fennema and J. Sherman. "Sex-Related Differences in Mathematics Achievement and Related Factors: A Further Study." *Journal for Research in Mathematics Education* 9:3 (1978), 189–203.

[13] J. Fleishman and R. Dusek. "Reliability and Learning Factors Associated with Cognitive Tests." *Psychological Reports* 29 (1971), 523–530.

[14] B. Franco. *Unfolding Mathematics with Unit Origami*. Emeryville, CA: Key Curriculum Press, 1999.

[15] L. Friedman. "A Meta-Analysis of Correlations of Spatial and Mathematical Tasks." Techncial Report, No. TM 018 973, University of Chicago, 1992. (ERIC Document Reproduction Service No. ED 353 270.)

[16] W. Higginson and L. Colgan. "Algebraic Thinking through Origami." *Mathematics Teaching in the Middle School* 6:6 (2001), 343–350.

[17] J. Hyde, E. Fennema, and S. Lamon. "Gender Differences in Mathematics Performance: A Meta-analysis." *Psychological Bulletin* 107:2 (1990), 139–155.

[18] E. Johnson and A. Meade. "Developmental Patterns of Spatial Ability: An Early Sex Difference." *Child Development* 58:3 (1987), 725–740.

[19] M. Linn and A. Petersen. "Emergence and Characterization of Sex Differences in Spatial Ability: A Meta-analysis." *Child Development* 56:6 (1985), 1479–1498.

[20] National Center for Education Statistics. "The Nation's Report Card." Available at http://nces.ed.gov/nationsreportcard/itmrls/, accessed August 10, 2005.

[21] National Council of Teachers of Mathematics. *Principles and Standards for School Mathematics*. Reston, VA: National Council of Teachers of Mathematics, 2000.

[22] R. Robichaux and P. Rodrigue. "Using Origami to Promote Geometric Communication." *Mathematics Teaching in the Middle School* 9:4 (2003), 222–229.

[23] I. Smith. *Spatial Ability: Its Educational and Social Significance*. San Diego, CA: Robert R. Knapp, 1964.

[24] S. Sundberg. "Effect of Spatial Training on Spatial Visualization Ability and Mathematics Achievement as Compared to Traditional Geometry Instruction." PhD dissertation, UNIVERSITY, 1994.

[25] Florence Temko. "Leaping Frog." In *Origami Toys*, by Florence Temko, Barbara Poeter, and Dave Kutchukian, pp. 30–31. Boston MA: Tuttle Publishing, 2003.

[26] A. Tubis. "A Brief Summary of Some Educational Benefits Associated with the Folding and Analysis of a Class of Origami Boxes." Unpublished manuscript, 2004.

[27] A. Tubis and C. Mills. *Unfolding Mathematics with Origami Boxes*. Emeryville, CA: Key Curriculum Press, 2006.

[28] US Department of Education, Office of Educational Research and Improvement, National Center for Educational Statistics. *The NAEP 1996 Technical Report*. Washington, DC: National Center for Educational Statistics, 1996.

[29] Z. Usiskin. "Resolving the Continuing Dilemmas in School Geometry." In *Learning and Teaching Geometry, K-12: 1987 Yearbook*, edited by M. Lindquist and A. Shulte, pp. 17–31. Reston, VA: National Council of Teachers of Mathematics, 1987.

[30] D. Voyer, S. Voyer, and M. Bryden. "Magnitude of Sex Differences in Spatial Abilities: A Meta-analysis and Consideration of Critical Variables." *Psychological Bulletin* 117:2 (1995), 250–270.

Understanding the Effect of Origami Practice, Cognition, and Language on Spatial Reasoning

Michael Wilson, Robin Flanagan,
Rona Gurkewitz, and Laura Skrip

1 Discussion

There is ample evidence to suggest that US students are not performing as well as they might in mathematics. This evidence comes in the form of the less than stellar performances on the TIMSS and National Assessment of Educational Performance (NAEP) in mathematics [18]. Vail [24] notes that the results of the NAEP suggest that mathematics learning is not moving forward. Cavanagh [5] asserts that the US government needs to establish policies that generate an improvement in the quality of the mathematics in US schools. Field [8] stresses that higher education in the US should have mathematics education as one of its top priorities.

In an initial study, Flanagan et al. [11] found that participants who experienced a treatment that involved several diagram-based origami activities were significantly faster on a mental rotation task than the students who had not experienced the treatment ($M = 1519$ ms and $SD = 868$ ms versus $M = 1783$ ms and $SD = 993$ ms, where M is mean and SD is standard deviation). The standardized coefficients of the regression equation generated from this analysis were as follows: estimated reaction time = (participants $\times -.115$) + (primed $\times$ .08) + (treatment $\times$ .144). In addition, there are a number of other studies that suggest a significant relationship

between mental rotation like that experienced by students in Flanagan's study and students' performance in mathematics [4, 13, 19]. Hence, the relationship found in the Flanagan et al. study, if understood, might provide some insights into improvement of mathematics performance.

There is also ample evidence to show a connection between origami and mathematics. For example, Alperin [1] discusses the origami in the context of Euclidean number systems using origami axioms for Pythagorean numbers, midpoint bisectors, and trisector axioms. Demaine and Demaine [6] provide an overview of the work accomplished in computational origami that includes a discussion of 37 articles on the subject. In addition, origami has been incorporated into educational instruction in mathematics. In the instructional realm it is used primarily in areas associated with geometry and trigonometry [14,21]. Yet, relatively little research could be found that specifically supports the use of origami in the development of cognitive operations associated with mathematical problem solving. The only article found was by Bart et al. [3], who investigated the extent to which origami practices affected the ability of four- to six-year-old Japanese and American children to judge the size of triangles and squares after manipulating these shapes during origami experiences. There is clearly room for more of this research.

1.1 Problem Solving and Problem Space

Both the mental rotation activity studied by Flanagan [11] and much of the support for mathematics education involves the complex activities involved in problem solving. According to Anderson [2], *problem solving* occurs whenever people become involved in a sequence of related mental behaviors with the intent of achieving a goal. A problem occurs when the goal is obstructed and requires some process to obtain, or is not obtainable given existing processes, behaviors, or routines. Jonassen [15] notes that for these mental behaviors involved in problem solving to be successful, they must occur within a cognitively defined *problem space* that is relevant to the problem. This space, according to Jonassan, involves the use of mental representations. The space established in these mental representations are multimodal composites that may consist of elements such as "structural knowledge, procedural knowledge, reflective knowledge, images, metaphors of the system and executive strategic knowledge" [15, p. 5]. Zhang and Zhang [25] discuss how mathematical problem space includes a universe of the problem, its structure, and its attributes. That is, the problem solver must be able to create a mental representation or replica of the circumstances and qualities associated with the problem with enough fidelity and dimensionality to make that representation consistent with the actual problem to be solved, and thereby attain the goal at hand. Mental

rotation as mental representation presents problems in a geometric/spatial format [22]. Roberts, Gilmore, and Woods [20] and Fisk and Sharp [9] also suggest that the problem space for spatial problems contain a verbal component in which the respondent organizes and modulates the mental representations associated with the mental aspects of spatial representations.

The Flanagan et al. [11] results suggest that the students involved in origami had some enhancements to their problem space that those who had not experienced the origami did not have. Understanding the differences between the two groups, as well as characteristics of those who performed better on the mental rotation task, should provide some insight into the cognitive composition of problem space as experienced by students in Flanagan's origami study.

1.2 Origami and Motivation

Let us also make the assumption that the problem space has some volitional qualities. For if one is to make the effort to construct the space and step into it when it becomes relevant, there must be something to compel the user in that direction, i.e., something to drive the problem solver to use a problem space in solution of the problem. In this case as well, origami represents a constructive activity with inherently desirable characteristics that internally compels learners' participation in activities associated with the problem space described above and also associated with aspects of mathematics. There is some research that supports the compelling quality inherent in origami and the motivation it appears to invoke [16, 17, 23]. Without this force, learning does not tend to occur since without motivation, students do not focus their attention on the learning at hand and consequently do not accomplish the learning tasks that the instruction is designed to support, to wit, the mental representations associated with mental rotations. Is the problem space also inhabited by volitional qualities, as well as the cognitive ones suggested above?

2 Design

2.1 Purpose

The purpose of the investigation is to take the Flanagan et al. [11] results and examine them for insights into the composition of the problem space associated with the mental rotation task. The methodology and treatment described here are also described in [11]. Those results and analysis have shown that origami effectively supports the development of students' men-

tal representation. In this paper, we want to examine the student data analyzed in [11], as well as some data that were not part of the original paper, to understand how the origami might have affected those involved, enhancing their problem spaces well enough to provide some advantage in a mental facility shown to relate to mathematics performance. By extension, this understanding might also suggest areas that can generalize to other problem spaces of mathematics and perhaps similar mathematics-related spaces such as science and computer technology.

2.2 Methodology

The investigation described in this paper began with the intent to simply determine whether the relationship existed [11]. This paper is an attempt to extend the investigation into originally unintended territory. Because of the additional direction, there is a less than perfect fit between the methodology and the intended goals described here. Instead, this paper represents thinking that will be used not only to consider the results of the current study but to extend the thinking engendered through the study to further theorizing and investigations. Since the investigation is exploratory in nature, the alpha will be set rather high—at about .2. So it must be kept in mind that the results are extremely tentative and speculative, and the discussion of results must be followed with considerable caution. The alpha is set high in order to identify more readily the relationships that would be affected by considerable noise due to the original construction of the study.

2.3 Sample

The investigation used a group of 37 middle-school students who were involved in a summer enrichment program. Each student was randomly assigned to one of two groups. The control group ($n = 19$) worked on a computerized mental rotation problem before working on a set of origami tasks and the treatment group worked on the origami tasks before attempting the mental rotation. The origami task required the students to generate three origami constructions by following a set of pictures and explanatory text. Although they were randomly assigned, the control group was slightly older (12.42 to 12.19), reported a slightly higher sense of math success (4.79 to 4.38 on a scale of 1 to 10) and slightly better attitude toward math (7.75 to 7.57 on a scale of 1 to 10). These differences were not significant, and consistently favored the control group. Prior to becoming part of the investigation, consent forms were received for all students involved. Students whose parents did not give permission did not participate, and students who did not give their own assent did not participate, either.

2.4 Materials

The origami task consisted of following "standard" Yoshizawa-Randlett diagrams. This is in contrast to being shown how to fold by a teacher demonstration and was selected because it has more in common with the mental rotation tasks that were used.

The models being folded were a box, a picture frame, and a small book. The folding involved in these models would be classified as simple by OrigamiUSA. The first two models were each made from one sheet of 8 1/2 × 11 inch paper and the book was made from ten sheets of 3 inch square paper, color coded to simplify the assembly of the book. While the folding of the book modules is simple, the assembly into the book was not immediately obvious to the students and required considerable attention to complete.

The diagrams from which students worked showed a sequence of line drawings of a piece of paper being folded, starting with the original piece. Each drawing, in turn, showed the result of the folds made in the previous step and the folds to be performed in the next step. A possible connection between the origami diagrams and mental rotation may have resulted from the need to transform images. In origami this meant transforming images from the directions, and in the mental rotation this meant transforming one image to compare it to the other. In both cases, transformations were accomplished through the mental manipulations of lines, spaces, and angles.

The mental rotation task was internet based and produced by Cog Lab [12]; it requires respondents to determine whether two figures are the same or a mirror image when one of the figures is rotated 0, 45, 90, or 180 degrees. Each participant completed 80 mental rotation trials. In addition, prior research [10] suggested that priming might be a factor. The priming task involved a set of visualization problems and the nonpriming task involved reading a brief history of origami and answering questions. Both the treatment and control groups were further separated into priming and nonpriming groups.

2.5 Treatment

Each session of the investigation occurred on either a Friday or a Monday. Both measurements of mental rotation occurred on a Monday. During the first session, both groups of participants were given a brief introduction to origami and an explanation of the mental rotation task [22] that they would encounter during the investigation in the internet-based Cog Lab program. During the second session, the control group worked on a priming task and the Cog Lab program, and the treatment group worked on the first origami task. During the third session, the control group worked on the

first origami task and the treatment group on the second origami task. During the fourth session, the control group worked on the second origami task and the treatment group on a priming task and the Cog Lab program. The fifth session consisted of a debriefing for all participants and a final origami task.

After each session, the participants were asked to complete a questionnaire, which addressed their feelings about mathematics and the activity they had just experienced. They were also given the chance to explain the activity they had just experienced.

3 Results

From the Flanagan et al. results described above, the origami exercises appear to have had some impact on the participants' facility with the mental rotation. Because of this result, we will make the assumption that something about origami is enhancing that part of mathematical problem space. In that the solution to the mental rotation task was considered the single goal consistent across all participants, and the problem space is the mental area each participant constructed and used to support his or her solution to the mental rotation problem, an analysis of the effect of origami exercises on that space should provide us with some clues to its characteristics. This study is in effect an expedition, a search for possible explanatory clues. As such, the concern for beta errors outweighs those associated with alpha errors, hence the high alpha level (0.2).

The variables in this study were generated in two ways. The dependent variable is the speed with which the mental rotation problems were solved; this was collected using a computer program. The other means of collecting variable data was a questionnaire to which students responded at the end of each origami or mental rotation exercise. From this questionnaire came data for the following variables:

- *Origami-enjoy* was based upon the response of a 1–10 point rating to the question: "how much did you enjoyed working on this task?"
- *Origami-giveup* on origami task was a 1–10 point rating of the question: "how close did you get to giving up on this task?"
- *Math-attitude* was a 1–10 point rating of the question: "how much do you like math?"
- *Math-success* was a 1–10 point rating of the question: "how successful do you feel in math?"

- *Rotation-enjoy* was a 1–10 point rating of the statement: "enjoyed working on this task."

- *Rotation-giveup* was a 1–10 point rating of the question: "how close did you get to giving up on this task?"

Confusion was a categorical coding of the types of confusion expressed in writing by the participants in addressing the mental rotation task. Three types of confusion were observed:

- *image*: dealing with the visual aspects ("I couldn't tell whether it was mirror or not"),

- *process:* knowing what problem to address or how to address the problem ("to mentally flip the shapes to figure the art"),

- *feedback:* needing to know whether the response was correct or not (e.g., "the most confusing part is I thought I was wrong").

Challenge was the level of challenge the participant experienced with the rotation task. A rating of one was given to the highest level showing the most positive experience ("the most fun aspect was the final results"); a rating of four was given for less than positive comments describing the process ("it was kind of serious and not exciting").

Attention was the level of attention the participant paid to what he or she was doing or thinking to solve the rotation problem during the rotation task as reflected in the participant's comments. These ranged from the lowest-level attention response ("I did what I had to do") to the highest-level attention response ("at first I was just guessing if the shapes were similar or mirror images, then I started randomly rotating the shapes to see if they were similar or mirror images. I would tell someone who was trying this cognitive reasoning task to rotate the shape in your head into different directions, until it looked similar or mirrored to the other shape").

Language was a simple counting of the number of words used in response to the three open-ended questions. *Mechanics* was the number of words used in responses that could be used to refer to aspects of the process or components involved in both the origami and the mental rotation tasks, such as aspects of line and angle comparison.

The following analyses were conducted to obtain a sense of the configuration of a problem space that could support a mental rotation task that we have assumed was established by the origami experiences. These analyses examine both how the treatment and control group may differ and

how the available variables may have influenced participants' solutions to the rotation problem.

The first analysis was conducted to gain some insight into whether the enjoyment of origami could have had any effect on the treatment group's performance on the mental rotation task. In this analysis, the Origami-enjoy and Origami-giveup levels are taken as reflections of participants' feelings associated with the problem space in their origami experience. These were the only two variables that clearly differentiated the treatment group from the control groups.

From the overall F test ($p = .023$), there does appear to be a relationship between the enjoyment that students experienced in the origami and the extent to which they felt like giving up on the mental rotation tasks. From the beta weights ($B = -.986$ and $-.491$) and t-test statistics ($p = .010$ and $.151$), it appears that both the enjoyment and sense of giving up on the rotation problems had some impact on students' ability to address the mental rotation. In addition, the enjoyment aspect was clearly more effective than the sense of giving up.

When the same analysis was conducted on the control group, the $F = 1.146, p = .343$) is not significant. Therefore, the effect appears to exist for the treatment group and does not exist for the control group. Furthermore, the control group R-squared accounts for considerably less variance than those shown for the experimental group (control $R^2 = .125$, treatment $R^2 = .496$). In the control group statistics, the beta statistics suggest a stronger sense of giving up compared to enjoyment ($B = -.337$ and $-.073$). Since the control group did not experience their origami until after they had been involved in the mental rotation, these results suggest that the sense of giving up on the mental rotation task may be a general effect on problem space, whereas the enjoyment is a specific result of the origami experiences.

The second set of analyses was conducted to gain some insights into how the control and treatment participants might be different and how these differences might be associated with or could have influenced the participants' performances on the mental rotation task. This portion of the analysis was accomplished through a series of t-tests.

The most significant difference between the treatment and control groups appears to be in the area of language ($p = .02$). This suggests that the treatment group wrote a great deal more than the control group. At a somewhat lower level of significance, the control group appears to be paying more attention ($p = .14$) to the rotation processes. These are the only two areas that met the rather liberal standards established for the alpha level. In the spirit of exploration, four additional variables appeared to be close to the significance criteria: Challenge ($p = .21$), Rotation-giveup ($p = .26$), Rotation-enjoy ($p = .27$), and Math-success ($p = .28$). The two

groups appear quite similar, however, in all of the rest of the variables—Mechanics, Origami-giveup, and Math-attitude, suggesting that these last variables had no impact on the origami treatment.

The third analysis addressed inherent qualities in both the treatment and control groups combined that might have had an effect on how rapidly they accomplished the mental rotation tasks. This analysis shows the predictor variables producing an R squared of .419 and an overall F of 2.166, $df = 8$, and a $p = .07$, suggesting a significant solution that explained slightly less than half of the variance associated with the response to the rotation task. The three variables with the most significant effect on the speed of rotation were Attention ($p = .009$), followed by Math-attitude ($p = .186$), and Challenge ($p = .187$). The Math-attitude variable is a relatively strong predictor but both groups appear about the same on this variable. Although the Language variable shows significant difference between the two groups in the t-test comparison, it was not a significant predictor of mental rotation performance. In these two sets of results together, only the Attention and Challenge variables have approached significance across the two tests, suggesting difference between treatment and control groups as well as significance in prediction discussed above. All of the other variables show neither any difference between the groups nor affect on the mental rotation task.

The fourth analysis examines the difference between the treatment and control groups in the kinds of confusion they experienced during the rotation task. This analysis is based on the written responses to a question about what confused participants the most. The result from this chi square analysis ($p = .08$) suggests that the participants in the treatment group, while solving the rotation task, are proportionately more involved in the image; and the participants in the control group are more involved in the process itself. This result tends to support the analysis above in which the treatment group seems to be placing less of their attention in the processes associated with the rotation task.

4 Conclusions

The treatment group appears to be paying less attention to the mental rotation tasks than the control group and this appears to be having some effect on the efficiency in solving the mental rotation problem. Since attention was coded as the level of conscious involvement in the process of problem solving, this result suggests that the treatment group members may have paid less conscious attention to the processes of solving the mental rotation task problems, which resulted in significantly higher speeds in their solution of each rotation problem.

In addition to the cognitive effects on mental rotation, the compelling nature of origami also seems to have played a role in the solution of the rotation problem. Those treatment group members who found enjoyment and the sense of a positive challenge in the origami subsequently performed better on the rotation task, as suggested by the multiple regression conducted on the treatment portion of the sample. When the two groups were compared, the treatment group showed a slightly larger mean, suggesting that it may have had a slightly better experience with the origami than the control group, who did not get to the origami until after they had experienced the rotation.

The results taken together suggest a problem space that is both cognitive and motivational. It appears to exclude, however, the function of language. Although a comparison of the two groups' level of language production in the Language variable showed a difference between the two groups, Language and the kinds of language used in the Mechanics variable appeared to not have any influence on the speed of the rotation response.

Origami may play a part in the way students pay attention to the rotation task, developing and supporting both the level of focus on task-related elements and perhaps some sort of automatic response associated with attention on the visual aspects of the tasks. These results considered in conjunction with those on language suggest that the effect on problem space is more associated with the visual than through language. The visual component seems to have supported a higher level of automatic behavior in the treatment group members compared to the response observed in the control group

Much of what experts do to solve problems is accomplished in the expert's unconscious [7]. In this way, much of the problem solving that experts do is automatic. Perhaps solving the origami problems produced in the treatment group a greater facility with the rotation problems in the development of underlying visual mental representational skills. Automatic reactions are also a function of attention, which is also supported by these results. Once acquired through origami, perhaps the treatment group members acquired, at an unconscious level, the skills needed to solve the rotation problem, thereby experiencing more positive reactions and ultimately more success without the effort needed by the control group participants.

The results in this study are consistent with the work of Bart et al. [3] on children's development of shape estimation in that they both show the influence of origami on mathematical thinking. The analysis goes beyond this study, however, by endeavoring to suggest some of the conditions of the problem space that seem to underlie the relationship between the origami and the mathematics-related cognition.

Before going too far with conjecture, however, caution must be an important concern here. We must be clear that the alpha level was set very

high in order to search for possible explanations among data with a substantial noise factor. The possible findings must be considered weak and must be followed with a great deal of additional work expanding and understanding both the potential and the ramification of origami as well as other practices that might be useful in the development of the capacity to solve problems supported by cognitive conditions described here as problem space. If we are to use origami to support mathematics and other learning, more investigations are needed to clarify and understand the underlying processes and effects involved in using origami as a problem space support. It is still too early in the investigative cycle to tell whether, or just how, to use origami in the development of solving problems in mathematics or related areas. Still, the road forward looks very promising from where we stand.

Bibliography

[1] Roger C. Alperin. "Trisections and Totally Real Origami." *American Mathematical Monthly* 112:3 (2005), 200–211.

[2] J. R. Anderson. *Cognitive Psychology and Its Implications*. New York: Freeman, 1980.

[3] W. M. Bart, M. Kataoka, L. J. Kinne, S. Sukemune, and M. Yuzawa. "The Effect of 'Origami' Practice on Size Comparison Strategy among Young Japanese and American Children." *Journal of Research in Childhood Education* 13:2 (1999), 133–43.

[4] M. B. Casey, R. Nuttall, E. Pezaris, and C. P. Benbow. "The Influence of Spatial Ability on Gender Differences in Mathematics: College Entrance Test Scores across Diverse Samples." *Developmental Psychology* 31:4 (1995), 697–705.

[5] S. Cavanagh. "NAEP Scores Show Few Budding Scientists." *Education Week* 25:39 (2006), 5–16.

[6] E. D. Demaine and M. L. Demaine. "Recent Results in Computational Origami." In *Origami^3: Proceedings of the Third International Meeting of Origami Science, Mathematics, and Education*, edited by Thomas Hull, pp. 3–16. Natick, MA: A K Peters, 2002.

[7] A. Dijksterhuis, M. B. Bos, L. F. Nordgren, and R. B. van Baaren. "On Making the Right Choice: The Deliberation-without-Attention Effect." *Science* 311:5763 (2006), 1005–1007.

[8] K. Field. "Federal commission Gears up for the Home Stretch." *Chronicle of Higher Education* 52:33 (2006), A32–A34.

[9] J. E. Fisk and C. A. Sharp. "The Role of the Executive System in Visuospatial Memory Functioning." *Brain and Cognition* 52 (2003), 364–381.

[10] R. Flanagan, R. Gurkewitz, M. Wilson, and L. Skrip. "Improving Spatial Reasoning through Experience: A Pilot Study." Poster presented at the annual meeting of the American Psychological Society, Los Angeles, CA, May 27, 2005.

[11] R. Flanagan, R. Gurkewitz, M. Wilson, and L. Skrip. "IImproving Spatial Reasoning through Experience: Evidence of Priming and Long-Term Effects." Poster presented at the annual meeting of the Association for Psychological Science (formerly American Psychological Society), New York, NY, May 26, 2006.

[12] G. Francis, I. Neath, A. MacKewn, and D. Goldthwaite. *CogLab on a CD*. Belmont, CA: Wadsworth, 2004.

[13] A. Gagatsis and M. Shiakalli. "Ability to Translate from One Representation of the Concept of Function to Another and Mathematical Problem Solving." *Educational Psychology* 24:5 (2004), 645–657.

[14] T. Hull. "Origami Quiz." *Mathematical Intelligencer* 26:4 (2004), 38–63.

[15] D. H. Jonassen. "Toward a Design Theory of Problem Solving." *Educational Technology Research and Development* 48:4 (2000), 63–85

[16] K. A. Lawless and S. W. Brown. "Multimedia Learning Environments: Issues of Learner Control and Navigation." *Instructional Science* 25:2 (1997), 117–131.

[17] D. C. McClelland and A. S. Alschuler. "Achievement Motivation Development Project: Final Report, Appendix IV, Part 2." Technical report, Education Ventures, Inc., 1971. (ERIC Document No. ED052481.)

[18] T. Neidorf, M. Brinkley, and M. Stephens. "Comparing Science Content in the National Assessment of Educational Progress (NAEP) 2000 and Trends in International Mathematics and Science Study (TIMSS) 2003 Assessments." Technical report, National Center for Education Statistics, 2006. Available at http://hub.mspnet.org/entry.cfm/12886.

[19] M. Reuhkala. "Mathematical Skills in Ninth-Graders: Relationship with Visuo-spatial Abilities and Working Memory." *Educational Psychology* 21:4 (2001), 387–399.

[20] M. J. Roberts, D. J. Gilmore, and D. J. Woods. "Individual Differences and Strategy Selection in Reasoning." *British Journal of Psychology* 88 (1997), 473–492.

[21] Rebecca R. Robichaux and Paulette R. Rodrigue. "Using Origami to Promote Geometric Communication." *Mathematics Teaching in the Middle School* 9:4 (2003), 222–229.

[22] Shepard and Metzlar. "Mental Rotation of Three-Dimensional Objects." *Science* 171 (1971), 701–703.

[23] J. Y. Smith. "The Origami Game." In *Activities Handbook for the Teaching of Psychology*, Vol. 2, edited by Vivian Parker Makosky, Linda Genevieve Whittemore, and Anne M. Rogers, pp. 235–238. Washington, DC: American Psychological Association, 1987.

[24] K. Vail. "Federal Commission Gears Up for the Home Stretch." *American School Board Journal* 193:8 (2006), 6.

[25] L. Zhang and B. Zhang. "The Quotient Space Theory of Problem Solving." *Fundamenta Informaticae* 59:2–3 (2004), 287–298.

Modular Origami in the Secondary Geometry Classroom

Margaret Cagle

1 Introduction

In the current climate of increasingly demanding standards and high-stakes testing, it may be hard to believe that there is an area of school mathematics not receiving sufficient attention, but that is indeed the case with three-dimensional geometry. While other areas of the K-12 school mathematics curriculum are characterized by long lists of concepts and skills to be mastered, three-dimensional geometry is often reduced to a single line item requiring students to calculate the surface area and volume of a variety of solids. The National Council of Teachers of Mathematics has identified four overarching geometry standards for students in grades K-12:

1. Analyze characteristics and properties of two- and three-dimensional geometric shapes and develop mathematical arguments about geometric relationships.
2. Specify locations and describe spatial relationships using coordinate geometry and other representational systems.
3. Apply transformations and use symmetry to analyze mathematical situations.
4. Use visualization, spatial reasoning, and geometric modeling to solve problems [5].

These standards clearly encompass a broad view of geometry, including the need for students to develop conceptual understanding and problem-solving abilities in a three-dimensional environment.

2 Issues Faced by Students in Secondary Geometry

Meeting the standards proposed by NCTM requires students to move from description to analysis, abstraction, and finally formal proof, as described in the Van Hiele Model Levels of Geometric Thinking:

- Level One: Visualization

  Children at this level can recognize figures by their physical appearance.

- Level Two: Analysis

  At this level, children can classify to some extent and can discern some characteristics. They still cannot see interrelationships between figures.

- Level Three: Informal Deduction

  Children can establish interrelationships between figures and derive relationships among figures. Simple proofs can be followed, though not understood completely.

- Level Four: Formal Deduction

  Students at this level understand the significance of deduction and the role of postulates, theorems, and proofs. They are able to write proofs with understanding.

- Level Five: Rigor

  Students understand how to work in an axiomatic system, and are able to make abstract deductions. Non-Euclidean geometry can be understood at this highest level.

By the time students are in a secondary high school course, they are expected to be operating at Van Hiele level three and moving to level four. Yet most of the curricula they have encountered in their K-8 mathematics preparation only address geometry at level one, focusing on naming shapes and relationships such as parallel or perpendicular, with, at best, infrequent opportunities to develop geometric reasoning. Today's children do not play in the same ways as children of past generations and this is having a significant negative impact on the development of their spatial

reasoning and visualization abilities. People of earlier generations grew up routinely engaged in activities that built spatial reasoning. They learned to sew, following diagrams and using patterns to transform two-dimensional fabric into three-dimensional garments. They played with Lincoln Logs, Tinkertoys, and other blocks well past the age of four and may have even graduated to Erector sets complete with motors and gears. They assembled jigsaw puzzles and built scale models. They climbed trees, played on jungle gyms, and built impromptu forts from card tables and sofa cushions rather than playing with prefabricated plastic environments. Wood, metal and plastics shop classes were a staple in junior high schools across the country, but are now virtually gone. While many of today's students play with simple puzzles and build with Lego blocks as young children, most quickly move to video games, where they spend their time manipulating two-dimensional images of three-dimensional worlds. As a result, they arrive in secondary geometry classrooms with weak spatial reasoning and poor visualization skills.

3 The Role of Modular Origami in the Secondary Geometry Classroom

Given this seemingly daunting confluence of issues, it is reasonable to ask why origami should be added to the already overcrowded curriculum. The answer is that origami can provide multiple opportunities to remediate these areas of weakness in an inherently engaging manner. It is accessible, affordable, nonroutine, and allows students to produce objects of their own. Building a model for one's self provides a profoundly deeper understanding of the geometry of an object than engaging in a study of either a premade model or a two-dimensional representation. Educators need to intentionally move students from concrete to abstract and in order to do that, students need to be provided with support along the way with intermediate steps. Before it is possible to visualize accurately in three dimensions, students need to be taught to look at and analyze three-dimensional objects. Developing this ability does not happen overnight, but can be built over time through repeated exposure to meaningful exercises.

Origami builds other mathematical capacities as well. If students are to use mathematical vocabulary with precision, then they need to be provided with rich environments in which to use that vocabulary in meaningful ways. Concepts are reinforced when dealt with in concert with the correct vocabulary, using concrete examples. Constructing origami models provides a setting to reinforce both the correct vocabulary and underlying concepts because students are using the words as they are using the con-

cepts to fold a model. Educators should be prepared to take advantage of unexpected opportunities to review and reinforce important mathematical concepts while using origami in their classrooms. Something as basic as asking students to fold a square in half can easily lead to a deep discussion of the number of ways in which this can be achieved. Most students will suggest two possibilities and will be amazed when through discussion they realize that there are infinite possibilities, provided the fold passes through the center of the square. Such opportunities rarely arise when performing routine tasks. The construction of origami models also provides a natural environment in which to develop accuracy. Students may have different personal standards for how accurately they fold. As an educator, it is important to allow students to determine their own criteria for their finished models. Remember that the goal is not to produce finely crafted end products, but rather to develop students' spatial reasoning, visualization, and three-dimensional problem-solving abilities. The fact that some students are tolerant of a great deal of imprecision may lead to problems in completing final models, but it also presents a natural opportunity to discuss the concept of accumulated error. Some models also rely on visual estimation. Estimation is an important life skill, but like so many topics that are not easily assessed using multiple choice tests, it is being stripped out of the K-12 curriculum.

4 Modular Polyhedral Models

While all origami models provide an opportunity to build spatial reasoning and visualization skills, focusing on polyhedra creates finished models that can themselves be used in further study of three-dimensional geometry. One possible classification of origami polyhedral models divides them into four families; face models, skeleton models, edge models, and other or miscellaneous models. (See Figure 1.) In face models, each face or seat of the polyhedra is built as a single piece. This means that there is exactly one piece composing each face or a single piece may be manipulated to construct all of the faces, but any individual face is monolithic, with no seams or joints. Skeleton models rely on constructing some of the internal or underlying characteristics of the polyhedra. This typically means that the model is made of portions of certain of the planes of symmetry, which then end at the edges of the polyhedra. In edge models, each edge is constructed individually and then assembled at the vertices to produce the polyhedra. There is a wide variety of types of edge models that have been engineered for this purpose. Some are specific to a particular polyhedron, while others have end variations that allow for them to be used to construct various models. Tom Hull's PHIZZ unit [3] has the flexibility, both literal and

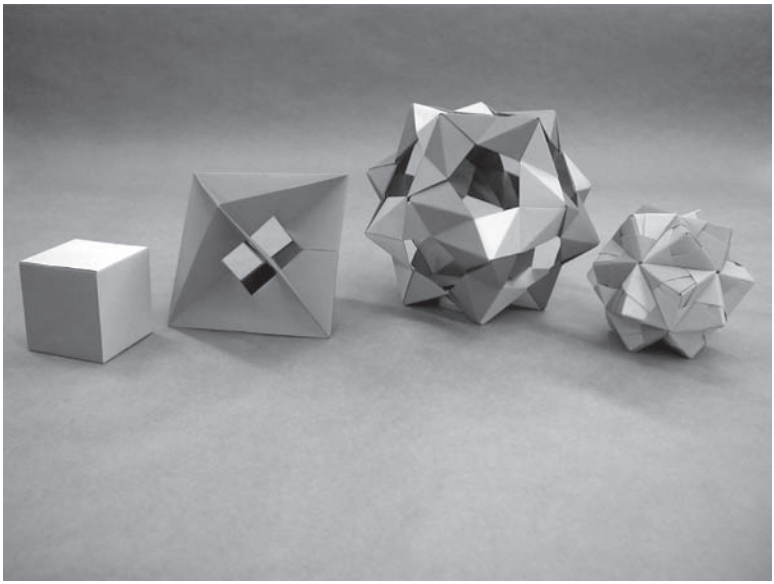

Figure 1. Models from all four families. From left to right: face model (Miyuki Kawamura's cube [4]), skeleton model (Lewis Simon's octahedron [1]), edge model (Tom Hull's PHIZZ dodecahedron [3]), and miscellaneous model (Mitsunobu Sonobe's augmented icosahedron [2]).

figurative, to build pentagonal, hexagonal, or heptagonal faces, allowing its use in a wide range of models. Other or miscellaneous models are comprised of modules that make only part of a face or edge such as the Sonobe unit or its many variations [2]. While they produce beautiful end products and have much to recommend them, in general this family of models does not provide as clear an opportunity for direct study of polyhedra and they do not readily justify the amount of time required to construct them, as compared to models from the other three families.

4.1 Face Models

Because face models are solid, they are well suited for study of attributes of the individual faces of a polyhedron, and the relationships between those faces. This can include investigations about the number of colors required to ensure that a given model has no adjacent faces (those sharing a common edge) of the same color, or about the case in which no faces of the same color meet at any given vertex. The creation of numerous models can be used by students to investigate space packing with polyhedra. This investigation can be used as a means of discovering the dihedral angles of the solids as an

analogy to looking at interior angles of regular polygons and their planar tessellations.

4.2 Skeleton Models

The inherent characteristics of the skeletal construction present opportunities to explore the underlying structure of individual polyhedra and related polyhedra, especially looking at planes and axes of symmetry. Most skeleton models are based on a particular arrangement of planes of symmetry for a polyhedron. By examining one set of planes of symmetry, students are typically able to visualize other sets of planes and axes of symmetry. This family of models can also be used as a means of discussing the concept of polyhedral duals. Duals are formed by replacing each face of a polyhedron with a vertex at the center of that face and then connecting those new vertices across the edges of the original polyhedron. The resultant polyhedron shares the same planes and axes of symmetry with the original. Building skeleton models of a polyhedron and its dual allows students to see this relationship in a very concrete way. Skeleton models also clearly indicate the center of regular and semiregular polyhedra; the point of intersection of all the planes and axes of symmetry. This allows students to develop a better understanding of the ability to inscribe every Platonic and Archimedean polyhedron inside a sphere so that each vertex lies on the surface of the sphere.

The structure of skeleton models provides a means for examining polyhedra from another perspective, namely, their possible congruent dissections. The fact that most skeleton models are based on planes of symmetry allows students to see one possible way of slicing a polyhedron into congruent parts. This can be used to further study related polyhedra, such as the cube and the rhombic dodecahedron. One possible interpretation of a rhombic dodecahedron is as originating from a three-dimensional checkerboard of cubes, redistributed using Dirichlet domains. Alternating cubes are capturing volume from each of the adjacent cubes on all six of their faces. This means that each cube that is being cannibalized is divided along its planes of symmetry to create six congruent square-base pyramids, which are then added onto the faces of the cubes that remain intact. The resultant polyhedra are rhombic dodecahedra. When students build a skeleton model of a cube, they clearly see how any cube can be sliced into six congruent square-base pyramids and how each of those pyramids could be added onto the faces of another cube.

4.3 Edge Models

Edge models are especially well suited for the study of relationships between different sides of a polyhedron because they are typically open. Students

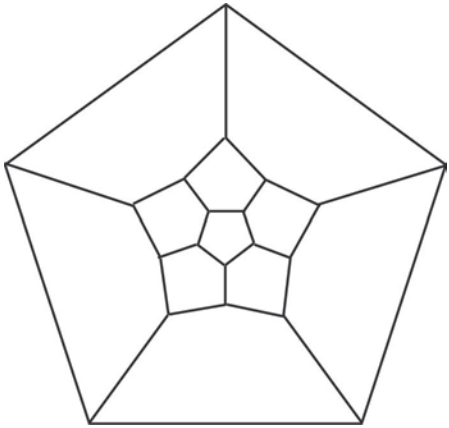

Figure 2. Schlegel diagram of a dodecahedron.

can actually look through a model to examine the relationships of opposite sides. Until they have held up an edge model and looked through the center, students rarely notice that the opposite faces of a dodecahedron are not only parallel, but are also 180 degrees rotated from each other. Most edge models rely on joining individual modules at the vertices, which provides for a discussion about the relationship between the edges and the vertices. Euler's formula for the relationship between vertices, edges, and faces of a polyhedron is arrived at as a natural extension of building a particular number of edges and then assembling them at a given number of vertices to create a given number of faces. In a traditional geometry course, students may be given the formula, but as with most mathematics that is taught without a meaningful context, it is rarely understood or remembered. Because an edge model reduces a polyhedron to a frame, it can be effectively used to help students see the connections between three-dimensional geometry and graph theory. Looking at a frame representation of a polyhedron makes it easy to connect it to a Schlegel diagram (Figure 2), which is a type of planar graph, topologically equivalent to the polyhedron. Schlegel diagrams can be used to examine relationships between the vertices, edges, and/or faces of a polyhedron. They are also useful in making decisions about different types of edge colorings for the three-dimensional models. It may be desirable to have a dodecahedron made with five colors such that each color forms one side of every pentagonal face. It may also be desirable to have a dodecahedron made with three colors such that each color is present at every vertex. Both of these coloring schemes are more efficiently explored in a two-dimensional environment before they are used to guide the actual assembly of an origami model.

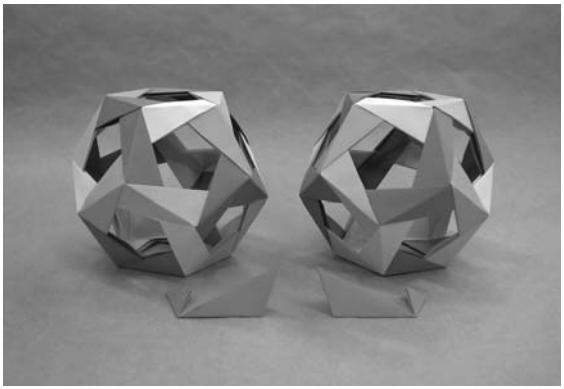

Figure 3. Right-handed and left-handed dodecahedra and their modular units. (Unit designed by Robert Neale [6].)

4.4 Modular Models

The fact that all modular models are assembled from numerous congruent pieces, provides another opportunity to strengthen students' ability to reason spatially. The number of pieces used to construct a model can be used to inform discussion about the underlying structure of the polyhedron. Face and edge models typically have a one to one correspondence between the number of pieces and either the number of faces or the number of edges. The number of edges that meet at a vertex can be used by students to make sense of the assembly process. If they know that three edges meet at a vertex, students can imagine a projection of the vertex with each edge forming 120 degree angles with the other edges. As the model is assembled, students must be constantly adjusting and updating their understanding of the model as it evolves. Few other classroom activities provide opportunities for students to problem-solve in three dimensions within a changing environment.

Most modular constructions rely on pieces that have either a right-handed or left-handed bias (see Figure 3), presenting an opportunity to introduce and discuss the concept of chirality. While chirality or handedness is present in geometry, appearing in the snub Archimedean polyhedra, it plays an important role in many other fields. Many chemical structures are defined by their handedness. Students often stumble across the issue of handedness when working cooperatively with others to build a model. Despite explicit instruction, many students will produce modular units with the orientation opposite from what they are shown. This disparity will only be noticed when students attempt to assemble pieces that have different chirality.

5 Conclusion

Perhaps the most powerful arguments for incorporating modular origami models into the secondary geometry classroom are that it creates a forum for active discussion among students and it connects to so many branches of mathematics while appearing to students to have nothing to do with math. Sense making is tied to language and when students engage in explaining to each other the means to assemble a model, they are also enriching and solidifying their own understanding of the underlying structure and characteristics of the polyhedra that they are building. Students do not learn the most by watching or by doing, but rather they learn the most by reflecting on and talking about the work in which they are engaged. As more and more is expected of students at younger and younger ages, they are tending to compartmentalize their learning. Students are given neither the time nor the encouragement to connect ideas between disciplines or even within disciplines. This may be most egregiously apparent in mathematics classrooms where students typically view each topic, concept, and skill as distinct and separate from other parts of the curriculum. Origami can serve as an effective bridge to help students see mathematics as a far-reaching and interconnected discipline with numerous facets, rather than a series of unrelated skills to be practiced and tasks to be performed in isolation from each other and from the world at large.

Bibliography

[1] Bennett Arnstein, Rona Gurkewitz, and Lewis Simon. *Modular Origami Polyhedra*. New York: Dover Publications, 1999.

[2] Tomoko Fuse. *Unit Origami, Multidimensional Transformations*. Tokyo: Japan Publications, Inc., 1990.

[3] Thomas Hull. *Project Origami*. Wellesley, MA: A K Peters, Ltd., 2006.

[4] Miyuki Kawamura. *Polyhedron Origami for Beginners*. Tokyo: Japan Publications, Inc., 2002.

[5] National Council of Teachers of Mathematics. *Principles and Standards for School Mathematics*. Arlington, VA: National Council of Teachers of Mathematics, 2000.

[6] James Plank. "Jim Plank's Origami Page (Modular)." Available at http://www.cs.utk.edu/~plank/plank//origami/origami.html, March 1996.

On the Effective Use of Origami in the Mathematics Classroom

V'Ann Cornelius and Arnold Tubis

1 Introduction

Origami is a valuable (and largely untapped) resource for supplementing and strengthening school mathematics curricula. Because it encompasses elements of both the arts and mathematics, it is ideal for augmenting and enriching the current educational focus on reading and mathematics. To date, origami has been used in the mathematics classroom mainly as a tool for: (1) doing geometric constructions via folding as an alternative to traditional straight-edge and compass ones, (2) determining area formulae for simple polygons, (3) developing manual dexterity and spatial visualization, (4) studying some aspects of line and point symmetry, and (5) studying properties of polyhedra. (For references see, e.g., Cornelius and Tubis [1] and Tubis and Mills [8]).

In this paper, we show how origami can be a very effective aid in guiding students in grades K-8 through the first three van Hiele [4, 9] levels of geometric understanding (*visualization*, *analysis*, and *abstraction/informal deduction*) that are crucial for success in subsequent studies at the *formal deduction* level in high-school geometry and *rigor* in later university studies. We also propose origami-mathematics activities in which students relate key dimensions and angles of a folded model to the mathematical details of the model crease pattern, and show that these activities strongly support mainstream mathematics standards. These standards are typically

classified under the headings of *number and operation*, *algebra*, *geometry*, and *measurement/data analysis/probability*. (See [5] for recently proposed key focal points of the K-8 mathematics curriculum.) The limited length of this paper allows only a cursory presentation of the many ways in which origami can enhance mathematics education.

2 General Procedure

Our general procedure is outlined below. The associated van Hiele levels of geometric understanding and mathematics standards are given in square brackets.

1. Select object to be folded (e.g., a box, envelope, or picture frame).
2. Identify constant features (e.g., size of paper, number of walls, and bottom face of an open box). [Geometry (Visualization)]
3. Identify variable features (e.g., shapes and sizes of walls and bottom face of an open box). [Geometry (Visualization)]
4. Fold model.
5. Identify shapes, angles, and symmetries in the crease pattern. [Geometry (Visualization, Analysis)]
6. Mathematically relate features of the model to those of the crease pattern. [Geometry (Abstraction/Informal Deduction); Number and Operation; Algebra]
7. Use mathematics to design and fold a form of a model that satisfies various requirements. [Geometry (Abstraction/Informal Deduction); Number and Operation; Algebra]
8. Check design by measuring dimensions of the folded model. [Measurement/Data Analysis]

We illustrate some of the above points in the next section in connection with the generalization of the traditional *Magazine Box* and its crease pattern. In subsequent sections, we give typical examples of other models that we have found effective in workshops on origami-mathematics for students in various grade levels. Except for the *Pythagorean Theorem* picture frames and boxes (Figures 6 and 7) and *Triangle Boxes* (Figure 8), the models are appropriate for K-8 grades. For fairly obvious reasons, it is usually desirable for models used in mathematics classes to be foldable in a short amount of time, be interesting from a utilitarian and/or novelty

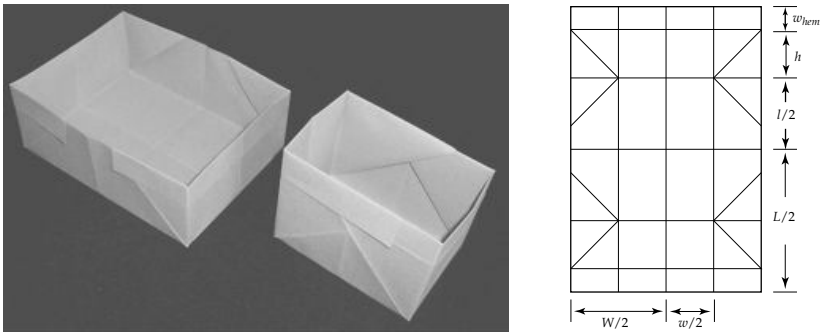

Figure 1. The generalized *Magazine Box* and its crease pattern.

perspective, be analyzable with the mathematical knowledge that is appropriate for the grade level of the students, and help students focus on the important mathematics standards.

3 The Magazine Box

In Figure 1 are displayed a photograph, crease pattern, and design equation of the generalized *Magazine Box* made from a rectangular sheet of paper. Both boxes in the photograph are folded from the same size rectangle. The design equations relate the features–length l and width w of the box face, width of the rim hem w_{hem}, and box height h—to the length L and width W of the starting rectangle. Like many other models, the *Magazine Box* may be used at various grade levels. In the early grades, the focus should be on the properties of the various shapes, lines, angles, bisections (angle and line), and symmetries (line and point) in the crease pattern (van Hiele levels of visualization and analysis). In higher grades, the mathematics standards—number and operation, algebra, and geometry (van Hiele level of abstraction/informal deduction)—come into play in the derivation of the design equations and in their application to the designing of boxes that will hold specified objects, as well as the calculation of areas, perimeters, and volume. Finally, by measuring the dimensions of a folded box and noting that they differ slightly from the "theoretical" ones implied by the design equations (measurement and data analysis), students gain a first-hand appreciation of the distinction between origami models folded with paper of finite thickness and stiffness, and the box (folded from idealized infinitely thin paper) described by the design equations.

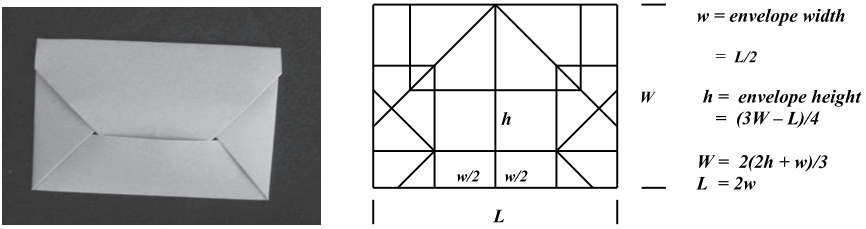

Figure 2. *Envelope* and its crease pattern.

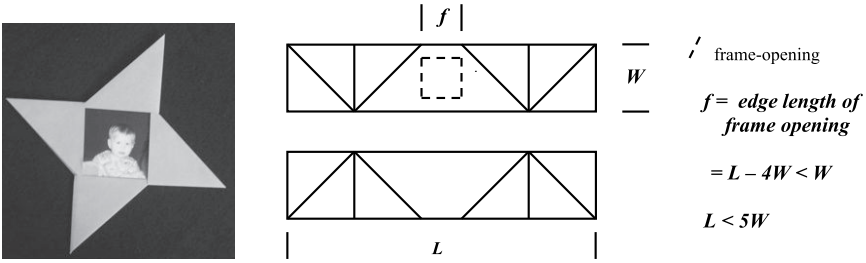

Figure 3. *Ninja Star* picture frame and its crease pattern.

4 The Envelope

The *Envelope* (Figure 2), like the *Magazine Box*, has a crease pattern with simple symmetries and angles (of measure 45° and 90°), and similar associated mathematical activities. However, the derivation of its design equations is somewhat more challenging.

Another model with similar attributes is the traditional *Ninja* (or *Throwing*) *Star* made from two identical rectangular strips that is generalized so as to serve as a square picture frame (Figure 3). The fact that the edge length of the frame cannot exceed the strip width presents an interesting problem that may be used as part of an introduction to inequality problems.

5 The Generalized Traditional Masu

We now present the first of a series of models in which the Pythagorean Theorem plays a significant role in relating model features to those of the crease pattern. The theorem may be first introduced in lower grades by having students simply verify that the length of the diagonal of a square is equal to approximately 1.4 times the edge length of the square. After

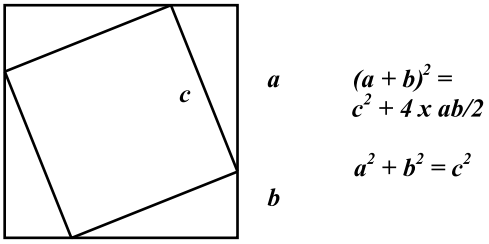

Figure 4. Crease pattern for informal proof of the Pythagorean Theorem. The congruence of the four right triangles bordering the inside square can be easily verified by folding (see, e.g., [6,8]).

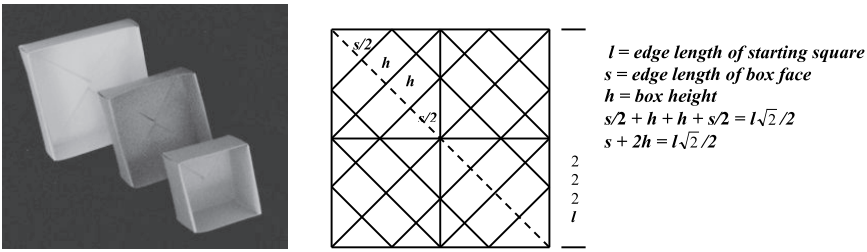

Figure 5. Generalized masu and its crease pattern. All three boxes in the photograph are folded from the same size square.

students learn about the areas of squares, rectangles, and triangles, informal paper-folding "proofs" of the theorem [6,8] can be based on forming the crease pattern in Figure 4. The generalized traditional Japanese *masu* ("box") (Figure 5) is one of the simplest models that illustrate the application of the theorem, and we have successfully used it for this purpose for five years with students in grades four through nine. For an extensive set of mathematical activities based on the masu and its generalizations, see Tubis and Mills [8].

6 Pythagorean Theorem Picture Frames and Boxes

The *Pythagorean Theorem* crease pattern of Figure 4 can serve as the starting point for numerous interesting models such as picture frames (Figure 6) and boxes (Figure 7). The crease pattern analyses of these two models would constitute instructive exercises in high-school trigonometry.

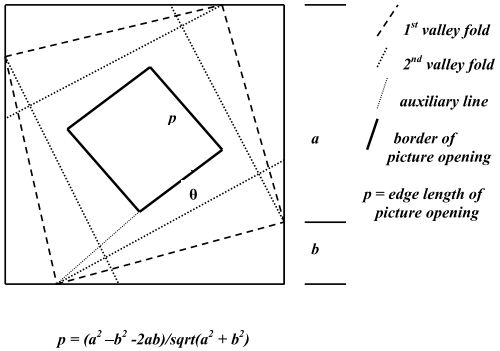

Figure 6. *Pythagorean Theorem* picture frames and their crease pattern. Both frames in the photograph are folded from the same size square. The edges of the picture opening are *not* crease lines.

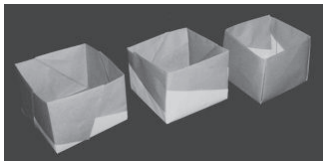

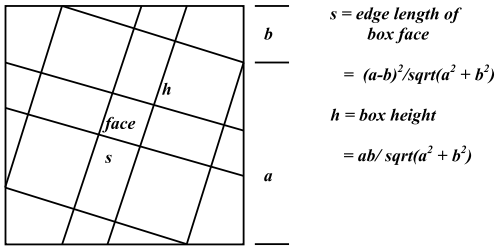

Figure 7. *Pythagorean Theorem* boxes and their crease pattern. All three boxes in the photograph are folded from the same size square.

7 Isosceles Triangle Boxes from Arbitrary Rectangles

Another model that would be very effective in a high-school trigonometry class is an *Isosceles Triangle Box* (Figure 8) with an arbitrary apex angle θ folded from an arbitrary starting rectangle [1].

8 Washington Crossing the Delaware Model from a Dollar Bill

Our final example (Figures 9(a) and (b)) is one that has mathematical significance (involving the construction of angles of 30° and 60°, the Pythagorean Theorem, and the altitude/base ratio of the equilateral triangle), and and is also relevant to American history (George Washington and the Revolutionary War). Note that 1732, Washington's birth year,

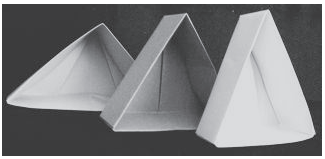

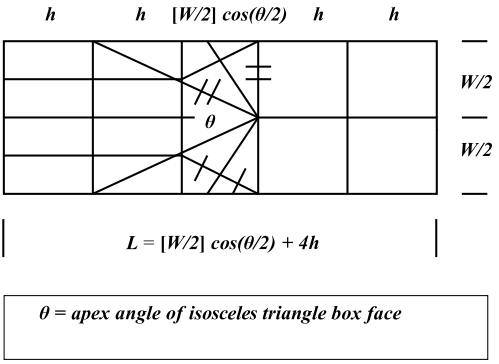

Figure 8. *Isosceles Triangle Boxes* from an arbitrary rectangle and their crease pattern. All three boxes in the photograph are folded from the same size rectangle.

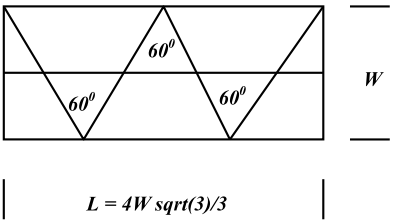

(a)

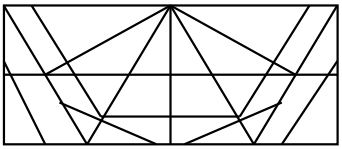

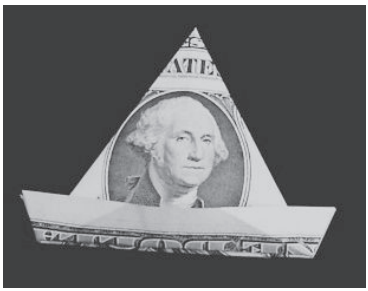

(b)

Figure 9. *George Washington Crossing the Delaware* and its crease pattern. (a) Part I: framing George in an equilateral triangle. (b) Part II: forming the boat.

contains the first four digits of the square root of 3 (twice the altitude/base ratio of the equilateral triangle). For an informal geometric approach to angles of 30° and 60°, see, e.g., Tubis and Mills [7].

9 Summary and Concluding Remarks

We advocate the origami-mathematics approach of this paper as a practical vehicle for: (1) providing learners with immediate applications of mathematical concepts via the folding/analysis of functional objects (which in turn serve as catalysts for future learning); (2) guiding students through the first three van Hiele stages (visualization, analysis, and abstraction/informal deduction) of geometric understanding; and (3) promoting competence in general mathematics standards. Aside from the relatively short time required for teaching the folding steps, the classroom studies associated with mathematically connecting model features to those of the crease patterns are all in line with mainstream mathematics classroom activities. "Visual-tactile" learners [3] might benefit in particular from this type of curricular content.

An initial trial of the approach outlined here is planned to take place in the school district of Long Beach, California, in collaboration with an organization called Dramatic Results—Academic Success Through Art [2].

Bibliography

[1] V'Ann Cornelius and Arnold Tubis. "Using Triangular Boxes from Arbitrary Rectangular Paper to Enrich Trigonometry and Calculus." In *Origami^3: Proceedings of the Third International Meeting of Origami Science, Mathematics, and Education*, edited by Thomas Hull, pp. 299–305. Natick, MA: A K Peters, 2002.

[2] Dramatic Results website. Available at http://www.dramaticresults.org, 2009.

[3] Howard Gardner. *Multiple Intelligences: The Theory in Practice*. New York: Basic Books, 1993.

[4] National Council of Teachers of Mathematics. *Navigating through Geometry*. Reston, VA: National Council of Teachers of Mathematics, 2001.

[5] National Council of Teacher of Mathematics. "Curriculum Focal Points for Prekindergarten through Grade 8 Mathematics," *National Council of Teacher of Mathematics*. Available at http://www.nctm.org/focalpoints, 2009.

[6] Arnold Tubis and Crystal Mills. "Eight Paper-Folding Steps to the Pythagorean Theorem." *California Mathematics Council ComMuniCator* 28:3 (2004), 51–56.

[7] Arnold Tubis and Crystal Mills, "Mathematical Paper Folding Explorations Based on 30° and 60° Angles." *California Mathematics Council ComMuni-Cator*, "More Standards-Based Activities for the Classroom K–12," Special Edition (2004), 40–46.

[8] Arnold Tubis and Crystal Mills. *Unfolding Mathematics with Origami Boxes*. Emeryville, CA: Key Curriculum Press, 2006.

[9] Pierre M. van Hiele. *Structure and Insight*. Orlando, FL: Academic Press, 1986.

Using Origami to Promote Problem Solving, Creativity, and Communication in Mathematics Education

Sue Pope and Tung Ken Lam

1 Introduction

The use of origami in mathematics education has long been known [2, 3, 7, 11]. (The last reference was originally published over 100 years ago.) However, such paper-folding activities are generally little known and not widespread [8].

If origami is used at all in mainstream lessons, it tends to be for demonstrating a small number of geometric principles and ideas [1]. Otherwise, origami is seen purely as a "fun end of term" activity. Furthermore, the pedagogic approach in both cases is for the teacher to instruct students one step at a time. There are few opportunities for creativity and problem solving; students are hardly ever encouraged to ask why methods work.

There are other teaching and learning strategies besides students following a teacher's instructions. Some presented here are based on those advocated by Wollring [12].

- *Whole class teaching and challenges are implemented.* Only the very simplest folds are introduced to the whole class. Students then investigate the properties of the resultant shapes and justify their findings.

Students are challenged to develop their shape into something more interesting.

- *Students in groups are challenged to make an existing origami object.* Each group has *two* examples of a folded object. Students are advised to dismantle just one object and figure out how it is made. As the objects are modular (i.e., made of more than one piece), once they have decided how one unit is made they can then work together to produce the units they need. By having one intact model they can figure out how to reconstruct the model.

Teachers can follow up on each of these activities by asking students to communicate their findings by preparing posters. One aim of these posters is to communicate to other groups of students how to make the same object. In order to emphasize visual and geometric understanding, the constraint of using as few words as possible was given. The use of *step folds* allows students who cannot draw neatly with pencils and rulers to produce quality work.

A third origami activity does not involve instructing students or giving students existing origami objects:

- *Students are challenged to design shapes to have given properties.* For example, students might be asked to produce the largest octagon from a square. Alternatively, students may be shown a tiling and asked to reproduce it by folding paper units.

In contrast with students following a teacher's instructions, these activities allow students to think for themselves and to solve problems. A benefit for the teacher and students is that students can work at their own pace. This avoids the frustration of some students having to wait for others to catch up, and some students struggling to keep up. The poster-making activity ensures that students probe the structure of an origami design.

Another advantage is that students can work at their own level. For example, there are a number of methods for finding the center of an equilateral triangle. Some may use their visual judgement; others might be able to work out a more precise folding method.

2 Examples of the Strategies

Examples of these teaching and learning strategies activities are now shown. They are drawn from a number of contexts including in-service training, mathematics masterclasses, and summer schools for gifted and talented children.

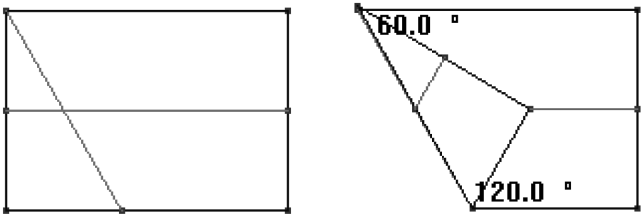

Figure 1. Crease lines on a paper, and trapezium with angles marked.

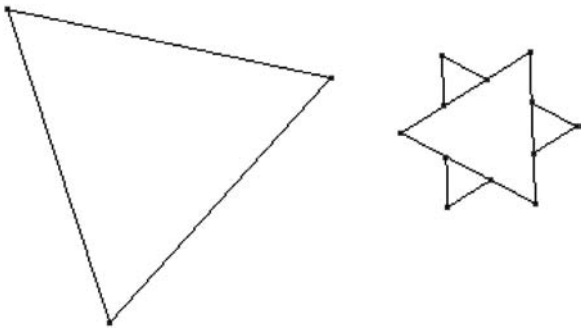

Figure 2. Fold a regular hexagram from an equilateral triangle.

2.1 Whole Class Teaching and Challenges

Folding a hexagram. Students were asked to fold the paper in half along the long mirror line, unfold, and to then fold one corner of the shortest edge onto the original crease to make a new crease through the adjacent corner (Figure 1). Students were asked to find out all they could about the resultant quadrilateral.

Once students had agreed and come up with reasons for the properties of the trapezium, they were asked if it would be possible to make an equilateral triangle. Students found out for themselves how to fold their equilateral triangle into a triangle whose sides are half the length (what happens to the area?) and into a regular hexagon (what fraction of the area of the equilateral triangle is its area?).

They were then shown a folded regular hexagram (Figure 2) and asked how they might develop their equilateral triangle into such a shape. The students worked in groups to develop a poster for other students about how to make the hexagram (Figure 3).

Further development of this origami included folding frustums of tetrahedra and assembling an icosahedron.

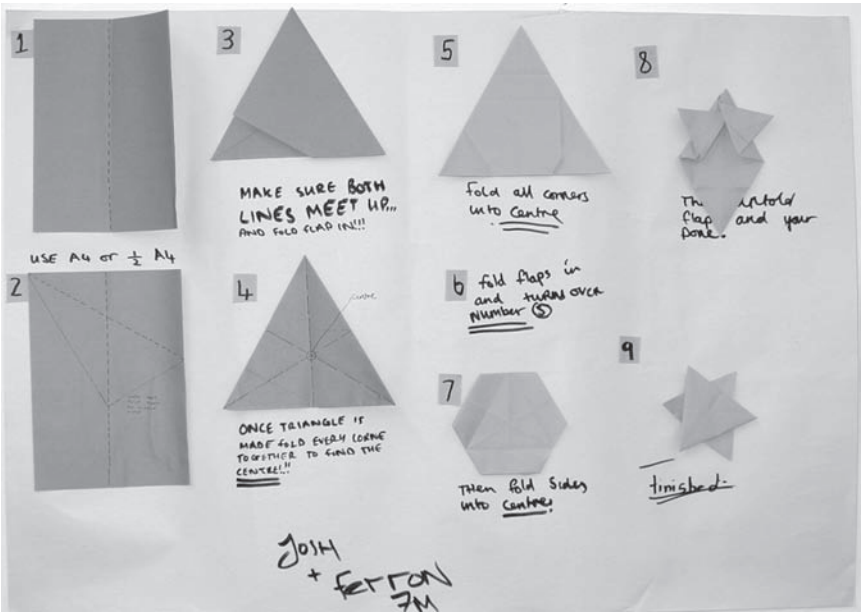

Figure 3. Typical poster of instructions for folding the hexagram.

2.2 Challenge to Make an Existing Origami Object

Folding a shuriken star. Pairs of prefolded stars (Figure 4) were distributed to small groups. They were challenged to work out how to make the star. Students were advised to pull one star apart and to keep one intact. The star is a classic origami model which, unlike many modular origami objects, uses two units that are mirror images of one another.

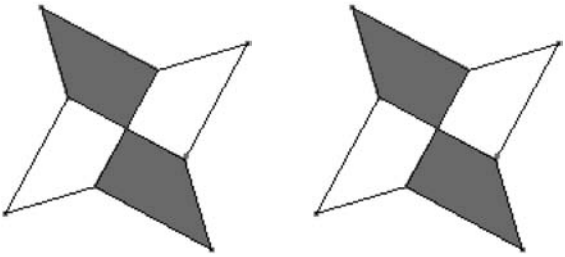

Figure 4. A pair of four-pointed stars. Each is made from two pieces that are mirror images.

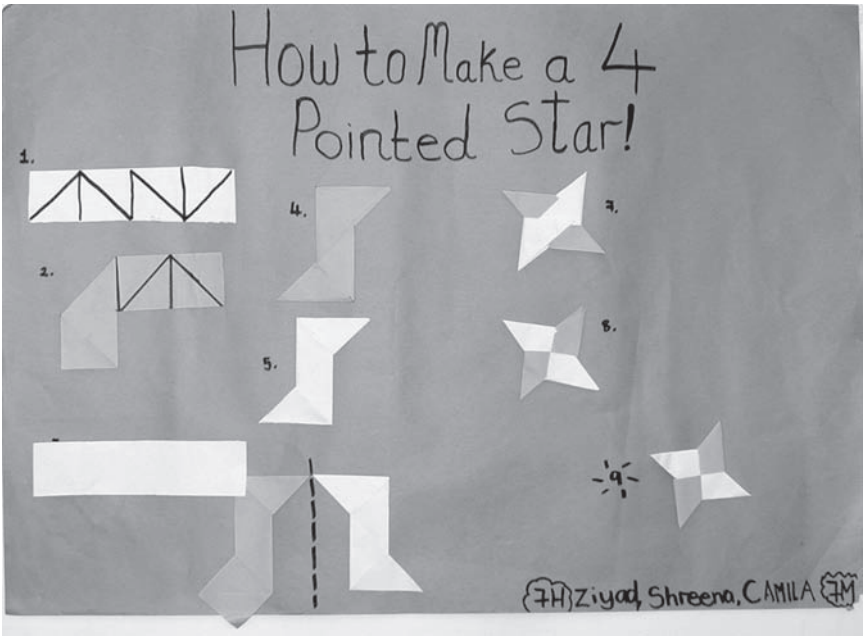

Figure 5. Typical poster of instructions for folding the four-pointed star.

Students were challenged to determine the properties of this star and then, in their groups, to prepare a poster that showed how to make the star that could then be used with other students (Figure 5).

Another good choice of origami for this type of activity is Robert Neale's action origami *Pinwheel–Ring–Pinwheel*, which can change shape and illustrate rotational symmetry [10].

In addition to two-dimensional origami models, students worked on three-dimensional modular origami, e.g., Paul Jackson's *Cube* and Robert Neale's *Skeletal Octahedron* [9].

2.3 Challenge to Design Shapes with Given Properties

Creating stained glass windows. Using images of stained glass windows and other tiling designs [4–6], students were challenged to recreate the designs. Each piece in the design had to be folded as accurately as possible from square pieces of paper. Figure 6 shows a number of different designs completed by different groups of students. These required students to work creatively and to solve their own problems.

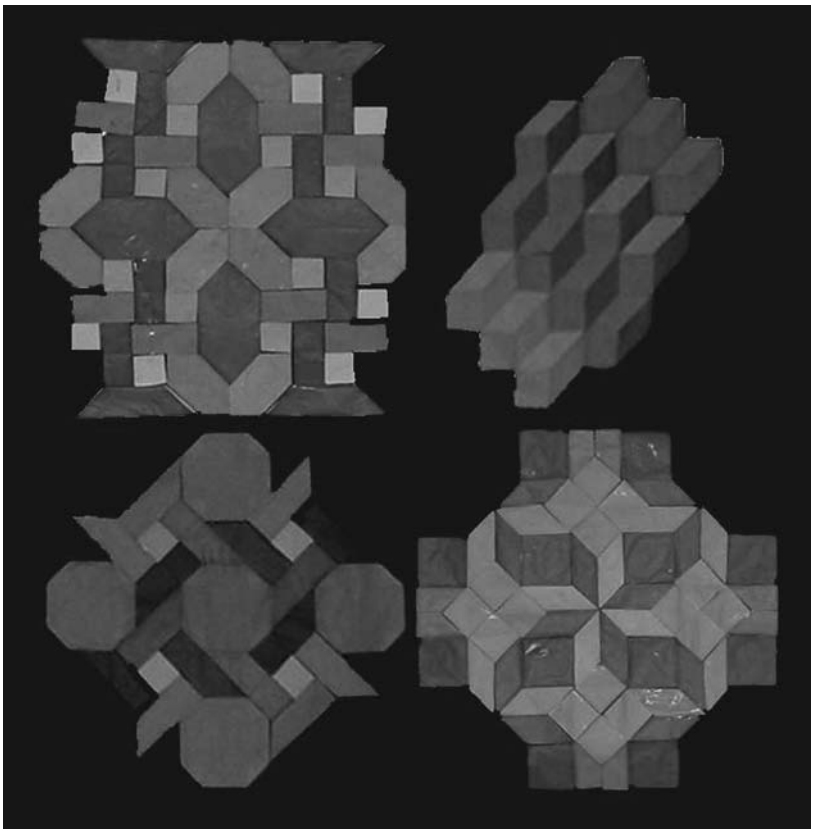

Figure 6. Stained glass window designs.

3 Outcomes

Specific outcomes of this study are described more fully in [8].

Generally, on the affective level, students are engaged and enjoy the folding activities. Students even make the origami outside of the sessions!

The social aspect of the activities encourage teamwork and communication. Students realize that their posters sometimes do not contain all the information needed to make an origami design.

The cognitive and mathematical content of the activities allows students to appreciate the connections between topics in mathematics that are taught at different times. Indeed, the memorable learning experience is often revealed later in more formal lessons on geometry. They see that there are a number of methods for doing something, some having disadvantages as well as advantages.

4 Implications for the Classroom

The use of origami allows a wide range of mathematics to be covered in a stimulating and enjoyable way. Along with the development of mathematical understanding, students develop their problem-solving and creative skills and their ability to work cooperatively with others. Producing posters challenged students to succinctly communicate their methods to a defined audience.

Acknowledgment. We are grateful to the teachers and students who participated in this work.

Bibliography

[1] J. A. Carter and B. J. Ferrucci. "Instances of Origami within Mathematics Content Text for Preservice Elementary School Teachers." In *Origami^3: Proceedings of the Third International Meeting of Origami Science, Mathematics, and Education*, edited by Thomas Hull, pp. 337–344. Natick, MA: A K Peters, 2002.

[2] V. Cornelius (editor). *Proceedings of the First International Conference on Origami in Education and Therapy*. New York: OrigamiUSA, 1995.

[3] D. A. Donovan. *Paper Folding for the Mathematics Class*. Washington, DC: National Council of Teachers of Mathematics, 1957.

[4] R. Field. *Geometric Patterns from Churches & Cathedrals*. Diss, England: Tarquin Publications, 1996.

[5] R. Field. *Geometric Patters from Tiles & Brickwork*. Diss, England: Tarquin Publications, 1996.

[6] R. Field. *Geometric Patters from Islamic Art & Architecture*. Diss, England: Tarquin Publications, 1998.

[7] T. Hull (editor). *Origami^3: Proceedings of the Third International Meeting of Origami Science, Mathematics, and Education*. Natick, MA: A K Peters, 2002.

[8] T. K. Lam and S. Pope. "The Use of Origami in the Teaching of Geometry." In *Proceedings of the International Symposium Elementary Mathematics Teaching (SEMT'03)*, edited by J. Novotna, pp. 120–125. Prague: Charles University, 2003.

[9] D. Mitchell. *Mathematical Origami*. Diss, England: Tarquin Publications, 1997.

[10] R. Neale and T. Hull. *Origami, Plain and Simple*. New York: St. Martin's Griffin, 1994.

[11] T. Sundara Row. *Geometric Exercises in Paper Folding*. New York: Dover, 1966. (Reprint of 1905 second edition.)

[12] B. Wollring. "Working Environments for the Geometry of Paper Folding in the Primary Grades." In *Proceedings of the International Symposium Elementary Mathematics Teaching (SEMT'03)*, edited by J. Novotna, pp. 177–178. Prague: Charles University, 2001.

Redundancy of Verbal Instructions in Origami Diagrams

Koichi Tateishi

1 Introduction

This paper discusses characteristics of the informational contents of verbal instructions in origami diagrams. We claim that verbal "instructions" are not real instructions, as the instructional role can be handled by the diagrams themselves. Rather, the words below the diagrams are for observational and/or confirmational purposes, that is, the words basically repeat information that is already shown in the diagrams. Individual diagrams are only shapes and figures that do not speak and they often incorporate vague information. The words below the diagrams help us clarify ambiguities and make sure that in such cases, folders can believe that they are doing the right thing.

With such goals in mind, we list several questions to address:

1. Do diagrams stand by themselves? Can we understand diagrams without words and still fold models without difficulty?

2. Do we need words below the diagrams? Do words help us clarify difficulties that folders may face when they fold models?

3. If so, then why can't words stand alone? In other words, what is the role they play in the comprehension of folding procedures? Do they instruct us how to fold, confirm what the diagrams tell us, explain

the details of what the diagrams tell us, or just observe the process that the diagrams show?

There has been one previous study on the informational contents of diagrams, an article by Komatsu Hideo in *Origami Tanteidan Magazine* [2]. As the title of the article, "Orizu Hyogenni Tsuite [Expressions in Diagrams]," suggests, Komatsu explored what kind of information the drawings and symbols in diagrams tell us.

Our paper, on the other hand, focuses on the words below the diagrams. What do they tell us in terms of informational content, and what do they *not* tell us? Thus, the current study is *not* about how to draw good diagrams. For that topic, you are referred back to Komatsu's paper [2], or carefully study the many and varied diagrams you can find in the origami literature.

2 Redundancy in Diagrams

Consider Figure 1, which shows a typical diagram of the first step of various models, including the traditional crane. It tells you to fold the bottom corner up to the top corner and make a triangular shape, nothing technically hard or special. In fact, though, even such a simple diagram incorporates too many information pieces.

The first unnecessary informational piece is an arrow and the word "upwards." The two elements tell us the same thing, so either one of the two is unnecessary; saying "fold corner to corner" is kinder, information-wise.

The second redundancy can be found in the dashed line indication for a valley fold and the phrase "valley fold." Here, too, one or the other is not necessary.

Moreover, the dashed line for the valley fold is redundant, too. This is because "a diagram never stands by itself." There is always the next diagram so folders can (and must) refer to that to make sure of what they are doing.

Also, there are some "grammars" of diagrams. For example, when someone sees a white square followed by a colored triangle, the most natural interpretation is that the square has been folded along a diagonal, not cut in half and turned over. So, when one sees a series of diagrams like that shown in Figure 2, one can and should interpret them as specifying to fold the square in half along the diagonal. Diagrams and the grammars behind them provide enough information to follow the instructions. Words below the diagrams are thus redundant in most cases.

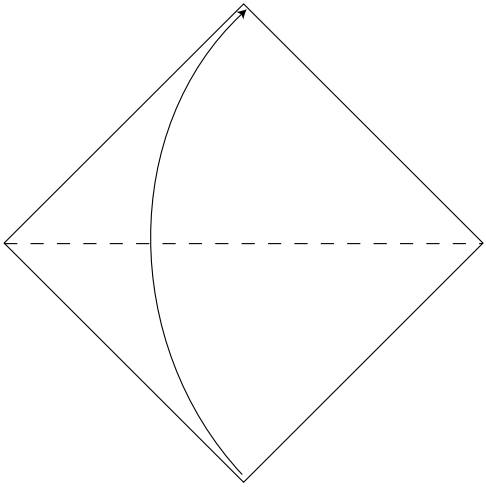

Figure 1. Diagram with too much information?

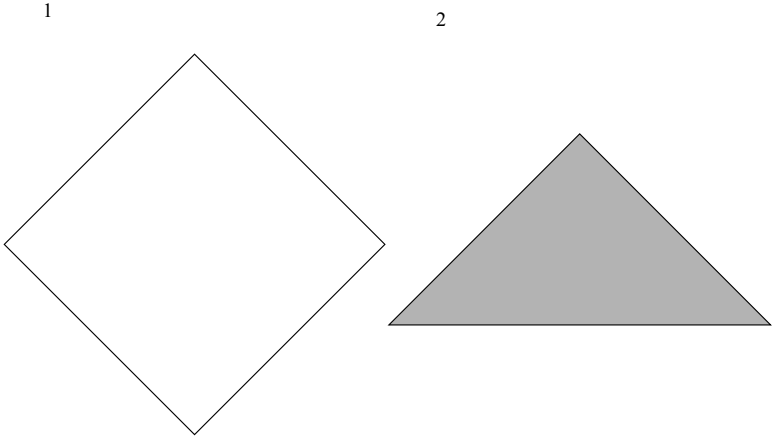

Figure 2. Diagrams with enough information?

3 Unnecessity of Verbal Instructions

In fact, the use of words below diagrams is not universal. I counted the use of words throughout all the diagrams in the *OrigamiUSA Origami Collection 2004* [1], and found that the authors' nationalities affect their use of words. Table 1 shows that more than 75% of American folders

	Average	Top 25%-Tile	Median	Bottom 25%-Tile
Americans	88.86%	100%	100%	75%
Non-Americans	56.35%	100%	84.12%	3.81%

Table 1. Ratio of verbal instructions per diagram in an OrigamiUSA publication.

	Average	Top 25%-Tile	Median	Bottom 25%-Tile
Japanese	62.23%	82.86%	66.15%	46.15%
Americans	78.98%	100%	100%	79.33%
Others	46.48%	84.07%	62.22%	30.05%

Table 2. Ratio of verbal instructions per diagram in a JOAS publication.

use words below most of their diagrams, while the non-Americans (mostly Europeans) do not use words as much but rather depend more heavily upon the drawings.

Table 2 shows the result of the same search through *The 10th Origami Tanteidan International Convention Book* from JOAS [3]. The same contrasts between Americans and non-Americans can be found there, too, with Japanese authors falling between the two. This is by itself a very interesting topic sociologically, but I am aware that we have to take into consideration factors like complexity of the model and the use of English as an instructional language, among others. Also, we have to know how the artist's quality of drawing in the diagrams affects his/her own usage of words. However, at the least we can say that, in terms of providing sufficient information, words below diagrams are not necessary.

4 Insecurity Issues

There still remains the question: are diagrams really enough for instruction? It is true that we have sufficient information with diagrams such as those in Figure 2, but we tend to feel somehow insecure about such diagrams.

The cause of this insecurity is perhaps lack of predictability, that is, we really do not know what is going on and what will come next. Without the aid of the third diagram, we cannot see what these first two steps of the diagrams will lead us to. That is, we need words *to make sure that we are doing the right thing.*

As for the drawings, Komatsu [2] correctly points out that symbols within diagrams do not always provide full information. For example, when we perform an inside reverse fold, there are cases where we would like to describe the action as "pulling down the corner from inside," while in other

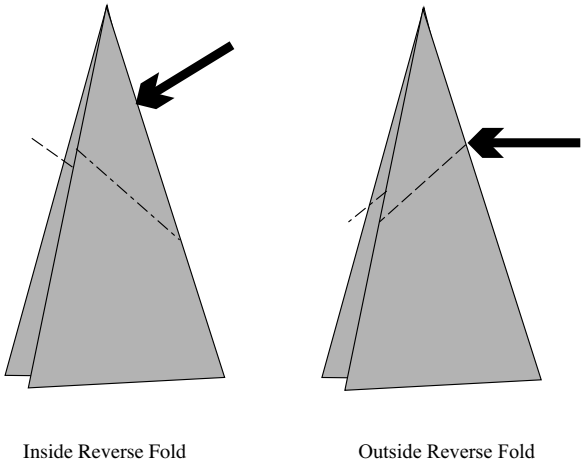

Figure 3. The same symbol, folded in opposite directions.

cases it should be carried out as "pushing down the corner from the back." Symbols perhaps cannot make such subtle distinctions.

For example, suppose someone used the symbolic system shown in Figure 3. The arrow in this system means "push the edge inside." On the left diagram, pushing in the back edge of the corner with this angle pushes the corner inside, so this is an inside reverse fold. On the other hand, on the right diagram, the angle and crease lines cross with a different angle and this move will reverse the edge itself, so that it will be an outside reverse fold. So far, there is no contradiction, and the system can give precise instructions.

However, how can we interpret Figure 4? Does this mean to inside-reverse-fold along the edge? It appears that this is the only possible interpretation, but, when you look at the diagram carefully, you can find that the inner layers are colored. This means that we can interpret this instruction as a sink. Moreover, in this case, the next diagram may not help, because the corner pushed in by this move may not be visible from the outside. Thus, we cannot show everything with symbols and diagrams. Something that corresponds to verbal instructions is necessary in many cases.

The problem here is very simple: lines and symbols cannot be universal. People differ even in how they express valley and mountain folds. When we see a symbol as in Figure 5, for example, we can interpret it as "rotate the model," "turn the sheet over," or "flip the flap/layer over"—or several other things. At the very least, we need some confirmation of what move we should take, even when this move is indicated by lines and symbols.

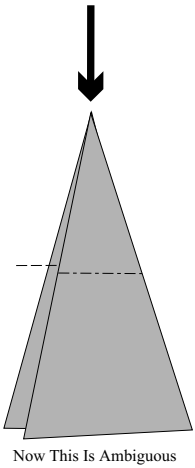

Figure 4. Which fold?

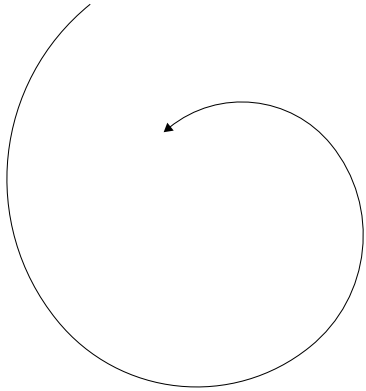

Figure 5. An ambiguous symbol.

5 Words Can't Suffice

5.1 Verbal Undercommunication

A problem also lies in the fact that words cannot be sufficient in and of themselves. For example, consider the following instruction without visual aid and diagrams:

> Fold corner to corner and make a triangle, and fold this triangle in half. There is a pocket on the bottom of the triangle so open it, and squash into a square. Repeat this on the other side. Pull up the corner of this square and swivel the edges to the center line. Flatten the model then. Repeat the same procedure on the back. Fold the four edges of the flaps to the center line, so that the flaps become thinner. Fold up the two thin flaps from inside as far as they go. Fold down a tip of one of them from inside. Open the wide flaps to the sides.

Experienced folders might perhaps fold and complete a crane successfully with this form of instruction, but for laymen, words are often ambiguous and vague. Open? Squash? How? Open completely, or just pull down? Words just can't convey everything. This is even more evident in so-called super-complex models.

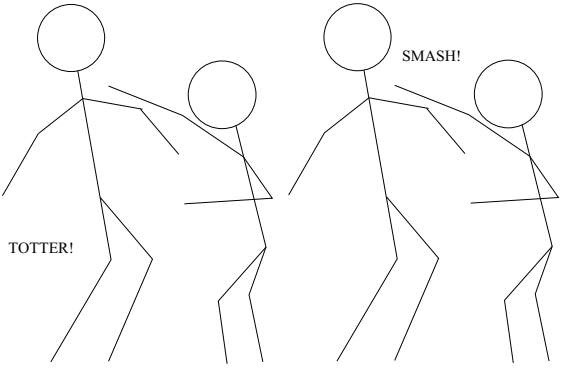

Figure 6. This figure contains a violent expression!

5.2 Complementary Distribution of Information Pieces

The fact is that words and diagrams complement each other to describe events in the world outside of origami. For example, in Figure 6, the position and types of the added words, "totter" and "smash," make us imagine completely different events. However, if a series of diagrams provides enough information, then we do not necessarily need words.

5.3 Verbal Overcommunication

Nevertheless, in some cases, words tell us too much. For example, the "Open the wings" instruction in Figure 7 is correct, but misleading. The words "open the wings" may persuade the folders to create a simple origami crane rather than the action that is indicated by the lines and symbols.

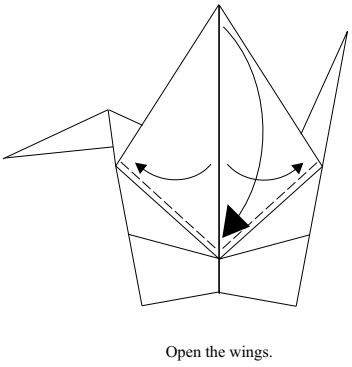

Figure 7. This is *not* a crane!

To make such cases clear, we need to add further (and thus unnecessary) precision, by saying something like "Open the edges of the wings and squash"; perhaps it is better if we simply present the diagram without words, to avoid such unnecessary confusion.

5.4 Printed Words Do Not Tell Us Anything

Given the discussion so far, we can say the following: words below diagrams do not exist primarily for instructional and explanatory purposes. To accomplish such purposes, words are in some ways powerless and in others they are too powerful. The real purpose of words, then, is observational and confirmational. They do not instruct directly, but they confirm what diagrams tell us. The actual instruction in what to do is the proper role of the drawings and symbols.

6 Conclusion

Words below diagrams do not exist for instruction, and that's why we need aids from diagrams and real instructional languages in origami classes. Words below diagrams exist for observational and confirmational purposes. Because of these purposes, words below diagrams use technical terms and are written without referential terms like *this* and *that*, and often describe several moves at once.

However, this does not mean that we need a new instructional language with sufficient referential terms below diagrams, because it would both provide too much information and be redundant with what the diagrams themselves tell us.

The risk of ignoring such factors is that, uses of the technical terms in verbal instruction may make the world of origami remote from ordinary would-be-folders. The proper usage of verbal media in diagrams should be seriously considered, along with discussions of cross-linguistic origami terminology.

Bibliography

[1] M. Chang, M. Kirchenbaum, and D. Scher. *OrigamiUSA Annual Collection 2004*. New York: OrigamiUSA, 2004.

[2] H. Komatsu. "Orizu Hyogenni Tsuite" [Expressions in Diagrams]. *Origami Tanteidan Magazine* 78 (2003), 11–13.

[3] M. Yamaguchi. *The 10th Origami Tanteidan International Convention Book*. Tokyo: Japan Origami Academic Society, 2005.

Origami, Isometries, and Multilayer Tangram

Emma Frigerio

1 Introduction

If, as Galilei put it, the book of the Universe is written in the language of mathematics, this is even more the case for origami: when we fold an origami model, whether we notice it or not, we also engage in some form of mathematics. Thinking about the mathematical meaning of the folds is perhaps the main feature of the 20-hour workshops on origami and mathematics that I give at both universities in Milan, Italy (see also [2]). These workshops are addressed to prospective teachers at the elementary or middle school level. Coming in, none of them is particularly keen on abstract reasoning. They fall into two groups: the first group is made up of sophomores majoring in primary education, the second mainly of natural sciences or biology graduates with some experience in teaching. I believe that a hands-on approach, rather than a formal study of geometric constructions via paper folding, gives them more motivation to discover the mathematics underlying origami; besides, it allows a quicker start than a rigorous axiomatization. I often use nonmathematical models to promote mathematical thinking. Once we have folded the model, I hand out a worksheet with questions such as: identify the mathematical meaning of some creases, compute lengths of segments and amplitudes of angles, recognize geometric facts (equality of segments or angles, parallelism of lines, ...), and prove some of them. Or, as a final exam, I ask them to prepare a worksheet, suitable for their students, on an assigned model.

In this respect, models that use a rectangular sheet of paper are very interesting. Some can be folded from rectangles of any shape, others from rectangles of only one shape (e.g., the so-called silver rectangle, whose sides are in the ratio of $1 : \sqrt{2}$), and some from rectangles whose shape must lie within a certain range. This very easy folded envelope by Luisa Canovi [1], former president of Centro Diffusione Origami (the Italian origami association), is a wonderful example of a model that gives rise to interesting mathematical questions of various natures and is suitable for students at different levels. It is so easy to fold that even small children can do it, as shown in Figure 1.

The knowledge of the Pythagorean theorem and of similarity allows for a complete study of the geometry of its crease pattern (Figure 2); however, for younger students, this model can also be the basis for an activity of experimental mathematics, which can also serve as an introduction to the concept of a function. Moreover, if we fold the envelope with a sheet of tissue paper and hold it against a window, we would notice that it is evenly made of four layers. We could also cut the model apart along its folds and rearrange the pieces in a sort of multilayer tangram: in any case, the area of the envelope is one fourth that of the sheet with which we started.

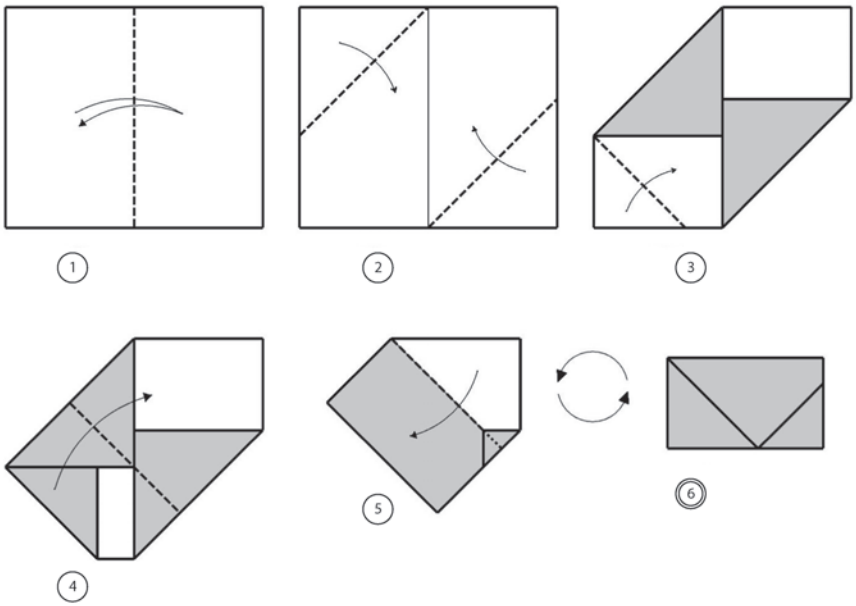

Figure 1. Instructions for folding Canovi's envelope.

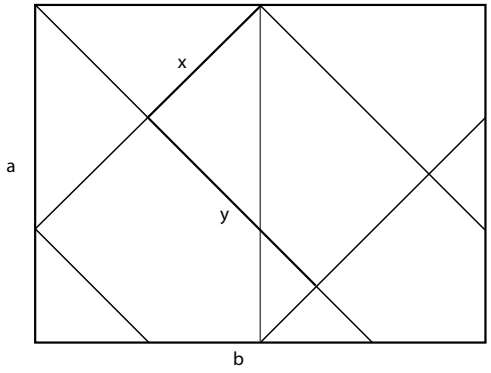

Figure 2. The crease pattern of the envelope.

Finally, on the crease pattern we can "read" the isometries associated with the folds; this allows us to prove rigorously that we really have a four-layer tangram.

This instance shows how much mathematics is hidden in an origami model; we just have to discover it.

2 The Mathematics of the Model

The first mathematical questions about the envelope that one thinks of are related to everyday life:

1. What size must the paper be if the envelope is to be of a given size?
2. Can the shape of the envelope be chosen at will?

The "dual" questions are somewhat easier:

3. What size will the envelope be if the paper is of a given size?
4. Can the shape of the paper be chosen at will?

Of course, a mathematical mind will immediately ask more questions, such as the following:

5. What is the ratio of the area of the envelope to the area of the sheet?
6. Is there a shape of the sheet for which the envelope has the same shape as (is similar to) the given sheet?

WORKSHEET

ENVELOPE (L. Canovi)

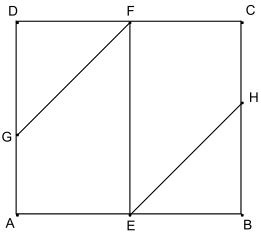

(a) Crease (1) is …… to AB and divides it into two ……. parts, hence it is the ……..……..…….. of AB.

(b) Creases made in (2) are the …….. of angle …… and of angle …… .

(c) Angle DGF measures …… .

(d) Mark on the picture the new positions of D and B after creases (2) and label D' and B' these new points. Triangles DGF and FGD' are …….. to each other.

(e) Describe in mathematical terms crease (3) …… .
Mark it on the picture and denote it by GI.

(f) Angle FGI is …… because ……
..…… .

(g) Describe in mathematical terms crease (4) …..…….. .
Mark it on the picture and denote by J, K, L its points of intersection with GF, EH, AB respectively.

(h) Crease (4) passes through D, D' because ……..……..……..……
……..…… .

(i) What is the ratio of JK to DL? …… Why? ……..……....
……...……..…… .

(j) Mark crease (5) on the picture and shade the rectangle representing the envelope.
Explain why, after crease (5), point C lies on the lower border of the envelope.
…..…….…… .

Use the back of the sheet to work out the answers to the following questions. If you prefer, you can ***first*** *answer question* (n)*,* ***then*** *use what you got in order to find the answers to* (k), (l), (m).

(k) If you use a 18 × 30 cm sheet, what size will the envelope have?

(l) If you want to get a 10 × 15 cm envelope, what size must the sheet have?

(m) Is it possible to get a 10 × 22 cm envelope?

(n) Set AD = a, AB = b. Find the measures of the envelope sides in term of a and b.
Find the ratio of the area of the envelope to the area of the sheet.
If you got everything right, you will find that this ratio does **not** depend on a and b.

(o) For which value of b/a is the envelope similar to the sheet used for the model?

Figure 3. Worksheet on the envelope.

If we look at the crease pattern of the model in Figure 2, we notice that these and similar questions can be answered once the Pythagorean theorem has been studied: all the creases, except the first one, are at a 45° angle to the sides. Thus, the dimensions x and y of the envelope can be easily related to the dimensions a and b of the sheet.

A worksheet that guides students through the study of this model is given in Figure 3.

But, perhaps, an experimental mathematics activity before the study of the Pythagorean theorem is more exciting than filling out a worksheet. Of course, my students do know the Pythagorean theorem, so I put the question in these terms:

> Pretend you are in fifth grade (no Pythagoras!). What size must the paper have if you want an envelope measuring 12×17 cm? Experiment with various sheets, working in groups of three to four persons; make a conjecture, verify it, and correct it if necessary. Explain your reasoning.

Generally speaking, students in Italy are not used to experimental mathematics. As a result, they did not know what to do and kept changing the sizes of both sides of the paper at once, thus not going very far. Had they kept a fixed, they would have easily noticed that y stays fixed, and as b increases, so does x; hence as b/a increases, y/x decreases (Figure 4).

Likewise, if b is fixed, x stays fixed; and as a increases, so does y; hence as b/a decreases, y/x increases (Figure 5).

I must admit, though, that I did not give them much time to work on the problem. Indeed, time is always a major problem in my workshops: in 20 hours I have to teach them how to fold, how to read origami diagrams, how to teach origami to their class and, most of all, how to use origami to do mathematics at school.

The following year, some groups (the A groups) received a set of sheets with a fixed and the others (the B groups) received sheets with b fixed; both also got an appropriate worksheet designed to guide their reasoning. The first steps were to fold an envelope from each of the four supplied sheets, measure its sides, and fill in the relative table. The theoretical results are summarized in Tables 1(a) and 1(b), respectively, but in reality they can vary a little, depending on accuracy in folding.

The A people noticed that a fixed implies y fixed, and that each time b increases by 2 cm, x increases approximately by 0.7 cm (see Table 1(a)); likewise, the B people noticed that b fixed implies x fixed, and that each time a increases by 2 cm, y increases approximately by 1.4 cm (Table 1(b)). Thus, at school, this model can also serve as an introduction to the concept of a function.

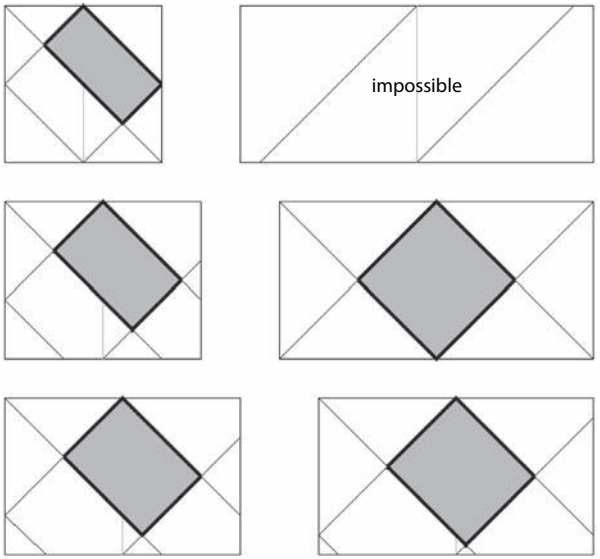

Figure 4. Comparing envelopes folded from sheets with a fixed.

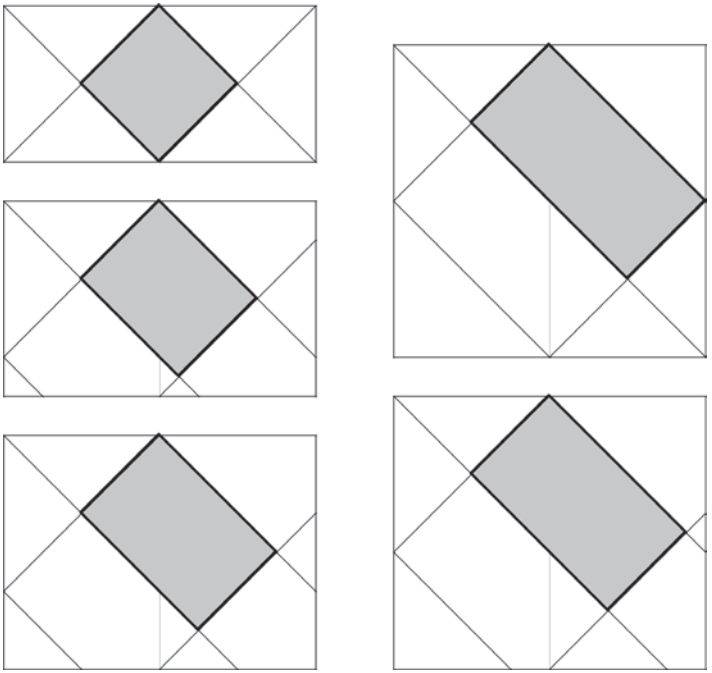

Figure 5. Comparing envelopes folded from sheets with b fixed.

$a \times b$	$x \times y$
12 × 14	*5.0 × 8.5*
12 × 16	*5.7 × 8.5*
12 × 18	*6.4 × 8.5*
12 × 20	*7.1 × 8.5*

(a)

$a \times b$	$x \times y$
10 × 18	*6.4 × 7.1*
12 × 18	*6.4 × 8.5*
14 × 18	*6.4 × 9.9*
16 × 18	*6.4 × 11.3*

(b)

Table 1. Measuring x and y for the folded envelopes. (a) Results from A group. (b) Results from B group. In order to distinguish between questions and answers, bold face has been used here for what was already printed in the tables, and italics for the answers.

In the second part of the worksheet, students were asked to make conjectures, based on the previous results, about the sizes of the envelope or of the sheet, verify them, and correct them if necessary. The A groups' questions can be summarized in Table 2. The analogous questions for the B groups will not be discussed here, being essentially the same as those for the A groups.

In the first two cases, with the same a as before, everybody gave the correct answer. This means they had detected the linearity of the function with which they were dealing. In the third question, they had to reverse their reasoning, which was hard for most of them. An easier approach would be to notice that the desired envelope has both sides approximately twice as big as the one obtained with a 12 × 18 cm sheet, hence this must hold for the sides of the paper as well. To this, some objected that similarity is not studied in fifth grade. This is true, but I believe that fifth graders have a basic knowledge of the concept from everyday life (clothes in different sizes, photos printed in different formats, maps in different scales, ...). In question 4, b is the same as in one case in Table 1(a) while a is increased by 2 cm. The best guess was that the envelope would measure 6.4 × 9.2 cm, which is wrong, but makes some sense: after all, to them a 2 cm increase of

	$a \times b$	$x \times y$
1	12 × 22	
2	12 × 17	
3		13 × 17
4	14 × 18	
5	18 × 24	
6		10 × 18.5

Table 2. Conjecturing on x and y or on a and b.

a side of the paper meant a 0.7 cm increase of a side of the envelope. Upon measuring the model, once they found out that their conjecture was wrong, they were surprised and unable to explain why. In the next questions, both sides (either of the paper or of the envelope) are different from those of the samples worked out before. However, in case 5 the sheet is similar to a previously used one, and this makes the question easier than in the last case, where some ingenuity is needed. Few participants answered question 5 correctly, while nobody was able to do so with the last question; it is likely that more time would have helped someone to argue correctly, but most of them really did not know what to do. Alternatively, to make the problem easier, each group should get both sets of sheets and fill in both Tables 1(a) and (b).

As I said earlier, it is easy to compute x and y in terms of a and b, once the Pythagorean theorem has been studied. Figure 6 shows that the sides of the envelope are the legs of isosceles right triangles whose hypotenuses measure $b/2$ and a respectively, so that

$$x = \frac{b}{2\sqrt{2}} = \frac{b\sqrt{2}}{4}, \quad y = \frac{a}{\sqrt{2}} = \frac{a\sqrt{2}}{2}, \tag{1}$$

hence

$$\frac{y}{x} = \frac{a\sqrt{2}}{2} \Big/ \frac{b\sqrt{2}}{4} = 2\,\frac{a}{b}.$$

This means that, if the sheet is a $1 \times k$ rectangle (i.e., $b/a = k$), then the envelope is a $1 \times k'$ rectangle, with $k' = 2/k$, thus making more precise the statement "as b/a increases, y/x decreases"; in fact, they are inversely

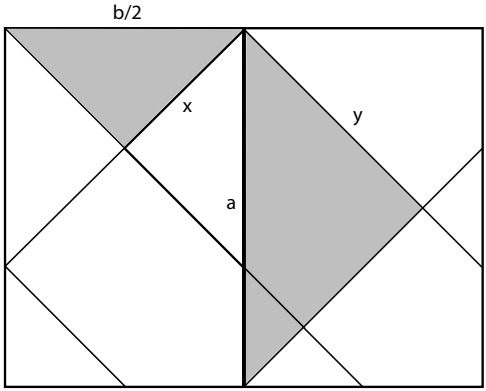

Figure 6. Computing x and y.

proportional, their product being equal to 2. Moreover, the envelope is similar to the sheet if, and only if,

$$k = \sqrt{2},$$

i.e., the paper is a silver rectangle, the standard size for paper in most European countries, including Italy.

The inverse formulas of Equations (1) are

$$a = y\sqrt{2}, \quad b = 2x\sqrt{2}.$$

Since we have assumed $a \leq b$, the above relations imply

$$y \leq 2x,$$

which means that it is not possible to obtain a $1 \times k'$ envelope for $k' > 2$.

Students accustomed to working with some kind of dynamic geometry software might prefer to simulate the folding procedure at the computer: they can start from a "dynamic" rectangle representing the sheet of paper, construct the crease pattern of the envelope, and figure out everything. Reversing the input with the output, they can start from a dynamic rectangle representing the envelope and construct the sheet of paper around it (Figure 7 (right)).

This allows one to answer the real-life questions we asked at the beginning; in particular, it makes very clear (Figure 7 (left)) that, if the desired envelope is "too long," it is impossible to fold it.

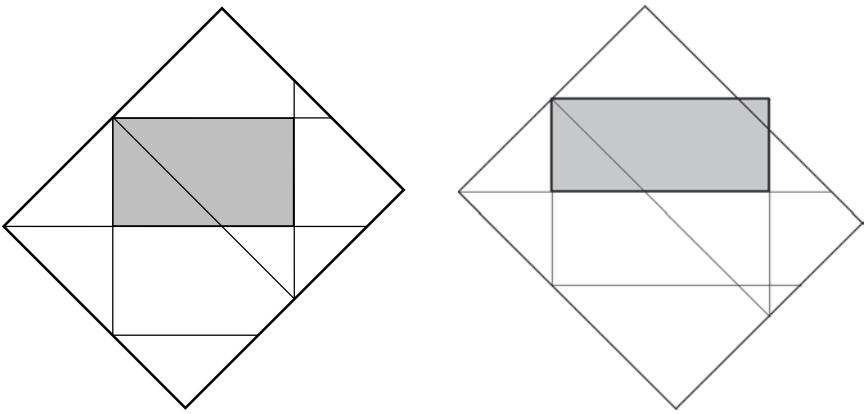

Figure 7. Constructing the sheet of paper around a given envelope: a possible case (left) and an impossible case (right).

Finally, whenever the envelope can be folded (which happens if, and only if, $a \leq 2\,b$), the area of the envelope is

$$x\,y = \frac{b\sqrt{2}}{4}\,\frac{a\sqrt{2}}{2} = \frac{a\,b}{4},$$

hence the ratio of the area of the envelope to the area of the sheet is always $1/4$.

This last result could be visually ascertained by younger students if they folded the envelope with a sheet of tissue paper. By holding it against a window, they would notice that it is evenly made of four layers. They could also cut the model along the folds and rearrange the pieces into a sort of multilayer tangram.

3 Isometries

Older students previously exposed to isometries can identify them on the crease pattern of the envelope. Indeed, the mathematical description of flat folding is reflection along the crease line of the part of the paper that we actually move (Figure 8). Moreover, the composition of two reflections is a translation if the axes are parallel—the vector of the translation is perpendicular to the axes, its length is twice the distance between them, and its direction is from the first to the second axis. If the axes intersect, then the composition of two reflections is a rotation; in particular, if the axes are perpendicular to each other, the rotation is by 180° about the intersection of the two axes.

The crease lines divide the sheet into regions, whose final position can be found by applying a composition of reflections to them.

In Figure 9, each part of the multilayer tangram created by the crease pattern of the envelope is labeled with a number, indicating the layer,

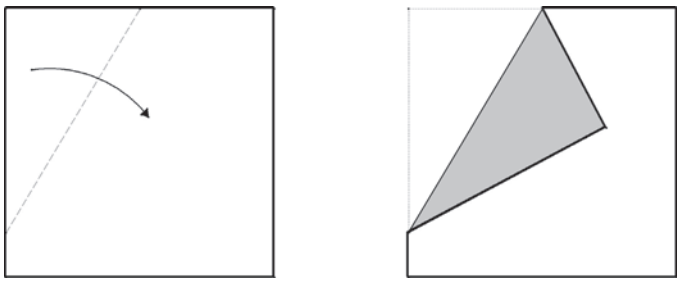

Figure 8. Flat folding = reflection of a part of paper along the crease line.

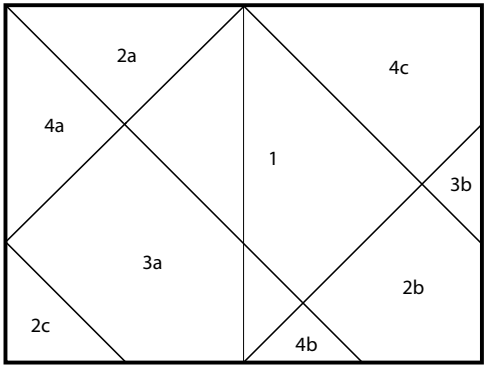

Figure 9. The multilayer tangram pieces.

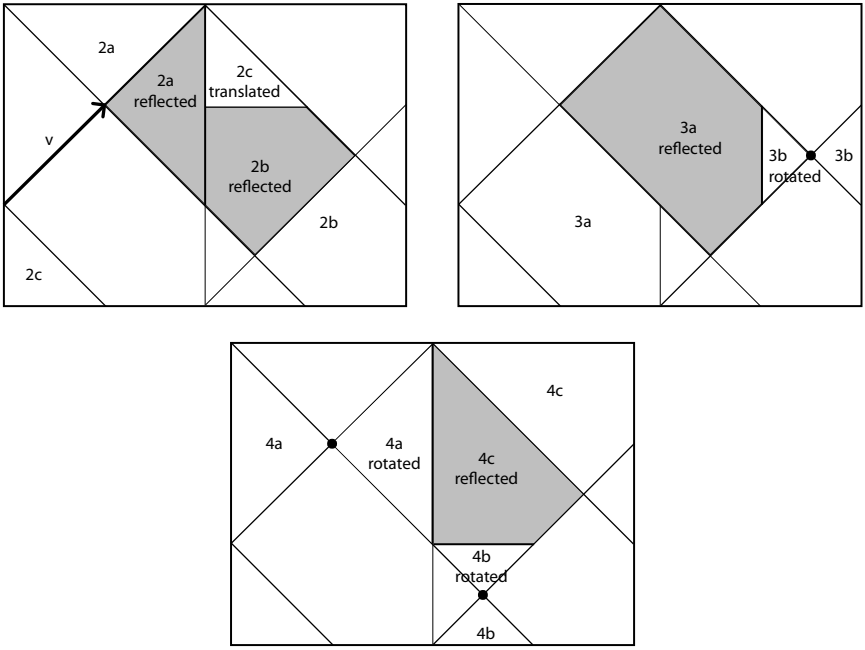

Figure 10. Reflections, translation, and rotations of the tangram pieces.

followed by a letter. Layer 1 is made of just one piece, so no letter is needed. Layers 2 and 4 are made of three pieces, while layer 3 is made of two. Observe that, in the folded model, pieces 4a and 4b are inside, between the second and the third layer, whereas 4c is outside, so it is not a real layer.

Then we can notice, as in Figure 10:

- 2a and 2b reflect themselves along the crease lines made in Step 2 (see Figure 1), while 2c, which reflects itself twice along parallel lines, translates by vector $\mathbf{v}$, determined by the folds in Step 2;
- 3a reflects itself along the crease line made in Step 4, while 3b rotates by 180° about the point of intersection of creases made in Steps 2 and 5;
- 4a and 4b rotate by 180° about the points of intersection of the creases made in Steps 2 and 4, while 4c reflects itself along the crease line made in Step 5.

The effect of these isometries on the tangram pieces can be easily demonstrated by using geometry software or can be proved rigorously from the crease pattern. Both approaches give students a valuable experience.

4 Final Remarks

In conclusion, this model provides so many opportunities to do mathematics that a teacher willing to use origami in geometry lessons should not overlook it.

A somewhat similar model by the late Humiaki Huzita was published in 1989 in the Centro Diffusione Origami newsletter [3]; however, it should be noted that it can be folded properly only from a silver rectangle, the result also being a silver rectangle. The folding sequence is much more complicated than in Canovi's model, but the envelope is self-locking. In Huzita's model (see Figure 11), the area of the envelope is one sixth the area of the sheet, as he himself pointed out in his diagrams; moreover, the sheet can be cut along the creases and the pieces rearranged tangram-style to demonstrate it. But the folded envelope is not a six-layer tangram, the number of layers at any given point ranging from four to eight.

Huzita was a pioneer in the field of origami and science and the beginner of these meetings, so we are all, in some sense, indebted to him. I was initiated into the study of the geometry of origami personally by him; his reasoning was often unusual and sometimes hard to follow due to a language barrier, but his insight was really deep. From him I learned to look at things from novel points of view, and now I regret not having more conversations with him on the subject. Thank you, Humi.

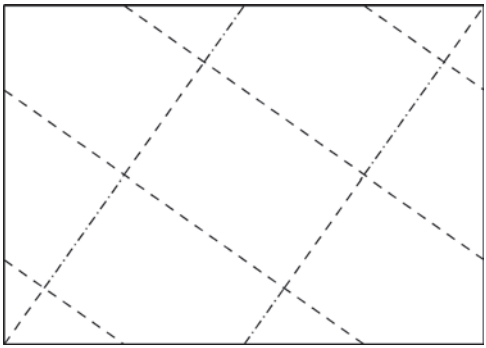

Figure 11. The crease pattern of Huzita's envelope with mountain-fold/valley-fold assignment indicated.

Bibliography

[1] L. Canovi. *Corso pratico di origami*. Milan: Fabbri Editori, 1999.

[2] E. Frigerio. "In Praise of the Papercup." In *Origami^3: Proceedings of the Third International Meeting of Origami Science, Mathematics, and Education*, edited by Thomas Hull, pp. 291–298. Natick, MA: A K Peters, 2002.

[3] H. Huzita. "Busta." *Quadrato Magico* 21 (1989), 13.

Contributors

- Roger C. Alperin, Department of Mathematics, San Jose State University, San Jose, CA, USA,
alperin@math.sjsu.edu
- Hideaki Azuma, 3-5-A-204, Koi-no-kubo, Nara-shi, Nara 630-8136, Japan,
azumahdk@syd.odn.ne.jp
- Devin J. Balkom, Computer Science Department, Dartmouth College, Hanover, NH, USA,
devin@cs.dartmouth.edu
- sarah-marie belcastro, Department of Mathematics and Statistics, Smith College, Northampton, MA, USA,
smbelcas@toroidalsnark.net
- Norma J. Boakes, School of Education, Richard Stockton College of New Jersey, Pomona, NJ, USA,
norma.boakes@stockton.edu
- Margaret Cagle, Lawrence Gifted Magnet, Los Angeles Unified School District, Los Angeles, CA, USA,
peg@cagle.com
- Chew Min Cheong, University of Tokyo, Tokyo, Japan,
cheongchewmin@gmail.com
- Timothy Y. Chow, Center for Communications Research, Princeton, NJ, USA,
tchow@alum.mit.edu

- V'Ann Cornelius, Mingei International Museum, San Diego, CA, USA, jc@hangarpilot.net (John Cornelius)
- Christoffer Cromvik, Department of Mathematical Sciences, Chalmers University of Technology and Department of Mathematical Sciences, University of Gothenburg, Gothenberg, Sweden, christoffer.cromvik@chalmers.se
- Erik D. Demaine, Computer Science and Artificial Intelligence Laboratory, Massachusetts Institute of Technology, Cambridge, MA, USA, edemaine@mit.edu
- Martin L. Demaine, Computer Science and Artificial Intelligence Laboratory, Massachusetts Institute of Technology, Cambridge, MA, USA, mdemaine@mit.edu
- Kenneth Eriksson, Department of Engineering Science, University West, Trollhättan, Sweden, kenneth.eriksson@hv.se
- C. Kenneth Fan, Girls' Angle: A Math Club for Girls, 27 Jefferson St. #6, Cambridge, MA, USA, ckfan@post.harvard.edu
- Jack Fastag, Lambertville, NJ, USA, jf52@cornell.edu
- Robin Flanagan, Department of Psychology, Western Connecticut State University, Danbury, CT, USA, flanaganr@wcsu.edu
- Emma Frigerio, Department of Mathematics, University of Milan, Milan, Italy, emma.frigerio@unimi.it
- Matthew Gardiner, Australian Network for Art and Technology, Adelaide, South Australia, Australia, matt@airstrip.com.au
- Robert Geretschläger, BRG Kepler Graz, Graz, Austria, robert.geretschlaeger@brgkepler.at
- Fadoua Ghourabi, Department of Computer Science, University of Tsukuba, Tsukuba, Japan, ghourabi@score.cs.tsukuba.ac.jp
- Miri Golan, Israeli Origami Center, Ramat-Gan, Israel, origami@netvision.net.il

- Rona Gurkewitz, Department of Computer Science, Western Connecticut State University, Danbury, CT, USA,
gurkewitzr@wcsu.edu
- Elias Halloran, Bard College, Annandale-on-Hudson, NY, USA,
e.t.halloran@gmail.com
- Alexander C. Huang, P.O. Box 16029, Stanford University, Stanford, CA, USA,
zhizhen@stanford.edu
- Thomas C. Hull, Department of Mathematics, Western New England College, Springfield, MA, USA,
thull@wnec.edu
- Tetsuo Ida, Department of Computer Science, University of Tsukuba, Tsukuba, Japan,
ida@score.cs.tsukuba.ac.jp
- Ushio Ikegami, Faculty of Mathematics, Kyushu University, Fukuoka, Japan,
foldable-at-its-lirnit@o.email.ne.jp
- Paul Jackson, Israeli Origami Center, Ramat-Gan, Israel,
origami@netvision.net.il
- Asem Kasem, Department of Computer Science, University of Tsukuba, Tsukuba, Japan,
kasem@score.cs.tsukuba.ac.jp
- Jien Kato, Department of Systems and Social Informatics, Graduate School of Information Science, Nagoya University, Nagoya, Japan,
jien@is.nagoya-u.ac.jp
- Ken-Ichi Kawaguchi, Department of Architecture, University of Tokyo, Tokyo, Japan,
kawaken@iis.u-tokyo.ac.jp
- Miyuki Kawamura, 3-10-521 Yaemizo Saga, Saga 849-0935, Japan,
myu3@beige.plala.or.jp
- Hidefumi Kawasaki, Faculty of Mathematics, Kyushu University, Fukuoka 33, 812-8581, Japan,
kawasaki@math.kyushu-ac.jp
- Toshikazu Kawasaki, Department of General Education, Anan National College of Technology, Tokushima 774-0017, Japan,
kawasaki@anan-nct.ac.jp

- Goran Konjevod, Department of Computer Science and Engineering, Arizona State University, Tempe, AZ, USA, goran@asu.edu
- Kaori Kuribayashi, Center for International Research on Micromechatronics, Institute of Industrial Science, University of Tokyo, Tokyo, Japan, kaorik@iis.u-tokyo.ac.jp
- Tung Ken Lam, HR Service, University of Cumbria, Bowerham Road, Lancaster, LA1 3JD, UK, ken.lam@cumbria.ac.uk and tklorigami@yahoo.co.uk
- Robert J. Lang, 899 Forest Lane, Alamo, CA, USA, robert@langorigami.com
- Arle Lommel, Department of Folklore and Ethomusicology, Indiana University, Bloomington IN, USA, fenevad@gmail.com
- Jun Maekawa, 1-1-21-805 Tobitakyu, Chofu, Tokyo 182-0036, Japan, maekawa@nro.nao.ac.jp
- Mircea Marin, Department of Computer Science, University of Tsukuba, Tsukuba, Japan, mmarin@score.cs.tsukuba.ac.jp
- Jun Mitani, Department of Computer Science, University of Tsukuba, Tsukuba, Japan, mitani@cs.tsukuba.ac.jp
- Koryo Miura, University of Tokyo (Emeritus), Tokyo, Japan, miurak@gakushikai.jp
- Charlene Morrow, SummerMath/Psychology and Education Department, Mount Holyoke College, South Hadley, MA, USA, cmorrow@mtholyoke.edu
- Jeannine Mosely, 32 Poplar St., Belmont, MA, USA, j9@alum.mit.edu
- John A. Ochsendorf, School of Architecture, Massachusetts Institute of Technology, Cambridge, MA, USA, jao@mit.edu
- Galen T. Pickett, Department of Physics and Astronomy, California State University, Long Beach, CA, USA, gpickett@csulb.edu

- Sue Pope, Lancaster, England, UK,
sa.pope@yahoo.co.uk

- Karl Schaffer, Dr. Schaffer and Mr. Stern Dance Ensemble, and DeAnza College, Cupertino, CA, USA,
karl_schaffer@yahoo.com

- Hiroshi Shimanuki, Department of Systems and Social Informatics, Graduate School of Information Science, Nagoya University, Nagoya, Japan,
simanuki@watanabe.ss.is.nagoya-u.ac.jp

- Laura Skrip, Department of Psychology, Western Connecticut State University, Danbury, CT, USA,
lauraskrip@yahoo.com

- Saadya Sternberg, 9 Hanoter Street, Beersheva, 84427, Israel,
saadya@saadya.net

- Hiromasa Suzuki, Research Center for Advanced Science and Technology, University of Tokyo, Tokyo, Japan,
suzuki@den.rcast.u-tokyo.ac.jp

- Tomohiro Tachi, Department of Architecture, University of Tokyo, Tokyo, Japan,
ttachi@siggraph.org

- Hidekazu Takahashi, Department of Computer Science, University of Tsukuba, Tsukuba, Japan,
hidekazu@score.cs.tsukuba.ac.jp

- Koichi Tateishi, Department of English, School of Letters, Kobe College, 4-1 Okadayama, Nishinomiya, Hyogo 662-8505, Japan,
koichi_tateishi_@kcc.zaq.ne.jp

- Sachio Teramoto, Service Platforms Research Laboratories, NEC Corporation, Tokyo, Japan,
s-teramoto@bx.jp.nec.com

- Arnold Tubis, Institute for Nonlinear Science, University of California, San Diego, CA, USA,
tubisa@aol.com

- Ryuhei Uehara, School of Information Science, Japan Advanced Institute of Science and Technology, Ishikawa, Japan,
uehara@jaist.ac.jp

- Tamara Veenstra, Department of Mathematics, University of Redlands, Redlands, CA, USA,
tamara_veenstra@redlands.edu

- Naohiko Watanabe, National Maritime Research Institute, Tokyo, Japan,
naohikowatanabe@gmail.com

- Toyohide Watanabe, Department of Systems and Social Informatics, Graduate School of Information Science, Nagoya University, Nagoya, Japan,
watanabe@is.nagoya-u.ac.jp

- Michael Wilson, Department of Education and Educational Psychology, Western Connecticut State University, Danbury, CT, USA,
wilsonm@wcsu.edu

- Zhong You, Department of Engineering Science, Oxford University, Oxford, UK,
zhong.you@eng.ox.ac.uk

- Hajijubok Zainodin, School of Science and Technology, Universiti Malaysia Sabah, Kota Kinabalu, Sabah, Malaysia,
zainodin@gmail.com

- Liudmila I. Zamiatina, 14711 NE 76th St., Redmond, WA, USA,
lucyzam@hotmail.com